Lecture Notes in Civil Engineering

Scott Walbridge · Mazdak Nik-Bakht · Kelvin Tsun Wai Ng · Manas Shome · M. Shahria Alam · Ashraf El Damatty · Gordon Lovegrove *Editors*

Proceedings of the Canadian Society of Civil Engineering Annual Conference 2021

CSCE21 Environmental Track

Springer

Lecture Notes in Civil Engineering

Volume 249

Lecture Notes in Civil Engineering (LNCE) publishes the latest developments in Civil Engineering - quickly, informally and in top quality. Though original research reported in proceedings and post-proceedings represents the core of LNCE, edited volumes of exceptionally high quality and interest may also be considered for publication. Volumes published in LNCE embrace all aspects and subfields of, as well as new challenges in, Civil Engineering. Topics in the series include:

- Construction and Structural Mechanics
- Building Materials
- Concrete, Steel and Timber Structures
- Geotechnical Engineering
- Earthquake Engineering
- Coastal Engineering
- Ocean and Offshore Engineering; Ships and Floating Structures
- Hydraulics, Hydrology and Water Resources Engineering
- Environmental Engineering and Sustainability
- Structural Health and Monitoring
- Surveying and Geographical Information Systems
- Indoor Environments
- Transportation and Traffic
- Risk Analysis
- Safety and Security

To submit a proposal or request further information, please contact the appropriate Springer Editor:

– Pierpaolo Riva at pierpaolo.riva@springer.com (Europe and Americas);
– Swati Meherishi at swati.meherishi@springer.com (Asia - except China, and Australia, New Zealand);
– Wayne Hu at wayne.hu@springer.com (China).

All books in the series now indexed by Scopus and EI Compendex database!

More information about this series at https://link.springer.com/bookseries/15087

Scott Walbridge · Mazdak Nik-Bakht ·
Kelvin Tsun Wai Ng · Manas Shome ·
M. Shahria Alam · Ashraf El Damatty ·
Gordon Lovegrove
Editors

Proceedings of the Canadian Society of Civil Engineering Annual Conference 2021

CSCE21 Environmental Track

Springer

Editors
Scott Walbridge
University of Waterloo
Waterloo, ON, Canada

Kelvin Tsun Wai Ng
University of Regina
Regina, SK, Canada

M. Shahria Alam
University of British Columbia - Okanagan Campus
Kelowna, BC, Canada

Gordon Lovegrove
University of British Columbia - Okanagan Campus
Kelowna, BC, Canada

Mazdak Nik-Bakht
Concordia University
Montreal, QC, Canada

Manas Shome
Matrix Solutions Inc.
Edmonton, AB, Canada

Ashraf El Damatty
University of Western Ontario
London, ON, Canada

ISSN 2366-2557 ISSN 2366-2565 (electronic)
Lecture Notes in Civil Engineering
ISBN 978-981-19-1060-9 ISBN 978-981-19-1061-6 (eBook)
https://doi.org/10.1007/978-981-19-1061-6

This Springer imprint is published by the registered company Springer Nature Singapore Pte Ltd.
The registered company address is: 152 Beach Road, #21-01/04 Gateway East, Singapore 189721, Singapore

Contents

About the Editors

Dr. Scott Walbridge Ph.D., P.Eng. (Alberta), is Professor at the University of Waterloo, where he has worked since completing his Ph.D. at the EPFL in Lausanne, Switzerland, in 2005/2006. He currently serves as Technical Committee (TC) Vice-Chair for the CSA S157 Design Code (Strength Design of Aluminum Structures) and TSC Chair for CSA S6 (Canadian Highway Bridge Design Code) Section 17 (Aluminum Structures). He is also Member of CSA W59 and W59.2 (Canadian structural steel and aluminum welding codes). In addition to his work on various structural design codes, he also currently serves as Program Director for the University of Waterloo's new undergraduate program in architectural engineering. His research has investigated topics in various areas including: fatigue of steel and aluminum welded connections, performance of steel and aluminum mechanical connections, vibration of aluminum pedestrian bridges, and stability of aluminum structures. He was awarded an Alexander von Humboldt Fellowship related to his research on metal fatigue in 2016–2017.

Dr. Mazdak Nik-Bakht is Associate Professor of Construction Engineering & Management in the Department of Building, Civil and Environmental Engineering at Concordia University, Montreal. He is Director of Compleccity Lab and Co-director of Centre for Innovation in Construction and Infrastructure Engineering and Management—CICIEM at Gina Cody School of Engineering and Computer Science. He has a Ph.D. in Construction Engineering and Management from the University of Toronto (2015), as well as a Ph.D. in Structural Engineering from Iran University of Science and Technology (2011). He is Licensed Professional Engineer with Professional Engineers Ontario and has years of professional experience as a structural designer, structural engineering division head, and project manager in structural and infrastructure rehabilitation projects. A new course called 'Big Data Analytics for Smart City Infrastructure' to train the next generation of construction and infrastructure engineering professionals was developed by him in 2019 and has been delivered annually ever since.

Dr. Kelvin Tsun Wai Ng is Professor of Environmental Systems Engineering at University of Regina, Canada. His major fields of interest are in waste management and environmental sustainability, particularly in development of (i) sustainable waste management system, (ii) evidence-based waste policy, and (iii) data-driven waste collection and disposal methods. His projects have been funded by a number of provincial and federal agencies, including NSERC, Mitacs, Communities of Tomorrow, Innovation Saskatchewan, Ministry of Environment, City of Regina, etc. He is Professional Engineer with Permission to Consult in Saskatchewan, Canada. He is also the instructor for a number of popular courses at the Faculty of Engineering and has received the 2017 President's Award for Teaching Excellence.

Manas Shome Ph.D., P.Eng., is Principal Engineer at Matrix Solutions, a Calgary-based environmental engineering consulting firm. Based in Edmonton, he provides technical leadership on water resources engineering projects. He obtained a B.Sc. and M.Sc. in Civil Engineering at the Bangladesh University of Engineering and Technology and earned his Ph.D. in Civil Engineering from the University of Alberta in 1995. His professional experience includes more than 30 years in sustainable water resources management, river engineering, computational modeling of rivers and drainage systems, design of hydraulic structures, and environmental impact assessment studies. An expert in the field of hydrology and hydraulic engineering, he frequently serves as an expert witness at regulatory hearings. Outside his consulting practice, he enjoys research, teaching, and watching sports. His research outcomes have been published in prestigious peer-reviewed journals and in conference proceedings. He is a co-recipient of the 2010 Keefer Medal Award and recipient of the 2015 Excellence in Teaching Award from the University of Alberta's Faculty of Extension. He has been elected to the grade of Fellow by the CSCE in 2019. He has been involved with CSCE since 2000 serving on the Edmonton section in various roles including Chair, and on the organizing committee of the 2012 Annual Conference in Edmonton, Alberta.

Dr. M. Shahria Alam is Professor of Civil Engineering at the University of British Columbia (UBC)'s Okanagan Campus and Director of Green Construction Research and Training Center (GCRTC) at UBC. He is currently serving as Chair of the Engineering Mechanics and Materials (EMM) division of the Canadian Society for Civil Engineering (CSCE). His research interests include applications of smart materials like shape memory alloys and sustainable construction materials, performance-based design, repair/retrofit of structures, and self-centering structures. He is Director of the Applied Laboratory for Advanced Materials & Structures (ALAMS) at UBC. He has authored over 250 peer-reviewed articles and holds several patents. He is the recipient of several national and international awards including CSCE's Pratley Award. He is also Active Member of several ACI and ASCE code committees.

Dr. Ashraf El Damatty is Professor and Chair of the Department of Civil and Environmental Engineering at the University of Western Ontario, London, Ontario, Canada. He is a Fellow of the Canadian Society of Civil Engineering and Fellow

of the Engineering Institute of Canada. He is Research Director at the WindEEE Research Institute. He holds the title of High-End Expert at Tongji University and Sichuan Universities, China. He obtained a B.Sc. and M.Sc. from Cairo University in 1986 and 1991, Ph.D. in Structural Engineering from McMaster University, Canada, in 1995, and an MBA in 2016 in Higher Education Management from University College, London, UK. He is Founder of the Canadian Society of Civil Engineering (CSCE) Steel Structures Committee and serves currently as Chair of the CSCE Structures Division. He has consulted on many projects in North America and the Middle East. He has written about 250 publications, supervised more than 30 Ph.D. and 20 M.Sc. students, and been invited as keynote speaker in many countries around the globe. He received several awards including the Alan Yorkdale Award by ASTM, Honourable Mention in 2014 Casimir Gzowski Medal Competition, 2015 CSCE Whitman Wright Award, 2016 CSCE Horst Leipholz Medal and Western University Faculty Scholar Award, and the 2018 Professional Engineers of Ontario Engineering Medal of Research of Development. His research work has influenced the international codes and engineering practice worldwide.

Dr. Gordon Lovegrove is MBA/Civil Engineer with over 30 years of experience in smarter growth, housing, sustainable transportation, safety, economics, and project management. He was the point man that got the award-winning Universal Transportation Pass (U-Pass) for UBC that tripled transit use at both campuses. His current research focus is on zero-emission, hydrogen-powered rail (hydrail), including several industry partnerships to develop Canada's first hydrail switcher locomotive. He is founding partner of the SMARTer Growth Partnership (smartergrowthpartnership.ca), Associate Professor/Founding Member of UBCO's School of Engineering (ok.ubc.ca), VP Technical Programs for the Canadian Society of Civil Engineering (csce.ca), and Co-author of several best practice guides on sustainable development, health, and safety. He brings 20 years of practical industry development experience plus 14 years of engineering research and design expertise. His research team includes electrical, mechanical, and civil engineering graduate students, plus computer science coders and research assistants.

Detecting NAPL in Unsaturated Soil

R. G. Zytner, A. Dawrea, and J. Donald

1 Background

Many traditional methods have been used to monitor TPH concentrations in the subsurface soil, including excavation grab samples, drilling of boreholes for sample collection and in situ vapour measurements. These in situ measurements and ex situ analysis are considered accurate, as they are normally done with advanced chemical analysis methods like gas chromatography and gas chromatography—mass spectrometry. However, they have many disadvantages, such as being intrusive, take time to execute and being expensive [5].

Geophysical techniques have developed over the last decades to overcome the limitations of the traditional methods due to their ability to observe into the subsurface soil. Options include time domain reflectometry, electrical resistivity, low-frequency electromagnetic induction and ground-penetrating radar (GPR). GPR is a non-destructive geophysical technique which can be used effectively to detect and monitor the presence of objects in the subsurface. One big advantage is that GPR can investigate larger areas at a lower cost [11].

GPR maps the electromagnetic properties of the subsurface soil by generating, emitting and sending high frequency electromagnetic (EM) waves through the soil and producing high-resolution images of the subsurface [3]. GPR does not directly detect and monitor the presence of TPH. Rather, the GPR survey records the discontinuity of the electromagnetic properties of the soil due to the presence of NAPL in the subsurface. Past research has shown that the GPR scans of known hydrocarbon

R. G. Zytner (✉) · A. Dawrea · J. Donald
University of Guelph, Guelph, Canada
e-mail: rzytner@uoguelpha.ca

A. Dawrea
University of Technology, Baghdad, Iraq

S. Walbridge et al. (eds.), *Proceedings of the Canadian Society of Civil Engineering Annual Conference 2021*, Lecture Notes in Civil Engineering 249,
https://doi.org/10.1007/978-981-19-1061-6_1

spill sites is ambiguous and appears to be site dependent [1, 6]. The main objective of this study is to improve GPR data interpretation to allow estimation of the TPH concentration in the unsaturated soil. Three types of soil were studied: silty loam, sandy loam and clay soil. The enhancement process focused on optimizing the operational parameters central antenna frequency and offset separation distance between the transmitter and the receiver. Sensitivity tests were used to optimize both parameters to provide confidence in the TPH threshold level for each soil. Synthetic GPR scans were generated using a MATLAB® based model, giving flexibility to the analysis process.

2 Approach

Method development focussed on ideal antenna frequency and offset distance between the transmitter and the receiver. The robustness of the proposed approach was then evaluated by analyzing synthetic GPR scans that were generated using the finite difference time domain approach (FDTD) with appropriate values of time and space discretization using a model developed on MATLAB®. The two-dimensional GPR scans represented the electrical and physical properties of the contaminated soil model for three types of soil, sandy loam, silty loam and clay. The developed 2D soil model consisted of a model to represent a water table at 0.5 m, giving a two-layer system consisting of an unsaturated contaminated Layer 1 and saturated Layer 2 to reflect the electromagnetic waves. The offset distance between the transmitter and receiver was 1 m with a frequency 1 GHz. The reference residual saturation values (S_N) in the soil varied from 0.01% V (20 mg/kg) to 30% V (62,100 mg/kg) (Table 1).

Determining the soil concentration in the synthetic GPR scan was based on the surface-based reflection process. The GPR scan was analysed to obtain the first breakpoint of the two-way travel time (TWT) that was corrected for zero-time. The time-zero correction of the arrival time of the reflected signal is essential to correct for the extra travel time at the beginning of each measurement. The extra travel time is caused by the travel time in the cables of the radar system. The correction process

Table 1 Soil properties [4, 9]

Soil type	Elora silty loam	Delhi sandy loam	Clay
Permeability (m^2)	$1.22e^{-13}$	$1.10e^{-11}$	$1.0e^{-17}$
Water content (%V)	0.12	0.12	0.12
Porosity	0.55	0.48	0.59
Bulk density (g/cm^3)	1.18	1.73	1.09

includes setting the arrival time of the airwave to correct for drift in the zero time [2].

The corrected TWT was then converted to velocity for reflected signal using Eq. 1:

$$v^2 = \frac{(2d)^2 + x^2}{TWT^2} \tag{1}$$

where, v is velocity (m/ns), d is depth (0.5 m), TWT is two-way travel time of the reflected signal in ns, x is antenna spacing.

Velocity of the EM wave propagation was converted to the dielectric constant of the contaminated soil mixture by $v = c_o/K_{mix}$, where v is velocity of EM propagation (m/ns), c_o is velocity of light in the space (0.3 m/ns) and K_{mix} is the dielectric constant of the host material (7.6 unitless). Using the dielectric constant value allows calculation of the residual saturation (S_N) using Eq. 2:

$$S_N = \frac{\sqrt{K_{mix}} - V_s\sqrt{K_s} - V_a}{\eta\frac{V_w}{V_N}\sqrt{K_w} + \eta\sqrt{K_N}} \tag{2}$$

where, S_N is residual saturation (m^3/m^3), V_W is volumetric water content (m^3), V_N volumetric NAPL content (m^3), K_{mix} is dielectric constant of the contaminated soil model (unitless), K_N is dielectric constant of NAPL (unitless), V_S volume of solid mineral content (m^3), K_s is dielectric constant of the solid mineral (unitless), V_a is volumetric air content (m^3) and η is porosity of soil. The S_N values were then converted to mass units (mg/kg) to obtain the TPH concentration. The threshold level in TPH concentration was determined when the dielectric constant for the soil had negligible change.

3 Results and Discussion

The GPR scans were initially analyzed manually to determine the two-way travel time (TWT) of the reflected waves and then using EKKO v5 [10], with specialized GPR software, to improve accuracy of the results. The first goal was to determine the ideal antenna frequency and offset distance between the transmitter and the receiver. Analysis of the synthetic data showed that the optimum frequency for the GPR scan to penetrate the soil profile was 1 GHz. This frequency is consistent with information in the literature for organic contaminants in soil [7]. The optimal separation distance (S) between the transmitter and the receiver was determined at 1 m using the sensitivity analysis. Both parameters were determined by finding the lowest percentage of error between the measured residual saturation from the 2D-synthetic GPR data set and the initial residual saturation that was set as reference data.

Results showed that the GPR approach could measure TPH levels as lower than 40,000 mg/kg for both the silty loam and the sandy loam due to the system sampling

frequency of 0.05 ns. Due to attenuation of the GPR signal, the GPR technique could not detect TPH in the clay which was not unexpected [12]. These measurement thresholds are much higher than the concentrations typically set for regulatory cleanup levels. Lowering the detection level requires improvement in the signal-sampling rate. One option is increasing the signal frequency. Discussions with Sensors and Software Inc. [10] revealed that their work with a 25 GHz antenna could provide a sampling interval time about 0.002 ns. However, using the central frequency (25 GHz) in real field GPR reduce the penetration depth into the subsurface to millimeters at best and not practical for soil remediation activities.

3.1 Lessons Learned

GPR has the potential to measure TPH levels in soil. The theoretical approach in this study showed that current threshold levels are to high to use GPR for site delineation studies. Possibly, with equipment advancement, the threshold level can be lowered, providing important data on when a site is clean and remediation efforts can cease. However, it should be noted that even the elevated collected GPR data can also be used as input data for numerical models to predict remediation effectiveness [8].

The challenge with using GPR is that success is a function of soil type. As demonstrated in this study, clay could not be analysed as there is too much attenuation of the radar signal. Currently the adjustment of frequency and separation distance between transmitter and receiver does not help for challenging soils like clay.

Acknowledgements The authors are grateful for the scholarship funding received from the Republic of Iraq and the support of Natural Sciences and Engineering Research Council of Canada (NSERC) through the Discovery Grant program.

References

1. Bertolla L, Porsani JL, Soldovieri F, Catapano I (2014) GPR-4D monitoring a controlled LNAPL spill in a masonry tank at USP. J Appl Geophys 103:237–244
2. Bianchini Ciampoli L, Tosti F, Economou N, Benedetto F (2019) Signal processing of GPR data for road surveys. Geosciences 9(2):96
3. Busch S, van der Kruk J, Bikowski J, Vereecken H (2012) Quantitative conductivity and permittivity estimation using full-waveform inversion of on-ground GPR data. Geophysics 77(6):H79–H91
4. Cann D (2005) An experimental design and study of gas phase dispersion in disturbed and undisturbed unsaturated soil. MSc thesis, University of Guelph, Guelph, ON
5. Cassiani G, Binley A, Kemna A, Wehrer M, Orozco A, Deiana R, Boaga J, Rossi M, Dietrich P, Werban U, Zschornack L, Godio A, Gandomi A, Deidda G (2014) Noninvasive characterization of the Trecate (Italy) crude-oil contaminated site: links between contamination and geophysical signals. Environ Sci Pollut Res 21:8914–8931

6. Chen HW, Fan CC, Chen SY, Lu CM (2012) Detection and analysis of LNAPL contaminated site by integrated time-lapse GPR surveys. In: 14th international conference on ground penetrating radar (GPR), Shanghai, 4–8 June 2012, pp 764–768
7. Francisca F, Rinaldi V (2003) Complex dielectric permittivity of soil organic mixtures 20 MHz–1.3 GHz. J Environ Eng 129(4):347
8. Lenhard RJ, Rayner JL, Davis GB (2017) A practical tool for estimating subsurface LNAPL distributions and transmissivity using current and historical fluid levels in groundwater wells: effects of entrapped and residual LNAPL. J Contam Hydrol 205:1–11
9. Robertson PK (2009) Estimating in-situ soil permeability from CPT & CPTu. In: 2nd international symposium on cone penetration testing, Huntington Beach, CA, May 2009
10. Sensors and Software (2019) https://www.sensoft.ca, Oct 2019
11. Srigutomo W, Agustine E (2016) Investigation of underground hydrocarbon leakage using ground penetrating radar. J Phys Conf Ser 739(1):012137
12. Steelman C, Endres A (2012) Assessing vertical soil moisture dynamic using multi-frequency GPR common-midpoint soundings. J Hydrol 436–437:51–66

Odour Emission and Dispersion from a Cold Region Municipal Wastewater Treatment Plant

M. Asadi, A. Motalebi Damuchali, and K. N. McPhedran

1 Introduction

The collection and treatment of municipal wastewaters are high-energy demand processes which lead to the generation and emission of greenhouse (GHG), toxic, and odourous gases. Odours generated from municipal wastewater treatment plants (MWTPs) can negatively affect public health and/or be a nuisance for residents living near MWTPs. Interestingly, odour nuisance from MWTPs has been shown to adversely impact nearby housing prices with decreases up to 15% [24]. Enhanced public awareness and stricter environmental regulations have resulted in increasing public complaints in response to odour pollution in recent decades [6, 14]. The most typical odourous gases produced by MWTPs include the rotten egg smell of hydrogen sulphide (H_2S) and the pungent smell of ammonia (NH_3) [1, 13]. H_2S is a colourless, hazardous, and potentially toxic compound; while NH_3 is a toxic, corrosive and chemically active gas, which can react in the atmosphere creating a greenhouse effect and low visibility [27]. Each of these gases can be produced and emitted during various wastewater treatment processes, however, the highest emissions are typically from anaerobic processes that result in fat and protein degradation [8, 10].

Previous research conducted to address odour characterization, quantification, and abatement for MWTPs has been primarily focussed on processes including preliminary treatment, primary settlers, sludge digestion tanks, sludge thickening, and dewatering facilities [25]. However, field monitoring has shown that other

M. Asadi · K. N. McPhedran (✉)
Department of Civil, Geological, and Environmental Engineering, University of Saskatchewan, Saskatoon, Canada
e-mail: kerry.mcphedran@usask.ca

A. Motalebi Damuchali
Department of Mechanical, Aerospace and Civil Engineering, The University of Manchester, Manchester, UK

S. Walbridge et al. (eds.), *Proceedings of the Canadian Society of Civil Engineering Annual Conference 2021*, Lecture Notes in Civil Engineering 249,
https://doi.org/10.1007/978-981-19-1061-6_2

MWTP processes may also be significant emission sources such as aerobic and anoxic tanks [9]. Overall, field monitoring of emissions from individual processes is often difficult given the tanks are largely open-to-air making emissions sampling problematic. More recently, mathematical modelling has been coupled with empirical data to determine odour emission rate estimates (EREs) and to predict atmospheric concentrations downwind of MWTPs (and vice versa via estimating EREs from downwind sampling regimes). For example, Schauberger et al. [22] calculated H_2S EREs from a tannery WTP based on downwind ambient air sampling and Gaussian regulatory dispersion modelling. Baawain et al. [3] employed AERMOD modelling to investigate H_2S EREs from a MWTP and reported that local H_2S pollution was markedly reduced over the winter [3]. Zhang et al. [29] studied NH_3 EREs from various WTP processes including adsorption-biodegradation activated sludge treatment, sequencing batch reactor (SBR) activated sludge treatment, and two different anaerobic-anoxic-oxic treatment processes. Out of 12 sampling stations, NH_3 concentrations, pH, and temperature were recorded and coupled with the US EPA's WATER9 model to estimate NH_3 EREs. They found that the anaerobic-anoxic-oxic treatment process produced the highest NH_3 at 0.29 ± 0.06 g/m^3 of wastewater [29]. Despite previous research, MWTPs have unique combinations of treatment processes and climate conditions requiring the determination of site-specific EREs to best determine potential impacts of odourous gases on nearby residents.

Overall, the EREs for NH_3 and H_2S from different MWTP treatment processes has not been adequately addressed, especially for regions having widely varying regional temperatures such as MWTPs found in the Canadian prairie provinces. Thus, the main objective of this study was to estimate the NH_3 and H_2S EREs from the open-to-air treatment processes at the Saskatoon Wastewater Treatment Plant (SWTP), Saskatchewan, Canada, and use these EREs to predict the downwind air concentrations in summer and winter seasons using dispersion modelling. Laboratory scale reactors were employed to develop EREs rates from primary and secondary clarifiers, as well as the anaerobic, anoxic and aerobic basins of the bioreactors. Experiments were conducted at 13 and 17 °C to simulate the winter and summer operating temperatures, respectively, which are the result of seasonal temperature variations ranging from −40 to +30 °C. Using the EREs, AERMOD was used as a steady-state plume model to determine the downwind odour concentrations in residential areas near the SWTP.

2 Materials and Methods

The SWTP treats an average wastewater flow rate of 120 million litres per day (MLD) and has the capacity to treat a peak flow rate of up to 300 MLD. It is a Biological Nutrient Removal (BNR) advanced treatment plant and is designated as a Class IV facility. The SWTP treatment process technologies include a grit and screen facility, primary clarifiers, pump station, fermenters, dissolved air flotation (DAF) thickener, bioreactors, secondary clarifiers, ultraviolet disinfection system, nutrient recovery

Fig. 1 Saskatoon Wastewater Treatment Plant (SWTP). WASSTRIP = Waste Activated Sludge Stripping to Recover Internal Phosphate. Bioreactors include anoxic, anaerobic and aerobic processes in different basins. The orange squares represent the approximate sampling locations used for experiments

facility, and anaerobic digesters (Fig. 1) [5]. The primary and secondary clarifiers, and bioreactors are open-to-air facilities, and along with the anaerobic digesters, could potentially be sources of the odourous H_2S and NH_3 gases [2].

Figure 2 shows a schematic flow chart of the methodology for determination of NH_3 and H_2S EREs and dispersion modelling for the open-to-air treatment processes and anaerobic digesters at the SWTP over the summer and winter time periods. The odour EREs from the SWTP anaerobic digesters was recently investigated with H_2S being determined to be the only odourous gas of concern generated from the anaerobic digestion process with an average ERE of 59 kg/d [2]. The EREs for the remaining reactors are determined herein following a similar experimental protocol as Asadi et al. [2]. The dispersion modelling inputs were aggregate EREs including all sources to assess the air concentrations downwind of the SWTP.

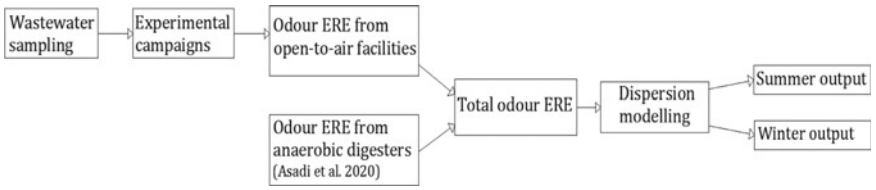

Fig. 2 Schematic flow chart of the study methodology for the determination of EREs and subsequent dispersion modelling using AERMOD from the SWTP. ERE = emission rate estimates

2.1 H_2S and NH_3 EREs from the Open-to-Air Facilities

Figure 3 shows the experimental setup of the batch reactors used for determining EREs for various SWTP processes. Wastewater samples were taken from each of the clarifiers and bioreactor basins on three occasions during each of the summer and winter seasons with six total sampling occasions for each process (Fig. 1). Samples were immediately used in experimental runs with durations of 24 h. The 5 L glass reactors were filled to a working volume of 3.0 L, sealed, and maintained at 13 and 17 °C to simulate the actual SWTP wastewater temperatures for the winter and summer, respectively. All individual experiments were done in triplicates.

For aerobic reactors, an aerobic environment was created by mixing the wastewater via magnetic stirrers and pumping air into the reactor at various rates to keep the dissolved oxygen (DO) concentrations between 1.0 and 2.0 ppm (typical DO

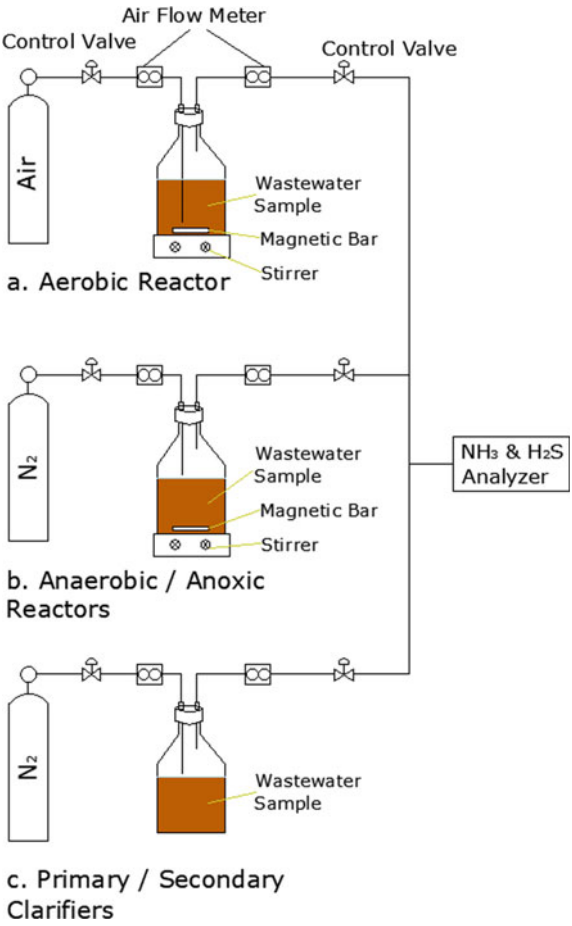

Fig. 3 Schematic experimental setup of batch reactors for simulation of **a** aerobic; **b** anaerobic and anoxic; and **c** primary and secondary clarifiers to estimate gas productions and emissions

Table 1 Characteristics of open-to-air treatment processes at the SWTP (Courtesy of SWTP)

Parameter	Primary clarifier	Anaerobic reactor	Anoxic reactor	Aerobic reactor	Secondary clarifier
HRT (min)	220	120	180	240	380
WFR (m^3/d)	93,000	275,400	275,400	275,400	189,000
Surface area (m^2)	4210	440	1760	3200	5500

range in the aeration basin of the SWTP). For anaerobic and anoxic reactors, the reactors' wastewaters were mixed by a magnetic stirrer and nitrogen gas (N_2) was pumped into the reactor headspaces to carry the produced gases into the gas analyser. The clarifier reactors were left unstirred and subjected to N_2 pumping of the reactor headspaces for gas analysis. The H_2S and NH_3 concentrations were measured using a Gas Alert Micro 5 (Honeywell, US) which was calibrated to measure 0–500 ppm with a resolution of 0.1 ppm.

The air and N_2 pumping rates into the reactors were controlled by valves and continuously monitored by airflow meters positioned before and after each reactor. The EREs from each reactor was determined using the monitored off-gas flowrate and measured H_2S and NH_3 concentrations by the gas analyzer. Thus, the total EREs for each process at the SWTP were computed using the reactor EREs as follows [11]:

$$\mathrm{ERE} = \mathrm{ERE}_{\mathrm{reactor}} \times \mathrm{HRT} \times \mathrm{WFR}/\mathrm{V}_{\mathrm{reactor}} \tag{1}$$

where, ERE = estimate of the gas emission rate from the actual SWTP treatment process; $\mathrm{ERE}_{\mathrm{reactor}}$ = monitored gas emission rate from the reactor; HRT = hydraulic retention time of the treatment process; WFR = wastewater flow rate of the treatment process; and $\mathrm{V}_{\mathrm{reactor}}$ = working volume of the batch reactor (Table 1).

2.2 Dispersion Modelling: AERMOD Model

The U.S. Environmental Protection Agency AERMOD [23] is a steady-state Gaussian dispersion model that is able to compute contaminant dispersion from multiple sources in rural and urban areas under both stable and convective conditions. AERMOD's inputs include source data such as emission rates, and terrain and meteorological data which are initially processed by the AERMAP and AERMET models, respectively. For full details on using this model, please consult [4]. Briefly, the downwind pollutant concentration can be calculated as follows:

$$\mathrm{C_T}\{\mathrm{x_r}, \mathrm{y_r}, \mathrm{z_r}\} = \mathrm{f} \cdot \mathrm{C_{c,s}}\{\mathrm{x_r}, \mathrm{y_r}, \mathrm{z_r}\} + (1 - \mathrm{f})\mathrm{C_{c,s}}\{\mathrm{x_r}, \mathrm{y_r}, \mathrm{z_p}\}, \ \mathrm{z_p} = \mathrm{z_r} - \mathrm{z_t} \tag{2}$$

where, $\{x_r, y_r, z_r\}$ = coordinate representation of a receptor; z_r = measured height relative to stack base elevation; z_p = height of a receptor above local ground; z_t = terrain height at a receptor (for flat terrain $z_t = 0$); C_T $\{x_r, y_r, z_r\}$ = total pollutant concentration; $C_{c,s}$ $\{x_r, y_r, z_r\}$ = contribution from the horizontal plume state in convective (c) and stable (s) conditions; and, $C_{c,s}$ $\{x_r, y_r, z_p\}$ = contribution from the terrain—following state in convective (c) and stable (s) conditions [4].

The AERMET model input included 5 years of hourly climate data that included wind direction and speed, temperature, relative humidity, cloud cover, and ceiling height [21]. The model calculates boundary layer parameters, entailing friction velocity, Monin–Obukhov length, convective velocity scale, temperature scale, mixing height, and surface heat flux, along with the vertical profiles of wind speed, lateral and vertical turbulence fluctuations, potential temperature gradients, and potential temperatures [4]. The AERMAP model input included the terrain characteristics of the City of Saskatoon available by the Canadian Digital Elevation Data [15]. The AERMET and AERMAP outputs were used to input into the AERMOD model to determine pollutant dispersion maps presented herein.

3 Results and Discussion

3.1 EREs

Overall, the experimental results for both summer and winter found that NH_3 emissions from all treatment processes were negligible. This result was somewhat expected as NH_3 emissions from similar treatment processes such as activated sludge-type MWTPs have been reported to be insignificant previously. For instance, Osada et al. [18] investigated five MWTPs across Japan between August 2014 and January 2015, and reported that the NH_3 emissions were negligible in all of the measurements from the wastewater treatment facilities [18]. The NH_3 is typically dissolved in wastewaters in the form of ammonium (NH_4^+) with concentrations dependent on temperature and pH. To release NH_3 into the atmosphere the NH_4^+ must be converted to NH_3. Currently, at a typical SWTP wastewater pH of 7.5 only 0.74% (13 °C) and 0.99% (17 °C) of the nitrogen would be available as NH_3 [7]. Given the maximum reported NH_4^+ influent concentration at the SWTP was around 40 mg/L, only 0.4 mg/L (0.53 ppm) of NH_3 would be expected to be released from the wastewater from any of the treatment processes. This value is negligible and below the detection limit of the gas analyzer used in the current study.

Figure 4 shows the results of H_2S EREs from the open-to-air facilities (determined herein) and anaerobic digesters (from Asadi et al. [2]) and their overall contributions to the total EREs from the SWTP. The winter H_2S emissions were negligible due to neutral pH = 7.5 and average wastewater temperature of 13 °C. Previous research has shown that both pH and temperature have high impacts on the formation and release of H_2S from wastewaters with release being significantly greater in acidic

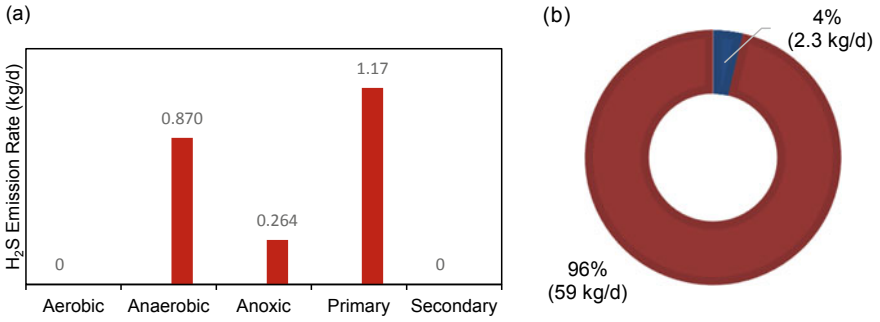

Fig. 4 **a** H_2S EREs for the primary and secondary clarifiers, and aerobic, anaerobic and anoxic bioreactors at a temperature of 17 °C (EREs were negligible at 13 °C); and **b** H_2S EREs for the anaerobic digesters (in orange) in comparison with the open-to-air sources combined (in blue)

conditions (pH < 7.0) [17, 28]. In addition, the solubility of H_2S in water is inversely correlated with the temperature resulting in 5.2 g/kg and 4.1 g/kg water, at 13 °C and 17 °C respectively [16]. Thus, the H_2S would be more readily released in summer months with the increased wastewater temperatures.

As shown in Fig. 4a, the summer H_2S emissions were highest from the primary clarifiers (1.17 kg H_2S/d) followed by the anaerobic and anoxic bioreactors (0.87 kg H_2S/d and 0.26 kg H_2S/d), respectively. Overall, the open-to-air processes total EREs were 2.3 kg/d (0.023 g/s) accounting for only 4–5% of the SWTP emissions (Fig. 4b). The dominant source of H_2S production (96%) was attributed to the anaerobic digesters at an ERE of 59 kg/d (0.68 g/s) [2]. The H_2S EREs from the SWTP open-to-air treatment processes were markedly lower in comparison with other MWTPs with similar capacity which highlights the potentially large variability of EREs between MWTPs in different regions. For example, Llavador Colomer et al. [12] studied H_2S emission rates from three MWTPs in Spain with capacity ranges of 38,962–61,821 m^3/d and reported that the average EREs varied between 0.09 and 2.47 g/s [12].

3.2 AERMOD

Figure 5 illustrates the results of AERMOD H_2S dispersion modeling of the aggregate SWTP H_2S EREs (from Fig. 4b) indicating maximum 24-h concentrations over the summer and winter of 5.67 μg/m^3 and 5.43 μg/m^3, respectively. Both of these values exceed Saskatchewan's ambient air quality standard for an average 24-h concentration of H_2S is 5.00 μg/m^3 [20]. However, it should be noted that gas produced by the anaerobic digesters is currently captured and used to produce heat for the on-site buildings and facilities; therefore, the open-to-air facilities should be considered as the primary sources of H_2S emissions from the plant. Based on this, the 24-h concentrations for both summer and winter would be well below the ambient air

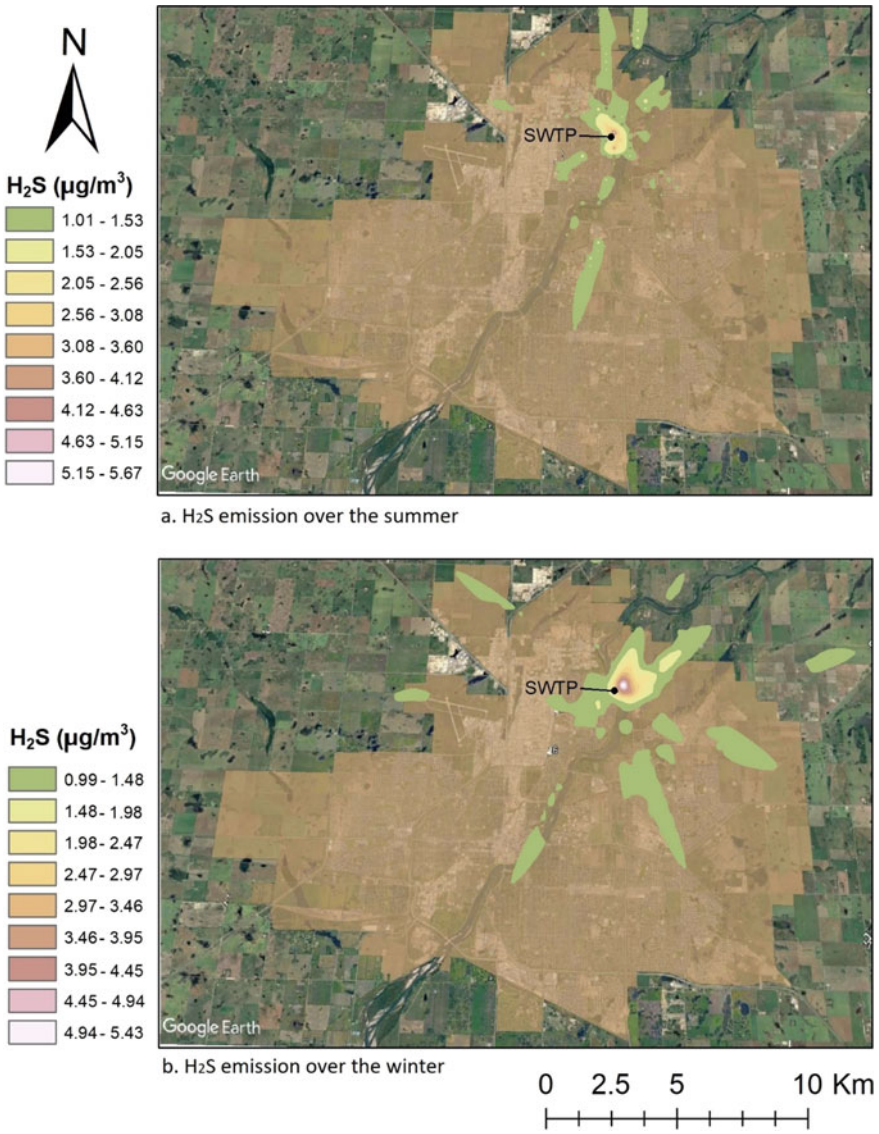

Fig. 5 Results of H_2S dispersion and maximum 24-h concentrations based on total EREs from all SWTP sources for **a** summer; and **b** winter

quality standards. However, it should be noted that other facilities that release gases directly from anaerobic digesters may create local exceedances of ambient air quality standards near other MWTPs.

Generally, the solar radiation intensity, and wind speed and direction are typically the most important factors impacting atmospheric stability and pollutant dispersion

behaviour [19]. The average winter and summer solar radiation intensities for the City of Saskatoon are reported to be 255 MJ/m^2 and 600 MJ/m^2, respectively [26]. In addition, the City of Saskatoon is considered to be a 'windy' location with wind speeds reaching 4.6 m/s. Thus, the summer atmospheric stability is categorised as an unstable atmosphere (Class B) that may result in a favourable conditions for vertical, then horizontal, mixing to be involved in H_2S (and other gas) dispersion [19]. These conditions resulted in the maximum H_2S concentrations close to the SWTP due to the vertical mixing, and other areas of increased concentrations to the south and north of the SWTP due to horizontal mixing (Fig. 5a). For winter, the atmospheric stability is more stable, and occasionally can be either neutral (Class D) or slightly unstable (Class C) [19]. Therefore, horizontal mixing and bulk motion as a function of wind speed would be dominant in the H_2S dispersion under these conditions. Winter results show that wider areas in the downwind of the SWTP could be affected by H_2S emission, and its maximum level was noticed at an approximate distance of 600 m away from the plant (Fig. 5b).

4 Conclusions

The accurate determination of odourous compound EREs and prediction of dispersion from MWTPs via air sampling efforts is difficult given the presence of a variety separate treatment processes that are open-to-air. Thus, the study of EREs and dispersion of odourous compounds, such as NH_3 and H_2S, via laboratory-scale reactors and dispersion modeling can be a useful and practical method to determine potential downwind odour issues. Overall, the NH_3 emissions from SWTP were negligible year-round while the H_2S emissions from the open-to-air processes were highest in the summer with EREs of 1.17, 0.870, and 0.264 kg/d for the primary clarifiers, anaerobic, and anoxic reactors, respectively. The aggregate H_2S EREs from the open-to-air facilities was 2.30 kg/d, however, was only about 4–5% of total produced H_2S at the SWTP with the anaerobic digesters producing 59 kg/d [2]. Downwind H_2S concentrations were dependent upon the meteorological parameters, such as solar radiation and wind speed and direction. Based on the total EREs, the H_2S maximum 24-h concentration exceeded the 5 $\mu g/m^3$ standard near the SWTP. However, this exceedance would only occur with the gas from the anaerobic digesters being released (currently captured). Overall, odourous emissions from the SWTP from are typically well below standards for both NH_3 and H_2S. However, in the summer the H_2S releases from the SWTP may impact nearby residents due to elevated EREs due to temperature, increased dispersion due to wind, and increased exposures due to enhanced activities in the summer months in addition to having windows open during the warmer months in Saskatoon.

Acknowledgements We would like to thank Mike Sadowski, Michael Beal, and Amanda Conway at the Saskatoon Wastewater Treatment Plant for their assistance in the fulfilment of this study. We would also like to extend our thanks to Helen Yin and Rlee Prokopishyn for their assistance in the

implementing of the experimental set-up. This research was financially supported by an NSERC Discovery Grant (K. McPhedran).

References

1. Agus E, Zhang L, Sedlak DL (2012) A framework for identifying characteristic odor compounds in municipal wastewater effluent. Water Res 46(18):5970–5980
2. Asadi M, Guo H, McPhedran K (2020) Biogas production estimation using data-driven approaches for cold region municipal wastewater anaerobic digestion. J Environ Manage 253:109708
3. Baawain M, Al-Mamun A, Omidvarborna H, Al-Jabri A (2017) Assessment of hydrogen sulfide emission from a sewage treatment plant using AERMOD. Environ Monit Assess 189(6):263
4. Cimorelli AJ, Perry SG, Venkatram A, Weil JC, Paine RJ, Peters WD (1998) AERMOD—description of model formulation. U.S. Environmental Protection Agency, North Carolina
5. City of Saskatoon (2018) Life in Saskatoon. https://www.saskatoon.ca/new-saskatoon/life-saskatoon
6. Easter C, Witherspoon J, Voigt R, Cesca J (2009) An odor control master planning approach to public outreach programs. In: Odours and VOCs: measurement, regulation and control techniques, vol31, p 53
7. Emerson K, Russo RC, Lund RE, Thurston RV (1975) Aqueous ammonia equilibrium calculations: effect of PH and temperature. J Fish Res Board Can 32(12):2379–2383
8. Fang J-J, Yang N, Cen D-Y, Shao L-M, He P-J (2012) Odor compounds from different sources of landfill: characterization and source identification. Waste Manage 32(7):1401–1410
9. Huber CV, Smeby KL (2010) Odor emissions from biological nutrient removal processes. Proc Water Environ Fed 2010(3):1–10
10. Lewkowska P, Cieślik B, Dymerski T, Konieczka P, Namieśnik J (2016) Characteristics of odors emitted from municipal wastewater treatment plant and methods for their identification and deodorization techniques. Environ Res 151:573–586
11. Lim Y, Kim D-J (2014) Quantification method of N_2O emission from full-scale biological nutrient removal wastewater treatment plant by laboratory batch reactor analysis. Bioresour Technol 165:111–115
12. Llavador Colomer F, Espinos Morato H, Mantilla Iglesias E (2012) Estimation of hydrogen sulfide emission rates at several wastewater treatment plants through experimental concentration measurements and dispersion modeling. J Air Waste Manag Assoc 62(7):758–766
13. Malhautier L, Gracian C, Roux J-C, Fanlo J-L, Le Cloirec P (2003) Biological treatment process of air loaded with an ammonia and hydrogen sulfide mixture. Chemosphere 50(1):145–153
14. Morales JJ, Köning H, Garcés J, Senante E (2008) Integrated odour control and management in WWTP of the región metropolitana of Santiago de Chile. In: Proceedings of the 3rd IWA international conference on odour and VOCs, Barcelona
15. Natural Resources Canada (2020) Canadian digital elevation model, 1945–2011. Government of Canada
16. Nielsen PH, Raunkjær K, Hvitved-Jacobsen T (1998) Sulfide production and wastewater quality in pressure mains. Water Sci Technol 37(1):97–104
17. Nielsen AH, Vollertsen J, Jensen HS, Madsen HI, Hvitved-Jacobsen T (2008) Aerobic and anaerobic transformations of sulfide in a sewer system—field study and model simulations. Water Environ Res 80(1):16–25
18. Osada T, Shiraishi M, Hasegawa T, Kawahara H (2017) Methane, nitrous oxide and ammonia generation in full-scale swine wastewater purification facilities. Front Environ Sci Eng 11(3):10
19. Pasquill F (1961) The estimation of the dispersion of windborne material. Met Mag 90:33

20. Saskatchewan Ministry of Environment (2012) Air monitoring guideline for Saskatchewan. Regina
21. Saskatchewan Ministry of Environment (2020) Saskatchewan regional meteorological data. Regina. http://www.environment.gov.sk.ca/Default.aspx?DN=d70d8af8-4f6d-4644-984d-c812e0ee261b
22. Schauberger G, Piringer M, Baumann-Stanzer K, Knauder W, Petz E (2013) Use of a Monte Carlo technique to complete a fragmented set of H_2S emission rates from a wastewater treatment plant. J Hazard Mater 263:694–701
23. USEPA (2019) User's guide for the AMS/EPA regulatory model (AERMOD). North Carolina. https://www3.epa.gov/ttn/scram/models/aermod/aermod_userguide.pdf
24. Van Broeck G, Bogaert S, De Meyer L (2009) Monetary valuation of odour nuisance as a tool to evaluate cost effectiveness of possible odour reduction techniques. In: Odours and VOCs: measurement, regulation and control techniques, vol31, p 42
25. Vincent AJ (2001) Sources of odours in wastewater treatment. In: Stuetz RM, Frechen F-B (eds) Odours in wastewater treatment: measurement, modelling and control. IWA Publishing, London
26. Wittrock V (2018) Climate reference station, Saskatoon, annual summary 2017. Saskatoon
27. Yongsiri C, Vollertsen J, Hvitved-Jacobsen T (2004) Hydrogen sulfide emission in sewer networks: a two-phase modeling approach to the sulfur cycle. Water Sci Technol 50(4):161–168
28. Yongsiri C, Vollertsen J, Hvitved-Jacobsen T (2004) Effect of temperature on air-water transfer of hydrogen sulfide. J Environ Eng 130(1):104–109
29. Zhang C, Geng X, Wang H, Zhou L, Wang B (2017) Emission factor for atmospheric ammonia from a typical municipal wastewater treatment plant in South China. Environ Pollut 220:963–970

Assessment of Agricultural Waste Products for Cost-Effective and Eco-Friendly Treatment of Arsenic Contaminated Waters

Kh. Zoroufchi Benis, J. Soltan, and K. N. McPhedran

1 Introduction

Arsenic (As) has a varied and historic relation to humankind. It has been a favorite homicide agent from long before the time of the Borgias (1400s) to the present, was responsible for the carcinogenic action of English chimney soot, caused sickness and death of cattle, and poisoned livestock after being widely used as an insecticide before being replaced by organic insecticides [3]. Nowadays, As is a global health and environmental risk, such that over 200 million people in more than 70 countries are exposed to As concentrations in drinking water that exceed the permissible level of 10 μg/L [40].

Canadians are exposed to As mainly through drinking water and food sources [42]. Typically, higher As concentrations are present in groundwater versus surface water [9] which is important in Canada given approximately one-third of the Canadian population relies on groundwater sources for their drinking water [38]. In addition, As can be ingested by people through consumption of food crops that are irrigated via As-contaminated water [34]. Elevated levels of As (>10 μg/L) in drinking water have been reported in most of the Canadian provinces [17] where naturally elevated levels of As have resulted from erosion and weathering of As-bearing rocks and soils. In the past decades, anthropogenic activities such as gold and uranium mining operations, coal-fired power plants, the use of As-containing wood preservatives and pesticides, and the disposal of industrial and municipal wastes have increased As input to the environment [21]. For example, Saskatchewan has become one of the world's premier uranium producers since 1953 with yields of approximately 350,000 tonnes of U_3O_8 per annum [32]. In 2004, about one-third of the world's annual uranium production was obtained from the Athabasca Basin, northern Saskatchewan, Canada

Kh. Zoroufchi Benis · J. Soltan · K. N. McPhedran (✉)
University of Saskatchewan, Saskatoon, Canada
e-mail: kerry.mcphedran@usask.ca

S. Walbridge et al. (eds.), *Proceedings of the Canadian Society of Civil Engineering Annual Conference 2021*, Lecture Notes in Civil Engineering 249,
https://doi.org/10.1007/978-981-19-1061-6_3

[20]. If the benefits of uranium production are the economic and strategic advantages for Saskatchewan and Canada, the legacy of its abandoned or decommissioned facilities, tailings, waste rocks, and flooded mines can be the drawbacks. These drawbacks also include the potential for releases of metals/metalloids, such as As, into receiving environments as they become available throughout the mining process. These waste streams must be treated prior to their release to safeguard both human and environmental health.

Treatment technologies depends on several key factors such as initial As concentrations, As speciation, target treatment levels, and regulatory requirements [10]; however, economic feasibility is the main factor for the selection of a technology for As abatement [13]. Among the presently available technologies for removal of As from water such as coagulation, filtration, membrane separation, reverse osmosis, sorption is considered to be one of the best methods due to its simplicity, low cost, and the potential for sorbent regeneration [36, 44, 49]. Sorption can occur due to van der Waals forces (i.e., physical sorption or physisorption) or chemical interactions (i.e., chemical sorption or chemisorption) between solute species/molecules (i.e., sorbate) and the solid surface of the sorbent [27]. A wide variety of sorbents derived from various sources such as modified activated carbons, metal oxides, gels, resins, and biomass have been utilized for As removal from water [35, 50]. Despite the relatively low costs of sorption versus other treatment methods, ongoing research is being conducted on biosorption using waste biomasses as a cheap alternative to more expensive commercial sorbents [5, 51].

Given the presence of elevated As concentrations in Canadian groundwaters and surface waters, in conjunction with an abundance of freely available agricultural waste biomasses, use of these biomasses for biosorption of As is an area of current research interest. Thus, the present study compares the sorption capacities of two abundant agricultural wastes in Saskatchewan, canola straw (CS) and wheat straw (WS), for the removal of As from water with consideration of solution pH and equilibration times.

2 Materials and Methods

2.1 Materials

Raw CS and WS were collected from a field in Saskatchewan, washed with tap water to remove soil, dried at 60 °C for 24 h, then ground and sieved using a 20–40 mesh. Then, they were washed with deionized water (DI) and dried at 60 °C for 24 h. Pentavalent As(V) stock solutions were prepared by dissolving sodium arsenate ($Na_2HAsO_4{\cdot}7H_2O$) in ultra-pure water (18.2 MΩ cm). The solution pH was adjusted to 3–10 using 0.1 M HCl and/or 0.1 M NaOH. All chemicals were purchased from Fischer Scientific (Canada).

2.2 Analysis

Solution pH was measured by pH meter (265, Beckman, Canada). The molybdenum blue method was applied to measure the As(V) concentration [26, 37] using a UV–vis spectrophotometer (DR6000, Hach, Canada). Briefly, for each 4.5 mL of sample, 0.05 mL of 98% H_2SO_4 acidifying solution, 0.2 mL of molybdate coloring reagent, and 0.1 mL of ascorbic acid solution were added in sequence, respectively. The absorbance at 844 nm was measured within 30 min using the UV–vis spectrophotometer.

The pH of zero-point charge (pH_{PZC}) of the sorbents was determined by the pH drift method [47]: 50 mL NaCl of 0.01 mol/L solution was placed in a 100 mL glass bottle. The pH of the solution was adjusted to 2–10 by adding 0.1 M HCl or NaOH solutions. Then, 0.1 g of the dried sorbent was added and the final pH was measured after 72 h agitation at 150 RPM. The pH_{PZC} of the sorbent is the point where the curve $pH_{initial}$ versus pH_{final} crosses the line of equality.

2.3 Batch Sorption Experiments

Batch sorption experiments were carried out in glass Erlenmeyer 250 mL flasks containing 150 mL As(V) solution with a sorbent dosage of 3 g/L. All experiments were performed at a constant temperature of 25 ± 0.2 °C. The required contact time to reach equilibrium was determined based on the Kinetic studies (see Sect. 2.5). The sorption capacity q_e (mg/g) of CS and WS were calculated via:

$$q_e = \frac{(C_0 - C_t)V}{W} \tag{1}$$

where C_0 (mg/L) and C_t (mg/L) are the As(V) concentrations at times (h) $t = 0$ and $t = h$, respectively; V (L) and W (g) are the volume of the As(V) solution and the mass of the sorbent, respectively.

2.4 FTIR Spectroscopy

The surface functional groups on the sorbents were determined using a Smith's Detection IlluminatIR FTIR microscope (Canada) accessory equipped with liquid nitrogen cooled MCT detector. The FTIR scans were collected in the wave number range of 4000–650 cm^{-1} with a spectral resolution of 4 cm^{-1}.

2.5 Kinetic Studies

The As(V) sorption kinetics were studied in batch mode, at 25 °C to elucidate the sorption mechanism and sorption characteristics of the sorbents. Sorbents (3 g/L) were suspended in an As(V) solution of 5 mg/L and stirred at 200 RPM, with samples taken at specific time intervals. The experimental data were modeled via pseudo-first-order (Eq. 2), pseudo-second-order (Eq. 3), intra-particle-diffusion (Eq. 4), and Elovich (Eq. 5) models [7, 39, 41, 48]:

$$\ln(q_e - q_t) = \ln q_e - k_1 t \tag{2}$$

$$\frac{t}{q_t} = \frac{1}{k_2 q_e^2} + \frac{t}{q_e} \tag{3}$$

$$q_t = k_p t^{0.5} + C \tag{4}$$

$$q_t = \frac{1}{b}\ln(ab) + \frac{1}{b}\ln(t) \tag{5}$$

where q_t (mg/g) is the As(V) sorbed per gram of sorbent at specific time intervals; k_1 (1/h), k_2 (mg/g.h), and k_p (mg/g.h$^{0.5}$) are pseudo-first order, pseudo-second order, and intra-particle diffusion rate constants, respectively; C is the intercept; a (mg/g.h) is the initial sorption rate; and b (g/mg) is the Elovich constant.

3 Results and Discussion

3.1 FTIR Spectra

Figure 1 shows the FTIR spectra of the sorbents in the range of 4000–650 cm^{-1}. Although there appear to be no significant spectra shifts for CS, WS, As(V)-loaded CS and WS samples, these spectra provide information on the presence of lignin,

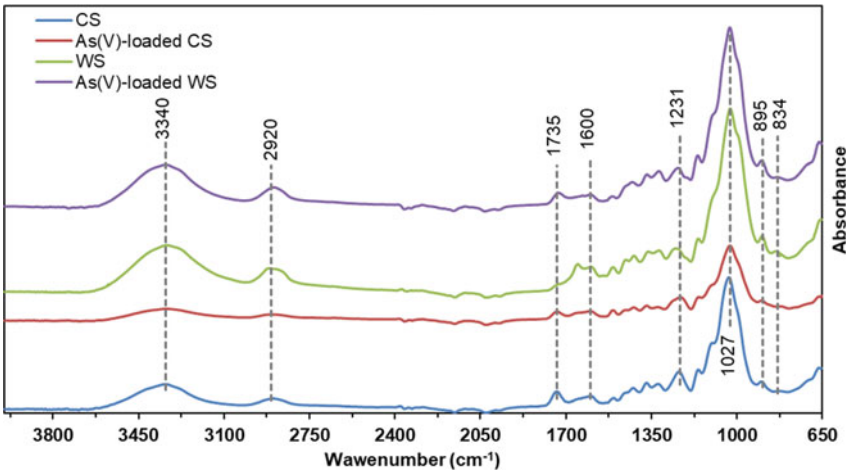

Fig. 1 FTIR spectra of the four sorbents including raw and As(V)-loaded CS and WS

hemicellulose, cellulose, and other functional groups [4, 6]. The spectra show broad and intense absorption bands at ~3340 cm^{-1} which indicates the presence of –OH surface functional groups [24]. Spectral peaks at ~2920 cm^{-1} could be attributed to the C–H aliphatic axial deformation in CH_2 and CH_3 groups from cellulose, lignin, and hemicellulose [4, 6]. The band at ~1735 cm^{-1} can be associated with the acetyl groups present in hemicellulose. The bands at ~1600 cm^{-1} indicate aromatic skeletal vibrations plus C=O stretch that is generally found in the lignin aromatic structure [2]. The band at ~1231 cm^{-1} can also be due to C–OH stretching of the phenolic groups, and the band at ~1027 cm^{-1} can be assigned to the C–O in cellulose [22]. The band at ~895 cm^{-1} is an asymmetrical stretching vibration of the C–O–C ring in cellulose [30], while the band at ~834 cm^{-1} might be associated with aromatic C–H out-of-plane vibration in lignin [11].

3.2 Effect of Initial pH

Solution pH plays an important role in As(V) sorption using biomaterials and affects not only the speciation of As in aqueous medium, but also the surface charge of the sorbent material. Distributing equations and pK_a values of As(V) are as follows [43]:

$$\begin{aligned} \text{As(V)} \quad & H_3AsO_4 \leftrightarrow H_2AsO_4^- + H^+ && pK_{a1} = 2.24 \\ & H_2AsO_4^- \leftrightarrow HAsO_4^{2-} + H^+ && pK_{a2} = 6.94 \\ & HAsO_4^{2-} \leftrightarrow AsO_4^{3-} + H^+ && pK_{a2} = 11.5 \end{aligned}$$

Based on the pK_a values, As(V) exists as oxyanions at pH values higher than 2.24. The pH drift method was applied to determine the pH_{PZC} values of the sorbents. As

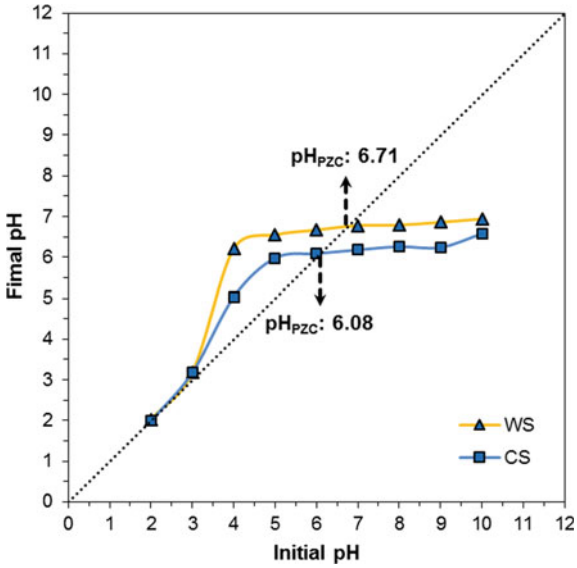

Fig. 2 Experimental results on pH_{PZC} determination

can bee seen in Fig. 2, the pH_{PZC} of WS was slightly higher than that CS that might be attributed to the presence of a higher amount of basic functional groups on the surface of WS. The pH_{PZC} plays a crucial role in the As(V) sorption process since the sorption of As oxyanions can effectively take place at pH values below pH_{PZC} due to electrostatic attraction between positively charged sorbent and negatively charged As(V) anions. As the pH of the solution increases up to pH_{PZC}, the As(V) sorption decreases due to the increasing the repulsion between the As species and the surface of the sorbent [46].

Figure 3 shows the sorption capacities obtained for WS and CS under different pH conditions. The maximum As(V) sorption on WS (1.32 mg/g) was found at pH 4–5, which is below the corresponding pH_{PZC}. However, the sorbed As(V) become negligible at pH < 3 (0.04 mg/g) which can be attributed to the dissolution of the substrate and, subsequently, reduction in the number of active sites [8]. Clearly, the sorption of As(V) to WS follows the expectations based on the measured pH_{PZC} with a peak at pH 4–5.

In contrast to WS, the sorbed As(V) on CS increased sharply from 0.02 mg/g at pH 3 to 1.28 mg/g at pH 7 where it then plateaued to 1.30 mg/g at pH 10. Interestingly, the sorption capacity of the CS at pH > pH_{PZC} was higher than pH < pH_{PZC}, which conflicts with the expected electrostatic repulsion between the As(V) oxyanions and negatively charged surface of the sorbent in this pH range. Thus, electrostatic attractions appear to not have an important role in the As(V) sorption for CS as compared to WS. The presence of polar functional groups on the CS surface such as alcoholic, carbonyl, carboxylic, and phenolic groups can be potential sites for As(V) sorption [28]. Although the sorption sites and the sorbate are both negatively charged at pH > pH_{PZC}, sorption may still occur due to geometric configurations.

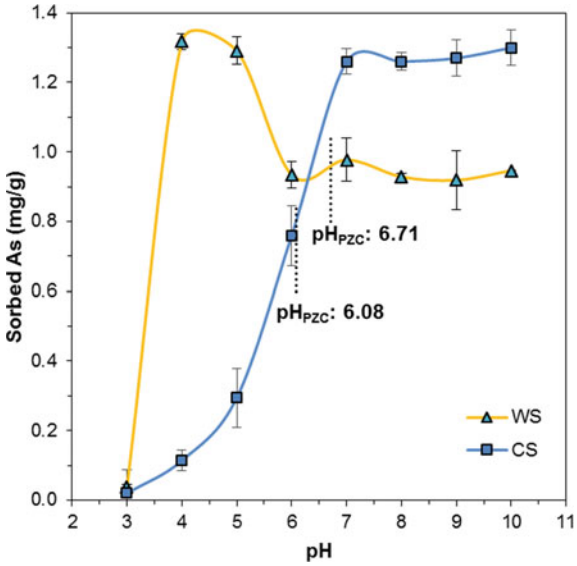

Fig. 3 Sorption capacities of CS and WS at different pH values

For example, As is a positively charged atom in the center of As oxyanion, which can be attracted to the carboxyl group on the surface of the CS while overcoming the electrostatic repulsion between the negatively charged sorbent and sorbate surfaces [8].

3.3 Sorption Kinetics

Investigation of the effect of contact time on As sorption plays an important role in modeling and designing industrial of sorption processes as it can reveal equilibrium times, and rates/mechanisms of sorption [31]. The kinetics of As(V) sorption onto the sorbents were investigated through batch experiments with parameters of kinetic models shown in Table 1 and sorption capacities in Fig. 4. Generally, the removal of As(V) by sorption on both CS and WS was found to be negligible at the initial stage with a lag period up to about 24 h, rapid from 72 to 96 h, and slowing to negligible after 120 h.

The pseudo-first-order model resulted in low R^2 values for both CS (0.84) and WS (0.86) and failed to explain the experimental data with the calculated sorption capacity (q_e cal.) being higher than the experimental value (q_e exp.) for both CS and WS. The pseudo-second-order model, on the other hand, was unable to describe the experimental kinetic data since negative sorption capacities were obtained for both CS and WS indicating that the conditions that represent this model were not applicable currently.

Table 1 Kinetic parameters of kinetic models for sorption of As(V) by CS and WS

Model	Parameter	CS	WS
Pseudo-first order	k_1 (1/h) q_e cal. (mg/g) q_e exp. (mg/g) R^2	0.02 2.01 1.39 0.84	0.03 2.61 1.44 0.86
Pseudo-second order	k_1 (mg/g.h) q_e cal. (mg/g) R^2	Unable to predict	Unable to predict
Intra-particle diffusion	k_p (mg/g.h$^{0.5}$) C (mg/g) R^2	0.17 0.71 0.93	0.18 0.68 0.94
Elovich	a (mg/g.h) b (g/m) R^2	0.03 1.62 0.93	0.05 1.78 0.93

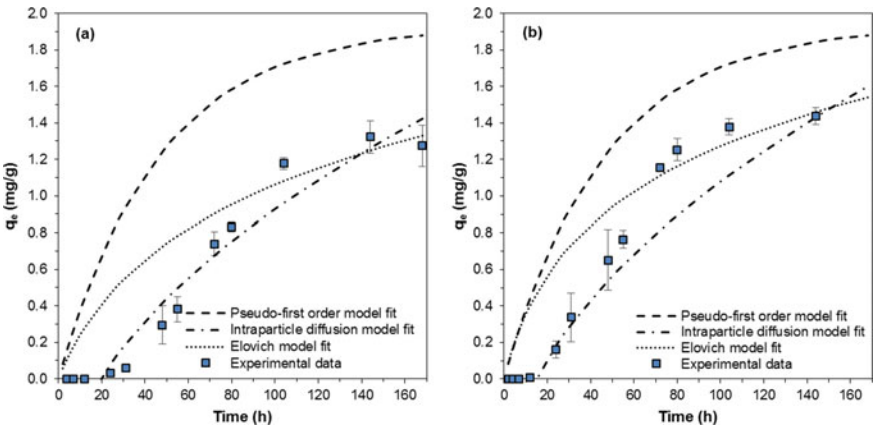

Fig. 4 As(V) sorption capacity of CS (**a**) and WS (**b**) as a function of contact time (sorbent dose = 3 g/L, C_0 = 5 mg/L, T = 25 °C)

In contrast, both the intra-particle diffusion and Elovich models performed reasonably overall (Table 1 and Fig. 4). Although the R^2 values obtained for these models were all >0.93 for both CS and WS, neither of these models predicted the long lag period in which negligible sorption occurred. This lag period can be attributed to a slow swelling of sorbents which limits the initial sorption of As(V) for both CS and WS. For instance, it was found previously that a rapid rate of swelling of sorbent can result in access to functional groups of the sorbent and subsequent increase the sorption rate [19, 25, 29]. Clearly, the swelling of CS and WS is being limited currently and further study is needed to determine the reason for this lag period for these sorbents.

In the case of the intra-particle diffusion model, if the regression of q_t versus $t^{0.5}$ was linear and it passed through the origin, then intra-particle diffusion would be considered to be the sole rate-limiting step [15, 45]. For both CS and WS, the regressions were linear, but the linear plots did not pass through the origin, suggesting that intra-particle diffusion is not the only rate-determining step, and the sorption process may be controlled by more than one mechanism.

The Elovich model assumes that the surface of the sorbent is heterogeneous, the activation energy increases with sorption time and the rate of sorption decreases exponentially with an increase in the amount of sorbate adsorbed [12, 41]. In the case of this model, the relatively high R^2 values obtained for both sorbents suggests that the rate-limiting step in sorption of As(V) onto CS and WS is probably the chemisorption step [1].

The obtained sorption capacities for CS (~1.2 mg/g) and WS (~1.4 mg/g) were higher than some biomasses such fungal biomass (0.001 mg/g) [14] and lemon residues (0.475 mg/g) [16]. However, the sorption capacities were much lower than chemically treated biomasses such as orange peel (81 mg/g) [18] and hardwood sawdust (12 mg/g) [33]. In addition, the time required to reach equilibrium in these studies was faster than the current biomasses ranging from 1 to 38 h. This significant equilibrium time of about 140 h is an issue that would likely hinder use of these materials in industry treatment processes. Therefore, treatment of these agricultural biomasses using different chemicals may be useful to increase their porosities and surface areas by extracting soluble organic compounds, changing or introducing new functional groups, and helping to eliminate colouration of the treated water [23].

4 Conclusions

The FTIR analysis of the sorbents showed the presence of lignin, hemicellulose, cellulose, and other functional groups; however, there was no significant shift or change in the spectra after As(V) sorption. Overall, the As(V) sorption by CS and WS were strongly affected by solution pH with the highest As(V) sorption capacities obtained at pH values of 7–10 for CS and 4–5 for WS. The batch sorption kinetics for As(V) were best described by the intra-particle diffusion and Elovich models; however, neither model predicted the initial lag periods found for both sorbents. Generally, sorption kinetic study results suggest the sorption process may be controlled multiple mechanisms and that chemisorption can play a significant role in sorption of As(V) by CS and WS. Overall, the issues with lag time, long equilibration times, and low sorption capacities of CS and WS indicate the need for further research into these biomasses to improve their efficiencies. Chemical treatment can potentially enhance the sorption capacity of these materials and make them more suitable for consideration in industrial sorption processes.

Acknowledgements This research was financially supported by two NSERC Discovery Grants (K. McPhedran and J. Soltan). We would also like to extend our thanks to the College of Graduate and Postdoctoral Studies, the University of Saskatchewan, for financial support in the form of a Dean's Scholarship (K. Benis).

References

1. Aranda-García E, Cristiani-Urbina E (2019) Effect of pH on hexavalent and total chromium removal from aqueous solutions by avocado shell using batch and continuous systems. Environ Sci Pollut Res 26:3157–3173. https://doi.org/10.1007/s11356-017-0248-z
2. Baker MJ, Trevisan J, Bassan P, Bhargava R, Butler HJ, Dorling KM, Fielden PR, Fogarty SW, Fullwood NJ, Heys KA, Hughes C, Lasch P, Martin-Hirsch PL, Obinaju B, Sockalingum GD, Sulé-Suso J, Strong RJ, Walsh MJ, Wood BR, Gardner P, Martin FL (2014) Using Fourier transform IR spectroscopy to analyze biological materials. Nat Protoc 9:1771–1791. https://doi.org/10.1038/nprot.2014.110
3. Carson R (1962) Silent spring. Houghton Mifflin Harcourt
4. Corrales RCNR, Mendes FM, Perrone C, Sant'Anna C, de Souza W, Abud Y, da Silva Bon EP, Ferreira-Leitão V (2012) Structural evaluation of sugar cane bagasse steam pretreated in the presence of CO_2 and SO_2. Biotechnol Biofuels 5:36. https://doi.org/10.1186/1754-6834-5-36
5. De D, Aniya V, Satyavathi B (2019) Application of an agro-industrial waste for the removal of As(III) in a counter-current multiphase fluidized bed. Int J Environ Sci Technol 16:279–294. https://doi.org/10.1007/s13762-018-1651-9
6. Gautam SB, Alam MS, Kamsonlian S (2017) Adsorptive removal of As(III) from aqueous solution by raw coconut husk and iron impregnated coconut husk: kinetics and equilibrium analyses. Int J Chem React Eng 15. https://doi.org/10.1515/ijcre-2016-0097
7. Gupta A, Vidyarthi SR, Sankararamakrishnan N (2015) Concurrent removal of As(III) and As(V) using green low cost functionalized biosorbent—*Saccharum officinarum* bagasse. J Environ Chem Eng 3:113–121. https://doi.org/10.1016/J.JECE.2014.11.023
8. Haque MN, Morrison GM, Perrusquía G, Gutierréz M, Aguilera AF, Cano-Aguilera I, Gardea-Torresdey JL (2007) Characteristics of arsenic adsorption to sorghum biomass. J Hazard Mater 145:30–35. https://doi.org/10.1016/J.JHAZMAT.2006.10.080
9. Health Canada (2006) Guidelines for Canadian drinking water quality: guideline technical document-arsenic. Ottawa
10. Henke K (2009) Arsenic: environmental chemistry, health threats and waste treatment. Wiley
11. Huang Z, Liang X, Hu H, Gao L, Chen Y, Tong Z (2009) Influence of mechanical activation on the graft copolymerization of sugarcane bagasse and acrylic acid. Polym Degrad Stab 94:1737–1745. https://doi.org/10.1016/j.polymdegradstab.2009.06.023
12. León G, García F, Miguel B, Bayo J (2016) Equilibrium, kinetic and thermodynamic studies of methyl orange removal by adsorption onto granular activated carbon. Desalin Water Treat 57:17104–17117. https://doi.org/10.1080/19443994.2015.1072063
13. Litter MI, Armienta MA, Villanueva Estrada RE, Villaamil Lepori EC, Olmos V (2020) Arsenic in Latin America: part II. In: Arsenic in drinking water and food. Springer, Singapore, pp 113–182. https://doi.org/10.1007/978-981-13-8587-2_5
14. Littera P, Urík M, Ševc J, Kolenčík M, Gardošová K, Molnárová M (2011) Removal of arsenic from aqueous environments by native and chemically modified biomass of *Aspergillus niger* and *Neosartorya fischeri*. Environ Technol 32:1215–1222. https://doi.org/10.1080/09593330.2010.532510
15. Mahmood T, Aslam M, Naeem A, Siddique T, Din SU (2018) Adsorption of As(III) from aqueous solution onto iron impregnated used tea activated carbon: equilibrium, kinetic and thermodynamic study. J Chil Chem Soc 63:3855–3866

16. Marín-Rangel VM, Cortés-Martínez R, Cuevas Villanueva RA, Garnica-Romo MG, Martínez-Flores HE (2012) As(V) biosorption in an aqueous solution using chemically treated lemon (*Citrus aurantifolia* Swingle) residues. J Food Sci 77:T10–T14. https://doi.org/10.1111/j.1750-3841.2011.02466.x
17. McGuigan CF, Hamula CLA, Huang S, Gabos S, Le XC (2010) A review on arsenic concentrations in Canadian drinking water. Environ Rev 18:291–307. https://doi.org/10.1139/A10-012
18. Meng F, Yang B, Wang B, Duan S, Chen Z, Ma W (2017) Novel dendrimerlike magnetic biosorbent based on modified orange peel waste: adsorption-reduction behavior of arsenic. ACS Sustain Chem Eng 5:9692–9700. https://doi.org/10.1021/acssuschemeng.7b01273
19. Mo J, Yang Q, Zhang N, Zhang W, Zheng Y, Zhang Z (2018) A review on agro-industrial waste (AIW) derived adsorbents for water and wastewater treatment. J Environ Manage 227:395–405. https://doi.org/10.1016/J.JENVMAN.2018.08.069
20. Moldovan BJ, Jim HM, Harrington GA (2008) The arsenic source term for an in-pit uranium mine tailings facility and its long-term impact on the regional groundwater. Appl Geochem 23:1437–1450. https://doi.org/10.1016/J.APGEOCHEM.2007.12.037
21. Mulligan CN, Wang S (2006) Remediation of a heavy metal-contaminated soil by a rhamnolipid foam. Eng Geol 85:75–81. https://doi.org/10.1016/J.ENGGEO.2005.09.029
22. Nadeem R, Manzoor Q, Iqbal M, Nisar J (2016) Biosorption of Pb(II) onto immobilized and native *Mangifera indica* waste biomass. J Ind Eng Chem 35:185–194. https://doi.org/10.1016/j.jiec.2015.12.030
23. Ngah WW, Hanafiah MM (2008) Removal of heavy metal ions from wastewater by chemically modified plant wastes as adsorbents: a review. Bioresour Technol 99(10):3935–3948
24. Niazi NK, Bibi I, Shahid M, Ok YS, Shaheen SM, Rinklebe J, Wang H, Murtaza B, Islam E, Farrakh NM, Lüttge A (2018) Arsenic removal by Japanese oak wood biochar in aqueous solutions and well water: investigating arsenic fate using integrated spectroscopic and microscopic techniques. Sci Total Environ 621:1642–1651. https://doi.org/10.1016/J.SCITOTENV.2017.10.063
25. Niu CH, Volesky B, Cleiman D (2007) Biosorption of arsenic (V) with acid-washed crab shells. Water Res 41:2473–2478. https://doi.org/10.1016/J.WATRES.2007.03.013
26. Ociński D, Mazur P (2020) Highly efficient arsenic sorbent based on residual from water deironing—sorption mechanisms and column studies. J Hazard Mater 382. https://doi.org/10.1016/j.jhazmat.2019.121062
27. Pal P (2015) Groundwater arsenic remediation: treatment technology and scale UP. Butterworth-Heinemann
28. Pehlivan E, Tran TH, Ouédraogo WKI, Schmidt C, Zachmann D, Bahadir M (2013) Removal of As(V) from aqueous solutions by iron coated rice husk. Fuel Process Technol 106:511–517. https://doi.org/10.1016/J.FUPROC.2012.09.021
29. Pholosi A, Naidoo EB, Ofomaja AE (2019) Sequestration of As(III) pollutant from water using chemically activated pine cone biomass: evaluation of interaction and mechanism. Int J Environ Sci Technol 1–14. https://doi.org/10.1007/s13762-019-02283-w
30. Qu G, Huang X, Yin Q, Ning P (2014) Dissolution of garlic stem in the 1-butylrpridinium bromide ionic liquid. J Chem Eng Jpn 47:435–441. https://doi.org/10.1252/jcej.13we163
31. Saraeian A, Hadi A, Raji F, Ghassemi A, Johnson M (2018) Cadmium removal from aqueous solution by low-cost native and surface modified Sorghum x drummondii (Sudangrass). J Environ Chem Eng 6:3322–3331. https://doi.org/10.1016/J.JECE.2018.05.018
32. Saskatchewan Ministry of the Economy (2014) Uranium mining supply chain requirement guide
33. Setyono D, Valiyaveettil S (2014) Chemically modified sawdust as renewable adsorbent for arsenic removal from water. ACS Sustain Chem Eng 2:2722–2729. https://doi.org/10.1021/sc500458x
34. Shakoor MB, Nawaz R, Hussain F, Raza M, Ali S, Rizwan M, Oh S-E, Ahmad S (2017) Human health implications, risk assessment and remediation of As-contaminated water: a critical review. Sci Total Environ 601–602:756–769. https://doi.org/10.1016/J.SCITOTENV.2017.05.223

35. Siddiqui SI, Chaudhry SA (2017) Iron oxide and its modified forms as an adsorbent for arsenic removal: a comprehensive recent advancement. Process Saf Environ Prot 111:592–626. https://doi.org/10.1016/j.psep.2017.08.009
36. Singh R, Singh S, Parihar P, Singh VP, Prasad SM (2015) Arsenic contamination, consequences and remediation techniques: a review. Ecotoxicol Environ Saf 112:247–270. https://doi.org/10.1016/J.ECOENV.2014.10.009
37. Tsang S, Phu F, Baum MM, Poskrebyshev GA (2007) Determination of phosphate/arsenate by a modified molybdenum blue method and reduction of arsenate by $S_2O_4^{2-}$. Talanta 71:1560–1568. https://doi.org/10.1016/J.TALANTA.2006.07.043
38. Uppal JS, Zheng Q, Le XC (2019) Arsenic in drinking water—recent examples and updates from Southeast Asia. Curr Opin Environ Sci Health 7:126–135. https://doi.org/10.1016/J.COESH.2019.01.004
39. Vieira BRC, Pintor AMA, Boaventura RAR, Botelho CMS, Santos SCR (2017) Arsenic removal from water using iron-coated seaweeds. J Environ Manage 192:224–233. https://doi.org/10.1016/J.JENVMAN.2017.01.054
40. WHO (2011) Guidelines for drinking-water quality, 4th edn. World-Health-Organization, pp 315–318
41. Wang J, Guo X (2020) Adsorption kinetic models: physical meanings, applications, and solving methods. J Hazard Mater 390:122156. https://doi.org/10.1016/J.JHAZMAT.2020.122156
42. Wang S, Mulligan CN (2006) Occurrence of arsenic contamination in Canada: sources, behavior and distribution. Sci Total Environ 366:701–721. https://doi.org/10.1016/J.SCITOTENV.2005.09.005
43. Xiong Y, Tong Q, Shan W, Xing Z, Wang Y, Wen S, Lou Z (2017) Arsenic transformation and adsorption by iron hydroxide/manganese dioxide doped straw activated carbon. Appl Surf Sci 416:618–627. https://doi.org/10.1016/J.APSUSC.2017.04.145
44. Yadav LS, Mishra BK, Kumar A, Paul KK (2014) Arsenic removal using bagasse fly ash-iron coated and sponge iron char. J Environ Chem Eng 2:1467–1473. https://doi.org/10.1016/J.JECE.2014.06.019
45. Yao Y, Bing H, Feifei X, Xiaofeng C (2011) Equilibrium and kinetic studies of methyl orange adsorption on multiwalled carbon nanotubes. Chem Eng J 170:82–89. https://doi.org/10.1016/j.cej.2011.03.031
46. Yazdani M (Roza), Tuutijärvi T, Bhatnagar A, Vahala R (2016) Adsorptive removal of arsenic(V) from aqueous phase by feldspars: kinetics, mechanism, and thermodynamic aspects of adsorption. J Mol Liq 214:149–156. https://doi.org/10.1016/J.MOLLIQ.2015.12.002
47. Zhou Y, Cao S, Xi C, Li X, Zhang L, Wang G, Chen Z (2019) A novel Fe_3O_4/graphene oxide/citrus peel-derived bio-char based nanocomposite with enhanced adsorption affinity and sensitivity of ciprofloxacin and sparfloxacin. Bioresour Technol 292:121951. https://doi.org/10.1016/J.BIORTECH.2019.121951
48. Zhu N, Yan T, Qiao J, Cao H (2016) Adsorption of arsenic, phosphorus and chromium by bismuth impregnated biochar: adsorption mechanism and depleted adsorbent utilization. Chemosphere 164:32–40. https://doi.org/10.1016/J.CHEMOSPHERE.2016.08.036
49. Zoroufchi BK, Motalebi DA, McPhedran KN, Soltan J (2020) Treatment of aqueous arsenic—a review of biosorbent preparation methods. J Environ Manage 273:111126. https://doi.org/10.1016/j.jenvman.2020.111126
50. Zoroufchi BK, Motalebi DA, Soltan J, McPhedran KN (2020) Treatment of aqueous arsenic—a review of biochar modification methods. Sci Total Environ. https://doi.org/10.1016/j.scitotenv.2020.139750
51. Zoroufchi BK, Shakouri M, McPhedran K, Soltan J (2020) Enhanced arsenate removal by Fe-impregnated canola straw: assessment of XANES solid-phase speciation, impacts of solution properties, sorption mechanisms, and evolutionary polynomial regression (EPR) models. Environ Sci Pollut Res. https://doi.org/10.1007/s11356-020-11140-0

Using the STP-EX Model for a Screening Level Assessment of Chemicals of Emerging Concern During the Municipal Wastewater Treatment Plant Process

S. Minaei, J. Soltan, R. Seth, and K. N. McPhedran

1 Introduction

Thousands of inorganic and organic compounds are present in commerce, including pharmaceuticals and personal care products (PPCPs), that are continually released into the environment. Given the possibility of negative ecosystem and human health effects due to these releases, increased efforts are needed in the assessment of persistence, bioaccumulation, toxicity, and long-range transport potential of these chemical compounds [4]. Over the past two decades, the focus of research efforts has shifted to newly developed chemical compounds which can be collectively grouped and designated as chemicals of emerging concern (CECs). Many industrial and household products contain various CECs that are released into receiving water bodies via municipal wastewater treatment plant (MWTP) effluents. The typical MWTP processes are not inherently designed to remove these newly emerging (as well as historic) chemical compounds. Thus, MWTP effluents are recognized as major sources of introduction of these compounds as environmental pollutants into receiving surface waters.

Given the potential ecosystem risks associated with CECs, many countries now require the assessment of new commercially developed CECs for their treatability in MWTPs through various sewage treatment models [11]. The fate and transport of CECs through various MWTP processes could be assessed using screening-level fate models such as the STP model [2, 11], SimpleTreat 3.0 [12], and ASTREAT [7]. More recently, the STP model has been updated (STP-Extended or STP-EX) to not only incorporate most of the features of the above mentioned models, but

S. Minaei · J. Soltan · K. N. McPhedran (✉)
University of Saskatchewan, Saskatoon, Canada
e-mail: kerry.mcphedran@usask.ca

R. Seth
University of Windsor, Windsor, Canada

S. Walbridge et al. (eds.), *Proceedings of the Canadian Society of Civil Engineering Annual Conference 2021*, Lecture Notes in Civil Engineering 249,
https://doi.org/10.1007/978-981-19-1061-6_4

also to include consideration of ionizable chemicals, such as pharmaceuticals, which was not an option available in the original STP model [11]. Besides, the STP-EX model includes both facultative and aerobic lagoon MWTPs that are still being used extensively worldwide and throughout Canada [11].

Generally, screening-level models can be useful for the elucidation of chemical fate through the various MWTP processes. Chemicals including CECs, can be removed prior to release in wastewater effluents via processes like volatilization, sorption to solids, and degradation (predominately biodegradation but may also be photodegradation). The MWTP process input model parameters (e.g., flow rates, tank volumes, sludge recycle rates, etc.) may be difficult to obtain and vary considerably among various MWTP processes. However, 'typical' MWTP processes can be useful for modelling for the determination of a general understanding of CECs fate and transport. In addition to MWTP process parameters, CEC-specific physico-chemical parameters are needed for MWTP modeling [11]. Of these parameters, the air–water (K_{aw}) and octanol–water (K_{ow}) partitioning coefficients are primary parameters needed for accurate model outputs. The K_{aw} is important to determine the potential for chemical volatilization (i.e., loss to atmosphere) and the K_{ow} is needed for determination of the sorption potential to MWTP organic matter (i.e., loss to sludges). Although most of the physico-chemical CEC parameters are generally available in the literature (or from manufacturers), the biodegradation rates are often not readily available and/or have unacceptably wide ranges that prevent accurate model outputs [9]. Given the lack of biodegradation rates for various CECs (amongst other chemicals), especially during MWTP processes, determination of at least 'guideline' biodegradation rates would be useful for MWTP modeling purposes. Wang et al. [13] proposed the scaling of biodegradation rates to various treatment processes (based on half-lives) starting from available aqueous biodegradation rates [13]. Unfortunately, even aqueous biodegradation rates are scarce in the literature, especially for CECs.

In the absence of laboratory determined biodegradation rates, a range of values may be used to determine the potential impacts of slow or fast biodegradation rates in various MWTP processes via modeling. Thus, the current study uses the STP-EX model for the creation of partitioning maps using 'typical' activated sludge-type, facultative lagoon, and aerated lagoon MWTP process parameters. These maps follow an analogous approach to Meyer et al. [9] and Meyer and Wania [8] in the development of chemical spaces that allow for the 'sensitivity analysis' of model parameters [8, 9]. These maps may be used to determine the potential fate of CECs based on their Log K_{aw} and Log K_{ow} values, both of which are typically available in the literature for most CECs. After creation of these maps without consideration of biodegradation, the second set of maps includes both slow (recalcitrant) and fast (readily biodegradable) biodegradation rates to help determine the impact that biodegradation may have on the various MWTPs. Lastly, five chemicals of interest including di-2-Ethylhexyl phthalate (DEHP), fluoranthene, toluene, cyclooctane, and dimethyl phthalate (DMP) are presented as case studies to discuss their fate and transport both with and without inclusion of either 'recalcitrant' or 'readily biodegradable' biodegradation rates.

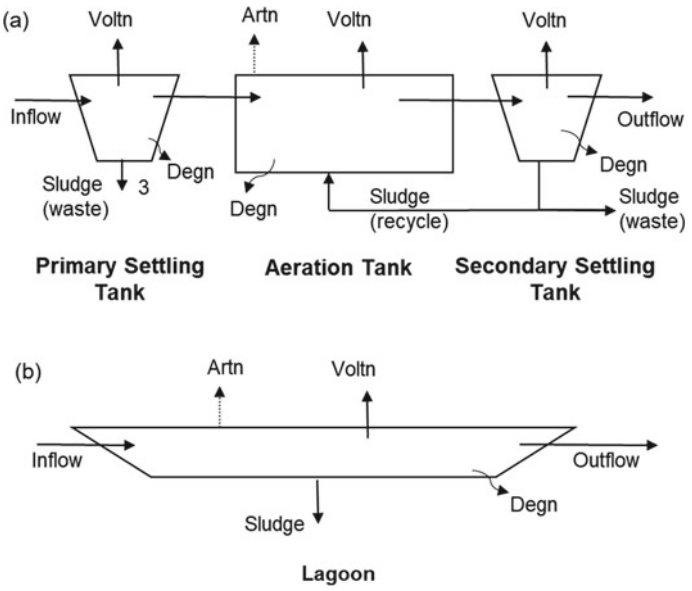

Fig. 1 **a** Schematic of a typical activated sludge-type municipal sewage treatment plant with chemical fate and transport processes. **b** Schematic of a typical lagoon-type municipal sewage treatment plant with chemical fate and transport processes. Voltn = volatilization; Artn = aeration loss; Degn = biodegradation. Adapted from [11]

2 Model Background and Inputs

2.1 STP-EX Model

The STP-EX model [11] is a relatively recent update of the original STP model originally developed by Clark et al. [2] that integrates many of the features found in similar MWTP models including SimpleTreat 3.0 [12] and ASTREAT [7]. The MWTP process flow diagrams used for the STP-EX model are shown for a typical activated sludge-type (Fig. 1a) and typical lagoon-type (Fig. 1b) processes. The chemical removal processes include sorption to suspended solids (loss to sludges), volatilization (loss to air), and biodegradation. For a complete description of the STP-EX model refer to the original model [2] and the updated model [11].

2.2 Model Input Parameters

The model input parameters include the operational parameters of the MWTPs and the physiochemical properties of the chemicals. The MWTP operational parameters are included in Table 1 for activated sludge-type, facultative lagoon and aerated

Table 1 STP-EX input parameters for each treatment process

Process		Parameter	Units	Value
Activated sludge	Influent	Flow rate	m^3/h	1000
		TSS	g/m^3	200
		Chemical conc.	g/m^3	0.01
	Primary tank	Surface area	m^2	266.7
		Depth	M	3.8
		Solids removal	%	60
		TSS (sludge)	g/m^3	50,000
	Aeration tank	Surface area	m^2	2000
		Depth	M	4
		MLSS	mg/L	2500
		Air flow rate	m^3 air/m^3 inflow	1.12
		Sludge recycle	(Influent fraction)	0.8
		Waste sludge	(Influent fraction)	0.015
	Secondary settler	Surface area	m^2	727.3
		Depth	M	3.8
		Effluent TSS	g/m^3	15
Facultative lagoon		Surface area	m^2	2,160,000
		Depth	M	2
		Effluent TSS	g/m^3	15
Aerated lagoon		Surface area	m^2	240,000
		Depth	M	2
		Effluent TSS	g/m^3	15
		Air flow rate	m^3 air/m^3 inflow	1

lagoon. Although these are considered to be 'typical' values for these MWTPs, it should be noted that variations in hydraulic and solid retention times for MWTPs will markedly affect chemical partitioning. However, modification of these variables was not considered in the current study. The physicochemical properties of chemicals were created for a 'hypothetical' suite of chemicals to create the partitioning maps. For this exercise, the Log K_{aw} (air–water partitioning coefficient) and Log K_{ow} (octanol–water partition coefficient) were the only two variable parameters considered. These parameters were varied incrementally from 2 to −9 and 1 to 9, respectively creating a 9 × 12 grid (108 'hypothetical' chemicals within each partitioning map); these values are representative of the majority of organic chemicals available in commerce [4] which include the CECs.

2.3 Biodegradation

As mentioned previously, there is both of lack of biodegradation data available, especially for CECs, while available data is often given in large ranges and for matrices dissimilar to wastewaters. Thus, the biodegradation rates were set for recalcitrant chemicals at 100 h for the aeration tank of the activated sludge-type MWTP and 25,000 h for both facultative and aerobic lagoon MWTPs. The biodegradation rates for readily biodegradable chemicals were set to 1 h for the aeration tank of the activated sludge-type MWTP and at 250 h for both facultative and aerobic lagoon MWTPs. This range can be considered as an approximate range in the absence of available experimental values and may be used as a first approximation for the fate analysis of the CECs.

3 Results and Discussion

3.1 Partitioning Maps

Partitioning maps of the Log K_{ow} versus Log K_{aw} partition coefficients without consideration of biodegradation are shown in Fig. 2a for activated sludge-type, aerated lagoon, and facultative lagoon MWTPs. These maps outline areas that exhibit dominant fate processes (>80% of chemical mass being volatilized, sorbed to solids, or found in effluents), two fate processes (when summed >80% of chemical mass), and all three fate processes (centre section showing 1:1:1 between processes). Generally, each of the individual MWTP partitioning maps show similar partitioning behaviors. This is especially the case for the aerated and facultative lagoons where there appears to only be a slight shift in mainly the volatilized areas with more chemicals within the >80% volatilized area for the facultative lagoons versus the aerated. This would be expected based on the much larger surface area of the facultative lagoon (2,160,000 m^2) versus the aerated lagoon (240,000 m^2), increasing the amount of volatilized chemicals in this MWTP process.

Overall trends for each process are shown in Fig. 2, with further discussion of the individual fate processes given below. The smaller surface areas and shorter residence times of the activated sludge-type MWTP show only a small area for volatilization focused where Log K_{ow} is <3.0 and Log K_{aw} is <0.5, while the majority of chemicals were bound to solids when Log K_{ow} > 5.0 (Table 2). Both the aerated lagoon and facultative lagoon had similar areas of sorbed chemicals from Log K_{ow} > 5.5 up to Log K_{aw} < −3, however, increased volatilization at Log K_{aw} > −3 reduced the chemicals sorbed to solids for both of these MWTPs (Table 2). The areas were fates were 1:1:1 for volatilized: effluents: solids were similar sizes for each MWTP, and in similar locations for the lagoons (about Log $K_{ow} = 4.5$ and Log $K_{aw} = -3.5$) while being shifted for the activated sludge-type MWTP to about Log $K_{ow} = 4.5$ and Log $K_{aw} = -0.5$ (Fig. 2a).

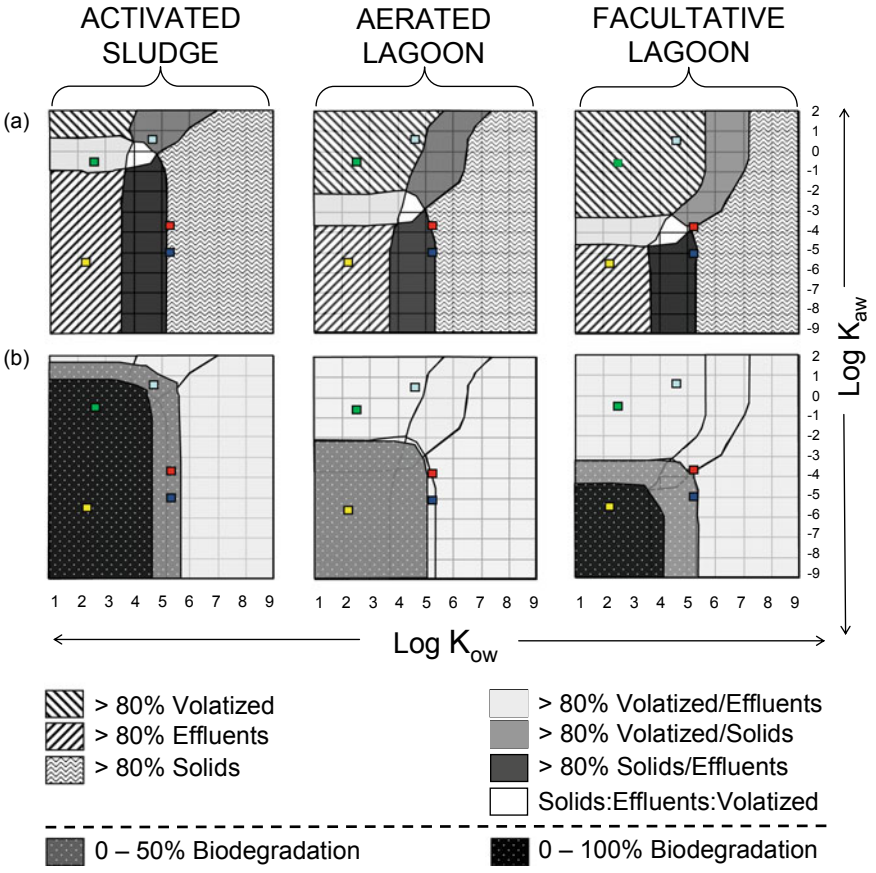

Fig. 2 **a** Partitioning maps of chemical fate (solids, volatilized, effluents) during each treatment process without biodegradation. *Note* Areas with no shading contain all three fate processes. **b** Biodegradation map indicating potential areas in which biodegradation may be important. *Note* Partitioning map areas shown in panel (a) have shaded to a single colour for clarity. Case study chemicals are shown in each panel with: DEHP (dark blue); fluoranthene (red); toluene (green); cyclooctane (light blue); and DMP (yellow)

3.1.1 Sorption to Solids

For all three of the MWTP processes, the sorption to solids dominates for high Log K_{ow} chemicals (Fig. 2a). Such behavior is expected due to the strong binding affinity of these chemicals to organic carbon. These bound chemicals, including CECs, would not readily available for biodegradation or volatilization and will accumulate in sludges and on suspended solids in wastewater effluents. For activated sludge processes, high log K_{aw} and high Log K_{ow} chemicals remain sorbed due to small process surface areas, shorter residence times, and chemicals entering the MWTP already bound (thus unlikely to be available for volatilization or biodegradation

Table 2 Partitioning maps (Fig. 2a) overall behavior trends based on Log K_{ow} and Log K_{aw} values

Process	Parameter	Log K_{ow}	Log K_{aw}
Activated sludge	Solids	>5.0	All
	Volatilized	<3.0	>0.5
	Loss in effluents	<3.5	<−1.0
Aerated lagoon	Solids	>5.5	<−3.0
		>6.5[a]	>−3.0[a]
	Volatilized	<4.5	>−2.0
	Loss in effluents	<4.0	<−4.5
Facultative lagoon	Solids	>5.5	<−4.0
		>7.5[a]	>−4.0[a]
	Volatilized	<6.0	>−3.0
	Loss in effluents	<4.0	<−5.5

[a]Two distinct zones, refer to Fig. 2a

where chemicals need to be freely-dissolved). Both lagoon types show decreasing sorption to solids at higher Log K_{aw} in comparison due to increased surface areas and residence times allowing the volatilization loss to increase for these chemicals. As the chemicals volatilize during longer duration treatment processes, further chemicals may have time to desorb from solids allowing them to then be volatilized or biodegraded. Additionally, it has been shown that partitioning can decrease due to the degradation of organic matter over time, thereby releasing chemicals including CECs in the process [3].

3.1.2 Volatilization

For all processes, high Log K_{aw} and low Log K_{ow} chemicals are lost to volatilization (Fig. 2a). This behavior is expected, since these chemicals will not readily sorb to solids (thus are likely to be freely-dissolved) and do not have a high affinity for water, despite the low Log K_{ow}, given the high Log K_{aw}. Similar to the solid's sorption, the volatilization for both lagoon MWTP processes are higher due to increased process surface area and residence times in comparison to the MWTP activated sludge-type process.

3.1.3 Loss in Effluents

Chemicals with lower Log K_{ow} and Log K_{aw} values remain in the wastewaters and are released via effluents for each of the MWTP processes (Fig. 2a). These chemicals do not readily sorb to solids and have higher vapour pressures; therefore, they preferentially remain in the wastewater matrix. The activated sludge-type MWTP processes have a greater amount of loss in effluents due to the decreased losses due

to volatilization. The higher Log K_{aw} chemicals that are lost in lagoon processes remain in the activated sludge effluents since they are not easily sorbed to solids but are not able to be volatilized due to short residence times and smaller surface areas of the activated sludge-type MWTP process.

3.1.4 Biodegradation

The partitioning maps modified to include chemical biodegradation are presented in Fig. 2b. For simplicity, the biodegradation rates plotted included 50 and 100% biodegraded areas for each of the various MWTP types. Although somewhat obvious, it should be noted that the 100% area overlaps the 50% for the activated sludge-type and facultative lagoon MWTP plots. For the activated sludge-type plots, biodegradation impacts are quite significant, with almost half of the plot area showing 50% of the chemicals being biodegraded (chemicals with Log $K_{ow} < 5.5$) and a large portion with 100% biodegraded (chemicals with Log $K_{ow} < 4.5$). In contrast, the lagoons only indicate impacts of biodegradation for chemicals that would typically be released via effluents and overlapping regions. In particular, the aerated lagoon MWTP only has 50% biodegradation being predicted in this region with no chemicals being 100% biodegraded.

Clearly, the choice of biodegradation rates impacts the chemical fate and partitioning maps, significantly for each of the three MWTP processes. However, the faster biodegradation rates in the activated sludge-type MWTP lead to much higher chemical losses for this process. This would be expected as this MWTP aeration basin promotes the development of his bacteria concentrations that would be able to degrade many of these chemicals. In contrast, the lagoons would be expected to have lower bacterial concentrations. However, the longer duration for treatment in facultative lagoons allows for higher biodegradation as compared to the shorter duration for treatment in the aerated lagoons.

3.2 Case Studies

Although partitioning maps may be useful in the determination of general chemical fate, chemicals such as CECs found in the transitional zones may be most important for future study. These chemicals may exhibit variable behavior in each process and their subsequent fate may be most important for ensuring appropriate monitoring efforts. Facilitating ease in understanding of the partitioning chemical spaces, five CECs (DEHP, fluoranthene, toluene, cyclooctane, DMP) with their physio-chemical properties given in Table 3 are considered as case studies for the description of fate in each of the processes.

Table 3 Physicochemical properties of organic chemicals selected for representing chemical distributions based on Log K_{ow} and Log K_{aw} values [6]

Chemical	Molecular mass (g/mol)	Water solubility (g/m^3)	Vapor pressure (Pa)	Log K_{ow}	Log K_{aw}
DEHP	390.4	2.65E−01	1.33E−05	5.11	−5.13
Fluoranthene	202.3	2.60E−01	1.23E−02	5.22	−3.41
Toluene	92.13	5.15E+02	3.80E+03	2.69	−0.56
Cyclooctane	112.2	7.90E+00	7.53E+02	4.45	0.63
DMP	194.2	4.00E+03	2.20E−01	2.12	−5.37

3.2.1 Di-2-Ethylhexyl Phthalate (DEHP)

Di(2-Ethylhexyl) phthalate (DEHP) as a plasticizer has enforcing disrupting properties [5]. It has been used as a plasticizer in the production of polyvinyl chloride (PVC) and is characterized by low solubility in water and subsequent high Log K_{ow} value of 5.11 (Table 3). In the absence of biodegradation, DEHP is almost exclusively sorbed to solids for all treatment processes (80–100%) (Fig. 2). With the addition of biodegradation, losses to biodegradation are approximated 20–40% for the activated sludge and facultative lagoon processes and remains unchanged for the aerated lagoons. It has been noted previously that sorbed chemicals are not available for biodegradation; thus, CECs fate in this region should be considered for further evaluation, given the potential impacts of biodegradation in this area.

3.2.2 Fluoranthene

Fluoranthene is a polycyclic aromatic hydrocarbon (PAH) that is found in both raw fuel and fuel combustion products [1]. It has a high Log K_{ow} value of 5.22 and low water solubility (Table 3). Fluoranthene is mainly sorbed to solids for the activated sludge process and is close to the >80% sorbed to solids range for both lagoon processes (Fig. 2). Once biodegradation is considered, fluoranthene is considered to be biodegradable in the activated sludge process, while little to no biodegradation would be expected for either of the lagoon processes. This chemical is in a similar zone as DEHP; therefore, further assessment of biodegradation should be determined for CECs that are found to be in this region.

3.2.3 Toluene

Toluene is a water-soluble aromatic hydrocarbon applied as a solvent in industry and can be released in air, water, and soils where it is produced or used [14]. Toluene is not easily sorbed to solids given its low Log K_{ow} value of 2.69 and has relatively high volatility at Log $K_{aw} = -0.56$ (Table 3). In the absence of biodegradation, it will

volatilize in both lagoon processes and either volatilize or, more likely, remain in effluents for activated sludge-type MWTP treatment processes (Fig. 2). As mentioned previously, increased volatilization would be expected in the lagoon treatments given their larger surface areas and longer retention times (as for DEHP) and will increase with increasing both of these parameters within an activated sludge-type MWTP. Biodegradation does not affect the fate of toluene in either lagoon process. However, during the activated sludge-type process, biodegradation may account for 0–100% of the chemical fate. Accurate measurements for biodegradation rates in this map area are needed for CECs since biodegradation will markedly influence chemical release via effluents and subsequent environmental loading.

3.2.4 Cyclooctane

Cyclooctane applied as a coating, plastic roofing materials, and pesticide [10]. Despite markedly different Log K_{ow} and Log K_{aw} values than toluene (Table 3), the cyclooctane fate in the various MWTPs is quite similar overall (Fig. 2). Without biodegradation, the toluene fate in lagoon processes is analogous to toluene while having marginally higher volatilization than toluene in the activated sludge-type MWTP. With biodegradation, cyclooctane fate is not impacted by either of the lagoon processes. However, for the activated sludge-type process 0–50% of cyclooctane fate may be biodegradation. This result is interesting since biodegradation would have to occur before volatilization and an appreciable amount of desorption from solids would also be needed to have higher biodegradation overall.

3.2.5 Dimethyl Phthalate (DMP)

DMP is water soluble chemical applied in the production of plastics [15]. Given its low volatility (Log $K_{aw} = -5.37$) and sorption capabilities (Log $K_{ow} = 2.12$) (Table 3), DMP is found almost exclusively in the effluents for all three treatment processes in the absence of biodegradation (Fig. 2). DMP would be predominantly freely-dissolved, and thus, available for biodegradation. With the inclusion of biodegradation, approximately 100% of DMP would be lost due to biodegradation for the activated sludge-type and facultative lagoon processes. Interestingly, this value drops to only 0–50% for aerated lagoons. Aerated lagoon biodegradation is lower than facultative lagoons due to the decreased residence time for available biodegradation. Effluents of aerated lagoons may be a source for DMP release to the environment.

4 Conclusions

The MWTP effluents have been a continual source of both historic chemicals and new CECs. The fate of these chemicals in the activated sludge-type, aerated lagoons, and facultative lagoons was assessed in this study using the STP-EX model. This model was used for the development of partitioning maps using 108 hypothetical chemicals that were defined by Log K_{ow} and Log K_{aw} values. Overall, these partitioning maps were similar for the three MWTP processes without consideration of biodegradation. Once biodegradation was included there was a clear difference between the three processes with the activated sludge-type being the most impacted by biodegradation, followed by the facultative lagoon and lastly the aerated lagoon. However, all three MWTP processes were impacted by biodegradation; thus, it is important to properly consider biodegradation impacts for other chemicals used in the STP-EX model, including CECs. The five case study chemicals highlight the need for proper assessment of chemicals found in the 'overlap' zones where fate and transport can be more difficult to assess.

Acknowledgements This research was financially supported by two NSERC Discovery Grants (K. McPhedran and J. Soltan). In addition, we would also like to extend our thanks to the College of Graduate and Postdoctoral Studies, the University of Saskatchewan, for financial support in the form of a Dean's Scholarship (S. Minaei).

References

1. Balmer JE, Hung H, Yong Y, Letcher RJ, Muir DCG (2019) Sources and environmental fate of pyrogenic polycyclic aromatic hydrocarbons (PAHs) in the Arctic. Emerg Contam 5:128–142
2. Clark B, Henry GLH, Mackay D (1995) Fugacity analysis and model of organic chemical fate in a sewage treatment plant. Environ Sci Technol 29(6):1488–1494
3. Gobas FAPC, MacLean LG (2003) Sediment−water distribution of organic contaminants in aquatic ecosystems: the role of organic carbon mineralization. Environ Sci Technol 37(4):735–741
4. Gouin T, Mackay D, Webster E, Wania F (2000) Screening chemicals for persistence in the environment. Environ Sci Technol 34(5):881–884
5. Halden RU (2010) Plastics and health risks. Annu Rev Public Health 31:179–194
6. Mackay D, Shiu W-Y, Lee SC (2006) Handbook of physical-chemical properties and environmental fate for organic chemicals. CRC Press
7. McAvoy DC, Shi J, Schecher W, Rittmann B, Lee KC (1999) ASTREAT: a model for calculating chemical loss with in an activated sludge treatment system (version 1) [computer software]. The Procter & Gamble Company, Cincinnati, OH
8. Meyer T, Wania F (2007) What environmental fate processes have the strongest influence on a completely persistent organic chemical's accumulation in the Arctic? Atmos Environ 41(13):2757–2767
9. Meyer T, Wania F, Breivik K (2005) Illustrating sensitivity and uncertainty in environmental fate models using partitioning maps. Environ Sci Technol 39(9):3186–3196
10. Richardson SD (2008) Environmental mass spectrometry: emerging contaminants and current issues. Anal Chem 80(12):4373–4402

11. Seth R, Webster E, Mackay D (2008) Continued development of a mass balance model of chemical fate in a sewage treatment plant. Water Res 42(3):595–604
12. Struijs J (1996) SimpleTreat 3.0: a model to predict the distribution and elimination of chemicals by sewage treatment plants. RIVM rapport 719101025
13. Wang J, McPhedran KN, Seth R, Drouillard KG (2007) Evaluation of the STP model: comparison of modelled and experimental results for ten polycyclic aromatic hydrocarbons (PAHs). Chemosphere 69(11):1802–1806
14. Weelink SAB, van Eekert MHA, Stams AJM (2010) Degradation of BTEX by anaerobic bacteria: physiology and application. Rev Environ Sci Bio/Technol 9(4):359–385
15. Xu B, Gao N-Y, Cheng H, Xia S-j, Rui M, Zhao D-D (2009) Oxidative degradation of dimethyl phthalate (DMP) by UV/H_2O_2 process. J Hazard Mater 162(2–3):954–959

Biofiltration Optimization Strategies—Operational and Water Quality Adjustments

A. Piche, H. P. Hamidi, S. Cleary, and O. D. Basu

1 Introduction

Conventional granular filtration removes small particulates from water to reduce turbidity to acceptable levels (typically 0.1 NTU as a legislated requirement in North America). Biofiltration practice is the allowance of a granular filtration media to develop a localized beneficial microbial population on the media surface to facilitate the removal of organics present in the water source in addition to small particulates. Reducing organic carbon during filtration has the benefit of decreasing chlorine demand and decreasing the potential for disinfection by-product formation during the final disinfection stage [8, 12]. Furthermore, reducing organic carbon during the treatment process reduces the potential for bacterial regrowth which can otherwise lead to discoloured water, and odour issues in the distribution system. It holds the promise of a sustainable technology that decreases chemical needs for removal of organic material in water systems and is therefore highly attractive. However, although the process appears quite simple to implement recent reviews of literature indicate that the removal of the organic portion by biofiltration is somewhat low [1, 13]. For instance, the median range of organic carbon removal by biofilters in *full scale plants* is only 10–17% with the higher removals for WTPs that pre-ozonate waters ahead of the biofilters [13]. Thus, more research on optimization and/or design of biofiltration is required to improve organic carbon removal.

A. Piche · H. P. Hamidi · O. D. Basu (✉)
Department of Civil and Environmental Engineering, Carleton University, 1125 Colonel By Dr, Ottawa, ON K1S 5B6, Canada
e-mail: onita.basu@carleton.ca

S. Cleary
Faculty of Applied Sciences and Technology, Humber Institute of Technology and Advanced Learning, 205 Humber College Blvd, NX201, Toronto, ON M9W 5L7, Canada

S. Walbridge et al. (eds.), *Proceedings of the Canadian Society of Civil Engineering Annual Conference 2021*, Lecture Notes in Civil Engineering 249,
https://doi.org/10.1007/978-981-19-1061-6_5

Biofiltration studies to increase natural organic matter (NOM) removal include filter media selection, hydraulic loading rates, EBCT, and pre-oxidation [1] with more recent studies examining nutrient supplementation and backwash. Research on nutrient supplementation have reported conflicting results with some studies noting small increases to organic carbon removal while others report no change at all; hinting at a more complex system than anticipated. Nutrient supplementation may also require complex changes to the WTP at full scale which would hinder its implementation. Meanwhile, simple water quality adjustments such as pH remain under explored.

Furthermore, operations staff remain concerned about increases in headloss development with biofiltration in comparison to conventional granular filtration [3, 6]. Biofilters inherently have additional buildup of microorganisms and it's associated biofilm matrix both of which can contribute to headloss development. Backwash strategy with biofilters has only recently received attention and requires further investigation to develop biofilter specific appropriate backwash procedures and protocols. This research examines the potential for adjusting pH and also investigates the influence of several backwash strategies on organic carbon removal, ammonia removal, particle counts and headloss development.

2 Methods

2.1 Laboratory Biofilter Column Methodology (Carleton University, Ottawa)

Two dual media lab scale biofilter columns were operated at 3 m/h and an EBCT of 14 min. The media consisted of 520 mm GAC over 180 mm sand with a 15 mm synthetic underdrain in place to support the media. The GAC effective size (ES) was 0.7 mm and the sand ES = 0.5 mm. Columns were acclimated for several months before experimental trials were started. The lab scale columns were utilized to assess for the impacts of pH adjustment and any influence from alkalinity level. The water pH was adjusted to values of 6, 7.5, 9 and 10 while alkalinity levels were tested at 25–50 mg/L (Low Level) and 180–220 mg/L (High Level) as $CaCO_3$. The biofilter columns were fed a synthetic water comprised of a C:N:P ratio of 25:5:1 [5] for an overall DOC $\cong$ 10 mg/L. The background DOC was 3 mg/L and the remainder was comprised of equivalent C mass amounts of glyoxal, formic acid and acetic acid [4]. The lab scale experiments were intended to assess for impacts of pH and alkalinity on biofilter performance in terms of DOC, ammonia, and headloss development.

2.2 Pilot Scale Methodology (Britannia Water Treatment Plant, Ottawa)

Two pilot scale biofiltration columns were operated for approximately 18 months at the Britannia Water Treatment Plant (Ottawa, ON, Canada). The biofilter columns were operated at 2.67 m/h (EBCT = 23 min). Both biofilters contained dual media consisting of 635 mm anthracite over 375 mm sand with a typical gravel underdrain for media support. Biofilter 1 contained sand media more than 50 years and anthracite media more than 25 years old with sand ES = 0.52 mm and UC = 1.3 and anthracite ES = 0.94 mm and UC = 1.6. Biofilter 2 contained media that was approx. 3 years old at the time of testing with sand ES = 0.5 mm and UC < 1.6 and anthracite ES = 1.03 mm and UC = 1.4. Britannia's source water comes from the Ottawa River which is a soft water (25–30 mg Ca/L), low in alkalinity (18–35 mg $CaCO_3$/L), high in colour (26–47 TCU) and with a moderate raw water DOC (6–8 mg/L). The feed water source is nutrient limited, with average organic carbon, nitrogen and phosphorous concentrations to the biofilters, post coagulation/flocculation/sedimentation, of 3.44, 0.18 and 0.0033 mg/L respectively. This corresponds to a C:N:P ratio of approximately 1000:55:1 on a weight basis and would be considered nutrient limited. The pilot scale experiments were to assess impacts of backwashing practices on biofilter performance in terms of DOC removal, disinfection by-product formation potential, turbidity, headloss control and particle counts.

Backwash experiments were conducted under 5 conditions: (I) water only with a 30% bed expansion, (II) water with air scour and a 30% bed expansion, (III) I + an extended terminal subfluidization wash (ETSW), (IV) II + ETSW, and (V) II + a double stage ETSW procedure. The ETSW backwash velocities were 13.2 m/h in the single stage procedures and were 19.2 m/h followed by 13.2 m/h during the double stage procedure [10].

2.3 Microbial Measurements

Both adenosine tri-phosphate (ATP) and extra polymer saccharides (EPS) were measured from both biofilter column setups in order to examine correlations between headloss and organic carbon removal with ATP and/or EPS.

ATP measurements were collected from media sample using the Deposit and Surface analysis (DSA) test kit (LuminUltra® Technologies Ltd). To determine ATP (pg ATP/g media) concentration on the media using the following equation:

$$tATP\left(\frac{pgATP}{g}\right) = \frac{RLU_{tATP}}{RLU_{ATP1}} \times \frac{50,000(pgATP)}{m_{sample}(g)} \tag{1}$$

where *RLU* is relative light units and *m* refers to the media sample mass. RLU_{ATP1} value is determine during the calibration step where 100 μL of the UltraCheck™1

standard is added to an assay tube, followed by 100 μL of Luminase™ enzyme reagent. The assay tube is gently swirled and inserted into the luminometer to record the RLU_{ATP1} value. Sample preparation is completed by weighing out 1 g of the media sample and adding it to a 5 mL UltraLyse™7 extraction tube. The tube is capped and vigorously shaken to disperse the media throughout followed by 5 min incubation time. Pipette 1 mL to a 9 mL UltraLute™ dilution tube; cap and invert several times. Next take 100 μL from the UltraLute™ tube and transfer to an assay test tube. Add 100 μL of Luminase™ to the assay tube and gently mix. Insert the tube right away in the luminometer and measure the RLU_{tATP} value.

EPS was attracted from the top of biofilter media (either GAC or Anthracite) by means of Cation Exchange Resin (CER) [3]. This method was selected as it has been demonstrated to minimize cell lysis. This is accomplished by preparing a 1 L phosphate buffer solution with Milli-Q water containing: 0.76 g Na_3PO_4, 0.55 g NaH_2PO_4, 0.53 g NaCl and 0.075 g KCl. Mix 2 g of wet media with 0.5 g CER (Dowex® Marathon™ C Sodium form) and 10 mL of buffer. Centrifuge the mixture at 3600 rpm for 30 min followed by vacuum filtration of the supernatant. Polysaccharides and proteins were then subsequently analyzed as follows: polysaccharides were analyzed using a phenol–sulphuric acid assay [2] and proteins by a modified Lowry assay using the Peirce™ BCA test kit.

3 Results and Discussion

3.1 Water Quality Impacts of pH and Alkalinity on Biofilter Column Performance

Biofiltration optimization studies within surface water sources have previously examined the addition of an upstream oxidant (commonly ozone) and/or nutrient supplementation [7, 11]; meanwhile simple pH adjustment has not been a factor that has been regularly considered within the context of organic carbon removal within biofilters. This research examined pH adjustment as well as the potential influence of water alkalinity on both organic carbon and ammonia removal in biofilters.

The adjustment of pH resulted in two opposing trends for TOC and ammonia removal in the biofilters. TOC removal decreased and ammonia removal increased as pH increased, respectively (refer to Fig. 1). In addition, it appears as though TOC removal in low alkalinity waters is not impacted by changes in pH from 6 to 9 with DOC removal in the range of 60–65%. Larger changes in DOC removal with pH are observed with the higher alkalinity waters. At the moderate pH of 6 and 7.5 overall DOC removal is in the range of 60–65% regardless of alkalinity. At a pH of 10 DOC removal drops to 30–50% which is associated with an adverse impact of the high pH on the heterotrophic microbes. Meanwhile ammonia removal is lowest at pH 6 with a median removal value of 12.5%. This low ammonia–nitrogen uptake appears to be related to nitrogen requirements for cellular growth with heterotrophic

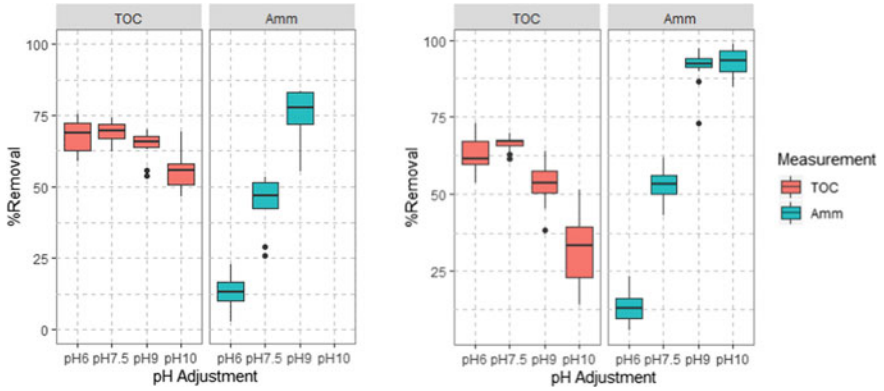

(a) Low Alkalinity Water (25-50 mg/L $CaCO_3$) (b)High Alkalinity Water (180-220 mg/L $CaCO_3$)

Fig. 1 TOC and ammonia removal with pH adjustment and alkalinity changes in the water

uptake of carbon in the system versus nitrification occurring within the system. Ammonia removal increases at pH 7.5 to approximately 45–55% and the lack of higher removal is likely due to the inability of the autotrophic nitrifiers to outcompete the heterotrophic carbon removing microbes. At pH 9 and 10, ammonia removal increases to greater than 90%; at the pH of 10 it is assumed that the ammonia is predominantly removed through volatilization. At pH 9 it is assumed some nitrification is occurring in conjunction with volatilization since as pH > 9.25 there is an equilibrium shift from ammonium to ammonia which is more volatile [9].

A two way anova on DOC and ammonia with pH and alkalinity was conducted. Both pH ($p < 0.000185$) and alkalinity ($p < 0.002058$) had significant effects with DOC removal levels. In comparison, ammonia removals were significantly different with pH ($p < 6.22e{-}08$) but alkalinity only demonstrated a moderate impact on ammonia removal ($p < 0.0127$). The influent ammonia into the system was about 2 mg/L NH_3–N while the alkalinity requirement for nitrification is 7.14 mg $CaCO_3$/mg NH_3–N; and as the Low Alkalinity Level was 25–50 mg/L $CaCO_3$ then sufficient alkalinity was present in the system.

The growth of bacteria on the filter media are known to increase headloss development within biofilters. One reluctance to adopt biofiltration is due to the increased headloss development that results and thus the potential for it to lead to higher demands on backwashing the filter systems for proper operational control. Both EPS and ATP were monitored along with headloss in this study under the various water quality parameters analyzed to assess for any potential correlations (refer to Fig. 2). The lowest headloss development levels were observed at pH 7.5 (high alkalinity) and pH 10 (high alkalinity). The lower headloss at pH 10 is not unexpected given that it corresponds with the lowest TOC removal; however this was also when the measured EPS was the highest recorded. Of note both EPS and ATP were only monitored within the top 5 cm of the biofilter columns and thus may indicate that full column sampling is required to better assess EPS and/or ATP for correlations

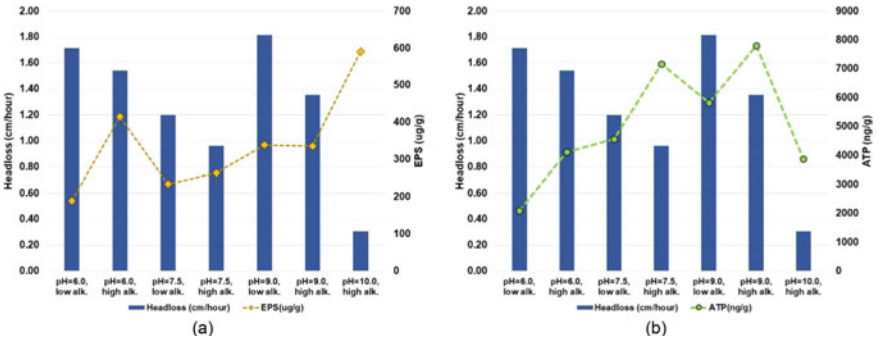

Fig. 2 Headloss, EPS, and ATP changes with pH adjustment and alkalinity changes in water

with headloss development [4]. However, depth sampling is likely not a practical task at most full-scale WTPs and is thus not recommended as a feasible procedure. It is interesting to observe that at pH 7.5 under low and high alkalinity conditions lower headloss development occurred compared to pH 6 and pH 9. This pH range is of particular interest as it is also the pH with both high DOC removal and reasonable ammonia removal; while the biofilter conditions at pH 6 has limited ammonia removal and at pH 9 the DOC removal begins to drop. Thus, there may indeed be a happier medium for the bacterial species at the pH 7.5 condition that indicates an optimal pH for TOC removal, nitrification, and control of headloss development.

3.2 Backwashing Impacts on Biofilter Column Performance

Previous research at the Carleton biofilter columns demonstrated that backwashing above a certain bed expansion demonstrated an adverse impact on removal of organic carbon in biofilters [5]. However, this research was under lab conditions with synthetic water and headloss control was not assessed at that time. A subsequent backwash study was undertaken at the City of Ottawa's Britannia Water Treatment Plant that assessed for several water quality parameters including headloss, DOC removal, DBPs, turbidity and particle counts.

Table 1 summarizes the results of the backwash experiments on headloss development. Headloss development improved in all cases when compared to the control case of a water only wash. Interestingly, when adding one extra step in the backwashing procedure (i.e. air scour or ETSW) similar but marginal improvements to headloss control in the biofilters were observed. When only air scour or ETSW was added the reduction in headloss was between 4 and 9%. When the air scour step was combined with the ETSW step the development of headloss was further reduced by 11–19%, indicating that each step facilitates removal of differing materials that otherwise contribute to headloss development. ETSW in the past has focused primarily on filter ripening with analysis of turbidity and particle counts; thus it is useful to also

Table 1 Improvement in headloss development with backwash strategy

Biofilter	Headloss reduction (%)				
	Water only (control)	Water + air scour	Water + ETSW	Water + air + ETSW	Water + air + 2-ETSW[a]
Biofilter 1	–	8	9	11	19
Biofilter 2	–	9	4	18	15

[a]2 ETSW = double stage ETSW

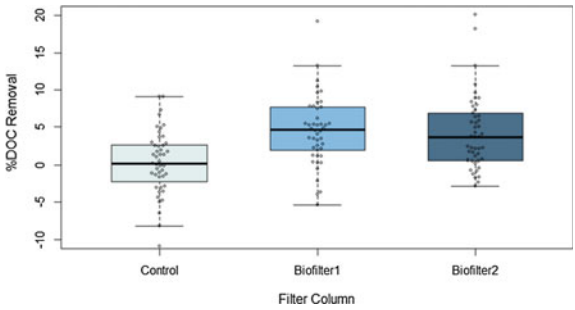

Fig. 3 DOC removal in biofilters and a control filter at the City of Ottawa Pilot WTP. Biofilters contained same material, Biofilter 1 media >50 years, Biofilter 2 media <5 years

consider that ETSW can be a helpful step with regards to headloss control in a filter column as well. Notably, there were some media age related observations, wherein Biofilter 2 which contained younger media had a higher headloss rate than Biofilter 1 with older media (additional details can be found in Piche et al. [10]).

DOC and DBP removals were not found to be influenced by backwash condition ($p > 0.05$). Thus, modifying the backwash in these cases did not influence water quality objectives with respect to these two parameters. It is however important to point out that the DOC removals for the biofilters provided only marginal gains with average DOC removal values close to 4% under all conditions (refer to Fig. 3). However, it can be noted that the DOC removal in the biofilters was better than a control filter which demonstrated a 0% removal of DOC. In addition, the influent to the biofilter columns were assessed for DBP formation potential for both HAA5s and TTHMs and then compared to the biofilter effluent. The biofilters were capable of reducing the HAA5 formation potential by almost 30% and the TTHMs by 18% (refer to Fig. 4).

Filter ripening with respect to effluent turbidity and particle release was examined with the various backwash strategies. The conventional backwash without the ETSW step shows the classic turbidity spike post backwashing when filters are placed back in service. Both the single stage and double stage ETSW demonstrate improvements in filter ripening, which would allow for filters to be place in service immediately following backwash. The pilot biofilter columns do demonstrate a higher turbidity NTU than allowable at close to 0.1 NTU in the filter effluent—however this observation is not reflected by the full scale plant itself. Total particle counts are also observed to decrease with single and double ETSW steps in comparison with the

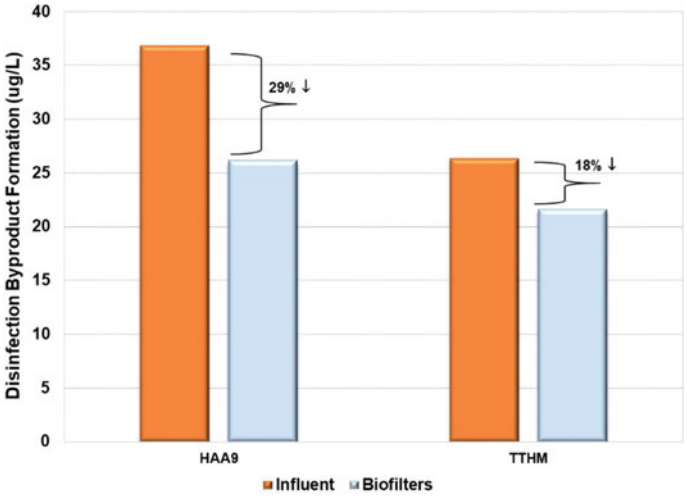

Fig. 4 Removal of disinfection by-products before and after biofiltration

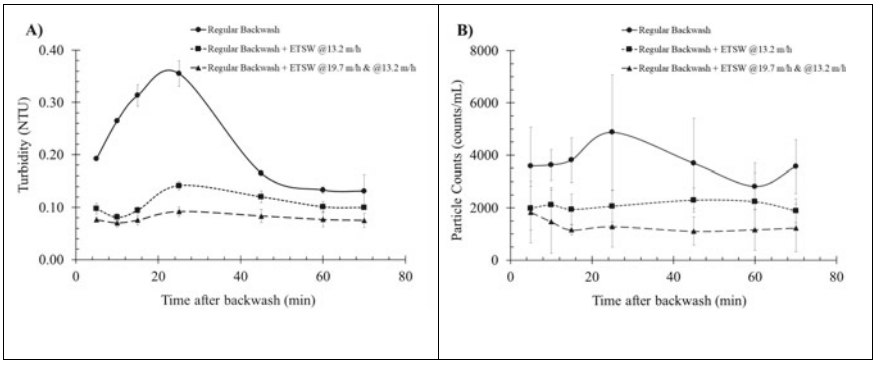

Fig. 5 Turbidity and particle counts during filter ripening and backwash strategy (Pilot Plant Data, Britannia WTP)

standard backwash procedure. The inclusion of ETSW as part of the backwash step is a relatively easy plant modification since it is based on existing infrastructure and does not require capital investment (Fig. 5).

4 Conclusion

The objectives of this research were to examine relatively easy modifications to biofilter operations to assess for improvements in various water quality parameters.

Lab scale testing conducted with a synthetic water source achieved optimal conditions at a water pH of 7.5 with respect to DOC and ammonia removal, as well as headloss control. Pilot Scale testing at a local water treatment plant demonstrated that the backwashing methods examined did not impact DOC or DBP removal and were useful with respect to controlling headloss development. Additionally, the backwash strategies, and in particular a two stage extended terminal subfluidization wash (ETSW), examined improved filter ripening outcomes with respect to turbidity and particle release.

Acknowledgements The authors would like to acknowledge the Natural Sciences and Engineering Research Council (NSERC) of Canada for funding this project. The authors also thank the members of the Basu Research Group that supported the project: Sahil Dhawan, Chamathka Varushawithana, Steve Lee, and Umar Hafeez. We also wish to thank all the staff at the Ottawa Britannia Water Treatment Plant and in particular Ian Douglas and notably Andy Campbell who showed us the ropes for operating the pilot plant and for whom we could not have completed this project without his advice and patience.

References

1. Basu OD, Dhawan S, Black K (2016) Applications of biofiltration in drinking water treatment—a review. J Chem Technol Biotechnol 91:585–595
2. DuBois M, Gilles KA, Hamilton JK, Rebers PA, Smith F (1956) Anal Chem 28(3):350–356
3. Elhadidy AM, Van Dyke MI, Chen F, Peldszus S, Huck PM (2017) Development an application of an improved protocol to characterize biofilms in biologically active drinking water filters. Environ Sci Water Res Technol 3:249–261
4. Hamidi HP, Kenari SLD, Basu OD (2020) Simultaneous TOC and ammonia removal in drinking-water biofilters: influence of pH and alkalinity. ASCE J Environ Eng 146(8):04020080
5. Ikhlef S, Basu OD (2017) Influence of backwash regime on biofilter performance in drinking water treatment. J Chem Technol Biotechnol 92(7):1777–1784
6. Keithley SE, Kirisits MJ (2018) An improved protocol for extracting extracellular polymeric substances from granular filter media. Water Res 129:419–427
7. Lauderdale C, Chadik P, Kirisits M, Brown J (2012) Engineered biofiltration: enhanced biofilter performance through nutrient and peroxide addition. J Am Water Works Assoc 104(73):289–309
8. McKie MJ, Taylor-Edmonds L, Andrews SA, Andrews RC (2015) Engineered biofiltration for the removal of disinfection by-product precursors and genotoxicity. Water Res 81:196–207
9. Metcalf & Eddy (2013) Wastewater engineering: treatment and resource recovery, 5th edn
10. Piche A, Campbell A, Cleary S, Douglas I, Basu OD (2019) Investigation of backwash strategy on headloss development and particle release in drinking water biofiltration. J Water Process Eng 32:100895
11. Rahman I, Van Dyke MI, Anderson WB, Jin X, Ndiongue S, Huck PM (2016) Effect of phosphorus addition on biofiltration pre-treatment to reduce ultrafiltration membrane fouling. Desalin Water Treat 57:25057–25069
12. Stoddart AK, Gagnon GA (2015) Full-scale prechlorine removal: impact on filter performance and water quality. J Am Water Works Assoc 638–647
13. Terry LG, Summers RS (2018) Biodegradable organic matter and rapid-rate biofilter performance: a review. Water Res 234–245

Evaluation of Arsenic and Iron Transport from Sediments of a Potable Water Treatment Wastewater Pond System

Ali Ekhlasi Nia, Harrison Bull, Ali Motalebi Damuchali, and Kerry McPhedran

1 Introduction

Drinking water treatment plants (DWTPs) create various types of wastes and wastewaters such as sludges, backwash waters, and concentrate waters, which have varying physicochemical characteristics depending on the raw source water. Groundwater is the primary source of drinking water for at least 50% of the world's population and is often the only source of raw water in many small communities [17]. The concentration of metal(loid)s, such as arsenic (As) and iron (Fe), are usually higher in groundwaters than in surface waters due to both anthropogenic and geogenic inputs [6, 20]. Arsenic is a widely recognized human carcinogen and exists in a variety of species of organic and inorganic compounds. However, inorganic species of trivalent arsenite and pentavalent arsenate are dominant in water due to their relatively high solubilities [12]. Iron is one of the essential nutrients for most living organisms; however, excessive Fe ingestion can result in significant health effects such as hereditary hemochromatosis (causing joint pain, extreme tiredness, weight loss, abdominal pain, and loss of sex drive), Fe overloading anemias, and trans-fusional Fe overloaded or other secondary forms of hemochromatosis [7, 8, 22]. Both As and Fe are typically found in elevated concentrations in many Canadian groundwaters used as raw water sources for DWTPs, especially for small communities in Saskatchewan and the other prairie provinces.

Residual wastewaters resulting from DWTP facilities with groundwater as their raw source water often contain high concentrations of As and Fe, thus, they must be treated prior to discharging into recipient water bodies. According to the Canadian Council of Ministers of the Environment [5], the limit for As in effluent waters is 5 μg/L. For Fe, the new Federal Water Quality Guideline is about 4.91 mg/L for

A. E. Nia · H. Bull · A. M. Damuchali · K. McPhedran (✉)
University of Saskatchewan, Saskatoon, Canada
e-mail: kerry.mcphedran@usask.ca

S. Walbridge et al. (eds.), *Proceedings of the Canadian Society of Civil Engineering Annual Conference 2021*, Lecture Notes in Civil Engineering 249,
https://doi.org/10.1007/978-981-19-1061-6_6

the current pond system but varies based on the pH and the DOC (dissolved organic carbon) levels in the final effluents. Wastewater stabilization ponds (WSPs), or a series of these ponds, can be effective treatment processes for residual wastewaters coming from DWTP facilities, especially for smaller facilities such as those found in many small communities. However, the effectiveness of these systems in treating residual wastewaters should be monitored over time as it could be reduced considerably due to the variety of reasons. One of the important parameters that could cause treatment effectiveness reduction in the WSPs is their sediments' contamination. Sediments exposed to wastewaters containing metal(loid)s become concentrated with these pollutants over time by particulate settling from the overlying wastewater as part of the treatment process. The sediments can then become a source of contamination to the future pond wastewaters, releasing metal(loid)s through desorption with a rate depending on the overlying effluent characteristics such as pH, temperature, and salinity, among others [10, 14].

Generally, the metal(loid) mass transfer between water and sediments (and vice versa) is a function of various physicochemical parameters. For example, diel (over 24 h) effects such as variation in water pH and temperature have been shown to cause changes in the concentrations of metal(loid)s in streams. These changes were considered to be significant in streams with neutral to alkaline pH over 24 h regardless of changes in flow rate and the significance of the concentration [16]. In addition to daily variations, seasonal metal(loid)s concentration variations occur in sediments because of changes in wastewater flow rates, nutrients, dissolved oxygen, and other physicochemical parameters [1]. For example, As concentrations have been found to vary by as much as 290% on a seasonal timeline with higher concentrations in summer vs. winter months [15]. In addition, Fe concentrations and As speciation have also been found to impact As concentrations on a seasonal timeline [13, 23].

Along with physicochemical parameters, the microbial activities in sediments have been shown to increase As mobilization by the reduction of arsenate to arsenite, which is a more soluble As species. Through this process, As is liberated by altering sorbed arsenate to arsenite compounds, which are uncharged and will be released to the aqueous phase [9]. In addition to the release of As by microbial arsenate reduction, Fe-reducing bacteria have been found to cause a release of co-precipitated As from Fe compounds by reducing the Fe in the minerals [11, 18, 19]. There are also compounds competing with As and Fe for adsorption sites in sediments such as phosphorus, selenium, and molybdate. Therefore, these compounds can cause a high rate of As leaching from sediments by replacing As in the available adsorption sites. Sediment adsorption capacity also plays a role itself given leaching of As will be increased when most of the adsorption sites are occupied [5]. Thus, metal(loid) concentrations in sediments and wastewaters of WSPs used for treatment of residuals from DWTPs should be monitored regularly to monitor treatment effectiveness over time.

The objective of this study was to monitor As and Fe concentrations in the sediments of a WSP system consisting of five sequential ponds used to treat residual wastewaters of a DWTP (Fig. 1). This facility is located in Saskatchewan and was using a combination of groundwater and surface water as its raw source water until

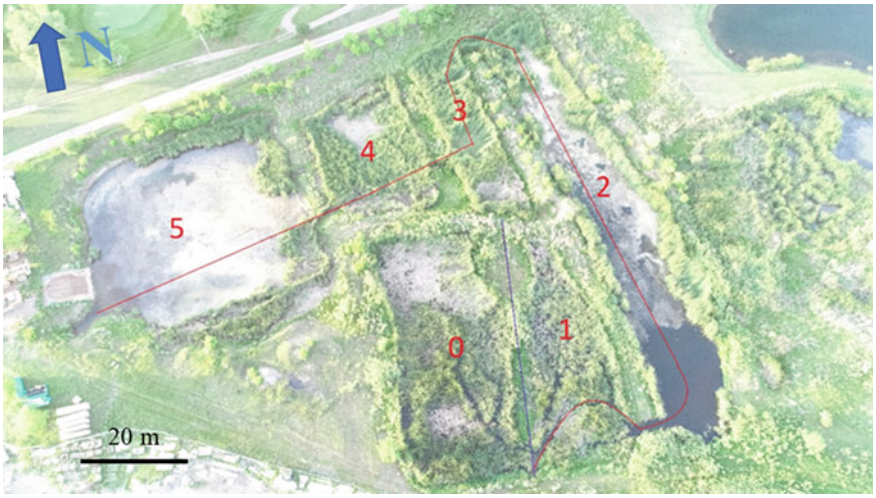

Fig. 1 Settling pond system with five settling ponds (labelled 1 through 5) that sequentially treat the DWTP effluents. The flow path is indicated via the red line starting from the bottom middle of the figure and exiting through Pond 5. *Note* Pond 0 is a part of Pond 1 that is no longer in the flow path

the end of 2019. Samples from the effluents of the WSPs have been shown to exceed guidelines previous to the start of this study which necessitated the need to better assess the individual ponds to evaluate their effectiveness including both the wastewater (as part of a parallel study; [3]) and the sediments (current study). In early 2020, a new treatment system using reverse osmosis was being commissioned that will be using 100% groundwater as the raw water source. It is expected that this new system will produce higher concentrations of both As and Fe contaminated residual wastewaters that could affect the WSP system treatment efficiency. In this study, As and Fe concentrations were measured in the sediments of the five ponds of the WSP system in on three occasions during 2019 (July, August, and October) and the variations among the ponds and over time are presented and discussed.

2 Methodology

2.1 DWTP and Settling Pond System

The studied DWTP has been in use since 1959 when it was first constructed to treat only surface water contained in a nearby reservoir. In 1989, an electro-dialysis reversal (EDR) system using groundwater as the raw source water was added to the DWTP and both systems remained active until the end of 2019. Prior to 2017, the EDR backwash waters were sent to a deep injection well; after this time, the

EDR residuals were released into the WSP system. This combined DWTP system generated wastewater that was concentrated in metals such as As and Fe which was discharged into the WSP system consisting of a series of five ponds (Fig. 1). This pond system has been in use for more than 50 years receiving wastewaters from the DWTP during which there have been a number of unrecorded changes in pond configuration. This includes impacts of heavy rainfall in the area in the early 2010s that flooded all ponds and a large portion of the DWTP municipality.

These ponds allow for oxidation and sedimentation of wastewater contaminants before releasing the effluents into a nearby waterbody. This receiving waterbody is a low-flow creek that contains fish species during the spring and summer, while the creek is largely frozen over in winter months. Historic monitoring by the DWTP operator of the WSP system effluents shows that the As concentrations were often exceeding the CCME guidelines of 5 μg/L [4]. As Fig. 1 shows, the system consists of five dissimilar ponds that largely covered by cattails and bulrushes and are habitat to some bird and animal species in the spring and summer months. The residual wastewater enters the pond system through a pipe to Pond 1, and it passes all the ponds to the end of Pond 5 where a pipe discharges the effluent to the creek. Currently, Pond 1 has been considered as consisting of two separate ponds due to the inactivity of half of the Pond 1 occurring over time due to sedimentation and short-circuiting of the pond into Pond 1. Thus, the inactive portion of this Pond 1 has been designated Pond 0 for recording purposes.

2.2 Sampling and Analysis

Sampling of the five ponds was completed on three occasions during 2019 during the months of July, August, and October. Random sediment sampling was performed for surficial (0–15 cm) sediment samples. Initially, the ponds were each divided into grids with intersected nodes sequentially numbered. The ponds were to be randomly sampled via the grid pattern with three samples for Ponds 1, 3, and 4 and five samples for Ponds 3 and 5 based on pond sizes. Unfortunately, access to pond locations was limited due to vegetation, so the ponds were each sampled in random, accessible locations determined at the site. In addition, due to pond vegetation, the use of typical sampling apparatus such as a Ponar sampler was not feasible (although it was attempted). Instead, at each site, a sampling scoop was used to collect the surficial sediments to a volume of 2 L per sampling location (6–10 L of the total sample for each pond). This comprehensive sample was mixed thoroughly in a container and 2-2 L ziplock bags (average of 3.2 kg each) were filled with sediments from each pond. One bag was processed for shipping to ALS Environmental (Saskatoon, SK, Canada) for analysis, while the second was transported in a cooler to the Environmental Engineering laboratory at USask and stored at 4 °C for use in future research experiments. All samples were transported at <10 °C in under 72 h to ALS labs for analysis as per guidelines (actual 4 °C and 48 h). Samples transported to USask

also followed the temperature guideline prior to long-term storage as they were not analyzed immediately.

In addition to sediment samples, wastewater samples were also taken from each of the ponds as part of a parallel study on the wastewater characterization [3]. These samples were taken from the outlets of each pond on the same day as the sediment samples. The ALS Environmental Laboratory provided the necessary sample containers and cooler for wastewater samples and all procedures they provided were followed as for the sediment samples. Metal(loid) analysis of wastewaters and sediments at ALS Environmental was conducted using collision/reaction inductively coupled plasma mass spectrometry (CRC ICP-MS) according to the Method 6020A of U.S. Environmental Protection Agency [21]. All wastewater samples were filtered using a 0.45 μm glass-fibre filter prior to analysis. All sediment samples were dried, disaggregated, and sieved using a 2 mm mesh. Then, they were digested with nitric and hydrochloric acids and analyzed using the CRC ICP-MS method. Although a suite of metal(loid)s were examined for all of the wastewater and sediment samples, only As and Fe are presented herein as they are considered to be contaminants of interest based on the historic DWTP monitoring indicating they could be present at concentrations that exceed CCME guidelines.

3 Results and Discussion

3.1 As Sediment and Wastewater Concentrations

Figure 2 shows the concentrations of As in the wastewater (mg/L on left y-axis) and sediment (mg/kg on right y-axis) samples for each of the ponds in July, August, and October, respectively. In general, the sediment As concentrations decreased from Pond 1 to Pond 5 on each sampling occasion with about 300–450 mg/kg and about 50 mg/kg, respectively. Interestingly, the sediments in Pond 2 had lower concentrations than Pond 1, however, the concentrations then increased in for both Ponds 3 and 4 before decreasing again in Pond 5. The only outlier was the July Pond 3 sample that was lower than the Pond 3 concentration. This low As concentration in the sediments of Pond 3 could be explained by development of vegetation including cattails and bulrushes that covered a large area of the pond which impeded sample collection from the centre of the ponds (a safety issue for sampling access). Despite the ponds being sampled in multiple locations, the concentrations of metal(loid)s would be expected to be higher in the deeper, centre sections of each pond where more settling may have occurred over time [2]. In general, sampling the entire ponds' sediments is not an option and the sub-sampling and mixing protocol used currently should provide for a representative sample for each pond.

For comparative purposes, the sediment concentrations may also be compared to the aqueous concentrations. For July and August, the aqueous concentrations generally increased from Pond 1 to Pond 5, while in October the concentrations were

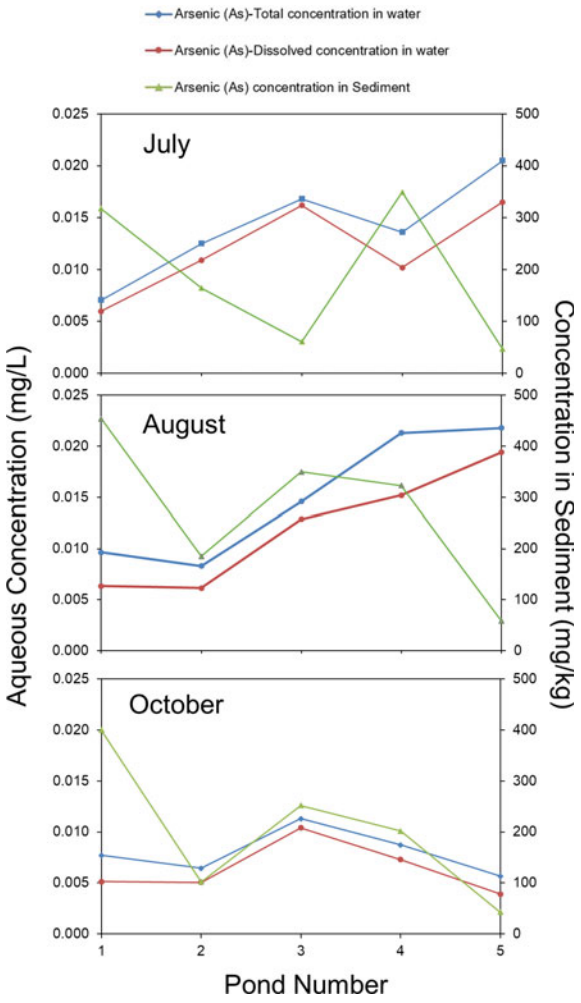

Fig. 2 The As concentrations in wastewater and sediments for each of the five ponds as determined for three sampling events in 2019

largely the same throughout the pond system. The increase of As concentrations from Pond 1 to Pond 5 may be the result of leaching of As from sediments into the wastewater in July and August. The determination of this leaching, including calculation of desorption rates, was assessed through desorption experiments using the collected sediments in the second stage of the study in 2020.

3.2 Fe Sediment and Wastewater Concentrations

Figure 3 shows the concentrations of Fe in the wastewater (mg/L on left y-axis) and sediment (mg/kg on right y-axis) samples for each of the ponds in July, August, and October, respectively. Similar to As, the general trend for Fe concentrations is a

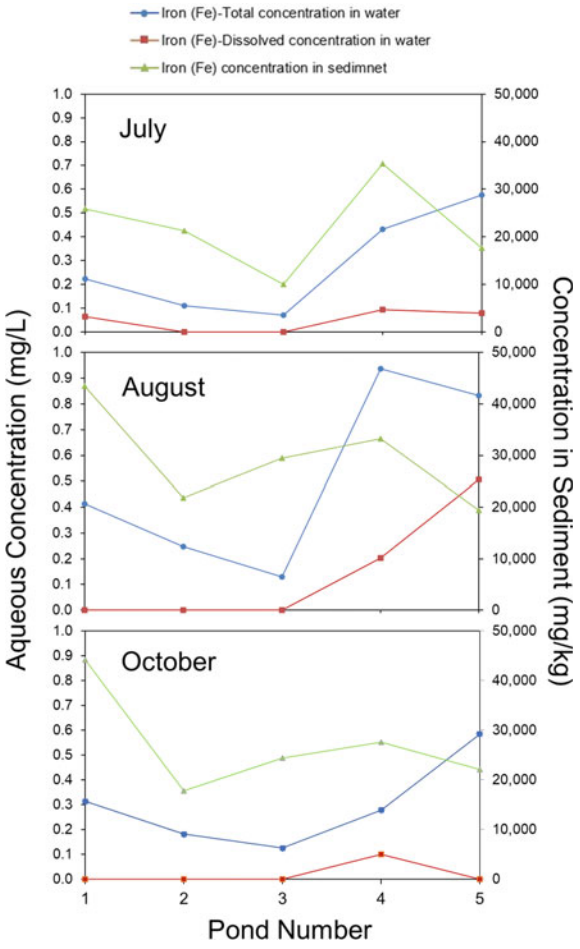

Fig. 3 Fe concentrations in wastewater and sediments for each of the five ponds as determined for three sampling events in 2019

decrease from Pond 1 to Pond 5 with 25,000 to 45,000 mg/kg and about 20,000 mg/kg, respectively. In addition, the same trends for Ponds 2, 3, and 4 are also apparent for Fe. In general, this would appear to indicate that As and Fe concentrations in sediments are correlated to each other. The Fe wastewater aqueous concentrations show a similar trend as As for July and August; however, unlike As, the Fe concentration also increasing from Pond 1 through Pond 5 in October.

3.3 As and Fe Variations in Ponds

Figure 4 shows the sediments As and Fe concentration variations in the individual ponds (including Pond 0) from July, August, and October, respectively. In general,

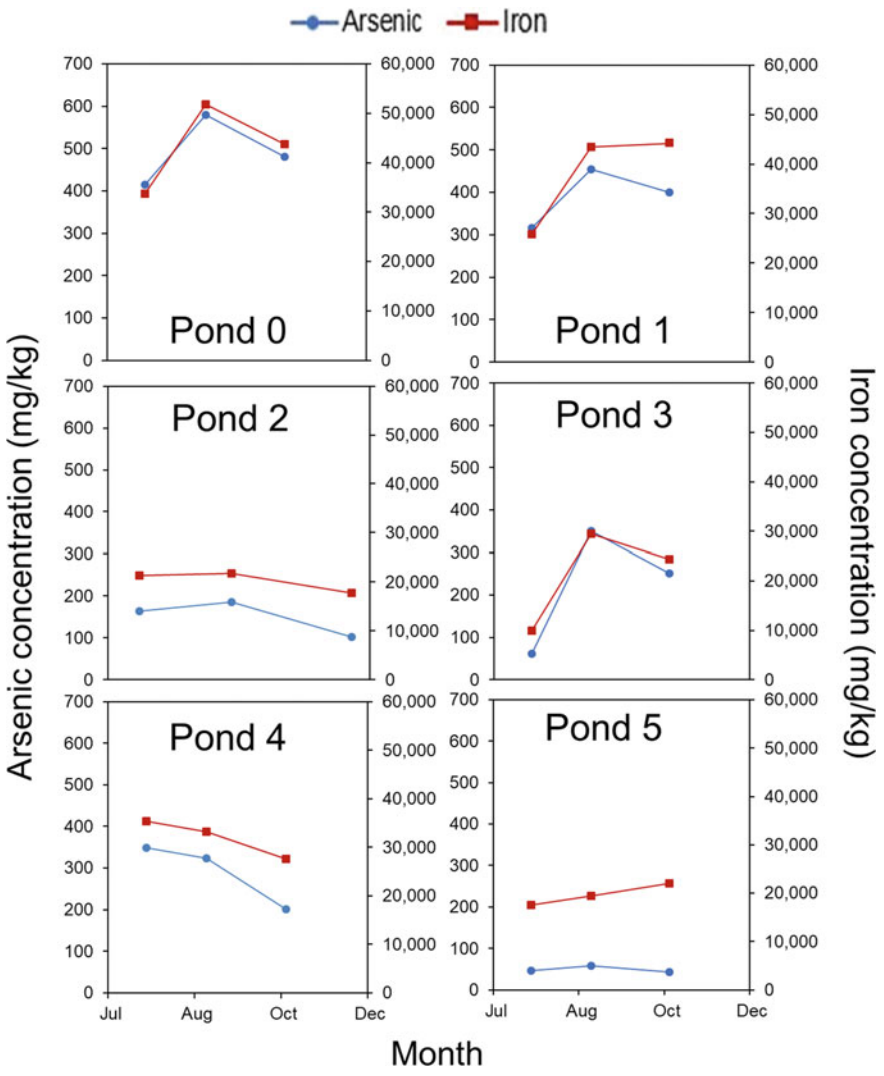

Fig. 4 As and Fe concentrations in sediments for each pond (including Pond 0) over time with samples collected in July, August, and October 2019

variations in As and Fe concentrations in the sediments of each pond over time were much lower than their variations from pond to pond. The As concentration increased from July to August and then decreased in October in all ponds except Pond 4, where As decreased over time. The lowest As concentrations were observed in the sediments of Pond 5 where As fluctuated from 40 to 60 mg/kg. In contrast, the highest As contaminations were observed in the Pond 0 where As ranged from 400 to 600 mg/kg; while the Pond 1 was also high at about 350 to 450 mg/kg. The

Fe concentrations had similar trends to As in Ponds 2, 3, and 4 but increased over time in Ponds 1 and 5. Pond 5 that had the lowest As-contaminated sediments, also had the lowest sediment Fe concentrations (although they were similar to Pond 2). The Fe concentrations ranged from 17,000 to 22,000 mg/kg and from 18,000 to 22,000 mg/kg in the sediments of Ponds 5 and 2, respectively. Similar to As, the Pond 0 had the highest Fe concentrations that ranged from 34,000 to 52,000 mg/kg.

4 Conclusions

In general, DWTPs that use groundwater as a raw source water produce wastewaters that are elevated in metal(loid)s, such as As and Fe. The As and Fe in the current study often exceed regulatory guidelines, thus, these wastewaters need to be treated before releasing to the environment. The DWTP WSP systems are typically designed to treat such wastewaters; however, the efficiency of these ponds needs to be monitored as the ponds can accumulate contaminants within their sediments and, therefore, become a source of wastewater contamination over time rather than a sink. This study monitored As and Fe concentrations in the wastewaters and sediments of a WSP system containing five sequential ponds for a Saskatchewan DWTP over three sampling events. The sediments contained As and Fe concentrations in the range of about 45–600 and 10,000–52,000 mg/kg, respectively. The concentrations varied among the ponds and over time, however, the variations between the ponds were greater than in each of the individual ponds over time. Of most interest are Ponds 3 and 4 that appear to have a potential for release of sediment bound As and Fe back into the wastewater stream. This release can then impact the pond system effluents and potentially leading to exceedances of CCME guidelines. This year 2019 research was preliminary research prior to a more intensive assessment of these ponds in 2020, including assessment of the sediment leaching potentials and impacts of the new treatment system on the pond systems.

Acknowledgements The authors would like to acknowledge funding through the Mitacs Accelerate program and SaskWater. In addition, research support has been provided by SaskWater personnel including Sumith Kahanda, Enisa Zanacic, Dale Hreshka, and Timo Jansen.

References

1. Adeyemo OK, Adedokun OA, Yusuf RK, Adeleye EA (2008) Seasonal changes in physico-chemical parameters and nutrient load of river sediments in Ibadan City, Nigeria. Glob Nest J 10(3):326–336
2. Andreas V, Irvine K, Jindal R, Thongdara R, Chatterji NN, Sheng WB (2019) Spatial patterns of heavy metals in the sediments of a municipal wastewater treatment pond system and receiving waterbody, Cha am, Thailand. J Water Manag Model 27:465–465

3. Bull H, Eklasi Nia A, McPhedran KN (2022) Evaluation of the efficacy of a treatment pond system for removal of concentrated iron and arsenic produced from water treatment plant (WTP) wastewater. Proceedings of the Canadian society of civil engineering. Springer, Boston, MA, USA
4. CCME (2001) Canadian water quality guidelines for the protection of aquatic life: Canadian water quality index 1.0 technical report. Canadian environmental quality guidelines. Winnipeg, MB, Canada
5. CCME (Canadian Council of Ministers of the Environment) (1997) Canadian soil quality guidelines for the protection of environmental and human health—arsenic (inorganic). ISBN 1-896997-34-1
6. Chakravarty S, Dureja V, Bhattacharyya G, Maity S, Bhattacharjee S (2002) Removal of arsenic from groundwater using low cost ferruginous manganese ore. Water Res 36(3):625–632
7. Dev S, Babitt JL (2017) Overview of iron metabolism in health and disease. Hemodial Int 21:S6–S20
8. Drakesmith H, Schimanski LM, Ormerod E, Merryweather-Clarke AT, Viprakasit V, Edwards JP, Sweetland E, Bastin JM, Cowley D, Chinthammitr Y, Robson KJ (2005) Resistance to hepcidin is conferred by hemochromatosis-associated mutations of ferroportin. Blood 106(3):1092–1097
9. Drewniak L, Sklodowska A (2013) Arsenic-transforming microbes and their role in biomining processes. Environ Sci Pollut Res 20(11):7728–7739
10. Duncan AE, de Vries N, Nyarko KB (2018) Assessment of heavy metal pollution in the sediments of the River Pra and its tributaries. Water Air Soil Pollut 229(8):272
11. Gounou C, Bousserrhine N, Varrault G, Mouchel JM (2010) Influence of the iron-reducing bacteria on the release of heavy metals in anaerobic river sediment. Water Air Soil Pollut 212(1–4):123–139
12. Jain CK, Ali I (2000) Arsenic: occurrence, toxicity and speciation techniques. Water Res 34(17):4304–4312
13. La Force MJ, Hansel CM, Fendorf S (2000) Arsenic speciation, seasonal transformations and co-distribution with iron in a mine waste-influenced palustrine emergent wetland. Environ Sci Technol 34(18):3937–3943
14. Li H, Shi A, Li M, Zhang X (2013) Effect of pH, temperature, dissolved oxygen, and flow rate of overlying water on heavy metals release from storm sewer sediments. J Chem 1–11
15. Nimick DA, Cleasby TE, McCleskey RB (2005) Seasonality of diel cycles of dissolved trace-metal concentrations in a Rocky Mountain stream. Environ Geol 47(5):603–614
16. Nimick DA, Gammons CH, Cleasby TE, Madison JP, Skaar D, Brick CM (2003) Diel cycles in dissolved metal concentrations in streams: occurrence and possible causes. Water Resour Res 39(9):1247–1264
17. Nouri J, Mahvi AH, Jahed GR, Babaei AA (2008) Regional distribution pattern of groundwater heavy metals resulting from agricultural activities. Environ Geol 55(6):1337–1343
18. Quantin C, Becquer T, Rouiller JH, Berthelin J (2001) Oxide weathering and trace metal release by bacterial reduction in a New Caledonia Ferralsol. Biogeochemistry 53(3):323–340
19. Saup CM, Williams KH, Rodríguez-Freire L, Cerrato JM, Johnston MD, Wilkins MJ (2017) Anoxia stimulates microbially catalyzed metal release from Animas River sediments. Environ Sci Process Impacts 19(4):578–585
20. Stollenwerk KG (2003) Geochemical processes controlling transport of arsenic in groundwater: a review of adsorption. Arsenic in Ground Water. Springer, Boston, MA, USA, pp 67–100
21. US EPA (United States Environmental Protection Agency) (1998) Inductively coupled plasma-mass spectrometry. EPA 6020A (SW-846)
22. Wessling-Resnick M (2017) Iron: basic nutritional aspects. Molecular, genetic, and nutritional aspects of major and trace minerals. Academic Press, Cambridge, MA, pp 161–173
23. Yan C, Che F, Zeng L, Wang Z, Du M, Wei Q, Wang Z, Wang D, Zhen Z (2016) Spatial and seasonal changes of arsenic species in Lake Taihu in relation to eutrophication. Sci Total Environ 563:496–505

Conceptualizing a Stress-Tolerant Bioremediation Strategy for Petroleum Hydrocarbon-Contaminated Soils in Cold Climates: A Preliminary Review

J. Kim and W. Chang

1 Introduction

Petroleum hydrocarbons (PHCs) are the most commonly identified contaminants in cold environments, including in polar and sub-polar regions in Canada [27]. They are a mixture of toxic and carcinogenic organic compounds that have spilled in various environments and threaten human health and ecosystems [32]. PHC spills in cold environments have occurred due to oil extraction, storage and transportation, and resulted from infrastructure failure and human error [6]. Spills in cold soils are considered more harmful than in temperate soil environments due to the separation and mobility of PHCs during seasonal freezing and thawing [4]. The high costs of remediating PHC-contaminated sites in polar regions are associated with remote site locations [11]. For example, the remediation costs for abandoned and contaminated Distant Early Warning (DEW) sites, which are remotely located throughout the Arctic and sub-Arctic in northern Canada, can be more than $500 million [12].

Bioremediation, which is the use of living organisms to reduce or remove contaminants such as PHCs, has been applied at cold contaminated sites as an eco-friendly and cost-effective remediation technology [1, 18]. Due to the remote locations with limited accessibility and the harsh cold environments, bioremediation in cold regions has mostly been applied during summer treatment periods [36]. However, summers in cold regions are only 2–4 months long, which is insufficient for meeting environmental criteria through significant biodegradation [23, 35]. The limitations in cold climates have implied longer timeframes for remediation practices at PHC-contaminated sites [6].

Cold-adapted, indigenous hydrocarbon degraders have been isolated from cold PHC-contaminated sites and characterized [8, 34]. They are able to survive and grow

J. Kim · W. Chang (✉)
University of Saskatchewan, Saskatoon, Canada
e-mail: Wonjae.chang@usask.ca

S. Walbridge et al. (eds.), *Proceedings of the Canadian Society of Civil Engineering Annual Conference 2021*, Lecture Notes in Civil Engineering 249,
https://doi.org/10.1007/978-981-19-1061-6_7

under cold conditions [22] and have therefore been utilized for biostimulation and bioaugmentation [36]. Based on recent work, the use of cold-adapted hydrocarbon degraders is expected to facilitate the extension of biodegradation from positive to subzero temperatures [7, 16].

This study reviews the recent advances in bioremediation in cold climates. The specific objectives of this study are to address PHC biodegradation performance at low temperatures in the laboratory and the field, summarize the kinetics of biodegradation related to low temperatures, and review sustainable microbial activity in freezing and frozen soils.

2 Bioremediation of PHC-Contaminated Soils in Cold Climates

PHC biodegradation has been examined at summer treatment temperatures in the laboratory. In cold regions such as the Alpine, Antarctic and Arctic, contaminated soils are nutrient-deficient. Biostimulation, the addition of nutrients to stimulate biodegradation, has therefore been used. Margesin and Schinner [17] performed PHC biodegradation experiments at a fixed 10 °C. They showed over 155 days that 90% of total petroleum hydrocarbons (TPH) was removed by adding nutrients to the Alpine soils. Aislabie et al. [2] investigated hydrocarbon biodegradation using ^{14}C-labelled hexadecane and naphthalene at a fixed 8 °C. Their results indicated 20% of the ^{14}C-hexadecane and 45% of the ^{14}C-naphthalene were removed over 90 days in nutrient-treated Antarctic desert soils. Mohn and Stewart [23] also studied PHC biodegradation at a fixed 7 °C. They demonstrated that approximately 30% of TPH were removed from Arctic tundra soils over 180 days. Whyte et al. [35] set the experimental temperature as low as 5 °C for PHC biodegradation. They noted that TPH removals reached 47% in 16 weeks following nutrient addition to the Arctic soils. The above studies showed the feasibility of biodegradation at low temperatures between 5 and 10 °C.

PHC biodegradation tests in the field have also focused on summer periods. Biodegradation field studies have been conducted in both the Arctic [20, 33, 37] and Antarctic [3, 19, 30]. As mentioned, the summer periods in cold regions are too short to meet the environmental criteria [7, 35], and field experiments have therefore been carried out over multiple years [9, 21, 24, 26, 29, 31]. McWatters et al. [21] showed the PHCs were significantly removed over 5 years by adding nutrients to contaminated soils in Antarctica. Robichaud et al. [29] also demonstrated significant PHC removal over five years in northern Canada using phytoremediation with compost. These studies substantiate that PHC removal at large scales in cold climates has been achieved.

The feasibility of PHC biodegradation at subzero temperatures has been discussed. Rike et al. [28] measured soil gases (O_2 and CO_2) in the field during winter, and indirectly demonstrated that PHC-biodegradation activity was measurable between

−1 and −3 °C in freezing contaminated soils. However, their study only claimed the possibility of biodegradation at subzero temperatures without TPH analysis. In a laboratory experiment using nutrients and biochar at a fixed −5 °C, the significant removal of PHCs was reported [13–15]. Nevertheless, applying a fixed subzero temperature to study cold-climate biodegradation has limitations for real contaminated sites, which are subjected to the temperature variations associated with seasonal freezing and thawing [25]. PHC biodegradation in the field, in freezing and frozen contaminated soils, remains largely unexplored.

PHC biodegradation under seasonally freezing and thawing conditions has been investigated rarely. Chang et al. [7] demonstrated significant TPH removal under site-representative seasonal freezing and thawing conditions in a pilot-scale biodegradation experiment. They conducted the experiment in a laboratory by using a site-temperature scenario: slow seasonal freezing (−0.12 °C/day) followed by thawing (+0.16 °C/day). That study correlated changes in unfrozen water content to soil respiration activity (CO_2 and O_2). Also in the field during seasonal freezing and thawing, Kim et al. [16] investigated the feasibility of PHC biodegradation using pilot-scale biopiles. Ambient temperatures reached −30 °C in the winter and the soil temperature decrease to −10 °C. Greater retention of unfrozen water content was observed in the treated biopile (nutrients and humate), compared to the untreated control biopile. The enhanced PHC biodegradation in the treated biopile was observed in the freezing and frozen soils, at subzero temperatures during the winter. This study indicates that *enhanced* and *extended* biodegradation in freezing and frozen soils, beyond conventional summer treatment periods, is feasible in the field. Table 1 summarizes the PHC biodegradation results achieved at various temperature ranges in previous studies.

3 PHC-Degradation Kinetics at Low Temperatures

PHC degradation kinetics at summer temperatures in cold regions have been analyzed using linear and first-order analyses in the laboratory and in the field. Under rapid and repeating freezing and thawing conditions between −5 and 7 °C, the linear rate constant for TPH degradation was reported to be 12.9 mg TPH/kg/day over 48 days [10]. Using a landfarm in the sub-Arctic subjected to varying field temperatures between 2 and 25 °C, Zytner et al. [37] reported a first-order TPH-degradation constant of 0.022–0.0043 d^{-1} over 30 days. In another on-site biodegradation study using a biopile, Thomassin-Lacroix et al. [33] recorded a linear TPH-degradation rate constant of 90 mg TPH/kg/day over 14 days at field temperatures between 0 and 10 °C. Paudyn et al. [26] conducted PHC biodegradation experiments using a landfarm in the Canadian Arctic. When average summer temperatures were 3 °C, the first-order TPH degradation rate constant was 0.015–0.026 d^{-1}. McWatters et al. [21] also performed PHC-biodegradation tests using large-scale on-site biopiles in the Antarctic. Within 100 days, the TPH-degradation rate constant was 2.6–60 mg TPH/kg/day. After 100 days, the TPH-degradation constant was lower at 13–26 mg TPH/kg/day.

Table 1 Bioremediation studies at low temperatures (F2: C10–C16, F3: C16–C34)

Laboratory/Field	Temperature	Experiment duration	PHC removal	References
Laboratory	Fixed at 10 °C	155 d	90%	Margesin and Schinner [17]
Laboratory	Fixed at 8 °C	90 d	45%	Aislabie et al. [2]
Laboratory	Fixed at 7 °C	180 d	30%	Mohn and Stewart [23]
Laboratory	Fixed at 5 °C	112 d	47%	Whyte et al. [35]
Field	Variable in summer	60 d	58%	Zytner et al. [37]
Laboratory	Variable from −5 to 7 °C	48 d	3.5 mg TPH/kg/day	Eriksson et al. [10]
Field	Variable in summer	365 d	92%	Mohn et al. [24]
Field	Variable from 0 to 10 °C	65 d	90 mg TPH/kg/day	Thomassin-Lacroix et al. [33]
Field	Variable from −2 to 10 °C	50 d	75%	Ruberto et al. [30]
Field	Variable from 0 to 20 °C	730 d	95%	Delille et al. [9]
Field	Variable from 1.3 to 4.9 °C	55 d	From 8300 to 500 mg Diesel/kg	McCarthy et al. [20]
Laboratory	Variable from −5 to 5 °C	48 d	54 mg hexadecane/kg/day	Børresen et al. [5]
Field	Variable	725 d	80%	Paudyn et al. [26]
Field	Variable	1460 d	73%	Sanscartier et al. [31]
Laboratory	Variable from −5 to 14 °C	160 d	F2: 32% F3: 16%	Chang et al. [7]
Field	Variable from −30 to 10 °C	1825 d	From 3531 to 907 mg TPH/kg	McWatters et al. [21]
Field	Variable from 0 to 10 °C	50 d	75%	Martínez Álvarez et al. [19]
Laboratory	Fixed at −5 °C	90 d	From 266 to 61 mg F3/kg	Karppinen et al. [13]
Laboratory	Fixed at −5 °C	90 d	From 656 to 473 mg F3/kg	Karppinen et al. [14]
Field	Variable from −30 to 30 °C	270 d	F2: 57% F3: 58%	Kim et al. [16]
Laboratory	Fixed at −5 °C	90 d	84%	Karppinen et al. [15]
Field	Variable	1825 d	75%	Robichaud et al. [29]
Field	Variable from 0 to 10 °C	50 d	75%	Álvarez et al. [3]

Table 2 PHC degradation rate constant related to low temperatures

Laboratory/Field	Temperature	PHC degradation rate constant	References
Laboratory	Variable from −5 to 7 °C	12.9 mg TPH/kg/day	Eriksson et al. [10]
Field	Variable	TPH: 0.022–0.0043 d^{-1}	Zytner et al. [37]
Field	Variable from 0 to 10 °C	90 mg TPH/kg/day	Thomassin-Lacroix et al. [33]
Field	Variable	TPH: 0.015–0.026 d^{-1}	Paudyn et al. [26]
Laboratory	Variable from −5 to 14 °C	TPH: 0.0046 d^{-1}	Chang et al. [7]
Field	Variable from −30 to 10 °C	2.6–60 mg TPH/kg/day (<100 days) 13–26 mg TPH/kg/day (>100 days)	McWatters et al. [21]
Laboratory	Fixed at −5 °C	F3: 0.0036 d^{-1}	Karppinen et al. [13]
Field	Variable from −30 to 30 °C	F3: 0.0066 d^{-1} (freezing) F3: 0.0013 d^{-1} (thawing)	Kim et al. [16]

Biodegradation rate constants at subzero temperatures have also been investigated. Chang et al. [7] applied seasonal freezing and thawing temperature conditions and reported TPH-degradation rate constants between 0.0046 and 0.017 d^{-1} when soil temperatures ranged from −5 to 10 °C. Fixed at −5 °C, Karppinen et al. [13] showed a degradation rate constant for F3 (C16–C34) hydrocarbons of 0.0036 d^{-1}. Kim et al. [16], in their field experiment during seasonal freezing and thawing, reported a degradation rate constant of 0.0066 d^{-1} for F3 hydrocarbons between November and mid-January. That was approximately five times higher than during the thawing period (0.0013 d^{-1}) from January to May. Their results are promising and suggest that the efficiency of PHC degradation can be significant beyond the short summer seasons. As summarized in Table 2, PHC degradation in freezing and frozen soils is still compatible with above-zero temperature conditions.

4 Summary

The remediation of contaminated sites in cold regions has been considered a very difficult challenge due to the cold environment, the limited access to sites, and other logistical and engineering factors. This preliminary review highlights the recent development of PHC biodegradation practices adapted to cold regions. Recent studies have brought up the possibility of enhanced PHC biodegradation in the winter, which will help overcome the limitations associated with cold temperatures and the remoteness of the contaminated sites. However, further understanding of biodegradation activity in freezing and frozen contaminated soils is required.

Acknowledgements This research was funded by Natural Sciences and Engineering Research Council (NSERC; RGPIN 05902-2014).

References

1. Aislabie J, Foght J (2008) Hydrocarbon-degrading bacteria in contaminated cold soil. In: Filler DM, Snape I, Barnes DL (eds) Bioremediation of petroleum hydrocarbons in cold regions. Cambridge University Press, New York, pp 69–83
2. Aislabie J, McLeod M, Fraser R (1998) Potential for biodegradation of hydrocarbons in soil from the Ross Dependency, Antarctica. Appl Microbiol Biotechnol 49(2):210–214
3. Álvarez LM,. Ruberto L, Gurevich J, Mac Cormack W (2020) Environmental factors affecting reproducibility of bioremediation field assays in Antarctica. Cold Reg Sci Technol 169:102915
4. Barnes D, Biggar K (2008) Movement of petroleum through freezing and frozen soils. In: Filler DM, Snape I, Barnes DL (eds) Bioremediation of petroleum hydrocarbons in cold regions. Cambridge University Press, New York, pp 55–68
5. Børresen M, Barnes D, Rike A (2007) Repeated freeze-thaw cycles and their effects on mineralization of hexadecane and phenanthrene in cold climate soils. Cold Reg Sci Technol 49(3):215–225
6. Camenzuli D, Freidman BL (2015) On-site and in situ remediation technologies applicable to petroleum hydrocarbon contaminated sites in the Antarctic and Arctic. Polar Res 34(1):1–19
7. Chang W, Klemm S, Beaulieu C, Hawari J, Whyte L, Ghoshal S (2011) Petroleum hydrocarbon biodegradation under seasonal freeze–thaw soil temperature regimes in contaminated soils from a sub-Arctic site. Environ Sci Technol 45(3):1061–1066
8. Chang W, Akbari A, David C, Ghoshal S (2018) Selective biostimulation of cold- and salt-tolerant hydrocarbon-degrading *Dietzia maris* in petroleum-contaminated sub-Arctic soils with high salinity. J Chem Technol Biotechnol 93:294–304
9. Delille D, Coulon F, Pelletier E (2004) Effects of temperature warming during a bioremediation study of natural and nutrient-amended hydrocarbon-contaminated sub-Antarctic soils. Cold Reg Sci Technol 40(1–2):61–70
10. Eriksson M, Ka J, Mohn WW (2001) Effects of low temperature and freeze-thaw cycles on hydrocarbon biodegradation in Arctic tundra soil. Appl Environ Microbiol 67(11):5107–5112
11. Harvey AN, Snape I, Siciliano SD (2012) Changes in liquid water alter nutrient bioavailability and gas diffusion in frozen Antarctic soils contaminated with petroleum hydrocarbons. Environ Toxicol Chem 31(2):395–401
12. Hird M (2016) The dew line and Canada's Arctic waste: legacy and futurity. North Rev 42:23–45
13. Karppinen EM, Siciliano SD, Stewart KJ (2017) Application method and biochar type affect petroleum hydrocarbon degradation in northern landfarms. J Environ Qual 46(4):751–759
14. Karppinen EM, Stewart KJ, Farrell RE, Siciliano SD (2017) Petroleum hydrocarbon remediation in frozen soil using a meat and bonemeal biochar plus fertilizer. Chemosphere 173:330–339
15. Karppinen EM, Mamet SD, Stewart KJ, Siciliano SD (2019) The charosphere promotes mineralization of ^{13}C-phenanthrene by psychrotrophic microorganisms in Greenland soils. J Environ Qual 48(3):559–567
16. Kim J, Lee AH, Chang W (2018) Enhanced bioremediation of nutrient-amended, petroleum hydrocarbon-contaminated soils over a cold-climate winter: the rate and extent of hydrocarbon biodegradation and microbial response in a pilot-scale biopile subjected to natural seasonal freeze-thaw temperatures. Sci Total Environ 612:903–913
17. Margesin R, Schinner F (1997) Bioremediation of diesel-oil-contaminated alpine soils at low temperatures. Appl Microbiol Biotechnol 47(4):462–468

18. Margesin R, Schinner F (1999) Biological decontamination of oil spills in cold environments. J Chem Technol Biotechnol 74(5):381–389
19. Martínez Álvarez L, Ruberto LL, Balbo A, Mac Cormack W (2017) Bioremediation of hydrocarbon-contaminated soils in cold regions: development of a pre-optimized biostimulation biopile-scale field assay in Antarctica. Sci Total Environ 590:194–203
20. McCarthy K, Walker L, Vigoren L, Bartel J (2004) Remediation of spilled petroleum hydrocarbons by in situ landfarming at an Arctic site. Cold Reg Sci Technol 40(1–2):31–39
21. McWatters R, Wilkins D, Spedding T, Hince G, Raymond B, Lagerewskij G, Terry D, Wise L, Snape I (2016) On site remediation of a fuel spill and soil reuse in Antarctica. Sci Total Environ 571:963–973
22. Miri S, Naghdi M, Rouissi TK, Brar S, Martel R (2019) Recent biotechnological advances in petroleum hydrocarbons degradation under cold climate conditions: a review. Crit Rev Environ Sci Technol 49(7):553–586
23. Mohn WW, Stewart GR (2000) Limiting factors for hydrocarbon biodegradation at low temperature in Arctic soils. Soil Biol Biochem 32(8–9):1161–1172
24. Mohn W, Radziminski C, Fortin M-C, Reimer K (2001) On site bioremediation of hydrocarbon-contaminated Arctic tundra soils in inoculated biopiles. Appl Microbiol Biotechnol 57(1–2):242–247
25. Or D, Smets BF, Wraith J, Dechesne A, Friedman S (2007) Physical constraints affecting bacterial habitats and activity in unsaturated porous media—a review. Adv Water Resour 30(6–7):1505–1527
26. Paudyn K, Rutter A, Rowe RK, Poland JS (2008) Remediation of hydrocarbon contaminated soils in the Canadian Arctic by landfarming. Cold Reg Sci Technol 53(1):102–114
27. Princz JI, Moody M, Fraser CV, der Vliet L, Lemieux H, Scroggins R, Siciliano SD (2012) Evaluation of a new battery of toxicity tests for boreal forest soils: assessment of the impact of hydrocarbons and salts. Environ Toxicol Chem 31(4):766–777
28. Rike AG, Haugen KB, Engene B (2005) In situ biodegradation of hydrocarbons in Arctic soil at sub-zero temperatures—field monitoring and theoretical simulation of the microbial activation temperature at a Spitsbergen contaminated site. Cold Reg Sci Technol 41(3):189–209
29. Robichaud K, Stewart K, Labrecque M, Hijri M, Cherewyk J, Amyot M (2019) An ecological microsystem to treat waste oil contaminated soil: using phytoremediation assisted by fungi and local compost, on a mixed-contaminant site, in a cold climate. Sci Total Environ 672:732–742
30. Ruberto L, Vazquez SC, Mac Cormack WP (2003) Effectiveness of the natural bacterial flora, biostimulation and bioaugmentation on the bioremediation of a hydrocarbon contaminated Antarctic soil. Int Biodeter Biodegr 52(2):115–125
31. Sanscartier D, Laing T, Reimer K, Zeeb B (2009) Bioremediation of weathered petroleum hydrocarbon soil contamination in the Canadian high Arctic: laboratory and field studies. Chemosphere 77(8):1121–1126
32. Siciliano SD, Schafer AN, Forgeron MA, Snape I (2008) Hydrocarbon contamination increases the liquid water content of frozen Antarctic soils. Environ Sci Technol 42(22):8324–8329
33. Thomassin-Lacroix E, Eriksson M, Reimer K, Mohn W (2002) Biostimulation and bioaugmentation for on-site treatment of weathered diesel fuel in Arctic soil. Appl Microbiol Biotechnol 59(4–5):551–556
34. Whyte LG, Hawari J, Zhou E, Bourbonnière L, Inniss WE, Greer CW (1998) Biodegradation of variable-chain-length alkanes at low temperatures by a psychrotrophic *Rhodococcus* Sp. Appl Environ Microbiol 64(7):2578–2584
35. Whyte L, Goalen B, Hawari J, Labbé D, Greer C, Nahir M (2001) Bioremediation treatability assessment of hydrocarbon-contaminated soils from Eureka, Nunavut. Cold Reg Sci Technol 32(2):121–132
36. Yang S, Jin H, Wei Z, He R, Ji Y, Li X, Yu S (2009) Bioremediation of oil spills in cold environments: a review. Pedosphere 19(3):371–381
37. Zytner R, Salb A, Brook T, Leunissen M, Stiver W (2001) Bioremediation of diesel fuel contaminated soil. Can J Civ Eng 28(S1):131–140

Soil Treatment Towards Stress-Tolerant Bioremediation Strategy for Petroleum Hydrocarbon-Contaminated Soils in Cold Climates Using Zeolite as a Remediation Agent: A Preliminary Study

Tasnim Nayeema, Aslan Hwanhwi Lee, Darshdeep Singh, LuVerne Hogg, and Wonjae Chang

1 Introduction

Petroleum hydrocarbons (PHC) are the most frequently occurring contaminants in Canada [19, 20], where over 22,000 contaminated and suspected sites have been identified [7]. Approximately 60% of federal contaminated sites are directly or indirectly impacted by PHC contamination. This has been a significant environmental concern in northern soil environments, where cold-climate soils are fragile and susceptible to PHC contamination [22]. Generally, PHC contamination occurs due to uncontrolled, accidental and chronic contamination associated with intensified industrial and anthropogenic activities [1]. Unfortunately, the cost of remediation for remote cold sites, including sub-polar and polar regions, is often prohibitively high due to low temperatures, short summers, harsh environments, remoteness, and associated field logistics [3, 16].

Bioremediation has been frequently considered a viable tool to clean up PHC-contaminated soils in cold climates [1, 6, 8, 15]. These soils are often deficient in inorganic nutrients such as nitrogen (N) and phosphorus (P) [1] and it has been reported that stimulating *cold-adapted*, indigenous, hydrocarbon-degrading bacteria (psychrophilic and psychrotolerant) is feasible by adding N and P (i.e., biostimulation). Biostimulation strategies have produced many successful outcomes

T. Nayeema · A. H. Lee · D. Singh · W. Chang (✉)
Civil, Geological and Environmental Engineering, University of Saskatchewan, Saskatoon, Canada
e-mail: wonjae.chang@usask.ca

L. Hogg
ZMM® Canada Minerals Corp., Peachland, Canada

S. Walbridge et al. (eds.), *Proceedings of the Canadian Society of Civil Engineering Annual Conference 2021*, Lecture Notes in Civil Engineering 249,
https://doi.org/10.1007/978-981-19-1061-6_8

for PHC degradation in cold climates, from laboratory treatability studies to field implementations [1, 3].

Most biostimulation studies have been conducted in the range of 0–15 °C, or at a fixed sub-zero temperature (e.g., −5 °C) at the laboratory microcosm-scale [2, 3, 6, 24]. Recently, our group has produced new biostimulation *field* data showing extended biodegradation activity into the winter season in a cold climate region where ambient temperatures reached −35 °C [13]. The outdoor biopile experiment was conducted at a pilot scale (~3 tonnes) and over the winter near Saskatoon, Saskatchewan. Both treated and untreated (control) biopiles were subjected to in situ seasonal freezing, deep freezing and subsequent thawing [13]. In the biologically treated biopile, microbial respiration activity was detected in both the partially frozen and deeply frozen soil phases. Significant biodegradation of petroleum hydrocarbons occurred in the biostimulated PHC-contaminated soils. It is speculated that unfrozen liquid water in freezing and frozen contaminated soils plays a key role in extending the sub-zero microbial activity to the long freezing months [4, 13]. Detectable unfrozen water was more abundant in biologically enhanced, PHC-contaminated soils, than in the untreated PHC-contaminated soils (control soils) [4, 13]. Therefore, in the present study, we focused on a freezing-tolerant biostimulation strategy based on increasing the retention of *unfrozen* water using Canadian analcime zeolites.

Zeolites are natural clay minerals that are abundant in nature in over 50 different species [12]. They have a three-dimensional structure composed of silicate and aluminate [18]. The most common species of zeolite are clinoptilolite, chabazite, phillipsite, analcime, modernite, stilbite and laumontite [25]. Origin and formation determine the different species of zeolite [12] and different species have slightly different chemical compositions and physical properties, which dictate their efficiency for a particular use [18]. Zeolite is of great interest to researchers because of its unique cage-like structures and properties, such as cation exchange capacity, adsorption capacity, nutrient-holding capacity, and ability to act as a molecular sieve [17]. Such properties make zeolite a practical material in a range of applications, and it has already been widely considered for various environmental purposes: dye removal from waste effluents [26], wastewater treatments [25], heavy metal soil pollution [21], nuclear waste site remediation [5], improving soil grading and fertilizer efficiency and preventing nutrient leaching [17], the construction of permeable bio-reactive barriers to remove PHC from soil water [9], the desalination of salinized groundwater [10], and many more.

However, the compatibility and potential roles of zeolites in treating PHC-contaminated cold-climate soils, along with conventional biostimulation nutrients (N and P), have not yet been extensively understood. The specific objective of this study is to investigate the effects of the Canadian analcime zeolite on biostimulation and unfrozen water retention. Using PHC-contaminated cold-climate site soils, this study has produced positive results showing enhanced microbial activity and water retention under water-stressed conditions (both soil drying and freezing), due to the zeolite amendment combined with inorganic nutrients.

2 Materials and Methods

2.1 Site Soil Characterization

The site soils are field aged, PHC-contaminated cold-climate soils. The site soils are poorly graded sandy soils with gravels based on the Unified Soil Classification System (USCS). The pH of the site soils was determined using $CaCl_2$ extract [11]. Viable heterotrophs were enumerated using R2A agar plates and hydrocarbon-degrading bacteria were enumerated using Bushnell Hass agar spiked with 0.5% diesel.

2.2 Zeolite-Assisted Water Retention During Soil Drying

The soil drying process is analogous to soil freezing in terms of changing water availability [14, 23]. We conducted a soil drying experiment using the diesel-spiked sands that were inoculated with hydrocarbon-degrading bacteria (*Dietzia maris*) and amended with zeolite. Water retention was assessed by measuring time-variable water content during soil drying as well as the growth of viable hydrocarbon-degrading bacteria inoculated to the diesel-spiked Ottawa sands with *and* without zeolite (control). All of the microcosms were amended with Bushnell Hass (BH) media as nutrient sources except carbons. The spiked diesel provides a sole carbon source for the growth of bacteria. The Canadian analcime zeolite was obtained from ZMM Canada Minerals Corp. (BC, Canada). The dosage of the zeolite as the soil amendment was 2% by weight. The initial water content in the control soil microcosms without the zeolite amendment was successfully maintained. The control microcosm (0% zeolite) was served as the baseline for comparison with the zeolite-amended soils. The experiment was run for 11 days. Corresponding soil samples were aseptically collected on Day 11. Viable hydrocarbon-degraders were enumerated (CFU/g; colony forming unit per gram of soil). The viable microbial populations in the diesel-spiked sands amended with zeolite represent the survivors from soil drying (water scarcity) due to water retention.

2.3 Zeolite-Assisted Water Retention During Soil Freezing

Soil freezing experiment was carried out to determine how the zeolite amendment in PHC-contaminated soils influences the retention of unfrozen liquid water. Field-aged, PHC-contaminated soils were amended with 2% (w/w) analcime zeolite. The particle size of the zeolite was ~44 μm (mesh size-325). The soil microcosms were subjected to freezing temperatures from 4 to −10 °C at a seasonal rate of −1 °C/day.

Volumetric unfrozen water content and soil temperature were measured using 5TM-EM50 probes (Decagon Devices, Pullman, USA). The soil freezing characteristics curve (SFCC) of the soil microcosms were generated.

2.4 Zeolite-Assisted Biostimulation

We also examined the compatibility of the analcime zeolite with the conventional nutrient-amendment. A commercial 20:20:20 N-P-K fertilizer (20% total N: 20% P_2O_5: 20% K_2O; Plant Prod®) was employed for the nutrient amendment. Zeolite along with a carbon amendment (ZMM Canada Mineral's T-Carbon), were used for the additional soil amendment. Field-aged, PHC-contaminated soils were treated with the 20:20:20 N-P-K fertilizer (200 mg N/kg), 2% (w/w) analcime zeolite and 2% (w/w) carbon amendments at a microcosm-scale. The soil microcosms, including untreated control microcosms, were incubated at 22 and 10 °C for 14 days. The soil samples were aseptically collected for downstream analyses, including the viability assessment for estimating the growth of heterotrophs at 22 and 10 °C.

3 Results and Discussions

3.1 Zeolite-Assisted Biostimulation Potential

The site soils showed significant numbers of indigenous heterotrophs (4.3×10^7 CFU/g) and hydrocarbon-degrading bacteria in the diesel range (2.2×10^7 CFU/g). The presence of indigenous hydrocarbon-degrading populations in the site soils suggests the biostimulation potential of the site soils by supplying the inorganic nutrient solutions. It is speculated that zeolites positively influence in retaining water, immobilizing nutrients, and providing the additional surface areas for microbial habitats in the site soils.

3.2 Zeolite-Assisted Water Retention for Microbial Survivors During Soil Drying

The diesel-spiked sand microcosms with zeolite additions of 2% (w/w) showed the significant survival of *D. maris* (2.9×10^6 CFU/g). The double asterisks in Fig. 1 (**) refers to data that was statistically different from the control soils ($p < 0.0001$). The diesel-spiked sand microcosms *without* zeolite that were exposed to drying showed significant inhibition in the growth of the hydrocarbon degraders under water-stressed conditions.

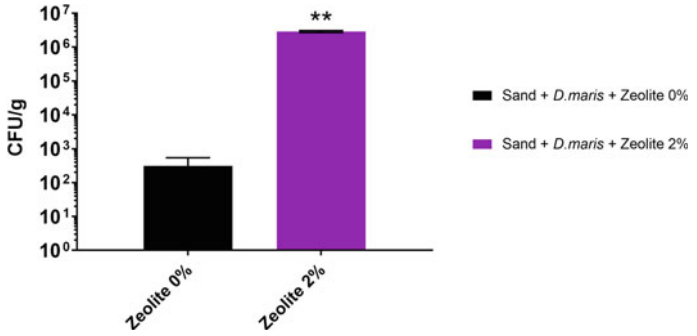

Fig. 1 Improved bacteria viability due to zeolite in water stressed condition

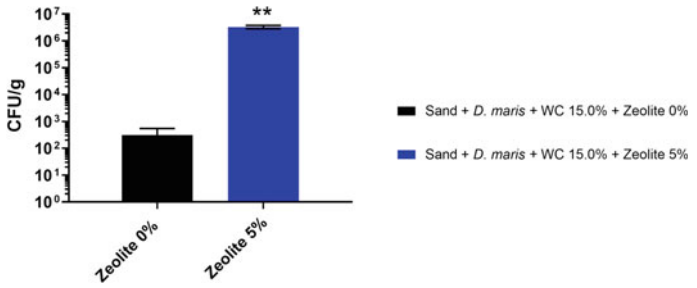

Fig. 2 Improved water retention due to zeolite additions

The zeolite dosage in the second experiment setup (Fig. 2) was 5% (w/w), and other factors (bacteria, nutrient concentration, diesel and soil matrix) were the same as those in the first setup (Fig. 1). The initial water content was maintained at 15%. Water content during soil drying was estimated by weight loss (water evaporation). The Canadian zeolites hold more water, supporting the growth of hydrocarbon-degrading bacteria in diesel-contaminated sands. Soil drying does not inhibit the growth of hydrocarbon-degrading bacteria when the zeolites are applied to diesel-contaminated soils. This is likely due to the delayed rates of soil drying caused by the retention of water available for bacterial growth. Retaining water in the zeolite-soil matrix is important in extending the contact time between bacteria and the substrate (oil contaminant) and other nutrients, which may support the formation of biofilms under water-stressed conditions (e.g., during drying and freezing).

3.3 Zeolite-Assisted Unfrozen Water Retention

Figure 3 shows the soil freezing characteristics curves (SFCC) for the zeolite-amended PHC-contaminated soils, along with the control set (without zeolites).

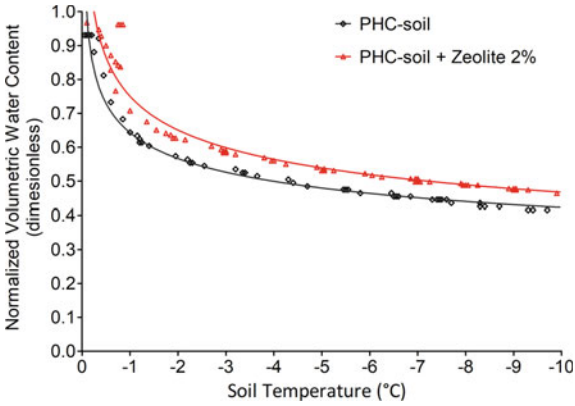

Fig. 3 Non-linear regression analyses (curve-fitting) for the generation of SFCC for the PHC-contaminated soils amended with zeolite

Zeolites are beneficial in shifting the freezing characteristics of PHC-contaminated soils, significantly improving the retention of unfrozen liquid water in freezing and frozen contaminated soils. We will continue to analyze the effects of surface area and particle size distributions of the variety of the Canadian zeolites to accurately understand the effect of the different zeolites on soil freezing characteristics. Based on the current datasets and SFCC for the PHC-contaminated soils amended with the Canadian analcime zeolite, optimizing the dosage and type of zeolites is a promising approach for maximizing the effectiveness of the amendments in a stress-tolerant bioremediation strategy for PHC-contaminated soils in cold climates.

3.4 Excellent Compatibility of Zeolite with Inorganic Nutrient Supply for Biostimulation

We examined the compatibility of the Canadian analcime zeolite with the water-based nutrient supply and additional carbon amendments for enhancing microbial activity. The zeolite amendment improved water retention and provides additional surface areas. But, zeolites might significantly adsorb some cations in the nutrient solution, potentially reducing the nutrient availability for microbial stimulation. As shown in Fig. 4, the viability assessment, however, showed the excellent compatibility of analcime zeolite with the nutrient supply (20:20:20 N-P-K fertilizer) and carbon amendments at 22 and 10 °C.

4 Conclusion

The site soil characterization indicated significant presence of indigenous hydrocarbon degraders suggesting the potential for using a bioremediation strategy assisted

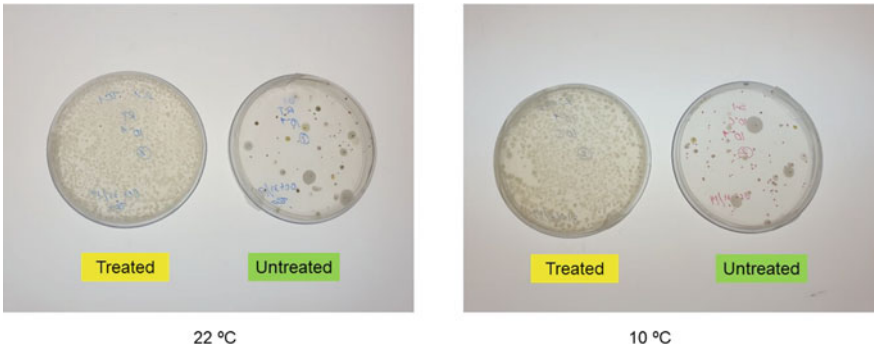

Fig. 4 Significant growth of bacteria in response to amendments

by nutrient addition. This study shows that the Canadian analcime zeolite exhibits excellent compatibility with indigenous hydrocarbon-degrading bacteria, and its addition likely introduces protective habitats for them under extreme water-stressed conditions (very low water content). Zeolite application may have multiple advantages for the bioremediation of PHC-contaminated soils, such as nutrient retention, unfrozen liquid water retention, and improved soil grading for the formation of protective microbial habitats. We will further investigate the effects of the analcime zeolite on enhancing bioremediation potential for PHC-contaminated soils in freezing and frozen soil phases under the sub-zero temperature regime. Overall, the current data suggest the significant potential of applying zeolites to enhance the bioremediation of oil-contaminated soils under water-stressed conditions.

Acknowledgements This research was funded by ZMM Canada Minerals Corp, Natural Sciences and Engineering Research Council (NSERC; RGPIN 05902-2014) and a Mitacs Accelerate Grant (IT04529).

References

1. Aislabie JM, Balks MR, Foght JM, Waterhouse EJ (2004) Hydrocarbon spills on Antarctic soils: effects and management. Environ Sci Technol 38(5):1265–1274
2. Børresen M, Barnes D, Rike A (2007) Repeated freeze–thaw cycles and their effects on mineralization of hexadecane and phenanthrene in cold climate soils. Cold Reg Sci Technol 49(3):215–225
3. Braddock JF, Ruth ML, Catterall PH, Walworth JL, McCarthy KA (1997) Enhancement and inhibition of microbial activity in hydrocarbon-contaminated Arctic soils: implications for nutrient-amended bioremediation. Environ Sci Technol 31(7):2078–2084
4. Chang W, Klemm S, Beaulieu C, Hawari J, Whyte L, Ghoshal S (2011) Petroleum hydrocarbon biodegradation under seasonal freeze− thaw soil temperature regimes in contaminated soils from a sub-Arctic site. Environ Sci Technol 45(3):1061–1066
5. Cortés-Martínez R, Olguín M, Solache-Ríos M (2010) Cesium sorption by clinoptilolite-rich tuffs in batch and fixed-bed systems. Desalination 258(1–3):164–170

6. Eriksson M, Ka J-O, Mohn WW (2001) Effects of low temperature and freeze-thaw cycles on hydrocarbon biodegradation in Arctic tundra soil. Appl Environ Microbiol 67(11):5107–5112
7. Federal Contaminated Sites Inventory (2019) Federal contaminated sites inventory 2019. Cited 28 Oct 2019. Available from https://www.tbs-sct.gc.ca/fcsi-rscf/home-accueil-eng.aspx
8. Filler DM, Snape I, Barnes DL (2008) Bioremediation of petroleum hydrocarbons in cold regions. Cambridge University Press
9. Freidman BL, Terry D, Wilkins D, Spedding T, Gras SL, Snape I, Stevens GW, Mumford KA (2017) Permeable bio-reactive barriers to address petroleum hydrocarbon contamination at subantarctic Macquarie Island. Chemosphere 174:408–420
10. Gibb NP, Dynes JJ, Chang W (2017) Synergistic desalination of potash brine-impacted groundwater using a dual adsorbent. Sci Total Environ 593:99–108
11. Gregorich EG, Carter MR (2007) Soil sampling and methods of analysis, 2nd edn. CRC Press
12. Hedström A (2001) Ion exchange of ammonium in zeolites: a literature review. J Environ Eng 127(8):673–681
13. Kim J, Lee AH, Chang W (2018) Enhanced bioremediation of nutrient-amended, petroleum hydrocarbon-contaminated soils over a cold-climate winter: the rate and extent of hydrocarbon biodegradation and microbial response in a pilot-scale biopile subjected to natural seasonal freeze-thaw temperatures. Sci Total Environ 612:903–913
14. Koopmans RWR, Miller R (1966) Soil freezing and soil water characteristic curves. Soil Sci Soc Am J 30(6):680–685
15. Lovley DR (2003) Cleaning up with genomics: applying molecular biology to bioremediation. Nat Rev Microbiol 1(1):35
16. McCarthy K, Walker L, Vigoren L, Bartel J (2004) Remediation of spilled petroleum hydrocarbons by in situ landfarming at an Arctic site. Cold Reg Sci Technol 40(1–2):31–39
17. Ming DW, Allen ER (2001) Use of natural zeolites in agronomy, horticulture and environmental soil remediation. Rev Mineral Geochem 45(1):619–654
18. Mumpton FA (1999) La roca magica: uses of natural zeolites in agriculture and industry. Proc Natl Acad Sci 96(7):3463–3470
19. Princz JI, Moody M, Fraser C, Van der Vliet L, Lemieux H, Scroggins R, Siciliano SD (2012) Evaluation of a new battery of toxicity tests for boreal forest soils: assessment of the impact of hydrocarbons and salts. Environ Toxicol Chem 31(4):766–777
20. Sanscartier D, Zeeb B, Koch I, Reimer K (2009) Bioremediation of diesel-contaminated soil by heated and humidified biopile system in cold climates. Cold Reg Sci Technol 55(1):167–173
21. Shi W-Y, Shao H-B, Li H, Shao M-A, Du S (2009) Progress in the remediation of hazardous heavy metal-polluted soils by natural zeolite. J Hazard Mater 170(1):1–6
22. Siciliano SD, Schafer AN, Forgeron MA, Snape I (2008) Hydrocarbon contamination increases the liquid water content of frozen Antarctic soils. Environ Sci Technol 42(22):8324–8329
23. Spaans EJ, Baker JM (1996) The soil freezing characteristic: its measurement and similarity to the soil moisture characteristic. Soil Sci Soc Am J 60(1):13–19
24. Walworth J, Braddock J, Woolard C (2001) Nutrient and temperature interactions in bioremediation of cryic soils. Cold Reg Sci Technol 32(2–3):85–91
25. Wang S, Peng Y (2010) Natural zeolites as effective adsorbents in water and wastewater treatment. Chem Eng J 156(1):11–24. https://doi.org/10.1016/j.cej.2009.10.029
26. Wang S, Zhu Z (2006) Characterisation and environmental application of an Australian natural zeolite for basic dye removal from aqueous solution. J Hazard Mater 136(3):946–952

Evaluation of the Efficacy of a Treatment Pond System for Removal of Concentrated Iron and Arsenic Produced from Water Treatment Plant (WTP) Wastewater

H. Bull, A. Ekhlasi Nia, and K. McPhedran

1 Introduction

Drinking water treatment plants (DWTPs) typically use a suite of treatment processes to improve the quality of their source waters to meet relevant drinking water standards. However, these treatment processes generate wastes in the form of backwashes, sludges, and concentrates. The nature of the wastes generated depends in large part on the characteristics of the source water with surface waters generally containing higher organics concentrations and groundwater higher metal(loid)s concentrations. For groundwaters, metal(loid)s such as arsenic (As) and iron (Fe) are present because of the more intensive contact of groundwaters with rocks and mineral species [8]. Reverse osmosis (RO) is one of the most common treatment processes used today for groundwater sources, however, it generates a substantial residual wastewater stream that is typically 10–50% of the raw water feed volume [18]. The residual wastewaters contain magnified concentrations of the contaminants present in the source water as they are removed from the potable water stream, thus, disposal and/or treatment of these residual wastewaters an ongoing challenge.

Arsenic and Fe are often present together and interact in water and related sediments. For example, the mobility of As in sediments has been proposed to be controlled by the reduction of As(V) coupled with the reductive dissolution of Fe(III) hydroxide [17]. In addition, the microbial respiration of Fe(III) can play a significant role in the speciation, and thus the solubility, of both As and Fe [7]. Arsenic is a toxic substance and a known carcinogen [11], while Fe in water can contribute to free radical production and oxidative damage in organisms [1]. Arsenic exposure in

H. Bull (✉) · A. Ekhlasi Nia · K. McPhedran
University of Saskatchewan, Saskatoon, Canada
e-mail: Harrison.Bull@usask.ca

K. McPhedran
e-mail: Kerry.mcphedran@usask.ca

S. Walbridge et al. (eds.), *Proceedings of the Canadian Society of Civil Engineering Annual Conference 2021*, Lecture Notes in Civil Engineering 249,
https://doi.org/10.1007/978-981-19-1061-6_9

mammals and some fish is known to induce oxidative stress and can affect signaling pathways, leading to harm in the organism [20]. Less complex life is also negatively impacted by As including it being poisonous to microorganisms and lower aquatic organisms [13]. Iron can adversely affect macroinvertebrates by reducing habitat quality and structure and by constraining food access by reducing visibility [9].

The World Health Organization recommends that drinking water should have maximum As and Fe concentrations of 10 μg/L and 300 μg/L, respectively [21]. For effluent waters, the Federal Environmental Quality Guidelines (FEQGs) in Canada for the protection of aquatic life for As and Fe are 5 μg/L [2] and 604 μg/L (at a pH of 7.5 and DOC of 0.5 mg/L) [5], respectively. Interestingly, the recently developed guideline for Fe is no longer static with the standards changing dependent on the water pH and dissolved organic carbon (DOC) concentrations. The formula for the Federal Water Quality Guideline (FWQG) for Fe concentrations is: FWQG (μg/L) = exp(0.671[ln(DOC)] + 0.171[pH] + 5.586) [5].

Overall, the direct disposal of As and Fe containing residual wastewaters from DWTPs into surface waters is impossible as they generally do not meet guidelines, making further treatment being required before their release. Thus, the objective of this study was to monitor aqueous As and Fe concentrations in a waste stabilization pond (WSP) system consisting of five sequential evaporation/settling ponds used to treat residual wastewaters of a local DWTP (Fig. 1). Firstly, the historic and current study monitored WSP inflow and outflow As and Fe concentrations are presented. Second, the potential for daily fluctuations in Fe concentrations are assessed (As daily fluctuations could not be assessed due to lack of available instrumentation on site). Lastly, the monthly pond-to-pond variations in As and Fe concentrations are

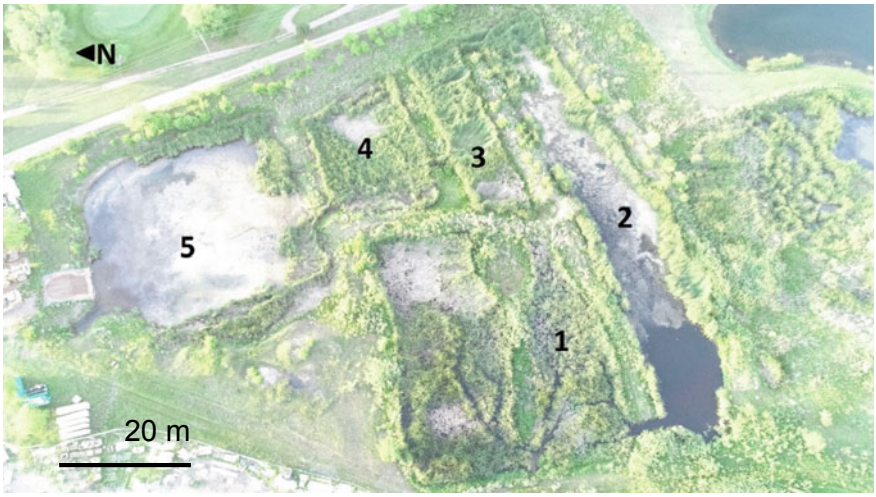

Fig. 1 Settling pond system with five settling ponds (labelled 1 through 5) that sequentially treat the DWTP effluents. *Note* Influent enters Pond 1 and outflow exits Pond 5

discussed. The current study will be extended into 2020 when a new DWTP facility is commissioned at this site as discussed in the Site Conditions section below.

2 Methods

2.1 Site Conditions

The DWTP site is located in Saskatchewan within the Great Plains region of North America. Typical climate for the region is cold and temperate. The average annual temperature is 1.3 °C, and winters (i.e., months with average temperatures below freezing) last from November to March. The average air temperature in the coldest month is −19 °C, which means the site lies in a cold region characterized as having a "very cold winter" [16]. The Köppen-Geiger climate classification is Warm-Summer Humid Continental climate. The annual precipitation at the site is 424 mm [3].

The DWTP has been in operation since 1958 and underwent major upgrades in 1985 and 1990. The DWTP used a mixture of groundwater and surface water as its raw source water until the end of 2019. The DWTP used an electro-dialysis reversal (EDR) system that was installed in 1990 which had been operating beyond its designated 20-year lifespan. Samples from the effluents of the WSP system often exceeded environmental guidelines for As and Fe (using older guidelines) prior to the start of this study. These exceedances necessitated the need to better assess the individual ponds and overall WSP system to evaluate their treatment efficiencies and potential need for upgrades. This assessment has included both the wastewater (this study) and sediments (parallel study) over the open-water seasons of 2019 and 2020. In early 2020, a replacement DWTP system using reverse osmosis was being commissioned that will use 100% groundwater as the raw water source. It is expected that this new system will produce higher concentrations of both As and Fe in WSP effluents, potentially impacting the ability of the WSPs to meet environmental protection guidelines for its wastewater effluents.

The site WSPs have been in service for the past 60+ years and have been receiving a variety of residual wastewaters since their introduction. The WSP system consists of an initial temporary storage pond followed by flow through natural wetlands and discharge into a low flow creek (Fig. 1). The WTP wastewaters are discharged into Pond 1 and progress through the WSP before flowing into a pipe discharge pipe connecting the Pond 5 and the creek. This creek can contain fish at certain times of the year, necessitating the need for the WSP effluents to meet CCME guidelines for their release into freshwater fish habitats.

A major flood event short-circuited the pond system in 2014, and all available aerial imaging for sizing was performed prior to this event. Factors such as the current size of the ponds, flow path, and the progress of treatment between ponds are unknown. More data needs to be collected to inform the new treatment process, and

remedial action taken, if necessary. Physically expanding the footprint of the WSPs is not feasible at the site, instead improving the current system is strongly preferred.

2.2 Overview of WSP Evaluation

Prior to commencing this study, a methodology for assessment of the WSPs needed to be determined. Lloyd et al. [12] describe a methodology of four steps for evaluating waste stabilization ponds:

1. **Desk study**: Review official quality monitoring and WSP performance data, together with local meteorological data, including wind, rainfall and temperature. Review of consulting engineering reports describing the original designs, treatment objectives and engineering specifications for each WSP system.
2. **On-site preliminary diagnostics**: Provide rapid assessment of operational status of WSP systems for comparison with archive data, and identification of plants for rehabilitation.
3. **Intensive performance and field evaluations**: Identify defective treatment stages of selected plants and causes of under-performance.
4. **Rehabilitation projects**: Develop a rehabilitation strategy, including design, implementation and evaluation of upgraded system to assess whether performance meets wastewater effluent standard.

Currently, the first two components of the methodology proposed by Lloyd et al. [12], namely the desk study and preliminary diagnostics, are presented in the current study. The remaining two components are to be published following further study of the WSPs in 2020 which is being conducted after the new DWTP is commissioned and under operation.

2.3 Sampling Procedure

Wastewater samples were collected for five months (May, June, July, August, and October) during 2019 from the five pond outlets within the WSP using approximately 1 L plastic containers. Sampling of the system occurred at regular time intervals between 8:00AM and 8:00PM. These samples were immediately tested for at the DWTP for pH, TDS, conductivity, and temperature. Iron testing for assessment of diel fluctuations included measuring both the total Fe concentration and the dissolved Fe concentration. Dissolved Fe was measured by filtering samples through standard 0.45 μm filters in a vacuum filtration apparatus prior to analysis using a DWTP site laboratory spectrophotometer. Monthly samples were also processed for analysis by an external laboratory as discussed below.

Regular sampling of the WSP inflows and outflows is conducted by the DWTP staff with analyses for As and Fe (and other contaminants not presented herein) via

ALS Environmental (Saskatoon, SK, Canada). ALS provided the necessary sample containers and coolers for wastewater sample collection and all procedures they provided were followed. All samples were transported at < 10 °C in under 72 h to ALS labs for analysis as per guidelines (actual 4 °C and 48 h). Metal(loid) analysis of 0.45 μm filtered wastewaters was conducted by ALS using collision/reaction inductively coupled plasma mass spectrometry (CRC ICP-MS) according to the Method 6020A of U.S. Environmental Protection Agency [19].

2.4 Groundwater Versus Surface Water Sources

Concentrated metal(loid)s are a common problem as groundwater sourced DWTPs typically use RO as their treatment option. The degree of concentration in the DWTP concentrates can be represented by the concentration factor (CF; Eq. 2), a relationship governed by the recovery percentage (%R; Eq. 1) of the plant [10]. The CF represents the increase in concentration compared to the source water (Eq. 3).

$$\%R = \frac{Permeate\ Flow\ Rate}{Feed\ Flow\ Rate} * 100 \tag{1}$$

$$CF = 1/(1 - R) \tag{2}$$

$$CF = \frac{Feed\ Flow\ Rate}{Concentrate\ Flow\ Rate} \tag{3}$$

3 Results and Discussion

3.1 WSP Inflow and Outflow Fe and As

The historic and current monitoring of Fe and As are presented in Fig. 2. Overall, the Fe concentrations for both the inlet and outlet samples do not exceed the current FWQG levels. Interestingly, they did sometimes exceed the previous guidelines making the new guidelines less stringent based on the WSP pH and DOC concentrations. In contrast, the As concentrations for both inlet and outlet regularly exceed the 5 μg/L guideline. The increases for both Fe and As in concentrations from the inlet to outlet indicate the movement of both of these compounds from the sediments into the wastewater. Historically, the DWTP does not have comprehensive data on the individual ponds, thus, the condition of the WSP has largely been assessed via monthly inflow/outflow water quality tests at their inlet and discharge. As the current WSP design does meet the environmental guidelines for As, the future ability of the ponds

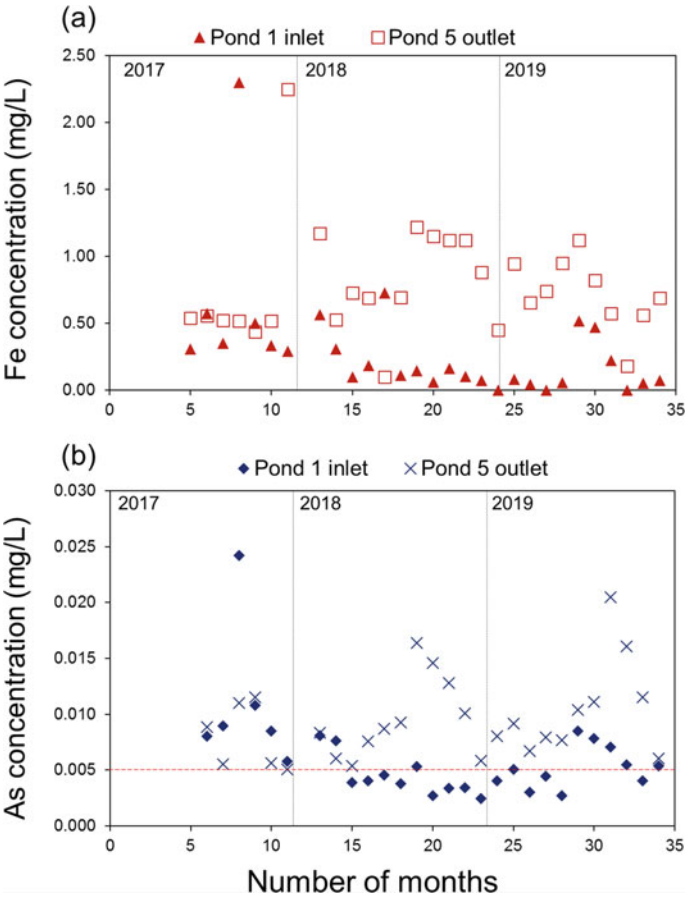

Fig. 2 The Fe (Panel a) and As (Panel b) concentrations for the WSP inlet (Pond 1 inlet) and outlet (Pond 5 outlet). Monitoring data was made available starting July 2017 through the duration of the current study

to remove sufficient As in their current state is uncertain. This may also become an issue for Fe as leaching from sediments and increased residual wastewaters from the new DWTP may increase WSP Fe outflows.

As of the end of 2019, the DWTP used a mixture of groundwater and surface water sources (approximately 1:3 surface water to groundwater) to generate an average of 25 L/s of treated water. The RO facility will have an expected average flow rate projected at 20 years of 34.5 L/s treated water, with an expected generation of 19.7 L/s effluents from the WSP system into the nearby creek. The calculated CF at this projected flow rate would be 2.75. Thus, it is anticipated that the wastewaters generated at the DWTP plant will continue to have high metal(loid) concentrations (including Fe and As), in addition to ammonium, and a high electric conductivity.

Iron and As concentrations are not static, they can vary over the course of a given day and throughout the seasons of the year. For example, seasonal variations have been noted in some natural bodies of water, including As concentrations in Poyang Lake, which were 7 times greater in the summer than in winter samples [4]. At the current DWTP, historically the wastewater samples were only collected during the morning, so the potential for consistent daily concentration variability (diel cycles) is unknown. To be fully aware of the changing conditions of the important species, diurnal testing must also be done, with samples being collected at various times over the same day and their concentrations compared. This diurnal testing was done currently using Fe as an example given the availability of instrumentation on site to determine dissolved and total Fe concentrations as presented in Sect. 3.2. To supplement the Pond 1 and Pond 5 data, all ponds were sampled on a monthly basis to determine if there was seasonal variation for the spring/summer/fall seasons of the WSPs as presented in Sect. 3.3.

3.2 Diel Fe Evaluation

Diel variations in Fe over the course of daylight hours were determined on multiple days during 2019 with a representative sampling day of July 24 shown for demonstrative purposes (Fig. 3). The dissolved Fe concentrations showed little to no variation from Pond to Pond during the day with concentrations under 0.1 mg/L. In addition, there was only marginal variability in the dissolved Fe concentrations on a monthly basis (results not shown). As for the dissolved Fe, the total Fe concentrations in Ponds 2, 3, and 5 showed little variation over the day with concentrations around 0.2, 0.1, and 0.5 mg/L, respectively. In contrast, temporal variation of total Fe concentrations were most pronounced in the outflows for Ponds 1 and 4. Pond 1 has a shorter retention time than the other ponds as it 'short circuits' almost directly into Pond 2 (Fig. 1). Thus, it is hypothesized that the total Fe variations in Pond 1 are most likely due to variable wastewater flow rates and backwash timings. For Pond 4, it is hypothesized that sediment dissolution/deposition is the dominant source of variability within this Pond. Additionally, the marked increase in total Fe concentrations between Ponds 3 and 4 indicates that sediment-aqueous mass transfer is occurring within Pond 4.

Generally, metals concentrations in streams and wetlands can vary markedly over the course of a day. Some proposed mechanisms for this variation include differing temperature, pH, or biofilms on the streambed [6]. Diel effects can be quite large in certain cases with changes on the order of 500% being shown in literature [15]. In one case, for the same water source, zinc had maximum variation of 500%, nickel had variation of 300%, and As had variation of 54% [15]. In multiple locations As has been known to vary as much as 50% in streams with neutral to alkaline pH [6, 14], which is the same pH range as in the WSPs. Clearly, although Fe is presented currently further research into other metal(loid) variability throughout the day would be beneficial for this WSP system.

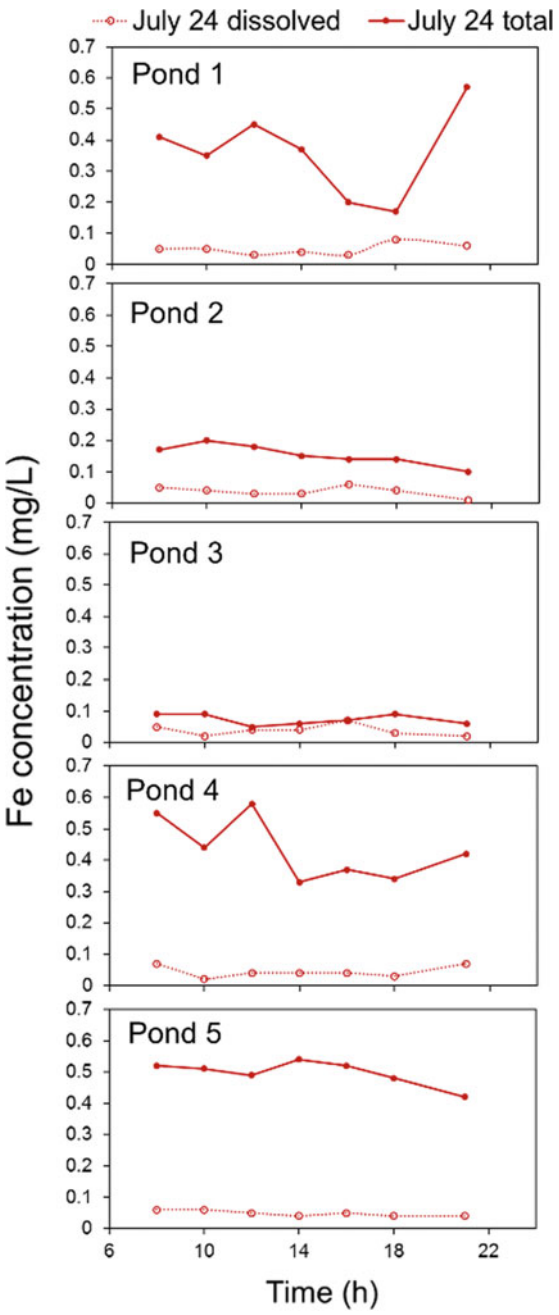

Fig. 3 Dissolved and total Fe concentrations as determined on July 24, 2019 (8:00 AM to 9:00PM) for the five ponds within the WSP system

3.3 Monthly Pond-to-Pond Concentration Profiles

The concentrations for total Fe and total As are presented in Fig. 4. Each of these samples were collected at 8:00 AM for all ponds on a monthly basis to avoid any diel variations in sample concentrations. For Fe, there was a decreasing trend for the first three ponds from May to July with total concentrations have low variability (Fig. 4a). In contrast, Ponds 4 and 5 showed an increasing trend in Fe concentrations with a high variability between the sample months. The Pond 4 concentrations (0.22 to 0.94 mg/L) were in a similar range as Pond 1 (0.22–0.52 mg/L), while the Pond 5 concentration range was the highest at 0.58 to 1.12 mg/L. In general, it appears that Fe concentrations were higher in the 'cooler' months of May and October as

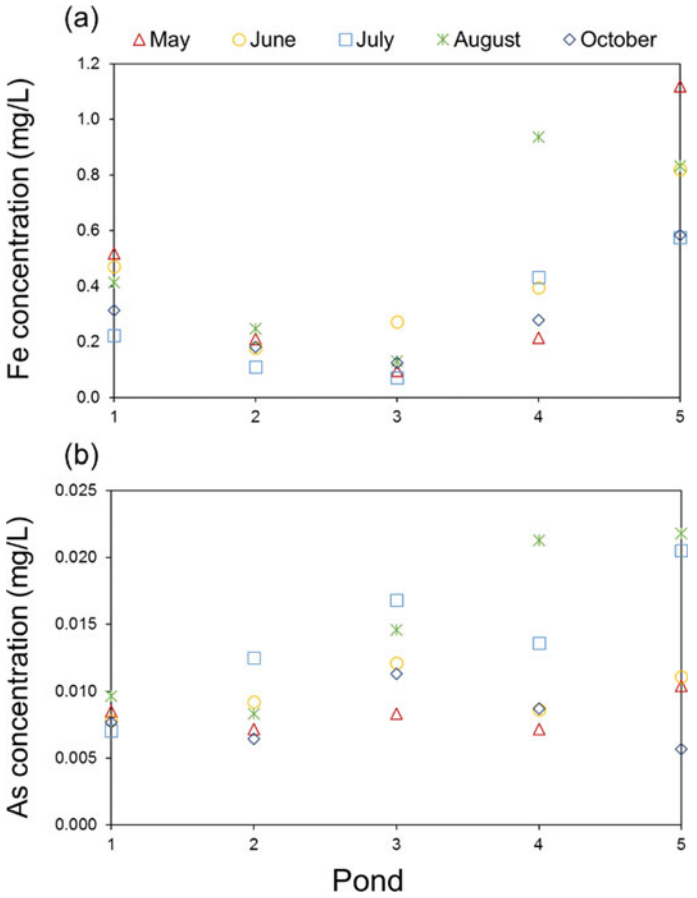

Fig. 4 The total Fe **a** and As **b** concentrations for each of the five WSP ponds over five months of sampling including May, June, July, August, and October 2019

compared to the 'warmer' months of June, July, and August. However, the Fe concentrations did not exceed FWQG guidelines, either within the individual ponds or at the WSP effluents, for any samples taken in 2019. However, further evaluation of these results with consideration of the other measured physico-chemical parameters (especially temperature) is ongoing to determine if these parameters are impacting Fe concentrations in the WSP system.

For As, there is no similar decrease and increase in the pond concentrations as compared to the total Fe concentrations (Fig. 4b). However, there is a statistically significant increasing trend in As concentrations from Pond 1 through Pond 5 during the months of July ($R^2 = 0.77$) and August ($R^2 = 0.87$) (trendlines not shown in Fig. 4b for clarity). In contrast, there is no statistical difference between the concentrations of the ponds for the months of May ($R^2 = 0.21$), June ($R^2 = 0.28$), and October ($R^2 = 0.02$). Clearly, the higher temperatures in July and August led to increasing concentrations through the WSP with desorption from sediments being the likely source of the As concentration. During these months, the As concentrations in the WSP effluents were almost double those of the other three months. In general, the As concentrations in the WSP effluents were above the CCME guideline values for every sampling period with July and August having values exceeding guidelines by a factor of 4.

Overall, the Fe and As monthly trends were mixed for the individual WSP ponds indicating that there may not be a correlation between these two elements. However, further research of the WSP system in 2020 will help to better understand the Fe and As, as well as other compounds, within this system.

4 Conclusions

Overall, the WSP effluents did not exceed guidelines for Fe concentrations, while typically exceeding guidelines for As concentrations since sampling results from the DWTP became available in 2017. Interestingly, changes to the Fe guidelines led to the guidelines moving from some exceedances to no exceedances given the inclusion of pH and DOC factors in the new FWQG. Thus, the As is the element of major interest for the WSP going forward as the system will need to meet the 5 μg/L guideline in the future. The Fe was used to determine if diurnal variations in concentrations were occurring for the individual ponds. Results indicated that dissolved Fe concentrations were not changing, while Ponds 1 and 4 variations were apparent. In general, further assessment of diurnal changes for other compounds of interest may be valuable. For seasonal variability, the Fe concentrations appeared to decrease with increasing temperature for all Ponds. In contrast, the As showed increasing concentrations from Pond 1 to Pond 5 in the warmer months indicating more As was being released from the WSP system during these months. It is expected the new DWTP RO system will result in higher influent Fe and As concentrations to the WSP. This will be monitored in 2020 using a similar methodology as the current study. If the WSP effluents continue to exceed guideline values, solutions will be

proposed for modification of the WSP to reduce Fe and As effluents in order to meet the FEQGs over the new plant's projected 40-year life cycle.

Acknowledgements The authors would like to acknowledge funding provided through the Mitacs Accelerate program and the financial and research support of SaskWater. In addition, research support has been provided by SaskWater personnel including Sumith Kahanda, Enisa Zanacic, Dale Hreshka, and Timo Jansen.

References

1. Bury NR, Boyle D, Cooper CA (2012) Iron. In: Wood CM, Farrell AP, Brauner CJ (eds) Homeostasis and toxicology of essential metals. Elsevier, Amsterdam, pp 201–251
2. Canadian Council of Ministers of the Environment (CCME) (2001) Canadian water quality guidelines for the protection of aquatic life: arsenic. Canadian council of ministers of the environment, Winnipeg, Manitoba, Canada
3. Climate-Data.org (2015) Saskatchewan climate. August 9. https://en.climate-data.org/north-america/canada/saskatchewan/
4. Deng T, Wu Y, Yu X, Guo Y, Chen Y, Belzile N (2014) Seasonal variations of arsenic at the sediment–water interface of Poyang Lake, China. Appl Geochem 47(C):170–76. https://doi.org/10.1016/j.apgeochem.2014.06.002
5. Environment and Climate Change Canada (ECCC) (2019) Canadian environmental protection act, 1999 federal environmental quality guidelines. Environment and Climate Change Canada
6. Gammons CH, Grant TM, Nimick DA, Parker SR, DeGrandpre MD (2007) Diel changes in water chemistry in an arsenic-rich stream and treatment-pond system. Sci Total Environ 384(1):433–51. https://doi.org/10.1016/j.scitotenv.2007.06.029
7. Handley KM, Mcbeth JM, Charnock JM, Vaughan DJ, Wincott PL, Polya DA, Lloyd JR (2013) Effect of iron redox transformations on arsenic solid-phase associations in an arsenic-rich, ferruginous hydrothermal sediment. Geochim Cosmochim Acta 102:124–142. https://doi.org/10.1016/j.gca.2012.10.024
8. Khatri N, Tyagi S, Rawtani D (2017) Recent strategies for the removal of iron from water: a review. J Water Process Eng 19:291–304. https://doi.org/10.1016/j.jwpe.2017.08.015
9. Linton TK, Pacheco MAW, Mcintyre DO, Clement WH, Goodrich-Mahoney J (2007) Development of bioassessment-based benchmarks for iron. Environ Toxicol Chem 26(6):1291–1298
10. Litter MI, Ingallinella AM, Olmos V, Savio M, Difeo G, Botto L, Torres EMF, Taylor S, Frangie S, Herkovits J, Schalamuk I, González MJ, Berardozzi E (2019) Arsenic in Argentina: technologies for arsenic removal from groundwater sources, investment costs and waste management practices. Sci Total Environ 690:778–789
11. Litter MI, Morgada ME, Bundschuh J (2010) Possible treatments for arsenic removal in Latin American waters for human consumption. Environ Poll 158(5):1105–18. https://doi.org/10.1016/j.envpol.2010.01.028
12. Lloyd BJ, Leitner AR, Vorkas CA, Guganesharajah RK (2003) Under-performance evaluation and rehabilitation strategy for waste stabilization ponds in Mexico. Water Sci Technol 48(2):35–43
13. National Research Council (US) Committee on Medical and Biological Effects of Environmental Pollutants (1977) Arsenic: medical and biologic effects of environmental pollutants. National Academies Press, Washington
14. Nimick DA, Cleasby TE, McCleskey RB (2005) Seasonality of diel cycles of dissolved trace-metal concentrations in a rocky mountain stream. Environ Geol 47(5):603–614. https://doi.org/10.1007/s00254-004-1178-x

15. Nimick DA, Gammons CH, Cleasby TE, Madison JP, Skaar D, Brick CM (2003) Diel cycles in dissolved metal concentrations in streams: occurrence and possible causes. Water Resour Res 39(9):1247–1264. https://doi.org/10.1029/2002WR001571
16. Shen H (2015) Cold regions science and marine technology. EOLSS Publishers Company Limited, Encyclopedia of Life Support Systems
17. Sun Q, Ding S, Wang Y, Xu LV, Wang D, Chen J, Zhang C (2016) In-Situ characterization and assessment of arsenic mobility in lake sediments. Environ Poll 214(C):314–23. https://doi.org/10.1016/j.envpol.2016.04.039
18. U.S. Department of Energy (2013) Reverse Osmosis optimization. Pacific Northwest National Laboratory
19. US EPA (United States Environmental Protection Agency) (1998) Inductively coupled plasma—mass spectrometry. EPA 6020A (SW-846)
20. Ventura-Lima J, Bogo MR, Monserrat JM (2011) Arsenic toxicity in mammals and aquatic animals: a comparative biochemical approach. Ecotoxicol Environ Saf 74(3):211–218
21. World Health Organization (2008) Guidelines for drinking-water quality incorporating 1st and 2nd addenda, vol1, Recommendations, 3rd edn. WHO Press, Geneva

Variable Rate Ion Exchange in Contaminant Transport

Fonstad Terrance and Rinas Crystal

1 Introduction

The intent of this paper is to offer a general review of the source of ion exchange potential in clayey soils and to outline the various methods available to calculate/model the effect during transport. An additional method proposes the determination of exchange coefficients as functions of solution characteristics and variable retardation factors that are a function of the ion solution concentration is presented.

Both isomorphous substitution plus lattice imperfections result in permanent charges in clay minerals. Permanent negative charges of illites, smectites and vermiculites (mol sites/kg) ranges from 1.9 to 2.8, 0.7 to 1.7, and 1.6 to 2.5 respectively [8]. Broken or unsatisfied bonds are important in all clays but significantly effect the charge on large particle clays such as kaolinite. At low pH values hydrogen (H^+) ions can compete for exposed oxygen (O^{2-}) and hydroxyl (OH^-) sites and at very low pH values can result in a net positive charge.

Several models used for calculations of absorption in natural waters (e.g. MINTEQA2) use a measurement of these surface absorbing sites (Γ_s) that gives the concentration of sorbing surface sites in units of moles of monovalent sites exposed to a liter of solution [4].

$$\Gamma_s(molesites/L) = \frac{N_s(sites/\mathrm{m}^2) \times S_A(\mathrm{m}^2/\mathrm{g}) \times C_S(\mathrm{g/L})}{N_A(site/molsites)} \quad (1)$$

F. Terrance (✉) · R. Crystal
University of Saskatchewan, Saskatoon, Canada
e-mail: Terry.Fonstad@usask.ca

R. Crystal
e-mail: Crystal.Rinas@usask.ca

S. Walbridge et al. (eds.), *Proceedings of the Canadian Society of Civil Engineering Annual Conference 2021*, Lecture Notes in Civil Engineering 249,
https://doi.org/10.1007/978-981-19-1061-6_10

where

N_S surface site density,
S_A surface area per weight of sorbent,
C_S weight of sorbent in contact with a liter of solution, and
N_A Avogadro's number (6.022×10^{23} sites/mol of sites).

Observation reveals that if we divide the answer by the weight of sorbent in contact with a liter of solution (C_S), then we find the concentration of sorbing surface sites in units of moles of monovalent sites per gram of sorbent. This is the convention preferred by soil scientists termed cation exchange capacity (CEC) given as milli-equivalents per 100 g of dry soil (sorbent) (meq/100 g) or as centimoles per kg of soil (sorbent) (cmol/kg). Langmuir [4] gives the following relation between the above mentioned variables and CEC:

$$\mathrm{CEC(meq/100\,g)} = \mathrm{N_s}(site/\mathrm{nm^2}) \times S_A(\mathrm{m^2/g}) \times 0.1661 \tag{2}$$

2 Ion Exchange

For solutions in contact with an exchanger, the tendency for ions to leave the solution and be sorbed to exchange sites at the same time an equal "activity" of ions leaves the exchange sites and goes into solution is affected by many factors including:

- the charge of the ions,
- the size of the ion or hydrated radius,
- the properties of the exchanger (e.g. clay mineral),
- quantity and ratios of the various valence of ions present, and
- the total solution concentration (affect of ion interactions).

If an exchanger with all sites occupied by a monovalent cation is placed in a solution with ions of only one different monovalent cation, exchange will take place. For the Law of Mass Action this exchange takes the form:

$$A^+ + BX = B^+ + AX \tag{3}$$

where A + and B + represent ions in solution and BX and AX represent absorbed ions.

Then:

$$K_{eq} = \frac{[B^+]}{[A^+]}\left(\frac{(AX)}{(BX)}\right)^n \tag{4}$$

if one assumes thermodynamic equilibrium applicable or

$$\frac{[A^+]}{[B^+]}K_C = \frac{(AX)}{(BX)} \tag{5}$$

if one assumes the quantity of each ion on the exchange sites is a proportional to the ratio of the ions in solution [9].

where

K_{eq}	the reaction constant or K_C = the distribution coefficient,
n	is an exponent,
$[A^+]$	activity of ion A in solution,
$[B^+]$	activity of ion B in solution,
(AX)	"activity" of ion A on the exchange sites, and
(BX)	"activity" of ion B on the exchange sites.

Activities for each ion in solution can generally be calculated using the Debije-Huckel equations but there is no agreed way to calculate ion activities on exchange sites. To remedy this, one can write the "activities" of the ions as a functions of the fraction of the total number of exchange sites the ion occupies multiplied by a "rational activity coefficient" giving the value of:

$$(AX) = \lambda_A \beta_A CEC \tag{6}$$

where

λ_A	the rational activity coefficient for the solid phase,
β_A	the equivalent fraction of ion A, and.
CEC	the cation exchange of the exchanger.

Substituting this into Eq. (4) and canceling the CEC gives:

$$K_{eq} = \frac{[B^+]}{A^+}\left(\frac{(\lambda_A \beta_A)}{(\lambda_B \beta_B)}\right)^n \tag{7}$$

Difficulties or shortcomings of this approach include that if K_{eq} is by definition a constant, then changes in selectivity need to be accounted for in changes in the rational activity coefficients for the solid phase (λ_A and λ_B). Changes in these coefficients are similar to that observed in solution activities as ionic strength increases. That is that at high ionic strengths the surface activity for certain ions may be negligible [5]. McBride [5] suggest the reasons for this may be:

- increased entropy associated with the more hydrated ion (more mobile ion) causes a decrease in the exchanger preference for the less hydrated ion (less mobile ion) as the exchange sites become more occupied with the more hydrated ion,
- solutions of higher ionic strength could alter the chemical potential of water to decrease the size of the hydration shell of strongly hydrated ions reducing the

distance between the charge sources and increasing the attraction between the charges,
- cation-cation repulsion forces, or
- changes in clay site geometry.

Boldt (1982) explains this phenomenon by assuming the absorbent charge exists as a uniform surface volume or density of charge. This approach indicates that the absorbent charge is either changing with distance from the center of the absorbent particle or constant throughout this charged volume around the particle. If one writes the selectivity coefficient (K_N) in terms of:

$$K_N = \sqrt{\frac{2}{V^\alpha}} \frac{\sqrt{(1 - 1/\overline{u}^3}}{\sqrt{(1 - 1/\overline{u}^2}} \tag{8}$$

where

V^α volume of homogeneous phase per equivalent of charge (m^3/keq), and.
$\overline{u}$ the Boltzman accumulation factor for counterions in a diffuse double layer in a phase with a constant electrical potential. (This accumulation factor is proportional to the electrical potential and inversely proportional to the kinetic energy per molecule).

One can see that an increase in concentration of the solution results in a decrease in the Boltzman accumulation factor and causes an increase in the selectivity coefficient. Then for a given ratio of monovalent cations to divalent cations (i.e. analogues to Sodium Adsorption Ratio), the amount of absorbed divalent cations will increase with increasing ionic strength/electrolyte concentration. For adsorbents with a constant charge density, the surface potential vanishes at very high electrolyte concentrations Bolt (1982).

A further explanation is to consider the decrease in size of the hydration shell as the collapse of the diffuse double layer (DDL) on hydrated ions and surfaces. Debije-Huckel theory for ion activities uses a parameter $1/\kappa$ termed the Debije length. This parameter can be given with ionic strength as a variable giving:

$$\frac{1}{\kappa} = \sqrt{\frac{\varepsilon \cdot RT}{2(N_a q_e)^2} \cdot \frac{1}{1000I}} \tag{9}$$

where

ε dielectric constant (for water 7.08×10^{-10} F/m at 25 8 °C).
R 8.314 J/K mol,
T absolute temperature,
N_a Avogadro's number (6×10^{23}/mol),
q_e is the charge of the electron (1.6×10^{-19} C), and.
I ionic strength in mol/L.

Inspection of this equation indicates that, at 25 °C, $1/\kappa = 3.09/\sqrt{I}$. The thickness of the diffuse double layer is considered the position away from the ion where the potential (ψ) is equal to the potential at the ion surface divided by e [1]. This is the position where the thickness of the DDL (x) is equal to $1/\kappa$. Therefore the thickness of the DDL at 25 °C can be given by $x = 3.09/\sqrt{I}$ and we can see that as the ionic strength increases the DDL collapses exponentially. This collapse of the DDL will affect the ability for ions to compete for exchange sites and thus cause variability in $K_{A/B}$.

Compounding the use of activity coefficients for the solid phase is the lack of experimental data. McBride [5], however, lists three "General Rules of Cation Exchange":

1. Adsorption of the high charge ions is associated with increases in entropy and enthalpy of the clay–water system.
2. An increase in solution concentration of the low-charge ion causes the selectivity coefficient to increase, suggesting a greater preference for the high-charge ion.
3. Increased loading of exchange sites with the high-charge ion generally shifts the value of the selectivity coefficient in favor of the high-charge ion.

3 Use of Equivalent Fractions

A more common method of calculating ion partitioning is to assume the exchange ions from an ideal solution. That is the "rational activity coefficients" (λ_A and λ_B) are equal to one (1), then Eq. (7) reduces to:

$$K'_{eq} = \frac{[B^+]}{[A^+]}\left(\frac{(\beta_A)}{(\beta_B)}\right)^x \tag{10}$$

where x is a function of "n" or an adjusted "n" and therefore $K_{eq}{}' = K_{eq} = K_{A/B}$. This also implies that the adsorbed concentration of the ion on the exchanger can be calculated as:

$$meq_A = \beta_A \cdot CEC \tag{11}$$

Application of the above theory to exchange of a monovalent cation for a divalent cation can be written as:

$$A^+ + 0.5BX_2 = 0.5B^{2+} + AX \tag{12}$$

and

$$K_{A/B} = \frac{[B^{2+}]^{0.5}}{[A]}\frac{(AX)}{(BX_2)^{0.5}} \tag{13}$$

and for calculation using equivalent fractions:

$$K_{A/B} = \frac{[B^{2+}]^{0.5}}{[A^{+}]} \frac{\beta_A}{\beta_B^{0.5}} \tag{14}$$

Values of $K_{A/B}$ have been published by numerous researchers for various ions and many of these results compiled by Bruggenwert and Kamphorst (1982). The published values appear to be useful for some situations depending on exchanger and solutions concentrations.

The exchange of various ions in solution is easier if written with respect to only one ion for all ions in solution. This is usually sodium as values of $K_{Na/I}$ are available without further calculation [1].

For example if we have Na, Ca, Mg, K, and NH_4 in a solution in contact with an exchanger, we can write the following equations:

$$\beta_{Ca} = \frac{\beta_{Na}^2}{K_{Na/Ca}^2} \frac{\left[Ca^{2+}\right]}{\left[Na^{+}\right]^2} \tag{15}$$

$$\beta_{Mg} = \frac{\beta_{Na}^2}{K_{Na/Mg}^2} \frac{\left[Mg^{2+}\right]}{\left[Na^{+}\right]^2} \tag{16}$$

$$\beta_{K} = \frac{\beta_{Na}}{K_{Na/K}} \frac{[K^{+}]}{[Na^{+}]} \tag{17}$$

$$\beta_{NH_4} = \frac{\beta_{Na}}{K_{Na/NH_4}} \frac{[NH_4^{+}]}{[Na^{+}]} \tag{18}$$

and

$$\beta_{Ca} + \beta_{Mg} + \beta_{Na} + \beta_{K} + \beta_{NH_4} = 1 \tag{19}$$

This gives a quadratic equation that can be solved for β_{Na} and then the remainder can be solved through substitution. Knowing the values of $K_{Na/I}$ we can now calculate the fraction of each ion on the exchanger for every point in the system where know the concentrations of the ions in solution. Bruggenwert and Kamphorst (1982) and Appelo and Postma [1] give values and ranges for various exchange coefficients for numerous ions with respect to Na^+ (i.e. $K_{Na/I}$). These values have been used by several researchers and yielded successful results [2, 6] but may not be valid for all solutions and concentrations. Fonstad (2004) showed that sufficient data allows for plotting of $K_{Na/I}$ as a function of the factors suggested by McBride [5] above.

If sufficient data is available we can write Eq. (4) as:

$$\frac{[A^{+}]}{[B^{+}]} = K_C \left(\frac{(AX)}{(BX)} \right)^n \tag{20}$$

which leads to:

$$\log \frac{[A^+]}{[B^+]} = \log K_C + n \log \frac{(AX)}{(BX)} \tag{21}$$

So that plotting the logarithm of the ratio of the ion activities in solution against the logarithm of the ratio of the quantity (concentration) of the ions on exchanger yields a slope of "n" and an intercept equal to log K_C (log $K_{A/B}$). $K_{A/B}$ is affected by solution concentration, ratio of the divalent to monovalent ions, and various other factors. This means that $K_{A/B}$ is not actually a reaction constant but can it's self be a variable (Fonstad 2004).

4 Correction Factors Based on Experimental Data

Several researchers have modified Eq. (4) to reflect a best fit to experimental data and to satisfy assumptions regarding ion exchange made by the researchers. The first of these was Kerr who had first proposed:

$$K_K = \frac{[B^{n+}]^m}{[A^{m+}]^n} \frac{\left(A^{m+}\right)^n}{(B^{n+})^m} \tag{22}$$

where all quantities are in molar units for the reaction:

$$nA^{m+} + mBX_n = mB^{n+} + nAX_m \tag{23}$$

Vanselow [10] conducted experiments with ammonium and calcium and proposed a modification of the Kerr equation due to the fact he could not accept the idea that the activity of the solid phase was unity. He modified the Kerr equation by using solution ion activities and a correction factor based on the absorbed ions expressed as:

$$K_V = \frac{[B^{n+}]^m}{[A^{m+}]^n} \frac{(A^{m+})^n}{(B^{n+})^m} \cdot [A^{m+} + B^{n+}]^{m-n} \tag{24}$$

or for monovalent-divalent exchange

$$K_V = \frac{[B^{2+}]}{[A^+]^2} \frac{(AX)^2}{(BX)} \cdot \frac{1}{[(BX) + (AX)]} \tag{25}$$

where solution phase quantities are in activity and absorbed phase are molar.

Both Krishnamoorthy and Overstreet [3] and Gaines and Thomas (1953) felt the Vanselow correction factor was somewhat over simplified and added a factor to

account for charge of the ions on the absorbed phase within the correction factor term. The Krishnamoorthy and Overstreet equation can be represented by:

$$K_{KO} = \frac{[B^{n+}]^m}{[A^{m+}]^n} \frac{(A^{m+})^n}{(B^{n+})^m} \cdot [aA^{m+} + aB^{n+}]^{m-n} \tag{26}$$

where "a" is 1 for monovalent ions, 1.5 for divalent ions and 2 for trivalent ions. The Gaines and Thomas equation can be represented by:

$$K_{GT} = \frac{[B^{n+}]^m}{[A^{m+}]^n} \frac{(A^{m+})^n}{(B^{n+})^m} \cdot \frac{n}{m}[mA^{m+} + nB^{n+}]^{m-n} \tag{27}$$

where solution quantities are expressed as activities and solid phase quantities are molar. A more extensive review of the various exchange equation can be found in White and Zelazny [9].

Soil scientists commonly prefer the Vanselow method of calculating exchange coefficients while geochemists have recently tended toward use of the Gaines and Thomas equation [6]. With the lack of exhaustive experimental data for exchange of numerous ions with numerous absorbents, it would appear there is still work to be done to determine appropriate correction factors for use in reactive transport modeling of solutes involving ion exchange. Although with data for both the absorbed and solution phases, one could calculate a partitioning coefficient ($K_{A/B}$) and then using a best fit method determine a correction factor. These values may only be valid for the absorbent and solution used but could possibly be used to predict equivalent fractions for each ion given or predicting solution chemistry at an individual location.

5 Use of Exchange as a Retardation Factor in Transport

The use of equivalent fractions, while useful for visual representation of ion fractions on exchangers, may not particularly useful in calculation of reactive transport of ions through a porous medium of an exchanger. For this we need the function of how the moles of ions on the exchange sites per weight of sorbent (C) changes with the moles of ions per volume of solution (S). This function we require is termed the distribution coefficient (Kd′) which can be a constant and the equation becomes:

$$C = Kd' \cdot S^n \tag{28}$$

where "n" is simply an exponent. If we plot log C versus log S, and a strait line results, then the slope is equal to the exponent "n" and the intercept is equal to log Kd'. If the result is a strait line the behavior is termed to follow a Freundlich isotherm. The Freundlich isotherm assumes there is an unlimited amount of unreacted sorption

sites. Another common isotherm is the Langmuir isotherm which assumes a finite number of sorption sites (N_{max}) and can be written as:

$$C = \frac{N_{\max} K d' S}{(1 + K d' S)} \tag{29}$$

For exchange with trace elements were the major ion on the exchange site is not affected, the value of Kd' can also be obtained from calculations of equivalent fraction by multiplying the equivalent fraction of the ion exchanging from the solution to the solids by CEC divided by 100 to give mille-equivalents per gram and multiplying the activity of the ion by the charge of the ion. Thus for:

$$1/mA^{m+} + 0.5BX_2 = 0.5B^{2+} + 1/mAX_m \tag{30}$$

gives:

$$Kd' = \frac{CEC \cdot 100}{m}\left(K_{A/B}\frac{\beta^{0.5}{}_B}{[B^{2+}]^{0.5}}\right)^m \tag{31}$$

Kd' thus far has been in units of (moles/g)/(mole/L) or L/g which are not conducive as inclusion as a retardation factor. We must therefore make Kd' dimensionless by expressing both the amount sorbed per kg sorbant and the solution concentration on a total volume basis. The easiest was to do this is to multiply the solution concentration by porosity and multiplying the sorbant concentration by the bulk density (g/L). This gives:

$$Kd = Kd'\frac{\rho_b}{\eta} \tag{32}$$

where

ρ_b bulk density, and
η porosity.

1 + Kd indicates the relative transport of an ion to a non-attenuated ion so that 1 + Kd = R where R is the retardation factor. This is also equal to the difference between the actual velocity of an ion (v) and the velocity of a constant concentration of an ion (v_c). That is to say:

$$R = \frac{v}{v_c} \tag{33}$$

where R = 1 + Kd.

For the advection–dispersion equation with retardation [1]:

$$(1 + Kd)\left(\frac{\partial C}{\partial t}\right) = -v\left(\frac{\partial C}{\partial x}\right) + D_L\left(\frac{\partial^2 C}{\partial t^2}\right) \tag{34}$$

where

C concentration,
t time,
x distance,
v apparent velocity, and
D_L dispersivity.

Retardation affects both the apparent velocity and the dispersivity as shown in:

$$\left(\frac{\partial C}{\partial t}\right) = -\frac{v}{R}\left(\frac{\partial C}{\partial x}\right) + \frac{D_L}{R}\left(\frac{\partial^2 C}{\partial t^2}\right) \tag{35}$$

This means the numerical solution for a front spreading in an infinite column becomes:

$$C(x,t) = C_i + 1/2(C_0 - C_i)erf\left(\frac{\frac{x-vt}{R}}{\sqrt{\frac{4D_L t}{R}}}\right) \tag{36}$$

One solution consistent with the other methods suggested in this paper is to define R as a decreasing or increasing value dependant on some characteristic in the solution-exchanger system.

6 Use of Ion Exchange in Modeling of Transport

Inclusion of ion exchange in aqueous geochemical models varies both in the equations used and in the method of inclusion during calculations. Most models calculate a transport step first, then calculate all equilibrium and kinetically controlled reactions including ion exchange, precipitation, dissolution, and decay, and then calculate the diffusive component prior to transporting the next step. PHREEQC [6] differs in that it calculates all equilibrium and kinetically controlled reactions before and after the diffusion step. This author could find no references that used variable exchange coefficients in the calculation of equivalent fractions or retardation factors. This may imply that all of the models reviewed to date may be limited to a range of solution concentrations and the results should be considered qualitative rather than quantitative. If data were available, most models did allow the user to define their own values for exchange coefficients within the database.

7 Conclusions

Several solutions exist for determination of general ion exchange behavior. Numerous distribution coefficients have been determined for a specific set of ions on a specific absorbent within a limited ionic strength. The use of solution activities along with molar values and a correction factor for the absorbed phase is more common than the use of activity coefficients for ions on the absorbed phase. To date, ion exchange and absorption calculations can only be considered qualitative rather than quantitative without laboratory data using the solution and absorbent in question. Further, the idea that selectivity coefficients and retardation factors are functions of characteristics of the solution-exchanger system opens the possibility of reactive transport of systems with higher ionic strengths.

References

1. Appelo CAJ, Postma D (1996) Geochemistry, groundwater and pollution. A.A. Balkema, Rotterdam, Netherlands, p 536
2. Beekman HE, Appelo CAJ (1990) Ion chromatography of fresh- and salt-water displacement: laboratory experiments and multicomponent transport modelling. J Contam Hydrol 7:21–37
3. Krishnamoorthy C, Overstreet R (1950) An experimental evaluation of ion exchange relationships. Soil Sci 69:41
4. Langmuir D (1997) Aqueous environmental geochemistry. Prentice Hall, Upper Saddle River, p 600
5. McBride MB (1994) Environmental chemistry of soils. Oxford University Press, Inc., New York, p 406
6. Parkhurst DL, Appelo CAJ (1999) User's guide to PHREEQC (version 2)- a computer program for speciation, batch reaction, one-dimensional transport, and inverse geochemical calculations. U.S. Department of the Interior, U.S. Geological Survey, Denver, Colorado, p 312
7. Shackelford CD (1995) Cumulative mass approach for column testing. J Geotech Eng 121(10):696–703
8. Sposito G (1979) Cation exchange in soils: an historical and theoretical perspective. In: Proceedings of a symposium by division S-2 of the American Society of agronomy and the soil science of America, Fort Collins, Colorado, August 5–10, 1979, ASA Special Publication Number 40, pp 13–28
9. Vanselow AP (1932) Equilibria of base exchange reactions of bentonite permutites soil colloids and zeolites. Soil Sci 33:95–113
10. White GN, Zelazny LW (1986) "Charge properties of soil colloids. In: Sparks DS (ed) Soil physical chemistry. CRC Press Inc., Boca Raton, Florida, p 308

Integrated Framework for Identifying Energy-Use Behavior of Hotel Guests

Palani Hevar and Karatas Aslihan

1 Introduction

In the United States, there are about 47,000 hotels, spending an average of $2196 per room on energy each year [10]. Studies have found that guests' energy-related behavior is one of the main factors that affects energy consumption in hotel buildings [8, 30-31, 32, 39]. However, there are many challenges that result in imprecise prediction on the energy consumption level of occupants in hotel buildings: (1) guests are not responsible for paying electrical bills [35]; (2) guest satisfaction is the number one priority in hotels to provide maximum comfort, convenience, and the positive brand experience of their guests [52]; (3) guests feel less restricted with their daily life routine [35], and (4) guests in the same room may behave differently due to diversity in guests' behavioral patterns [7, 49]. To overcome these challenges, there is a need for a model that investigate and analyze hotel guests' energy-use behavior to effectively reduce energy consumption in hotel buildings.

There are several studies investigated various energy reduction strategies primarily focusing on the observation, understanding, and prediction of occupants' energy-use behavior in commercial and residential buildings [8, 30–32]. These strategies include: (i) competition/challenge to increase knowledge of occupants about energy-related issues by encouraging them to change their behaviors for the better depending on the nature of competitions/challenges in monitoring and assessing occupants' energy-related behaviors in a short or limited period of time [20]; (ii) occupant energy use data/feedback to compare occupants' current energy use with their historical use and monitor progress [8, 19, 26, 41] (iii) rewards/penalties to offer incentives to change occupants' behavior or to force extra administrative cost of regulations and sanctions

P. Hevar (✉) · K. Aslihan
Department of Civil, Material, and Environmental Engineering, University of Illinois at Chicago, Chicago, USA
e-mail: hpalan2@uic.edu

S. Walbridge et al. (eds.), *Proceedings of the Canadian Society of Civil Engineering Annual Conference 2021*, Lecture Notes in Civil Engineering 249,
https://doi.org/10.1007/978-981-19-1061-6_11

on occupants [23, 30, 31, 45]; and (iv) technologies to save energy without any human involvement by retrofitting of existing buildings and/or installing high energy-efficient products (e.g., energy-efficient light bulbs, and occupancy sensors) [23, 30, 51]. Despite the significant contributions of these research studies on analyzing the impact of occupants' behavior on energy performance, they primarily focus on residential and office buildings. Therefore, there is little or no research study that provides practical and efficient energy-use reduction strategies based on occupants' energy-related behavior in hotel buildings.

Accordingly, this study focuses on developing an integrated energy-use framework that is efficient in identifying energy-use behavior of hotel guests. This study provides decision-makers (e.g., hotel owners and hotel managers) with better understanding to identify hotel guests' energy-use behavior and thus, reduce energy consumption in hotel buildings and reduce CO_2 and greenhouse gas emissions.

2 Objectives

The goal of this study is to develop an integrated energy-use framework that is capable of assisting decision-makers in hospitality industry to come up with effective energy saving strategies to reduce hotel guests' energy consumption. To achieve this, two objectives are developed to: (1) identify and synthesize the most effective energy-related behavior models (i.e., Motivation-Opportunity-Ability, Norm Activation Model, Theory of Planned Behavior, and Pro-Environmental Behavior) to understand the influential factors that impact hotel guests' energy-use behavior; and (2) develop a set of hypotheses and their relevant measures to examine the relationship among the energy-related behavior models and hotel guests' energy-use behavior.

3 Energy-Use Behavior Models Review

The Motivation-Opportunity-Ability (MOA) Model was originally developed and implemented to understand individual's engagement in processing brand information and purchasing behaviour [4, 17, 37]. In this study, the MOA model was adopted to investigate and understand hotel guests' energy-related behavior in hotel buildings. The MOA model is divided into three main constructs: (1) Motivation refers to occupant's desire and interest to process energy saving information and to implement the required energy conservation behavior [23, 30, 31, 33, 46]; (2) Opportunity refers to the occupant's surrounding environmental factors that are not under his control to enable desired actions [4, 30, 33], and (3) Ability refers to occupant's prior knowledge about energy consumption behavior and knowledge about possible conservation strategies [5, 23, 30].

The Norm Activation Model (NAM) was developed by Schwartz [44] to explain altruistic behaviors (e.g., recycling, volunteering), and other pro-social behaviors (e.g., driving and traveling style, environmental protection and energy-saving behaviors) [31, 44, 50, 53]. NAM is an important theory to understand the influential factors on environmental behavior to reduce energy consumption of buildings [50]. NAM is divided into three main categories: (1) Personal Norms represents the behaviors that are influenced by "expectations, obligations, and sanctions anchored in the self" [31, 53], (2 Awareness of Consequences represents an individual being aware of the consequences of his actions that are caused by energy use [31, 50, 53], and (3 Ascription of Responsibility represents the assignment of responsibility for taking actions or attribution of responsibility for the negative consequences of not acting proactively [53].

The Theory of Planned Behavior (TPB) states that the main antecedent of an individual's behavior is his/her intention toward the behavior. The Theory of Planned Behavior (TPB) was used to capture the rational aspects of individual energy behaviors to strengthen the MOA model [8, 14]. TPB is divided into four main categories: (1) Attitude refers to occupant's overall evaluation of the behavior that is either positively or negatively valued by the occupant [22], (2) Subjective Social Norms apply to energy consumption when an occupant believes that he is under social pressure by surrounding people towards action(s) whether or not engaging in energy saving behaviors [14, 31], (3 Descriptive Social Norms captures the perceptions of others' actual wasting or saving energy behaviors [11, 31, 43], and (4 Perceived Behavioral Control represents a function of occupant's perception of how easy or difficult it would be to perform the desired energy-related behavior [2, 31].

The Pro-Environmental Behavior (PEB) is a behavior that intentionally seeks to reduce the negative impact of an occupant's actions on the environment [27]. In this study, three main categories of PEB were used: (1) Environmental Perceived Knowledge describes behaviors that change toward PEB as a function of an occupant's self or existing environmental knowledge [15, 22], (2 Environmental Concern refers to the evaluation of facts, or an attitude towards facts with consequences for the environment [47], and (3) Effort refers to the physical demonstration of the occupant toward conducting a specific action/behavior [27].

4 Integrated Energy-Use Framework

4.1 Synthesizing Energy-Related Behavior Models

The identified energy-related behavior models (i.e., MOA, NAM, TPB, and PEB) were combined to provide a comprehensive approach on identifying hotel guests'

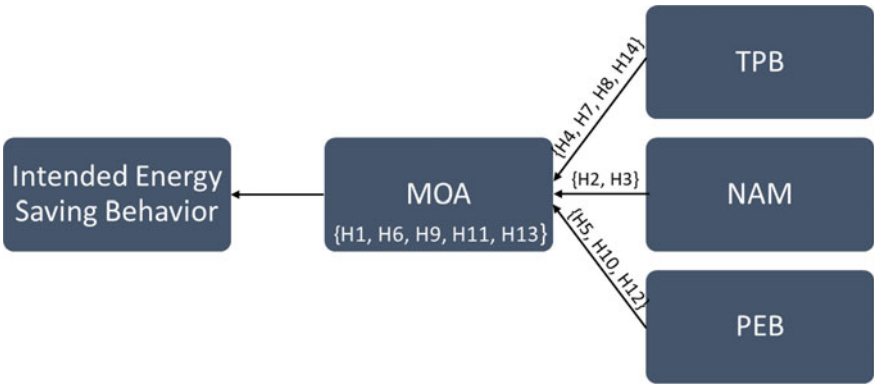

Fig. 1 Integrated energy-use framework

energy-use behavior. The integrated energy-use framework assigned the Motivation-Opportunity-Ability (MOA) model to act as a moderator for the other three energy-related behavior models: Norm Activation Model (NAM), Theory of Planned Behavior (TPB), and Pro-environmental Behavior (PEB) (see Fig. 1). The three main levels of MOA model (i.e., Motivation, Opportunity, and Ability) were designed to have high impact on intended energy saving behavior by combining the energy-related behavior models in this study as discussed in details below.

Motivation (M) Level is directly associated with intended energy saving behavior of the occupant [30, 36]. In this study, hotel guests' concerns and desire for energy reduction in hotel buildings were investigated as a measure of their Motivation level. Moreover, NAM was used to extend several important psychological measurements to capture the essential aspects of hotel guests' Motivation level in hotel buildings. Therefore, in order to capture the social-psychological factors of hotel guests in Motivation, this study adopted: (i two NAM categories of "Personal Norms" and "Ascription of Responsibility"; (ii one TPB category of "Attitude"; and (iii one PEB category of "Environmental Concern". The Personal Norms category of NAM was designed as an internalized need to commit to pro-environmental behavior on hotel guests in hotel buildings. The Ascription of Responsibility category of NAM was adopted on hotel guests to measure their degree of responsibility toward energy saving behavior in hotel buildings. The Attitude category of TPB was developed to evaluate hotel guests' energy saving performance level in hotel buildings. This is based upon the hotel guests' expectations about the outcomes of a particular energy saving behavior and whether these outcomes are desirable from the hotel guest's perspective. Furthermore, the Environmental Concern category of PEB was designed to activate a hotel guest's sense of responsibility to perform energy-related behavior.

Opportunity (O) Level measured the controllability and accessibility of hotel guests to hotel room energy systems (e.g., lighting, HVAC, appliances, electronics) in hotel buildings. The Opportunity level adopted four categories in this study: (i) two TPB

category of "Subjective Social Norms" and "Descriptive Social Norms"; (ii) one MOA category of "Hotel Management Support; and (iii) one PEB category of "Physical Effort." The Subjective Social Norms category of TPB was designed to affect a hotel guest's energy consumption behaviors when the guest tends to perform a particular behavior in the room if it is approved by the room companion(s). The Descriptive Social Norms category of TPB was designed to capture the perceptions of hotel room companion's actual wasting or saving energy consumption behaviors [11, 42]. The Hotel Management Support category of MOA was designed to reflect the hotel management's commitment level in promoting energy saving behavior in hotel buildings such as hotel management rewards for guests saving energy [48]. The Physical Effort category of PEB was designed to evaluate hotel guests' level of tendency to make changes in their energy-related behavior in hotel buildings when the energy-related behavior is easy and convenient to perform from guests' perspective [27].

Ability Level depended on two main factors in this study: individuals' perception of their energy consumption level, and individuals' knowledge about energy consumption facts [30]. In the context of energy consumption behaviors in hotel buildings, the authors in this study adopted three main categories to capture hotel guests' Ability: (i one PEB category of "Environmental Perceived Knowledge"; (ii one MOA category of "Actual Knowledge"; and (iii one TPB category of "Perceived Behavioral Control". Environmental Perceived Knowledge of PEB referred to hotel guests' perception of their energy-related knowledge about reducing energy consumption in hotel buildings. The Actual Knowledge category of MOA measures an individual's mental capabilities [1, 31]. In this study, it measured hotel guests' facts and actual energy-related knowledge in hotel buildings. The Perceived Behavior Control category of TPB measures an individual's Ability level on his physical capability and perceived knowledge on how easy to conduct a behavior [31]. In this study, this category was adopted to measure hotel guests' existing knowledge and their overall evaluation about the simplicity of conducting energy-related behavior in hotel rooms.

It is also remarkable to mention that both Opportunity (O) and Ability (A) affect energy saving behaviors only when Motivation (M) is present [31]. This means that both Opportunity and Ability levels moderate the impact of Motivation level on energy saving behaviors of hotel guests in hotel buildings.

4.2 Developing Energy-Use Behavior Hypotheses and Their Relevant Measures

In this section, 14 hypotheses with their relevant measures were developed to find the relationship among the aforementioned energy-related behavior models and energy-use behavior of hotel guests, as presented in Fig. 1 and Table 1.

Hypothesis 1 (H1), Hypothesis 2 (H2), Hypothesis 3 (H3), Hypothesis 4 (H4), and Hypothesis 5 (H5), were designed to test the Motivation level of hotel guests.

Table 1 Integrated framework hypothesis and their measures

Hypothesis #	Measures	Hypotheses representative studies
H1 Energy conservation motivation	• Adjusting lighting control	[9, 13, 24, 30, 31]
	• Adjusting indoor climate conditions	
	• Adopting energy conservation strategies	
	• Personal motivation	
H2 Personal norms	• Hotel guest's moral obligation to reduce energy consumption in his/her hotel room	[3, 6, 18, 28, 31, 38, 50, 53]
H3 Ascription of responsibility	• Hotel guest's degree of responsibility	[16, 18, 31, 38, 53]
H4 Attitude	• Positive and negative energy conservation attitudes of hotel guests	[2, 6, 18, 31, 40]
H5 Environmental concern	• Environmental concern levels of hotel guests	[6, 12, 25]
H6 Energy conservation opportunity	• Availability and accessibility of energy saving information and energy control systems to hotel guests	[23, 24], [30, 31]
H7 Subjective social norms	• Hotel management's expectations toward hotel guest's energy conservation behavior (e.g., lighting control, adjusting indoor climate conditions, window blinder control)	[2, 6, 18, 31, 40]
	• Room companion(s) expectations toward hotel guest's energy conservation behavior (e.g., lighting control, adjusting indoor climate conditions. window blinder control)	
	• Peer pressure	
H8 Descriptive social norms	• Room companion(s) concern level about energy consumption in the hotel room	[2, 11, 31] [40, 43]
H9 Hotel management support	• Hotel management's policy, regulations, and/or recommendations provided to hotel guests about reducing their energy consumption	[31]

(continued)

Table 1 (continued)

Hypothesis #	Measures	Hypotheses representative studies
H10 Physical effort	• Physical efforts to conduct energy saving behaviors that are not bothersome or inconvenient to the hotel guest in the hotel room	[27, 29, 35]
H11 Energy conservation ability	• Hotel guest's prior knowledge in energy-savings and skills in interpreting information received from behavioral interventions	[4, 23, 24, 30, 31]
H12 Environmental perceived knowledge	• Perceived self-knowledge capacity of energy conservation	[9, 13, 21, 24, 30, 31, 34, 53]
	• Perceived self-knowledge capacity of adjusting indoor climate conditions (HVAC system)	
	• Perceived self-knowledge capacity of lighting usage	
H13 Actual knowledge	• Knowledge of plug loads	[9, 13, 30, 31]
	• Knowledge of adjusting indoor climate conditions (HVAC)	
	• Knowledge of lighting control	
	• Knowledge of energy conservation strategies	
	• Knowledge of renewable resources	
H14 Perceived behavioral control	• Hotel guest's physical capability and perceived ease to enact a behavior	[6, 31]
	• Hotel management's physical capability and perceived ease to enact a behavior	

H1 was designed to predict if guests' high motivation levels have an impact on their energy reduction behavior. This hypothesis measures: (1) adjusting lighting control; (2) adjusting indoor climate conditions; (3) adopting energy conservation strategies; and (4) personal motivation. H2 was designed to investigate if guests with high personal norms have an effect on their energy reduction behaviors in the presence of energy reduction motivation. This hypothesis measures hotel guests' moral obligation to reduce energy consumption in their hotel rooms. H3 was designed to predict if guests' ascription of responsibility has an effect on their energy reduction behaviors in the presence of energy reduction motivation. H3 measures hotel guests'

degree of responsibility to reduce their energy consumption in hotel rooms. H4 was designed to determine whether guests' positive attitude can change their energy consumption behavior when they are also motivated to reduce energy. H4 measures hotel guests' positive and/or negative energy reduction attitudes. H5 was designed to investigate if guests' environmental concern levels have impact on their energy reduction behaviors in the presence of energy reduction motivation. This hypothesis measures hotel guests' concern level toward reducing their energy consumptions in hotel rooms.

Hypothesis 7 (H7), Hypothesis 8 (H8), Hypothesis 9 (H9), and Hypothesis 10 (H10), were designed to test the Opportunity level of hotel guests. H7 was designed to predict if guests' subjective social norm levels have an impact on energy-related conservation behaviors in the presence of energy conservation motivation. This hypothesis measures the expectations of hotel management, expectations of hotel room companion(s), and peer pressure to reduce energy consumption of hotel guests. H8 was designed to predict if guests' descriptive social norm levels have an impact on energy-related conservation behaviors in the presence of energy conservation motivation. This hypothesis measures the hotel room companion(s) concern levels to reduce guests' energy consumption. H9 was designed to investigate if support from hotel management would have an impact on energy-related conservation behaviors when energy motivation is high. H8 measures general policy, regulations, and recommendations of hotel managements provided to hotel guests to reduce their energy consumption. Finally, H10 was designed to predict if guests' physical effort levels have an impact on energy-related conservation behaviors in the presence of energy conservation motivation. This hypothesis measures the opportunities provided by hotel management to hotel guests that provided true expectations for easier and less need for physical effort from hotel guests to conduct energy-related conservation behavior.

Hypothesis 12 (H12), Hypothesis 13 (H13), and Hypothesis 14 (H14), were designed to test the Ability level of hotel guests. H12 was designed to predict if guests' environmental perceived energy-related conservation knowledge level would affect their energy conservation behaviors when they are motivated to conserve energy. H12 measures guests' self-assessed knowledge levels to reduce energy consumptions, self-assessed knowledge level to adjust indoor climate conditions, and adjusting lighting usage. H13 was designed to determine if guests' knowledge levels of energy consumption facts (actual knowledge on energy consumption) would have an impact on energy-related conservation behaviors when energy motivation is high. H13 measures guests' actual energy reduction knowledge including knowledge of: (1) plug loads; (2) adjusting indoor climate conditions; (3) lighting controls; (4) energy conservation strategies; (5) renewable resources. H14 was designed to investigate whether guests perceived behavioral control levels have an impact on energy-related conservation behaviors when energy motivation is high. This hypothesis measures both hotel guests' and hotel management's physical capability to reduce their energy consumption.

Finally, Hypothesis 6 (H6) and Hypothesis 11 (H11) were designed. H6 was designed to determine if hotel guests' accessibility and availability to environmental

energy reduction information and control systems have an impact on their energy-related conservation behaviors in hotel buildings. H6 measures if guests' opportunity level is mediated by their motivation. H11 was designed to predict if hotel guests' existing environmental knowledge and skills are effective in reducing energy consumption in hotel buildings. H11 measures if guests' ability level is mediated by their motivation.

5 Conclusion

This paper aims to present a holistic approach to identify energy-use behavior of hotel guests in hotel buildings. To achieve this, a comprehensive literature review was conducted on energy-related behavior models in the field of social psychology to develop an integrated energy-use framework (see Fig. 1). The integrated energy-use framework was developed in two stages. First, four energy-related behavior models were identified and investigated: (1) Motivation-Opportunity-Ability (MOA); (2) Norm Activation Model (NAM); (3) Theory of Planned Behavior (TPB); and (4) Pro-environmental Behavior (PEB) to design the integrated energy-use framework of this paper. Second, 14 hypotheses and their relevant measures were designed to predict the relationship among the energy-related behavior models (i.e., MOA, NAM, TPB, and PEB) and hotel guests' energy-use behavior as presented in Table 1. This integrated energy-use framework will assist researchers and hospitality industry decision-makers, including hotel owners and hotel management personnel, to develop effective strategies to reduce hotel guests' energy consumption in hotel buildings. Decision makers can develop a cost-effective occupancy-focused intervention programs that prioritize hotel guests' energy saving behaviors and encourage them for more sustainable behavior pattern in hotel buildings. Decision-makers in hospitality industry should provide aggressive incentive strategies to hotel guests that have dark energy consumption behavior. For example, providing non-financial incentives such as free hotel room upgrade and free VIP parking or providing financial incentives such as discount for future stays and meal coupon. The proposed integrated energy-use framework is expected to deepen and broaden the concept and understanding of human behaviors to identify hotel guests' energy-use behavior and thus, to reduce energy consumption of hotel guests in hotel buildings.

6 Future Work

The authors of this study will conduct an energy-use survey to analyze the effect of each determined measure on hotel guests' energy-use behavior. Then, the energy-use survey results will be analyzed to test and validate the 14 hypotheses of the integrated energy-use framework. This will help to identify energy-use behavior (e.g., low Motivation level, high Ability level) and energy-use profiles (e.g., good

energy consumption behavior, dark energy consumption behavior) of hotel guests in hotel buildings. After that, a set of interventions and incentives will be developed in collaboration with a US hotel chain to achieve win–win operation for hotel stakeholders (i.e., hotel owners, hotel managements, and hotel guests).

References

1. Abrahamse W, Steg L (2009) How do socio-demographic and psychological factors relate to households' direct and indirect energy use and savings? J Econ Psychol 30(5):711–720
2. Ajzen I (1991) The theory of planned behavior. Organ Behav Hum Decis Processes Theor Cogn Self-Regul 50(2):179–211
3. Bamberg S, Hunecke M, Blobaum A (2007) Social Context, Personal Norms and the Use of Public Transportation: Two Field Studies. J Environ Psychol 27(3):190–203
4. Bigné E, Hernandez B, Ruiz C, Andreu L (2010) How motivation, opportunity and ability can drive online airline ticket purchases. J Air Transp Manag 16(6):346–349
5. Celsi RL, Olson JC (1988) The role of involvement in attention and comprehension processes. J Consum Res 15(2):210–224
6. Chen M, Tung P (2014) Developing an extended theory of planned behavior model to predict consumers' intention to visit green hotels. Int J Hosp Manag 36(1):221–230
7. Csoknyai T, Legardeur J, Abi Akle A, Horváth M (2019) Analysis of energy consumption profiles in residential buildings and impact assessment of a serious game on occupants' behavior. Energy Build 196(8):1–20
8. D'Oca S, Chen C, Hong T, Belafi Z (2017) Synthesizing building physics with social psychology: an interdisciplinary framework for context and occupant behavior in office buildings. Energy Res Soc Sci 34(12):240–251
9. Eccles M, Grimshaw J, Walker A, Johnston M, Pitts N (2005) Changing the behavior of healthcare professionals: the use of theory in promoting the uptake of research findings. J Clin Epidemiol 58(2):107–112
10. Energy Information Administration (EIA) (2020). https://www.eia.gov/tools/faqs/faq.php?id=87&t=1
11. Forward SE (2009) The theory of planned behaviour: the role of descriptive norms and past behaviour in the prediction of drivers' intentions to violate. Transp Res F Traff Psychol Behav 12(3):198–207
12. Fujii S (2006) Environmental concern, attitude toward frugality, and ease of behavior as determinants of pro-environmental behavior intentions. J Environ Psychol 26(4):262–268
13. Geller ES (1995) Integrating behaviorism and humanism for environmental protection. J Soc Issues 51(4):179–195
14. Greaves M, Zibarras LD, Stride C (2013) Using the theory of planned behavior to explore environmental behavioral intentions in the workplace. J Environ Psychol 34(6):109–120
15. Grob A (1995) A structural model of environmental attitudes and behaviour. J Environ Psychol Green Psychol 15(3):209–220
16. Groot JD, Steg L (2007) General beliefs and the theory of planned behavior: the role of environmental concerns in the TPB. J Appl Soc Psychol 37(8):1817–1836
17. Gruen TW, Osmonbekov T, Czaplewski AJ (2005) How e-communities extend the concept of exchange in marketing: an application of the motivation, opportunity, ability (MOA) theory. Mark Theory 5(1):33–49
18. Han H, Hwang J, Kim J, Jung H (2015) Guests' pro-environmental decision-making process: broadening the norm activation framework in a lodging context. Int J Hosp Manag 47(5):96–107
19. Houwelingen JH, Raaij WF (1989) The effect of goal-setting and daily electronic feedback on in-home energy use. J Consum Res 16(1):98–105

20. Johnson PM, Xu Y, Brewer RS, Lee GE, Katchuck M, Moore CA (2012) Beyond KWh: myths and fixes for energy competition game design. Proc Meaningful Play 1–10
21. Kaiser FG, Fuhrer U (2003) Ecological behavior's dependency on different forms of knowledge. Appl Psychol 52(4):598–613
22. Kaiser FG, Wölfing S, Fuhrer U (1999) Environmental attitude and ecological behaviour. J Environ Psychol 19(1):1–19
23. Karatas A, Menassa CC, Stoiko A (2015) A framework for delivering targeted occupancy interventions to reduce energy usage in buildings. Procedia Eng Defining Future Sustain Resilience Des Eng Constr 118(1):752–759
24. Karatas A, Stoiko A, Menassa CC (2016) Framework for selecting occupancy-focused energy interventions in buildings. Build Res Info 44(5–6):535–551
25. Kim Y, Choi SM (2005) Antecedents of green purchase behavior: an examination of collectivism, environmental concern, and pce. ACR North American Advances NA-32. https://www.acrwebsite.org/volumes/9156/volumes/v32/NA-32
26. Klein L, Kwak J, Kavulya G, Jazizadeh F, Becerik-Gerber B, Varakantham P, Tambe M (2012) Coordinating occupant behavior for building energy and comfort management using multi-agent systems. Autom Constr 22(3):525–36
27. Kurisu K (2015) Pro-Environmental Behaviors. Springer, Tokyo, Japan
28. Lam S (1999) Predicting intentions to conserve water from the theory of planned behavior, perceived moral obligation, and perceived water right. J Appl Soc Psychol 29(5):1058–1071
29. Lee H, Kurisu K, Hanaki K (2013) Influential factors on pro-environmental behaviors—a case study in tokyo and seoul. Low Carbon Economy 4(3):104–116
30. Li D, Menassa CC, Karatas A (2017) Energy use behaviors in buildings: towards an integrated conceptual framework. Energy Res Soc Sci 23:97–112
31. Li D, Xu X, Chen C, Menassa C (2019) Understanding energy-saving behaviors in the american workplace: a unified theory of motivation, opportunity, and ability. Energy Res Soc Sci 51(5):198–209
32. Lutzenhiser L (1993) Social and behavioral aspects of energy use. Annu Rev Energy Env 18(1):247–289
33. MacInnis DJ, Moorman C, Jaworski BJ (1991) Enhancing and measuring consumers' motivation, opportunity, and ability to process brand information from ads. J Mark 55(4):32–53
34. McMakin AH, Malone EL, Lundgren RE (2002) Motivating residents to conserve energy without financial incentives. Environ Behav 34(6):848–863
35. Miao L, Wei W (2013) Consumers' pro-environmental behavior and the underlying motivations: a comparison between household and hotel settings. Int J Hosp Manag 32(3):102–112
36. Moorman C (1990) The effects of stimulus and consumer characteristics on the utilization of nutrition information. J Consum Res 17(3):362–374
37. ölander F, ThØgersen J (1995) Understanding of consumer behaviour as a prerequisite for environmental protection. J Consum Policy 18(4):345–85
38. Onwezen MC, Antonides G, Bartels J (2013) The norm activation model: an exploration of the functions of anticipated pride and guilt in pro-environmental behaviour. J Econ Psychol 39(12):141–153
39. Palani H, Karatas A (2021) Identifying Energy-Use Behavior and Energy-Use Profiles of Hotel Guests. Applied Sciences 11(13):6093
40. Perugini M, Bagozzi RP (2001) The role of desires and anticipated emotions in goal-directed behaviours: broadening and deepening the theory of planned behaviour. Br J Soc Psychol 40(1):79–98
41. Peschiera G, Taylor JE, Siegel JA (2010) Response-relapse patterns of building occupant electricity consumption following exposure to personal, contextualized and occupant peer network utilization data. Energy Build 42(8):1329–1336
42. Rai V, Beck AL (2015) Public perceptions and information gaps in solar energy in Texas. Environ Res Lett 10(7):074011
43. Rivis A, Sheeran P (2003) Descriptive norms as an additional predictor in the theory of planned behaviour: a meta-analysis. Curr Psychol 22(3):218–233

44. Schwartz SH (1977) Normative influences on altruism. In: Advances in experimental social psychology, Elsevier, 10:221–79
45. Seyrfar A, Ataei H, Movahedi A, Derrible S (2021) Data-Driven Approach for Evaluating the Energy Efficiency in Multifamily Residential Buildings. Practice Periodical on Structural Design and Construction. American Society of Civil Engineers 26(2):04020074.
46. Steg L, Vlek C (2009) Encouraging pro-environmental behaviour: an integrative review and research agenda. J Environ Psychol Environ Psychol Move 29(3):309–317
47. Takala M (1991) Environmental awareness and human activity. Int J Psychol 26(5):585–597
48. Thøgersen J (2014) The mediated influences of perceived norms on pro-environmental behavior. Revue d'economie politique 124(2):179–193
49. Wang J, Zhu J, Ding Z, Zou PXW, Li J (2019) Typical energy-related behaviors and gender difference for cooling energy consumption. J Clean Prod 238(11):117846
50. Werff EVD, Steg L (2015) One model to predict them all: predicting energy behaviours with the norm activation model. Energy Res Soc Sci 6(3):8–14
51. Wong NH, Cheong DKW, Yan H, Soh J, Ong CL, Sia A (2003) The effects of rooftop garden on energy consumption of a commercial building in Singapore. Energy Build 35(4):353–364
52. Yao Z, Zhuang Z, Gu W (2015) Study on energy use characteristics of hotel buildings in Shanghai. In: Procedia engineering, the 9th (ISHVAC) joint with the 3rd international (COBEE), 12–15 July 2015, Tianjin, China, 121(1):1977–82
53. Zhang Y, Wang Z, Zhou G (2013) Antecedents of employee electricity saving behavior in organizations: an empirical study based on norm activation model. Energy Policy 62(11):1120–1127

A 3D Bioventing Model to Estimate Closure Time

M. Khodabakhshi Soureshjani, R. G. Zytner, and H. J. Eberl

1 Background

Petroleum hydrocarbons as soil contaminants endanger human health because of their potential to migrate from contaminated soil into the groundwater. Therefore, it is crucial to understand how to remediate petroleum hydrocarbons-contaminated sites. Soil vapor extraction (SVE) is a popular in situ remediation approach, but it faces a tailing issue. Tailing increases mass transfer resistance, which in turn increases the clean-up time. Additionally, tailing allows the contaminant concentrations to stay higher than the clean-up standard. Therefore, substituting SVE with an appropriate bioremediation method can eliminate these drawbacks (Khan and Zytner 2013). Bioventing is usually an appropriate alternative to implement after SVE since the physical system is the same; air flow is reduced, and nutrients are added to the subsurface.

Bioventing (BV) as an in situ method that can economically clean up motor oil, diesel fuel, jet fuel, and gasoline contaminated soils and overcome the tailing effects caused by the SVE process [1]. Bioventing is a biological degradation technique where native aerobic microorganisms are stimulated by adding oxygen and nutrients (phosphorus and nitrogen) to bioremediate the petroleum hydrocarbons [6].

Some experimental studies have been completed on the bioventing treatment of the hydrocarbon-contaminated soils in micro-scale, meso-scale, and large-scale reactors to estimate bioremediation rate constants and scale-up factors [1, 3, 5].

A meso-scale bioventing reactor was developed by Khan et al. [3] and (2013). Regression models were developed and identified a two-stage rate constant. Faster biodegradation rate occurred during the first 8 days of process, while a slower degradation rate happened in the remaining 22 days. The rate constant was positively

M. Khodabakhshi Soureshjani · R. G. Zytner (✉) · H. J. Eberl
University of Guelph, Guelph, Canada
e-mail: rzytner@uoguelpha.ca

S. Walbridge et al. (eds.), *Proceedings of the Canadian Society of Civil Engineering Annual Conference 2021*, Lecture Notes in Civil Engineering 249,
https://doi.org/10.1007/978-981-19-1061-6_12

affected by the initial population of degraders and the amount of silt, whereas the extent of clay and organic matter negatively impacted the rate.

The biodegradation correlations and scale-up factors obtained so far in our research group for a 4 kg reactor will be imposed to the model [3]. The first simulation will be based on the meso-scale bioventing reactor developed by Khan et al. [3] and (2013), and the second step will be the modeling of large-scale (80 kg) reactor [5].

Various modeling studies on bioremediation of hydrocarbon-contaminated soils have been completed, but they include several assumptions to simplify the system: sorption between the solid and gas phases was neglected; biodegradation was assumed to occur just in the aqueous phase; microorganisms were homogeneously dispersed in one phase; and soil was considered as a homogeneous media [2, 4, 8]. In addition, most of the current models were developed in 1 or 2 dimensions while the conditions in the third dimension may not be consistent with those of the other dimensions. For instance, some physical properties such as permeability of soil and dispersion coefficient may be different in the third direction. Those assumptions reduce the accuracy of the predictions.

The main purpose of this study is to develop a 3-D axisymmetric bioventing model to obtain accurate closure time predictions. By incorporating accurate soil characteristics along with a rate constant correlation, the bioventing model would be improved, providing better predictions of closure time. The model considers multiphase fluid (gas, aqueous, NAPL) interactions in the unsaturated soil environment, gas flow through a porous medium, and transport equations including convection, dispersion, diffusion, interphase mass transfer and a biodegradation rate correlation for a BV system.

2 Model Development

A three-dimensional bioventing model was developed by considering multiphase flow (aqueous, NAPL, gas) in unsaturated soil environment, multicomponent transport (contaminant, water, oxygen, nutrient) and equilibrium mass transfer phenomena (partitioning) along with biodegradation. The contaminated site was considered as a homogenous region in the model, with the geological (e.g., permeability) and operational properties (e.g., airflow rate) of contaminated sites will be simulated by the proposed 3-D model using OpenFOAM®. The volatile characteristics of the contaminants were accounted in the model based on mass transfer between dissolved, adsorbed and free phases available in the vapor phases and also in the soil. Equilibrium conditions were assumed for this stage of the development. The rate constants were determined at 25 °C, but can be adjusted for any typical subsurface temperature.

The multiphase flow and multicomponent interaction of the system was based on the mass balance Eq. (1) [7]:

$$\frac{\partial}{\partial t}\left(\varphi\rho_\beta S_\beta\right) = \nabla\left[\frac{\rho_\beta k_{ij} k_{r\beta}}{\mu_\beta}\left(\nabla p_\beta - \rho_\beta g e_j\right)\right] + E_\beta^\alpha + p_\beta Q_\beta \tag{1}$$

where φ is the porosity of soil, β represents the phases, S_β and ρ_β (kg/m^3) are the saturation and density of phase β, respectively. The parameters k_{ij} (m^2) and $k_{r\beta}$ are intrinsic permeability of porous medium and relative permeability of phase β, respectively. e_j are the components of a unit vector (0,0,1). Q_β (mol/m^{3}s), p_β (Pa), and μ_β (kg/m.s) show the source/sink, pressure, and viscosity of phase β, respectively. E_β^α is the total mass transfer of the components from other phases to phase β.

The components considered in the bioventing system were nutrients (n), Oxygen (O_2), water vapor and the contaminant (C). The non-linear advective–dispersive conservation equation was applied to the model to represent the transport of component k in the gas phase (β):

$$\frac{\partial}{\partial t}(\varphi S_\beta C_{\beta,k}) = \nabla\left(\varphi S_\beta D_{\beta,k} \nabla C_{\beta,k}\right) - \nabla\left(q_\beta C_{\beta,k}\right) + \gamma_{\alpha\beta,k} + Q_{\beta,k} \tag{2}$$

where $C_{\beta,k}$ (mol/m^{3}s) and $D_{\beta,k}$ (m^2/s) are molar concentration and dispersion coefficient tensor of species k in gas phase β, respectively. q_β (m/s) represents the velocity of phase β, and $Q_{\beta,k}$ (mol/m^3.s) is source/sink of the component k in phase β. $\gamma_{\alpha\beta,k}$ is the mass transfer of component k from phase α to phase β.

It was assumed that only the gas phase was flowing. This was based on the assumption that the contaminated area was unsaturated soil, with the aqueous and NAPL phases immobile. The first-order biodegradation kinetics was considered and incorporated into the model.

The system of equations was solved by coupling the governing equations and the constraining equations. Mass transfer coefficients will be the first choices as fitting parameters to adjust the results to the experimental data. After fitting the model, the time needed to reach to a specific concentration of contaminant in soil will be estimated (closure time).

3 Results and Discussion

The bioventing system was mathematically modeled and simulated using open source code OpenFOAM® for the computational fluid dynamics (CFD) with free deployment on parallel computers. Unlimited customisation is an advantage of OpenFOAM® which means users can extend the collection of solvers, utilities and libraries in OpenFOAM®, using some prerequisite knowledge of the underlying method, physics and programming techniques involved. The software is code based, with the base language C++. As a result, modelling is highly flexible, making it easy to adjust parameters and equations as required.

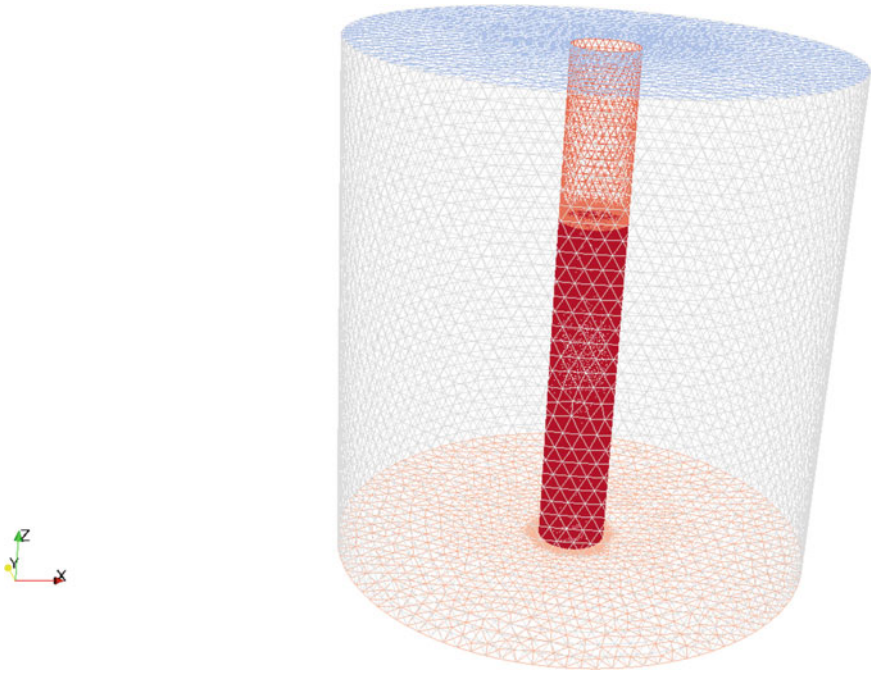

Fig. 1 CFD mesh in Paraview (OpenFOAM)

Using a preliminary compressible fluid (gas) flowing model in porous media, the efficiency of the mesh was assessed. The mesh as shown in Fig. 1 was built in FluentAnsys and then converted to the format compatible with OpenFOAM.

The next step will be to add the phases and the governing interphase mass transfer equations to the main solver to simulate the process. The mesh size will be optimized after running the simulations, imposing the axisymmetric system and optimized mesh size will significantly decrease the computational time.

The model will be fitted and then validated using three independent set of experimental data at 200 g system [1], 4 kg reactor (Khan and Zytner 2013 and 2015) and 80 kg reactor [5]. The initial fitting will be with the 4 kg reactor using the fitting parameters.

A parameter sensitivity analysis will be done to find out which parameters have the largest influence on the sensitivity of the numerical solutions of the model. One choice can be mass transfer coefficient from NAPL to gas phase since experimentally and theoretically, mass transfer between the NAPL and vapour phase has been demonstrated to have a critical influence on SVE and bioventing. Based on the assumption that the biodegradation occurs only in the aqueous phase, mass transfer coefficient from NAPL phase to aqueous phase which controls the biodegradation can be another choice.

Best fit will be identified with a log transformation mean squared difference between the experimental and simulated data (Harper et al. 2003).

4 Summary

The clean-up of contaminated sites with petroleum hydrocarbons is an expensive and long-term process. When remediation predictions are incorrect or take too long, site owners abandon cleanup efforts. Consequently, choosing the proper remediation method and estimating the corresponding clean-up time is significant. Accordingly, it is vital to have an accurate 3D model that is robust and includes many parameters affecting the bioremediation of petroleum hydrocarbons, something current models cannot do. The current work on a 3-D bioventing model to predict the closure time will address this deficiency.

Acknowledgements The authors would like to thank NSERC for a Discovery Grant to fund this research.

References

1. Eyvazi MJ, Zytner RG (2009) A correlation to estimate the bioventing degradation rate constant. Bioremediat J 13(3):141–153
2. Fernández EL, Merlo EM, Mayor LR, Camacho JV (2016) Kinetic modelling of a diesel-polluted clayey soil bioremediation process. Sci Total Environ 557–558:276–284
3. Khan AA, Zytner RG, Feng Z (2015) Establishing correlations and scale-up factor for estimating the petroleum biodegradation rate in soil. Bioremediat J 19(1):32–46
4. McClure PD, Sleep BE (1996) Simulation of bioventing for soil and ground-water remediation. J Environ Eng 122(11):1003–1012
5. Mosco MJ, Zytner RG (2017) Large-scale bioventing degradation rates of petroleum hydrocarbons and determination of scale-up factors. Bioremediat J 21(3–4):149–162
6. Nikolopoulou M, Kalogerakis N (2008) Enhanced bioremediation of crude oil utilizing lipophilic fertilizers combined with biosurfactants and molasses. Mar Pollut Bull 56:1855–1861
7. Nguyen VT, Zhao L, Zytner RG (2013) Three-dimensional numerical model for soil vapor extraction. J Contam Hydrol 147:82–95
8. Rathfelder KM, Lang JR, Abriola LM (2000) A numerical model (MISER) for the simulation of coupled physical, chemical and biological processes in soil vapor extraction and bioventing systems. J Contam Hydrol 43(3–4):239–270
9. Wu M, Li W, Dick WA, Ye X, Chen K, Kost D, Chen L (2017) Bioremediation of hydrocarbon degradation in a petroleum-contaminated soil and microbial population and activity determination

Optimizing Waste Management Regions Spanning Inter-Provincial Boundaries

A. Richter, K. T. W. Ng, and N. Karimi

1 Introduction and Literature Review

Canadians have one of the highest rates of waste generation in the world, generating 973 kg/cap in 2016 [26, 27]. Of this generated waste, most is sent to landfills for permanent disposal [4, 30]. In 2016, the percentage allocation of waste management budgets to collection and transportation of waste at the local government level was 41.3% [28]. This represents the largest single expenditure category on any type of waste management service. Regionalization of waste management systems includes municipalities working together and delegating responsibilities to a central authority within a defined geographic boundary [12]. A number of Canadian jurisdictions have already employed regionalized waste management systems, including Alberta [9] and Nova Scotia [11]. Following suit, the Government of Saskatchewan is also intending to regionalize their waste management system [13]. It is believed that regionalization will have the following benefits: providing efficient and economical waste disposal and diversion services, improving the environmental performance of the system, improving landfill operations while reducing municipal liability of landfill operations, and enhancing waste minimization [12]. Richter and Ng [22] explored the unique demographic and infrastructure demands in Saskatchewan, and found that they may pose an extra challenge with respect to regionalized waste management systems in the province.

Typical waste system optimization studies apply GIS to find the optimal placement of waste management facilities in an area, not the design of specific regions which encapsulate the waste management system. For example, [29] use overlay analysis and buffering in order to define suitable areas for landfills. Khan et al. [17] used GIS

A. Richter (✉) · K. T. W. Ng · N. Karimi
Faculty of Engineering and Applied Science, University of Regina, Regina, Canada
e-mail: richamy1@uregina.ca

S. Walbridge et al. (eds.), *Proceedings of the Canadian Society of Civil Engineering Annual Conference 2021*, Lecture Notes in Civil Engineering 249,
https://doi.org/10.1007/978-981-19-1061-6_13

methods such as location allocation and analytical hierarchical process (AHP) to site waste conversion facilities in the province of Alberta.

Chalkias and Lasaridi [5] used ArcGIS Network analyst tools to improve the efficiency of waste collection and transportation in a Greek municipality. In their study, they improved efficiency by reallocation of waste bins to different sectors (essentially creating sectors that are optimized for waste management), as well as applying vehicle routing to optimize distance and time travelled. They noted the importance of sectorisation of larger waste collection areas, and the importance of spatial analysis over empirical approaches when it comes to designing waste management and collection systems.

Adamides et al. [1] discuss the importance of spatial analysis and topology of waste management regions. In their study, they consider population distribution along with estimated production volumes of solid waste, which are used to determine end treatment facilities in each of the five administrative regions in the study area (Greece). They note the importance of multi-methodological intervention in developing regional waste management systems, combining both social and economic aspects.

With respect to the actual development of regions, [6] noted that the attractive characteristics of service areas were: [i] connectivity and [ii] compactness. By improving the shape characteristics of regions, arc or node routing problems within each region can be solved more optimally [6].

Richter et al. [21] proposed and applied a novel recursion algorithm to optimize the shape of waste management regions in Saskatchewan and Nova Scotia, which is applied in this study. Using the proposed methodology, significant reductions in standard deviation were observed in both Nova Scotia (9.6–30.4%) and Saskatchewan (4.9–46.1%).

With respect to waste management, there are few studies on interprovincial or transboundary movement of solid waste from an optimization perspective. Li et al. [18] examined interprovincial movement of waste electrical and electronic equipment (WEEE) in China. In applying a Minimum Distance Maximum Receiving (MDMR) model, they found that there is room for optimization with respect to interprovincial movement of WEEE in China. Furthermore, they found that certain provinces are underserved in terms of recycling of WEEE, while others are overserved.

Agovino et al. [2] noted that administrative data are aggregated on the basis of arbitrary geographical boundaries that reflect political and historical changes. They further concluded that the choice of spatial aggregation unit is essential in their study on spatial proximity effects. For example, in Nova Scotia, waste management regions are the amalgam of Federal Subdivision [11]. Richter et al. [21] questioned the use of administrative boundaries in the development of waste management regions in Canada, however, they failed to consider whether interprovincial analysis yielded any further optimization. As a result, the objectives of this paper are to: (i) apply the recursive Thiessen Polygon algorithm in an interprovincial comparison of Saskatchewan and Manitoba using Federal subdivisions as the input tessellation, and (ii) compare the results to see if optimization occurs across interprovincial boundaries.

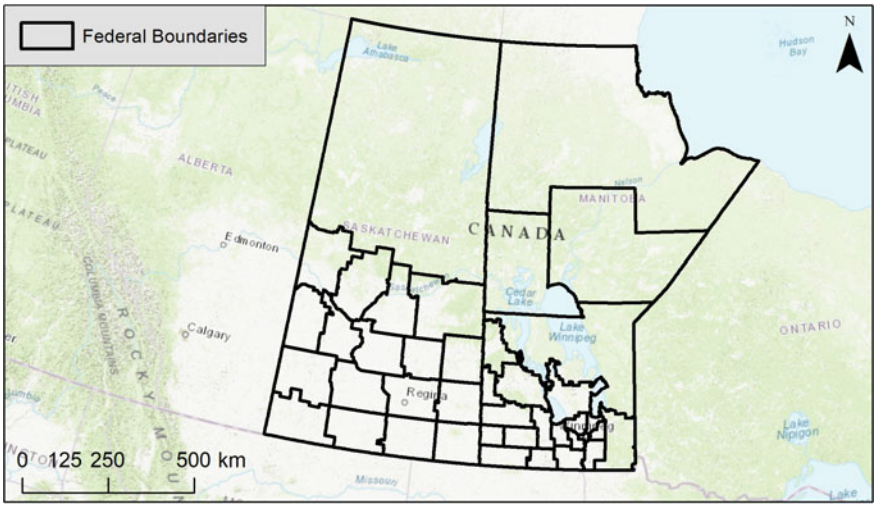

Fig. 1 Input tessellations—Federal Subdivision in Manitoba and Saskatchewan

2 Methodology

2.1 Study Area

The input tessellation to the recursive Thiessen polygon algorithm is shown in Fig. 1. This represents the Federal census Subdivisions for Saskatchewan and Manitoba. In order to determine whether optimization occurs in the interprovincial analysis, Federal Subdivisions in both Saskatchewan and Manitoba were considered separately, followed by the interprovincial analysis. One should note the distinct differences in shape and size of Federal census boundaries in the two provinces, along with the distinct large size of northern regions in both provinces. A total of 18 Federal Subdivisions are located in Saskatchewan, whereas 23 Federal Subdivisions are located in Manitoba. Federal census subdivisions are municipalities or areas that are treated as municipal equivalents for statistics purposes by the Federal government [23].

2.2 Data Acquisition and Pre-processing

The data obtained for this study is shown in Table 1, with the majority of the data being obtained directly from local government open data portals. Where required, data was clipped to the study area using ArcMap (v.10.5.1).

Table 1 Data type and acquisition

Province	Data	Data type	References
Saskatchewan	Federal subdivisions	Polygon	[24]
Saskatchewan	Roads	Line	[8]
Saskatchewan	Populated places	Point	[7]
Saskatchewan	Landfills	Point	[14]
Manitoba	Federal subdivisions	Polygon	[24]
Manitoba	Roads	Line	[8]
Manitoba	Populated places	Point	[7]
Manitoba	Landfills	Point	[10]

2.3 Workflow and Optimization

The workflow used in this study is presented in Fig. 2, after [21]. First, the centroid of each polygon in the input tessellation (shown in Fig. 1) is calculated. This is used as the seed for the development of the Thiessen polygon mesh. Once completed, the intersection of the vector datasets is calculated. Three different parameters were used to check the optimization of the mesh: landfills (LFs), populated places (Pop), and road length (road). In this case, that is the 'count' or sum of number of landfills and populated places, along with the sum of length of road within each respective polygon in the newly developed mesh. The vector data is also intersected with the input tessellation in order to compare the data. The standard deviation of the number of populated places and landfills (point datasets) and length of road (linear vector datasets) are then calculated for each of the new polygons in the Thiessen polygon mesh developed in the previous step. Optimization occurred when the standard deviation for each of the parameters (landfills, populated places, and road length) was minimized, which did not necessarily occur at the same iteration. In this study, ten iterations were carried out, though all optimization occurred well before the 10th iteration.

2.4 Thiessen Polygons

This study makes use of Thiessen polygons and the Centroidal Voronoi Tessellation algorithm (also known as Lloyd's Algorithm) to define the new boundaries of waste management regions. Thiessen (or Voronoi) polygons are derived from a topological relationship between a set of points in x, y two-dimensional space [20]. They are a common structure in geographic information systems, and are built using Delaunay triangulation in ArcMap (v. 10.5.1.). They have been applied in waste management studies [17, 21], geology [15], and transportation [3].

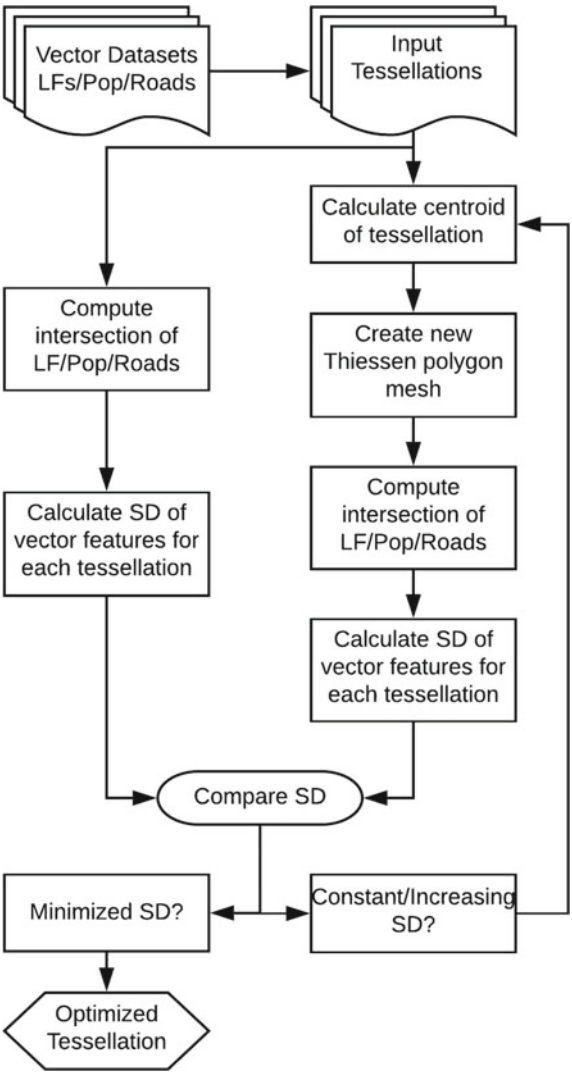

Fig. 2 Workflow used in this study. Adapted from [21]. (LFs: Landfill, Pop: Populated Places, Roads: Road length)

2.5 Minimization Parameters

In this study, similar to [21], standard deviation is used as the minimization parameter. It is defined in Eq. (1), [19].

$$SD = \sqrt{\frac{\sum_{i=1}^{n}(y_i - \overline{y})^2}{n-1}} \tag{1}$$

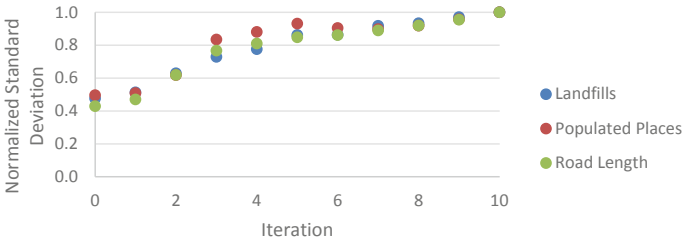

Fig. 3 Results of Thiessen polygon recursion on Federal Subdivisions in Saskatchewan

where y_i is any number in the set, $\bar{y}$ is the mean of the set, and n is the sample size (in this case, the number of polygons in the tessellation). The stopping criteria for the iterative process described in Sect. 2.3 is minimization of the SD, indicating that the allocation of chosen parameters (landfills, populated places, and roads) is as equal as possible in all subdivisions. Richter et al. [21] believe that this equalization will help to create practical and efficient waste management regions. Normalization (division of respective values against the maximum value in a set) was used in order to be able to compare results from different areas.

3 Results and Discussion

3.1 Saskatchewan

Results from the application of the recursive Thiessen polygon tool on Saskatchewan Federal Subdivisions yielded no optimization, and are reported in Richter et al. [21]. The implication is that the current topology of Saskatchewan Federal subdivisions is already optimized when considering landfills, populated places, and road length. The optimized tessellation is shown in Fig. 1 (Saskatchewan only) and is not included here for conciseness. Figure 3 shows the results of the optimization process, and the minimum SD occurring at the zeroth iteration, with a steady increase in the normalized SD as the number of iterations increased. Although Richter et al. [21] found that optimization did occur when Federal Subdivisions were split vertically and horizontally, the main finding was that specialized approaches were required to address the large remote northern division of the province.

3.2 Manitoba

Unlike Saskatchewan, optimization did occur in Manitoba, albeit at different iterations (IT) for roads/populated places (IT = 1) and landfills (IT = 5) as shown in

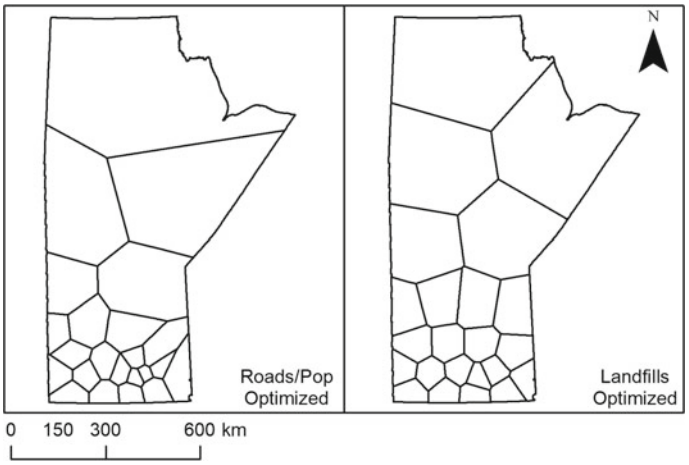

Fig. 4 Optimized regions in Manitoba

Fig. 4. Road and population tend to optimize at the same iteration, indicating that the two parameters may be more related to each other compared to landfills. This finding was also evident in Richter et al. [21]. The size distribution of the regions is similar to that of Saskatchewan, owing to the sparsely populated northern regions of the province. Like Saskatchewan, specialized approaches to waste management may be required in Northern and rural areas of Manitoba.

Figure 5 shows the normalized minimization of parameters. Unlike in Fig. 3, where each curve had roughly the same shape, we see variation in the shape of the curves in Manitoba, especially between landfills and populated places/roads. From Fig. 1, the input tessellation appears much more regular in Saskatchewan (uniform squares for the most part) compared to the more oddly shaped polygons present in Manitoba's input tessellation. It is likely that this causes the shape of the respective curves to be more volatile in Manitoba compared to Saskatchewan. As discussed by Richter et al. [21], the choice of best tessellation (in the event that optimization doesn't occur at the same iteration) would depend on which factor is more important: landfills, populated places, or roads. This is a decision that would have to be made

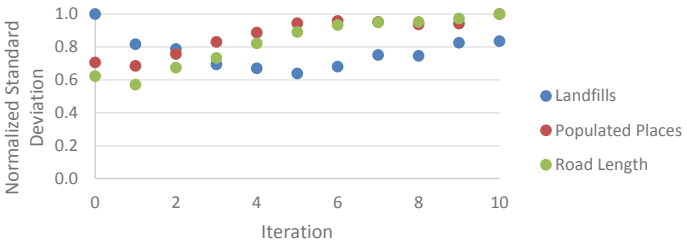

Fig. 5 Results of Thiessen polygon recursion on Federal Subdivisions in Manitoba

by policy makers in the respective province and would depend on a number of other factors.

Considering the relative magnitude of standard deviation however, we see that the SD is smaller in Saskatchewan (Fig. 3) compared to Manitoba (Fig. 5), indicating that the parameters are spread more equally (closer to the mean, less deviation) in Saskatchewan compared to Manitoba. This may indicate that the proposed 'optimized' tessellation for Saskatchewan is more optimized than that of Manitoba, an interesting finding considering that Saskatchewan Federal subdivisions were optimized at the input tessellation.

3.3 Interprovincial Analysis

Results from the interprovincial analysis indicate that, when considering Federal subdivisions in Saskatchewan and Manitoba concurrently, optimization occurs at the first iteration for all parameters. The optimized regions are shown in Fig. 6. It is interesting to note that the optimized tessellation for the inter-provincial analysis is quite different from the optimized tessellations for Saskatchewan and Manitoba considered separately. The total number of Federal census boundaries remains constant at 41, while there is some overlap of regions across the Saskatchewan-Manitoba border. This is especially pronounced in Northern regions, which may indicate that regionalization is more beneficial in Northern regions compared to the more populated southern regions. As an area of future work, it is suggested that sub-regions within the provinces be considered separately.

Fig. 6 Optimized inter-provincial regions

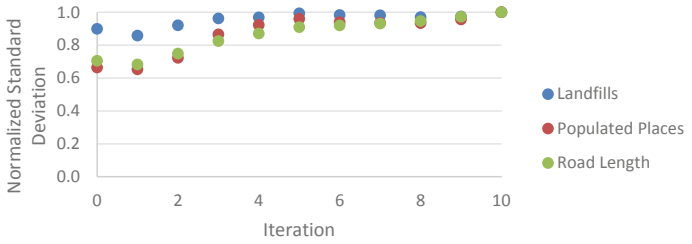

Fig. 7 Results of Thiessen Polygon recursion on Federal Subdivisions in an inter-provincial analysis

Table 2 Optimized absolute standard deviations

Parameter	SK	MB	Average	Inter-provincial
Landfills	7.72	5.13	6.43	11.30
Populated Places	66.56	61.63	64.10	72.55
Road Length	2286.29	1436.71	1861.50	2942.28

Figure 7 shows the normalized standard deviation for each iteration. We observe that the shape of the curves are generally similar, despite landfills being slightly elevated for iterations 0–4. For each different set of input tessellations (Saskatchewan, Manitoba, and interprovincial), the highest normalized standard deviation occurs at the tenth iteration, which may indicate that a more regular pattern in the input tessellation is likely to lead to optimization within ten iterations. In order to confirm this finding, a study should be done which uses input tessellations with a less regular pattern.

In order to determine whether the results from the interprovincial analysis are better than those from the separate analysis of Saskatchewan and Manitoba, non-normalized data are explored. A summary table of absolute standard deviation is shown in Table 2.

Given the similarities between Saskatchewan and Manitoba with respect to their waste generation characteristics, recycling behaviors, and management of waste systems, one would expect the potential benefits of using jointed waste facilities between the provinces. However, the results suggest that the standard deviations for Saskatchewan, Manitoba, and the average of both provinces considered separately (Average, shown in column 4 of Table 2) is less than that of the inter-provincial analysis for all of the parameters considered. This indicates that using this methodology, it is advantageous to create waste management regions that respect current provincial boundaries rather than an inter-provincial system, at least for Manitoba and Saskatchewan.

Richter et al. [21] noted that remote northern regions of Saskatchewan required a specialized approach to development of waste management regions. The authors believe that the same is true in this study, since both Manitoba and Saskatchewan are

similar in terms of distribution of population in the northern parts of the province. It is believed that a similar approach, whereby the interprovincial input tessellation is divided into vertical and horizontal subdivisions may improve the results of this interprovincial analysis.

3.4 Practical Implications and Areas of Future Work

This study attempts to optimize waste management regions from an interprovincial perspective for Manitoba and Saskatchewan. Future work involves the integration of waste policies and laws related to interprovincial movement of waste. Richter et al. [21] reported that the optimization results are sensitive to input tessellations. In a future study, the boundaries for the combined SK-MB region will be first re-defined before optimization. Furthermore, it may be possible to re-configure the number of regions in each province after applying the recursion algorithm. From the interprovincial analysis, it was observed that the newly defined waste management regions tended to 'cross-over' the provincial border more often in Northern regions compared to the southern regions. Studies have suggested that waste management in Northern Canadian regions is more complex [16] and may require specialized approaches [21].

An area of future work may include a temporal analysis of optimization. As noted in the study, Saskatchewan Federal Subdivisions did not optimize, while Manitoba did, possibly owing to temporal changes in populated places, roads, and landfill locations. Recall that Federal census subdivisions, as defined by Statistics Canada [23] are areas treated as municipal equivalents for statistical purposes. The fact that Saskatchewan Federal Subdivisions were already optimized using this methodology, while Manitoba Federal Subdivisions were not, may indicate temporal changes in these parameters over time. Region development should perhaps not be static, but rather a dynamic system that changes over time. It appears that interprovincial analysis is complex, and may benefit from other approaches, such as that presented by Li et al. [18]. In the future, techniques such as Minimum Distance Maximum Receiving (MDMR) may shed light on improvements to interprovincial movement of waste in Canada.

4 Conclusions

In this paper, a novel recursion algorithm first introduced by Richter et al. [21] is applied to an interprovincial analysis of waste management regions in Saskatchewan and Manitoba in order to optimize the system. The results suggest that when considering Saskatchewan alone, Federal census subdivisions are already optimized based on the distribution of landfills, populated places, and roads in the province. However, it appears that specialized approaches are required in the province, due to the remote

and rural nature in areas of the province. On the other hand, an optimized tessellation of waste management regions in Manitoba is presented, indicating that there is room for improvement with respect to waste management in Manitoba. The input tessellations for Saskatchewan and Manitoba are significantly different, indicating the input tessellation is important to the optimization process. Furthermore, when comparing results from Saskatchewan and Manitoba, it is observed that the standard deviation is smaller in Saskatchewan compared to Manitoba, indicating that the parameters are more equally spread in Saskatchewan. For the interprovincial analysis, an optimized tessellation is presented. However, the results show that it is best to create waste management regions that respect current provincial boundaries rather than an inter-provincial system, at least when considering Manitoba and Saskatchewan. A number of suggestions for future work are provided. It is believed that this work will help to drive and contribute to evidence-based waste policy in Canada.

Acknowledgements The research reported in this paper was supported by a grant from the Natural Sciences and Engineering Research Council of Canada (RGPIN-2019-06154) to the corresponding author, using computing equipment funded by FEROF at the University of Regina. The authors are grateful for their support. The views expressed herein are those of the writers and not necessarily those of our research and funding partners.

References

1. Adamides ED, Mitropoulos P, Giannikos I, Mitropoulos I (2009) A multi-methodological approach to the development of a regional solid waste management system. J Oper Res Soc 60(6):758–770
2. Agovino M, Crociata A, Sacco PL (2016) Location matters for pro-environmental behavior: a spatial Markov Chains approach to proximity effects in differentiated waste collection. Ann Reg Sci 56:295–315
3. Ai T, Yu W, He Y (2015) Generation of constrained network Voronoi diagram using linear tessellation and expansion method. Comput Environ Urban Syst 51:83–96
4. Bruce N, Asha AZ, Ng KTW (2016) Analysis of solid waste management systems in Alberta and British Columbia using provincial comparison. Can J Civ Eng 43:351–360
5. Chalkias C, Lasaridi K (2011) A GIS based model for the optimization of municipal solid waste collection: the case study of Nikea, Athens, Greece. WSEAS Trans Environ Dev 10(5):640–650
6. Constantino M, Gouveia L, Candida Mourao M, Catarina Nunes A (2015) The mixed capacitated arc routing problem with non-overlapping routes. Eur J Oper Res 244:445–456
7. Esri Canada (2014) Canada populated places. From https://www.arcgis.com/home/item.html?id¼49858f881b31c4187bd95c74ab46be44b. Accessed on 12 Dec 2019
8. Esri (2018) World street map. Accessed from https://www.arcgis.com/home/item
9. Government of Alberta (2018) Landfills. From https://www.alberta.ca/landfills.aspx. Accessed on 4 Nov 2019
10. Government of Manitoba (2020) Solid Waste Sites in Manitoba. From https://www.gov.mb.ca/sd/wastewise/landfill.html. Accessed on 18 Feb 2020
11. Government of Nova Scotia (1995) Solid waste-resource management strategy. From https://novascotia.ca/nse/waste/swrmstrategy.asp#section02. Accessed on 4 Nov 2019
12. Government of Saskatchewan (2016). Starting a Regional Waste Management System. From http://www.environment.gov.sk.ca/ on Accessed 18 Feb 2020

13. Government of Saskatchewan (2017) Saskatchewan Solid Waste Management Strategy—discussion paper. From http://publications.gov.sk.ca/documents/. Accessed on 4 Nov 2019
14. Government of Saskatchewan (2018) Landfills. From http://www.saskh2o.ca/landfills.asp. Accessed on 5 Mar 2019
15. Huang L, Huang S, Lai Z (2020) On the optimization of site investigation programs using centroidal Voronoi tessellations and random field theory. Comput Geotech 118:103331
16. Keske CMH, Mills M, Godfrey T, Tanguay L, Dicker J (2018) Waste management in remote rural communities across the Canadian North: Challenges and opportunities. Detritus 2:63–77
17. Khan MM, Vaezi M, Kumar A (2018) Optimal siting of solid waste-to-value-added facilities through a GIS-based assessment. Sci Total Environ 610–611:1065–1075
18. Li J, Song X, Yang D, Li B, Lu B (2020) Simulating the interprovincial movements of waste mobile phones in China based on the current disassembly capacity. J Clean Prod 244:118776
19. Mendenhall W, Sincich T (2007) Statistics for engineering and the sciences, 5th edn. Pearson Prentice Hall, Upper Saddle River
20. Mu L (2009) Thiessen polygon. International encyclopedia of human geography. Elsevier, Amsterdam, pp 231–236
21. Richter A, Ng KTW, Karimi N, Wu P, Kashani AH (2019) Optimization of waste management regions using recursive Thiessen polygons. J Clean Prod 234:85–96
22. Richter A, Ng KTW (2018) Landfill regionalization: a strategic move for all provinces? Technical short paper, Canadian Civil Engineer, "CIVIL" magazine. Can Soc Civil Eng 35(4):18–20
23. Statistics Canada (2011) Census dictionary—census subdivisions. Accessed from https://www12.statcan.gc.ca/census-recensement/2011/ref/dict/index-eng.cfm
24. Statistics Canada (2016) Census Boundary Files, p. 2011. Accessed from https://www12.statcan.gc.ca/census-recensement/2011/geo/bound-limit/bound-limit-2011-eng.cfm
25. Statistics Canada (2019) Table 38-10-0032-01 Disposal of waste, by source. https://doi.org/10.25318/3810003201-eng
26. Statistics Canada (2020a) Table 38-10-0033-01. Materials diverted, by source. https://doi.org/10.25318/3810003301-eng
27. Statistics Canada (2020b) Table 38-10-0032-01. Disposal of waste, by source. https://doi.org/10.25318/3810003201-eng
28. Statistics Canada (2020c) Table 38010-0036-01. Local Government Characteristics of the waste management industry. https://doi.org/10.25318/3810003601-eng
29. Sumathi VR, Natesan U, Sarkar C (2008) GIS-based approach for optimized siting of municipal solid waste landfill. Waste Manage 28(11):2146–2160
30. Wang Y, Ng KTW, Asha AZ (2016) Non-hazardous waste generation characteristics and recycling practices in Saskatchewan and Manitoba. Can J Mater Cycles Waste Manage 18:715–724

Stacking Different Spatial Statistics in a Novel Recursion Algorithm to Improve the Design of Waste Management Regions in Saskatchewan

A. Richter, K. T. W. Ng, and N. Karimi

1 Introduction and Literature Review

Canadians have one of the highest waste generation rates in the world, generating 973 kg/cap in 2016 [32, 33]. Landfilling continues to be the most prevalent choice for final disposal of waste in Canada [4, 36]. Low population density contributes, in part, to increased costs for waste management [23]. In 2016, Canadians paid $1.4 billion to collect and transport waste, accounting for 41.3% of total expenditure on all parts of the waste management system [34]. In Saskatchewan, expenditure on waste collection and transportation totalled $77 million [34].

Regionalization is the process of encouraging municipalities to work together and share resources to reduce costs and risks [12]. Regionalized waste management systems have been implemented in some Canadian provinces [10, 11] and these systems are common around the world [22, 35]. Regionalizing WMSs is a complex and politically challenging task, involving factors such as population density, costs, location of waste management infrastructure and environmental constraints [30].

The idea of regionalization has existed in Saskatchewan for quite some time, but not solely in the context of waste management. Stabler and Olfert [31] introduced a methodology to create labour market areas for economic regionalization of the province to improve the efficiency of municipal government systems. They noted that an inverse relationship existed between population density and region size. With respect to healthcare systems Marchildon [18] noted that the creation of health regions in the province was undertaken to save money and reallocate resources for preventive care measures. With respect to waste management, Bolton and Curtis [3] developed an environmental assessment method of siting landfills on a regional basis

A. Richter (✉) · K. T. W. Ng · N. Karimi
University of Regina, Saskatchewan, Canada
e-mail: richamy1@uregina.ca

S. Walbridge et al. (eds.), *Proceedings of the Canadian Society of Civil Engineering Annual Conference 2021*, Lecture Notes in Civil Engineering 249,
https://doi.org/10.1007/978-981-19-1061-6_14

in Saskatchewan, but noted that the highly autonomous nature of communities in the province made regional cooperation difficult.

Sectorizing, the process of diving a region into smaller parts [28], for administrative, political, or economic activities is common [7], and is important from both a planning and operational standpoint. Often the development of regions for these various uses is simply based on pre-existing natural or administrative boundaries and lacks a scientific and theoretical basis [27, 37]. Furthermore, when considering the design of regionalized waste management systems, geospatial dependency adds to the complex nature of the problem. In Canada, low population density [23], and other economic and social challenges in rural and remote northern communities [16, 17, 25] require approaches that differ from those in more populated areas.

Around the world, a small group of researchers have worked on the problem of best defining regions for waste management. Chalkias and Lasaridi [5] used spatial analysis to re-allocate bins to different sectors and therefore improve waste management collection efficiency. Adamides et al. [1] noted the importance that spatial analysis and topology played in their multi-methodological analysis and development of waste management regions. Using population distribution and estimates of waste generation, they developed efficient waste management regions. Other researchers have found that the design of regions and collection costs will vary depending on urban and rural areas [6], location and demographics [15], and country influences [21].

A large amount of research on regional co-operation has been carried out in Italy, likely due to the high population density and topographical differences in the country. Sarra et al. [29] used multi-stage data envelopment analysis to find the optimal dimensions for cooperation for waste collection services in Italy. It was found that the optimal number of inhabitants for this type of cooperation would not exceed 55,000 [29]. Agovino et al. [2] studied the performance of different Italian regions using data envelopment analysis. The results suggest that waste management performance is optimized when citizens and local governments act jointly. The results further indicate the importance of the topography and the local dimension of waste management in the country.

Richter et al. [27] applied Centroidal Voronoi Tessellation to develop waste management regions, thereby questioning the use of pre-existing administrative boundaries for waste management purposes. Centroidal Voronoi Tessellation relies on the geometric centroid of a region to create future iterations and tessellation development. There are, however, different spatial statistics that can be used in place of the geometric centroid to develop these tessellations. Furthermore, once optimization has been reached using one spatial statistics, other spatial statistics may be able to further optimize the tessellation, directly building on the prior optimization. The objectives of this study are to: (i) stack different spatial statistics (mean and median center) on top of the initial CVT algorithm and (ii) compare the results to those using only the CVT algorithm to determine if the stacking method proposed in this study can further improve the results of the CVT algorithm. The results from this study may help to further develop data driven regions for waste management in Saskatchewan and Canada.

2 Methodology

2.1 Study Area

In this study Transportation Planning Committee areas (TPCs) are used to investigate the ability of the so-called 'stacking' algorithm to better optimize waste management regions. First, the Centroidal Voronoi Tessellation (CVT) algorithm was applied to the transportation planning committees (shown in Fig. 1a). Optimization using the CVT algorithm has been reported in previous work [27]. The optimization results from the previous study suggest that landfills and populated places optimized at the fourth iteration (shown in Fig. 1b), while roads optimized at the first iteration (Fig. 1c). Area transportation planning committees have been used in Saskatchewan since the late 90's to help influence planning for transportation in the province [20]. There are 11 sub-regions in the area.

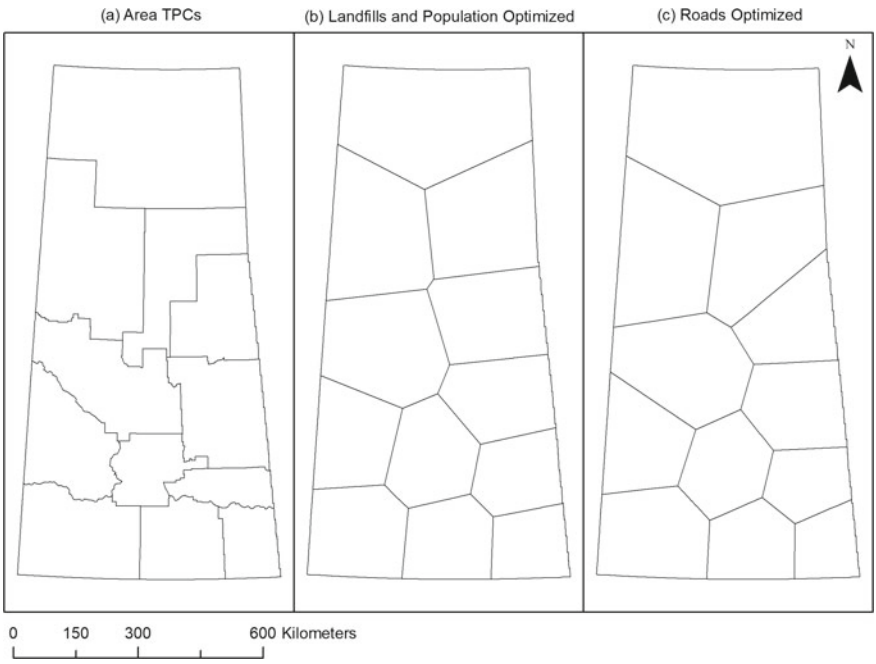

Fig. 1 **a** Area transportation planning committees (TPCs) prior to the CVT algorithm; and after applying the CVT algorithm to optimize for **b** landfills and population places, and **c** roads

Table 1 Data type and acquisition

Data	Data type	References
Area TPCs	Polygon	Derived from [14]
Roads	Line	Esri [8]
Populated places	Point	Esri Canada (2014)
Landfills	Point	Government of Saskatchewan [13]

2.2 Data Acquisition and Pre-Processing

The data obtained for this study is shown in Table 1, with the majority of the data being obtained directly from local government open data portals. Where required, data was clipped to the provincial boundary using ArcMap (v. 10.5.1).

2.3 Workflow and Spatial Statistics

The workflow for this study is similar to that used by Richter et al. [27]. In this study, the starting tessellations are not the original area transportation planning committees, but rather the tessellations that have already been optimized using CVT (Fig. 1b, c). Instead of using the geometric centroid (shown in Fig. 2b), used by Richter et al. [27], the mean and median center (shown in Fig. 2c, d) are applied. Mean Center is a point constructed from the average x and y coordinates for all input features within the study area. It is calculated using Eq. (1) [9]:

$$\overline{X} = \frac{\sum_{i=1}^{n} x_i}{n}, \overline{Y} = \frac{\sum_{i=1}^{n} y_i}{n} \quad (1)$$

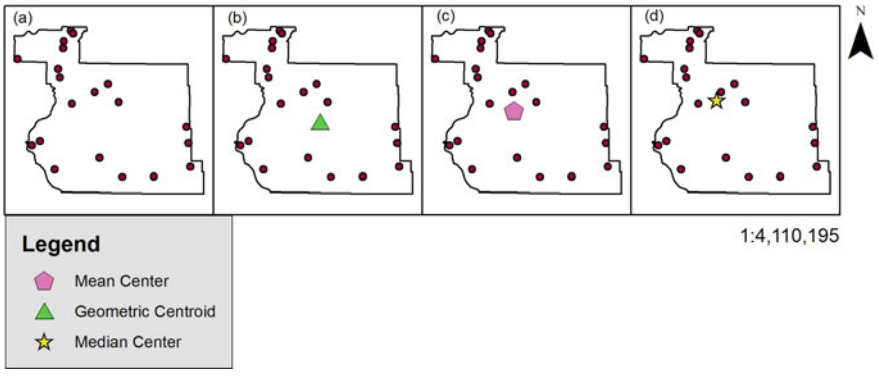

Fig. 2 **a** Graphical set of points for which, **b** geometric centroid, **c** mean center, and **d** median center are shown

where x_i, y_i are the coordinates for features i and n is the total number of features, and $\bar{X}$ and $\bar{Y}$ are the point coordinates of the averaged x and y coordinates in the set.

The median center is a measure of central tendency that minimized travel from itself to all other features in the dataset. The median center (d^t_i) is calculated iteratively, where at each step 't' in the algorithm, a candidate point (X^t, Y^t) is found, and then refined until it minimizes the Euclidean distance 'd' to all feature 'I' in the dataset [9]. Mathematically it is expressed by Eq. (2) [9].

$$d_i^t = \sqrt{(X_i - X^t)^2 + (Y_i - Y^t)^2} \tag{2}$$

Unlike the mean center (Eq. 1), the median center is robust to outliers [9]. Although the location of the mean and median centers are similar (Fig. 2c, d), median center accounts for travel distance, which may be important in the design of waste management regions for minimized transportation costs.

The maroon points shown in Fig. 2 represent the populated places dataset, used to calculate the mean and median center. The geometric centroid is independent of the dataset, and relies solely on boundary geometry, while both the mean and median center rely on the points and are independent of the boundary. For each sub-region in the tessellations (shown in Figs. 1b, c), the mean and median centers are calculated and used as input to the centroidal Voronoi tessellation algorithm. In other words, the spatial statistic that is calculated is used as the 'seed' to create a mesh of Thiessen polygons which are then clipped to the provincial boundary. This process is repeated until the optimization criteria (explained in the next section) are met.

2.4 Optimization Criteria and Minimization Parameters

Three different parameters were used to check the optimization of the mesh of Thiessen polygons: landfills (LFs), populated places (pop), and road length (road). The number of landfills and populated places, and the length of road within each created sub-region are calculated using the 'summarize within' tool in ArcMap (v. 10.5.1). The standard deviation of the number of landfill, populated places, and road length are calculated in order to compare the data to the results from the previous tessellation. Optimization occurs when the standard deviation for each of the parameters (landfills, populated places, and roads) are minimized. This does not necessarily occur at the same iteration. This optimization method was used in keeping with Richter et al. [27] who supposed that optimized regions were those where the spread of landfills, populated places, and roads were most equally spread across each region in the province.

Similar to Richter et al. [27], standard deviation is used as the minimization parameter. It is defined in Eq. (3) [19].

$$SD = \sqrt{\frac{\sum_{i=1}^{n}(y_i - \overline{y})^2}{n-1}} \tag{3}$$

where y_i is any number in the set, $\bar{y}$ is the mean of the set, and n is the sample size (in this case, the number of polygons in the tessellation).

3 Results and Discussion

3.1 Applying Mean Center to CVT Iteration 1

Recall from Fig. 1 that landfills and populated places were optimized at iteration 1. Applying the mean center spatial statistic to the tessellation shown in Fig. 1b yielded improvement from the CVT algorithm. The resulting decrease in optimization metrics (percent standard deviation, % SD) is shown in Fig. 3.

A percent decrease in percent standard deviation (% SD) of 5.2% was observed for landfills, 6.7% for populated places, and 2.2% for roads. Only three iterations using the mean center were required before increases in the % SD were observed. Results reported using another spatial statistic [24], the central feature, yielded much larger optimizations. We conclude that in this case, the stacking methodology proposed can further optimize the tessellations than the original CVT algorithm which uses the geometric centroid. However, the results suggest that the Central Feature Method proposed by Richter et al. [24] is still superior to the method proposed herein. Next, we look to see if further improvements can be made when using the tessellation where roads were optimized using the CVT approach.

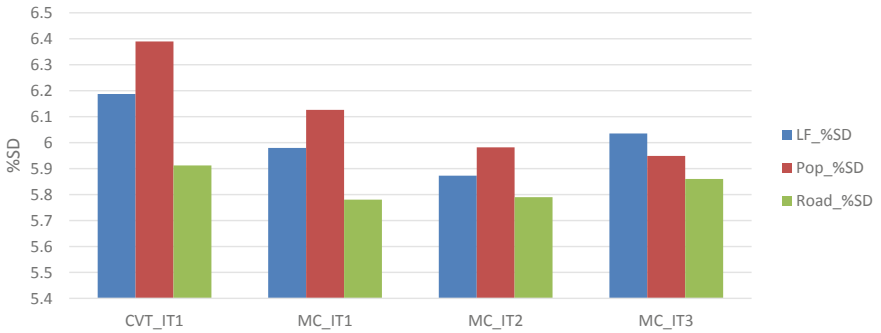

Fig. 3 Optimization results applying the mean center algorithm to the first CVT optimized tessellation

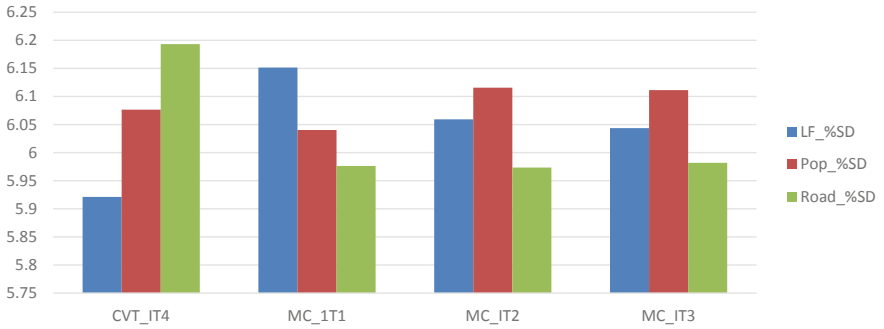

Fig. 4 Optimization results applying the mean center algorithm to the fourth CVT optimized tessellation

3.2 Applying Mean Center to CVT Iteration 4

Applying the mean center algorithm to the tessellation presented in Fig. 1c, where roads optimized using the CVT algorithm, a reduction in % SD is observed for roads, but not landfills or populated places. This is shown in Fig. 4, and similar to the results in Sect. 3.1, only 3 subsequent iterations are required. Recall that this application uses the optimized tessellation for roads, which occurred at the fourth iteration using the CVT algorithm. This is likely the reason that only roads are observed to optimize when applying the mean center to the tessellation, unlike in Sect. 3.1 where all parameters were observed to optimize further, despite the fact that the only landfills and populated places were CVT optimized in that tessellation. The proposed stacking algorithm may be more efficient at making improvements when the first algorithm used (in this case, CVT) optimizes at a relatively low (less than four in this case) number of iterations. Unfortunately, despite the reduction of % SD by 3.6%, the proposed stacking algorithm still fails to have better results that than of the central feature method proposed by Richter et al. [24]. Although the mean and median center spatial statics are similar (see Fig. 2), we will explore and compare the results using the median center in the next sections.

3.3 Applying Median Center to Iteration 1

When applying the Median Center spatial statistics to the optimized tessellation for landfills and populated places via CVT algorithm, shown in Fig. 1b, we note that all parameters are capable of further reduction in % SD. This is similar to those results presented in Sect. 3.1, however, more iterations are required (Fig. 5). Percent reductions in % SD of 10.3, 7.4, and 2.7 percent are observed for landfills, populated places, and roads, respectively. This indicates that although the use of the Median Center is more computationally demanding (ie. requires more iterations),

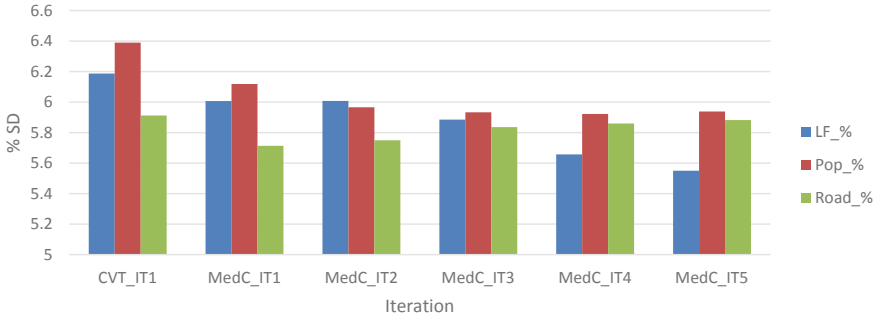

Fig. 5 Optimization results applying the median center algorithm to the first CVT optimized tessellation

it is better able to reduce the % SD, yielding more efficient waste management regions. One possible reason for this improvement in optimization is that the median center is robust to outliers and can better account for travel distances [9], which may be important for waste management problems [26]. Nonetheless, the proposed method once again fails to improve upon the results using the central feature method, presented by Richter et al. [24]. Next, we will investigate the results when considering the fourth.

3.4 Applying Median Center to Iteration 4

The results when applying the Median Center spatial statistic to the optimized tessellation for roads using the CVT method are more complex than those previously presented. Most notably is the amount of iterations required for optimization to occur, shown in Fig. 6. In total, 18 iterations were required before the algorithm

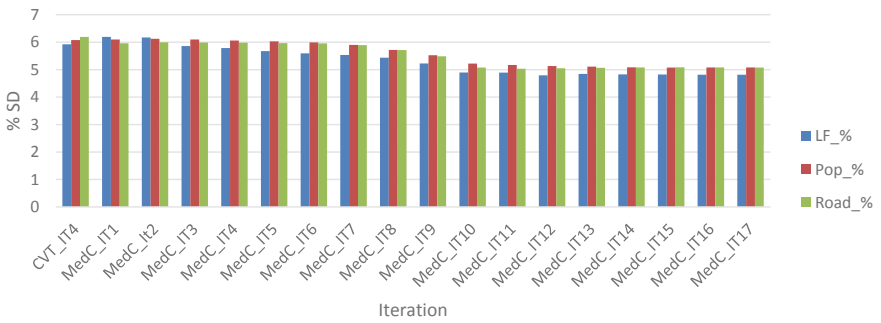

Fig. 6 Optimization results applying the median center algorithm to the fourth CVT optimized tessellation

optimized. Unlike the previous results which showed some improvement, but failed to improve upon the Central Feature Method proposed by Richter et al. [24], landfills were better able to be optimized. The absolute standard deviation for landfills using the method proposed in this study was 21.19, slightly less than the standard deviation of 22.08 for landfills using the central feature method [24]. Populated places has a similar SD of 177.91 (this method) compared to 177.63 using the central feature method. Roads continued to be better optimized by the central feature method (SD = 6675.56).

Figure 7 presents the different optimized tessellations for landfills in a side-by-side comparison. Despite the different path used to obtain the results, and the computational complexity and demand of the algorithm proposed in this paper, there are some striking resemblances between the two figures. Of special note is the resemblance of the northern divisions via the different methods. Larger differences in the tessellation are observed in the southern part of the province. These results suggest that there could be an infinite amount of different optimized tessellations through different optimization algorithms. The computational demand and efficiency of the algorithms may dictate their useability in future applications.

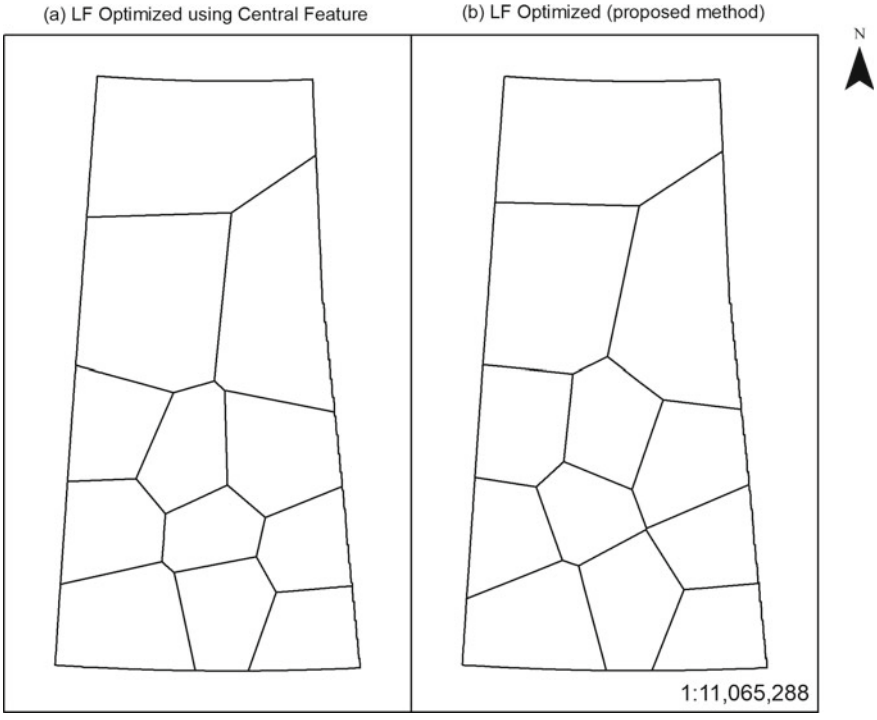

Fig. 7 Comparison of optimized tessellations for landfills using central feature method [24] and the newly proposed stacking algorithm

4 Conclusions

This paper continues to build on methods first presented by Richter et al. [27], by using different spatial statistics, namely the mean and median center, which are applied to previously optimized tessellations in order to see if these spatial statistics can further improve the optimization. The results show that the mean and median center spatial statistics are able to slightly improve the optimization compared to the results of CVT. However, in most cases they are unable to improve the results when comparing to the results presented by Richter et al. [24], which uses the central feature method. When applying the median center to the fourth iteration CVT optimized tessellation, however, landfills were better optimized (absolute SD = 21.19 compared to 22.08 using the central feature method). Comparing the two tessellations reveals two very similar tessellations, indicating that there may be an infinite number of optimized tessellations. The computational demand for the proposed method is much higher than that of the central feature method proposed by Richter et al. [24], indicating that the efficiency of algorithms may dictate their use in certain circumstances. In the future, using different types of population data that can better account for urban versus rural areas and differences in population density would be useful from an engineering and decision-making point of view. The results of this study have practical importance in the development of regions for waste management. However, they are widely applicable to many different regionalization problems.

Acknowledgements The research reported in this paper was supported by a grant from the Natural Sciences and Engineering Research Council of Canada (RGPIN-2019-06154) to the corresponding author, using computing equipment funded by FEROF at the University of Regina. The authors are grateful for their support. The views expressed herein are those of the writes and not necessarily those of our research and funding partners.

References

1. Adamides ED, Mitropoulos P, Giannikos I, Mitropoulos I (2009) A multi-methodological approach to the development of a regional solid waste management system. J Oper Res Soc 60(6):758–770. https://doi.org/10.1057/palgrave.jors.2602592
2. Agovino M, D'Uva M, Garofalo A, Marchesano K (2018) Waste management performance in Italian provinces: efficiency and spatial effects on local governments and citizen action. Ecol Ind 89:680–695. https://doi.org/10.1016/j.ecolind.2018.02.045
3. Bolton KF, Curtis FA (1990) An environmental assessment procedure for siting solid waste disposal sites. Environ Impact Assess Rev 10:285–296. https://doi.org/10.1016/0195-9255(90)90043-Y
4. Bruce N, Asha AZ, Ng KTW (2016) Analysis of solid waste management systems in Alberta and British Columbia using provincial comparison. Can J Civ Eng 43:351–360
5. Chalkias C, Lasaridi K (2009) A GIS based model for the optimization of municipal solid waste collection: the case study of Nikea, Athens, Greece. WSEAS Trans Environ Dev 10(5):640–650
6. Cubillos M, Wøhlk S (2020) Solution to the maximal covering tour problem for locating recycling drop-off stations. J Oper Res Soc. https://doi.org/10.1080/01605683.2020.1746701

7. Eagleson S, Escobar F, Williamson I (2002) Hierarchical spatial reasoning theory and GIS technology applied to the automated delineation of administrative boundaries. Comput Environ Urban Syst 26:185–200
8. Esri (2018) World Street Map. Accessed from https://www.arcgis.com/home/item
9. Esri (2020) Tool References, Spatial Statistics Toolbox. From https://pro.arcgis.com/en/pro-app/tool-reference/spatial-statistics/an-overview-of-the-spatial-statistics-toolbox.htm. Accessed on 9 Sep 2020
10. Government of Alberta (2018). Landfills. From https://www.alberta.ca/landfills.aspx. Accessed on 4 Nov 2019
11. Government of Nova Scotia (1995) Solid waste-resource management strategy. From https://novascotia.ca/nse/waste/swrmstrategy.asp#section02. Accessed on 4 Nov 2019
12. Government of Saskatchewan (2016) Starting a regional waste management system. From http://www.environment.gov.sk.ca/. Accessed on 18 Feb 2020
13. Government of Saskatchewan (2018) Landfills. From http://www.saskh20.ca/landfill.asp. Accessed on 5 Mar 2019
14. Government of Saskatchewan (2021) Area transportation planning committee map. https://geohub.saskatchewan.ca/datasets/area-transportation-planning-committe-map. Accessed 15 Feb 2021
15. Kayakutlu G, Daim T, Kunt M, Altay A, Suharto Y (2017) Scenarios for regional waste management. Renew Sustain Energy Rev 74:1323–1335. https://doi.org/10.1016/j.rser.2016.11.147
16. Keske CMH, Mills M, Godfrey T, Tanguay L, Dicker J (2018) Waste management in remote rural communities across the Canadian North: challenges and opportunities. Detritus 2:63–77. https://doi.org/10.31025/2611-4135/2018.13641
17. Lakhan C (2015) North of the 46° parallel: obstacles and challenges to recycling in Ontario's rural and northern communities. Waste Manage 44:216–226. https://doi.org/10.1016/j.wasman.2015.06.044
18. Marchildon GP (2006) Chapter in health services restructuring in Canada: new evidence and new directions. In: Beach CM, Chawkowski R, Deutsch J (eds)
19. Mendenhall W, Sincich T (2007) Statistics for engineering and the sciences, 5th edn. Pearson Prentice Hall, Upper Saddle River
20. Nixon D (1997) Government of Saskatchewan news release. Funding support program for area transportation planning committees. https://www.saskatchewan.ca/government/news-and-media/1997/december/18/funding-support-program-for-area-transportation-planning-committees. Accessed 15 Feb 2021
21. Noll D, Wiedenhofer D, Miatto A, Singh SJ (2019) The expansion of the built environment, waste generation and EU recycling targets on Samothraki, Greece: An island's dilemma. Resour Conserv Recycl 150:104405. https://doi.org/10.1016/j.resconrec.2019.104405
22. Okuda I, Thomson V (2007) Regionalization of municipal solid waste management in japan: balancing the proximity principle with economic efficiency. Environ Manage 40:12–19. https://doi.org/10.1007/s00267-006-0194-x
23. Richter A, Ng KTW (2018) Landfill regionalization: a strategic move for all provinces? Technical short paper, Canadian Civil Engineer, 'CIVIL' magazine. Can Soc Civil Eng 35(4):18–20
24. Richter A, Ng KTW, Karimi N, Li RYM (2021a) An iterative tessellation-based analytical approach to the design and planning of waste management regions. Article submitted for publication
25. Richter A, Ng KTW, Karimi N, Chang W (2021) Developing a novel proximity analysis approach for assessment of waste management cost efficiency in low population density regions. Sustain Cities Soc 102583. https://doi.org/10.1016/j.scs.2020.102583
26. Richter A, Ng KTW, Karimi N (2021b) Meshing Centroidal Voronoi Tessellation with spatial statistics to optimize waste management regions. J Clean Prod 295:126465. https://doi.org/10.1016/j.jclepro.2021.126465

27. Richter A, Ng KTW, Karimi N, Wu P, Kashani AH (2019) Optimization of waste management regions using recursive Thiessen polygons. J Clean Prod 234:85–96. https://doi.org/10.1016/j.jclepro.2019.06.178
28. Rodrigues AM, Ferreira JS (2015) Sectors and routes in solid waste collection. CIM Ser Math Sci 4. Springer. https://doi.org/10.1007/978-3-319-20328-7_20
29. Sarra A, Mazzocchitti M, Nissi E (2020) A methodological proposal to determine the optimal levels of inter-municipal cooperation in the organization of solid waste management systems. Waste Manage 115:56–64. https://doi.org/10.1016/j.wasman.2020.07.024
30. Shmelev SE, Powell JR (2006) Ecological-economic modelling for strategic regional waste management systems. Ecol Econ 59:115–130
31. Stabler J, Olfert R (2002) Functional economic areas of the Canadian Prairie Region. Study commissioned by Agriculture and Agrifood Canada. https://www.semanticscholar.org/paper/Functional-Economic-Areas-of-the-Canadian-Prairie-Stabler-Olfert/ae1b146253739adc86128ff6de2e84e113f2d135. Accessed 29 Dec 2020
32. Statistics Canada (2020a) Table 38-10-0033-01. Materials diverted, by source. https://doi.org/10.25318/3810003301-eng
33. Statistics Canada (2020b) Table 38-10-0032-01. Disposal of waste, by source. https://doi.org/10.25318/3810003201-eng
34. Statistics Canada (2020c) Table 38010-0036-01. Local Government Characteristics of the waste management industry. https://doi.org/10.25318/3810003601-eng
35. Wang C, Lin M, Lin C (2008) Factors influencing regional municipal solid waste management strategies. J Air Waste Manag Assoc 58(7):957–964. https://doi.org/10.3155/1047-3289.5-7-957
36. Wang Y, Ng KTW, Asha AZ (2016) Non-hazardous waste generation characteristics and recycling practices in Saskatchewan and Manitoba. Can J Mater Cycles Waste Manage 18:715–724
37. Zhang K, Yan H, Zeng H, Xin H, Tao T (2019) A practical multi-objective optimization sectorization model for water distribution network. Sci Total Environ 656:1401–1412. https://doi.org/10.1016/j.scitotenv.2018.11.273

Temporal and Spatial Assessment of Landfill Gas Emission Near the City of Regina Landfill

Nima Karimi, Amy Richter, and Kelvin Tsun Wai Ng

1 Introduction

Urbanization and population growth lead to an increase in solid waste generation worldwide. As an example, populated regions in the Caribbean and Latin America were responsible for generating around 131 million tons of waste by 2005 which is estimated to have a significant jump to around 179 million tons by 2030. Consequently, need for engineered landfills seems clearer than ever before [17]. On the other hand, there are countries like Germany that take new policies regarding 3R approaches (reduce, reuse, recycle) seriously and planned to end landfilling practice by 2020. Some developing countries like Brazil also increasing its separation and recycling rate both in municipalities and the private sector. On the other hand, increasing population lead to a significant increase in waste generation as well. It is also believed that larger countries with lower population densities are more likely to use landfills than countries with higher population densities due to lower average landfilling costs [17]. Considering the major countries in North America shows that Canada also has around 16 times more landfills per hundred thousand people compared to USA [4, 19]. Hence, landfilling is known as the first solution for Canada's solid waste. Therefore, landfills have to be designed in a way to prevent hazardous environmental effects [2, 20]. Even by aiming to minimize the environmental damage, there are hidden inherited threats in landfill practice which are regarded to be inevitable [1, 10, 11]. Such effects can be included but not limited to water resources contamination adjacent to landfills [12] and health issues for neighboring population [15]. In addition, one of the major concerns for such sites could be the excessive landfill gas (LFG) release which in turn may cause hazardous consequences as explosions [16].

N. Karimi (✉) · A. Richter · K. T. W. Ng
University of Regina, Regina, Canada
e-mail: NKG797@UREGINA.CA

S. Walbridge et al. (eds.), *Proceedings of the Canadian Society of Civil Engineering Annual Conference 2021*, Lecture Notes in Civil Engineering 249,
https://doi.org/10.1007/978-981-19-1061-6_15

LFG is the by-product of waste decomposition in landfills. The proportion of methane is around 50 percent of the entire LFG [3]. Methane basically comes from anaerobic decomposition stage after a provided environment which takes regularly less than one year. On the other hand, it could be more efficient if it can be captured, converted and used as an energy resource instead of being released to the atmosphere and be a part of local air pollution issue and global climate change [3].

Landfills should be monitored using in situ sampling for soil, water and released gases. Certainly, ground monitoring is cost and time consuming. This is where remote sensing imagery could be a suitable substitute for in-situ monitoring and has been vastly used in solid waste management within the recent years [7, 13, 14]. For example, [7] used night time light satellite imagery in extracting suitable regions for landfill sites. On the other hand, some literature used satellite images in defining the attributable environmental changes within the disposal sites. For example, [9] used land surface temperature (LST), normalized difference vegetation index (NDVI), soil adjusted vegetation index (SAVI) and modified soil adjusted vegetation index (MSAVI) to estimate the fluctuation of temperature as well as vegetation health. They found an increase around 4 degrees centigrade in temperature within the agricultural land adjacent to the disposal site and a drop in vegetation health due to the mentioned vegetation indices. Increased land surface temperature in landfills was also observed using remote sensing imagery in a local landfill in Glina, Romania [5].

For the current study, LST has been used to extract out probable methane release spots to properly and efficiently locate the gas extraction system within Regina Landfill. Since the association between methane emission and land surface temperature (LST) is estimated to be positive [6], LST could be used as a proxy in determining potential gas extraction spots [7, 8].

2 Methodology

For the current study, Regina Fleet Street landfill located in northeastern part of Regina, Saskatchewan is selected. With regard to the boundaries of the current landfill, the maximum occupied area is estimated to be 1,182,427 square meters. The exact location of landfill with regard to the coordination system and boundaries is shown in Fig. 1.

Details of the downloaded satellite imagery for the study area are shown in Table 1. The Landsat imagery was captured from February 5th to November 27th, 0–3 images per month and no images in January, June and December due to cloud cover and atmospheric haziness.

After downloading satellite imagery and clipping out the area of interest, land surface temperature was calculated using Landsat-8 handbook [18]. Based on the handbook, prior to the calculation of LST, TOA (top of atmosphere radiance), BT (brightness temperature), NDVI (normalized difference vegetation index), PV (proportion of vegetation) and e(emissivity) were extracted out using Eqs. (1)–(6).

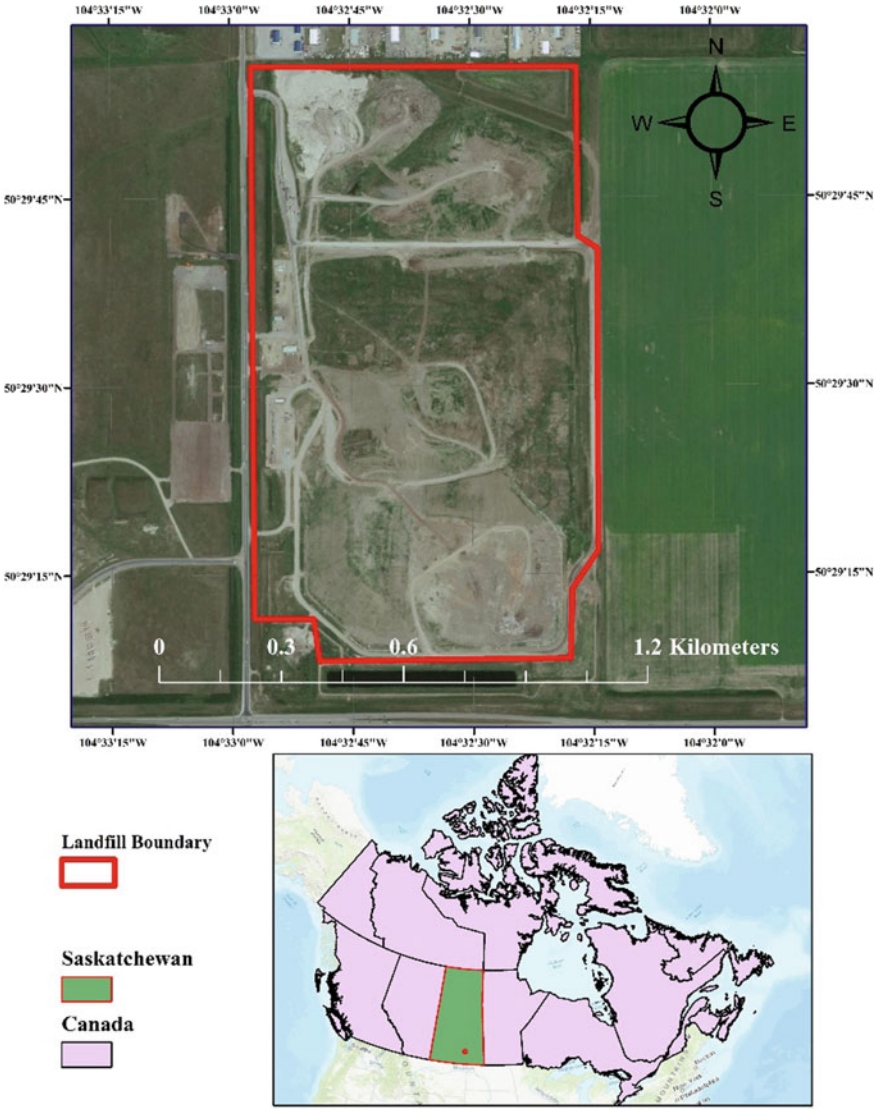

Fig. 1 Regina landfill boundaries and location in the province of Saskatchewan, Canada

$$L_\lambda = M_L \times Q_{Cal} + A_L \tag{1}$$

where

L_λ spectral radiance (watts/m^2 × sr × μm)

Table 1 Type of satellite imagery, location and date of images used in the current study

Satellite details and spatial resolution: Landsat 8 OLI (operational land imager) and TIRS (thermal infrared sensor) level-1 data products/30 × 30 m			
Path/Row	Captured date YYYY.MM.DD	Path/Row	Captured date YYYY.MM.DD
36/25	2018.02.05	36/25	2018.07.04
36/25	2018.02.20	36/25	2018.08.28
35/25	2018.03.20	35/25	2018.08.29
36/25	2018.04.17	35/25	2018.09.12
35/25	2018.05.01	36/25	2018.10.30
36/25	2018.05.02	35/25	2018.10.31
35/25	2018.05.16	35/25	2018.11.27

M_L Band-specific multiplicative rescaling factor for the band (RADIANCE_MULT_BAND_n, from the metadata of each downloaded Lansat8 scene)

A_L Radiance additive scaling factor for the band (RADIANCE_ADD_BAND_n, from the metadata)

Q_{cal} Level 1-pixel value in DN.

Using the computed spectral radiance, the BT is then computed:

$$\mathrm{BT} = \frac{K_2}{\ln\left(\frac{K_1}{L_\lambda} + 1\right)} \tag{2}$$

where

BT Temperature in kelvin where:

L_λ TOA spectral radiance (Watts/(m^2 × srad × μm))

K_1 Band-specific thermal conversion constant from the metadata (K1_CONSTANT_BAND_x, where x is the thermal band number)

K_2 Band-specific thermal conversion constant from the metadata (K2_CONSTANT_BAND_x, where x is the thermal band number)".

$$\mathrm{NDVI} = \frac{Band5(near\ infrared\ band) - Band4(red\ band)}{Band5(near\ infrared\ band) + Band4(red\ band)} \tag{3}$$

$$\mathrm{PV} = \left(\frac{NDVI - NDVImin}{NDVImax - NDVI\,min}\right)^2 \tag{4}$$

$$\mathrm{Emissivity(e)} = 0.004 \times \mathrm{PV} + 0.986 \tag{5}$$

$$\mathrm{LST} = \frac{BT}{1 + \left(\frac{\lambda \times BT}{\rho}\right) \times \ln(e)} \tag{6}$$

where, λ, is equal to 10.8 μm which is the centre of thermal band wavelength. Reflectance (ρ) is related to Boltzmann's constant (σ), Planck's constant (h), and speed of light (c) as follows:

$$\rho = \frac{h \times c}{\sigma\left(1.438 \times 10^{-2} m \cdot k\right)} \tag{7}$$

After calculating LST, the sites with increased surface temperature separated from rest of the landfill based on one standard deviation. Sites with surface temperature higher than (Average + 1STDEV) have LST values thatare higher than over 80 percent of the landfill. In other words, such sites assumed to be suitable representative for fugitive emissions. Therefore, areas with LST values over (Average + 1STDEV) were reclassified as 1; and the remaining areas were set to 0. Finally, 14 binary maps were overlaid and provided an integer map that its values range between 0 and 14. Higher values show the higher frequency of continuous higher relative temperatures and higher probability of being a methane flux source. A schematic map of the entire procedure is shown in Fig. 2.

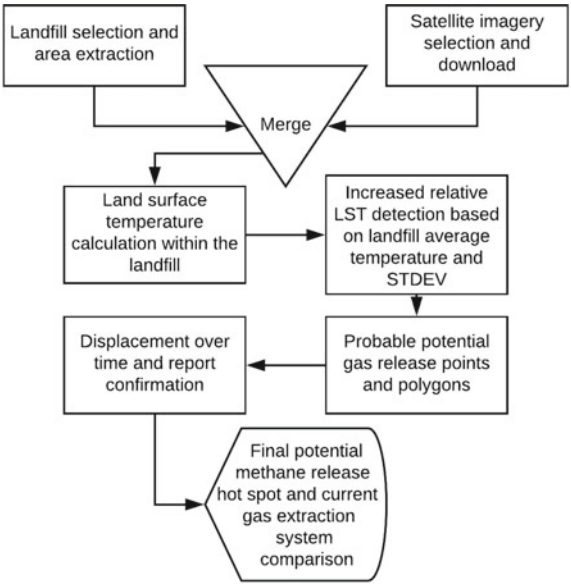

Fig. 2 Entire process of the current study

3 Results and Discussion

Since regions with higher LST were aimed to be filtered from the lower ones, values over (average + 1standard deviation) were separated accordingly and shown in Fig. 3. Lowest estimated temperature is around -20 °C for November whilst the highest one was recorded for August which is over 30 °C. A considerable temperature difference (around 10 degrees centigrade) between two adjacent days occurred on 30th and 31st October which could be probably local temperature variations.

Final LST map for 4 scenes as the representatives of all seasons and 14 images (Table1) are shown in Fig. 4. For winter, there is a relative increase in LST at the southern central part that was drawn to the southern western parts with lower temperatures. By going into the warmer seasons, for example in the spring season, the northern central part also was detected as one of the probable methane sources. The pattern of southern detected region also was shrunk and moved to southern edges of the landfill. The STDEV for temperature changes in the winter was calculated to be 0.77 degree centigrade whilst in the spring time it was 2.86 degree centigrade. In other words, the lower ranges of variation (below 1 centigrade) probably couldn't be enough to differentiate relative higher surface temperatures. In summer and fall seasons, the same pattern of relative higher temperatures was recorded for southern and northern central part of the landfill and these sources have been linked through the eastern edge of landfill. Not only the source of methane for landfill, but also the location of the piled solid waste can be recognized by LST pattern.

As it is shown in Fig. 4 frequency of the occurrence (FO) map, the central part of landfill was covered with vegetation areas. At the same time, there are visible access roads to the northern and southern central parts of the landfill which could be the path of trucks to unload waste along those detected sites. Ultimately, the FO map shows the consistency of relative increased temperature for sources. Due to this map, the major source for methane release is southern central and western region along with north central eastern region. By comparison, the detected northern region has a

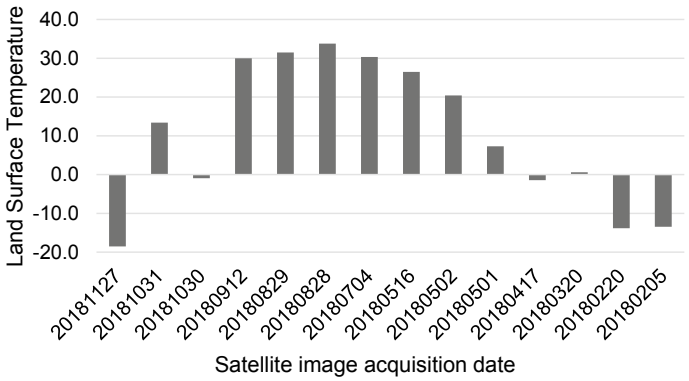

Fig. 3 Values of land surface temperature + STDEV acquired for all 14 dates within Regina landfill

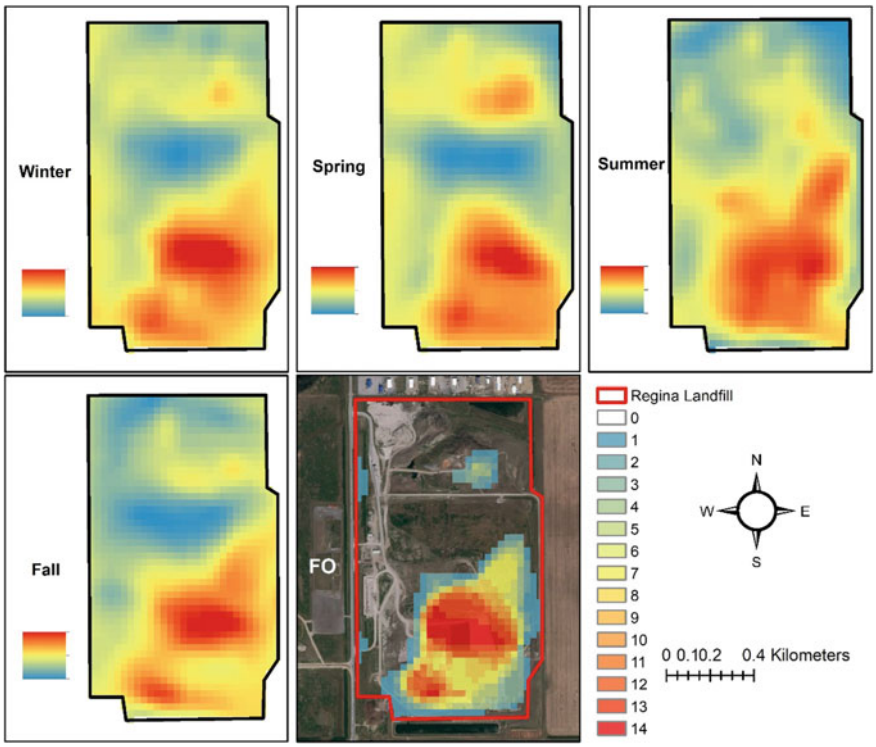

Fig. 4 Location of relatively high surface temperature within Regina landfill for four seasons and FO (frequency of occurrence) map that shows the major detected sources of methane

lower FO than the southern one. This could be due to the aging, type and volume of waste. Since the methane emissions occur mostly due to the anaerobic decomposition process for organic materials and it takes a relatively longer time than the aerobic process, the southern part of landfill may fill earlier with a higher volume and contain more organic materials than the northern part. This algorithm also could be used in determining the capped (covered) and active sites of the landfills since capped ones are filled earlier and may have higher LST.

4 Conclusion

In the current study, remote sensing imagery used to extract LST and monitor its variation within Regina landfill. LST used to detect methane sources due to high association between these two parameters. seasonal LST shows somehow similar location of methane sources with negligible displacements. In order to take all LST into account, relatively high surface temperature locations were separated from the

rest of the landfill and reclassified as one. Summation of reclassified images shows pretty much the same results as seasonal LSTs. The FO map discovered two major sources located in the southern central-western and northern central eastern regions. The FO for southern part (14) doubled the ones located in the northern sites (7). It is believed that higher FO could be probably because of solid waste maturity, high organic proportion and the higher volume of piled waste. Finally, the proposed method could be used as a primary estimation factor for designing a gas extraction network in an efficient way.

Acknowledgements The research reported in this paper was supported by a grant from the Natural Sciences and Engineering Research Council of Canada (RGPIN-2019-06154) to the third author (K.T.W. Ng), using computing equipment funded by the FEROF at the University of Regina. The authors are grateful for their support. The views expressed herein are those of the writers and not necessarily those of our research and funding partners.

References

1. Butt TE, Lockley E, Oduyemi KO (2008) Risk assessment of landfill disposal sites–state of the art. Waste Manage 28:952–964
2. Cointreau S (2006) Occupational and environmental health issues of solid waste management: special emphasis on middle-and lower-income countries. Urban papers, 2 pages?
3. EPA (environmental protection agency) (2020) Basic information about landfill gas from https://www.epa.gov/lmop/basic-information-about-landfill-gas. Retrieved by 24 Feb 2020
4. Government of Saskatchewan (2017) Saskatchewan solid waste management strategy – discussion paper March 2017. Accessed on http://publications.gov.sk.ca/documents/66/97825-Solid%20Waste%20Management%20Strategy%20Discussion%20Paper.pdf by 25 Mar 2022
5. Iacoboaea C, Petrescu F (2013) Landfill monitoring using remote sensing: a case study of Glina, Romania. Waste Manage Res 31:1075–1080
6. Javadinejad S, Eslamian S, Ostad-Ali-Askari K (2019) Investigation of monthly and seasonal changes of methane gas with respect to climate change using satellite data. Appl Water Sci 9:180
7. Karimi N, Richter A, Ng KTW (2020) Siting and ranking municipal landfill sites in regional scale using nighttime satellite imagery. J Environ Manage 256:109942
8. Karimi N, Ng KTW, Richter A, Williams J, Ibrahim H (2021) Thermal heterogeneity in the proximity of municipal solid waste landfills on forest and agricultural lands. J Environ Manage Elsevier. Manuscript ID.: JEMA-D-20-09480R1
9. Mahmood K, Batool SA, Chaudhry MN (2016) Studying bio-thermal effects at and around MSW dumps using satellite remote sensing and GIS. Waste Manage 55:118–128
10. Mahmood K, Batool A, Faizi F, Chaudhry MN, Ul-Haq Z, Rana AD, Tariq S (2017) Bio-thermal effects of open dumps on surroundings detected by remote sensing—influence of geographical conditions. Ecol Ind 82:131–142
11. Manfredi S, Tonini D, Christensen TH (2010) Contribution of individual waste fractions to the environmental impacts from landfilling of municipal solid waste. Waste Manage 30:433–440
12. Pasalari H, Farzadkia M, Gholami M, Emamjomeh MM (2019) Management of landfill leachate in Iran: valorization, characteristics, and environmental approaches. Environ Chem Lett 17:335–348
13. Richter A, Ng KTW, Karimi N (2019) A data driven technique applying GIS, and remote sensing to rank locations for waste disposal site expansion. Resour Conserv Recycl 149:352–362

14. Shaker A, Faisal K, El-Ashmawy N, Yan W (2010) Effectiveness of using remote sensing techniques in monitoring landfill sites using multi-temporal Landsat satellite data. Al-Azhar Univ Eng J 5:542–551
15. Tansel B, Inanloo B (2019) Odor impact zones around landfills: delineation based on atmospheric conditions and land use characteristics. Waste Manage 88:39–47
16. Toro R, Morales L (2018) Landfill fire and airborne aerosols in a large city: lessons learned and future needs. Air Qual Atmos Health 11:111–121
17. UN, 2020. Waste management from https://www.un.org/esa/dsd/resources/res_pdfs/publications/trends/trends_Chemicals_mining_transport_waste/ch4_waste_management.pdf. Retrieved by 24 Feb 2020
18. USGS (2020) Calculating land surface temperature from Landsat imagery, section 5 conversion of DNs to physical units; Landsat 8 (L8) data users handbook from https://www.usgs.gov/media/files/landsat-8-data-users-handbook. Retrieved by 23 Feb 2020
19. University of Michigan (2017) Municipal solid waste. Center for sustainable systems—university of Michigan. Accessed from: http://css.umich.edu/factsheets/municipal-solidwaste-factsheet. On 8 Sept 2018
20. Vergara SE, Tchobanoglous G (2012) Municipal solid waste and the environment: a global perspective. Annu Rev Environ Resour 37:277–309

Environmental and Economic Assessment of Municipal Landfill Locations in Saskatchewan and Manitoba

Karimi Nima, Richter Amy, and Kelvin Tsun Wai Ng

1 Introduction

Canada is using landfills as the most regular method for waste disposal [13, 21]. From 2002 to 2016, the entire amount of solid waste that collected in Canada had 11% or 3.5 million tonnes increase. On the other hand, diversion rate also had a relative increase around 39% or 2.9 million tonnes. Thus, increased rate of disposal (tonnage) overweighs diversion rate, which consequently lead to an increase in landfilling practice [23]. It is also verified that landfilling is the first selection for solid waste treatment in Prairie Provinces of Canada [20]. Particularly, the number of landfills per hundred thousand people is around 7.9 [7], which is a considerable amount compare to 0.5 in US reported by 2015 [29].

Siting, managing and monitoring engineered landfills could be of major concern in Prairie Provinces of Canada. Regarding to potential hazardous impacts of landfills in many environmental, economical and societal aspects, site suitability should be implemented to consider the best places in locating such facilities. Since many decision factors are engaged to select a better location, failure of such process could result in unfavorable issues including adjacent soil and aquifer pollution from landfills leachate [19], uncontrolled toxic gas emission [2, 24] and health and aesthetic issues for neighboring inhabitants [5, 25].

Due to all those concerns, a number of approaches were taken into action for landfill site selection. This includes analytic hierarchy process (AHP) and fuzzification techniques implemented to prioritize and normalize the output layers [3, 6, 16]. Furthermore, a major number of literatures applying Geographical information system (GIS) with AHP and generally MCDM (Multi Criteria Decision Making) functions has increased during the recent years [1, 12, 16]. For example, Kamdar

K. Nima (✉) · R. Amy · K. T. W. Ng
University of Regina, Regina, Canada
e-mail: NKG797@UREGINA.CA

S. Walbridge et al. (eds.), *Proceedings of the Canadian Society of Civil Engineering Annual Conference 2021*, Lecture Notes in Civil Engineering 249,
https://doi.org/10.1007/978-981-19-1061-6_16

et al. [12] combined morphological, environmental and societal parameters to obtain the best possible sites for landfilling, Kamdar et al. [12] used GIS and AHP to assess their data accessed from online portals and governmental organizations. The main objective of current study is to estimate whether the active landfill sites in both Saskatchewan and Manitoba provinces are well located considering major environmental and economic issues or not. It is believed that comparing these two provinces may clarify their potential weaknesses and help policy makers to focus on some specific parameters that are being underweighted so far. On the other hand, current study makes the best use of night time light satellite imagery in defining populated areas rather than using authorized predefined boundaries for urban areas. This application can clearly detect active anthropogenic sites which may remain hidden in making decisions in favour of human being.

2 Methodology

For current study, two Prairie Provinces namely Saskatchewan and Manitoba that are located in central part of Canada have been analyzed. Saskatchewan has borders with Alberta from the west and Manitoba from the east. Most of its southern lands covered by wheat agricultural areas and prairies whilst some forest lands covered the northern parts. Its population is around 1,178,657 by the end of September 2019 which shows about one percent increase compare to its past year [10]. Manitoba located at the eastern side of Saskatchewan with a population of 1,360,396 as of 2019 and its population density is around 2 people per square kilometer. Its largest city is Winnipeg with a population of 665,000. Northern part of it mostly covered by forest land whilst the southern part of it covered with scrublands, savannas and croplands. Figure 1a shows the location of both provinces and Fig. 1b shows the precise land use classification system in these two provinces. These classes obtained from Collection 6 MODIS Land Cover namely MCD12Q [26]. Details for classification systems can be found from mcd12-user guide, V6 [27].

Since protected areas are those reserved for purposes like saving biodiversity and nature, forest lands could be considered as a part of it [30]. Forest lands and water bodies separated from MODIS classification system.

All mentioned three factors as urban areas, protected areas and water bodies detected to assign a buffer zone for further protection whilst land surface temperature functions individually and suitable zones are the ones with higher recorded surface temperature. In other words, operating in landfill sites that are more likely to freeze are less favorable and may increase the costs which in turn couldn't be economically feasible [3, 16]. Similar siting approach, using urban areas, protected areas; and water bodies, were implemented in the literature [13, 14].

Land surface temperature (LST) retrieved from Collection-6 MODIS Land Surface Temperature Product. This product provides mean monthly pixel based LST by 200 $\times$ 200 km tiles and with a spatial resolution of around 5600 m [17]. For current study, LST downloaded for July 2019. The entire area of interest (province

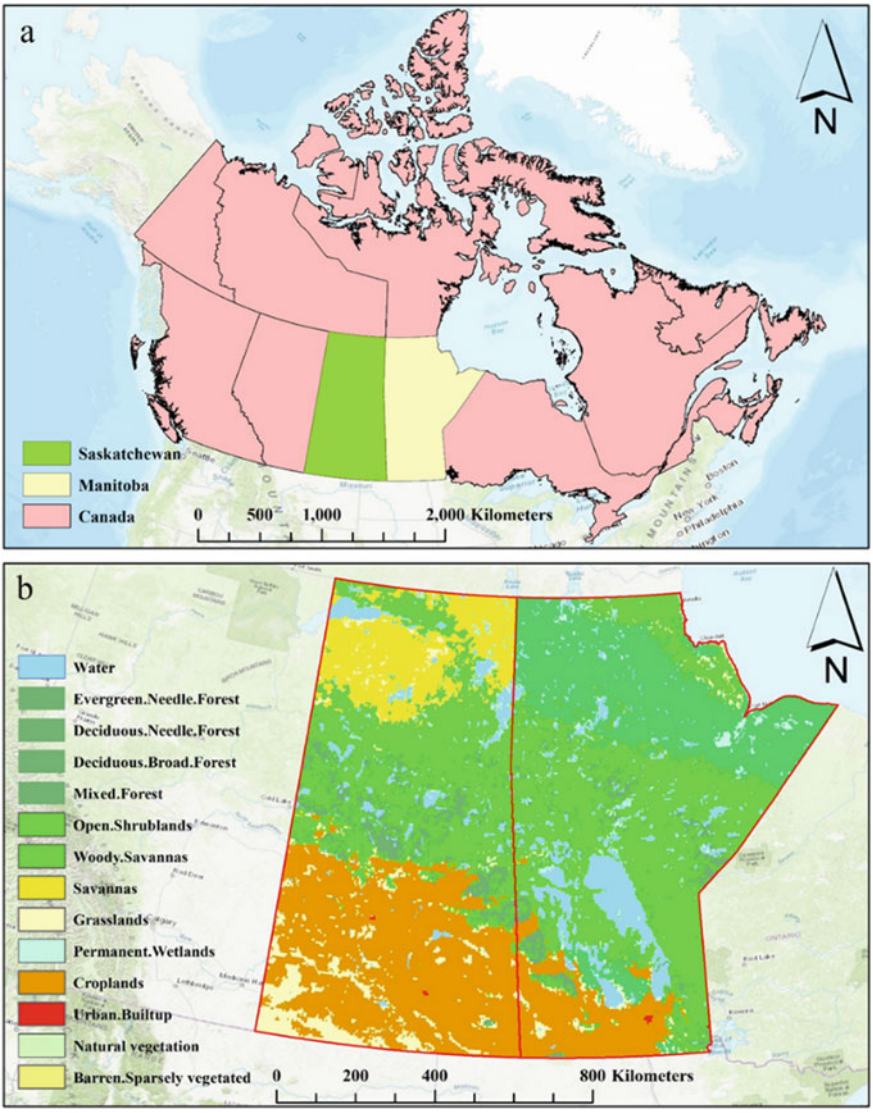

Fig. 1 **a** Study area covers the prairie provinces of Canada namely Saskatchewan and Manitoba, **b** separate detailed classes for Modis MCD12Q classification of two provinces

of Saskatchewan and Manitoba) is covered within 8 tiles. These tiles then mosaicked to an aggregated unit layer. Final layer DN values changed to regular land surface temperature in centigrade using Eq. (1) (MODIS 11 user guide 2020).

$$\text{LST in centigrade} = (\text{DN values from MOD11B3} - \text{v006} \times 0.02) - 273.15 \quad (1)$$

The basic circumstance in developing a multi criteria decision making tool is assigning membership grade for each individual layer. This membership grade is higher when the site is far away from a predefined under risk environment and thus would be recognized as suitable. On the other hand, it is prevented to construct a landfill up to a certain adjacent distance. This distance may vary based on locations and regulations. For current study, prevented distance for landfill construction selected to be 1000, 500 and 1000 m for urban, protected areas and water resources respectively [13]. Provided four fuzzified layers that ranges from 0 to 1 were overlaid with equal 0.25 weight to create the final rasterized suitability map, called as simple additive weighing method-SAW [15]. Since raster-based map couldn't be practical for defining the level of suitability for current active landfills, it is changed to regional suitability map. The number of regions were selected by the number of populated points. These points were defined earlier in nighttime light time series image as lighter regions. Conversion of points to polygons (regions) were done by using Thiessen polygons [4].

Location of all active landfills in Saskatchewan and Manitoba retrieved from government of Saskatchewan and Manitoba respectively [8, 9]. The entire process of current study shown in Fig. 2.

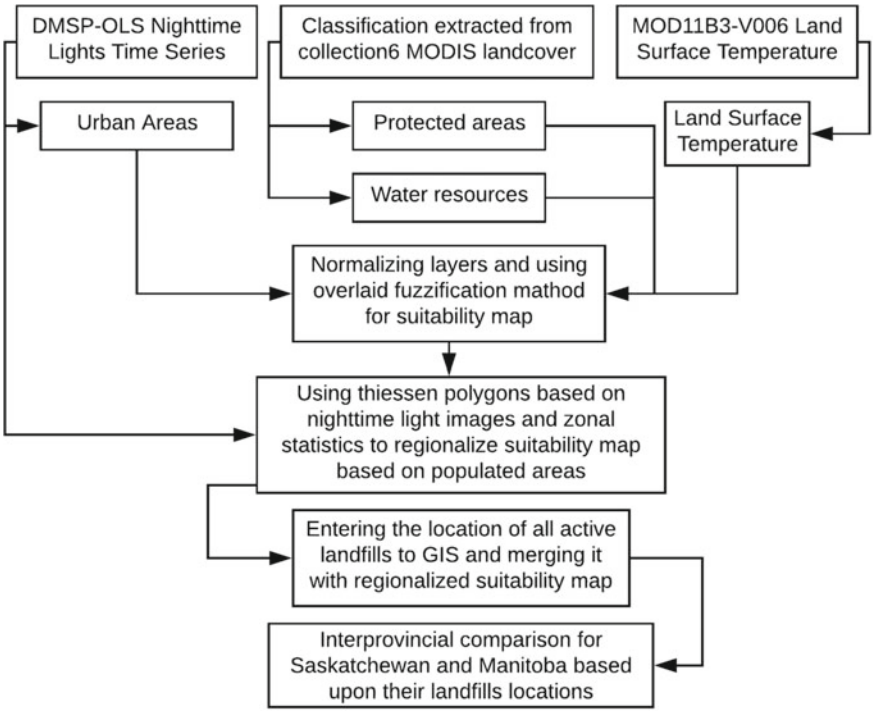

Fig. 2 A schematic flowchart of total procedure for current study

3 Results and Discussion

As shown in Fig. 3, since there is no landfill that its suitability drops below 0.75, both provinces are likely operating satisfactorily. Due to relative interprovincial comparison, Manitoba located its landfills in better places compare to Saskatchewan as 87% of its landfills' suitability ranking is above 0.9 and located at southern central part of province. Most of these parts covered with grassland and croplands, are away from protected areas and water resources that located in northern and central part of Manitoba respectively. On the contrary, the landfills that their suitability range from 0.8 to 0.9 located mostly in south eastern part of Saskatchewan. A strip of mixed forest and shrub lands which considered as protected areas drawn from central west to east of Saskatchewan that could be the reason of dropped suitability below 0.8 for this region. Higher suitability ranking for landfills in Manitoba compare to Saskatchewan in this study has been rooted in four decisive factors. In other words, summation of circumstances provides better sites within Manitoba for managers to locate their landfills. Presence of two major cities in Saskatchewan (Regina and Saskatoon) compare to one in Manitoba (Winnipeg) also could be another factor in dropping overall ranking of landfills in Saskatchewan while they have to be far off from urban areas. In furtherance, built up areas originates from night time light maps and the lighter areas, the

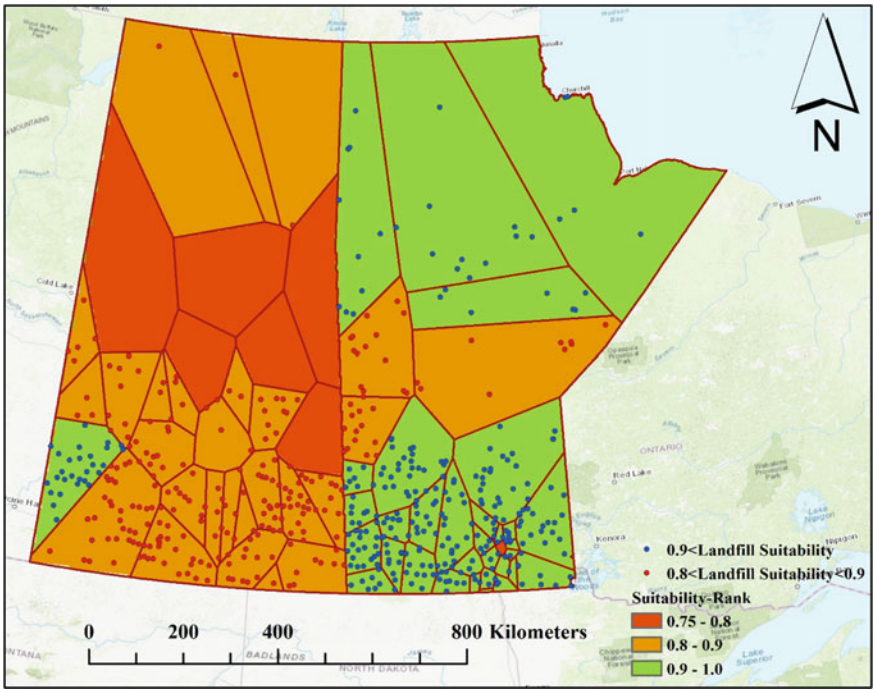

Fig. 3 Suitability map of active landfills in Provinces of Saskatchewan and Manitoba

more decrease in ranking for landfills that are in vicinity of such sites. Therefore, it could also be implied that there are many hidden populated regions in Saskatchewan rather than Manitoba and they naturally may locate their local landfills close to them for a better accessibility, which in turn results in decreased suitability for landfills. Suitability over 0.90 in province of Saskatchewan belongs to a region that located in southwestern part and include 9.3% of the entire landfill in province. This region is far away from protected areas, water resources, urban areas and may have had higher relative surface temperature.

Despite the results of current study that suggests the more remote regions as the more suitable regions, additional factors such as accessibility should be taken into account, since collected solid waste have to be transferred properly through road network to their final landfill sites. In other words, without any provided accessibility, it may increase the primary costs for infrastructure which in turn may not be interest of decision makers and managers.

With that being mentioned, closer regions to road network may have had higher suitability score, whilst closest regions couldn't be suitable because of aesthetic, safety and road obstruction issues. Hence, a monotonic suitability algorithm has to be defined for such parameters that is out of scope of current study. Thus, there are several other major factors imbedded in landfilling practice to make the most feasible decisions.

Figure 3 shows that night time light imagery is functioning good in separating populated regions. The association between the number of polygons (higher in southern part and lower in northern part for both provinces) and the density of landfills (higher in southern and lower in northern part) implies that populated regions locate their landfills closer to themselves. In furtherance, there are separate polygons in central part of Saskatchewan which shows that populated regions located in central parts, but there are no detected landfills in these polygons. Therefore, these populations may either transfer their solid waste to the closest southern landfills or use another alternative way such as illegal dumpsites for their solid waste which is not registered as an engineered landfill.

4 Conclusion

A multi criteria decision making tool used in conjunction with fuzzification method to rank the site suitability of current landfills in provinces of Saskatchewan and Manitoba. In addition, satellite imagery used for the first time in determining urban and built-up areas and it is believed that such method could bring more authentic results rather than classification results. The results suggest that such methods could be applied in coarser scales to compare the overall score of all landfills and bring up the most suitable sites. Higher suitability ranking belongs to those that are far off from protected areas (mixed forest and shrub lands), water resources, populated regions and with higher land surface temperature. These parameters are highly satisfied in landfills that are located in southern part of Manitoba. Central parts of both provinces

known to be relatively low suitable compare to the rest of them. The reason behind it could be interpreted differently. For example, water resources in central part of Manitoba may lower down the suitability whilst intensive forest lands in Saskatchewan may be the dominant factor in decreasing the overall suitability. Thus, according to findings, more parameters should be added to environmental and economical criteria as decisive factors to make much more feasible comparisons.

Acknowledgements The research reported in this paper was supported by a grant from the Natural Sciences and Engineering Research Council of Canada (RGPIN-2019-06154) to the third author (K.T.W. Ng), using computing equipment funded by FEROF at the University of Regina. The authors are grateful for their support. The views expressed herein are those of the writers and not necessarily those of our research and funding partners.

References

1. Alavi N, Goudarzi G, Babaei AA, Jaafarzadeh N, Hosseinzadeh M (2013) Municipal solid waste landfill site selection with geographic information systems and analytical hierarchy process: a case study in Mahshahr County, Iran. Waste Manage Res 31(1):98–105. https://doi.org/10.1177/0734242x12456092
2. Bruce N, Ng KTW, Richter A (2017) Alternative carbon dioxide modelling approaches accounting for high residual gases in LandGEM. Environ Sci Pollut Res 24(16):14322–14336. https://doi.org/10.1007/s11356-017-8990-9
3. Demesouka OE, Vavatsikos AP, Anagnostopoulos KP (2013) Suitability analysis for siting MSW landfills and its multicriteria spatial decision support system: Method, implementation and case study. Waste Manage 33(5):1190–1206. https://doi.org/10.1016/j.wasman.2013.01.030
4. ESRI (2020) Create Thiessen Polygons (Analysis) from https://pro.arcgis.com/en/pro-app/tool-reference/analysis/create-thiessen-polygons.htm. Retrieved by 25 Feb 2020
5. Elliott P, Briggs D, Morris S, de Hoogh C, Hurt C, Jensen TK, Maitland I, Richardson S, Wakefield J, Jarup L (2001) Risk of adverse birth outcomes in populations living near landfill sites. BMJ 323(7309):363
6. Gorsevski PV, Donevska KR, Mitrovski CD, Frizado JP (2012) Integrating multi-criteria evaluation techniques with geographic information systems for landfill site selection: a case study using ordered weighted average. Waste Manage 32(2):287–296. https://doi.org/10.1016/j.wasman.2011.09.023
7. Government of Saskatchewan (2017) Saskatchewan solid waste management strategy – Discussion paper accessed onhttp://publications.gov.sk.ca/documents/66/97825-Solid%20Waste%20Management%20Strategy%20Discussion%20Paper.pdf
8. Government of Manitoba (2019) Solid waste sites in Manitoba from https://www.gov.mb.ca/sd/wastewise/landfill.html. Accessed by 23 Nov 2019
9. Government of Saskatchewan (2019). Landfills section from https://www.saskatchewan.ca/government/directory?ou=672d0e8d-1935-4642-9e6c-c05e24c7eff7. Retrieved by 13 Nov 2019
10. Government of Saskatchewan (2020) Population from https://dashboard.saskatchewan.ca/people-community/people/population. Retrieved by 19 Feb 2020
11. IPCC (2018) Waste management (Chapter 10) from https://www.ipcc.ch/site/assets/uploads/2018/02/ar4-wg3-chapter10-1.pdf. Retrieved by 10 Nov 2019
12. Kamdar I, Ali S, Bennui A, Techato K, Jutidamrongphan W (2019) Municipal solid waste landfill siting using an integrated GIS-AHP approach: a case study from Songkhla, Thailand. Resour Conserv Recycl 149:220–235. https://doi.org/10.1016/j.resconrec.2019.05.027

13. Karimi N, Richter A, Ng KTW (2020) Siting and ranking municipal landfill sites in regional scale using nighttime satellite imagery. J Environ Manage 256:109942. https://doi.org/10.1016/j.jenvman.2019.109942
14. Karimi N, Richter A, Ng KTW (2019) Improving the selection process for future landfills: an approach combining RS, GIS, and MCDA tools—applied for Vancouver, BC. Sardinia'19. In: 17th international waste management and landfill symposium, Santa Margherita di Pula, Cagliari, Italy, September 30–October 4. In: Cossu R, He P, Kjeldsen P, Matsufuji Y, Stegmann R (eds) CISA, Environmental Sanitary Engineering Centre, Cagliari, Italy
15. Kontos TD, Komilis DP, Halvadakis CP (2005) Siting MSW landfills with a spatial multiple criteria analysis methodology. Waste Manage 25(8):818–832. https://doi.org/10.1016/j.wasman.2005.04.002
16. Moeinaddini M, Khorasani N, Danehkar A, Darvishsefat AA, Zienalyan M (2010) Siting MSW landfill using weighted linear combination and analytical hierarchy process (AHP) methodology in GIS environment (case study: Karaj). Waste Manage 30(5):912–920. https://doi.org/10.1016/j.wasman.2010.01.015
17. NASA (The National Aeronautics and Space Administration) (2020) MODIS land surface temperature and emissivity (MOD11) from https://modis.gsfc.nasa.gov/data/dataprod/mod11.php. Retrieved by 20 Feb 2020
18. NOAA (National Oceanic and Atmospheric Administration) (2019) Version 4 DMSP-OLS Nighttime Lights Time Series archived and from https://ngdc.noaa.gov/eog/dmsp/downloadV4composites.html. Accessed by 10 Nov 2019
19. Pasalari H, Farzadkia M, Gholami M, Emamjomeh MM (2019) Management of landfill leachate in Iran: valorization, characteristics, and environmental approaches. Environ Chem Lett 17(1):335–348
20. Richter A, Ng KTW, Karimi N (2019) A data driven technique applying GIS, and remote sensing to rank locations for waste disposal site expansion. Resour Conserv Recycl 149:352–362. https://doi.org/10.1016/j.resconrec.2019.06.013
21. Richter A, Ng KTW, Karimi N, Wu P, Kashani AH (2019) Optimization of waste management regions using recursive Thiessen polygons. J Clean Prod 234:85–96. https://doi.org/10.1016/j.jclepro.2019.06.178
22. Richter A, Ng KTW (2018) Landfill regionalization: a strategic move for all provinces? Technical short paper, Canadian Civil Engineer "CIVIL" magazine. Can Soc Civil Eng 35(4):18–20
23. Statistics Canada (2017) Canada at a Glance, environment edition, waste accessible from https://www150.statcan.gc.ca/n1/pub/12-581-x/2017001/sec-5-eng.htm by 10 Nov 2019
24. Talaiekhozani A, Nematzadeh S, Eskandari Z, Dehkordi AA, Rezania S (2018) Gaseous emissions of landfill and modeling of their dispersion in the atmosphere of Shahrekord, Iran. Urban climate 24:852–862
25. Tansel B, Inanloo B (2019) Odor impact zones around landfills: Delineation based on atmospheric conditions and land use characteristics. Waste Manage 88:39–47
26. USGS (2020) Collection 6 MODIS Land Cover namely MCD12Q from https://modis.gsfc.nasa.gov/data/dataprod/mod12.php. Retrieved by 10 Jan 2020
27. USGS (2020) Details of Modis classification system from https://lpdaac.usgs.gov/documents/101/MCD12_User_Guide_V6.pdf. Retrieved by 25 Dec 2019
28. United Nations (2019) Report for waste management from https://www.un.org/esa/dsd/resources/res_pdfs/publications/trends/trends_Chemicals_mining_transport_waste/ch4_waste_management.pdf. Retrieved by 07 Nov 2019
29. University of Michigan (2017) Municipal solid waste. Center for sustainable systems – university of Michigan. From http://css.umich.edu/factsheets/municipal-solidwaste-factsheet. Accessed on 8 Sept 2018
30. Yale school of forestry and environmental studies, 2020. Protected areas; Global forest atlas from https://globalforestatlas.yale.edu/conservation/protected-areas. Retrieved by 19 Feb 2020

Utilization of Organic Wastes as a Bio-Resource: A Case Study of Corn Cobs in Nigeria

Osezele Stephen Anuge, Abhijeet Ghosh, and Kelvin Tsun Wai Ng

1 Introduction and Background

Nigeria has a land area of over 923,000 km^2 and is one of the most populous country in the world. Waste management issues are of great importance in Nigeria, and these issues have been reported by several studies [2, 7, 11, 23]. Nigeria bordering Niger in the north, Cameroon in the east, and Benin in the west, as shown in Fig. 1.

Nigeria is a major corn producer in Africa and the 10th largest producer of corn in the world, harvesting 9.2 million tonnes in 2011 [3]. Corn is grown in six geopolitical zones of the country, and Northern Nigeria is the leading production base of corns. In 2006, the production of corn in the North-central geopolitical zone was about 31% of the national production and increased to 44% in 2009 [15]. The main objectives of this case study are to (i) identify various means of proper utilization of corn cobs as a bio-resource in Nigeria, and (ii) discuss its benefits as well as the challenges with respect to the Nigerian bio-resource industry.

Corn is a popular food in Nigeria which can be boiled, roasted, crushed, or processed into other food products by locals. It is also regarded as the most important cereal crop in Nigeria [3]. As a result of the popularity of corn crops in Nigeria, corn agricultural wastes such as crop residues is high. If the crop residues are not properly managed or utilized, it could pose serious threat to the environment and to the health of the residents [15]. Utilizing the corn crop residues as bio-resource would reduce the waste generated and generate revenue for the farmers [3].

Corn is a resourceful crop with a high socio-economic worth as all its derivatives (grain, stalk, leaves and cob) can be processed into other food and non-food

O. S. Anuge · A. Ghosh (✉) · K. T. W. Ng
Faculty of Engineering and Applied Science, University of Regina, Regina, Canada
e-mail: abhijeeg@uregina.ca

K. T. W. Ng
e-mail: kelvin.ng@uregina.ca

S. Walbridge et al. (eds.), *Proceedings of the Canadian Society of Civil Engineering Annual Conference 2021*, Lecture Notes in Civil Engineering 249,
https://doi.org/10.1007/978-981-19-1061-6_17

Fig. 1 Major cities in Nigeria [6]

related products [3]. The use of corn residues has been studied and reported by many others, as discussed below. Corn crop residues are versatile, and they are used as raw materials in many developed countries either as a source of energy generation or construction materials [15].

In this case study, we will specifically explore the use of corn cobs as bio-resource. Corn cobs are readily available in Nigeria compared to other biomass resources and reusing these agricultural wastes would reduce waste management issue and lessen the environmental impact in Nigeria.

2 Utilization of Nigerian Corn Cobs

A total of four potential reuse of corn cobs are identified from our literature review, including (i) energy generation, (ii) construction and engineering applications, (iii) animal feeds, and (iv) industrial effluent treatment. They are separately discussed below.

2.1 Energy Generation

As a result of the over dependence on crude oil, alternative energy source in Nigeria is much less explored. Corn cobs, or other crop residues, are good sources of energy. Table 1 summarised heating values from various crops. Corn cob has a heating value of 17.39–19.14 MJ/kg [15, 22], making it a potential thermo-chemical feedstock. Compared to sesame stalks, corn cobs are at least 21.2% higher in heating value (Table 1). As it is generated in large amounts in Nigeria, corncobs could serve as a good potential feedstock for biofuels. The use of coal can be substituted with corn cobs or blended with corncobs, reducing the reliance of conventional fossil fuels. This would reduce air pollutants as harmful emissions from coal combustion are significantly reduced. Compared with coal (0.8–1.9% N and 0.7–1.2% S), corncobs (0.41–0.57% N and 0.7–1.2% S) contain lower amounts of nitrogen and sulphur [15]. Hence, less sulphur oxides are emitted during corncob combustion than coal combustion. This is especially important in Nigeria, where its population is much higher than other African countries.

Instead of direct combustion, corn cobs can also be used to generate fuel gas with minimum processing such as drying and cutting. According to Ogunjobi and Lajide [18], biochar generated from the pyrolysis of corncob can contribute 83.6 billion MJ to the energy generation in Nigeria, and simultaneously preventing about 6.8 million tonnes of CO_2 emission into the environment. According to Yu et al. [27], biochar derived from the pyrolysis of corncob can also serve as direct carbon fuel cell yielding a maximum power of 185 mW/cm^2 at a current density of 340 ^{mA}/cm^2 and at 750 °C.

Hydrogen fuel can also be derived from corn cobs. A recent study by Tang et al. [25] investigated hydrogen production from corncob using mesophilic bacterium clostridium hydrogeniproducens. They found that corncobs pretreated with alkali soaking, steam explosion, and acid explosion produce 90%, 86%, and 65%, hydrogen, respectively, using enzymatic hydrolysates as the biocatalyst. Given the abundance of corn cobs, they can be regarded as a potential hydrogen fermentation substrate. Hydrogen can be used as alternative energy resource to drive zero-emission vehicles with the use of hydrogen fuel cell [13].

Biagini et al. [4] studied gasification of corncob in a demonstration plant using a downdraft reactor. It was reported that a satisfactory plant operability was obtained with potential net power efficiency from 21.1–21.6%, gas specific production at 2 m^3/kg, and gas heating value at 5.6–5.8 MJ/m^3. The reported results are comparable

Table 1 Heating values from various crops

Crop residue	Heating values, MJ/kg	Reference
Corn cob	17.39–19.14	[15, 22]
Cotton stalk	17.40	[9]
Wheat stalk	17.15	[22]
Rice straw	15.54	[8]
Sesame stalk	14.35	[28]

to those of wood materials (chips, briquettes, and pellets) used as a feedstock in most studies in downdraft gasifiers.

A recent study by Sulaiman et al. [24] examined the production of biomass as energy source using plant residue pellets. The residues investigated were granulated corn cob residues, granulated corn stalks, and an equal mix of granulated corn stalk and corncob residues. The residues were compacted at a pressure of 200 MPa and pelletized using cassava starch as a binder. The pellets were analyzed using emission, proximate, ultimate, and calorimetry analyses. They reported that the equal mix of corn cob and stalk residues exhibited the best properties with a low nitrogen content of 0.64% and a hydrogen content of 6.22%. It also had a high heating value of 32.9 kJ/kg. Hence, it can be concluded that corn residues, regardless of residue types, are good biofuels for energy generation. The results are significant given the growth of population and its associated energy demand in Nigeria.

2.2 Construction and Engineering Applications

Corncobs can be used in manufacturing of low-cost particle boards, which can be used in building construction. The use of corn cobs in construction applications has the potential of using large amount of these agricultural waste. The use of waste materials in engineering projects saves valuable virgin construction materials and supports sustainable infrastructure. Faustino et al. [5] investigated the use of particle boards made from corncobs as a sound-proofing material. They reported that particle boards made from corncobs have comparable acoustic insulation properties when compared to other conventional materials such as expanded polystyrene and glass wool. Particle boards made from corn cobs could also serve as partition walls in buildings [19]. Ecological characteristics of construction materials are increasingly valued by architects and engineers. Concrete containing corncob-based aggregates can be used in various building and construction applications.

As discussed in Sect. 2.1, energy generation appears to be an attractive use of the corn cobs. Combustion and gasification of corn cobs produce ashes, and these ashes could then be utilized as additives to improve engineering performance of Portland cement. According to Adesanya and Raheem [1], ashes derived from burnt corn cobs can served as pozzolanic material to produce blended cement. The ash derived could also serve as a supplementary material for developing high performing and low-cost aluminum hybrid composites [15].

The literature review results suggest that corn cobs are versatile and has great potential in construction and engineering applications.

2.3 Animal Feeds

The third identified use is the use of corn cobs as animal feeds [14, 16, 17]. Crop residues are commonly used as feed for the livestock across the globe. Corn cobs can be used as an ingredient pig feeds in Nigeria. A Nigerian study reported the effect of corn cob meal on the growth and nutrient digestibility of 36 pigs [17]. They found that up to 10% of corn cobs in pig ration has no negative impacts on the livestock weight gain and other performance indicators. The major challenge associated with the use of corn cobs as pig feeds is the lignocellulosic nature (20–30% lignin, 45–55% cellulose, 25–35% hemicellulose) of the crop residue [10].

High fiber content in corn cobs, and a lack of specialized digestive in pig's digestive track may reduce the digestion rate [10]. On the other hand, Kanengoni et al. [10] also claimed that high dietary fiber associated with corn cobs hinders the production of pathogenic bacteria in the intestines, promotes the growth of lactic acid bacteria, and improves intestinal health of the pigs. Kanengoni et al. [10] further suggested that alternation of the structure of the fibrous components in maize cobs can be achieved by fermentation, heating, and grinding of corn cobs. The processed corn cobs can then be used as feed for pigs.

Millet et al. [14] reported that a balanced diet using corn cobs can be used to produce comparable meat and carcass traits with common feeding practice for organic pork. The literature review results generally support the use of corn cobs as ingredient for pig feeds. However, processing of corn cobs is typically required, and may increase the material overall cost.

2.4 Industrial Effluent Treatment

The last identified use of corn cobs is for water and wastewater treatment. Due to rapid population growth, clean water is a precious resource in Nigeria. Corn cobs, as well as corn stalks, have been investigated for their suitability in the removal of copper ion (Cu^{2+}) from wastewater effluents. According to Mohlala et al. [15], corn cob is more effective in the removal of copper than the corn stalk.

It appears that processed corn cobs offer wider range of applications in wastewater remediation. Uranium is toxic, and weakly radioactive. According to Mahmoud [12], powdered corncob can remove Uranium (VI) from an aqueous solution when applied in a batch and a fixed bed system. However, uptake rate of uranium ion in a fixed bed system is dependent on the bed height, the feed flow rate, and the initial concentration of the solution [12].

A study by Shim et al. [20] investigated the use of silica extracted from corn cob for treatment of contaminated water. They found that 84–88% Cu and 83–87% Cd were removed from the contaminated water within 24 h. The corn cob silica beads displayed are more effective in removing Cu and Cd from wastewater compared to zeolite beads. In their study, the removal efficiency of Cd, Cu, and phenol were

99%, 98% and 93%, respectively. However, it was also suggested that regeneration of the silica beads for reuse could be a challenge [20]. Ultrafine amorphous silica in nanoscale (50 nm) obtained from corncob could serve as potential future materials for controlled release applications, wastewater treatment technology catalyst, as well as dielectric materials [26].

2.5 Project Feasibility and Processing Cost

Figure 2 summaries the identified use of corn cobs with respect to the degree of processing. Literature on waste reuse and recycling generally indicate that project success depends on the required material processing cost, time, and expertise. As such, we recommend reusing Nigerian corn cobs with no, or minimum processing such as drying, cutting, and/or grinding. Specifically, we recommend the following five corn cobs applications: (i) ingredient for animal feeds, (ii) fuel gas production, (iii) insulation materials for construction projects, (iv) filtration materials for wastewater treatment, and (v) bio-char production.

3 Benefits and Challenges of Utilizing Bio-Resources in Nigeria

As a highly populous country, proper utilization of bio-resources in Nigeria is important socio-economically as it serves as a means of employment and income generation. Bio-energy industries would require skilled labor, contribute to a knowledge-based economy, and establish new markets. These new bio-resource businesses are likely to be in the rural area to take advantage of the cheaper land price and higher availability of crop residue. Rural agriculture and meat and livestock industrials might also benefit from these newly established bio-resource businesses. This would increase the number of jobs in the rural sectors, improve the income of the locals, and create wealth.

It is believed proper utilization of bio-resources would lead to development of rural areas in Nigeria. The bio-resource industry would attract investments, resulting development in rural infrastructure [21]. Roads, railways, schools, power stations, clinics, and research institutions are all important elements for a thriving rural community. As shown in Fig. 3, commercialization of the corn cobs would attract other investors and entrepreneurs for development of the Nigerian rural areas.

Some challenges are identified with the development of bio resource industries in Nigeria. Lack of basic amenities in the rural areas may hinder the development of the industries, especially at the beginning stage. Development of the bio resource industry in Nigeria would likely require subsidiary funding from the government either as long-term loans or through incentives [21]. However, getting these loans

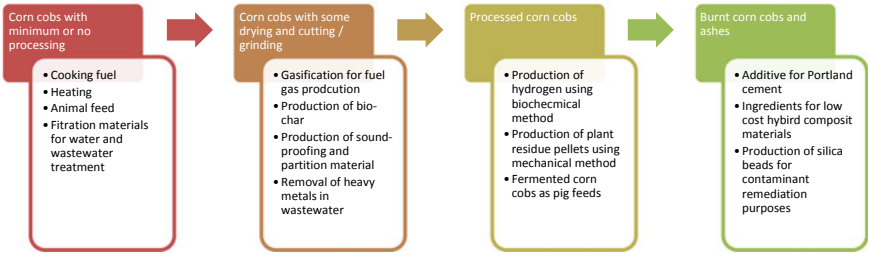

Fig. 2 The use of corn cobs as resource in Nigeria

Fig. 3 Potential benefits of the establishment of the bio-resource sector in Nigeria

may be difficult because of the lower level of income within the rural communities. Another issue would be the availability of skilled workers with adequate technical knowledge in the bio resource industry in rural Nigeria [21].

Competing use of corn cobs could also be a potential challenge. In this case study, several corn cob reuse approaches are identified. In the short term, approaches with minimum processing are recommended. In the long term, a comprehensive study on the economic and environmental performance of the alternatives should be conducted to select the most appropriate approach to corn cobs. At a minimum, the following three studies are recommended for implementation of a given project: cost effectiveness study, product life-cycle analysis, and full environmental impact assessment.

4 Conclusions

In Nigeria, corn cobs are used mainly for domestic cooking in rural areas, with a large amount improperly disposed or left to decay in soil. Research efforts have been made to use corn cobs in various applications. In this case study, potential reuse of corn cobs is identified, including energy generation, construction and engineering applications, animal feeds, and industrial effluent treatment. Literature review results suggest that corn cobs are versatile and can be used in several applications with or without further processing. We recommend reusing Nigerian corn cobs with no, or minimum processing. Specifically, we recommend the following five corn cobs applications: (i) ingredient for animal feeds, (ii) fuel gas production, (iii) insulation materials for construction projects, (iv) filtration materials for wastewater treatment, and (v) bio-char production.

Generated in large quantities, corn cobs may be an important resource in Nigeria. Utilizing corn cobs as bio resource in Nigeria would be very rewarding as it is largely available across the country. Unfortunately, a comprehensive study on the use of corn cob is not yet available. This case study represents the first step in this area. Reusing corn cobs contributes to local economy, reduces solid waste generated, and lessens greenhouse gas emission.

Acknowledgements The research reported in this paper was supported by a grant from the Natural Sciences and Engineering Research Council of Canada (RGPIN-2019-06154) to the third author (K. T. W. Ng), using computing equipment funded by FEROF at the University of Regina. The authors are grateful for their support. The views expressed herein are those of the writers and not necessarily those of our research and funding partners.

References

1. Adesanya D, Raheem A (2009) A study of the workability and compressive strength characteristics of corn cob ash blended cement concrete. Constr Build Mater 23(1):311–317
2. Akpeimeh GF, Fletcher LA, Evans BE (2019) Exposure to bioaerosols at open dumpsites: a case study of bioaerosols exposure from activities at Olusosun open dumpsite, Lagos Nigeria. Waste Manage 89:37–47. https://doi.org/10.1016/j.wasman.2019.03.058
3. Awoyale A, Lokhat D (2018) Harnessing the potential of bio-ethanol production from lignocellulosic biomass in Nigeria—a review. Biofuels Bioprod Biorefin 13(1):192–207
4. Biagini E, Barontini F, Tognotti L (2014) Gasification of agricultural residues in a demonstrative plant: corn cobs. Biores Technol 173:110–116
5. Faustino J, Pereira L, Soares S, Cruz D, Paiva A, Varum H, Ferreira J, Pinto J (2012) Impact sound insulation technique using corn cob particleboard. Constr Build Mater 37:153–159
6. Google Map (2020) Map data 2020. https://www.google.com/maps/place/Nigeria/@8.9826439,4.6310689,6.25z/data=!4m5!3m4!1s0x104e0baf7da48d0d:0x99a8fe4168c50bc8!8m2!3d9.081999!4d8.675277. Accessed on 26 Feb 2020
7. Hammed TB, Wandiga SO, Mulugetta Y, Sridhar MKC (2018) Improving knowledge and practices of mitigating green house gas emission through waste recycling in a community, Ibadan, Nigeria. Waste Manage 81:22–32. https://doi.org/10.1016/j.wasman.2018.09.044

8. Hiloidhari M, Baruah DC (2011) Rice straw residue biomass potential for decentralized electricity generation: a GIS based study in Lakhimpur district of Assam, India. Energy Sustain Dev 15:214–222
9. Jekayinfa SO, Scholz V (2009) Potential availability of energetically usable crop residues in Nigeria. Energy Sources Part A Recovery Utilization Environ Effects 31:687–697
10. Kanengoni A, Chimonyo M, Ndimba B, Dzama K (2015) Potential of using maize cobs in pig diets—a review. Asian Australas J Anim Sci 28(12):1669–1679
11. Kofoworola OF (2007) Recovery and recycling practices in municipal solid waste management in Lagos, Nigeria. Waste Manage 27(9):1139–1143. https://doi.org/10.1016/j.wasman.2006.05.006
12. Mahmoud M (2016) Kinetics studies of uranium sorption by powdered corn cob in batch and fixed bed system. J Adv Res 7(1):79–87
13. Manoharan Y, Hosseini SE, Butler B, Alzhahrani H, Fou Senior BT, Ashuri T, Krohn J (2019) Hydrogen fuel cell vehicles; current status and future prospect. Appl Sci 9(11):2296. https://doi.org/10.3390/app9112296
14. Millet S, Raes K, De Smet S, Janssens G (2005) Evaluation of corn cob mix in organic finishing pig nutrition. J Sci Food Agric 85(9):1543–1549. https://doi.org/10.1002/jsfa.2148
15. Mohlala L, Bodunrin M, Awosusi A, Daramola M, Cele N, Olubambi P (2016) Beneficiation of corncob and sugarcane bagasse for energy generation and materials development in Nigeria and South Africa: a short overview. Alex Eng J 55(3):3025–3036
16. Ndou SP, Gous RM, Chimonyo M (2013) Prediction of scaled feed intake in weaner pigs using physico-chemical properties of fibrous feeds. Br J Nutr 110:774–780
17. Ndubuisi EC, Iheukwumere FC, Onyekwere MU (2008) The effect of varying dietary levels of maize cob meal on the growth and nutrient digestibility of grower pigs. Res J Anim Sci 2:100–102
18. Ogunjobi JK, Lajide L (2013) Characterization of bio-oil and biochar from slow-pyrolysed Nigerian yellow and white corn cobs. J Sustain Energy Environ 4:77–84
19. Paiva A, Pereira S, Sá A, Cruz D, Varum H, Pinto J (2012) A contribution to the thermal insulation performance characterization of corn cob particle boards. Energy Buildings 45:274–279
20. Shim J, Lim J, Shea P, Oh B (2014) Simultaneous removal of phenol, Cu and Cd from water with corn cob silica-alginate beads. J Hazard Mater 272:129–136
21. Simonyan KJ, Fasina O (2013) Biomass resources and bioenergy potentials in Nigeria. Afr J Agric Res 8(40):4975–4989
22. Singh J, Panesar BS, Sharma SK (2008) Energy potential through crop biomass using geographical information system—a case study of Punjab. Biomass Bioenergy 32:301–307
23. Solomon UU (2009) The state of solid waste management in Nigeria. Waste Manage 29(10):2787–2799. https://doi.org/10.1016/j.wasman.2009.06.030
24. Sulaiman M, Adetifa B, Adekomaya S, Lawal N, Adama O (2019) Experimental characterization of maize cob and stalk based pellets for energy use. Eng J 23(6):117–128
25. Tang X, Ren N, Xu J (2013) Evaluation of hydrogen production from corn cob with the mesophilic bacterium clostridium hydrogeniproducens HR-1. Int J Hydrogen Energy 38(22):9104–9110
26. Velmurugan P, Shim J, Lee K, Cho M, Lim S, Seo S, Cho K, Bang K, Oh B (2015) Extraction, characterization, and catalytic potential of amorphous silica from corn cobs by sol-gel method. J Ind Eng Chem 29:298–303
27. Yu J, Zhao Y, Li Y (2014) Utilization of corn cob biochar in a direct carbon fuel cell. J Power Sources 270:312–317
28. Zabaniotou A, Ioannidou O, Antonakou E, Lappas A (2008) Experimental study of pyrolysis for potential energy, hydrogen, and carbon material production from lignocellulosic biomass. Int J Hydrogen Energy 33:2433–2444

Applications of Geographic Information Systems to Site Waste Facilities in Saskatchewan—Phase 1

Abhijeet Ghosh, Amy Richter, and Kelvin Tsun Wai Ng

1 Introduction and Literature Review

Solid waste in most scenarios meets its end in a landfill site. Canadians have chosen land disposal or landfilling as the most popular way of disposing waste due to huge availability of undeveloped land [12]. Most of the generated waste in Canada is sent to landfills for permanent disposal [2, 25]. This has made Saskatchewan's demand for landfills grow considerably over the years. Without any restrictions from local government on the per capita number of landfills in the province, Saskatchewan has the highest number of waste disposal grounds, with approximately 454.4 landfills per million people. Also, with increasing growth in the provincial population and urbanization, the waste generated and disposed has constantly increased. As per Ravindra et al. [17], the consequence of rapid urbanization is a large increase in population density and as such, a large increase in the amount of municipal solid waste being produced in urban centers around the world. Environmental impacts associated with the use of landfill technology includes the generation of landfill gas and groundwater contamination due to leachate, both are well documented in various Canadian studies [3, 14, 19].

To deal with the high number of landfills, the concept of regionalization has grown over the years. Regionalization of waste management systems includes municipalities working together and delegating responsibilities to a central authority within a defined geographic boundary [9]. Several Canadian jurisdictions have already employed regionalized waste management systems, including Alberta [8]. The Government of Saskatchewan also intends to regionalize their waste management system [10, 19]. Transfer stations or facilities have showed the maximum potential to help in regionalization of these landfills. A Transfer station is an intermediate station between

A. Ghosh (✉) · A. Richter · K. T. W. Ng
University of Regina, Regina, Canada
e-mail: abhijeeg@uregina.ca

S. Walbridge et al. (eds.), *Proceedings of the Canadian Society of Civil Engineering Annual Conference 2021*, Lecture Notes in Civil Engineering 249,
https://doi.org/10.1007/978-981-19-1061-6_18

final disposal options and generation sources to increase the efficiency of the MSW management system [16]. Management and study of spatial distribution of these transfer stations in relation to existing operational landfills will play a vital role in future planning and construction of new transfer stations.

Geographical Information System (GIS) approaches have been successfully applied to site waste disposal sites and landfills. Geographical Information Systems (GIS) have moved mapping from a historical role of provider of input, to an active and vital ingredient in the "throughput" process of decision-making [22]. Faisal [6] has mentioned the importance of remote sensing (RS) techniques in various aspects of landfill management and Manzo et al. [11] has given importance to aerial photography, space-borne, and air-borne sensors in continued improvement in planning and management of solid waste sites. These newer methods have replaced the costlier and time driven manual ground measurements.

Using GIS to site landfills and transfer stations have been conducted separately on many occasions [23, 24]. This study combines siting of both and map all the closed and open landfills and transfer facilities across the province. This enables study of the relationship between the spatial distribution of both landfills and transfer facilities in the province. As per Ramachandra [15], choosing best locations for the transfer facilities is always challenging. Transfer facilities play an important role in waste collection system such as: (i) reduction in transportation cost, (ii) reduction in the volumes of solid waste because of the compaction process; (iii) reduction in the traffic of the city [5], and hence newer locations for transfer facilities must be examined in relation to existing landfill locations to make the locations economically sustainable.

1.1 Objective

The key objective of this study is to examine the spatial distribution of waste facilities (active landfills, closed landfills, active Transfer Facilities, all closed facilities) in Saskatchewan using Federal Census Subdivision. The use of transfer facilities will be also evaluated using a new ratio known as LTR.

2 Methodology

2.1 Data Acquisition

The spatial data of the waste facilities used in this study have been obtained from the official website of Government of Saskatchewan [7]. In this study, a landfill refers to any permanent disposal site for municipal, industrial, and commercial solid waste storage. Waste transfer stations are defined as facilities where municipal solid waste

or other waste, is temporarily held and stored before heading to a landfill or waste-to-energy plant. Usually, waste transfer stations follow a regular process flow starting with arrival of waste, unloading, sorting, and processing in case it is connected to a material recovery facility and finally compacting and reloading waste to outbound trailers which in most cases end up at landfills.

The Federal Census Subdivision data is obtained for the censor year 2011. According to official designations adopted by provincial/territorial or federal authorities, census subdivisions are classified into multiple types. As per Statistics Canada, (2017) the province of Saskatchewan is divided in 18 subdivisions [21]. Under the Planning and Development Act, 2007, (the PDA) "subdivision" means, "a division of land that will result in the creation of a surface parcel or the rearrangement of the boundaries or limits of a surface parcel" [13].

2.2 Study Area

Saskatchewan, a prairie province in Canada is bordered by Alberta to the west, Northwest Territories to the north, Manitoba to the east and to U.S. states North Dakota and Montana to the South. Saskatchewan is selected because it has the highest number of landfills per capita than other Canadian provinces. As per coker, (2019) Saskatchewan has the highest number of waste disposal grounds (500), with approximately 454.4 landfills per million people [4]. Saskatchewan has the lowest population density (1.9 cap/km^2) and the lowest waste diversion rate (154 kg/cap in 2016) among Alberta, Ontario, and Manitoba. The province's population has seen a constant growth and is estimated by the World Population Review to be around 1.12 million, where most of the population resides in the southern half of the province [20]. Thus, with increasing population, the amount of waste generated will always increase, demanding better waste management tools.

2.3 Landfill to Transfer Facilities Ratio

A landfill to transfer facilities ratio (LTR) is proposed in the present study to examine the use of transfer facilities in Saskatchewan (Eq. 1). It is hypothesized that the use of transfer station can reduce the total number of landfills by combining smaller landfills to mega or regional landfills. Given the fact that Saskatchewan has the highest number of landfill sites per capita, the use of LTR allows better waste management planning and facilitate efficient use of landfills. The ratio is computed for each subdivision to identify possible location for potential transfer facilities.

$$LTR = \frac{Number\ of\ operational\ landfills}{Number\ of\ operational\ transfer\ facilities} \tag{1}$$

3 Results and Discussion

3.1 Waste Facilities in Saskatchewan

Figure 1 shows the waste facilities and the 18 census divisions in the Province of Saskatchewan. As mentioned above, Saskatchewan has the highest number of landfills per capita than other Canadian provinces. Many factors such as available land area, low population density, scattered population centers throughout the province, lack of governance and less stricter regulations, and municipal politics can be the reason for the high number of landfills in Saskatchewan. Thus, the number of landfills and their geographical distribution is of importance to further analyze the associated factors and implement waste management strategies.

As shown in Fig. 1a, more operational landfills are in the southern part of the province, probably due to high population density. The number of operational landfills per subdivision ranged from nine to ten landfills to as high as thirty-four to thirty-seven landfills, with an average of eighteen landfills per subdivision. In general, higher operational landfill density subdivisions are located near the Alberta-Saskatchewan and Saskatchewan-Manitoba borders. This suggests the possibilities of shared waste facilities across inter-provincial borders. From Alberta and Manitoba's point of view, the available space on the other side of the border; and being close to the border thus reducing the transportation cost are other factors which could have led to the huge number of landfills.

Figure 1b shows the spatial distribution of the closed landfills in Saskatchewan. The number of closed landfills per subdivision ranged from two to five with few subdivisions having about fifteen to twenty closed landfills. This averages out to be about five closed landfills per subdivision. Unlike the spatial distribution of operational landfills, a considerably higher number of closed landfills are located at the west side of the Province. The locations of these closed landfill site may represent the spatial distribution of population in the past. It is hypothesized that the locations of these closed landfills are closely related to the activities from the mining and gas sector in the province. Another factor to be considered is Alberta's population, which increased by 40% between 1970 and 2000 [1]. This meant there was less available space for landfills in Alberta, and more waste may have been transported to other provinces. Given the presence of topographical constraint such as the mountains between the British Columbia-Alberta borders, it is expected that several wastes were transported to Saskatchewan landfills, particularly waste generated near the interprovincial border. Further, the landfills close to Alberta-Saskatchewan border met their end life much earlier than expected and thus had to be shut down. However, more data is needed before a definite conclusion can be made.

Figure 1c shows the spatial distribution of the operational transfer facilities or stations. The number of operational transfer facilities per subdivision ranged from one to five with few subdivisions having about twenty transfer stations, averaging around seven transfer stations per subdivision. No operational transfer station is identified in northern Saskatchewan, which represents more than half of the total

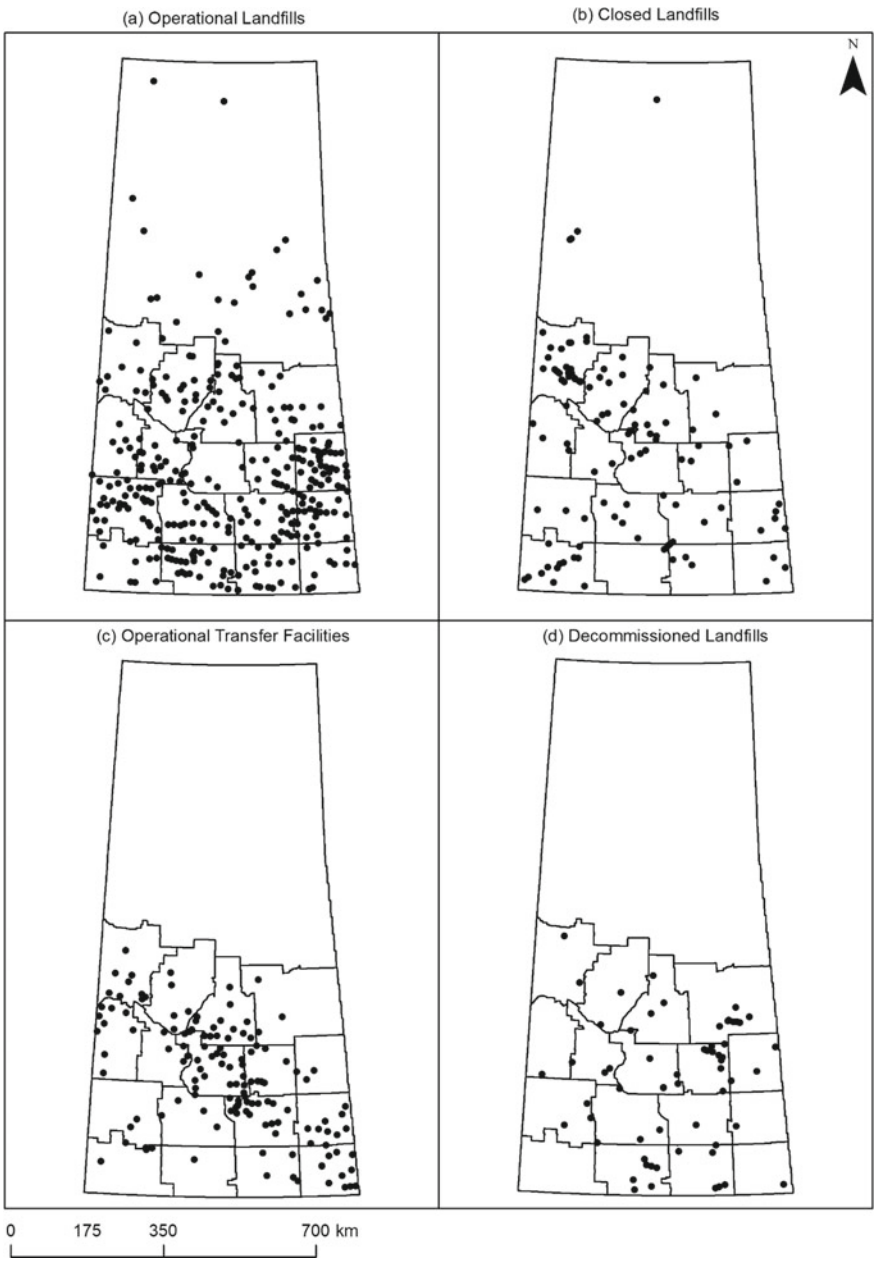

Fig. 1 Locations of various waste facilities in Saskatchewan

area in Saskatchewan. The transfer stations in Saskatchewan as shown in Fig. 1c, are not evenly distributed. A considerable high number of transfer facilities are in the central region of Southern Saskatchewan. Transfer station is used for the temporary deposition of waste, and this allows efficient use of waste collecting vehicle. When both Fig. 1a and c are studied together, it is observed that the transfer facilities are present in the areas of with minimum of operational landfills. The results suggest that the present location of transfer facilities is appropriately located spatially.

Figure 1d shows the spatial distribution of the decommissioned landfills. The number of decommissioned landfills per subdivision ranged from one to seven, with an average of three decommissioned per subdivision. No decommissioned landfills are identified in the Northern and South-west corner of the province.

3.2 The Use of Transfer Facilities to Reduce Landfill Number

A landfill to transfer facilities ratio (LTR) is used to examine the use of transfer facilities in Saskatchewan. LTR for each subdivision is computed to identify possible locations for additional transfer facilities. The LTR ranged from one to four except for Northern Saskatchewan subdivision which had no transfer stations and two subdivisions in South Saskatchewan having about twenty landfills but only one and two transfer stations, respectively. The average LTR is about six. Lower than average LTR concludes the subdivision has moderate distribution of landfills and transfer stations. However, it is recommended that more transfer facilities be used in areas with a higher-than-average LTR, which, in this case would include northern Saskatchewan and three other subdivisions. Richter et al. [18] noted the importance of a specialized approach to waste management in Northern regions. It is important to note that the design of solid waste management system is complex, and the proposed LTR is only applicable when assessing waste facilities spatial design within a predetermined boundary. The project is on-going, and the spatial distribution of these waste facilities will be further investigated in a future publication.

3.3 Heat Maps of Waste Facilities in the Province

Figure 2 graphically illustrates the spatial densities of operational and closed landfills, operational transfer facilities, and decommissioned landfills in Saskatchewan. The heat maps are derived from the spatial densities, which equal to the number of the facilities per unit area. The results suggest that the waste facilities are not evenly distributed across the province. The hotspots (shown in red) are mostly located in the southern part. The heat maps are consistent with the waste facilities count present in Fig. 1. The results are important to waste managers and policy makers for siting these waste facilities. This study suggests few subdivisions in the province which

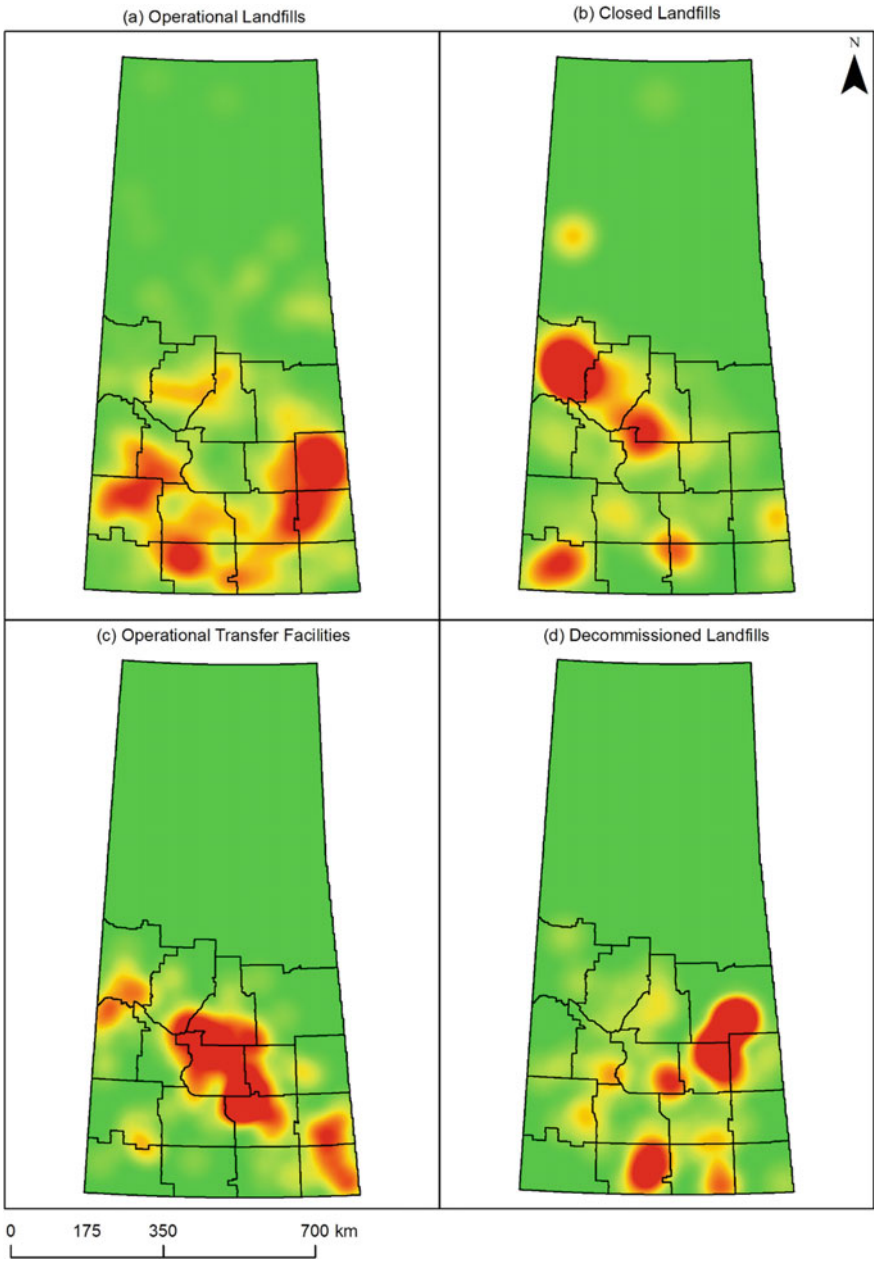

Fig. 2 Heat maps on waste facility density in Saskatchewan

need newer transfer stations as described by the corresponding high operational landfill to active transfer facilities ratio (LTR) ratios.

4 Conclusion

In this paper, all open and closed landfills and waste transfer facilities in the province of Saskatchewan are mapped using Geographical information system (GIS) to examine the special distribution and relationship between them. Solid waste management is complex and there are many factors like accessibility, volume, per capita production, and many more which are used in evaluating system design; however, this paper focuses on analysis based on spatial distribution of landfills and transfer stations within the defined boundary of Federal Census Division using a Landfill Transfer Station Ratio.

The results presented in this study represent the first stage of a more comprehensive study on the use of GIS to study the efficiency of landfill technology in the province. On average, there are about eighteen operational landfills and five closed landfills per subdivision. There are about seven transfer station per subdivision. The average decommissioned landfills per subdivision is three. More operational landfills are located near the Alberta-Saskatchewan and Saskatchewan-Manitoba borders. It was found that a higher number of closed landfills are located on the west side of Saskatchewan. Transfer station and decommissioned landfills are not identified in northern Saskatchewan, which consist of almost half of the total land area. Thus, it is believed this is probably due to the spatial distribution of the populated places in the province.

Operation Landfill to all the operational transfer facility ratio (LTR) is introduced, to identify the subdivisions in the province which are more feasible to construct a new transfer facility. Spatial densities of operational and closed landfills, operational transfer facilities, and decommissioned landfills in Saskatchewan are shown using heat maps. The results suggest that the transfer facilities are not evenly distributed across the province. The LTR ratio calculated shows most of the subdivisions being below the average LTR with exception of three subdivisions. These subdivisions are more favourable for construction of newer transfer facilities.

Acknowledgements The research reported in this paper was supported by a grant from the Natural Sciences and Engineering Research Council of Canada (RGPIN-2019-06154) to the third author (K. T. W. Ng), using computing equipment funded by FEROF at the University of Regina. The authors are grateful for their support. The views expressed herein are those of the writers and not necessarily those of our research and funding partners.

References

1. Alberta Population Estimates—Data Tables (2018). Retrieved February 18, 2020, from https://open.alberta.ca/dataset/alberta-population-estimates-data-tablesMunicipalities%20and%20the%20Subdivision
2. Bruce N, Asha AZ, Ng KTW (2016) Analysis of solid waste management systems in Alberta and British Columbia using provincial comparison. Can J Civ Eng 43:351–360
3. Bruce N, Ng KTW, Vu HL (2018) Use of seasonal parameters and their effects on FOD landfill gas modeling. Environ Monit Assess 190:291. https://doi.org/10.1007/s10661-018-6663-x
4. Coker C (2019) GIS tools to streamline organics diversion. Retrieved February 22, 2020, from https://www.biocycle.net/2010/04/22/gis-tools-to-streamline-organics-diversion/
5. Cui L, Chen LR, Li YP, Huang GH, Li W, Xie YL (2011) An interval-based regret-analysis method for identifying long-term municipal solid waste management policy under uncertainty. Retrieved February 24, 2020, from https://www.sciencedirect.com/science/article/pii/S0301479710004470
6. Faisal KS (2011) Environmental monitoring of landfill sites using multi-temporal remote sensing images. Master's Thesis. King Abdul Aziz University, Jeddah, Saudi Arabia
7. Government of Saskatchewan (2018) Landfills. http://www.saskh2o.ca/landfills.asp. Accessed on 5 March 2019
8. Government of Alberta (2018) Landfills. https://www.alberta.ca/landfills.aspx. Accessed on 15 Feb 2020
9. Government of Saskatchewan (2016) Starting a regional waste management system. http://www.environment.gov.sk.ca/adx/aspx/adxGetMedia.aspx?DocID=523,424,252,94,88,Documents&MediaID=0be8d1ff-9d60-42ff-a7f8-2468b06a3283&Filename=Waste+-+Regional+Waste+Management+System.pdf&l=English. Accessed on 12 Feb 2020
10. Government of Saskatchewan (2017) Saskatchewan solid waste management strategy—discussion paper. http://publications.gov.sk.ca/documents/. Accessed on 14 Feb 2020
11. Manzo C, Mei A, Fontinovo G, Allegrini A, Bassani C (2016) Integrated remote sensing for multi-temporal analysis of anthropic activities in the south-east of Mt. Vesuvius National Park
12. Ministry of the Environment [MOE] (2004) Ontario's 60% diversion goal—a discussion paper. Queen's Printer for Ontario, Toronto
13. Municipalities and the Subdivision Process (n.d.) Retrieved February 21, 2020, from https://www.saskatchewan.ca/government/municipal-administration/community-planning-land-use-and-development/subdivision-zoning-and-land-use/municipalities-and-the-subdivision-process
14. Pan C, Ng KTW, Richter A (2019) An integrated multivariate statistical approach for the evaluation of spatial variations in groundwater quality near an unlined landfill. Environ Sci Pollut Res 26(6):5724–5737. https://doi.org/10.1007/s11356-018-3967-x
15. Ramachandra T (2006) Management of municipal solid waste. TERI Press
16. Ramachandra T, Bachamanda S (2007) Environmental audit of municipal solid waste management. Int J Environ Tech Manag. Retrieved February 18, 2020 from https://www.researchgate.net/publication/228654976_Environmental_audit_of_Municipal_Solid_Waste_Management
17. Ravindra K, Kaur K, Mor S (2015) System analysis of municipal solid waste management in Chandigarh and minimization practices for cleaner emissions. Retrieved February 22, 2020, from https://www.sciencedirect.com/science/article/pii/S0959652614010786
18. Richter A, Ng KTW, Karimi N, Wu P, Kashani AH (2019) Optimization of waste management regions using recursive Thiessen polygons. J Clean Prod 234:85–96
19. Richter A, Ng KTW (2018) Landfill regionalization: a strategic move for all provinces? Technical short paper, Canadian Civil Engineer "CIVIL" magazine, Canadian Society for Civil Engineering, vol 35(4), pp 18–20
20. Saskatchewan Population 2020 (2020) Retrieved February 21, 2020, from http://worldpopulationreview.com/canadian-provinces/saskatchewan-population/

21. Statistics Canada (2017) Canada at a glance, 2017. Population and Dwelling Count Highlight Tables, 2016 Census. https://www12.statcan.gc.ca/census-recensement/2016/dp-pd/prof/index.cfm?Lang=E. Accessed on 21 Feb 2020
22. Tsou M-H, Buttenfield BP (2002) A dynamic architecture for distributing geographic information services. Trans GIS 6(4):355–381. https://doi.org/10.1111/1467-9671.00118
23. Vu HL, Bolingbroke D, Ng KTW, Fallah B (2019) Assessment of waste characteristics and their impact on GIS vehicle collection route optimization using ANN waste forecasts. Waste Manage 88:118–130. https://doi.org/10.1016/j.wasman.2019.03.037
24. Vu HL, Ng KTW, Bolingbroke D (2018) Parameter interrelationships in a dual phase GIS-based municipal solid waste collection model. Waste Manage 78:258–270. https://doi.org/10.1016/j.wasman.2018.05.050
25. Wang Y, Ng KTW, Asha AZ (2016) Non-hazardous waste generation characteristics and recycling practices in Saskatchewan and Manitoba. Can J Mater Cycles Waste Manage 18:715–724

Biomass and MSW to Energy Technology Options for Distributed Electricity Generation in Canada

E. M. Bartholameuz, G. Doluweera, and I. D. Gates

1 Introduction

Rapid growth of the integration of distributed energy resources (DER) is one of the most significant and important trends in the electricity industry worldwide. DER encompasses electricity generation systems, storage systems, and controllable loads (i.e., demand response) connected to the distribution system at or closer to the final consumers of electricity [3, 11]. Distributed Electricity Generation (DG) refers to technologies that produce electricity at or near the final electricity consumers [1]. DG may serve a single facility (e.g., house, commercial building, college campus), part of the microgrid, feed electricity to the distribution network, or a combination of all of the above.

DG is gaining increased attention and proponents attribute many benefits to it. These include increased reliability of supply, increased resiliency of the electricity system [8], not being exposed to electricity price volatility, lower overall electricity losses, and environmental benefits [17]. The economic and environmental benefits resulting from using existing, cost-effective renewable energy sources in homes and businesses are the main benefits cited by the proponents of DG. Another major driver of DG is the advancement of new small-scale power generation technologies. The examples include more efficient solar photovoltaic (PV) technologies, the advancement of small-scale incinerators and gasifiers, micro-hydropower plants, and natural gas technologies. Other technological advancements, such as the development of advanced battery storage systems and improved cogeneration technologies, have further strengthened the case for DG. Technologies that can be used for DG may

E. M. Bartholameuz (✉) · I. D. Gates
University of Calgary, Calgary, Canada
e-mail: embartho@ucalgary.ca

G. Doluweera
Canadian Energy Research Institute, Calgary, Canada

S. Walbridge et al. (eds.), *Proceedings of the Canadian Society of Civil Engineering Annual Conference 2021*, Lecture Notes in Civil Engineering 249,
https://doi.org/10.1007/978-981-19-1061-6_19

rely on locally extracted primary energy resources (for example, wind, solar, hydro, biomass, or geothermal) or locally purchased, such as natural gas. Globally, many jurisdictions are promoting the implementation of DG (and DER in general) through supportive policies and program [7].

In Canada, DER is being promoted through federal, provincial, and territorial policies and programs. Among other objectives, the federal and provincial governments are considering the promotion of DG technologies as a complementary policy tool to achieve GHG emissions reduction targets. In Canada, the growth of DG is also starting to scale. For example, in Ontario, the province with the most extensive set of policies to support DER, over 4000 MW of DG has been installed and contracted over the past ten years [12]. As of May 2020, the number of sites with DG in Alberta was about 5553 [2]. Since 2004, over 1800 customers have invested in DG and joined British Columbia's net-metering program.

Despite the growing interest and cited benefits, DG is not without challenges and criticism [6]. These challenges depend on the specific electric power system that hosts DG and the policies that support the incorporation of DG. One of the main challenges frequently cited is whether the compensation mechanisms for DG would lead to challenges for the utilities in recovering the cost of electricity generation and delivery assets [6].

Among the potential DG feedstock, biomass and MSW remain relatively unexplored resources. The burning of biomass to produce energy is one of the first human power uses, specifically for heating. Over the years, the usage of biomass to produce both electricity and heating has increased several folds. In addition, biomass and MSW feedstocks are considered green resources. Using locally available biomass and MSW for electricity production could add to already available DG options.

According to Canada Energy Regulator (CER), as of 2014, Canada had approximately 70 biomass generating power plants with a total installed capacity of 2.408 MW. Most of these facilities rely on wood, wood by-products, and landfill gas. B.C., Ontario, Alberta, Quebec, and New Brunswick have the largest biomass-based energy production. The presence of active pulp and paper and forestry industries has been a key factor for biomass power generation. Other than the pulp and paper and forestry industry, agricultural biomass residue and MSW has been identified by many industry experts as a potential feedstock for biomass power generation. Both biomass and MSW electricity generation are mainly based on thermal methods such as incineration and gasification. Recovery of Landfill Gas (LFG) and using anaerobic digesters are also viable alternatives to develop energy from biomass and MSW. Biomass and MSW contribute to around 1.9% of Canada's power generation and has seen a growth of 54% between the years 2005 and 2015.

This study assesses the production potential of several Biomass and MSW to Energy technologies for DG. The analysis is conducted for all population centers surveyed by Statistic Canada's 2016 Census of Population [16]. The analysis excludes population centers with low feedstock capacity.

2 Methodology

Eight technologies are selected based on the potential to apply the technology at a smaller scale. These 8 technologies include; Biomass Incineration Stoker System with a steam turbine (BMSIST), Biomass Integrated Gasification with combined cycle (BMIGCC), Biomass Integrated Gasification with an internal combined engine (BMIGICE), Biomass Anaerobic Digestion with an internal combined engine (BMADICE), Biomass Anaerobic Digestion with a gas turbine (BMADGT), MSW Incineration Stoker System with a steam turbine (MSWSIST), MSW Anaerobic Digestion with an internal combined engine (MSWADICE), MSW Anaerobic Digestion with a gas turbine (MSWADGT). Table 1 highlights the capacities, efficiencies, and cost information for each of the technologies.

The analysis is conducted for 1009 population centers across Canada. For BM analysis, agricultural waste biomass availability of a 25 km radius from the population center or district boundary is used. Data is collected through the Agriculture Canada BIMAT database and other independent sources. The biomass generated inside a capture area is analyzed under 9 different categories, Barley Straw, Corn Stover, Wheat Straw, Feedstock_1, Feedstock_2, Forest Residue, Mill Residue, Urban Wood Residue, and Other Wood waste. Feedstick_1 includes Barley chaff and stubble, oat chaff and stubble, wheat chaff and stubble, and corn stubble. Feedstock_2 includes flax and oat straw.

MSW Generation information: MSW generation and MSW diversion information of each population center or district are used for MSW technology assessment. Where specific information is not available, national and provincial averages are used. The national waste diversion percentage used for the analysis is 20%. 50% of the not diverted waste is assumed to be available for power generation.

The following parameters are calculated for all technologies and different power plant capacities; Energy output potential for each scenario (kW/tonne), Power Generation Capacity (MW), and Levelized Cost of Electricity (LCOE). The energy potential is analyzed under 4 different categories, MB Thermal Energy Potential, BM Biological Energy Potential, MSW Thermal Energy Potential, and MSW Biological Energy Potential. The calculation of the annual thermal Energy Potential for biomass is as follows:

$$EP_{BM}^{T}\left(\frac{\text{kW}}{\text{tonne}}\right) = \frac{1}{8760}\frac{Q^{CW}HHV^{CW} + Q^{SW}HHV^{SW} + Q^{WW}HHV^{WW}}{Q^{CW} + Q^{SW} + Q^{WW}} - Latent\ Heat\ Loss \quad (1)$$

where, EP_{BM}^{T} is Biomass Thermal Energy Potential (kW/tonne), Q^{CW} is Quantity of Crop based agricultural biomass waste, chaff, and stubble (tonnes), Q^{SW} is Quantity of straw and stover based agricultural biomass waste (tonnes), Q^{WW} is Quantity of Wood Waste (Forest Residue, Mill Residue, Urban Wood Residue). For other wood waste (tonnes), HHV^{CW} is the Higher Heating value of crop based agricultural

Table 1 Technology attributes used for the analysis

Technology	Capacity (kW)	CapEx (CAD 1000/kW)	Fixed OpEx (CAD/kW/year)	Variable OpEx (CAD/kWh)	Efficiency (%)
BM SI ST	5000	8500.00	255.00	0.07	0.35
BM SI ST	2000	9500.00	380.00	0.07	0.33
BM SI ST	500	13,333.33	800.00	0.07	0.3
BM IGCC	5000	8000.00	240.00	0.05	0.55
BM IGCC	2000	9500.00	380.00	0.05	0.5
BM IGCC	500	12,000.00	720.00	0.05	0.45
BM IGICE	5000	4000.00	120.00	0.04	0.25
BM IGICE	500	7000.00	350.00	0.04	0.22
BM IGICE	50	8000.00	400.00	0.04	0.2
BM AD ICE	2000	4500.00	135.00	0.06	0.25
BM AD ICE	500	4500.00	225.00	0.06	0.22
BM AD ICE	50	5333.33	266.67	0.06	0.2
BM AD GT	2000	8000.00	160.00	0.06	0.4
BM AD GT	500	7000.00	210.00	0.06	0.35
BM AD GT	50	6000.00	240.00	0.06	0.3
MSW SI ST	5000	9500.00	380.00	0.08	0.35
MSW SI ST	2000	10500.00	525.00	0.08	0.33
MSW SI ST	500	14,901.96	1117.65	0.08	0.3
MSW AD ICE	2000	4500.00	225.00	0.07	0.25
MSW AD ICE	500	4500.00	270.00	0.07	0.22
MSW AD ICE	50	5333.33	320.00	0.07	0.2
MSW AD GT	2000	8000.00	400.00	0.07	0.4
MSW AD GT	500	7000.00	420.00	0.07	0.35
MSW AD GT	50	6000.00	450.00	0.07	0.3

Source International Renewable Energy Agency (IRENA) [13], Canadian Biogas Association [4], Kumar et al. [14]

waste (kWh/tonne), HHV^{SW} is the Higher Heating value of straw and stover bases agricultural waste (kWh/tonne), HHV^{WW} is the Higher Heating value of wood wastes (kWh/tonne), and 8760 is the number of hours in a year. Latent heat loss is calculated based on moisture content and combustion water produced by each biomass faction.

For the calculation of BM biological Energy potential, the maximum amount of straw and wood waste that can be mixed is assumed as 30% due to low biodegradability in straw and wood waste that can inhibit biological reactions. The potential to generate Renewable Natural Gas is calculated using the following formula.

$$RNG_{BM}(\mathrm{m}^3/\mathrm{tonne}) = \frac{Q^{CW} RNG_{CW} + Q^{SW\_1} RNG_{SW} + Q^{WW\_1} RNG_{WW}}{Q^{CW} + Q^{SW\_1} + Q^{WW\_1}} \tag{2}$$

where RNG_{BM} is Renewable Natural gas production potential of BM waste (m^3/tonne), RNG_{CW} is Renewable Natural gas production potential of Crop Wastes (m^3/tonne), RNG_{SW} is Renewable Natural gas production potential of straw and stover Wastes (m^3/tonne), RNG_{WW} is Renewable Natural gas production potential of wood Wastes (m^3/tonne), Q^{SW_1} is either 30% of BM crop wastes or the maximum available amount, whichever is the lowest value (tonnes), Q^{WW_1} is If BMSW is zero 30% of BM crop waste. If BMSW_1 is not zero, either the balance 30% or the maximum available amount, whichever is the lowest value (tonnes). The renewable gas generation is then converted to energy potential using the following equation.

$$EP^{B}_{BM}\left(\frac{\mathrm{kW}}{\mathrm{tonne}}\right) = \frac{1}{8760} RNG_{BM} HHV^{CH4} \rho_{CH4} y_{CH4} - Latent\ Heat\ Loss \tag{3}$$

where EP^{B}_{BM} is biomass biological energy potential (kW/tonne), HHV^{CH4} is the higher heating value of methane, ρ_{CH4} is density of methane, and $\%_{CH4}$ is the methane percentage of the biogas. The thermal energy potential of Municipal Solid Waste is found from:

$$EP^{T}_{MSW}\left(\frac{\mathrm{kW}}{\mathrm{tonne}}\right) = 8760 \frac{Q^{MSW}_{T}\ HHV^{MSW\_T}}{Q^{MSW}_{A}} - Latent\ Heat\ Loss \tag{4}$$

where Q^{MSW}_{A} is the available MSW for energy production after diversion (tonnes), Q^{MSW}_{T} is the thermally combustible volatile solids component of MSWA (assumed 60%) (tonnes), and HHV^{MSW_T} is the higher heating value of the thermally combustible fraction of MSW (kWh/tonne). The biological energy potential of MSW and heat of vaporization of water is calculated from:

$$RNG_{MSW}(\mathrm{m}^3/\mathrm{tonne}) = \frac{Q^{MSW}_{B} RNG_{MSW\_B}}{Q^{MSW}_{A}} \tag{5}$$

where Q^{MSW}_{B} is the biodegradable volatile solids component of Q^{MSW}_{A} (Assumed 50%) (tonnes), RNG_{MSW} is renewable natural gas production potential of MSW (m^3/tonne), and RNG_{MSW_B} is the renewable natural gas production potential of the biodegradable fraction of MSW (m^3/tonne). The renewable gas generation is then converted to energy potential by:

$$EP^{B}_{MSW}\left(\frac{\text{kW}}{\text{tonne}}\right) = \frac{1}{8760} RNG_{MSW} HHV^{CH4} \rho_{CH4} y_{CH4} - Latent\ Heat\ Loss \tag{6}$$

where EP^{B}_{MSW} is MSW biological energy potential (kW/tonne).

The energy potentials under the above 4 categories are calculated by using information collected from literature for all population centers. The values used for the analysis are as follows; the moisture content of crop wastes 30%, moisture content of wood wastes 60%, moisture content of MSW 40%, moisture in biogas 30%, biogas methane percentage 50%, biogas potential crop 600 m^3/tonne, biogas potential straw 350 m^3/tonne, biogas potential wood waste 250 m^3/tonne, biogas potential MSW 400 m^3/tonne, methane density 0.70 $^{kg}/m^3$, methane energy potential HHV 15.40 kWh/kg, biomass waste HHV 3.88 kWh/kg, and MSW HHV 3.22 kWh/kg [7, 9, 10, 15]. Once the energy potential is calculated, the energy output potential is determined from:

$$Power\ Output\ Potential\left(\frac{\text{kW}}{\text{tonne}}\right) = \frac{(Power\ genration\ potential)(Plant\ efficiency)}{Capacity\ factor} \tag{7}$$

The Power output potential is calculated for each capacity and technology. Power generation capacity is calculated by simply multiplying the power output potential and available feedstock quantity calculated as stated previously, for each population center and for each technology capacity combination. The LCOE of electricity is calculated using the cost values in Table 1 for each population center. Some parameters were determined using a generic module from the System Advisor Model of NREL (Version 2018.11.11), as highlighted in Table 2. Additional financial parameters were used in the analysis are an analysis period of 25 years, annual inflation of 2.0%, Internal Rate of Return (IRR) of 12.0%, project term debt of 50.0%, and nominal debt interest rate of 6.5%.

3 Results and Discussion

3.1 National Level Analysis

At the national level, three responses are used to determine the viability of using BM and MSW as DG technology options. The three responses are LCOE, the number of viable population centers, and the available power generation capacity, as highlighted in Fig. 1, Tables 3 and 4.

Table 2 Waste generation and financial parameter values

Province ID	Province	Per capita waste gen 2012 (kg/year)	Project financing factor (PFF)	Construction financing factor (CFF)	Capital recovery factor (CRF)	Provincial multiplier[a]
10	Newfoundland and Labrador	743.17	1.128	1.039	0.079	0.99
11	Prince Edward Island	728.34	1.134	1.039	0.079	0.99
12	Nova Scotia	386.39	1.134	1.039	0.079	0.99
13	New Brunswick	651.31	1.122	1.04	0.079	0.99
24	Quebec	748.52	1.108	1.041	0.08	1.01
35	Ontario	673.42	1.108	1.041	0.08	1.05
46	Manitoba	853.53	1.111	1.041	0.08	1.07
47	Saskatchewan	880.84	1.111	1.041	0.08	1.07
48	Alberta	1006.52	1.09	1.043	0.081	1.07
59	British Columbia	573.28	1.111	1.041	0.08	1
60	Yukon	728.34	1.111	1.041	0.08	1.07
61	Northwest Territories	728.34	1.108	1.041	0.08	1.07
62	Nunavut	728.34	1.111	1.041	0.08	1.07

[a] Provincial multiplier is the difference in capital cost across Canada respect to BC
Source Conference Board of Canada [5] and Author Generated Values

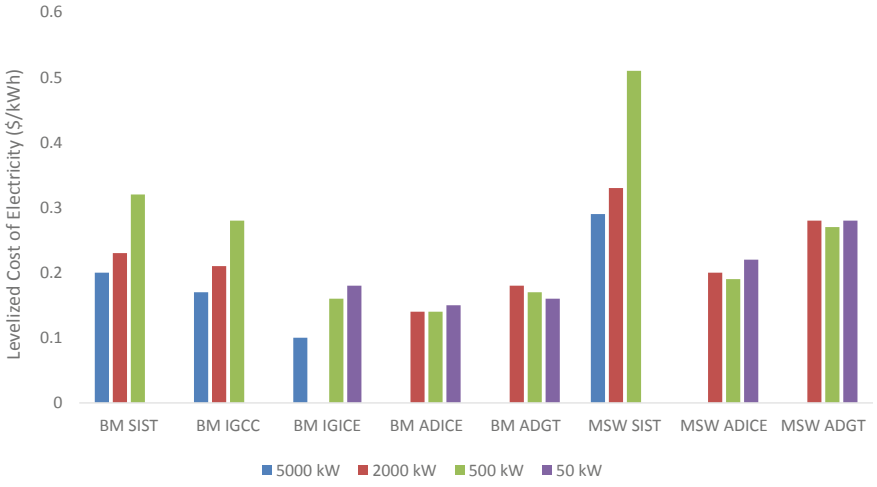

Fig. 1 LCOE, national averages for Canada ($/kWh)

Table 3 Number of viable population centers, national averages for Canada

Plant capacity, kW	BM SIST	BM IGCC	BM IGICE	BM AD ICE	BM ADGT	MSW SIST	MSW ADICE	MSW ADGT
5000	259	259	259			58		
2000	260	260		228	230	109	37	58
500	260	260	260	230	230	315	97	138
50			260	230	230		519	659

Table 4 Number of viable population centers, national averages for Canada (MW)

Plant capacity, kW	BM SIST	BM IGCC	BM IGICE	BM ADICE	BM ADGT	MSW SIST	MSW ADICE	MSW ADGT
5000	30,706	48,252	21,933			955		
2000	28,951	43,866		4,047	6,475	966	204	348
500	26,319	39,479	19,300	3,561	5,666	957	203	334
50			17,546	3,238	4,856		209	318

Based on LCOE, as seen in Fig. 1, the BM IGICE technology option at 5000 kW capacity is the cheapest technology option at 0.10 $/kWh. However, for lower capacities than 5000 kW, the BM ADICE option provided the cheapest LCOE values. For MSW options, ADICE options again proved to be the cheapest. In general, all technology options remained between 0.10 and 0.32 $/kWh. Current electricity prices in Canada varies between 0.07 and ~0.19 $/kWh in provinces [18]. The prices are ~0.35 $/kWh in some territories, suggesting competitive market entry prices for LCOE in most provinces. However, current electricity prices, especially compared to values for options with MSW feedstock, are lower. Technology options involving ICEs could be economically viable options for DG, especially for locations that cannot connect to the main power grid.

Availability of feedstock largely impacts the selection of a viable technology. Out of 1009 population centers studied, only 260 centers had adequate BM feedstock availability to meet at least 40% of plant capacity for at least one of the considered technology options. The number of potential population centers is lower for options with AD than thermal methods. MSW feedstock generally produced the lowest number of potential population centers at capacities above 500 kW. However, at the lower capacity of 50 kW, MSW AD technology options produced more than 500 potential population centers, as seen in Table 3. As expected, MSW feedstock is proportional to the population, and hence the number of potential population centers varies significantly with plant capacity. On the other hand, BM generation is proportional to the available BM feedstock, where feedstock availability will be determined by agricultural, forestry, and lumber industry.

Although, the ICE options had the lowest costs, they also had the lowest potential capacities due to lower efficiencies associated with the technology. Thermal conversion options (SI and IG), as expected, had higher capacities than biological (AD) options. BM IGCC with its expected higher efficiencies yields the highest capacities, with over 48 GW power generation potential in Canada. However, cost remains a concern at the studied capacities. For higher capacities >5000 kW, the costs are expected to be lower, and BM IGCC plants could provide an alternative green energy source.

Based on the above analysis, a collection of the cheapest technology options and capacities are selected for further study at the provincial level: BM IGCC at 5000 kW, BM IGICE at 5000 kW, BM ADICE at 2000 kW, BM ADICE at 500 kW, and MSW ADICE at 2000 kW.

3.2 Provincial Level Analysis

At the provincial level analysis, only five provinces are included due to other provinces and territories having no or low number of BM producing population centers. The studied provinces include Quebec with 46 potential population centers, Ontario with 73 potential population centers, Manitoba with 17 potential population centers, Saskatchewan with 46 potential population centers, and Alberta with 74 potential population centers. In Alberta, the 74 potential population centers account for 61% of the total population centers. Saskatchewan had the highest number of potential population centers as the percentage with 46 of its 61 (75%) population centers being viable locations for DG using BM. The number of potential populations centers reduces significantly in Saskatchewan and Alberta for AD based technology options. AD has lower energy recovery rates than thermal methods, and some population centers with lower feedstock capacity become not viable for energy recovery under AD. The total power generation capacity (MW) for all viable population centers is presented in Table 6, as shown from the Table, and as expected thermal methods have a significantly larger potential for power generation (Tables 5 and 6).

MSW analysis at the provincial level was conducted for the selected 5 provinces, as presented in Table 7. As can be seen, the potential population centers for the

Table 5 BM technology options provincial percentage of viable population centers

Province	BM IGCC 5000 kW (%)	BM IGICE 5000 kW (%)	BM ADICE 2000 kW (%)	BM ADICE 500 kW (%)
Quebec	17.1	17.1	17.1	17.1
Ontario	25.5	25.5	25.2	25.2
Manitoba	33.3	33.3	31.4	31.4
Saskatchewan	75.4	75.4	50.8	49.2
Alberta	60.7	60.7	48.4	47.5

Table 6 BM technology options provincial capacity (MW)

Province	BM IGCC 5000 kW plants	BM IGICE 5000 kW plants	BM ADICE 2000 kW plants	BM ADICE 500 kW plants
Quebec	6661	3028	206	182
Ontario	15,903	7229	1015	894
Manitoba	3624	1647	308	271
Saskatchewan	6833	3106	526	463
Alberta	15,199	6909	1985	1748

Table 7 MSW ADICE at 2000 kW provincial level details

Province	Viable population centers (%)	Available capacity (MW)
Quebec	2.2	44
Ontario	5.2	94
Manitoba	2.0	7
Saskatchewan	3.3	4
Alberta	2.5	22

selected MSW technology option remained a low percentage. This result is observed in all provinces. As expected, the available capacity was highest in the provinces with the highest populations.

A closer look reveals that the potential population centers for MSW technology options are the major cities in each province. For example, Alberta shows a 2.5% viable population centers. However, this accounted for the 3 largest cities in the province out of 122 population centers, where the 3 cities are Calgary, Edmonton, and Red Deer. This is observed in all provinces. Also, the largest cities are the ones that benefit least from DG, where these cities have direct access to a more stable main grid power supply.

Based on the above, it can be concluded that using MSW as a feedstock may not be economically viable. However, MSW could still be part of an integrated solution to DG, especially in remote locations. In addition, Landfill Gas (LFG) as a potential feedstock has not been evaluated. LFG capture is an essential operation throughout Canada, and this could provide a cheaper alternative to using MSW as a feedstock.

As for BM as a feedstock, current electricity prices in the province's suggests that some of the selected options could be viable options. Both Quebec and Manitoba currently have electricity prices lower than 0.1 $/kWh and do not provide an economic advantage to the DG technology options. Ontario has recently seen a reduction in electricity prices and currently stands around 0.13 $/kWh. Similar prices have been seen in recent years in Saskatchewan. On the other hand, Alberta electricity prices have seen recent upwards trends, with a current value of around 0.15–0.18 $/kWh. The electricity prices in Ontario, Saskatchewan, and Alberta are comparable to the DG technology options LCOE values. The values vary between

0.1 $/kWh and 0.17 $/kWh for the selected BM technology options. Both Alberta and Saskatchewan currently produce 39.2% and 42.9% of total electricity using coal power, respectively. DG-based BM technologies could be a green alternative to reduce dependence on coal. In addition, Canada currently produces ~5000 tonnes per year of biomass pellets, mainly from biomass waste feedstocks. The majority of biomass pellets are exported to the US. Taking advantage of the already established pelleting industry could make BM a more accessible feedstock. As stated, the current capture area analyzed for BM technology options is a 25 km radius around the population center. BM pallets could help enlarge this radius since the mobility of feedstock significantly increases with pelleting.

This analysis provides a general understanding of using BM and MSW as a potential feedstock for DG. It should also be noted that the analysis is based on theoretical maximum energy values which may not be attainable in field applications. In future work, the analysis will examine the city/population center level, where a deeper understanding of local limits and advantages could be considered.

4 Conclusions

The study evaluates technology options using biomass waste and MSW as a feedstock for distributed electricity generation in Canada. Current electricity prices in Canada are lower than 0.20 $/kWh for most provinces. Hence, technology options with lower prices are selected as viable technologies. For biomass waste feedstock, integrated gasification with a combined cycle (IGCC) power plant at a nameplate capacity of 5000 kW yielded the highest power generation potential. However, the cheapest technology option at nameplate capacity 5000 kW is integrated gasification with internal combustion engines (IGICE), with an LCOE value of 0.10 $/kWh. At lower capacities than 5000 kW, using anaerobic digestion with internal combustion engines (ADICE) is the cheapest technology option. Using MSW as a feedstock, the potential power generation capacities remained relatively low except in major cities. In addition, LCOE values are higher than 0.20 $/kWh for MSW technology options. MSW as a feedstock for power generation could be part of the integrated solution in remote communities. However, it may not be feasible when there is access to the main power grid due to higher costs.

At the provincial level, in Alberta and Saskatchewan, more than 50% of the population centers were suitable for distributed electricity generation at the studied capacities. The current electricity prices in both Alberta and Saskatchewan are also in the range of 0.15–0.20 $/kWh. Using the suggested technology options for distributed electricity generation in Alberta and Saskatchewan may provide a green alternative to coal as an energy source in the future.

Acknowledgements The authors would like to extend appreciation to the University of Calgary's Canada First Research Excellence Fund program, the Global Research Initiative (GRI) for Sustainable Low-Carbon Unconventional Resources and the Canadian Energy Research Institute for

providing funding and research support. In addition, the authors also appreciate insights provided by Doug Webb of AgriPower Inc.

References

1. Ackermann T, Andersson G, Söder L (2001) Distributed generation: a definition. Electr Power Syst Res 57(3):195–204. https://doi.org/10.1016/S0378-7796(01)00101-8
2. AESO (2020) Micro- and small distributed generation reporting. Alberta Electric System Operator. https://www.aeso.ca/market/market-and-system-reporting/micro-and-small-distributed-generation-reporting/
3. Akorede MF, Hizam H, Pouresmaeil E (2010) Distributed energy resources and benefits to the environment. Renew Sustain Energy Rev 14(2):724–734. https://doi.org/10.1016/j.rser.2009.10.025
4. Canadian Biogas Association (2013) Canadian biogas study—benefits to the economy, environment and energy
5. Conference Board of Canada (2016) Waste generation—environment provincial rankings—how Canada performs. https://www.conferenceboard.ca/hcp/provincial/environment/waste.aspx
6. Costello KW (2015) Major challenges of distributed generation for state utility regulators. Electr J 28(3):8–25. https://doi.org/10.1016/j.tej.2015.03.002
7. Doluweera G, Gallardo V, Rahmanifard H, Bartholameuz EM (2020) Opportunities and challenges for distributed electricity generation in Canada. Study No. 187. Calgary, AB: Canadian Energy Research Institute. https://ceri.ca/assets/files/Study 187 Full Report.pdf.
8. Driesen J, Katiraei F (2008) Design for distributed energy resources. IEEE Power Energ Mag 6(3):30–40. https://doi.org/10.1109/MPE.2008.918703
9. Environment and Climate Change Canada (2018) Canadian environmental sustainability indicators: solid waste diversion and disposal. http://epe.lac-bac.gc.ca/100/201/301/weekly_acquisitions_list-ef/2019/19-04/publications.gc.ca/collections/collection_2019/eccc/En4-144-71-2018-eng.pdf
10. Esposito G (2012) Bio-methane potential tests to measure the biogas production from the digestion and co-digestion of complex organic substrates. Open Environ Eng J 5(1):1–8. https://doi.org/10.2174/1874829501205010001
11. ETNO (2019) Structural options for Ontario's electricity system in a high-DER future. Energy Transformation Network of Ontario. http://ieso.ca/-/media/Files/IESO/Document-Library/etno/ETNO-StructuralOptionsHighDERFuture.pdf?la=en
12. IESO (2020) Distributed energy resources. Independent Electricity System Operator. http://www.ieso.ca/en/Learn/Ontario-Power-System/A-Smarter-Grid/Distributed-Energy-Resources
13. International Renewable Energy Agency (IRENA) (2012) Renewable energy technology analysis series: biomass for power generation
14. Kumar A, Cameron JB, Flynn PC (2003) Biomass power cost and optimum plant size in western Canada. Biomass Bioenergy 24(6):445–64. https://doi.org/10.1016/S0961-9534(02)00149-6
15. Nguyen H, Heaven S, Banks C (2014) Energy potential from the anaerobic digestion of food waste in municipal solid waste stream of urban areas in Vietnam. Int J Energy Environ Eng 5:1–10. https://doi.org/10.1007/s40095-014-0133-1

16. Statistics Canada (2017) Report on energy supply and demand in Canada. 2015 Preliminary. Catalogue No. 57-003-X. Annual Report. Ottawa, ON: Statistics Canada. http://www.statcan.gc.ca/pub/57-003-x/57-003-x2017002-eng.pdf
17. Sullivan JE, Cannon GD, Burton D, Johnson SD, White JM (2014) Why end users are investing (big) in distributed generation. Electr J 27(2):23–32. https://doi.org/10.1016/j.tej.2014.01.008
18. Urban R (2020) Electricity prices in Canada (Updated 2020). Energyhub.Org. https://www.energyhub.org/electricity-prices/

Mass Recovery for BTEX Stripping from Organic and Sandy Soil Using Soil Vapor Extraction Process

R. Ray, G. C. Hilbers, and N. Biswas

1 Introduction

Soil contamination is usually concealed under the ground and neglected. Contrary to air and water pollution, contaminated soil sites are finite in spatial extent, which makes them unique in some ways [5]. Prior to the twenty-first century, large contamination sites with hazardous waste were considered to be the priority and became a focus for most of the research and expenditure on soil remediation. The reality is that there are several forms of large soil contamination, including toxic leachate, industrial waste, heavy metals, and others are not as common as small oil spill sites [1]. EPA estimates that between 10 and 30% of the estimated 552,000 regulated underground storage tanks in the United States leak petroleum products [12]. According to Environment Canada, 3–5% of the roughly 225,000 registered underground storage tanks are leaking [2]. Gasoline is a common petroleum product that contains over 100 chemicals, many of which are volatile and partly soluble in water. A lot of gasoline components are very mobile in the natural environment. This makes the potential for contamination of groundwater or evaporation into surrounding structures high. As per Ontario regulations, contaminated soils must be cleaned up by landowners to be sold. Clean-up costs in 1999 averaged $50,000 US dollars in Ontario where the Federal groundwater remediation costs in Canada in 2011 averaged $64,000 CAD [8]. While there are many components to gasoline, but four in particular pose a particular health hazard and provide substantial concern with regard to water pollution and adverse health effects, commonly called BETX [3]. Different remediation methods exist for gasoline contaminated soils. Ex-situ remediation tends to be very expensive,

R. Ray (✉) · N. Biswas
University of Windsor, Windsor, Canada
e-mail: rayr@uwindsor.ca

G. C. Hilbers
Windsor Detroit Bridge Authority, Windsor, Canada

S. Walbridge et al. (eds.), *Proceedings of the Canadian Society of Civil Engineering Annual Conference 2021*, Lecture Notes in Civil Engineering 249,
https://doi.org/10.1007/978-981-19-1061-6_20

time-consuming and practically inefficient for small areas like gas stations. When in-situ technology is used, it tends to be much cheaper and more efficient [7].

In different locations in North America, the soil vapor extraction (SVE) method has been successfully applied by a variety of scientists, but most applications so far have been based on empirical data. There are often still a lot of questions about chemical and physical interactions that occur when this method is used. Furthermore, only a few case studies are available for use as a baseline feasibility study to determine its effectiveness in potential remedial sites. For large sites, computer modelling has become a standard design tool, with less reliance on empirical methods. Permeability, moisture content, grain size distribution, organic matter content and soil temperature influence rate of contaminant movement in different soil types. Other important parameters include solubility, vapour pressure, and density [10, 11]. There have been relatively few studies on the full-scale investigation of the SVE method, both on the bench and in the laboratory, where the air flow rate, mass removal rate, mass recovery time, and residual chemical distribution of BTEX have been examined.

This study sought to determine the relationship between stripping rates of BTEX under different air flow rates as well as quantify residual contaminant and moisture distributions in soil that has been stripped of pollutants.

2 Experimental Technique

The study was conducted using an apparatus that replicated SVE to determine the removal rates of benzene, toluene, ethylbenzene and xylene from two types of soil using bench scale experiments. There have been 10 sets of experiments, each including 3 separate experiments varying only with respect to the air flow rate. Four sets of experiments involved contaminated sandy and organic soil with benzene, toluene, ethylbenzene, and xylene individually. Four chemicals were used in another experiment on sandy soil. The last experiment was done using moisture-saturated air to blow through sand containing toluene. Temperature was kept constant at 23 $\pm$ 0.3 °C. Table 1 summarizes the experimental conditions. Table 2 summarizes different properties of sandy and organic soil.

2.1 Instrumentation

The stripping experiments were conducted with stainless steel columns, 100 mm in diameter and one meter in height. Each column had acrylic caps with one-inch compression fittings on both ends, and the bottom cap had two fittings, one in the centre and two off-centre. A schematic diagram of the experimental setup is provided in Fig. 1. In order to drain the columns once they were loaded, they were placed on specially designed benches, which held them 400 mm above the floor, allowing them to be removed by gravity. The pressure fittings on the bottom caps of the columns

Table 1 Experimental conditions

Experiment No.	Soil type	Chemical	Air moisture	Flow-1 (L/h)	Flow-2 (L/h)	Flow-3 (L/h)
1	Sand	Benzene	Dry	1.5	3.0	6.0
2	Sand	Toluene	Dry	1.5	3.0	6.0
3	Sand	Ethylbenzene	Dry	1.5	3.0	6.0
4	Sand	Xylene	Dry	1.5	3.0	6.0
5	Organic	Toluene	Dry	1.5	3.0	6.0
6	Organic	Xylene	Dry	1.5	3.0	6.0
7	Organic	Benzene	Dry	1.5	3.0	6.0
8	Organic	Ethylbenzene	Dry	1.5	3.0	6.0
9	Sand	BTEX	Dry	1.5	3.0	6.0
10	Sand	Toluene	Saturated	1.5	3.0	6.0

Table 2 Soil properties

Properties	Sandy Soil	Organic soil
Effective porosity, %	32.7 ± 0.6	67.8 ± 6.4
Organic content, %	1.6 ± 0.1	24.3 ± 1.55
Bulk mass density, g/cm^3	1.626 ± 0.031	0.647 ± 0.003
Particle mass density, g/cm^3	2.416 ± 0.046	2.009 ± 0.007
Moisture content, % (as received)	0.2 ± 0.01	30.4 ± 3.5

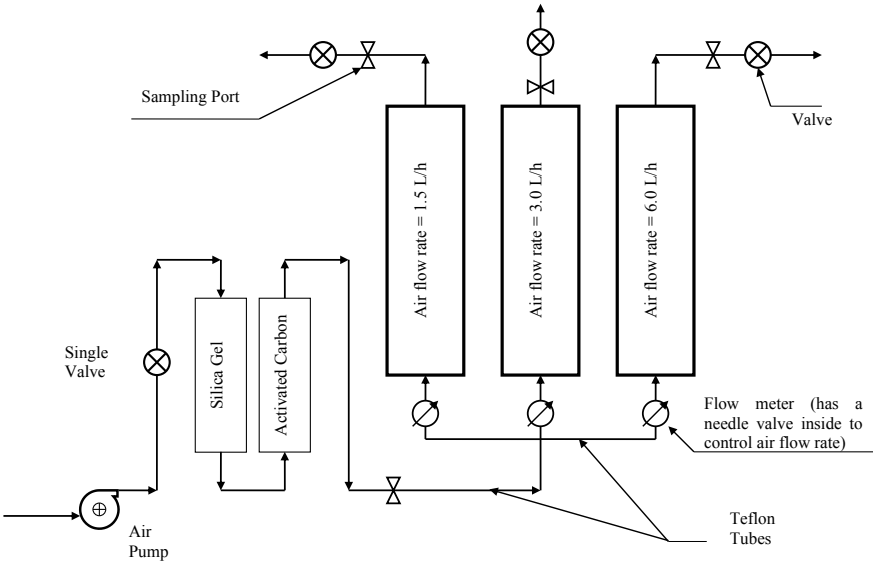

Fig. 1 Schematic diagram of the experimental setup

were accessed by drilling six holes in the bottom shelf of the bench. Three flow meters were attached to the side of the bench. A middle shelf, consisting of two removable pieces, secured the columns firmly in place.

2.2 Preparation of Contaminants and Columns

An aqueous solution containing the target compound(s) was prepared and added to the soil in the column. The target concentrations of all the solutions were the same—150 mg/L. All of the solutions were prepared in 20 L glass carboys. Therefore 2.25 g of chemical was required to achieve the target concentration. Based on the densities of each of the BTEX chemicals, approximately 2.5 ml of neat chemical was required to achieve the target concentration. 2.25 g of each compound were added to the carboy to conduct the experiment using all four compounds combined. Due to the low solubility of Ethylbenzene and Xylene in water, these two chemicals were allowed to mix for four hours before they became dissolved.

Following the column preparation described above, a flow meter was attached to each column. A single valve controlled the air flow into the system. The flow to the columns was controlled by throttling needle valves built into the flow meters. Air flow rates of 1.5, 3 and 6 L per hour were used for this study (Table 1). Those flow rates corresponded to an approach velocity of 5.30×10^{-05} m/s, 2.12×10^{-04} m/s and 1.06×10^{-04} m/s respectively and set on the flow meters at the beginning of each experiment. Over the course of five days, bubble flow meters were used to measure the flow rate in each column three times a day. Each column was provided with a short section of tubing that was attached to the top of the cap to interface with the column's sampling port. Gas samples were then taken directly.

A number of soil properties were examined with the objective of assessing the soil chemical properties. The effective porosity, organic content, bulk density, particle mass density and moisture content (as received) were evaluated in order to determine the soil's organic carbon content. All properties were determined by averaging six measurements for sandy soil and three measurements for organic soil. The samples of sand and organic matter (inorganic and native) were isolated for each set of experiments and analysed separately. For all subsequent calculations, the average of five sand samples and two organic samples was used.

2.3 Calculation of Exhaust Gas and Residual Contaminant Concentrations in Soil

Each gaseous sample collected was analysed on a gas chromatograph. Samples were injected manually through a split/splitless injection port. Sample separation was achieved using a 60 m capillary column. A standard Flame ionization Detector was

used with the GC. Nitrogen, the carrier gas, was provided at a flow rate of 200 mL per minute. Hydrogen and extra dry air fuelled the FID. Both the Injection Port and the Detector were operated at 250 °C and the column was held isothermally at 100 °C. The run time for the GC was four minutes, which was ample time to resolve the chemicals of interest.

For the injection of samples into the GC, first the syringe containing the sample was fitted with a blunt tipped needle which worked best because it caused the least wear on the injection port septa. Rheodyne needles, were used for this study. Once the needle was in place the syringe, with the valve still Closed, was inserted into the injection port. The valve was then opened, and the sample injected slowly. The results of the analysis were outputted to the Integrator and the instrument was ready to analyse another sample.

At the end of each experiment soil from each column was sampled in order to determine the residual concentrations. The analysis of the soil samples was conducted on a Gas Chromatograph equipped with a Mass Spectrometer. A purge and trap system were used for sample introduction.

3 Results and Discussions

When individual contaminants were applied to the sandy soil, at higher air flow rates, contaminants were removed at faster rates and resulted in lower residual concentrations. For all BTEX contaminants and flow rate, more than 95% of the applied mass was recovered within 24 h (Fig. 2). However, the contaminant mass fraction removal rate varied considerably. For both types of soil, benzene showed the highest mass

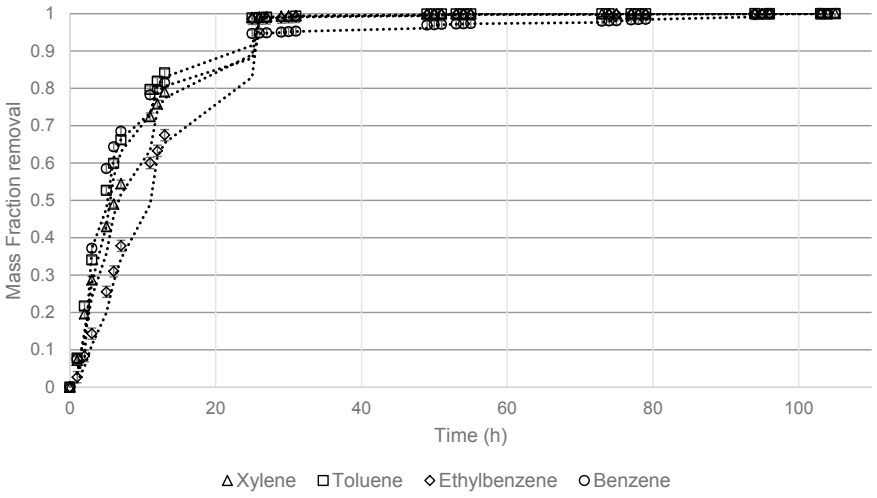

Fig. 2 Mass fraction of components removed from organic soil at medium flow rate

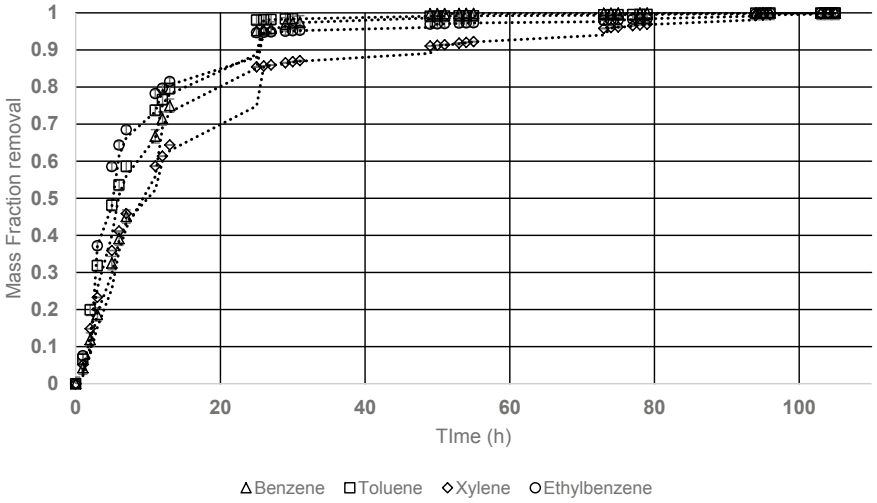

Fig. 3 Mass fraction of components removed from sandy soil at medium flow rate

fraction removal rate while ethylbenzene showed the lowest. Hu et al. [4] found that after 4 months of SVE application, the mass fraction removal of BTEX was 53%, 64%, 68% and 91% for ethylbenzene, xylene, toluene and benzine respectively. Other researchers also found similar type of results [13, 14]. Though the density is higher for benzine compare to other compounds of BTEX, it is postulated that higher vapor pressure for benzine is responsible for it [14].

Mass fraction recovery rate for each component from sandy soil (at medium flow rate) are shown in Fig. 3. While comparing to organic and sandy soil, the columns containing organic soils exhibit higher removable fraction as compared to the sandy soil. Kacem et al. [6] and Qin et al. [9] found that organic content in soil has direct positive relationship with removal efficiency in SVE process. Higher porosity and moisture content in organic content of soil is believed to be accountable for it [6].

For each of the experiments, with benzene, toluene ethylbenzene and xylene, air flow rate appeared to have no appreciable effect on the mass fraction recovery. The mass fraction recovered for all three air flow rates from the benzene columns were more than 98%, whereas for toluene and xylene recovery rates were nearly 90%. Recovery rate was only 84% for ethylbenzene. However, Kacem et al. [6] found that lower air flow rate has lower mass fraction removal rate. The recovery curves for xylene show faster removal at higher air flow rates. For all columns containing the organic soil, more than 95% of the easily removable contaminant mass fraction was removed within 20 h. The effect of stripping BTEX as a mixture from sandy soil, at three different flow rates was examined. No clear correlation between flow rate and mass fraction removal was observed.

The three experiments conducted using sandy soil at a medium flow rate, with toluene (both dry air and saturated air) resulted in nearly equal mass fractions removed in 24 h. The same is true for BTEX mixture with dry air and sandy soil at a medium

flow rate. After 24 h, the removal from the sandy soil, stripped with dry air, increased very slowly. However, both the column stripped with saturated air and the column containing BTEX continued to show further removal at a slow rate until the end of the experiments (100 h). The column stripped using saturated air was expected to show a slower rate of removal due to the lower relative concentration of pore water. The residual concentration of the saturated-air stripped column was expected to be lower, because the soil will not dry out and therefore adsorption to mineral surfaces is negligible.

4 Conclusions

Soil vapour extraction was simulated by using soil columns in the laboratory. The conditions were equivalent to those found at remedial sites which contained a dissolved NAPL contaminate plume or have been reinitiated to a point where all NAPL had already been extracted. Both the rate of contaminant removal and the residual chemical concentrations in the soils were determined and the following conclusions were drawn regarding the rate of contaminant removal:

1. An increase in air flow rate in columns containing sandy soil resulted in increased removal rates.
2. The air flow rates used in this study had no significant effect on the removal rate in an organic soil which had both high porosity and moisture content.
3. When moisture-saturated air was used to strip toluene from a sandy soil the recovery rates were approximately 50% of those observed when dry air was used.
4. Compounds with higher vapour pressures were stripped faster and were present at lower residual concentrations when stripped under similar conditions.

Acknowledgements This research was funded by Natural Sciences and Engineering Research Council Canada.

References

1. Asante-Duah K (2019) Management of contaminated site problems, 2nd edn. CRC Press, Boca Raton
2. CCME (2003) Environmental code of practice for aboveground and underground storage tank systems containing petroleum and allied petroleum products (PN 1326). Retrieved November 20, 2020, from https://www.canada.ca/content/dam/eccc/documents/pdf/cepa/ccme-pn-1326-eng.pdf
3. Chambers DM, Reese CM, Thornburg LG, Sanchez E, Rafson JP, Blount BCJRE, De Jesús R (2018) Distinguishing petroleum (crude oil and fuel) from smoke exposure within populations based on the relative blood levels of benzene, toluene, ethylbenzene, and xylenes (BTEX),

styrene and 2,5-dimethylfuran by pattern recognition using artificial neural networks. Environ Sci Technol ACS 52(1):308–316
4. Hu LM, Lo IM, Meegoda JN (2006) Centrifuge testing of LNAPL migration and soil vapor extraction for soil remediation. Pract Periodical Hazard Toxic Radioactive Waste Manage 10(1):33–40. https://doi.org/10.1061/(asce)1090-025x(2006)10:1(33)
5. Irshad M, Khan RU, Jadoon S, Hassan A, Eneji EA (2014) Effect of phosphate rock on the solubility of heavy metals in soils saturated with industrial wastewater. Can J Soil Sci 94:543–549
6. Kacem M, Esrael D, Benadda B (2017) Flowrate and water presence effect on venting/SVE process efficiency. Int J Energy Environ Eng 8(3):209–217. https://doi.org/10.1007/s40095-017-0238-4
7. Kuppusamy S, Palanisami T, Megharaj M, Venkateswarlu K, Naidu R (2016) Ex-situ remediation technologies for environmental pollutants: a critical perspective. In: de Voogt P (ed) Reviews of environmental contamination and toxicology (continuation of residue reviews), vol 236. Springer, Cham
8. Office of the parliamentary Budget Officer (OPBO) (2014) Federal contaminated sites cost. Ottawa, Canada April 10, 2014. Retrieved November 20, 2019 http://www.pbo-dpb.gc.ca/web/default/files/files/files/Federal%20Contaminated%20Sites%20Cost.pdf
9. Qin C, Zhao Y, Zheng W, Li Y (2010) Study on influencing factors on removal of chlorobenzene from unsaturated zone by soil vapor extraction. J Hazard Mater 176(1–3):294–299. https://doi.org/10.1016/j.jhazmat.2009.11.027
10. Rathfelder K, Lang JR, Abriola LM (1995) Soil vapor extraction and bioventing: applications limitations, and future research directions. Rev Geophys 33(2):1067–1081
11. US Army Crop of Engineers (2002) Soil vapor extraction and bioventing, army engineering manual
12. USEPA (2019) Underground storage tanks (USTs) (2019). Retrieved November 20, 2019, from https://www.epa.gov/ust
13. Yang Y, Li J, Xi B, Wang Y, Tang J, Wang Y, Zhao C (2017) Modeling BTEX migration with soil vapor extraction remediation under low-temperature conditions. J Environ Manage 203:114–122
14. Yu Y, Liu L, Yang C, Kang W, Yan Z, Zhu Y, Zhang H (2019) Removal kinetics of petroleum hydrocarbons from low-permeable soil by sand mixing and thermal enhancement of soil vapor extraction. Chemosphere 236:124319

Diversion of Electron in Mixed Microbial Culture to Treat the High Sulfate and LCFA Contaminated Wastewater Treatment

Rajan Ray, Mamata Sharma, and Nihar Biswas

1 Introduction

Sulfate concentrations are extremely high in wastewater from the chemical and metallurgical industries, while LCFAs are often high in diaries, food, and vegetable oil processing industries. There are numerous challenges associated with the treatment of these effluents, as a variety of different microorganisms are impacted by their toxicity effects. Even though LCFAs inhibit methanogens throughout anaerobic treatments, they disrupt electron fluxes in these processes. Several researchers have documented this diversion of electron fluxes [1, 14].

SRBs generate H_2S by dissimilatory sulfate reduction. However, the ability to use sulfate as an electron acceptor for an energy generating process involves large-scale reduction of sulfate (e.g., in anaerobic wastewater treatment processes) and is unique to SRBs [1, 9]. The type of the carbon source utilized for the reduction of an electron acceptor (SO_4^{2-} varies according to genus and SRBs utilize many different electron donors. The preferred carbon source for SRBs are always low-molecular-weight compounds such as organic acids (e.g., lactate, pyruvate, formate, and malate, VFAs (e.g. acetate, and alcohols (e.g., ethanol, propanol, methanol, and butanol and occasionally sugars and longer chain fatty acids [4, 6]. Most of these products come from the degradation of carbon, protein, and lipids under anaerobic conditions. The SRBs are terminal degraders, and their role is analogous to methanotrophs producing methane and carbon dioxide as final products of anaerobic degradation.

SRB and Methane producing bacteria (MPB) coexist in mixed anaerobic communities and typically, both of these microorganisms are terminal degraders, since they compete for electron donors [7]. In comparison to MPBs, SRBs are much more versatile in terms of substrate utilization. In environments where sufficient sulfate

R. Ray (✉) · M. Sharma · N. Biswas
University of Windsor, Windsor, Canada
e-mail: rayr@uwindsor.ca

S. Walbridge et al. (eds.), *Proceedings of the Canadian Society of Civil Engineering Annual Conference 2021*, Lecture Notes in Civil Engineering 249,
https://doi.org/10.1007/978-981-19-1061-6_21

is present, compounds such as propionate and butyrate, which require syntrophic consortia to degrade in methanogenic environments, are degraded directly [13]. SRBs also have a stronger affinity for acetate, formate, and hydrogen as substrates [2, 15]. In the presence of non-limiting sulfate concentrations, SRBs are believed to out-compete methanogens based on kinetic and thermodynamic properties.

The development of desired terminal products was examined in a mixed anaerobic microbial culture in which electron fluxes from glucose degradation and methane reduction were redirected. In these two instances, the electron flux pattern in mixed microbial communities was investigated in the current study. In the first case, the terminal electron acceptor was sulphate, while in the second case, the terminal electron acceptor was protons rather than sulphate. The electron fluxes were thus redirected to the desired terminal product generation by LCFAs with 18 carbons, which inhibited methanogenesis, the final act in the breakdown of organic matter by anaerobic bacteria.

2 Experimental Methods

The inoculum cultures were collected from the Little River Wastewater Treatment Facility in Windsor, Ontario, as well as a Chatham, Ontario-based ethanol manufacturing facility. To ensure a proper sulfidogenic population for the sulphate reduction studies, the ethanol cultures were blended with the primary municipal sludge in an 80:20 ratio.

Experiments were performed in batch reactors using inocula enriched in 4 L semicontinuous reactors with glucose plus sulfate or glucose only. The VSS concentration in all the batch cultures was 2000 mg/L at 37°C. In diverting electron fluxes to sulfate reduction, a COD/SO_4^{2-} ratio of 1.25 was chosen to establish glucose limiting conditions so that excess sulfate was available for SRBs in the presence of varying LCFA levels (100, 300, 500, 700 and 1000 mg/L) at pH 7.0–7.2. In these studies, the LCFAs under consideration were LA, OA and SA.

3 Results and Discussions

In cultures fed LA and OA, electron fluxes from glucose to SRBs (for sulphate reduction) were observed, while SA had no effect on sulphate elimination (Fig. 1). This is due to LA and OA's inhibitory effect on methanogenic populations. The inhibitory effect of C18 LCFAs on methanogens has been documented by several researchers [3, 11, 12]. OA and LA selectively suppressed methanogens at all concentrations and induced a metabolic change in the syntrophic electron intake pathway, relative to glucose plus sulphate controls. In cultures receiving glucose plus LA or OA, the highest sulphate reduction levels were 92% and 72%, respectively (Fig. 1). Only 24% of the sulphate was removed from cultures receiving glucose plus SA, whereas 31%

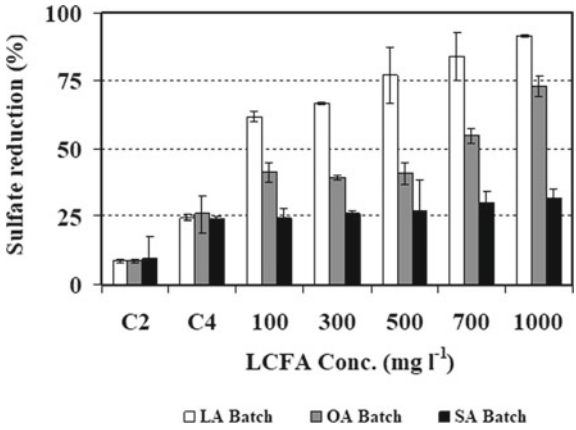

Fig. 1 Percentage of sulphate reduction (maximum removal) in cultures fed with 1870 mg/L glucose, 1500 mg/L sulphate and 100 to 1000 mg/L LCFA (C2 = Sulfate control; C4 = Glucose plus sulfate control). The values shown are mean and standard deviations for triplicate samples

of the sulphate was removed from cultures receiving glucose plus sulphate controls According to literature [3] the degree of inhibition of methanogenesis increases with the number of double bonds. The same pattern was observed in the case of sulphate reduction in the presence of C18 LCFAs.

C18 LCFAs (LA (C18:2), OA (C18:1), and SA (C18:0) are less soluble (3 mg/L) and hence inaccessible to microorganisms [8, 10]. The inhibition caused by LCFAs is likely due to their surfactant properties. LA decreases the interfacial stress between the bacterial membrane and the bulk aqueous phase of the growth medium, acting as a surfactant (surface-active agent) [5].

Compounds such as LA (C18:2) can reduce the interfacial tension on cell surfaces by lowering their surface tension. As a poorer surfactant than LA, SA (C18:0) was reported not to inhibit growth at 30 °C compared to LA [5]. This inhibition is mainly achieved through LCFA adsorption. Once adsorption occurs, the LCFAs begin the inhibition process by interfering with both extra- and intracellular processes.

The initial levels of sulphate and glucose degradation were affected by LA and OA. Sulfate removal data show that LA and OA helped reduce the sulphate while SA had no observable effect (Fig. 2a). Increased LA and OA levels decreased the initial glucose degradation rate compared to their effects on sulphate (Fig. 2b). Inhibition of Glucose degradation has been increased with increasing levels of unsaturation and LA and OA concentrations. LA inhibited more than SA on glucose degradation [11]. All the cultures examined for sulfate reduction contained higher amount of acetate and propionate from glucose degradation.

4 Conclusions

The use of LCFAs with unsaturated C–C double bonds resulted in a metabolic change in the syntrophic microbial pathway, diverting electron equivalents to SRBs, while SA

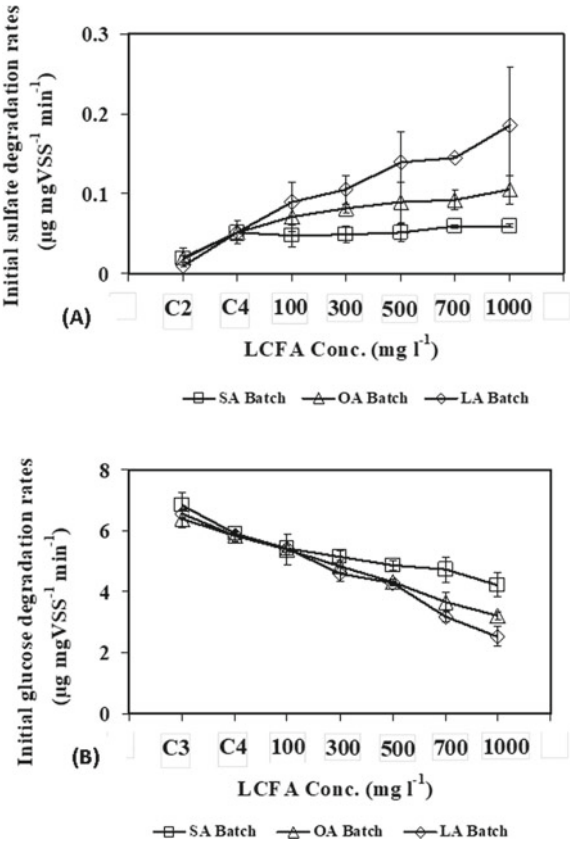

Fig. 2 Initial degradation rates (maximum elimination) for cultures fed with 1870 mg/L glucose, 1500 mg/L sulphate and 100 to 1000 mg/L LCFAs. (a = Initial rate of sulphate degradation; b = Initial rate of glucose degradation. The values shown are mean and standard deviations for triplicate samples. C2 = Control of sulphate; C4 = Control of glucose plus sulphate)

with no double bond had no impact on sulphate removal. With the use of OA (LCFA with one unsaturated C–C double bond) and LA (LCFA with two unsaturated C–C double bonds), methanogens were inhibited and electron equivalence competition between MPBs and SRBs decreased. The flow of electron fluxes towards sulfidogenesis was a factor of both LCFA concentration and types. As compared to cultures that only received glucose and sulphate. A maximum sulfate reduction of 1380 mg/L (92%) was observed in cultures receiving LA, while only 24% sulfate reduction was observed in cultures receiving glucose plus sulfate. Furthermore, up to 73% sulfate reduction and a 22% increase in overall electron flow were observed when OA was used to inhibit methanogenesis. The concentrations of OA and LA increased the percentage electron flow and the sulfate reduction.

Acknowledgements This study was sponsored by NSERC Canada.

References

1. Ahmed W, Rodríguez J (2018) Modelling sulfate reduction in anaerobic digestion: complexity evaluation and parameter calibration. Water Res 130:255–262
2. Cetecioglu Z, Dolfing J, Taylor J, Purdy KJ, Eyice Ö (2019) COD/sulfate ratio does not affect the methane yield and microbial diversity in anaerobic digesters. Water Res 155:444–454
3. Dasa KT, Westman SY, Millati R, Cahyanto MN, Taherzadeh MJ, Niklasson C (2016) Inhibitory effect of long-chain fatty acids on biogas production and the protective effect of membrane bioreactor. BioMed Res Int
4. Gibson GR (1990) Physiology and ecology of the sulfate-reducing bacteria. J App Bacteriology 69:769–797
5. Greenway KGA, Dyke KGH (1979) Mechanism and the inhibitory action of linoleic acid on the growth of Staphylococcus aureus. J Gen Microbiol 155:233–245
6. Hao OJ, Chen JM, Huang L, Buglass RL, (1996). Sulfate–reducing bacteria. Cri Rev Env Sci TechnoL 26:155–187
7. Lens P, Visser A, Janssen A, Hulshoff Pol L, Lettinga G (1998) Biotechnological treatment of sulfate rich wastewaters. Crit Rev Environ Sci Technol 28:41–88
8. Ma J, Zhao QB, Laurens LL, Jarvis EE, Nagle NJ, Chen S, Frear CS (2015) Mechanism, kinetics and microbiology of inhibition caused by long-chain fatty acids in anaerobic digestion of algal biomass. Biotechnol Biofuels 8:141
9. Madigan MT, Martinko JM, Parker J (2000) Brock biology of microorganisms. Prentice-Hall Inc.NJ, USA, pp 574–634
10. Ray S, Saady N, Lalman J (2009) Diverting electron fluxes to hydrogen in mixed anaerobic communities fed with glucose and unsaturated C18 long chain fatty acids. J Environ Eng 136(6):568–575
11. Shin HS, Kim SH, Lee CY, Nam SY (2003) Inhibitory effects of long-chain fatty acids on VFA degradation and β-oxidation. Water Sci Technol 47(10):139–146
12. Sousa DZ, Salvador AF, Ramos J, Guedes AP, Barbosa S, Stams AJ, Madalena Alves M, Pereira MA (2013) Activity and viability of methanogens in anaerobic digestion of unsaturated and saturated long-chain fatty acids. Appl Environ Microbiol 79(14):4239–4245
13. Stams AJM, Plugge CM, De Bok FAM, Van Houten BHGW, Lens P, Dijkman H, Weijma J (2005) Metabolic interactions in methanogenic and sulfate-reducing bioreactors. Water Sci Technol 52:13–20
14. Yang F, Bai L, Li P, Li Q, Luo L, Li W (2019) Improved methane production and sulfate removal by anaerobic co-digestion corn stalk and levulinic acid wastewater pretreated by calcium hydroxide. Sci Total Environ 691:499–505
15. Zan F, Hao T (2020) Sulfate in anaerobic co-digester accelerates methane production from food waste and waste activated sludge. Bioresour Technol 298:122536

Mitigating Fugitive Methane Emissions from Closed Landfills: A Pilot-Scale Field Study

B. R. Nelson, R. G. Zytner, Z. L. Kanmacher, A. Yochim, R. Vaillancourt, B. Boss, Y. Dulac, and A. R. Cabral

1 Introduction

Emissions from Canadian landfills account for 20% of national emissions [2], a portion of which is represented as fugitive methane (CH_4) emissions that are uncaptured by gas collection systems. The challenge continues following landfill closure, where capturing/treating fugitive gas emissions must continue, as small emissions of gas can occur for a period reaching 100 years. Designing landfill covers in a way that maximizes methane oxidation capacity provides a promising corresponding strategy for the control of emissions escaping gas collection systems [4]. Methane oxidation is particularly desirable for emission mitigation at closed sites where the methane production is too low for energy recovery or flaring, and where the use of a gas extraction system is less effective.

Passive methane oxidation biosystems (PMOBs) are considered a scientifically sound and cost-effective treatment system for fugitive CH_4 emissions. Microbial oxidation of methane gas is achieved by methanotrophic bacteria (or methanotrophs), a group of mostly mesophilic obligate aerobes [5]. Methanotrophs utilize CH_4 as a carbon and energy source, aerobically oxidising methane to carbon dioxide [3, 5]. Carbon dioxide formed inside landfills and released into the atmosphere produces a

B. R. Nelson · R. G. Zytner (✉) · Z. L. Kanmacher
School of Engineering, University of Guelph, Guelph, ON N1G 2W1, Canada
e-mail: rzytner@uoguelph.ca

A. Yochim · R. Vaillancourt
Waste Management, Regional Municipality of Waterloo, Waterloo, ON N2J 3Z4, Canada

B. Boss
Dillon Consulting Limited, Edmonton, AB T6X 1M5, Canada

Y. Dulac · A. R. Cabral
Department Civil and Building Engineering, Université de Sherbrooke, Sherbrooke, PQ J1K 2R1, Canada

S. Walbridge et al. (eds.), *Proceedings of the Canadian Society of Civil Engineering Annual Conference 2021*, Lecture Notes in Civil Engineering 249,
https://doi.org/10.1007/978-981-19-1061-6_22

negligible effect on the environment due to its biogenic origin and the insufficient quantities relative to other human-related CO_2 sources [4]. Conversely, the global warming potential of methane is described as 36 times greater than that of CO_2, over a period of 100 years [6].

The objective of this on-going study is to develop a design procedure for a PMOB capable of abating fugitive methane emissions that reach the surface of landfills. Factors considered include type of biofilter media, methane loading rates, impact of the hydraulic contrast between materials, and ambient temperature. The effectiveness of the design will be evaluated through a pilot-scale PMOB developed to assist the Region of Waterloo in creating a long-term solution to mitigate fugitive methane emissions at closed and active landfills. Performance is monitored via various sensors for water content, temperature, soil suction, and CH_4 concentrations at the surface and within several profiles. Successful completion of the project will provide a low-maintenance, high impact technology to abate landfill emissions, which could be applied by landfill designers and operators across Canada. The following sections present the steps taken to design, install and monitor the PMOB.

2 Materials and Methodology

2.1 Study Area

The pilot-scale PMOB was built at a closed landfill, now a popular public park located in Kitchener, Ontario. The landfill was active from 1958 to 1978, and thus has been closed for over 40 years. Environmental control infrastructure is in place to monitor and control landfill gas. Challenges exist throughout the park with methane mitigation, specifically, localized fugitive CH_4 emissions (hotspots).

2.2 PMOB Design

The methane oxidation layer (MOL) material pre-selection was based on geotechnical and hydraulic characteristics, as well as accessibility and cost. Three materials were pre-selected for testing based on availability from the Region of Waterloo: two types of soils and one compost. A decision was made to mix the compost with recycled plastic pellets (ratio of 2-parts compost to 1-part pellets), as the material required more structure. The geotechnical and hydraulic characteristics of the materials were determined, including the air permeability functions using the methodology described in Ahoughalandari et al. [1]. Saturated hydraulic conductivity tests were conducted using various apparatuses, and the water retention curves (WRC) were obtained using the HYPROP apparatus (Meter Inc.). The hydraulic permeability functions were obtained using the WRC and applying the van Genuchten–Mualem

formulation [7]. The geotechnical and hydraulic characteristics revealed the compost-recycled plastic pellets mixture as the most suitable MOL material. The hydraulic parameters were then modelled using Hydrus 2D to assess the overall hydraulic behaviour of the PMOB and help select the slope and length of the PMOB.

2.3 PMOB Construction

Construction of the PMOB began in October 2020. The PMOB, shown in Fig. 1a, is contained in a 10 × 3 × 1.2 m plywood box on an 8% slope, supported with 2 × 4 inch framing and outer bracing. A base fill consisting of 0–3/4 inch gravel was installed with a 3:1 slope on the outer edges to mitigate erosion and washout. Inside the box is a foam layer for insulating and a geomembrane liner for drainage. Water collected in the bottom is drained out through a heat-traced p-trap (to avoid unaccounted for inflow of air). The design includes a ¾ inch gravel base that serves as gas distribution layer (GDL). The GDL is placed upon a geotextile layer, which is placed above the geomembrane. The pipe distribution system integrated into the GDL (Fig. 1b) distributes the gas loading evenly throughout the surface of the PMOB. Two transitional layers were placed above the GDL: ¼ inch gravel and sand. A heating system (Heat-Line®) was installed in the sand layer to maintain optimal temperatures in the MOL throughout the colder months. The MOL consists of a 1 m-thick layer of the compost-plastic pellet mixture.

Three 4 m-deep wells were installed to supply landfill gas to the PMOB. The biogas connection system includes a sloped pipe with a condensate reservoir connecting to the three well heads. A capped Y-fitting is included for future mixing with the ambient air to provide oxygen to the PMOB to maintain appropriate CH_4 and O_2 levels. The addition of air depends on the landfill gas composition and will vary with time.

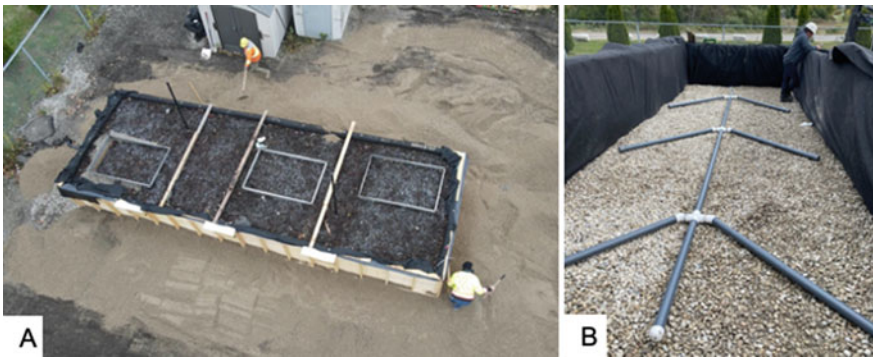

Fig. 1 **a** Aerial view of constructed PMOB. **b** Perforated pipe system in the gas distribution layer

A mass flowmeter was installed to monitor the CH_4 loading to the PMOB, which is to be controlled manually. There are sample ports at each well head and after the Y-fitting to measure CH_4 concentrations at the inlet to calculate system efficiencies.

2.4 PMOB Monitoring

The PMOB is a fully instrumented and monitored system on an x, y, z coordinate system with integrated sensors, measurement tools and environmental monitoring equipment. TEROS 10 (Meter Inc.) probes, used to measure water content, and TEROS 11 (Meter Inc.) probes, used to measure water content and temperature, are distributed at various depths to monitor conditions in the MOL profile. TEROS 32 (Meter Inc.) tensiometers, used to measure suction, will be installed during above-freezing temperature periods, providing information about the hydraulic behaviour of the compost mixture at the MOL-GDL interface. The field data collected will be used to reconstruct the WRC of the MOL for potential future design adjustments. Settlement plates were installed as a method to measure the settlement of the compost over time, permitting further adjustment of the hydraulic properties of the mixture. An ONSET weather station was installed near the PMOB to collect relevant atmospheric data, including precipitation.

Gas concentrations will be measured through two approaches: the first uses a micro gas chromatograph (Micro GC 3000 A, Agilent) using samples extracted from gas probes at four different depths within the three profiles; the second uses a flame ionisation detector (TVA 1000, Thermo Fisher) to measure CH_4 concentrations within three large-scale flux chambers, which permit surface flux calculations. The surface fluxes and CH_4 loading data will be used to calculate mass balances, therefore system efficiencies.

3 Discussion

This project is in the initial phase of operation. A limited database shows that optimal temperatures for CH_4 oxidation (25–35 °C) are being met. The heating system installed above the sand layer kept the MOL at optimal temperatures for methanotrophs during the winter months. As shown in Fig. 2a, at a depth of 95 cm (i.e., 5 cm above the heating system), the temperature was approximately 40 °C. Temperatures are maintained well within the ideal range as far as 20 cm deep (T ~20 °C). Only near the surface (10 cm; T ~6 °C) did temperatures fall below the ideal range.

Water content is an essential factor for microbial activity [5]. However, too much water accumulation at the bottom of the system impedes gas migration, forcing it to flow upslope or, in worst-case scenario, preferential flow along the edges of the PMOB. Preliminary air permeability test results revealed that the water content resulting in air occlusion is approximately 52%. Figure 2b shows that water content

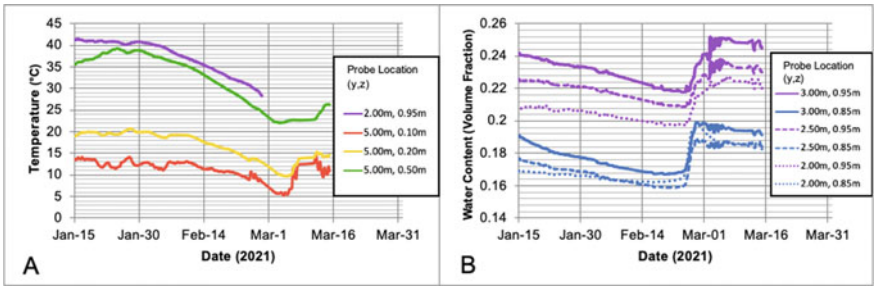

Fig. 2 **a** MOL temperature profile the center of the PMOB. **b** MOL water content at the MOL-GDL interface in the downslope region of the PMOB

was in the optimal range for methane oxidation, as it ranged from 16 to 25% in the downslope region, where the greatest accumulation of precipitation was expected.

4 Next Steps

Supply of landfill gas to the PMOB started in late February 2021. Loading will be increased slowly over several weeks to allow microbial community development. As spring approaches, temperatures will be monitored to ensure they do not rise over the optimal range. Subsequently, proper monitoring will start, with frequent measurements of surface CH_4 fluxes, inlet CH_4 concentrations, and MOL profile gas concentrations. Temperature and water content will be continuously monitored to assess design efficiency and necessary maintenance.

A future step includes stress tests to assess the capacity of the PMOB to respond to sudden changes in conditions such as temperature and CH_4 loading. Ultimately, this project will provide all the elements needed by the Regional Municipality of Waterloo for future implementation of PMOB systems for the mitigation of fugitive CH_4.

Acknowledgements The work presented in this paper received financial support from NSERC (ALLRP 548667-2019), Dillon Consulting Ltd. and the Regional Municipality of Waterloo.

References

1. Ahoughalandari B, Cabral AR, Leroueil S (2018) Elements of design of passive methane oxidation biosystems: fundamental and practical considerations about compaction and hydraulic characteristics on biogas migration. Geotech Geol Eng J 36(4):2593–2609
2. Environment Canada (2017) Municipal solid waste and greenhouse gases. Government of Canada, retrieved 02 11, 2020, from https://www.canada.ca/en/environment-climate-change/services/managing-reducing-waste/municipal-solid/greenhouse-gases.html

3. Gebert J, Groengroeft A, Miehlich G (2003) Kinetics of microbial landfill methane oxidation in biofilters. Waste Manage 23(7):609–619
4. Huber-Humer M, Roder S, Lechner P (2009) Approaches to assess biocover performance on landfills. Waste Manage 29(7):2092–2104
5. Scheutz C, Kjeldsen P, Bogner J, De Visscher A, Gebert J, Hilger H, Huber-Humer M, Spokas K (2009) Microbial methane oxidation processes and technologies for mitigation of landfill gas emissions. Waste Manage Res 27(5):409–455
6. Stocker T (2014) Climate change 2013: the physical science basis: working group I contribution to the fifth assessment report of the intergovernmental panel on climate change. Cambridge University Press, New York, USA
7. Van Genuchten MT (1980) A closed-form equation for predicting the hydraulic conductivity of unsaturated soils. Soil Sci Soc Am J 44:892–898

Improved NASM Framework for Food Processing Wash-Water and Solid Residuals

C. Dunlop, B. Abbassi, A. Costas, L. Dunnett, and R. G. Zytner

1 Background

Ontario's agri-food sector is challenged to meet the environmental regulations for land application of food processing wastewater, solids, and organic matter defined as NASM. Ontario Regulation 267/03 (O. Reg. 267/03) under the Nutrient Management Act (NMA) outlines the requirements that NASM has to meet to avoid any negative environmental and human health risks associated with land application of the different sources of material. O. Reg. 267/03 classifies NASM into three different categories. Currently, Category 2 NASM (waste and wash-water from processed fruits and vegetables) and Category 3 NASM (includes dairies and abattoirs) have stringent requirements that processors must follow. These categories require a NASM plan to be completed which outlines various parameters that need to be tested for prior to land application such as 11 heavy metals and additional criteria if specified under Section 98.0.16. (O. Reg. 338/09, S.70). Based on the Government of Canada's average costs for a laboratory analysis of a sample, the average price range per sample of heavy metals can range between $35 and $100 CAD [2]. Additionally, certified NASM plan developers must be continually retained by the facility to complete the required NASM documentation. It is estimated that the annual fees for staying compliant can add up to $25,000 per year in cost to the facilities. Many processors believe that these regulations are overly burdensome due to all the sampling and reporting which is not feasible for smaller wash-water facilities looking into land application of NASM.

C. Dunlop · B. Abbassi · A. Costas · L. Dunnett · R. G. Zytner (✉)
School of Engineering, University of Guelph, Guelph, Canada
e-mail: rzytner@uoguelpha.ca

C. Dunlop
e-mail: cdunlop@uoguelpha.ca

S. Walbridge et al. (eds.), *Proceedings of the Canadian Society of Civil Engineering Annual Conference 2021*, Lecture Notes in Civil Engineering 249,
https://doi.org/10.1007/978-981-19-1061-6_23

The Ontario government is committed to reducing regulatory burden for all businesses to help improve Ontario's economic competitiveness. Previous changes have already been made to the NMA and O. Reg. 267/03, which re-categorized lower risk manures from non-farm grazing animals such as zebras and elephants from Category 3 to Category 1. Category 1 NASM does not require the same sampling and analysis as Category 3 NASM. Amendments were also made to remove the automatic cessation on the Nutrient Management Strategy (NMS) after five years. The five-year cessation rule was currently applied even if no change in agricultural operation occurred and this amendment will help reduce administrative burden for farmers. The total expected benefits from these changes are estimated to provide cost savings as well as additional business opportunities totalling an average of $1.2 million per year for all phased-in farms [1]. In order for Ontario to continue its prosperous growth within the agri-food sector, the industry should continue to adopt sustainable and economically viable resource management for food based wash-waters and solid residuals that are being generated.

Therefore, the main goal for this case study project was to identify areas in the current O. Reg. 267/03 regulations, where regulatory burden can be reduced, and where regulatory oversight is still needed to protect public interest. The output of this project will be a comprehensive report that assembles all information obtained from existing practices in NASM management. Additionally, a LCA study is being completed on a representative agri-food processor, which will provide further information to help develop improved best management practices (BMPs). Completion of this project will enhance Ontario's database for a comprehensive analysis of the management of wash-waters and residuals for the Ontario context. Overall, improving Ontario's regulatory framework will help processors to be more economically competitive and will also help provide better utilization of NASM on Ontario farm fields, which is a direct fit with the Ontario Soil Strategy [3].

2 Approach

A detailed approach was created for the project to determine how the data would be obtained and how the research objectives would be accomplished. First, wash-waters across the Ontario agri-food sector were examined to characterize the solid residues produced. For this step, wash-water data was summarized from previous projects on residual management across provincial ministries such as the Ontario Ministry of Agriculture, Food and Rural Affairs (OMAFRA) to identify any trends or gaps within the available data. Next, a comprehensive literature review was completed on scientific studies of wash-water treatment and final disposal for the food processing industry to identify any further limitations within the current data. Once the literature review was completed, a jurisdiction scan was conducted to understand how food processing wash-water are being regulated in other provinces, U.S. states and across the world. Here, a survey was created that was used to obtain additional information on the regulatory practices from agronomists within various jurisdictions.

Next, NASM case studies were initiated with several processors who currently land apply their wash-water materials as NASM. Several sectors are being looked at, including, cheese, fresh cut fruit and vegetables and abattoirs. The case studies allow the team to understand and identify any challenges producers faced while they develop and implement a NASM plan. The case studies looked to show what works well, what could be improved, and what it costs these processors for their NASM plans and land application. The review will keep the processor anonymous, but the case history information will provide valuable input for developing best management practices (BMPs) as these processors will help to identify additional limitations of the current regulations.

Finally, a LCA study is being completed on representative NASM processors across the sector to help support the development of improved best management practices (BMPs) for Ontario. The data from the case studies discussed previously were used here as the initial data set and have been supplemented by information collected from literature or agencies. The LCA study will be carried out under the guidelines of ISO 14040, the international standard for life-cycle assessment. The software SimaPro 8.0.4.26 is the LCA model version that was used with all the databases included for the study. Furthermore, the TRACI assessment tool was used to calculate the environmental impacts. An important component of the LCA study is setting the boundary conditions, which helps decide the depth of the study. For this LCA study the boundary conditions are such that NASM disposal was considered. Completion of this LCA looks to provide additional information for the development of BMPs for Ontario.

3 Results and Discussion

The first step of the project was to examine previous project data on wash-water and residual management to identify any gaps and limitations. Data was made available from previous OMAFRA projects conducted on wash-waters and solid residuals including fruits and vegetables, abattoirs, cheese and dairy, brewery and food processing in general. The wash-water information was scattered in diverse reports, so it first had to be collected and organized. Additionally, the wash-water data was sampled from various locations throughout the facilities and had to be sorted for samples obtained from the end of the facility processes, as this would be the material that would be land applied at the end. Initially, there were around 700 wash-water samples from different locations throughout the facilities and for a variety of parameters. After sorting through the data for samples at the end of the facility in combination with samples containing heavy metal data, the final data set consisted of a total of 126 samples.

With the heavy metal wash-water data set organized, the next step was to analyze and summarize any trends or limitations within the samples. The focus on this step was analyzing the heavy metal parameters of the wash-water, as all these sources of NASM are required to be sampled for 11 heavy metals under O. Reg. 267/03. O.

Reg. 267/03 has two categories for heavy metals; CM1 and CM2, where CM1 is the lowest concentrations of heavy metals that can be applied. If the samples exceed any limits for CM1, the land application rate of the NASM will have to be lowered. If the CM2 regulations are exceeded, the NASM material cannot be applied. As shown in Table 1, out of a total of 126 wash-water samples, only 13 samples were detected that exceeded the CM1 values for heavy metals.

Based on the low occurrence of heavy metal values (Table 1), it is no surprise that producers question the need for on-going metal analysis. The repeated sampling incurs additional costs to the facilities, which is not feasible for smaller wash-water operations. Furthermore, as shown through this initial analysis, there is little evidence of any heavy metals within the wash-water. Sewage biosolid facilities are categorized with sources of food processing wash-water and therefore have similar sampling requirements prior to land application, but their influent material changes based on which industries are contributing wastewaters. When compared to food processing wash-water facilities, the influent material here is relatively consistent unless a completely new produce is being handled. Therefore, one major recommendation based on these preliminary results would be to decrease the sampling frequency that is required for wash-water facilities for heavy metals. Moreover, improvements such as a potential Category 4 NASM for food processing wash-waters are being looked into, where Category 4 NASM could have different requirements for sampling and reporting for their NASM plans based on the specific material.

After completing the initial analysis of previous wash-water data, the next goal for the project was to determine how other jurisdictions are currently handling their food-based wash-waters and residues. By understanding how other jurisdictions are handling their materials, Ontario can then evaluate where it could make further improvements to the regulatory framework. A focus for this step was on determining how the other jurisdictions are sampling for heavy metals, as this was a gap that was identified in the previous results. To obtain the jurisdiction information, regulations and associated with land application of wash-water or biosolids were searched for across the world. Additionally, a survey was created that was used to obtain further information from agri-food specialists within that jurisdiction if any contacts could be made. This survey was used to help better understand how the agronomists within that jurisdiction felt about the land application regulations and if there were any improvements that could be made.

The jurisdiction scan revealed that Ontario was one of the most advanced and stringent jurisdictions for regulations associated with wash-water or biosolid land application. First, it was found that out of all the jurisdictions that were evaluated, Ontario had the highest frequency of sampling for heavy metals. For example, Quebec omits all of the heavy metal sampling if the source of the material is agri-food biosolids, but heavy metals are required to be sampled if the source is sewage biosolids. Furthermore, it was identified that Ontario has the most stringent limits for heavy metal standards. For example, the limit for mercury that can be land applied within the material in states such as Wisconsin and Kentucky are 70 times greater than Ontario. As mentioned previously, the focus here was on the heavy metal standards as this was

Table 1 Summary of wash-water samples compared to CM1 standards (O. Reg. 267/03)

Heavy metal CM1 values from O. Reg. 267/03	As 0.13 (mg/L)	Cd 0.03 (mg/L)	Co 0.34 (mg/L)	Cr 2.1 (mg/L)	Cu 1.0 (mg/L)	Pb 1.5 (mg/L)	Hg 0.008 (mg/L)	Mo 0.05 (mg/L)	Ni 0.62 (mg/L)	Se 0.02 (mg/L)	Zn 5.0 (mg/L)
Total samples	126	126	126	126	126	126	126	126	126	126	126
Number of samples > CM1	0	2	0	4	1	0	1	2	3	0	0
Number of samples > CM2	0	0	0	0	0	0	0	0	0	0	0

found to be a limitation in the data from the previous step. However, additional information was also collected from the jurisdictions on soil health parameters (sodium, fats oils and greases (FOGs) and organic carbon content), setback distances and frequency of sampling which will be highlighted in the upcoming presentation and comparisons using GIS will be shown for visualization purposes.

3.1 Next Steps

The next steps for this project will be to complete additional processor case studies to understand and identify any challenges faced while they develop and implement a NASM plan. This step is currently being conducted and so far three case studies have been conducted on Ontario cheese processors. The current case studies have highlighted additional improvements that can be made to the regulations regarding decreased sampling frequency and increased land application timeframes, if the weather is permitting. Additional summaries of case studies are looking to be completed on fruit and vegetable and abattoir processors to understand if there are similar challenges across the different wash-water categories. Furthermore, the LCA study is also being completed, which will help to provide additional insight for the development of BMPs. The results of the wash-water data analysis, literature review, jurisdiction scan, processor case studies, and LCA study will be further discussed in the upcoming presentation.

Acknowledgements The authors would like to thank OMAFRA for funding through a special initiative project (SIP). Additionally, the authors are grateful for the support provided by Peter Doris, Environmental Specialist with OMAFRA, for input on the project and coordinating discussions with the various processors and OMAFRA colleagues.

References

1. DeVos G (2019) Proposed regulatory amendments to Ontario regulation 267/03 under the nutrient management act. https://www.ontariocanada.com/registry/view.do?postingId=28106
2. Government of Canada (2020) Average costs for the laboratory analysis of a sample. https://gost.tpsgc-pwgsc.gc.ca/fld_cst.aspx?lang=eng
3. OMAFRA (2019) Ontario's agricultural soil health and conservation strategy. http://www.omafra.gov.on.ca/english/landuse/soil-strategy.htm#intro1

Multifunctional PVDF Membrane Modified with Nanocomposites for Membrane Fouling Mitigation

Xiujuan Chen, Gordon Huang, Chunjiang An, and Yinghui Wu

1 Introduction

Membrane-based filtration technology has been extensively applied for water and wastewater treatment due to its advantages in high compactness, reliability, and efficiency [1]. Poly(vinylidene fluoride) (PVDF) membrane, one of the most robust membranes with high mechanical strength, excellent thermal stability, and great chemical resistance, has been commonly used for wastewater treatment processes [2]. However, due to the low surface energy and high hydrophobic property, they usually suffer from membrane fouling, particularly organic and biological fouling. Organic fouling involves the formation of cake layer through the accumulation of organic matters, and biological fouling associates with the growth of biofilm owing to the adhesion of microorganisms on membrane surface [3]. The problem of membrane fouling leads to dramatic decrease in permeate flux, thus increasing operation cost and shortening membrane lifetime [4]. Therefore, developing a PVDF membrane with both properties of hydrophilicity and antimicrobial is desired for its practical application.

Surface modification with hydrophilic materials has been regarded as a promising strategy to mitigate organic fouling and increase permeate flux for PVDF membrane,

X. Chen (✉)
Institute for Energy, Environment and Sustainable Communities, University of Regina, Regina, Canada
e-mail: xchen@iseis.org

G. Huang · Y. Wu
Faculty of Engineering and Applied Science, University of Regina, Regina, Canada
e-mail: huangg@uregina.ca

C. An
Department of Building, Civil and Environmental Engineering, Concordia University, Montreal, Canada

S. Walbridge et al. (eds.), *Proceedings of the Canadian Society of Civil Engineering Annual Conference 2021*, Lecture Notes in Civil Engineering 249,
https://doi.org/10.1007/978-981-19-1061-6_24

however, this method may not effectively prevent biofouling at the same time [3]. Recently, nanocomposites (NCPs) decorated with silver nanoparticles (Ag NPs) were loaded onto membrane surfaces to simultaneously improve membrane hydrophilicity and antibacterial activity, since Ag NPs have strong antimicrobial property to a variety of bacteria. For example, silver nanoparticle/multiwalled carbon nanotubes (Ag/MWNTs) were coated on polyacrylonitrile (PAN) membranes to act as a disinfection barrier and reduce biofilm formation [5]. Ag/SiO_2 NCPs were loaded onto a PVDF membrane surface, which reduced the water contact angle from 81.6° to 34.4° and enhanced its anti-fouling performance [6]. Silver functionalized graphene oxide (Ag–GO) NCPs were also applied for surface modifications of PVDF membranes to improve filtration performances [7]. However, these efforts may struggle with high cost and low efficiency because of the characteristics of mentioned NCPs. Few research involves modification of membrane surface with silver decorated zink oxide (ZnO–Ag) NCPs.

Therefore, a multifunctional PVDF membrane was developed through chemical binding with ZnO–Ag NCPs on commercial membrane surface. The obtained membrane was expected to have properties of surface hydrophilicity and organic/bio fouling resistance. The effects of NCPs on the membrane hydrophilicity and antimicrobial properties were investigated. The improvements in filtration performance and antifouling ability of the functionalized membrane were demonstrated through the treatment of secondary wastewater effluent.

2 Methods

A typical deposition–precipitation method was used to synthesize ZnO–Ag NCPs. PVDF microfiltration membrane with 0.1 μm of average pore size was purchased from TQX Membrane Technology Ltd. (Xiamen, China). A poly(acrylic acid) (PAA) layer was introduced on membrane surface through cold plasma-induced graft-polymerization to immobilize ZnO–Ag NCPs. Morphology and elementary composition of membrane surface were characterized by scanning electron microscopy (SEM) (JSM-6510; Rigaku) equipped with an energy dispersive X-ray spectroscopy (EDS). Surface contact angle measurements (OCA20; DataPhysics Instruments) were performed with the sessile drop method. The impacts of nanocomposite coating on membrane performances were assessed in a cross-flow filtration system (CF016 membrane test skid; Sterlitech Corporation). Feed water samples were collected from the secondary wastewater effluent in the Regina Water Treatment Plant, Canada. Membrane performances including water flux, permeate flux, and removal rates of total organic carbon (TOC), total nitrogen (TN), and bacteria were investigated. The live *E. coli* bacteria attached on the used membrane surface was measured by cfu enumeration. The concentrations of TOC and TN in feed and permeate solutions were monitored by a TOC/TN analyzer (TOC-L; Shimadzu).

The permeation flux (J_w, L/m^2·min) of membrane was defined as follows:

$$J_w = V/(A \times \Delta t) \tag{1}$$

where V is the permeate water volume (L), A is the effective membrane area (m^2), and Δt is the permeation time (min).

The removal rate R_i (%) was defined as follows:

$$R_i(\%) = \left(1 - C_{pi}/C_{fi}\right) \times 100 \tag{2}$$

where C_{pi} is the concentration of i in the permeate solution (mg/L), C_{fi} is the concentration of i in the feed water (mg/L), and $i = 1, 2$ which denotes TOC and TN, respectively. The quality assurance/quality control (QA/QC) program was followed to ensure the accuracy and reliability of the collected data.

3 Results

SEM images in Fig. 1 show the surface morphologies of the original and functional PVDF membranes. After modification, ZnO–Ag NCPs were immobilized to PAA-coated membrane surface through combining with carboxyl groups of PAA, forming a PAA-NCP coating (Fig. 1c). The result of EDS from the functional PVDF membrane surface in Fig. 1d also proved the successful formation of PAA-NCP coating, in which the elements of Zn and Ag were newly detected. This PAA-NCP coating was expected to endow excellent hydrophilicity and oleophobicity to the

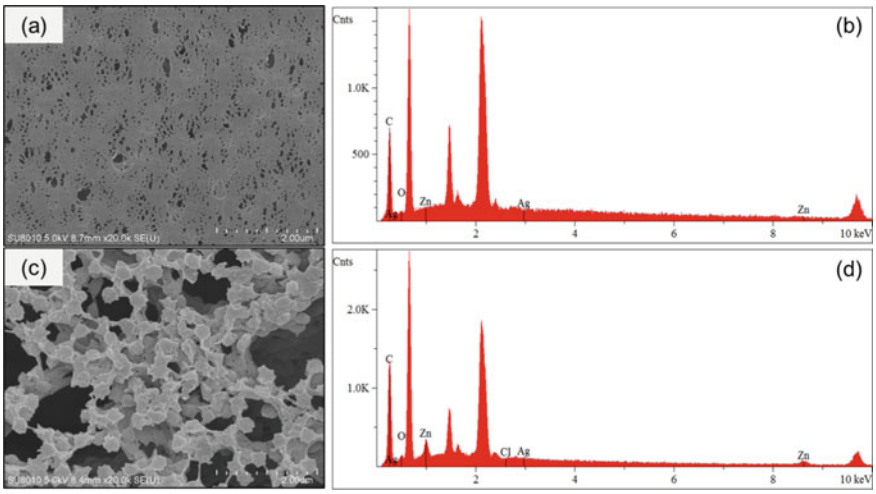

Fig. 1 Results of SEM images and EDX: **a–b** the original PVDF membrane, and **c–d** the functional PVDF membrane

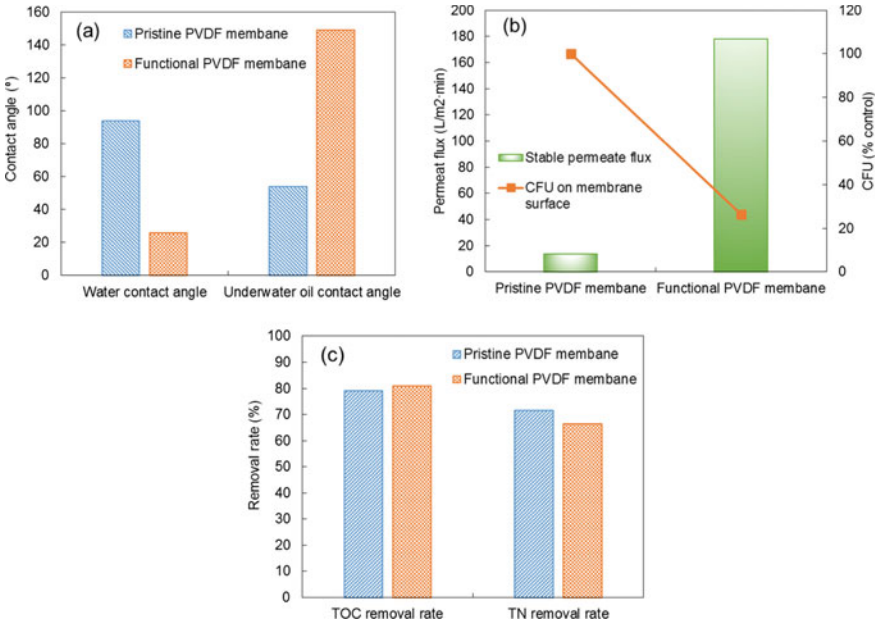

Fig. 2 Performance comparison of the original and functional PVDF membranes: **a** contact angle, **b** permeate flux and fouling resistance, and **c** TOC and TN removal rate

functional PVDF membrane surface. After modification, the water contact angle decreased from ~ 94° to ~ 26°, and the underwater oil contact angle dramatically increased from ~ 54° to ~ 150° (Fig. 2a). This brought about significant improvements of membrane performances both in permeate flux and fouling resistance.

The filtration performance of the membranes for was evaluated and compared through the treatment of secondary wastewater effluent under 3 bar of operating pressure, and the results were summarized in Fig. 2. As shown in Fig. 2b, the functional PVDF membrane showed much higher stable permeation flux which was about 180 L/m^2 min, while the stable permeation flux of the original PVDF membrane was lower than 20 L/m^2 min. Meanwhile, the relative numbers of viable *E. coli* cells on membrane surfaces after filtration experiments were compared in Fig. 2b. After filtration experiments, the attached *E. coli* cells on the membrane surfaces were detached through sonication in saline solution, and then incubated 24 h for cfu plate counting. The counted cfu data of the functional PVDF membrane was normalized to the data of the original PVDF membrane for analysis. It was found that the number of viable *E. coli* cells attached on the functional PVDF membrane surface was only ~26% of that on the original membrane, indicating much stronger antibacterial activity of the functional PVDF membrane. Moreover, the TOC and TN removal rates of the two membranes were comparable (Fig. 2c), demonstrating that the surface modification did not decrease the overall contaminant rejection rate.

4 Conclusion

In this study, a functional PVDF membrane was functionalized with ZnO–Ag NCPs to improve treatment efficiency and mitigate biofouling for water and wastewater treatment. The formation of PAA-NCP coating endowed properties of hydrophilicity, oleophobicity, and antibacterial activity to the modified membrane. The functional PVDF membrane thus exhibited strong biofouling resistance and superhigh permeate flux without sacrificing contaminant rejection rates during filtration process.

Acknowledgements This research was supported by Canada Research Chair Program, Natural Science and Engineering Research Council of Canada, Western Economic Diversification (15269), and MITACS.

References

1. Chen X, Huang G, Li Y, An C, Feng R, Wu Y, Shen J (2020) Functional pvdf ultrafiltration membrane for tetrabromobisphenol-a (tbbpa) removal with high water recovery. Water Res 115952
2. Chen X, Huang G, An C, Feng R, Wu Y, Huang C (2019a) Plasma-induced paa-zno coated pvdf membrane for oily wastewater treatment: Preparation, optimization, and characterization through taguchi oa design and synchrotron-based x-ray analysis. J Membr Sci 582:70–82
3. Sri Abirami Saraswathi MS, Nagendran A, Rana D (2019) Tailored polymer nanocomposite membranes based on carbon, metal oxide and silicon nanomaterials: a review. J Mat Chem A 7(15):8723–8745
4. Chen X, Huang G, An C, Feng R, Yao Y, Zhao S, Huang C, Wu Y (2019b) Plasma-induced poly(acrylic acid)-tio2 coated polyvinylidene fluoride membrane for produced water treatment: Synchrotron x-ray, optimization, and insight studies. J Clean Prod 227:772–783
5. Yoosefi Booshehri A, Wang R, Xu R (2013) The effect of re-generable silver nanoparticles/multi-walled carbon nanotubes coating on the antibacterial performance of hollow fiber membrane. Chem Eng J 230:251–259
6. Pan Y, Yu Z, Shi H, Chen Q, Zeng G, Di H, Ren X, He Y (2017) A novel antifouling and antibacterial surface-functionalized pvdf ultrafiltration membrane via binding ag/sio2 nanocomposites. J Chem Technol Biotechnol 92(3):562–572
7. Ko K, Yu Y, Kim M-J, Kweon J, Chung H (2018) Improvement in fouling resistance of silver-graphene oxide coated polyvinylidene fluoride membrane prepared by pressurized filtration. Sep Purif Technol 194:161–169

Monitoring Microbial Quality of Source Waters Using Bayesian Belief Networks

Atefeh Aliashrafi and Nicolas M. Peleato

1 Introduction

Fecal indicator bacteria (FIB), including *Escherichia coli (E. coli*), are commonly used as indicator organisms to determine microbial quality of drinking and recreational waters. However, the measurement of FIB takes more than 18 h resulting in significant time-delays in assessments [1]. During this time-delay, pathogens concentrations can exceed regulatory or operational limits for water treatment systems. As such, to provide real-time assessment of microbial water quality, there is interest in a modelling approach to predicting pathogen concentrations, without the need for routine measurement. To accurately predict pathogen concentrations in source waters, both historical weather and water quality parameters must be considered. Changes in water quality, including turbidity or conductivity, may indicate increased probability of contamination [2]. Short-term source water contamination due to severe weather conditions is often a significant factor in many major waterborne disease outbreaks. For example, the outbreak of *E. coli* 0157:H7 in Walkerton, Ontario, was due in-part to contamination of a well following a heavy rainfall event [3]. More generally, it has been observed that regions with high run-off potential and large daily pathogen productions are more likely to be the source of pathogenic contaminations [4]. Garcia-Aljaro et al. (2017) reported higher microbial load concentration of pathogens in river sediment samples after heavy rainfalls [5]. Incorporating weather impacts is especially important considering that climate change projections indicate increasing frequency and intensity of extreme weather events [6].

A. Aliashrafi (✉) · N. M. Peleato
School of Engineering, University of British Columbia Okanagan, 1137, Alumni Ave., Kelowna, BC, Canada
e-mail: ashrfi93@mail.ubc.ca

S. Walbridge et al. (eds.), *Proceedings of the Canadian Society of Civil Engineering Annual Conference 2021*, Lecture Notes in Civil Engineering 249,
https://doi.org/10.1007/978-981-19-1061-6_25

Although FIB levels can provide some indication of the overall microbial quality, they are not necessarily well correlated with concentrations of important pathogens that can cause severe disease outbreaks such as the protozoa *Cryptosporidium* spp. and *Giardia* spp. [7]. For example, *Cryptosporidium* contamination of Milwaukee's drinking water in 1993 resulted in more than 100 deaths and over 100,000 infections and weakened immune systems [8]. Protozoa are particularly important to consider when setting treatment objectives since they are small enough to penetrate some treatment barriers, and they are particularly resistant to disinfection by chlorine. Also, *Cryptosporidium* is environmentally robust, allowing it to stay dormant in water sources for prolonged periods [9]. Therefore, further to FIB concentrations, it is critical to understand the expected levels of *Cryptosporidium* in water sources used for drinking water. However, when considering the management of *Cryptosporidium* risk, the major challenge is enumeration or monitoring. Measurement of *Cryptosporidium* in water requires laborious morphometric or molecular techniques that are expensive and timeconsuming [10]. As such, it is virtually impossible to assess *Cryptosporidium* risk on a day-to-day basis using measured values.

Mathematical and data-driven models based on historical data have been used to address the challenges of time-delayed FIB measurements and difficulty monitoring protozoa by providing predictions of pathogen concentrations on a day-to-day basis. This approach has been investigated previously, with several models built to provide an early warning system of elevated levels of *Cryptosporidium* and other pathogens in source waters [2, 11–15]. While many distinct model types have previously been used, Bayesian approaches have not been utilized in this applifcation, but have attracted considerable attention for application to other environmental systems. Bayesian models have several characteristics that make them well suited for modelling environmental systems, including directly represent underlying uncertainty in predictions by defining probability distributions for each variable [16]. Due to this capability explicity dealing with uncertainties, a wide range of ecosystems and environmental systems has been successfully modeled with this framework (e.g. [16–19]). Bayesian Belief Networks (BBNs) are a Bayesian-type method that can represent variable relationships graphically, and can use a combination of historical and expert knowledge for building probability distributions [20]. While the use of BBNs has successfully modeled complex environmental systems, environmental data, which is often continuous, must be discretized to be applied in a BBN resulting in some degree of information loss. Furthermore, the value and of the model depends significantly on the quality of the historical dataset. Difficulty in the routine measurement of protozoa reduces the chance of building a complete dataset. Often datasets of protozoa concentrations are heavily skewed with non-detects (i.e., the vast majority of sample results are below detection limits). Unbalanced datasets will significantly reduce the sensitivity and accuracy in predicting positive cases when protozoa will be present [21].

This work aims to predict FIB (fecal coliforms and *E. coli*) as well as Cryptosporidium presence in water sources using water quality and weather parameters that can be monitored day-to-day. To address dataset unbalance, the adaptive synthetic sampling algorithm (ADASYN) is utilized. The ADASYN method

creates synthetic samples of specific classes (i.e., positive detection) to improve model performance. The modelling approach discussed in this paper is intended to provide accurate predictions of pathogen levels in water sources to enhance risk-based management of water resources.

2 Methods

2.1 Data Source and Case Study

For prediction of *Cryptosporidium*, source water quality and pathogen concentrations were obtained from New York City's open database reported from the Department of Environmental Protection. Monitored parameters were turbidity, fecal coliforms, and *Cryptosporidium* with a total of 238 samples from the summer of 2015 up to the summer of 2019. In addition to turbidity and microbial water quality data, weather data from a weather station located close to the reservoirs was obtained. Weather parameters included were precipitation on the sampling day, precipitation three days prior, maximum air temperature, and minimum air temperature.

The model for predicting fecal coliforms and *E. coli* used data from three different sites in British Columbia, obtained from Canada's National Long-term water quality monitoring dataset and Environment Canada Weather station [1]. The water quality parameters included: turbidity, conductivity, hardness FIB, *E. coli*, water temperature and the precipitation on day and three days prior as well as air temperature were selected weather parameters for considering impact of weather conditions on microbial quality.

2.2 Adaptive Synthetic Sampling

A significant challenge when dealing with *Cryptosporidium* is the low number of samples recording presence, or anything greater than zero. In the dataset used, the majority of reported values (220 out of 238 samples) were 'zero' concentrations of protozoa or below the detection limit. Unbalanced datasets with limited positive samples (i.e., presence of the organism) are difficult to use and often result in poor performing models. To address this issue, we investigated the use of ADASYN to generate a number of positive samples and balance the dataset (Fig. 1).

ADASYN uses the density distribution for balancing the number of samples in the minor and major classes of a dataset. Considering a full dataset with a binary target (i.e. presence/absence o *Cryptosporidium*), there would be m_x number of samples in the majority class (absence) and m_y number of samples in the minority classe (presence). ADASYN generated the $m_y - m_x$ number of samples to balance the dataset [21].

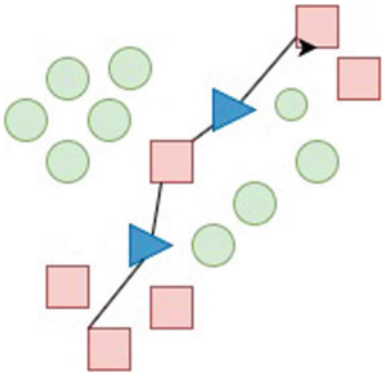

Fig. 1 A schematic of adaptive synthetic sampling; circle shapes indicate samples in majority class and square samples in minority class and triangle is indicating the synthesized samples 21

2.3 Bayesian Belief Network

BBNs are constructed based on Bayes theorem and capture variable relationships in a probabilistic structure [17]. BBNs can calculate the probability distributions of variables and represent other factors' impact on the probability of outcome. One of the main advantages of BBN is their graphical representation of variable relationships in Directed Acyclic Graphs (DAGs), where each node (variable) can be connected indicating one-way dependence [22]. The relation of each node with another has a conditional probability table that quantifies the dependency of variables on each other, calculated using Baye's theorem:

$$P(x_1|x_2) = \frac{P(x_2|x_1)P(x_1)}{P(x_2)} \tag{1}$$

where $P(x_n)$, $P(x_2|x_1)$ show the probability of outcome n and the conditional probability for $\times$ 2 given $\times$ 1 [1].

GeNIe (BayesFusion LLC, Pittsburgh, PA) software is used in this work for developing BBN and different algorithms was tried for finding the best structure of the model. Although the Tree Augmented Naive Bayes could improve the performance, the relationship of variables lacked logical order. Therefore, the structure was developed based on expert knowledge.

3 Result and Discussion

3.1 Prediction Using Bayesian Belief Network

The dataset obtained from three different monitoring sites in British Columbia was used for developing the BBN model. The model structure was developed based on

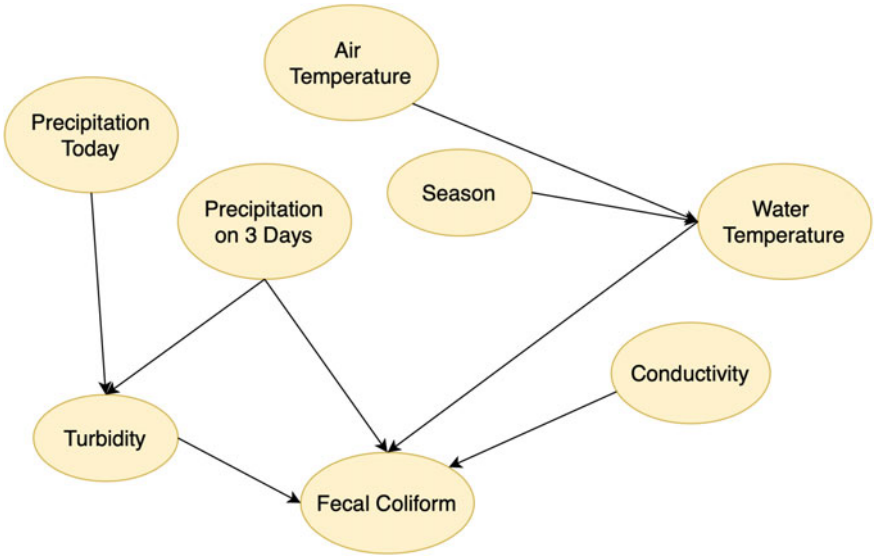

Fig. 2 Structure used for bayesian belief network modeling for FIB prediction

expert knowledge and is shown as Fig. 2. Each of the predictor variables considered was discretized into four classes of approximately equal size or sample number, with consideration of divisions being realistic and interpretable. The target variables were either fecal coliforms (as shown in Fig. 2) or *E. coli*. fecal coliforms were discretized into four equal bins due to the large range in values, however *E. coli* was discretized into two categories: < and > 20 CFU/100 mL. This threshold is a typical estimate of levels used to differentiate pristine and impacted water sources. Data was divided based on their recording day under category of season which affects the water temperature and indirectly can impact the activity of microorganism in water. Also, precipitation on day and three days prior can affect the fecal coliform direct or indirect since the result turbidity from washing out after each runoff can shift the FIB or other pathogens in water.

Performance of the model was assessed using a confusion matrix and overall accuracy (i.e., rate of true positive or true negatives). A summary results for predictions of FIB and *E. coli* is indicated in Table 1. As it can be seen from the results,

Table 1 Result summary of BBN model performance for predicting fecal coliforms and 20 CFU threshold of *E. coli*

Dataset	Target parameters	
	Fecal coliforms	*E. coli*
Fraser river	95.45	96.67
Englishman river	81.34	90.16
Cheakamus river	81.79	95.15

the model successfully predicted FIB with higher than 70% accuracy for all sites (Fig. 3).

The same method was applied to predict the presence or absence of *Cryptosporidium* in New York City drinking water reservoirs. The structure of BBN model was again created based on expert knowledge and available parameters (Fig. 4). Each

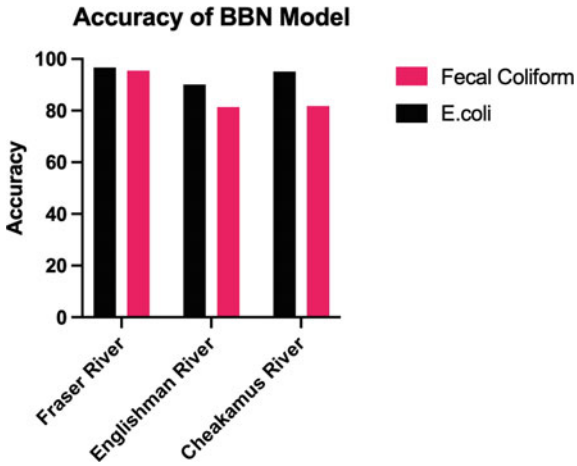

Fig. 3 Perfomance result for fecal colifrom and *E. coli* Prediction with BBN

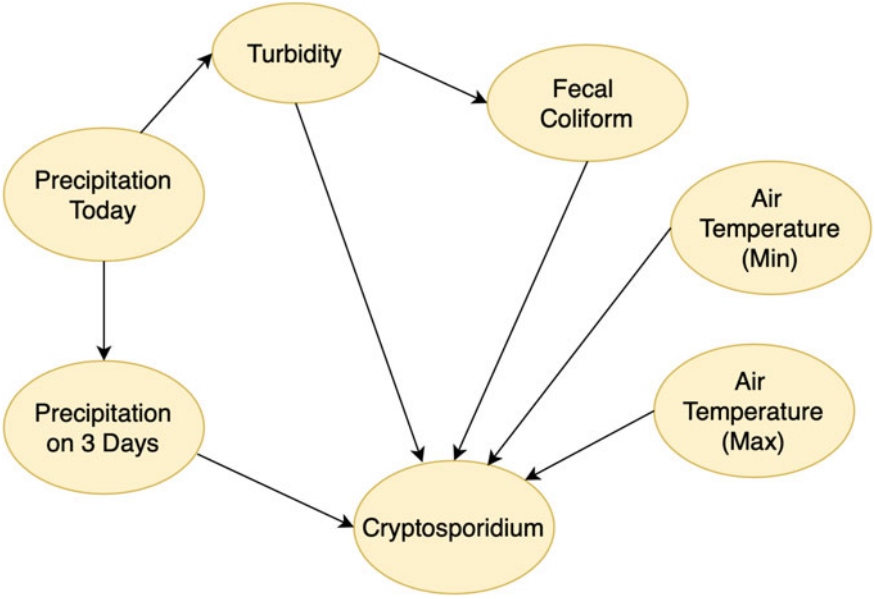

Fig. 4 Structure used for Bayesian belief network modeling for *Cryptosporidium* prediction

of the variables considered was discretized. Before developing the model, correlations between variables were determined to better understand the structure that should be developed (Table 2).

Correlation between all parameters was very poor and only coliform, turbidity and precipitation have a positive correlation with *Cryptosporidium.* Due to very poor relationships with precipitation over 7 *days* prior, this parameter was removed from dataset and it was assuming that precipitation on day can affect both turbidity, coliforms, and precipitation over three days prior. However, the impact of three days prior precipitation was connected directly to *Cryptosporidium.*

It is expected that the air temperature willwould impact water temperature, which results in affecting the activity or presence of *Cryptosporidium.*

The dataset included a significant number of *Cryptosporidium* non-detects. From 238 recorded data, only 18 samples indicated presence of *Cryptosporidium.* Due to this problem model was overfitted with higher than zero samples and failed to predict the days with positive *Cryptosporidium* values (Fig. 5). Therefore, the model only was able to predict the zero *Cryptosporidium* and never predicted the presence.

To overcome the issue of unbalanced datasets, the ADASYN algorithm was applied to the New York City *Cryptosporidium* dataset. The ADASYN method generated 206 samples were generated with 'presence' of *Cryptosporidium*, to now a total of 441 samples. The generated data were used to develop a new BBN model, and lifted the performance of the model in predicting 'presence of *Cryptosprodium* up 65%. Figure 5 indicates the comparison between both BBN and ADASYN-BBN model and it can be observed that the application of ADASYN ables BBN to predict the presence of *Cryptosprodium* with acceptable accuracy.

In particular there is a pronounced increase in true detection of *Cryptosporidium* presence, indicating the model has learned conditions that would result in pathogen loading in the reservoir. The observation in this study aligns with the result of the study conducted by Xu et al. (2020) where employing ADASYN improved prediction accuracies for other water quality parameters. The results show that the quality of data is important for developing accurate prediction models and the ADASYN algorithm can overcome issues associated with unbalanced datasets through synthesizing samples based on real data.

4 Conclusion

Monitoring the microbial quality of source waters is of great importance for informing drinking water treatment targets and protecting public health. Time-delays inherent to direct measurement of pathogens limits risk-based management of drinking water supplies and is not capable of reliably capturing short-term contamination events. Data-driven models that predict conditions based on historical observations and easy to measure variables are a viable alternative to assessing microbial water quality.

One of the most significant challenges in implementing data-driven modelling of source water quality is the quality of dataset and poor representation of adverse

Table 2 Correlation coefficient of water quality and weather parameters for Newyork data

	Crypto-sporidium	Turbidity	Fecal Coliform	Prec	Prec.(3 day)	Prec.(7 days)	Min. temp	Max. temp
Cryptosporidium	1.00	0.0	0.01	0.0	−0.04	0.08	−0.13	−0.15
Turbidity	0.0	1.00	−0.06	−0.02	−0.04	−0.16	−0.20	−0.23
Fecal Coliform	0.01	−0.06	1.00	0.11	0.27	0.22	−0.01	−0.05
Prec	0.0	−0.02	0.11	1.00	0.07	0.00	−0.03	0.06
Prec.(3 day)	−0.04	−0.04	0.27	0.07	1.00	0.63	−0.11	−0.01
Prec.(7 days)	0.08	−0.16	0.22	0.00	0.63	1.00	−0.02	0.06
Max. temp	−0.13	−0.20	−0.01	−0.03	−0.11	−0.02	1.00	0.93
Min. temp	−0.15	−0.23	0.05	0.06	−0.01	0.06	0.93	1.00

Prec Precipitation day-of; prec. *(3 day)* Precipitation over last 3 *days*; sprec. *(7 day)* Precipitation over last 7 *days*; *temp.* Temperature

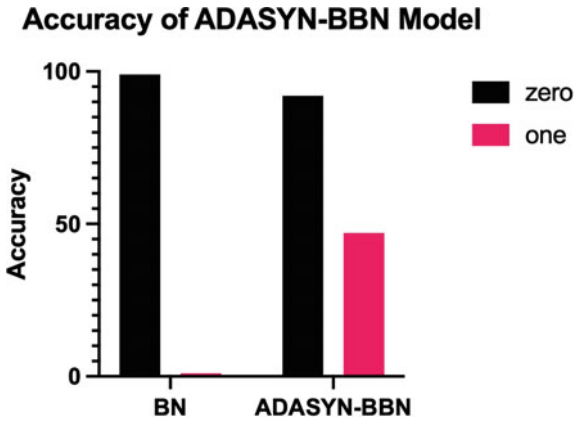

Fig. 5 Perfomance result for cryptosprodium prediction with BBN and ADASYN-BBN: Zero' refers to no Cryptosporidium and 'one' refers to the presence of Cryptosporidium in the sample

events (i.e., positive samples). For example, due to the difficulty and high expense of measuring pathogens of concern such as *Cryptosporidium*, available datasets reporting *Cryptosporidium* concentrations are highly unbalanced. In order to solve this issue, the ADASYN algorithm was applied to the dataset from New York City in order to improve model performance. The prediction of *Cryptosporidium* improved to 68% using ADASYN algorithm. This study provides a solution to better inform decision and policy makers on the microbial quality of source waters. The focus of future research can be the assessment of other potential data-driven models with balanced/unbalanced data.

References

1. Panidhapu A, Li Z, Aliashrafi A, Peleato NM (2020) Integration of weather conditions for predicting microbial water quality using Bayesian belief networks. Water Res 170:115349
2. Nevers MB, Whitman RL (2011) Efficacy of monitoring and empirical predictive modeling at improving public health protection at Chicago beaches. Water Res 45(4):1659–1668
3. Auld H, MacIver D, Klaassen J (2004) Heavy rainfall and waterborne disease outbreaks: the Walkerton example. J Toxi Environ Health, Part A 67 20–22(2004):1879–1887
4. Dorner SM, Huck PM, Slawson RM (2004) Estimating potential environmental loadings of *Cryptosporidium* spp. and Campylobacter spp. from livestock in the Grand River Watershed, Ontario, Canada. Environ Sci Technol 38(12):3370–3380
5. García-Aljaro C, Martín-Díaz J, Viñas-Balada E, Calero-Cáceres W, Lucena F, Blanch AR (2017) Mobilisation of microbial indicators, microbial source tracking markers and pathogens after rainfall events. Water Res 112:248–253
6. Mishra A, Alnahit A, Campbell B (2020) Impact of land uses, drought, flood, wildfire, and cascading events on water quality and microbial communities: a review and analysis. J Hydrol 125707
7. McClung RP, Roth DM, Vigar M, Roberts VA, Kahler AM, Cooley LA, Hilborn ED et al. (2017) Waterborne disease outbreaks associated with environmental and undetermined exposures to water—United States, 2013–2014. MMWR. Morb Mortal Wkly Rep 66(44):1222
8. Karanis P, Kourenti C, Smith H (2007) Waterborne transmission of protozoan parasites: a worldwide review of outbreaks and lessons learnt. J Water Health 5(1):1–38

9. Hamilton KA, Waso M, Reyneke B, Saeidi N, Levine A, Lalancette C, Besner M-C, Khan W, Ahmed W (2018) Cryptosporidium and Giardia in wastewater and surface water environments. J Environ Qual 47(5):1006–1023
10. Rossle NF, Latif B (2013) Cryptosporidiosis as threatening health problem: a review. Asian Pac J Trop Biomed 3(11):916–924
11. Benham BL, Baffaut C, Zeckoski RW, Mankin KR, Pachepsky YA, Sadeghi AM, Brannan KM, Soupir ML, Habersack MJ (2006) Modeling bacteria fate and transport in watersheds to support TMDLs. Trans ASABE 49(4):987–1002
12. Coffey R, Cummins E, Bhreathnach N, Flaherty VO, Cormican M (2010a) Development of a pathogen transport model for Irish catchments using SWAT. Agric Water Manag 97(1):101–111
13. Coffey R, Cummins E, O'Flaherty V, Cormican M (2010b) Analysis of the soil and water assessment tool (SWAT) to model *Cryptosporidium* in surface water sources. Biosys Eng 106(3):303–314
14. Rossi A, Wolde BT, Lee LH, Wu M (2020) Prediction of recreational water safety using Escherichia coli as an indicator: case study of the Passaic and Pompton rivers, New Jersey. Sci Total Environ 714:136814
15. Tang J, McDonald S, Peng X, Samadder SR, Murphy TM, Holden NM (2011) Modelling Cryptosporidium oocysts transport in small ungauged agricultural catchments. Water Res 45(12):3665–3680
16. Uusitalo L, Kuikka S, Romakkaniemi A (2005) Estimation of Atlantic salmon smolt carrying capacity of rivers using expert knowledge. ICES J Mar Sci 62(4):708–722
17. Bertone E, Sahin O, Richards R, Roiko A (2016) Extreme events, water quality and health: a participatory Bayesian risk assessment tool for managers of reservoirs. J oCleaner Prod 135:657–667
18. Herrig I, Seis W, Fischer H, Regnery J, Manz W, Reifferscheid G, Böer S (2019) Prediction of fecal indicator organism concentrations in rivers: the shifting role of environmental factors under varying flow conditions. Environ Sci Eur 31(1):1–16
19. Usitalo L (2007) Advantages and challenges of Bayesian networks in environmental modelling. Ecol Model 203(3–4):312–318
20. Marcot BG, Holthausen RS, Raphael MG, Rowland MM, Wisdom MJ (2001) Using Bayesian belief networks to evaluate fish and wildlife population viability under land management alternatives from an environmental impact statement. For Ecol Manage 153(1–3):29–42
21. Xu T, Coco G, Neale M (2020) A predictive model of recreational water quality based on adaptive synthetic sampling algorithms and machine learning. Water Res 177:115788
22. Fasaee MAK, Berglund E, Pieper KJ, Ling E, Benham B, Edwards M (2021) Developing a framework for classifying water lead levels at private drinking water systems: a Bayesian belief network approach. Water Res 189:116641

Environmental Remediation of a Shallow Mesotrophic Lake Water Using On-Site Non-woven Geotextile Filtration Treatment

Antonio C. Pereira, Dileep Palakkeel Veetil, Catherine N. Mulligan, and Sam Bhat

1 Introduction

Surface water is heavily affected due to new climate change patterns combined with anthropogenic actions. These patterns are characterized by precipitation increase in some regions [1, 2], dry period intensification in others [3], water temperature stratification changes in lake systems (i.e., affecting water mixing) [4] or simply the anthropogenic action of releasing waste in to those waters directly or indirectly without previous treatment [5].

By these variables, the concentration of nutrients and sediments in lake systems is increasing, resulting in the possible eutrophication and browning of those aquatic bodies [6]. This human-induced fertilization leads to an increase in water color and excessive cyanobacteria/algae growth possibly affecting the aquatic system's natural processes. In addition, it can bring potential recreational and health advisories by the government due to possible cyanotoxin release in to the water. As those stressors will not cease in the near future, the number of affected lakes will increase over the years [7] and may bring nutrient enrichment of lakes to be a rising concern soon.

Although nutrients from catchments are partly in the particulate form that settles in the water column (i.e., external loads) and are not directly used by phytoplankton until released from particles, internal loads are predominantly in the dissolved form directly available for algal growth [8]. In addition, the spatial distribution of those nutrients is not uniform throughout the whole lake [9], making it difficult to assess and remediate in a possible eutrophication case.

A. C. Pereira · D. P. Veetil · C. N. Mulligan (✉)
Concordia University, Montreal, Canada
e-mail: mulligan@civil.concordia.ca

S. Bhat
Titan Environmental Containment Ltd., Manitoba, Canada

S. Walbridge et al. (eds.), *Proceedings of the Canadian Society of Civil Engineering Annual Conference 2021*, Lecture Notes in Civil Engineering 249,
https://doi.org/10.1007/978-981-19-1061-6_26

The first methodology to combat eutrophication on shallow lakes is the reduction of phosphorus availability on the system either in the particulate or dissolved form. This element is considered the limiting nutrient [10]. Several methods in the literature address internal and external nutrient loads. For example, there are sediment dredging and lanthanum-modified bentonite addition [11], cement addition [12], water intake, and oxygen nanobubble aeration [13].

These remediation techniques can decrease the water volume, in the case of additives, and adversely disrupt lake biota in the water column and sediment and thus are not ideal remedial alternatives [14]. To answer this problem, geotextiles have been employed as membranes by our research group for lake/pond water remediation by nutrient and suspended solids removal using filtration [14–16], indicating its strong potential as a flexible and reactive environmental remediation technique that can be adapted to shallow lakes and other surface water types.

Therefore, over the years, our environmental engineering research team has been deploying a flexible and reactive approach, an on-site non-woven geotextile filtration treatment, for lake water remediation. In 2020, the on-site trials have been applied at Lake Johanne, a shallow mesotrophic lake, located in a Quebec municipality, which has suffered in the past recreational advisories due to water quality. Consequently, the objectives of this present study are to assess the lake water quality and evaluate the usefulness of the geotextile on-site filtration for nutrient and suspended solids removal.

2 Materials and Methods Schedule

2.1 Study Area

The study area of this project was Lake Johanne (45°50′23″ N; 74°08′19″ W), shown in Fig. 1, a shallow mesotrophic lake located in the *Sainte-Anne des-Lacs* municipality in Quebec. This is considered the head lake in the Masse watershed, composed of vegetation with few residents [17]. The approximate surface area of the lake is

Fig. 1 Lake Johanne with sampling stations

44,910 m^2, water volume is 74,900 m^3 also with a maximum and average depths of 3.5 and 1.7 m, respectively [18].

Increased phosphorus occurrence on the lake has been correlated to external loads as runoff from a nearby road (i.e., Station 9) and the forested area as well as plant decomposition in the water. Furthermore, internal loads are associated with wetland discharge at the lake inlet, possible diffuse contamination from septic tanks, and phosphorus sediment release. According to Veetil et al. [9], the sediment phosphorus concentration in this lake varied between 1186 and 1451 mg/kg.

2.2 Filter Media

Geotextiles were used in this onsite treatment as filtration media for capturing suspended solids and particulate nutrients to remediate this mesotrophic lake water. The filter selection and combination were based on the previous on-site studies during 2017–2018, corroborated by 2019 project results [14]. The geotextiles were made by Titan Environmental based on the particle size that 90% of solids in this lake water is under (D90). The characteristics of the five non-woven geotextiles membranes used (TE-GTX300, TE GTT100, TE-GTT120, TE-GTT200, and TE-GTN350B) are represented in Table 1.

With the exception of the nonwoven geotextile TE-GTX300 that was made with PET fibers, the four other geotextile membranes were made of polypropylene (PP) fibers. They were all extremely flexible with a dimensionally stable fabric that is an excellent material to be used as a filtration membrane.

For use in this research, geotextile layers were cut in a 22 cm diameter and arranged in decreasing order of their AOS (110, 100, 90, 70, and 65 μm) using one layer of each one. When combined the total thickness of the five layers was approximately 10.0 mm. Identical filter combinations were employed for both batch and continuous experiments. Also, the combined layers (CL) were entirely changed upon clogging or by the end of each experiment, whichever happened first. Figure 2 shows three non-woven geotextiles before the filtration process.

2.3 On-Site Geotextile Filtration Setup

The setup used on this project was based on a plastic tank of 543 L, width of 97.8 cm and height of 35.6 cm, placed in a cleared and leveled area near to the lakeshore (i.e., station 2) with a floating unit recirculating water to be filtered by the combined non-woven geotextile layers. Additionally, four small pumps were submerged in the tank with a very low flow rate to prevent short-circuiting in filtering the entire tank water.

The floating unit was made of plexiglass consisting of a square-shaped base, a filter holder, and a cylindrical tube with 20 cm, 25 cm of internal diameter and height,

Table 1 Non-woven geotextile characteristics used in this study

Filters	Material	Apparent opening size (AOS) (μm)	Flow rate (L/s/m^2)	Permittivity (sec $^{-1}$)	Mass per unit area (g/m^2)	Thickness (mm)
TE-GTX300	[a]PET	110	65	1.62	300	–
TE-GTT100	[b]PP	100	75	–	150	0.8
TE-GTT120	[b]PP	90	70	–	120	0.8
TE-GTT200	[b]PP	70	50	–	200	1.5
TE-GTN350B	[b]PP	65	45	0.56	350	–

[a] *PET* Polyester; [b] *PP* Polypropylene

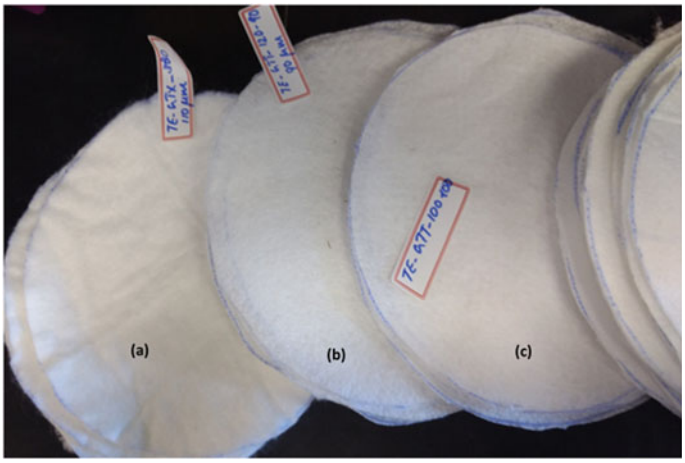

Fig. 2 Non-woven geotextiles before the filtration process **a** TE-GTX300-110 μm **b** TE-GTT120–90 μm **c** TE-GTT100–100 μm

respectively. shown in Fig. 3a. The circular void at the center, where the water column contacts the geotextiles, has a column diameter of 20 cm. The filtration column was placed on a square base to support a maximum hydraulic head of 18 cm. Screws were used to fix and attach the filtration column to the base and the membrane combination.

For the experiment deployment, the tank was filled up to 300 L of lake water using a submersible pump. After this, the filtration unit with the sandwiched geotextile combination was placed on the polystyrene foam sheet with a circular hole of 20 cm at the center, to float the component on the tank water and to permit the filtered water to return to the tank (Fig. 3b).

In this study, two different filtration tests were deployed: (i) 3 batch experiments, and (ii) 3 continuous filtration experiments with retention times of 2, 1, and 0.5 day.

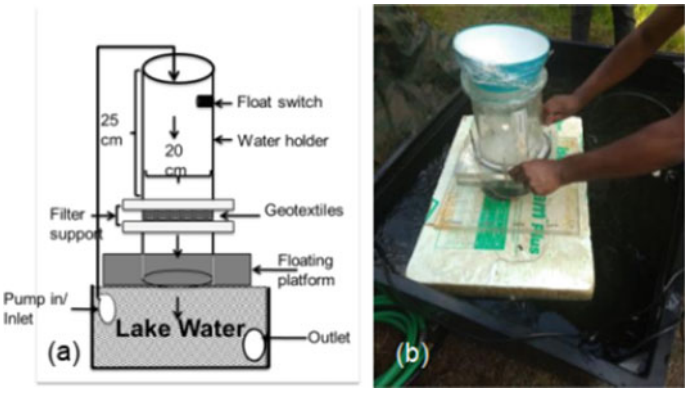

Fig. 3 **a** Schematic of filtration set up and **b** On-site filtration unit

While the continuous experiment was performed using an inlet (with a previously calibrated medium flow rate peristaltic pump fed by lake water) and outlet by overflow, the batch experiment only treated 300 L for an average of 6.6 days. The experiment was checked for geotextile clogging, pumping status, outlet and inlet clogging, sampling, and other external influences every 2–3 days. A tarpaulin was used for covering the system.

2.4 Water Quality Analysis

Water samples from the tank and the inlet (when the continuous experiment was deployed), were taken every 2–3 days. Also, water samplings of the entire lake were done at selected stations (St. 1, St. 4, St. 7, St. 9, and St. 11) for accessing water quality in the 2020 summer to-midfall. Water samples were collected in 1L high-density polyethylene (HDPE) amber bottles and 50 ml sterilized polypropylene test tubes. Both were stored at 4 °C in the dark prior to any physico-chemical analysis and all analyses were performed within 48 h.

The water samples were analyzed for the following parameters: particle size distribution (PSA), turbidity, total suspended solids (TSS), total phosphorus (TP), total nitrogen (TN), nitrate ($NO3^{-}$), and Chemical Oxygen Demand (COD). Test kits from Hach chemicals were used for analyzing TN (TNT 826, Method 10,208, persulfate digestion) and COD (TNT 820, Method 10,221, reactor digestion method). Particle size analysis (PSA) was performed with a laser diffraction particle analyzer (LA-960 Horiba laser particle size analyzer). Turbidity was measured with an Oakton turbidity meter, and TSS followed the APHA procedure (SM 2540D).

Nitrate was determined using a Metrohm Ion Chromatography applying isocratic conditions with a Metrosep A Supp 5—150/4.0 analytical column (150 × 4 mm) and suppressed conductivity detection. The eluent used was composed of 3.2 mM Na_2CO_3–1.0 $_{mM}$ $NaHCO_3$. The injection volume was 100 μL/ml, and the eluent flow rate was 7.0 $_{ml}$/min. Phosphorus, on the other hand, was determined by elemental analysis done by ICP-MS with a quadruple mass analyzer after partial acid-peroxide digestion (HNO_3–H_2O_2) of water samples [19].

3 Results and Discussion

3.1 Lake Johanne Water Quality Assessment

Using the MDDEP [20] trophic status classification, Lake Johanne (LJ) is a mesotrophic lake (13–20 μg/L) possible going towards the high range of mesoeutrophic classification in the future. Our results when only based on total phosphorus concentration have shown the same classification. It is worth commenting that LJ

Table 2 Lake Johanne water quality during July–Sep, 2020

Parameters	2020[a]
TP (μg/L)	15.1 ± 1.5
COD (mg/L)	21.0 ± 2.5
NO3-(mg/L)	0.4 ± 0.3
TN (mg/L)	1.0 ± 0.7
TSS (mg/L)	4.6 ± 1.1

[a] Average of 7 samplings of 5 lake stations

has an average depth of 1.7 m and no significant microscopic algae/cyanobacteria in suspension and other comprehensive methods used for trophic classification (chlorophyll-a and transparency) are not applicable for shallow lakes. Table 2 presents the results of samplings for the year 2020.

Regarding PSA results, the D90 was under the range of 60–74 μm and 50% of the particles have (D50) diameters under the 8–16 μm range over the 7 samplings of 2020. Large particle sizes were found at St.4, near the wetland as this is one of the internal sediments/nutrient inputs of the lake. Nitrate and TN concentrations are under Quebec guidelines (i.e., MDDEP [20]) for protecting aquatic life, and are 2.9 mg/L and 1.0 mg/L, respectively.

Related to the total suspended solids (TSS) concentration in this lake water, even though the guideline value for concentration presents a value of 13 mg/L in the IQBP (*l'indice de qualité bactériologique et physicochimique*), this parameter needs to be addressed because TSS is an excellent indicator of physical and esthetic degradation of this surface water. The COD concentration showed that LJ water is slightly elevated above the guideline of 20 mg/L according to Chapman and Kimstach [21]. All those results corroborate the MELCC [22] recommendation on *Réseau de surveillance volontaire des lacs* (RSVL) for the adoption of measures to limit nutrient inputs and avoiding further degradation of this lake and further loss of uses.

3.2 Filtration Experiments

Treatment experiments ran for 91 days from July 17 to October 15 of 2020 (i.e., divided into 3 batch experiments and 3 continuous experiments) shortly after the start of summer until the mid-fall season. For the whole experiment, 26 sets of filters cut 22 cm in diameter (5 layers) were used, totaling approximately 1 m^2 for each AOS in the experiment with a total cost of $5.05 for treating 34.5 m^3 of lake water. It is worth commenting that when the retention time was at the lowest value (0.5 day or 12 h), filters were changed every 3 days due to clogging.

Cake layer formation was observed on the top of the geotextile combination in all experiments. For a more graphic representation, Fig. 4 shows one set of used geotextile filters after 1 week of lake water filtration. As can been perceived, not only the straining filtration mechanism has occurred on this process but also depth

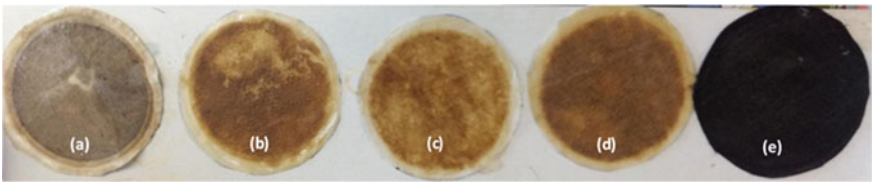

Fig. 4 Non-woven geotextiles after the filtration process in the AOS order: **a** 110 μm **b** 100 μm **c** 90 μm **d** 70 **μm** and **e** 65 μm

filtration due to the initial ripening and further cake formation. Those mechanisms were efficient in reducing the AOS of the membranes and further explain the reduction of particle size and quantity of suspended solids of treated lake water.

3.3 Batch Experiments

As with any filtration process, the first and foremost removal that occurs is the suspended particles. These mechanics were observed in this remediation technique showing the efficiency of this on-site non-woven geotextile filtration method. With an average of 6.6 days, three batch experiments were performed using 300 L of lake water. Due to the particle accumulation on the top of the filters and cake formation after the second day of deployment, those experiments presented an expressive reduction in the suspended particles. The TSS results and the diameter of 90% of the particles (D90) observed are shown, in Fig. 5a and b. This represented a 75% and 86% particle size and TSS reduction, respectively.

Furthermore, the removal of suspended particles in the water has caused the same reduction in the organic matter, represented by COD, and particulate phosphorus, represented by total phosphorus (TP), as shown in Fig. 6a and b. In other words, removing suspended particles from this lake water by this environmental treatment has demonstrated a reduction in the nutrient concentration in water. The direct remediation of this lake water allows removing particles that would settle with time to

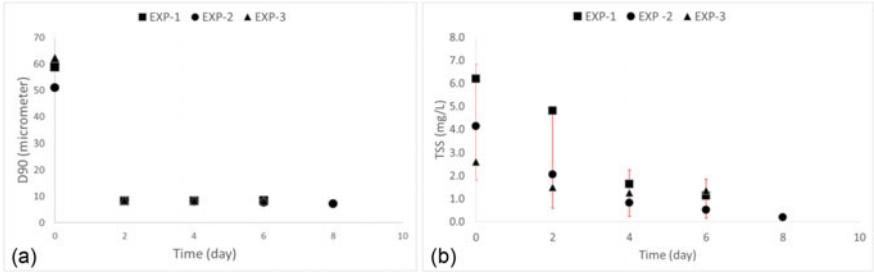

Fig. 5 **a** D90 diameter (μm) and **b** TSS concentration (mg/L) in the tank water

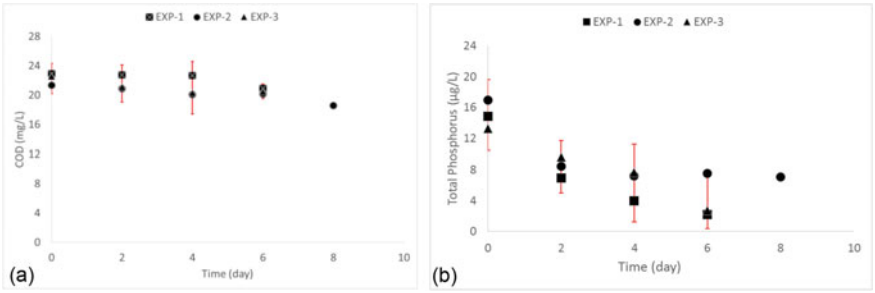

Fig. 6 **a** COD concentrations (mg/L) and **b** TP concentrations (μg/L) in the tank water

be uptaken by the phytoplankton. Total removal in the system was approximately an average removal of 75% of TP and 11% of COD in the experiments. By the end of batch experiments, the limit value for unpolluted oligotrophic surface waters was reached.

Throughout the experiments, no significant change in the concentrations of TN and nitrate was observed. The average value was kept below the values present in the raw water and within the Quebec regulated values. For TN, the value was kept at an average of 0.89 ± 0.14 mg/L, and for nitrate, its average was 0.18 ± 0.02 mg/L.

3.4 Continuous Experiments

To test the reactivity and adaptability of the system, 3 continuous experiments were performed, using a peristaltic pump for the inlet (lake water) and overflow for outlet (returning to the lake). This was a continuation of the experiments done in 2019. In the experiments, it was observed that a fast and stable removal of TSS brought a steady D90 reduction in the tank water proving that AOS reduction can improve filtration. This reduction in the geotextile's pore sizes, long after the second day of filtration can be seen in Fig. 7a and b with removals of TSS and particle sizes. The size of 90% of particles in the tank/outlet (D90) was kept below 8.45 ± 0.23 μm from the second day of the first experiment done (1-day) until the end with the other retention times (2 and 0.5 days). The average reduction on D90 was 99.9% in this experiment.

Likewise, the treated water discharged into the lake presented TSS values below 2.0 mg/L after two days of filtration in the 1-day retention time (Fig. 7b). For 2-day and 0.5-day retention times, the removal was maintained values even below 2.0 mg/L, realizing a cleaner output water at the same level. The average removal was 94%, for a 1-day retention time keeping the TSS values at 0.66 ± 0.67 mg/L until the end of the experiment. Removal of TSS in the lake water also reduced the turbidity (Fig. 8a, b, and c) in the returning lake water, presenting the values always below the initial values of the lake. For the retention time of 1 day, an average removal of 41%

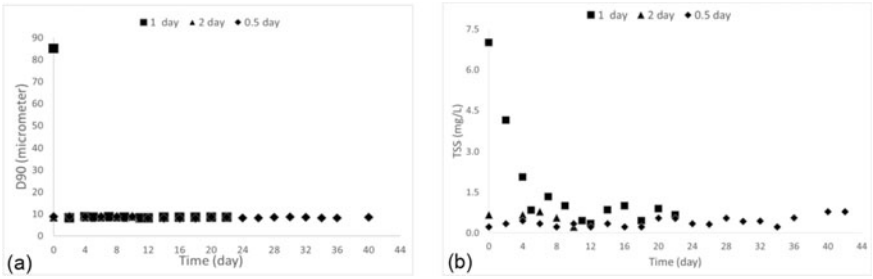

Fig. 7 **a** D90 (μm) in the tank water for specific retention time and **b** TSS concentration (mg/L) for 1-,2- and 0.5-day retention time in the tank water

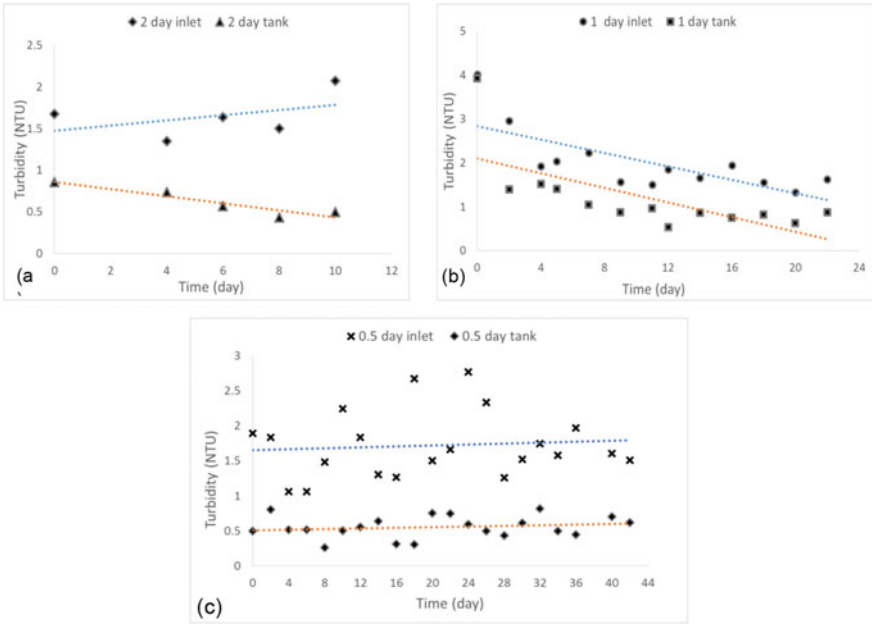

Fig. 8 **a** Turbidity removal (NTU) for 2-day retention time, **b** Turbidity removal (NTU) for 1-day retention time and **c** Turbidity removal (NTU) for a 0.5-day retention time

was achieved when comparing the inlet and outlet. Greater removal was achieved for the 2 day and 0.5-day retention times where the averages were 62% and 67%, respectively.

Oligotrophic water was returned to the lake shortly after 2 days of filtration remaining steady during the whole experiment, as can be seen in Fig. 9a, b, and c. Even with constant input going into the tank, the floating filter unit was able to achieve constant removal of particulate phosphorus. This was accomplished because as previously presented, removal of TSS, turbidity, and reducing particle size occurred. In

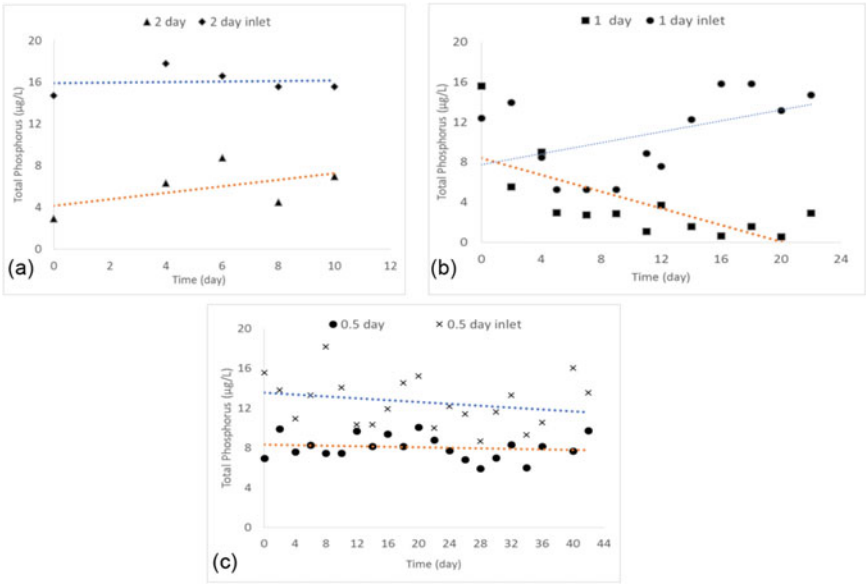

Fig. 9 **a** TP concentrations (µg/L) for 2-day retention time, **b** TP concentrations (µg/L) for 1-day retention time and **c** TP concentrations (µg/L) for a 0.5-day retention time

other words, suspended particles have phosphorus associated with it. It was noticed that average removal was 63, 63, 35% with decreasing retention. This lower value is explained because when water temperature started to drop the TSS level reduced.

Similar to the batch experiments, in the 3 continuous tests, no significant alteration of the concentrations of TN and nitrate were found. The TN value remained 0.95 ± 0.21 mg/L and for nitrate, the average value was 0.17 ± 0.05 mg/L which did not affect the experiment. On other hand, the COD presented continuous removal of approximately 12% in the 3 retention times presented. Figure 10a, b, and c demonstrates the removal of COD in the experiments. Due to the nature of the COD in this lake water, which is found mainly in the dissolved form, particle removal does not significantly affect this value. Additionally, the higher removal in batch experiments could be explained by the higher retention time that causes uptake of some dissolved COD.

4 Conclusions

With this adaptable, reactive, and environmentally-friendly remediation technique a representative amount of lake water was improved thus proving the method's feasibility. The combined non-woven geotextile thin layers in the floating unit have

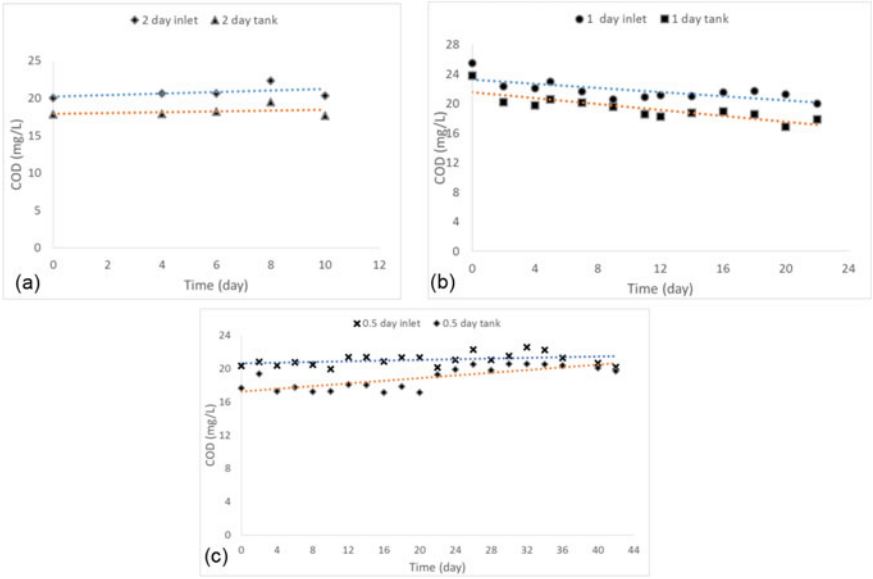

Fig. 10 **a** COD concentrations (mg/L) for 2-day retention time, **b** COD concentrations (mg/L) for 1-day retention time and **c** COD concentrations (mg/L) for a 0.5-day retention time

reduced the number of particles and their sizes in the water by sieving and cake filtration that lowers the membrane AOS. With reduced suspended particles and turbidity, lake levels of phosphorus and organic matter were lowered as well and cleaner water was returned to it. These on-site non-woven geotextile experiments have shown to be a potentially economically efficient and strong technique to be applied not only for preventing new sediment settling but also particulate phosphorus uptake that can be directly applied to water quality management in lakes. Incineration of clogged membranes (i.e., volume reduction) and final disposal in landfills is the most convenient way to dispose of used geotextiles membranes. However, in the direction of circular economy and sustainability to ensure waste reduction, routes to reuse, reduce, and recycle of membranes are being addressed. For future work, in situ filtration tests, dissolved COD removal, and clogged geotextile filter reuse will be investigated.

Acknowledgements The authors thank NSERC and Concordia University for the financial support of this project. The authors are also grateful to their industrial partner, Titan Environmental Containment Ltd., for supplying geotextiles and providing technical and financial support for this project.

References

1. De Wit HA, Valinia S, Weyhenmeyer GA, Futter MN, Kortelainen P, Austnes K, Hessen DO, Räike A, Laudon H, Vuorenmaa J (2016) Current browning of surface waters will be further promoted by wetter climate. Environ Sci Technol Lett 3(12):430–435
2. Morabito G, Rogora M, Austoni M, Ciampittiello M (2018) Could the extreme meteorological events in Lake Maggiore watershed determine a climate-driven eutrophication process? Hydrobiologia 824(1):163–175
3. Rocha Junior CAND, Costa MRAD, Menezes RF, Attayde JL, Becker V (2018) Water volume reduction increases eutrophication risk in tropical semi-arid reservoirs. Acta Limnol Bras 30. Retrieved from: https://doi.org/10.1590/S2179-975X2117
4. Woolway RI, Merchant CJ (2019) Worldwide alteration of lake mixing regimes in response to climate change. Nat Geosci 12:271–276. https://doi.org/10.1038/s41561-019-0322-x
5. Bhagowati B, Ahamad K (2019) A review on lake eutrophication dynamics and recent developments in lake modeling. Ecohydrol Hydrobiol 19(1):155–166
6. Hayden B, Harrod C, Thomas S, Eloranta A, Myllykangas J, Siwertsson A, Præbel K, Knudsen R, Amundsen P, Kahilainen K (2019) From clear lakes to murky waters—tracing the functional response of high-latitude lake communities to concurrent 'greening' and 'browning.' Ecol Lett 22(5):807–816
7. Le Moal M, Gascuel-Odoux C, Ménesguen A, Souchon Y, Étrillard C, Levain A, Moatar F, Pannard A, Souchu P, Lefebvre A, Pinay G (2019) Eutrophication: a new wine in an old bottle? Sci Total Environ 651:1–11
8. Bormans M, Maršálek B, Jančula D (2015) Controlling internal phosphorus loading in lakes by physical methods to reduce cyanobacterial blooms: a review. Aquat Ecol 50(3):407–422
9. Veetil DP, Mulligan CN, Bhat S (2018) Phosphorus speciation of sediments of a mesoeutrophic lake in Quebec, Canada. In: The international congress on environmental geotechnic, vol. 1, Springer, Singapore, pp 780–787
10. Søndergaard M, Lauridsen T, Johansson L, Jeppesen E (2017) Nitrogen or phosphorus limitation in lakes and its impact on phytoplankton biomass and submerged macrophyte cover. Hydrobiologia 795(1):35–48
11. Yin H, Yang C, Yang P, Kaksonen A, Douglas G (2021) Contrasting effects and mode of dredging and in situ adsorbent amendment for the control of sediment internal phosphorus loading in eutrophic lakes. Water Res 189:116644
12. Liu B, Liu L, Li W (2020) Effective removal of phosphorus from eutrophic water by using cement. Environ Res 183:109218
13. Zhang H, Chen J, Han M, An W, Yu J (2020) Anoxia remediation and internal loading modulation in eutrophic lakes using geoengineering method based on oxygen nanobubbles. Sci Total Environ 714:136766
14. Pereira AC, Veetil DP, Mulligan CN, Bhat S (2020) On-site non-woven geotextile filtration method for remediation of lake water. In: 2020 CSCE Annual Conference
15. Mulligan CN, Davarpanath N, Fukue M, Inoue T (2009) Filtration of contaminated suspended solids for the treatment of surface water. Chemosphere 74:779–786
16. Veetil DP, Arriagada E, Mulligan C, Bhat S (2021) Filtration for improving surface water quality of a eutrophic lake. J Environ Manag 279:111766
17. Couture HM, Gourlin B, Gutjjahr B, Mercier C (2013) Strategie de protection et de mise en valeur des milieux hummides sur le territoire de la Municipalite de Sainte-Anne-des-Lacs. Université de Sherbrooke. Retrieved from: https://www.sadl.qc.ca/wp-content/uploads/2016/01/Rapport-final-Strategie_milieu-humides2.pdf
18. ABVLACS (Agence des Bassin Versants de Sainte-Anne-des-Lacs) (2018). Retrieved from http://abvlacs.org/lac-johanne. Date: 1st Mar 2020
19. US EPA (1996) US EPA—EPA Method 3050B: acid digestion of sediments, sludges, and soils. Revision 2, p 12, Washington DC. Retrieved from: https://www.epa.gov/esam/epa-method-3050b-acid-digestion-sediments-sludges-and-soils. Date: 1st Nov 2020

20. Ministère du Développement durable, de l'Environnement et des Parcs (MDDEP) (2012) Portrait de la qualité des eaux de surface au Québec 1999 – 2008, Québec, Direction du suivi de l'état de l'environnement. Retrieved from: https://www.environnement.gouv.qc.ca/eau/portrait/eaux-surface1999-2008/Portrait_Quebec1999-2008.pdf
21. Chapman D, Kimstach V (1996) Water quality assessments: a guide to the use of biota, sediments, and water in environmental monitoring. CRC Press. 2nd ed. London
22. Ministère de l'Environnement et de la Lutte contre les changements climatiques (MELCC) (2018) Réseau de surveillance volontaire des lacs - Lac Johanne (0497A)- Suivi de la qualité de l'eau. Retrieved from: https://www.environnement.gouv.qc.ca/eau/rsvl/relais/fiches-bilans/2018/Johanne,%20Lac_0497A_2018_SA_SU.html

Artificial Intelligence-Based Prediction of Permeable Pavement Surface Infiltration Rates

A. Malik, K. Abogadil, U. T. Khan, and L. J. Butler

1 Introduction

1.1 Urban Stormwater Management and Low Impact Development

As population continues to grow around the world, it is expected that a larger fraction of people will live in urban areas. As a result of higher populations, cities are forced to expand and densify, leading to urban sprawl which can adversely affect the environment and more specifically, the hydrological cycle [1, 2]. As cities around the world become more urbanized, the number of impervious surfaces such as roads, rooftops, and other structures increases. These surfaces disrupt the natural hydrological cycle by preventing rainfall from infiltrating below ground as it should in predeveloped conditions, thus increasing stormwater runoff.

In recent years, source control and natural treatment methods such as Low Impact Development (LID) technologies have been gaining popularity as a way of capturing and treating urban stormwater runoff. The basic principle of LIDs is to maintain a site's post-development hydrology to the natural hydrology of the site before development [3–5], USA [6]. The main goal of implementing LIDs is to reduce the amount of impervious area, thereby reducing the amount of runoff generated. Several other

A. Malik (✉) · K. Abogadil · U. T. Khan · L. J. Butler
Department of Civil Engineering, Lassonde School of Engineering, York University, Toronto, ON, Canada
e-mail: amalik96@yorku.ca

U. T. Khan
e-mail: usman.khan@yorku.ca

L. J. Butler
e-mail: Liam.Butler@lassonde.yorku.ca

S. Walbridge et al. (eds.), *Proceedings of the Canadian Society of Civil Engineering Annual Conference 2021*, Lecture Notes in Civil Engineering 249,
https://doi.org/10.1007/978-981-19-1061-6_27

benefits of implementing LID include the ability to treat stormwater on-site through natural hydrological processes, a decrease in air pollution, and other socioeconomic benefits [7, 8]. LID technologies promote natural hydrological processes such as infiltration, evapotranspiration, on-site storage, absorption, adsorption, and percolation. By encouraging these processes to occur, the increased peak flow rates and high surface runoff volumes observed in urban land use types will decrease. Examples of LID infrastructure include bioretention cells, green roofs, rain gardens, grass swales, rain barrels, and pervious pavements [3].

1.2 Overview of Permeable Pavements

Permeable pavements are a type of LID technology that are an alternative to conventional impervious pavement surfaces such as asphalt and concrete. Permeable pavements in general have been shown to provide stormwater management by encouraging groundwater recharge, reducing surface runoff, and treating runoff pollutant loads through infiltration and storage [3, 9]. There are several types of permeable pavements but their overall goal is the same: to infiltrate stormwater [9]. Portland Cement Pervious Concrete (PCPC) are one type of permeable pavement. The design of PCPCs typically considers two parameters: structural adequacy and hydraulic performance. In PCPCs, these two characteristics are highly correlated. Typically, as the strength of PCPCs increases, the hydraulic performance (typically permeability or infiltration rate) decreases. A pervious concrete thickness of 5–6 inches (127–152.4 mm) has been seen to adequately handle expected traffic loads and thicker pavements of 8–12 inches (203.2–304.8 mm) have been used for higher traffic conditions [10, 11]. It should be noted that PCPCs beyond a thickness of 8 inches (203.2 mm) may be difficult to adequately compact [12].

1.2.1 Maintenance Concerns

Although newly installed permeable pavements can have sufficient (typically 100–10,000 mm/hr) surface infiltration rates (SIR) for even rare storm events [13], TRCA [14, 15] ACI [12, 16] over time, accumulation of pollutants (sediments, organic matter, and debris) within the voids of the concrete and on the surface causes the SIR of the pavement to decrease, reducing its performance in terms of both runoff reduction and pollutant load reduction. The accumulation of fine sediments in particular has been shown to severely affect SIR [14]. Factors such as, traffic, the nearby presence of fine sediments, sediment size distribution in runoff, presence of vegetation, the need for winter maintenance (salt/sanding, and age have indicated to influence clogging [14, 17].

Clogging of permeable pavement systems has been shown to greatly reduce the SIR. Bean et al. in [14] conducted an investigation of the SIR of different types of permeable pavements. The authors found SIRs in PCPC pavements as high as

7000 cm/hr where there was no visible clogging. Other locations with visible buildup of fine sediments had SIRs as low as 11 cm/hr. Winston et al. in [18] found that newly installed pervious asphalt pavements yielded SIRs up to 3000 cm/hr whereas pavements 25–30 years old had SIRs as low as 0.3 cm/hr. Valeo and Gupta in [16] conducted infiltration tests using the ASTM C1701 method on pervious asphalt and found SIRs as high as 302.4 cm/hr and as low as 0 cm/hr in clogged locations.

Due to this degradation of SIR, maintenance has been recommended to restore clogged pavements so that their long term hydraulic and environmental benefits can be fully realized. It has been suggested that clogging, in most cases, occurs near the pavement surface. 'Simulated maintenance' was conducted on concrete grid pavers where the first 13–19 mm of buildup was removed from the void spaces between the pavers resulting in significant improvements of SIR [14]. Cored samples were collected from various pervious concrete pavement systems and Computed Tomography (CT) scans were conducted to investigate clogging [17]. Results show that in general, the porosity of the top layer (25 mm) of the cored samples were generally lower, suggesting that clogging takes place near the top of the pavement system. The authors also found that age plays a significant role in pavement performance, and on average, older pavements had poorer performance than newer ones.

It is becoming increasingly understood that proper maintenance of these technologies is needed to maintain sufficient hydraulic performance [14]. The aforementioned methods to conduct maintenance are expensive and thus are either performed infrequently or not performed at all, leading to permeable pavement systems that no longer perform at their designed infiltration capacity [19]. Moreover, maintenance cannot be done optimally unless the degree of clogging of the pavement is known. Thus, determining the degree of clogging is a way of encouraging maintenance and therefore enabling the pavement to perform as it is originally intended.

1.2.2 Determining Permeable Pavement Performance

The most common performance metric for permeable pavement systems is the SIR which is inversely proportional to the amount of clogging and is likely dependant on the quality of the first 1″ (25.4 mm) of pavement depth [17]. Several methods of determining the SIR have been investigated. Early methods involved using permeameters in the field to determine the permeability of the pavement using either a constant head or falling head instead of destructive approaches that involved collecting cored samples [20, 21]. Other methods used double-ring infiltrometers that were adopted from the standard method of determining the infiltration rate of field-soils [14]. Brown and Borst [22] used single ring infiltrometers with a constant head on various types of permeable pavement systems. Custom methods of determining pavement performance have also been conducted. Lucke and Beechman [23] used double ring infiltrometers, but in locations where the infiltration rate was too high, an inundation method where a larger volume of water was used. Lucke et al. [24] used a custom infiltrometer to measure the performance of interlocking concrete pavers that showed to provide accurate results while being much more efficient than the standard method.

Other methods of rainfall simulation and large-scale surface inundation have also been investigated and shown to have promising results, although likely impractical for widescale adoption [25, 26]. The various methods and variability of results in these different methods lead to the establishment of standard methods for determining the SIR for two types of permeable pavement systems. ASTM C1701 and C1781 were developed for pervious concrete and interlocking concrete pavers, respectively. It has been shown that C1701 can be utilized for pervious asphalt pavements as well [16]. These contact-methods of determining permeable pavement performance can take hours to complete if a pavement is severely clogged [16]. Additionally, the logistics of bringing large amounts of water to a pavement site can be troublesome. Moreover, conducting multiple tests at different locations on-site for an accurate representation of the status of the pavement system is vital, however, it can be labour intensive and costly [22]. For these reasons, and the fact that maintenance is often overlooked, many installed permeable pavement systems no longer perform at their designed infiltration rate.

Other, non-contact methods, for determining SIR need to be explored that aim to remove some of these drawbacks. Several issues with PCPCs need to be further investigated. Mainly, these pavement systems are prone to clogging and eventually lose their ability to infiltrate stormwater. Contact methods of determining SIR are cumbersome, labour intensive, and time consuming. Thus, there is a need for easily determining the SIR of the pavement, which would lead to optimized maintenance of these systems. In this paper, we investigate the use of data-driven models to predict SIR using the relationship between the image of the pavement and the pavement's observed SIR.

Clogging has been identified as a major issue with permeable pavement systems. Current methods of obtaining a pavement's hydraulic performance are time consuming, labour intensive, and logistically challenging and thus, many PCPC systems no longer operate at their designed capacity. Maintenance has been seen to restore a pavement's infiltration capacity, however, determining when this maintenance should take place is challenging. Creating models to predict the clogging status of permeable pavement systems will be a quick, labour-free way of determining the infiltration rate of these systems and thus may result in more widespread maintenance, and thus may lead to the increased adoption of these pavement systems.

2 Method

2.1 Preliminary Field Investigation

Valeo and Gupta [16] conducted a brief regression analysis to investigate the relationship between the mean gray level of an image of the surface of a pervious pavement and the acquired infiltration rate of the pavement. Results from the study indicate that clogged pavements result in images with larger mean gray levels, or overall whiter

images. In this research, we investigated this relationship further by conducting a preliminary field investigation of permeable pavement parking lots located on and near York University's Keele Campus. Single-ring infiltrometer tests were performed in accordance to the ASTM C1701 standard for measuring the infiltration rate of in-place pervious concrete. The bottom of the infiltration ring, which measures approximately 300 mm in diameter, was lined with non-drying plumber's putty and then pressed into the surface to create a water-tight seal. The inner wall of the ring was marked with two lines at a distance of 10 mm and 15 mm from the bottom of the ring. Water was poured into the ring in accordance to ASTM C1701 and the time needed for the water to infiltrate the pavement was recorded. The infiltration rate is then calculated using Eq. (1) where I is the surface infiltration rate (mm/min), K is a constant with units (mm3*s/(kg*min), M is the mass of infiltrated (not pre-wet) water (kg), D is the inside diameter of the infiltration ring (mm), and t is the time for the water to infiltrate the surface (s). Prior to each test, the surface of the pavement was swept and a photograph was taken via iPhone 6S (12-megapixel camera) at approximately 0.5 m from the surface. This photograph was then later used for image analysis but is not required by the ASTM C1701 standard.

$$I = KM/(D^2t) \tag{1}$$

2.2 Lab Analysis

Results from the preliminary field investigation revealed that many locations of the parking lot were subject to high levels of clogging. To obtain a robust relationship between the image and infiltration rate of the pavement, controlled levels of clogging is necessary where the pavement is slowly clogged such that the progression of clogging is fully captured. To do this, small-scale pavement slabs were constructed. An iterative, experimental mixture design program was undertaken to obtain a pervious concrete mix design with similar physical properties of typical in-service PCPC systems. A 9.5 mm pea stone aggregate was used in addition to varying proportions of ordinary Portland cement, water, and a water reducing admixture to obtain an optimal mix. The 14 day and 28 day compressive strengths as well as the porosity of the hardened concrete specimens were obtained to help inform mixture design adjustments for subsequent mixes. Six 150 × 300 mm cylinders were cast for each mix where three cylinders were used for testing 14 day and 28 day tests. The compressive strength of the cylinders was obtained using a displacement-based loading rate of 0.02 mm/s which corresponded to a total test time of 5–7 min. Neoprene caps were installed at the ends of the cylinders prior to testing. The porosity of the cylinders was obtained in accordance to the ASTM C1754 standard for obtaining void content of hardened pervious concrete where the cylinders were weighed in both air and while submerged in water using a wire basket.

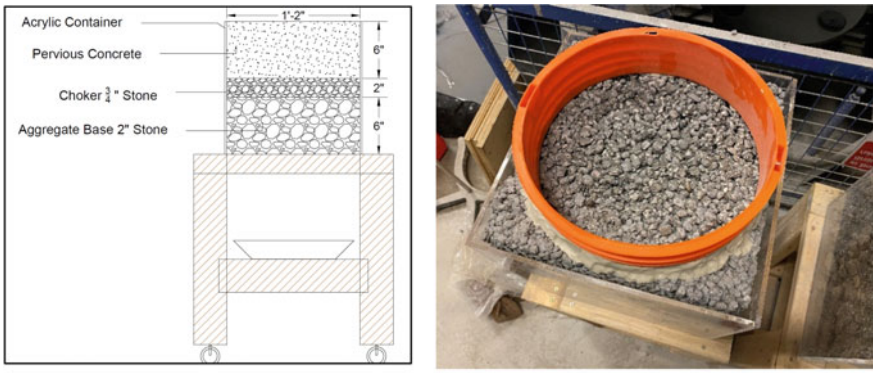

Fig. 1 Experimental setup for conducting infiltration tests on PCPC specimen. The schematic is shown in (**a**) and the top-view of the specimen with the installed infiltration ring is shown in (**b**)

Once the mix design process was completed, four PCPC slabs each with dimensions 335 mm × 335 mm × 150 mm deep were constructed. Infiltration rates of these slabs were measured and the concrete mixture design was once again adjusted such that high infiltration rates were obtained. As these slabs are subject to clogging, higher infiltration rates would yield more obtainable data. Acrylic containers with drainage holes were filled with gravel stone that acted as storage for the infiltrated water. These containers were placed on wooden stands with wheels for easy transport. A container was placed at the bottom of the stand, underneath the drainage holes, to capture the infiltrated water. Figure 1 shows the experimental setup. At the time of writing this paper, infiltration rate tests for the lab scale pavements were not yet conducted.

2.3 Data Analysis Techniques

Using MATLAB, properties of the images acquired during the field investigation were extracted. The images were first converted to greyscale and their individual histograms of the grey levels were acquired. In greyscale images, black pixels are represented as 0 while white pixels are represented as 255. In between are different shades of gray with increasing whiteness as the grey level increases to 255. Properties of the histograms were extracted including the mean grey level, variance, standard deviation, and skewness. These properties were then plotted with the measured infiltration rate to understand their correlation. The extracted properties were also used as input variables to a preliminary linear regression to investigate the potential of using these images to predict clogging. The linear regression used a data split of 60% where 60% of the data was used for training and 40% was used for testing the model.

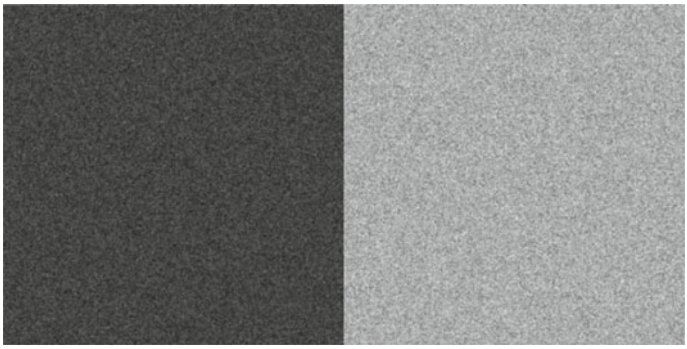

Fig. 2 Generated 'pavement' images where the left image represents an unclogged pavement with high infiltration and the right represents one that is clogged with low infiltration

Figure 2 shows samples of the generated images where the darker images represent less clogged pavements.

Artificial Neural Networks (ANNs) were also investigated for the purpose of predicting SIR. These models require large datasets for accurate predictions. Once calibrated, these models are well known for their predictive power and ability to model non-linearity in datasets [27, 28]. The acquired field data was not used in these models due to a low number of collected data. Instead, artificial images were generated using MATLAB to build proof of concept. Once sufficient lab measurements and photographs have been taken, they will be used as inputs to the models instead of the artificial images. The properties of these artificial images were extracted and used as inputs to predict SIR. The results were compared with a linear regression model with the same dataset.

3 Results

3.1 Preliminary Field Investigation

Images were acquired from various permeable pavement parking lots around York University's Keele Campus. Histograms of these images were obtained using MATLAB as well as the image's mean grey level, standard deviation, and skewness. Figure 3a shows a photograph of the surface of a pavement before conducting an infiltration test with the corresponding grayscale histogram in Fig. 3b. The histogram displays how many times a pixel value appears in the image. This count was normalized to provide a range from 0 to 1. The pavement was seen to be visibly clogged upon conducting the infiltration test and its corresponding mean grey level was seen to be relatively larger than the mean grey levels of other collected images which suggests that clogged pavements tend to produce whiter images, similarly found by

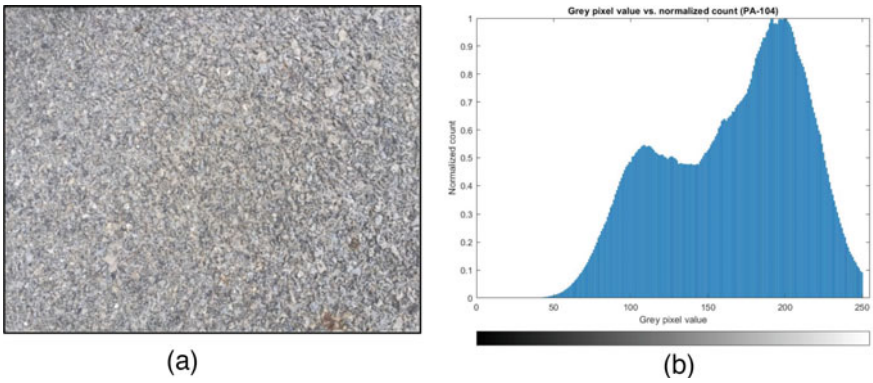

Fig. 3 Visibly clogged permeable pavement (**a**) and the extracted grayscale histogram (**b**)

Valeo and Gupta [16]. Many areas were already subject to high levels of clogging. Some areas were so clogged that the water for prewetting the pavement took over an hour to infiltrate. For these locations, infiltration rates were reported using the pre-wetting amount.

3.2 Data Analysis

3.2.1 Field Investigation

The extracted properties of the image were plotted with their associated infiltration rate to investigate their relationship. Figure 4a shows a plot of the inverse mean grey level with the associated infiltration rate. The mean grey level is suspected to be inversely proportional to the infiltration rate, meaning the larger the mean grey level, or the whiter the image, the smaller the pavement's infiltration rate. Thus, the inverse of the mean grey level was used to maintain a positive relationship, meaning the larger the inverse mean grey level, or the blacker the image, the higher the infiltration rate. The plots show different types of permeable pavement surfaces that were tested. These included Permeable Interlocking Concrete Pavers (PICP), pervious asphalt, and pervious concrete. Many locations that were tested were already subject to high levels of clogging, thus yielding infiltration rates close to 0. This means that many in service 'pervious' pavements behave similarly to ordinary asphalt pavement in where most stormwater ends up as runoff. Correlation between the inverse mean grey level and SIR resulted in a value of −0.1259. This means that the data is not very well correlated and the hypothesized positive relationship between the inverse of the mean grey level and the SIR is not true with this dataset. Variability in collecting field data may have affected the results. Some sources of this variability include the lighting condition when taking photos and inconsistencies in conducting

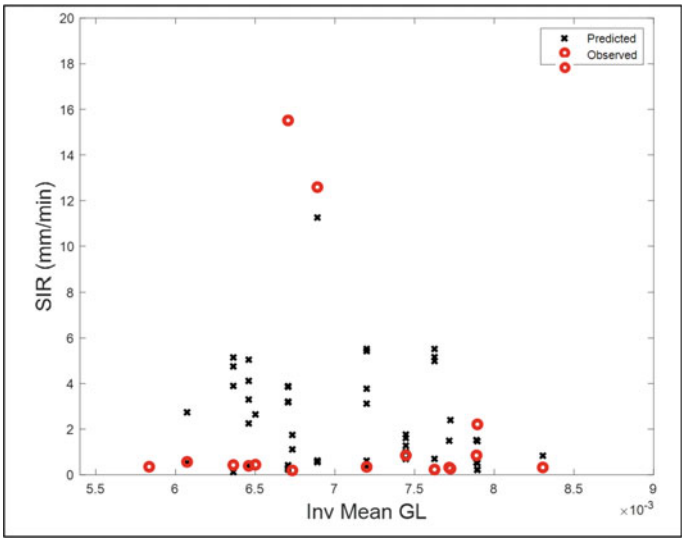

Fig. 4 Inverse mean grey level versus Observed SIR where observed data was obtained through the preliminary field investigation. The predicted points were obtained through linear regression

infiltration tests. This calls for conducting a similar lab-scale experiment where the pavement system is slowly clogged while simultaneously conducting infiltration tests and capturing images. This should provide the dataset necessary to thoroughly investigate the relationship between the infiltration rate of the pavement and the properties of the image.

A simple linear regression was conducted with the field images as seen in Fig. 4b. Only the pervious asphalt data points were used and some outliers were omitted due to suspicions of leakage during the infiltration test. The R^2 of the model was 0.55. Due to the high number of clogged observations and low number of observations in general, the model does not provide adequate predictive power. If the hypothesis that as pavements get clogged, the overall image shifts to a whiter image is to be thoroughly investigated, a larger, full-range dataset that captures the full lifecycle of the pavement as it clogs is required.

3.2.2 Artificial Pavement Images

An artificial dataset was used where 'pavement' images were generated using MATLAB to investigate the relationship between the properties of the image and theoretical SIRs. The properties (inverse mean grey level, standard deviation, and skewness) of these images were used as inputs to calibrate linear regression and artificial neural network (ANN) models. The ANN used a training-validation-testing data split of 55/22.5/22.5, nine neurons, an early stopping criteria of 6, the Levenberg–Marquardt training function, and a positive-linear transfer function. Figure 5

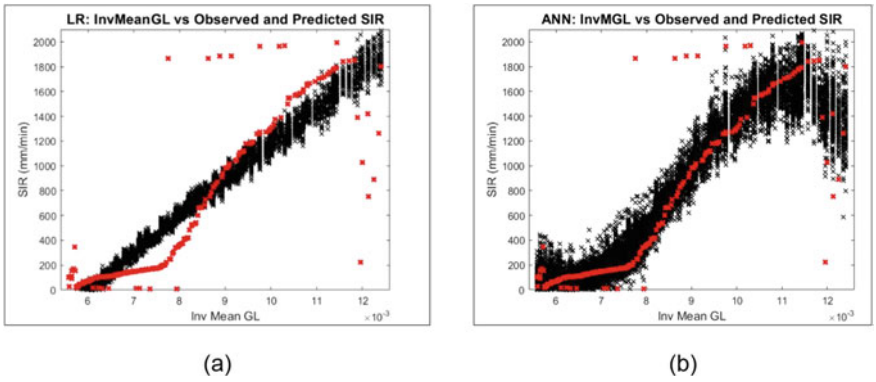

Fig. 5 Model results where black 'X' are the predicted values from the ensemble (100 runs) and red are the observed values. Figure 5a shows the linear regression results and Fig. 5b shows the artificial neural network results

highlights the predictive power of ANNs as they are able to capture the non-linearity of the data set as well as more of the extreme data points.

3.3 Future Work

One research challenge that was identified in the introduction and further verified was that many in-service pavement systems are already subject to high levels of clogging. This means that many systems no longer perform at their intended designed infiltration rate and some are so clogged that their infiltration is similar to a non-pervious asphalt pavement. This high-level of clogging resulted in difficulties in acquiring a dataset as they do not give the full clogging progression of the pavement. Thus, future research is going to focus on testing PCPC lab specimens with physical properties that resemble typical in-service PCPC pavements. These specimens will be subjected to artificial clogging while infiltration tests will be conducted simultaneously. Images of the pavements will be taken prior to each infiltration test. Properties of the images will be extracted and investigated to determine if there is a relationship between the surface of the image and its associated infiltration rate. This will allow for a complete dataset to be collected which will fully represent a pavement system's infiltration capacity for its entire lifespan from unclogged with high infiltration to clogged with low infiltration. This dataset will then be used as inputs to the aforementioned models such that the SIR of a given image of a pavement will be able to be predicted.

4 Conclusion

The preliminary field investigation revealed that many locations of different parking lots containing pervious concrete pavements were already subject to high levels of clogging. Due to this, obtaining a dataset of images and their associated infiltration rates proved difficult. Moreover, these locations required a large amount of time for water to infiltrate which added more logistical challenges in obtaining a large dataset due to time constraints. Although some images demonstrated the hypothesized relationship between the mean grey level and infiltration rate, the data collected to date cannot be used to statistically confirm it. This is due to the low quantity of collected data points, the low number of conducted tests that were able to actually infiltrate water, and variability in conducting field tests. The variability in the dataset include differences in lighting conditions, the angle at which the phone was held when taking photographs of the pavement, and human errors in conducting infiltration tests such as improper sealing of the infiltration ring or inconsistencies of pouring water for different tests. These challenges were propogated in the linear regression model as inadequate data resulted in an inaccurate model. The R^2 of the linear regression model was 0.55. Due to COVID-19, lab work was put on hold and artificial data was generated using MATLAB to calibrate models. This dataset was input to linear regression and artificial neural network models which resulted in R^2 values of 0.78 and 0.86, respectively. The ANN was found to produce a more accurate predictive model where it was able to capture the non-linearity in the dataset as well as predict more extreme points. The field investigation did not yield conclusive results between the relationship of the properties of the image of the pavement and its associated infiltration rate. A controlled lab investigation where pervious concrete slabs are slowly clogged as their images and infiltration rate are obtained may yield better results due to the elimination of some of the identified sources of error.

References

1. Booth DB, Jackson CR (1997) Urbanization of aquatic systems: degradation thresholds, stormwater detection, and the limits of mitigation. JAWRA J Am Water Resour Assoc 33(5):1077–1090
2. Wang L, Lyons J, Kanehl P, Bannerman R (2001) Impacts of urbanization on stream habitat and fish across multiple spatial scales. Environ Manage 28(2):255–266
3. Ahiablame LM, Engel BA, Chaubey I (2012) Effectiveness of low impact development practices: literature review and suggestions for future research. Water Air Soil Pollut 223(7):4253–4273
4. Fletcher TD, Shuster W, Hunt WF, Ashley R, Butler D, Arthur S, Trowsdale S et al (2015) SUDS, LID, BMPs, WSUD and more–The evolution and application of terminology surrounding urban drainage. Urban Water J 12(7):525–542
5. Khan UT, Valeo C, Chu AV, Van Duin B (2012) Bioretention cell efficacy in cold climates: Part 1—hydrologic performance. Can J Civ Eng 39(11):1210–1221
6. US EPA (2000) Low impact development (LID): A literature review (# EPA-841-B-00-005). Environmental Protection Agency, Office of Water, Washington, DC

7. Kaykhosravi S, Abogadil K, Khan UT, Jadidi MA (2019) The low-impact development demand index: a new approach to identifying locations for LID. Water 11(11):2341
8. Li J, Deng C, Li Y, Li Y, Song J (2017) Comprehensive benefit evaluation system for low-impact development of urban stormwater management measures. Water Resour Manage 31(15):4745–4758
9. Dietz ME (2007) Low impact development practices: A review of current research and recommendations for future directions. Water Air Soil Pollut 186(1):351–363
10. Obla KH (2010) Pervious concrete—An overview. Indian Concr J 84(8):9
11. Tennis PD, Leming ML, Akers DJ (2004) Pervious concrete pavements. Portland Cement Association, Skokie, IL, USA
12. ACI Committee 522 (2010) 522R-10: Report on pervious concrete. American Concrete Institute
13. Brattebo BO, Booth DB (2003) Long-term stormwater quantity and quality performance of permeable pavement systems. Water Res 37(18):4369–4376
14. Bean EZ, Hunt WF, Bidelspach DA (2007) Field survey of permeable pavement surface infiltration rates. J Irrig Drain Eng 133(3):249–255
15. TRCA Toronto and Region Conservation Authority (2006) Performance evaluation of permeable pavement and a bioretention swale. Toronto and Region Conservation Authority Interim Report #2. Seneca College, King City, ON, Canada
16. Valeo C, Gupta R (2018) Determining surface infiltration rate of permeable pavements with digital imaging. Water 10(2):133
17. Kayhanian M, Anderson D, Harvey JT, Jones D, Muhunthan B (2012) Permeability measurement and scan imaging to assess clogging of pervious concrete pavements in parking lots. J Environ Manage 95(1):114–123
18. Winston RJ, Al-Rubaei AM, Blecken GT, Viklander M, Hunt WF (2016) Maintenance measures for preservation and recovery of permeable pavement surface infiltration rate—the effects of street sweeping, vacuum cleaning, high pressure washing, and milling. J Environ Manage 169:132–144
19. Liu J, Li H, Wang Y, Zhang H (2020) Integrated life cycle assessment of permeable pavement: model development and case study. Transp Res Part D: Transport Environ 85:102381
20. Cooley AL, Brown RE (2000) Selection and evaluation of field permeability device for asphalt pavements. Transp Res Rec 1723(1):73–82
21. Fwa TF, Tan SA, Chuai CT, Guwe YK (2001) Expedient permeability measurement for porous pavement surface. Int J Pavement Eng 2(4):259–270
22. Brown RA, Borst M (2014) Evaluation of surface infiltration testing procedures in permeable pavement systems. J Environ Eng 140(3):04014001
23. Lucke T, Beecham S (2011) Field investigation of clogging in a permeable pavement system. Building Res Inf 39(6):603–615
24. Lucke T, White R, Nichols P, Borgwardt S (2015) A simple field test to evaluate the maintenance requirements of permeable interlocking concrete pavements. Water 7(6):2542–2554
25. Boogaard F, Lucke T, Van de Giesen N, Van de Ven F (2014) Evaluating the infiltration performance of eight Dutch permeable pavements using a new full-scale infiltration testing method. Water 6(7):2070–2083
26. Lucke T, Boogaard F, van de Ven F (2014) Evaluation of a new experimental test procedure to more accurately determine the surface infiltration rate of permeable pavement systems. Urban Plann Transp Res 2(1):22–35
27. Kia A, Wong HS, Cheeseman CR (2019) High-strength clogging resistant permeable pavement. Int J Pavement Eng 1–12
28. Samarasinghe S (2016) Neural networks for applied sciences and engineering: from fundamentals to complex pattern recognition. Crc Press

The Covid-19 Pandemic: An Exploration of Environmental Implications

Lynal Albert and Izaria Ferguson

1 Introduction

Today, the world faces a common enemy- SARS-CoV-2, frequently referred to as the corona virus. The on-going COVID crisis first identified in China in December 2019, has resulted in a global pandemic [1, 2] claiming more than 2,490,000 lives with over 500,000 deaths in the United States and over 20,000 deaths in Canada as of February 2021 as per the John Hopkins coronavirus resource center. The pandemic has unveiled unique social, economic and medical challenges that have threatened the well being of millions. As part of contingency measures to control the spread of the disease, various precaution measures and control strategies have been implemented globally. These include complete and partial lockdowns, short term and extended lockdowns, travel bans and restrictions, isolation and quarantine measures, limited service hours, remote working options and online learning in synchronous and asynchronous settings, control of mass gatherings and group activities, limited public transportation, the use of masks, gloves, sanitizers, frequent washing of hands, social distancing of at least 6 ft, regular temperature monitoring and disinfection of surfaces used by multiple people. The measures implemented within specific countries have largely been controlled by the respective governing bodies at the national, state and district or county and city levels [3–12]. These measures have triggered an avalanche of environmental effects. While some consequences are limited to certain regions or areas, we present in this paper an overview of global environmental implications of the COVID-19 pandemic.

L. Albert (✉) · I. Ferguson
Department of Engineering and Computer Science, Tarleton State University, Stephenville, TX 76402, USA
e-mail: albert@tarleton.edu

S. Walbridge et al. (eds.), *Proceedings of the Canadian Society of Civil Engineering Annual Conference 2021*, Lecture Notes in Civil Engineering 249,
https://doi.org/10.1007/978-981-19-1061-6_28

2 Methodology

To establish the critical environmental implications associated with the COVID pandemic, an integrated review of literature to collect information from various studies was performed. Publications related to environmental consequences published since the start of the crisis were included in the study. Broad searches were conducted to identify relevant publications using google scholar, scopus, web of science and databases associated with the John Hopkins Coronavirus Research Center, World Health organization, Center for Disease control, European Center for Disease Prevention and Control were utilized.

Due to the recent nature of the pandemic presenting unique circumstances, several studies examined the immediate environmental impacts. Each of these articles were reviewed and the environmental impacts were compiled. We have provided a review of various indirect environmental influences resulting from the COVID control strategies adopted worldwide. We also additionally present environmental consequences associated with the ripple effect of these outcomes that were synthesized based on community observations.

3 Results

The COVID response and control has varied significantly across various countries. Measures to control spread have ranged from short term stay at home orders to extended measures like social distancing, quarantine, and wearing of masks. For example, in the United States the first COVID-19 positive case was determined in January 2020 and several states including Pennsylvania, Texas, North Carolina, Alabama, Mississippi, issued stay at home orders in March and April of 2020 that lasted for varying times extending to April, May and June of 2020. Certain other states including Arkansas, Oklahoma, Nebraska, and South Dakota followed other control measures without a rigid stay at home order being issued. In Canada, by late March, the government strongly encouraged all people with the exception of non-essential workers to stay at home. In contrast, India reported the first positive case in January 2020 and a nation-wide lock down was imposed in March 2020 [3]. In Brazil the first COVID-19 infection was diagnosed in February 2020 and physical distancing and other confinement measures were implemented in March 2020. Additionally, in Russia lockdown measures were initiated towards the end of March. Nationwide lockdowns were implemented in Spain, France, UK, Italy, Peru, Argentina, Venezuela, Colombia, Ecuador, Bangladesh and others. The control strategies adopted worldwide, resulted in numerous indirect effects on the environment [13, 14]. While some outcomes on the environment are positive, others are negative. Figure 1 provides a summarized overview of these effects.

The following sections provide details on each of the positive and adverse outcomes listed above.

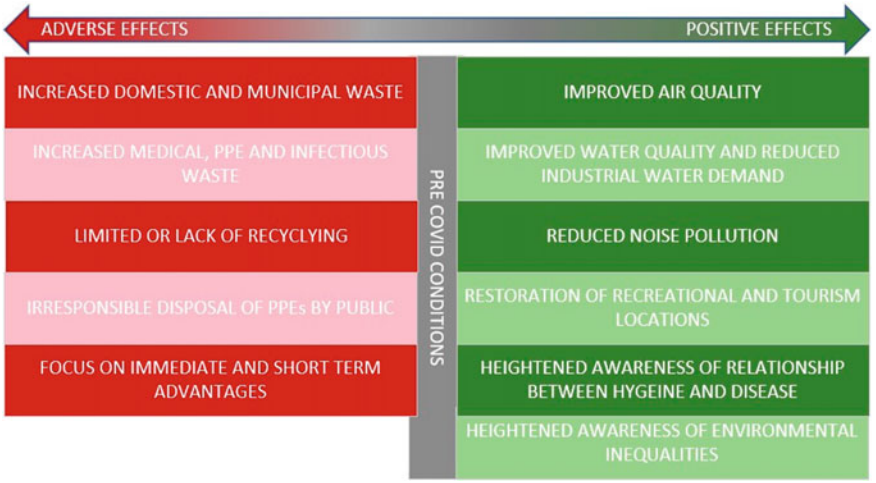

Fig. 1 A summarized depiction of the positive and negative environmental impacts of the COVID crisis

3.1 Improved Air Quality

Poor air quality is a major concern resulting in 8% of global deaths annually including thousands of premature deaths, as a result of respiratory and cardiovascular complications due to air pollution [15–17]. Moreover, it is widely accepted that sub-par air quality can increase lung disease that can heighten the predisposition of individuals from developing severe symptoms and complications associated with the COVID disease [18]. Although not a direct result of the spread of the pandemic, air quality has improved since the start of the crisis as an indirect consequence of contingency measures like lock downs, remote schooling and business, travel bans and limited industrial functioning [3, 18–20]. The most common air pollutants regulated under the Clean Air Act as criteria pollutants include carbon monoxide, ground level ozone, lead, nitrogen di oxide, sulfur dioxide and particulate matter ($PM_{2.5}$ and PM_{10}). These criteria pollutants have National Ambient Air Quality Standards (NAAQS) established by the EPA that are reviewed periodically based on public health while including a margin of safety for at-risk populations [21]. Table 1 summarizes the criteria pollutant sources, and effects summarized from EPA's website and [15, 16], Pinkerton 2016.

Although sources of pollution can also include natural sources like pollen, dust, volcano eruptions and forest fires, a higher incidence of these criteria pollutants is often associated with anthropogenic activities including transportation and vehicle exhaust, industrialization, fossil fuel consumption, construction, and incineration as listed in Table 1. Therefore, pandemic response actions like the lockdown and travel bans alone can indeed result in improved air quality. COVID control measures also limited other anthropogenic activities resulting in decreased socio-economic

Table 1 Criteria pollutants, summarized health effects and their recommended regulatory levels

Pollutant	Primary sources	Health effects
Carbon monoxide	Mobile sources from the transportation sector, fossil fuels	Mortality, heart attacks, cardiovascular disease, dizziness, confusion
Ozone	Photochemical reactions involving NO_x and Volatile Organic Compounds	Asthma, wheezing, bronchitis, eye irritation, pneumonia, chronic obstructive pulmonary disease, headaches, accelerated aging and other respiratory complications
Nitrogen dioxide	Mobile sources from the transportation sector, fossil fuel combustion	Edema, eye irritation, nasal irritation, pulmonary discomfort, lung cancer
Sulfur dioxide	Fossil fuel combustion	Sore throat, fatigue, shortness of breath, cough, bronchitis
Lead	Mineral ore processing, leaded fuel, incineration, lead smelting	Gastro-intestinal problems, vomiting, loss of appetite, kidney and liver damage, fertility issues, impaired mental development, nervous system complications
Particulate matter PM10	Mechanical crushing, grinding and abrasion of surfaces	Respiratory and cardiovascular diseases, infant mortality, hay fever, bronchitis, dermatitis
Particulate matter PM2.5	Combustion of fuel, gas and diesel engines and wood	Cardiovascular disease, respiratory complications, mortality

activities thereby resulting in a myriad of air quality changes that have been studied globally.

Studies have shown that reduced air pollution levels corelated with COVID response activity restriction periods. A reduction in PM2.5 and PM 10 have been identified and reported in various regions including China, Japan, India, the European Union, United States [7, 22]. Other studies show that NO_2, SO_2 and CO concentrations plummeted in Brazil, India, China, parts of North America, European cities like Barcelona, Madrid, Milan, Rome and Paris [14, 16, 20, 23, 24]. Satellite data from NASA reflect the improvements in NO_2, SO_2 and other contaminants in Korea, Spain, Germany, U.S and others by 20–38% [14, 20, 23, 25]. These improved air quality conditions manifested in decreased number of children developing respiratory problems when compared to the previous years and reduced other respiratory illness [22, 25].

In contrast to the above-mentioned criteria pollutants that predominantly showed a decrease in concentration due to COVID activity limitations, ground level ozone demonstrated no change or an increase in concentration. High levels of ozone are associated with severe lung disease, asthma and cardiovascular morbidity. Increase in ground level ozone has been attributed to variation in NOx- VOC ratios that have exhibited variation during recent air quality trends [3, 18, 19, 26].

Additionally, reduced industrialization and limited transportation including international and domestic flights resulted in a decrease in overall fossil fuel consumption thereby decreasing green house gases emissions. China, the world's largest consumer of coal reduced coal consumption by over 35% compared to the pre-COVID conditions. Further, studies have demonstrated a decline in CO_2 concentrations in the U.S, UK, Brazil, Japan and India [14, 16, 22, 24, 27].

3.2 Improved Water Quality and Reduced Industrial Water Use

Over two third of the world's population lives in water stressed areas magnifying our need to maintain surface water quality. Surface water serves multiple purposes including being used as a drinking water source, used for commercial and industrial applications (including cooling water), used for irrigation, used for regional transportation purposes, used as a source of food, and used for additional purposes including recreational and religious reasons. Pollution from various sources including urban, agricultural and cattle rearing run offs, continue to threaten the quality of our water resources. In developing countries other factors like industrial effluents, untreated sewage and illegal dumping continue to pose challenges to improving water quality of rivers and lakes [3, 14].

In the natural environment, the primary compartments of air, water and soil are interlinked through mass transfer and exchange thereby the benefits we have observed with air quality improvements combined with reduced industrial activities have resulted in improved surface water quality. Studies demonstrate significant improvements in water quality in various part of the globe due to reduced point source inputs and non-point source inputs [23]. In Grand canal, the primary waterway in Venice, Italy, the water in the canal has shown visual improvement in appearance due to reduced water traffic [14, 23]. The enhance in water quality has also been associated with the reappearance of aquatic life. Other studies have showed water quality improvement in the San Francisco Bay, California and the Vembanad lake, the longest fresh water lake in India. The overall amount of industrial, constructional and manufacturing related waste generation reduced during the COVID, thereby indirectly improving water quality in surface waters that are used as sinks for these waste effluents in developing nations.

Water pollution has also been documented to have reduced across a large number of beaches across the globe as discussed below. The reduction in water traffic due to reduced trade and travel bans also helped limit marine pollution.

The complete and partial lockdowns in different areas also resulted in decreased water usage in various industrial sectors [14, 28]. Studies show that water usage by the commercial, industrial and institutional sector reduced by 11.2%. Similar studies have shown a decrease in the industrial water demand in Brazil and other nations despite a slight increase in domestic water use.

3.3 Increase in Domestic and Municipal Waste

The COVID crisis and response measures encouraged and sometimes even required people to stay at home. This resulted in several life style changes including enhanced online shopping and delivery of grocery that causes an increase in packaging waste [27, 29]. Shoppers that often-used recycled bags and shoppers that reuse plastic bags started depending on single use plastic bags and disposing them with household waste after use thereby resulting in more packing related waste generation [30]. Social distancing practices coupled with limited hours and services in restaurants has also resulted in an increase in take away orders and online orders further contributing to the generation of packaging waste [27, 30].

The COVID contingency measures have included the requirement of face masks in stores, schools, recreational places, hospitals, places (airports and bus and train stations) and means of public transport, at work and all other places of public and religious services. The increase in demand for one time use plastics like masks and gloves, tissues and wipes has drastically increased severely impacting waste composition and increasing the environmental burden [3, 29]. To complicate matters, asymptomatic people and those that have contracted the disease and are following stay at home isolation and quarantine orders, continue to generate domestic waste that may be infectious. Waste handlers and processors are at risk of exposure through the infectious waste [3, 30, 31]. This can result in increasing spread of the disease in developing countries where waste collection sites and systems are poorly regulated, open dump sites exist and where handlers and rag pickers do not have access to appropriate protective equipment [31]. Furthermore, the increase in domestic waste has raised alarms for possible increase in incidence of waste fires. Waste fires increased by 10% in March 2020 when compared to previous years. The increase has been attributed to a high amount of packaging waste associated with the hike in online orders [24].

3.4 Increase in Medical, Personal Protective Equipment (PPE) and Infectious Waste

With the increase in the production of personal protective equipment to meet the needs of the medical industry due to the pandemic, comes the inevitable task of dealing with the increase in waste after use. The safe handling, collection, transportation, disinfection and disposal of medical and infectious waste is crucial to the well being of any society at all times. The pandemic situation has resulted in larger volumes of medical waste including personal protective equipment like masks, gloves and shields being generated at hospitals, clinics, dental offices, laboratories and other long-term care centers [13, 32]. An increase in plastic packaging of single use equipment, protective gear and other medical logistics will also contribute to solid waste generation [30]. In the city of Wuhan alone about 240 tons of medical waste was

generated per day compared to their general trend of close to 50 tons per day [27]. In Egypt the medical waste generation went from about 70 tons per day to around 300tons per day [26].

Studies have shown that the corona virus can live on different surfaces for varying durations from hours to days. For example, the virus has been identified to remain alive on glassware for 4 h and on plastic for about 3 days [30]. Thus, personnel handling waste require special protective gear and training to help in efficient and safe waste management. Studies have shown a higher prevalence of COVID spread among waste collectors in India, Brazil, Pakistan, Greece and Iran. Countries that had poor waste management practices in pre-COVID conditions will undoubtedly need to develop new and safe practices to combat the complications arising from higher medical waste generation rates [24].

3.5 Irresponsible Disposal of PPEs

The use of PPE like masks and gloves are critical to prevent and manage the spread of the COVID virus according to the Center for Disease Control. Although the disposal of used face masks generated in medical settings are overseen carefully, there is increasing evidence of irresponsible waste disposal particularly of masks and gloves in the environment by the public [22]. Face masks have been identified at nature trails, sidewalks, parks, water bodies and beaches due to improper and irresponsible disposal [3, 14, 32] (Fig. 2).

Apart from the possibility of being infectious, with the ability to trigger secondary infections, the waste results in clogging of storm water systems, accumulation

Fig. 2 This figure demonstrates the irresponsible disposal of PPEs by the public in parks, outside grocery stores, walkways, near trash cans, and in and around water bodies

by water bodies affecting aesthetics and aquatic health, contaminating soil and presenting environmental persistence issues. Inappropriate disposal of PPEs like masks can result in them being carried by wind or transported by rain water to waterbodies where they can be voluntarily or involuntarily ingested, or physically trap organisms like fish, turtles, corals and tadpoles causing a great threat to both wildlife and marine life. Further, there is a risk of toxins generation and meso and microplastics release from the polypropylene waste that can trigger another plethora of adverse outcomes if they enter the food chain. It is imperative to realise that these masks were mostly designed to be efficient barriers and not easily break down.

3.6 Limited Recycling of Waste

Reduced and prohibited recycling during the pandemic has resulted in short term and long-term environmental impacts. Due to the possible risk to handlers and sorters, and the increased possibility of cross contamination, several countries have suspended their recycling programs. In areas where recycling continues, it is to be noted that the value of recycled materials has decreased therefore despite the surge in single use plastics and disposables, these materials still end up with the municipal waste [30, 32]. The fact that recycling is mostly limited or suspended results in aggravating the already monumental problem of high municipal waste generation during the pandemic. The recycling industry not identified as essential service, is interrupting efficient waste management systems in parts of US, Brazil and Europe [27].

3.7 Reduced Noise Pollution

Noise pollution is ranked the third hazardous pollution problem after air and water pollution. Continual exposure to noise pollution can result in severe health complications. Studies show that hypertension, sleep disorders, cardiovascular disease, gestational diabetes, hormonal dysfunction and mental wellbeing problems are associated with noise pollution. Other studies have directed that anthropogenic activity related noise pollution can impact the behavior patterns and habitat quality associated with wildlife. The COVID response resulted in reduced socioeconomic activities, road, rail and air traffic thereby significantly reducing noise pollution in different regions [26, 27].

3.8 Restoration of Recreational and Tourist Locations

The pandemic has resulted in disrupted tourism and recreational travel for an extended time due to people prioritizing safety, social distancing requirements and restricted

travel [22, 33]. This has reduced pollution in popular locations that are frequented by people. Alleviated pollution linked with road traffic, boating, and trash that is associated with tourism has resulted in restoration of these overexploited locations. Reduced litter and plastics and improved water quality have primarily been attributed to regional bans from large gatherings, and limited opportunities for tourism. Reduced effects of anthropogenic activity have been observed in beaches in Maldives, Thailand, United States, Ecuador, Mexico, India and Barcelona [26, 27, 33].

3.9 Heightened Awareness of Environmental Inequalities

Environmental inequalities have long existed across the globe. These predispositions both increase the likelihood of spread of germs in these groups and enhance the vulnerabilities of certain populations to disease. These inequalities include lack of access to clean water, communal water supplies, sanitation and hygiene related deprivations, shared facilities, and high population density. Additionally, studies have demonstrated that exposure to air pollution can increase the possibility of complications arising from the COVID disease [18]. For example, an increase in 1 μg/m3 in PM 2.5 was linked to a 5% increase in death rate due to COVID. Similar observations have been made in India, Indonesia and China. Indoor air quality conditions in developing countries that rely on fuel sources like wood, charcoal, peat, wheat, rye etc. can be compromised and populations exposed to these prolonged poor air qualities may be at greater risk for complications. The crisis situation has elevated these problems as urgent and has triggered initiatives to address these inequalities in different ways. Understanding the interconnectedness between air quality, availability of clean water to wash hands and maintain clean surfaces and disease susceptibility is vital to building our defense against the disease. This heightened awareness is a step in the right direction to support these populations by providing temporary and long-term accommodations or solutions as feasible to decrease health risk of these populations.

3.10 Focus on Immediate and Short-Term Advantages

The COVID disease has threatened the sustenance of humanity and individuals, organizations and even nations that were streamlining sustainable initiatives can have a shift of focus. While facing health crisis situations, the priority is mostly immediate safety and short-term benefits. This includes increase in usage of disinfectants, plastics, and paper coupled with accelerated waste disposal without organization and sorting and neglection of recycling possibilities [30, 32]. Severe disruption in public health and socio-economic aspects tend to swing the attention of governing bodies, organizations and even individuals to focus available resources on improving the economy and strengthening their health-related options. Sustainable living and practices may take a backseat while we battle the negative consequences of COVID

despite the fact that sustainable living has long term impacts on both health and socioeconomics [30, 34].

Additionally, the use of disinfectants provides immediate and clear benefits of clean surfaces which are critical to control disease spread. However, the increase in amounts and frequency of disinfectants used by people across the globe can result in environmental consequences that may be detrimental but yet unknown.

3.11 Heightened Awareness of the Relationship Between Hygiene and Disease Spread

We have long understood the critical symbiotic relationship between hygiene and disease. Every year millions of people contract the flu due to lack of efficiently washing hands, touching contaminated surfaces and exposure to infected people. The COVID crisis is mounting with millions contracting the disease however seasonal infections remain at extremely low levels compared to previous years. This change highlights enhanced personal hygiene practices and the positive effects of social distancing and limited travel [35]. The decline in multiple seasonal and respiratory viral infections has been attributed to reduced travel domestically and worldwide [35]. Millions of people living in rural areas of developing countries do not have the privilege of adequate sanitation resources but the pandemic has resulted in awareness and promoted hygiene related services and practices in these areas.

4 Discussion and Conclusion

Some of the environmental implications presented above for example, improvement in air quality, decline in water pollution, reduced industrial water demand, decrease in noise pollution, restoration of recreational and tourism locations and increased domestic and medical waste have been identified as temporal changes to the environment while others related to lack of recycling, shift in the focus to immediate and short term benefits versus long term goals, heightened awareness of environmental inequalities are examples of more lasting impacts. While the COVID disease has provided an opportunity for the environment to rebound positively in many ways, the authors recognize and acknowledge the unfavorable, grim and tragic effects of the pandemic resulting in increased hospitalizations, high mortality, job losses and economic crisis are inescapable and cannot be marginalized. Other detrimental effects associated with the wellbeing of the society include increase use of marijuana and other substance abuse related products.

The positive outcomes have however taught us that reduced and controlled anthropogenic activities can provide significant environmental improvements, therefore measures should be adopted to increase the longevity of these desirable effects.

Although directing resources to address the needs of the health sector and to rebuild economic losses are crucial to recover from the pandemic mode, it also is necessary to continue to push towards achieving long term sustainability goals that will benefit public health and overall well being of the society. To champion efforts on sustainability, resources will have to be channelled to promote and prompt the society about pre-COVID sustainability goals. This can be achieved by focussing on sustainability related advertisements and workshops in schools, colleges and local communities. Industrial organizations and companies can be provided incentives to promote water and air quality improvements beyond that which is legally required. The crucial environmental related lesson we have learned is that controlled anthropogenic activities can go a long way in improving the quality of the environment. This experience can be particularly useful to bring about positive change when combined with collective efforts and definite sustainability goals when we are no longer fighting a pandemic situation.

References

1. Dong E, Du H, Gardner L (2020) An interactive web-based dashboard to track COVID-19 in real time. Lancet Infect Dis 20(5):533–534
2. Sohrabi C, Alsafi Z, O'Neill N, Khan M, Kerwan A, Al-Jabir A, Iosifidis C, Agha R (2020) World health organization declares global emergency: a review of the 2019 novel coronavirus (COVID-19). Int J Surg 76:71–76
3. Bhat SA, Bashir O, Bilal M, Ishaq A, Dar MUD, Kumar R, Bhat RA, Sher F (2021) Impact of COVID-related lockdowns on environmental and climate change scenarios: a case study of New Delhi in India. Environ Res 110839
4. Chaudhry R, Dranitsaris G, Mubashir T, Bartoszko J, Riazi S (2020) A country level analysis measuring the impact of government actions, country preparedness and socioeconomic factors on COVID-19 mortality and related health outcomes. EClinicalMedicine 25:100464
5. Chen Y-T, Yen Y-F, Yu S-H, EC-Y Su (2020) An examination on the transmission of COVID-19 and the effect of response strategies: a comparative analysis. Int J Environ Res Publ Health 17(16):5687
6. de Moura Villela EF, López RVM, Sato APS, de Oliveira FM, Waldman EA, Van den Bergh R, Fodjo JNS, Colebunders R (2021) COVID-19 outbreak in Brazil: Adherence to national preventive measures and impact on people's lives, an online survey. BMC Publ Health 21(1):1–10
7. Han E, Tan MMJ, Turk E, Sridhar D, Leung GM, Shibuya K, Asgari N, Oh J, García-Basteiro AL, Hanefeld J (2020) Lessons learnt from easing COVID-19 restrictions: an analysis of countries and regions in Asia Pacific and Europe. The Lancet
8. Liao H, Zhang L, Marley G, Tang W (2020) Differentiating COVID-19 response strategies. The innovation 1(1):100003
9. Patrikar S, Deepti Poojary DR, Basannar DSF, Kunte R (2020) Projections for novel coronavirus (COVID-19) and evaluation of epidemic response strategies for India. Med J Armed Forces India 76(3):268–275
10. Rohrich RJ, Hamilton KL, Avashia Y, Savetsky I (2020) The COVID-19 pandemic: changing lives and lessons learned. Plast Reconstr Surg Glob Open 8(4)
11. World Health Organization (2020) Coronavirus disease (COVID-19) technical guidance: infection prevention and control Wash, Who
12. Xiao Y, Torok ME (2020) Taking the right measures to control COVID-19. Lancet Infect Dis 20(5):523–524

13. Bashir MF, Benjiang MA, Shahzad L (2020) A brief review of socio-economic and environmental impact of covid-19. Air Qual Atmos Health 13(12):1403–1409
14. Cheval S, Adamescu CM, Georgiadis T, Herrnegger M, Piticar A, Legates DR (2020) Observed and potential impacts of the COVID-19 pandemic on the environment. Int J Environ Res Publ Health 17(11):4140
15. Ayala A, Brauer M, Mauderly JL, Samet JM (2012) Air pollutants and sources associated with health effects. Air Qual Atmos Health 5(2):151–167
16. Espejo W, Celis JE, Chiang G, Bahamonde P (2020) Environment and COVID-19: pollutants, impacts, dissemination, management and recommendations for facing future epidemic threats. Sci Total Environ 747:141314
17. Kurt OK, Zhang J, Pinkerton KE (2016) Pulmonary health effects of air pollution. Curr Opin Pulm Med 22(2):138–143
18. Ching J, Kajino M (2020) Rethinking air quality and climate change after COVID-19. Int J Environ Res Public Health 17(14):5167
19. Connerton P, Vicente J, de Assunção R, de Miranda M, Slovic AD, Pérez-Martínez PJ, Ribeiro H (2020) Air quality during COVID-19 in four megacities: lessons and challenges for public health. Int J Environ Res Public Health 17(14):5067
20. Ghosh S, Ghosh S (2020) Air quality during COVID-19 lockdown: blessing in disguise
21. Hartmanns A (2014) A comparative assessment of the environmental and human health-related legislation on mixture Toxicity, in the USA and the EU. University of Gothenburg
22. Rume T, Islam SMDU (2020) Environmental effects of COVID-19 pandemic and potential strategies of sustainability. Heliyon e04965
23. Hallema DW, Robinne F-N, McNulty SG (2020) Pandemic spotlight on Urban water quality. Ecol Process 9:1–3
24. Rupani PF, Nilashi M, Abumalloh RA, Asadi S, Samad S, Wang S (2020) Coronavirus pandemic (COVID-19) and its natural environmental impacts. Int J Environ Sci Technol 1–12
25. Isaifan RJ (2020) The dramatic impact of coronavirus outbreak on air quality: has it saved as much as it has killed so far? Glob J Environ Sci Manag 6(3):275–288
26. Mostafa MK, Gamal G, Wafiq A (2021) The impact of COVID 19 on air pollution levels and other environmental indicators-a case study of Egypt. J Environ Manag 277:111496
27. Zambrano-Monserrate MA, Ruano MA, Sanchez-Alcalde L (2020) Indirect effects of COVID-19 on the environment. Sci Total Environ 728:138813
28. Li D, Engel RA, Ma X, Porse E, Kaplan JD, Margulis SA, Lettenmaier DP (2021) Stay-at-home orders during the COVID-19 pandemic reduced urban water use. Environ Sci Technol Lett
29. Ouhsine O, Ouigmane A, Layati E, Aba B, Isaifan R, Berkani M (2020) Impact of COVID-19 on the qualitative and quantitative aspect of household solid waste. Global J Environ Sci Manag 6 (Special Issue (Covid-19)):41–52
30. Sharma HB, Vanapalli KR, Cheela VRS, Ranjan VP, Jaglan AK, Dubey B, Goel S, Bhattacharya J (2020) Challenges, opportunities, and innovations for effective solid waste management during and post COVID-19 pandemic. Resour Conserv Recycl 162:105052
31. Mol MPG, Caldas S (2020) Can the human coronavirus epidemic also spread through solid waste? Waste Manage Res 38(5):485–486
32. Sarkodie SA, Owusu PA (2020) Impact of COVID-19 pandemic on waste management. Environ Devel Sust 1–10
33. Zielinski S, Botero CM (2020) Beach tourism in times of COVID-19 pandemic: critical issues, knowledge gaps and research opportunities. Int J Environ Res Public Health 17(19):7288
34. Morgan AK, Awafo BA, Quartey T (2021) The effects of COVID-19 on global economic output and sustainability: Evidence from around the world and lessons for redress. Sustain Sci Pract Policy 17(1):77–81
35. Jones N (2020) How COVID-19 is changing the cold and flu season. Nature 588(7838):388–390

Insights into Effects of Tillage and Residue Management on the Growth of Canola in Canadian Prairie-A Case Study in Saskatchewan

J. Huang, G. Huang, X. Xin, and C. An

1 Introduction

Canola belongs to the Brassica genus and is a valuable seed crop in many countries throughout the world. From the beginning of the twenty-first century, Canola has been widely planted in Canadian farms because of its high yields and resistance to herbicides [1]. In 2017, canola production in Canada was 21.3 million tones and its economic value was up to 26.7 billion dollars [2]. Alberta, Manitoba, Saskatchewan and British Columbia are main areas of canola products in Canada. Canola products, including oil and meal, play an important role in agriculture, industry, animal husbandry and other fields. Among them, canola oil is widely used as the third largest vegetable oil after soybean oil and palm oil [3]. As a conventional co-product during extracting bio-oil production process, canola meal can be used in livestock and aquaculture industries for animals feed because it is rich in protein and amino acid [4]. Therefore, many researchers are interested in exploring effective strategies and methods to enhance canola yield and quality.

J. Huang (✉)
Institute for Energy, Environment and Sustainable Communities, University of Regina, Regina, Canada
e-mail: jhbamboo@outlook.com

G. Huang
Faculty of Engineering and Applied Science, University of Regina, Regina, Canada
e-mail: huang@iseis.org

X. Xin
Department of Civil Engineering, Memorial University of Newfoundland, St. John's, Canada

C. An
Department of Building, Civil and Environmental Engineering, Concordia University, Montreal, Canada

S. Walbridge et al. (eds.), *Proceedings of the Canadian Society of Civil Engineering Annual Conference 2021*, Lecture Notes in Civil Engineering 249,
https://doi.org/10.1007/978-981-19-1061-6_29

Previous studies have proved that high crop production is attributed to improved soil physical, chemical and biological properties. Water content and organic matter in soil can be influenced by various factors including management options for tillage, residue, and rotation length [5]. No-tillage and minimum tillage with standing stubble have been proved beneficial for conservation of nutrition and moisture of soil, and generally increase of crop production [6]. Canola seed yield and oil content are positively correlated with soil moisture availability, while unfavorable soil moisture condition particularly during flowering and bud development results in intensive assimilates, pod abortion and loss in seed weight [7]. In addition, favorable effects of conventional tillage practices on soil enzyme activities have been proved in previous studies [8].

However, no comprehensive study of characterization of canola growth within the plants was reported for Canadian prairie, where harsh natural conditions warrant special attention on cold resistance and water conservation in the processes of tillage and residue management.

Therefore, the objective of this study is to explore: (1) the features in canola growth within a Canadian prairie context under the interferences of tillage and residue treatment; (2) characteristics of canola at seedling and mature stages. Factorial analysis method will be presented to explore changes of these features of canola plants under different conditions.

2 Materials and Methods

2.1 Overview of Study Site

The trial field was located at a village called Spalding in the Canadian province of Saskatchewan. This study field was approximately 1 km^2, divided into four segments. This place was planted wheat in 2018. Before seeding canola in 2019, wheat was harvested on October 18, 2018 and residuals of wheat crops were left in the field. Two different combines were used to conduct the wheat harvest. A few days later, post-harvest treatments for the subsequent canola crop were carried out when wheat residue was dry and in good condition for the post-harvest operations. Three diverse post-harvest treatments (harrow, tillage and check) were applied in the trial field. In total, there were six combinations of chopper types and post-harvest treatments in each segment. Every combination replicated four times in this chosen trial filed. After post-harvest treatment, the canola of Invigor L233P variety were seeded at this field on May 21st, 2019.

2.2 Indicators

Plant emergence was used as an indicator to analyze the growth status of canola at seedling stage. The spring plant counting was carried out at 31 days after seeding (June 21st, 2019) in the growing season as a response (plant emergence) for the general factorial design experiment. At the same time, the soil temperature of each trial field part was measured and recorded.

For further analyses, more data about seedlings needs to be measured in laboratory by collecting seedling samples from all parts in the field. At 36 days after seeding (June 26th, 2019) three samples of canola seedlings were picked up in each field part. Totally 72 canola seedling samples were collected for measuring the leaf length which was used as another response in the general factorial design. For compared to seedling samples, 72 mature canola plants were reaped as samples from 24 parts in the trail field at the sampling points of canola seedling during the maturation period at 67 days after seeding (July 27th, 2019). At these same places, 72 wheat residues were also collected. Plant height was measured from the head of plant to the land as the third response in the general factorial design experiment. The root length as another response represented the length of main root grown below land. Pod numbers on each plant sample of mature canola were counted. The canola harvest took place at five months after seeding (October 23, 2019). After canola harvest, yield of canola in each part of the trail field was measured as the last response of the general factorial design experiment. The general factorial design was a universal approach used to analyze effects of different factors and their interactions on diverse responses in various fields [9]. Due to the systematic and comprehensive characteristics of this statistical analysis method, it was applied in this study to investigate the effects of chopper type and post-harvest treatment on the growth of canola. All the indicators will be used as responses in the following factorial experiments (Table 1).

Table 1 The general factorial design for field trial

Factor	Name	Level	Response	Unit
A	Copper machine type	OEM	Plant emergence	plants/sq ft
		Aftermarket	Leaf length	cm
			Plant height	cm
B	Post-harvest treatment	Tillage	Root length	cm
		Harrow	Pod numbers	pods/plant
		Check	Yield	bushels/acre

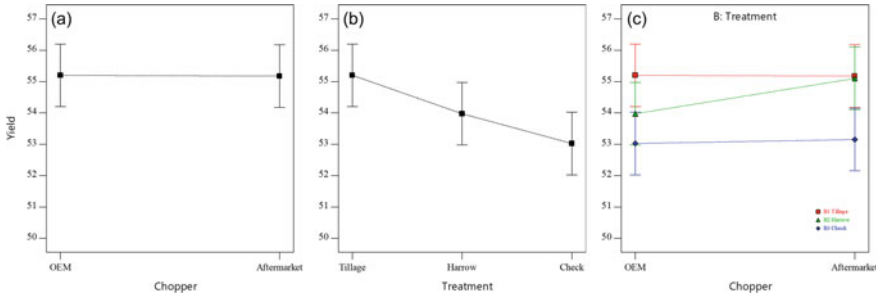

Fig. 1 Effects of different factors on the yield of canola

3 Results and Discussions

3.1 Growth States of Canola

According to ANOVA results, factor B affected significantly on the seedling emergence at the early development stage of canola at 0.95 confidence level with a P-Value of 0.02. Effects of harrow and check treatments on the growth of canola were similar while the growth of canola was the slowest under tilled treatment condition. In terms of leaf length of canola seedlings, the results showed that both factors A and B were significant at the 95% confidence level.

Height of mature canola plant above ground was chosen as a response to represent the growth state of canola plants. ANOVA results showed that the effect of factors B was significant for the height of mature canola plant at 0.95 confidence level with P-Value less than 0.001. Both factors A and B affected root length of mature canola plant significantly with P-Values less than 0.001. Interact effect of factors A and B was also significant with P-Value of 0.012. In terms of pod numbers of each plant, ANOVA results revealed that all the factors A, B and interact factor AB were significant at 0.95 confidence level. Yield of canola in each part of the experimental was measured and calculated after canola harvest. Analysis results indicated that the factor B showed significant effect on canola yield at 0.95 confidence level with P-Value of 0.017. Comparing with check treatment, both harrow and tilled post-harvest treatments resulted in higher canola yield (Fig. 1).

3.2 Correlation Among Growth Characteristics

There were six different indicators used as responses in general factorial analysis design experiments to signify the growth state of plants during the whole life cycle of canola. In order to identify the correlation among these responses, bivariate correlate analyses among these indicators were carried out in this section. According to

P-Values, plant emergence at seedling stage and height of mature plant were significantly related to the final yield of canola. Among these two indicators, seedling emergence was negatively related to yield with Pearson Correlation Coefficient of −0.517 (P-value = 0.01) while mature plant height was positively related to yield with Pearson Correlation Coefficient of 0.475 (P-value = 0.019). Since soil conditions relates to the growth of canola plants directly, the correlation of soil temperature and the other responses was analyzed. Although negative relationship between soil temperature and plant emergency with P-Value of 0.241 and Pearson Correlation Coefficient of -0.249, life length of canola seedling was positively related to soil temperature with P-Value of 0.623 and Pearson Correlation Coefficient of 0.106. Effects of soil temperature on germination percentage and leaf length of canola seedling was opposite while not significant. These results can be explained by previous studies which revealed that the temperature had little effect on canola seedling emergence percentage [10]. Soil temperature was positively related to the growth of mature canola except pod numbers on each plant. Among them, the positive correlation between soil temperature and root length of mature plant was significant with P-Value of 0.028. Root length of mature plant was longer with the increase of soil temperature.

4 Conclusions

In terms of seedling emergence of canola, the effects of harrow and check treatments on the growth of canola were similar while the growth of canola was the slowest under tilled treatment condition. The combination of harrow treatment and Aftermarket chopper were the best choice for the growth of canola seedlings at the early development stage. Soil temperature positively related to the growth of mature canola except pod numbers on each plant.

Acknowledgements The authors are thankful to Prairie Agricultural Machinery Institute (PAMI). Some research data in this paper comes from PAMI. Meanwhile, the authors would like to acknowledge Saskatchewan Canola Development Commission (SaskCanola) and Saskatchewan Wheat Development Commission (SaskWheat) for their supports. This research was supported by the following funding contributors to this project: Natural Science and Engineering Research Council of Canada (NSERC); the Canada Foundation for Innovation (CFI); the Canada Research Chairs Program (CRC).

References

1. Friesen LF, Alison GN, Rene CV (2003) Evidence of contamination of pedigreed canola (Brassica napus) seedlots in western Canada with genetically engineered herbicide resistance traits. Agron J 5(2003):1342–1347

2. Ni L, Punja ZK (2020) Effects of a foliar fertilizer containing boron on the development of Sclerotinia stem rot (Sclerotinia sclerotiorum) on canola (Brassica napus L.) leaves. J Phytopathol 168(1):47–55
3. Dizge N, Keskinler B (2008) Enzymatic production of biodiesel from canola oil using immobilized lipase. Biomass Bioenerg 32(12):1274–1278
4. Ismael A, Guevara-Oquendo VH, Refat B, Zhang H, Yu P (2019) Connection of inherent structure with nutrient profiles and bioavailability of different co-products and by-products after processing using advanced grading and vibrational molecular spectroscopy. Crit Rev Food Sci Nutr 59(17):2796–2806
5. Malhi SS, Lemke R, Wang ZH, Chhabra BS (2006) Tillage, nitrogen and crop residue effects on crop yield, nutrient uptake, soil quality, and greenhouse gas emissions. Soil Tillage Res 90(1–2):171–183
6. Bescansa P, Imaz MJ, Virto I, Enrique A, Hoogmoed WB (2006) Soil water retention as affected by tillage and residue management in semiarid Spain. Soil Tillage Res 87(1):19–27
7. Abdullah AS (2014) Minimum tillage and residue management increase soil water content, soil organic matter and canola seed yield and seed oil content in the semiarid areas of Northern Iraq. Soil Tillage Res 144:150–155
8. Mohammadi K, Heidari G, Nezhad MTK, Ghamari S, Sohrabi Y (2012) Contrasting soil microbial responses to fertilization and tillage systems in canola rhizosphere. Saudi J Biol Sci 19(3):377–383
9. Camacho LM, Fox JA, Ajedegba JO (2017) Optimization of electrodialysis metathesis (EDM) desalination using factorial design methodology. Desalination 403:136–143
10. Zheng GH, Wilen RW, Slinkard AE, Gusta LV (1994) Enhancement of canola seed germination and seedling emergence at low temperature by priming. Crop Sci 34(6):1589–1593

Enriching the Decision-Aiding Process for Asset Management Programs for Climate Change Preparedness in Small Municipalities on the Prairies

D. Lemieux and D. McMartin

1 Introduction

According to the IPCC [1], climate change impacts and responses are closely linked to the sustainable development which balances social well-being, economic prosperity, and environmental protection. Increasing financial investment into physical and social infrastructure will enhance the resilience and the adaptive capacities of societies. The investments are most effective when aligned with economic and sustainable development, and when local governments and decision makers are supported by national governments. Knowledge gaps exist where there is insufficient data to calculate specific climate resilience-enhancing investments from the current underinvested basic infrastructure [1]. How does a municipality make an informed decision on which infrastructure to address first? There are many layers of data that need to be considered when making informed decisions on the sensitivity ranking of each infrastructure within a municipality.

2 Background

A changing climate poses risks to economies, societies, environment, and infrastructure specifically when assessing climate related extremes. The extreme weather events lead to breakdown of infrastructure networks and critical services [2]. On the Prairies, there have been the strongest warming to date which is creating a shift in water resources, ecosystems and recourse and causing a change in precipitation

D. Lemieux (✉) · D. McMartin
University of Regina, Regina, Canada
e-mail: dnblemieux@gmail.com

S. Walbridge et al. (eds.), *Proceedings of the Canadian Society of Civil Engineering Annual Conference 2021*, Lecture Notes in Civil Engineering 249,
https://doi.org/10.1007/978-981-19-1061-6_30

Table 1 Municipality categories

Category	Population
Small	<5000
Medium	5000–30,000
Large	>30,000

Source Canadian Infrastructure Report Card [7]

[3]. These conditions, according to the Government of Canada, will put stress on infrastructure within municipalities but specifically, small municipalities [4].

According to Infrastructure Canada [5] much of the infrastructure has been build to a standard that did not consider a changing climate in its original design. The Canadian Infrastructure Report Card [6] determined that a concerning amount of municipal infrastructure is in poor or very poor condition which has left municipalities ill prepared for stresses to their infrastructure. Specifically, nearly 40% of roads and bridges, between 30 and 35% of recreational and cultural facilities and 30 percent of water infrastructure are in fair, poor or very poor condition.

3 Classification of Municipalities

In Canada, there are 3 main governance structures: Federal, Provincial/Territorial and Municipal. When considering the information from IPCC [1] and the understanding that climate resilience is driven by local governments, the focus on the layers of data is geared toward municipalities. According to the infrastructure report card, there are 3 different categories when considering municipalities and they are population based (Table 1):

4 Decision Considerations for Ranking Infrastructure

4.1 Infrastructure

Municipal infrastructure facilitates the movement of people and goods, provides safe drinking water, handles our solids waste and wastewater, provides spaces for sport and recreation, and helps safeguard our home from flooding and other natural disasters. Municipalities own the core infrastructure assets that are critical to the quality of life of Canadians and the competitiveness of Canada on the world stage [7].

Since early 2000s, the federal, provincial, and territorial governments have been working closely with municipalities to address their aging infrastructure [7]. In 2019, the CIRC surveyed approximately 2000 jurisdictions and received a 90% response

Table 2 Municipalities with a documented asset management plan

Category	Municipalities with a documented AMP (%)
Small	29
Medium	56
Large	70

Source Canadian Infrastructure Report Card [6]

rate to their study. From their survey, they determined that a concerning amount of municipal infrastructure in in poor or very poor condition.

According to Canadian Infrastructure Report Card [7], Canada's Infrastructure is aging and in poor condition. An Asset Management Plan (AMP) is the foundation to understand and mitigate climate risk within a community. Specifically, an AMP should lay out characteristics and condition of infrastructure assets, the expected level of service, and financing strategies to implement the planned actions. Asset management is still relatively new in Canada, but the concept is growing amongst municipalities. The following table presented from the Infrastructure Report Card [6] shows percentage of municipalities, from their 2019 survey, that have a documented AMP based on population (Table 2):

4.1.1 Climate Resilient Infrastructure

Climate resilient infrastructure is planned, designed, built, and operated in a way that anticipates and adapts to changing climate conditions. In addition, if extreme weather conditions are experienced by the infrastructure, a resilient infrastructure should rapidly withstand, respond and recover to disruptions caused by the extreme conditions. It is important to note that climate resilient infrastructure does not eliminate the disruptions, but they reduce the risk of climate related disruptions [8].

The climate resilience of individual infrastructure assets should be viewed in the context of the system as a whole. For this reason, efforts to ensure resilience at the project level should be embedded within a strategic approach to infrastructure network planning that accounts for the direct and indirect effects of climate change and climate variability [8].

Risk management requires making trade-offs between risk minimization and cost. The cost of risk minimization can become extremely expensive and increase the technical complexity in doing so. Building resilience ensures that the risks have been considered and managed to achieve an acceptable level of service to the users of the infrastructure. The costs of protection need to be weighed against the consequences of damage or disruption [8].

Table 3 Core infrastructure with reinvestment rates

Infrastructure grouping	Lower target reinvestment rate (%)	Upper target reinvestment rate (%)
Portable water (linear)	1.0	1.5
Portable water (non-linear)	1.7	2.5
Wastewater (linear)	1.0	1.3
Wastewater (non-linear)	1.7	2.5
Stormwater (linear)	1.0	1.3
Stormwater (non-linear)	1.7	2.0
Roads and sidewalks	2.0	3.0
Bridges	1.0	1.5
Buildings	1.7	2.5
Sport and recreation	1.7	2.5

Source Canadian Infrastructure Report Card [7]

4.1.2 Core Infrastructure

The Canadian Infrastructure Report Card [7] has identified core infrastructure for their project. The categories simplify the focus of infrastructure when considering the system of a municipality and they related to their report cards and outcomes. In maintaining these groupings, it allows for municipalities to compare themselves to the average Canadian municipality based on population. Associated with each infrastructure grouping are the target reinvestment rates. These rates are pivotal in understanding how much funding should be set aside for each infrastructure within a budget cycle (Table 3).

To address the aging of municipal infrastructure, the CIRC suggests increasing reinvestment rates to stop the deterioration. Reinvesting in infrastructure will save money in the long term because it will prolong the life of the asset. The CIRC identified that rates can be varied by factors such as age, level of service and risk tolerance. In this decision-aided process, reinvestment rates serve as a substitute for life cycle assessments as they generalize the ageing of infrastructure in relation to the funding required for maintenance and replacement over time.

4.2 Climate Risks of the Prairie Provinces

According to Sauchyn et al. [3], the Prairie Provinces, defined as Alberta, Saskatchewan, and Manitoba, have had the strongest warming to date across southern Canada. With climate change, the Prairie provinces are projected to be much less

cold than at present, with increased total precipitation, although mostly in winter and spring [9]. Evaporation and transpiration will also increase with warmer temperatures, leading to more frequent and intense droughts and soil moisture deficits over the southern Prairies during summer. There will be far fewer cold days, higher maximum temperatures, and heavier rainfall events, as warming amplifies the already wide variability in the prairie hydroclimate [3].

Extreme weather presents the most immediate climate risk for the Prairie provinces in Canada. The extremes in precipitation and temperature have led to 3 major risk impacts: floods, droughts, and wildfires. Extreme weather events, along with long term trends of a changing climate, create a significant impact on the economy and the challenges of creating a resilient municipality [3].

4.3 Climate Data

Climate models have been a difficult endeavor to create consistency for shared information and therefore increasing the reproducibility in data for quantitative analysis. In 2020, climatedata.ca was released and is a collaboration effort between Environment and Climate Change Canada (ECCC), Computer Research Institute of Montreal (CRIM), Ouranus, Pacific Climate Impacts Consortium (PCIC), Prairie Climate Centre (PCC), and Habitat Seven. The goal of the portal is to assist and support decision makers to incorporate climate change considerations into their decisions. By providing the most up to date reliable climate data, the data reduces the tedious task of sourcing reproducible climate data.

4.4 Political Opinion

When considering Canadian municipalities in the prairie provinces, there are several political factors that would contribute to the decision of which infrastructure should be upgraded first. It is important to understand that when it comes to municipal owned assets, very rarely are decisions around maintenance or replacement driven by expert opinion or asset management programs. Often the decisions regarding municipal assets can be politically driven.

One asset over another may be very public facing and therefore receive higher priority from public opinion. the public. It is important to not disregard the political layer when considering a rank of infrastructure because without political opinion, gaining acceptance of the rank is much more challenging to implement.

The unit of analysis that will be considered political opinion is the scheduled maintenance and a condition rating.

4.5 Subject Matter Expert

To incorporate climate considerations to the sensitivity of infrastructure, the judgement of a subject matter expert is required. The purposed to create a data layer that will be used to connect the characteristics with the climate condition assessed with a focus on public safety. The assessment will be on a linear scale from 1 to 5 with 5 being the most severe.

An example Potable Water (non-linear) versus Roads and Sidewalks when considering an increase in drought. A drought may impact a water supply for the municipality which in turn, may put a community at risk. Whereas for roads and sidewalks, a drought may impact the foundation causing surface damage. This observation would determine that a Potable Water (non-linear) facility is more sensitive to a drought than roads and sidewalks.

5 A Tool to Assist Municipalities

To address the aging of municipal infrastructure, the CIRC suggests increasing reinvestment rates to stop the deterioration. Reinvesting in infrastructure will save money in the long term because it will prolong the life of the asset. The understanding the three main risks of flooding, drought and wildfires on the Prairies, demonstrates that climate factors need to be considered when reinvesting into infrastructure to mitigated substantial damage to communities.

The size of community will determine if a rank is possible. Each scenario is applicable however, the larger the study area, the greater the complexity and the more likely that programs exist for the purpose of ranking infrastructure. In addition, the larger the municipality, the likely the governance structure includes engineers that can monitor assets on an ongoing basis. From the information presented in Sect. 3, it is imperative that to create resilient communities, small municipalities require a low-cost tool to help them make more informed decisions.

The data layers presented in Sect. 4 demonstrate that the decision on which core infrastructure enhance for climate resiliency is a multicriteria problem that requires a sophisticated analysis tool. Not all criteria are linear in nature and demonstrate a high level of complexity and therefore a tradition weighted sum method is not sophisticated enough to address and respect the intricacy of the criteria (Fig. 1).

Finally, it is important that this method be readily available to the small municipalities in a user-friendly format. An application should be developed to rank infrastructure and assist with making financial decisions for municipalities.

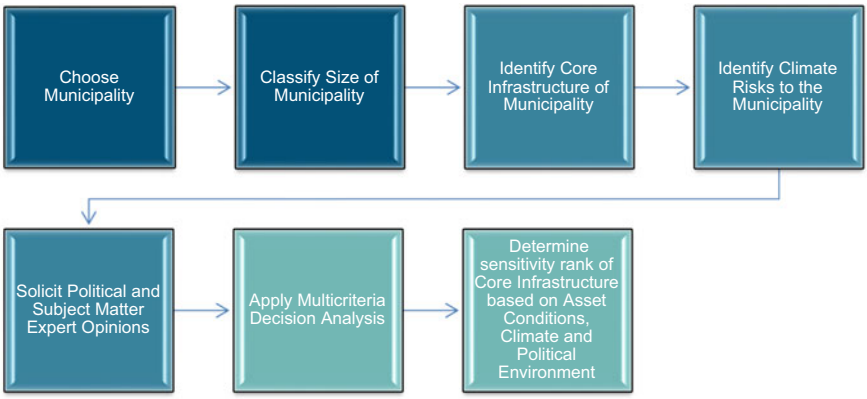

Fig. 1 General decision-aiding framework to determine sensitivity rank of core infrastructure

Acknowledgements Funding to support this project was received from the NSERC Discovery Grants (DWM 2020–04014) program.

References

1. IPCC (2012) Summary for policy makers managing the risks of extreme events and disasters to advance climate change adaptation [Field CB, Barros TF, Stocker TF, Qin D, Dokken DJ, Ebi MD, Mastrandrea MD, Mach KJ, Plattner G-K, Allen S, A special report of working groups I and II of the intergovernmental panel on climate change., 1-19. Cambridge University Press, New York, N.Y., USA and Cambridge, UK
2. IPCC (2014) Summary for policymakers. In: Climate change 2014: impacts, adaptation and vulnerability. Part a: Global and sectoral aspects. Contribution of working group II to the fifth assessment report of intergovernmental panel on climate change. Cambridge University Press, Cambridge, UK and New York, USA
3. Sauchyn D et al (2020) Prairie provinces; Chapter 4 in a changing climate: regional perspectives. Government of Canada, Ottawa, Ontario. Retrieved from https://changingclimate.ca/regional-perspectives/chapter/4-0/
4. Government of Canada (2019) Climate-resilient buildings and core public infrastructure initiative. Retrieved 2 Mar 2021, from Infrastructure Canada: https://www.infrastructure.gc.ca/plan/crbcpi-irccipb-eng.html
5. Infrastructure Canada (2006) Adapting infrastructure to climate change in Canada's cities and communities—A literature review. Res Anal Div
6. Canadian Infrastructure Report Card (2019) Monitoring the state of Canada's core public infrastructure. Retrieved from http://canadianinfrastructure.ca/downloads/canadian-infrastructure-report-card-2019.pdf
7. Canadian Infrastructure Report Card (2016) Informing the future: the Canadian infrastructure report card. Retrieved from http://canadianinfrastructure.ca/downloads/Canadian_Infrastructure_Report_2016.pdf

8. OECD (2018) Climate-resilient infrastructure. Retrieved 2 Mar 2021, from oecd.org: http://www.oecd.org/environment/cc/policy-perspectives-climate-resilient-infrastructure.pdf
9. Zhang X et al. (2019) Changes in temperature and precipitation across Canada. In: Bush E, Lemmen DS (eds) Chapter 4 in Canada's changing climate report. Government of Canada, Ottawa, Ontario. Retrieved 2 Mar 2021, from https://changingclimate.ca/CCCR2019/chapter/4-0/

Rapid and Cross-Source Detection of Naphthenic Acids and Phenol Using 3d Fluorescence Spectroscopy

Ziyu Li and Nicolas M. Pelesato

1 Introduction

Oil sands process-affected waters (OSPW) are produced in surface mining to recover bitumen from a mixture of sand, water, and clay [1]. With the growing volume of OSPW stored in tailing ponds, increasing attention is being paid to the potential migration of toxic substances and contamination in surface water and groundwater. Grewer et al. [2] indicated that the exposure of OSPW might lead to multiple physiological problems to a variety of organisms, such as compromised immunological function and impaired reproduction [3, 4]. Despite the variety in the composition of OSPW, the primary source of the toxic components is believed to be acid extractable organics, known as naphthenic acids (NAs) [5]. NAs are a mixture of organic compounds described by the general formula $C_nH_{2n+z}O_2$, where n represents the number of carbon atom and z represents the number of hydrogen deficiency (classical NAs), or $C_nH_{2n+Z}O_x$, where $x = 2$ to 5 (oxidized NAs) [2, 6]. Other contaminants such as phenols would also contribute to the toxicity of OSPW. The ambient levels of NAs and phenol in natural waters in the oil sand regions are typically less than 1 mg/L and 1.6 μg/L in the surface waters [7]. However, as reported, the concentration of NAs and phenol ranged widely from 12 to 43 mg/L and 8–83 μg/L in OSPW, which highly exceeds the Canadian Council of Ministers of the Environmental (CCME) guidelines (1 mg/L and 4 μg/L for NAs and phenol, respectively) [7]. Recent research has provided evidence of migration of OWSP and enter into surface water and groundwater nearby [8].

Currently, standard methods to quantify NAs and phenol include high-performance liquid chromatography (HPLC), gas chromatography coupled to mass

Z. Li · N. M. Pelesato (✉)
School of Engineering, University of British Columbia Okanagan, 1137 Alumni Ave., Kelowna, BC V1V 1V7, Canada
e-mail: npeleato@mail.ubc.ca

S. Walbridge et al. (eds.), *Proceedings of the Canadian Society of Civil Engineering Annual Conference 2021*, Lecture Notes in Civil Engineering 249,
https://doi.org/10.1007/978-981-19-1061-6_31

spectrometry, and Fourier transform infrared (FTIR) spectroscopy [9–11]. Although those methods are precise and selective to measure the contaminants, they are costly, and the steps for acquisition and sample preparation are time-consuming. It is imperative to regularly monitor those contaminants releasing into in the surface waters in the oil sand regions to protect public and aquatic ecosystem health.

Fluorescence spectroscopy is a fast and promising optical method that can characterize and quantify organic compounds and contaminants in the water. High dimensional fluorescence excitation-emission matrices (EEMs) measured at iterated excitation, and emission wavelengths could reflect the chemical composition of the organic matters in water [12, 13]. Previously, NAs have been successfully detected in pure water, OSPW, or other controlled background matrices [10, 11]. However, little is known about the actual detection of NAs and phenol in natural surface waters. It is challenging to interpret NA and phenol's fluorescence signals in the presence of natural organic matters (NOM), which fluoresces strongly in similar spectral regions. The composition and concentration of background NOM is varied and dependent on local environmental conditions [14]. As such, interference from complex and dynamic NOM fluorophores presents a significant challenge for building robust fluorescence-based NAs and phenol detection models. The standard way to deal with this issue is to develop site-specific corrections between contaminants and their concentrations, often relying on assumptions that fluorescence intensities will change linearly with concentration [15]. However, the need for site-specific calibration implies a significant burden on sampling and analysis [16].

This study investigates the use of fluorescence spectroscopy as a contaminant detection tool to monitor NAs and phenol in different water sources. Several dimensionality reduction methods were used to obtain underlying fluorescence components from high-dimensional EEMs. The most basic and widely applied method is the peak-picking approach, based on the intensity of fluorophores at pre-determined peak positions [17]. Principal component analysis (PCA) was also applied to interpret high-dimensional fluorescence data and extract relevant features. Fluorescence analysis for NAs and phenol was firstly applied to develop site-specific models of contaminants in two water sources (Lake Okanagan and Mission Creek). The ability to transfer model knowledge from one source to another was then examined.

2 Methods

2.1 Samples and Mixing Experiments

Natural water samples used in this study were collected from Lake Okanagan (Kelowna, Canada) and Mission Creek (Kelowna, Canada) over three months from October to December 2020. The study objective was to explore the applicability and sensitivity of the fluorescence technique for detecting target contaminants with the interference from NOM in surface waters. As such, two water sources were used

to explore the impact of varying NOM characteristics on detection methods. NOM variability over seasons could impact results, and a longer-term sampling program is planned for future work. High-density polyethylene containers were used for sampling and were triple rinsed using the respective natural water before sampling. All the natural samples were stored in the dark at 4 °C for a maximum of 20 days.

NAs and phenol were spiked in the range from 0 – 50 mg/L and 0 – 100 μg/L into natural water samples in the mixing experiments. The concentration range was chosen based on the studies from Holowenko et al. [18], and Belosevic et al. [7] to explore using fluorescence techniques to detect target contaminants. NAs stock solution of 10,000 mg/L and phenol stock solution of 10 mg/L were prepared by dissolving pure NAs and phenol purchased from Sigma-Aldrich (≥98%) in methanol (HPLC grade, Sigma-Aldrich) and Milli-Q® pure water, respectively.

2.2 Fluorescence

Fluorescence spectra were collected using an Aqualog spectrometer (Aqualog, HORIBA, Japan). The EEMs were collected with excitation and emission wavelengths that ranged from 240 to 600 nm in steps of 2 nm and 250–800 nm in steps of 2 nm. The blank of pure Milli-Q® water was subtracted from each sample to eliminate the fluorescence impacts from the background solvent. Inner-filter corrections were automatically applied using Aqualog® package software. Fluorescence EEMs were then normalized and converted into Raman Units (R.U.) using the integrated area under Raman peak (ex = 350) measured from the blank Milli-Q® pure water [19].

2.3 Dimensionality Reduction

2.3.1 Peak-Picking

The Peak-picking approach is considered the easiest and the most basic method to identify fluorescence components from high-dimensional fluorescence EEMs. Due to differences in molecular structures, each organic fluorophore has a unique absorbance and emission response [17]. Fluorescence intensity and corresponding concentration level are considered to have a linear relationship with each other, which could be used as a basis to distinguish them [14]. However, the challenges of the peak-picking approach in monitoring are the overlapping signals with background NOM and possible peak shifts, which may cause deviation from linearity [14, 20]. The wavelength pairs (ex/em) of NAs and phenol were determined relying on the peak of fluorophores in previous reports (Table 1). The peak-picking analysis was carried out using in-house developed Python scripts.

Table 1 Excitation/Emission (ex/em) wavelengths of NAs and phenol selected by the peak-picking method

Contaminant	Excitation wavelength (nm)	Excitation wavelength (nm)	References
Naphthenic acids	270	330	Mohamed et al. [11]
Phenol	272	298	Wang et al. [21]

2.3.2 Principal Component Analysis (PCA)

PCA is a multivariate analysis method that is widely used to interpret fluorescence EEMs to lower dimensions and reduce the number of variables. Several independent variables decomposed from fluorescence EEMs, referred to as principal components (PCs), can substitute the original dataset and account for a large proportion of the total variance [13]. The results of the decomposition of the data matrix X from PCA are shown in Eq. (1), usually given as outer products of score vectors t_i, loading vectors p_i and a noise residual matrix E [22]. Loading vectors indicate the relative importance of excitation-emission wavelength combinations for specific principal components. Scores are analogous to concentrations of the relative importance of each principal component to a specific sample. Scikit-learn, an open-source package for machine learning in python, was used for PCA analysis [23].

$$X = \sum_{i=1}^{k} t_i p_i + E \tag{1}$$

2.4 Cross-Source Model Transfer

While fluorescence spectra can represent a detailed fingerprint of contaminants in water, a remaining challenge is that the resulting models are site-specific and require frequent calibration to address the spatial and temporal variability in water composition. This study investigated a cross-source model transfer method to transfer a detection model from one water source to another. PCA was applied to the fluorescence EEMs of the target water to extract features in an unsupervised manner. The fluorescence EEMs of the source water were then interpreted using the target water's features. Therefore, both source water and target water would have similar latent variables after dimensionality reduction. The transfer approach is based on the hypothesis that fluorescence spectral characteristics of any given compound should be similar, but not identical, between water sources. Peak shifts and shape distortions possible due to environmental variations. Therefore, after applying features from another surface water, the whole data structure should not be changed radically and contribute to unified features between two surface waters (Fig. 1).

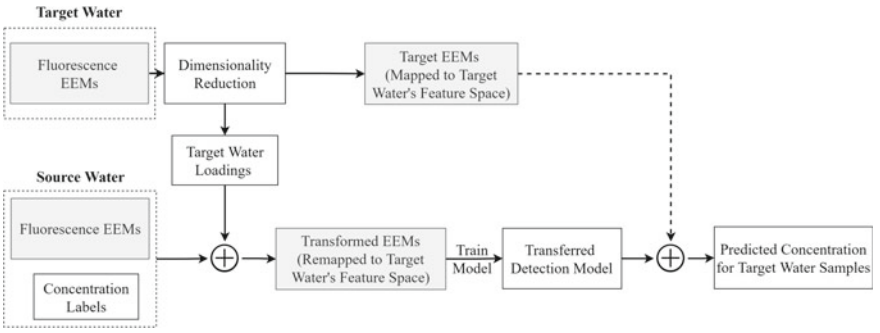

Fig. 1 Roadmap for model setup using fluorescence EEMs to predict the concentration of NAs and phenol in the target water samples

2.5 Regression Analysis

Linear regression analysis was employed using either intensity of NAs and phenol from pick-peaking or the output scores of principal components (PCs) from PCA analysis. The performance of linear regression models was evaluated using Mean Absolute Error (MAE) and Coefficient of Determination (R^2) according to the accuracy to predict the concentration of NAs and phenol spiked into samples. The equation of calculations of MAE and R^2 are listed in Eqs. (2) and (3). MAE calculates the error between the predicted concentration $\widehat{y_i}$ and the true concentration value y_i, while R^2 represents how well the regression model fits the observed concentration value.

$$\mathrm{MAE} = \frac{1}{N}\sum_{i=1}^{N}\left|y_i - \hat{y}_i\right| \tag{2}$$

$$R^2 = 1 - \frac{\sum_{i=1}^{N}\left(y_i - \hat{y}_i\right)}{\sum_{i=1}^{n}\left(\hat{y}_i - \overline{y}_i\right)} \tag{3}$$

3 Results and Discussion

3.1 PCA Components

PCA was applied to the fluorescence EEMs as a dimensionality reduction method to identify the underlying components. The 4 component PCA model had cumulative explained variance >99.70% while the first component explained 99.00% of the variance in the dataset. Loading plots of the 4 component PCA model derived from the creek water showed in Fig. 2. Most PC components showed spectra characteristics

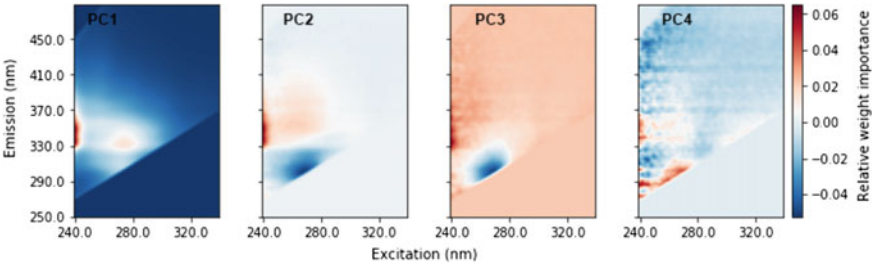

Fig. 2 Loading plots of the 4 component PCA model (PC1-4). PCs 1 to 4 represented >99.70% of the variance in the dataset

at excitation/emission regions of 240/350 nm, which matched the characteristics of protein-like compounds ubiquitous in the lakes and rivers [24, 25]. PC 1 also identified signals around 270/330 nm (ex/em) that conform well to characteristics of NAs. the low emission regions emphasized by PC4 may represent fluorophores of phenol around 272/298 nm. However, each PCA component is unlikely to be a one-to-one representation of individual fluorophores in the water, and therefore, most of them are challenging to interpret. Those decomposed components are the reconstructions of the original data to substitute original interrelated variables in fluorescence EEMs. The latent variables are expressed by the loading values showing the relative importance of spectral regions. Coefficients, or PCA scores, are analogous to individual PC importance or scores for any given sample. Scores were used in subsequent regression models.

3.2 Prediction of NAs and Phenol in Surface Waters

The bench-scale mixing experiments with NAs and phenol were performed to examine fluorescence spectroscopy as a surrogate for measuring contaminant concentrations in surface water. This hypothesis stems from an underlying assumption that excitation-emission maxima of fluorophores, which depended on compounds' molecular structure, weight, and functional groups, are linearly related to the concentration [26], Murphy et al. [13]. A total of 332 mixing samples were collected (112 mixing lake samples and 120 mixing creek samples) and then split into two parts: the training sets and the testing sets for each water source. A fivefold cross-validation approach was applied to the dataset to assess the model prediction performance accurately. This approach iteratively splits the original dataset into randomized training and test subsets but utilizes all available data. fivefold was chosen to maintain a common split of 80/20 for training/testing. The validation sets were not included in the dimensionality reduction and model building, making the model capable of testing its ability to predict new data that was not included in modelling.

Table 2 Mean absolute error (MAE) for peak-picking and PCA dimensionality reduction analysis to predict naphthenic acids (NAs) and phenol in site-specific waters and in transfer water sources

Dimensionality reduction	Site-specific (Creek)	Transfer from lake to creek		Site-specific (Lake)	Transfer from creek to lake	
		With transfer	No transfer		With transfer	No transfer
Naphthenic acids (mg/L)						
Peak-picking	2.83	–	5.70	2.74	–	4.86
PCA	1.82	2.90	7.60	1.46	2.28	7.69
Phenol (μg/L)						
Peak-picking	30.23	–	32.23	27.91	–	30.48
PCA	12.97	13.84	28.27	12.15	15.50	45.57

The predictability of both the peak-picking approach and PCA approach were compared to determine if the algorithm-based dimensionality reduction approach had better performance than using fluorescence intensity at fixed wavelengths. Linear regression models were trained to develop site-specific correction on each water source using the outputs from peak-picking and PCA analysis: (1) peak-picking fluorescence intensity, (2) PCA component scores. Mean absolute error (MAE) was used to measure the performance of the site-specific regression models (Table 2). It should be noted that MAE from naphthenic acids was given on a different scale (mg/L) than MAE from phenol (μg/L) according to the different concentration ranges spiked in samples. The concentration of NAs was randomized over a range of 0.1–50 mg/L, whereas the concentration of phenol was from 0.1 to 100 μg/L.

The accuracy of peak-picking based site-specific models were consistently lower compared to PCA-based site-specific detection models on both lake and creek water sources, especially for the prediction of phenol concentrations. The interaction with other fluorophores largely influences site-specific detection models constructed with only excitation-emission maxima. In this study, the fluorescence intensity of phenol was found to be weak, and fluorophores of phenol were easily hindered with the inclusion of NAs in the water. As such, the concentration of phenol might be overestimated with peak-picking method due to the overlapping peaks (Lake: 27.91 μg/L, Creek: 30.24 μg/L). The interference caused the relationship between fluorescence intensity and concentration of phenol to deviate from linearity. In contrast, the increased prediction accuracy of phenol was found after applying PCA dimensionality reduction in the collected dataset from the creek and the lake (Lake: 12.15 μg/L, Creek: 12.97 μg/L). PCA could reduce the high dimensionality of fluorescence EEMs and help to separate the overlapping signals in the complex mixtures to make fluorophores easier to interpret.

For the detection of NAs using site-specific models, both peak-picking and PCA approaches could produce sensitive regression models capable of predicting contaminant concentration with MAE < 2.83 mg/L. This is because of the strong fluorescence

fluorophores of NAs which may limit the impacts from overlapping signals of phenol and background NOM.

3.3 Contaminant Detection in Cross-Source Water

In this study, model transfer methods were also investigated to reduce the burden on collecting data for developing site-specific models. A remapping type of approach was taken to unify the features of two surface waters using feature loadings derived from target water fluorescence EEMs. We hypothesized that background NOM variability and peak shifts between sources would be minimized after unifying the features. Therefore, linear regressors trained on the remapped source fluorescence EEMs could also provide sensitive identification and quantification of contaminants on the target water.

We examined two situations: one is to develop the detection model in Lake Okanagan and transfer it to the creek, while another way is to transfer the detection model from the creek to the lake. MAE was applied to compare the transfer models' predictability to the site-specific baseline models and no transfer situation (Table 2). The 'no transfer method' represents directly applying the site-specific models trained in the source dataset and predicting contaminant concentrations in the target water samples. Peak-picking models were trained on the intensities at fixed and constant wavelengths for both sources, and therefore the concept of model transfer is not applicable.

After directly using a site-specific detection model to a new surface water, no transfer method resulted in the poorest performance to predict the concentration of NAs and phenol (NAs: 4.86–7.69 mg/L, phenol: 28.27–45.57 μg/L), which is also reflected in Fig. 3. Based on the variation in background water composition, especially natural organic matter (NOM), those models could not capture the relationship between the contaminants and background signals in another water site. This also explained the consistently better model performance of the site-specific models and the advantages of in-situ modeling or site-specific calibration to obtain site-specific relationships between variables effectively.

However, the performance of cross-source transferred models using PCA was competitive compared to site-specific models and showed significant improvements compared with no transfer models. It implied the substantial capability of PCA-based model transfer to discover universal cross-source underlying components. Predictive performance visualized in Fig. 3 further confirmed that after remapping and unifying the features, the transferred model more accurately quantified contaminants in the target water. Considering the significant burden for data collection to generate site-specific models, a cross-source model transfer approach may be a viable approach to the widespread implementation of fluorescence detection methods.

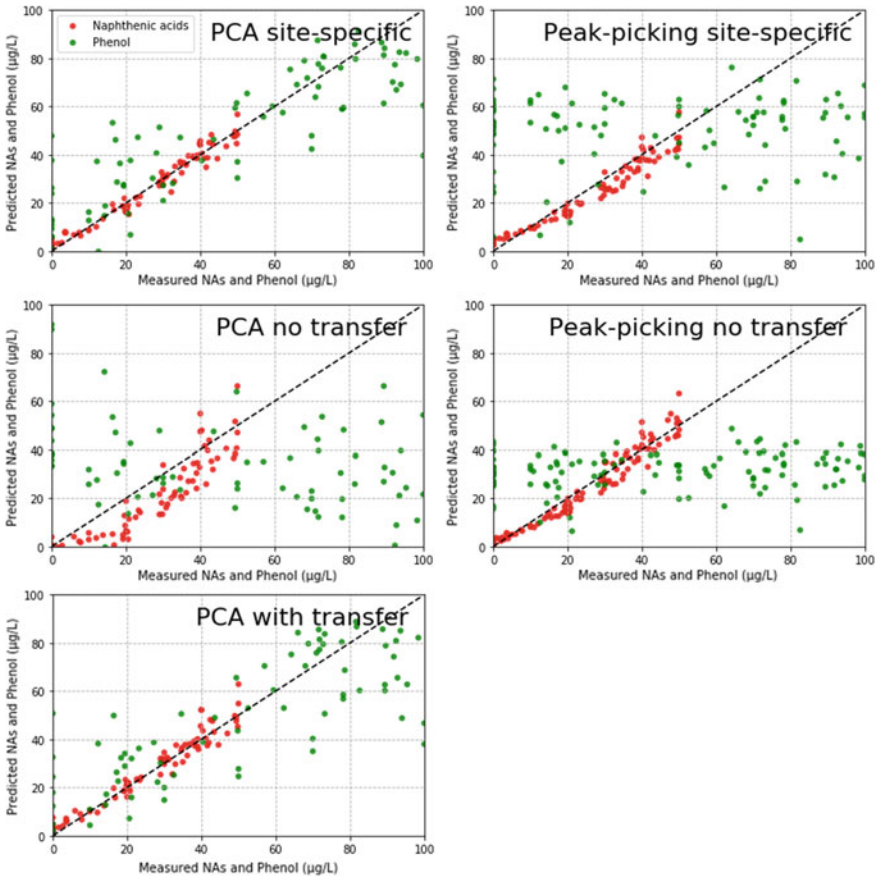

Fig. 3 Measured vs predicted PAHs and pesticides for test samples (the creek source) using peak-picking and PCA approaches

4 Conclusions

The application of fluorescence technique to quantify known NAs and phenol in surface waters was investigated in this study. Results showed that the PCA-based fluorescence model could provide sensitive detection with MAE < 1.82 mg/L and 12.97 µg/L for predicting concentrations of NAs and phenol, respectively. Compared to only using peak intensities, PCA analysis could better interpret fluorescence EEMs to deal with overlapping and interacting signals. Furthermore, an approach to transfer fluorescence-based contaminant detection models between water sources was also studied. Based on an already established model (from a source water), only a few additional unlabeled fluorescence EEMs from a new target water were required to unify features. The transferred models have comparable predictability to predict NAs and phenol in water samples and would reduce the burden for data collection.

The potential application to transfer the existing fluorescence model to other surface waters could aid in the broader implementation of fluorescence-based contamination detection models.

References

1. Li C, Fu L, Stafford J, Belosevic M, Gamal El-Din M (2017) The toxicity of oil sands process-affected water (OSPW): a critical review. Sci Total Environ 601–602:1785–1802. https://doi.org/10.1016/j.scitotenv.2017.06.024
2. Grewer DM, Young RF, Whittal RM, Fedorak PM (2010) Naphthenic acids and other acid-extractables in water samples from Alberta: what is being measured? Sci Total Environ 408(23):5997–6010. https://doi.org/10.1016/j.scitotenv.2010.08.013
3. Kavanagh RJ, Frank RA, Kent Burnison B, Young RF, Fedorak PM, Solomon KR, Van Der Kraak G (2012) Fathead minnow (Pimephales promelas) reproduction is impaired when exposed to a naphthenic acid extract. Aquat Toxicol 116:34–42
4. Rogers VV, Wickstrom M, Liber K, MacKinnon MD (2002) Acute and subchronic mammalian toxicity of naphthenic acids from oil sands tailings. Toxicol Sci 66(2):347–355
5. Mahaffey A, Dubé M (2017) Review of the composition and toxicity of oil sands process-affected water. Environ Rev 25(1):97–114. https://doi.org/10.1139/er-2015-0060
6. Samanipour S, Reid MJ, Rundberget JT, Frost TK, Thomas KV (2020) Concentration and distribution of naphthenic acids in the produced water from offshore Norwegian North Sea oilfields. Environ Sci Technol 54(5):2707–2714. https://doi.org/10.1021/acs.est.9b05784
7. Belosevic M, Singh A, Gamal El-Din M, Li C, McPhedran K, Chelme-Ayala P, Klamerth N (2014) Synthesis of toxicological behavior of oil sands process-affected water constituents. In: OSRIN technical reports
8. Frank RA, Roy JW, Bickerton G, Rowland SJ, Headley JV, Scarlett AG, West CE, Peru KM, Parrott JL, Conly FM (2014) Profiling oil sands mixtures from industrial developments and natural groundwaters for source identification. Environ Sci Technol 48(5):2660–2670
9. Hsu CS, Dechert GJ, Robbins WK, Fukuda EK (2000) Naphthenic acids in crude oils characterized by mass spectrometry. Energy Fuels 14(1):217–223
10. Lu W, Ewanchuk A, Perez-Estrada L, Sego D, Ulrich A (2013) Limitation of fluorescence spectrophotometry in the measurement of naphthenic acids in oil sands process water. J Environ Sci Health A Tox Hazard Subst Environ Eng 48(4):429–436. https://doi.org/10.1080/10934529.2013.729802
11. Mohamed MH, Wilson LD, Headley JV, Peru KM (2008) Screening of oil sands naphthenic acids by UV-Vis absorption and fluorescence emission spectrophotometry. J Environ Sci Health A Tox Hazard Subst Environ Eng 43(14):1700–1705. https://doi.org/10.1080/10934520802330255
12. Bridgeman J, Bieroza M, Baker A (2011) The application of fluorescence spectroscopy to organic matter characterisation in drinking water treatment. Rev Environ Sci Bio/technol 10(3):277–290. https://doi.org/10.1007/s11157-011-9243-x
13. Murphy KR, Bro R, Stedmon CA (2014) Chemometric analysis of organic matter fluorescence.In: Baker A, Reynolds DM, Lead J, Coble PG, Spencer RGM (eds) Aquatic organic matter fluorescence. Cambridge University Press, Cambridge, pp 339–375
14. Korak JA, Dotson AD, Summers RS, Rosario-Ortiz FL (2014) Critical analysis of commonly used fluorescence metrics to characterize dissolved organic matter. Water Res 49:327–338. https://doi.org/10.1016/j.watres.2013.11.025
15. Carstea EM, Baker A, Bieroza M, Reynolds D (2010) Continuous fluorescence excitation-emission matrix monitoring of river organic matter. Water Res 44(18):5356–5366. https://doi.org/10.1016/j.watres.2010.06.036

16. Li Z, Peleato NM (2021) Comparison of dimensionality reduction techniques for cross-source transfer of fluorescence contaminant detection models. Chemosphere 130064
17. Li L, Wang Y, Zhang W, Yu S, Wang X, Gao N (2020) New advances in fluorescence excitation-emission matrix spectroscopy for the characterization of dissolved organic matter in drinking water treatment: a review. Chem Eng J 381:122676
18. Holowenko FM, MacKinnon MD, Fedorak PM (2002) Characterization of naphthenic acids in oil sands wastewaters by gas chromatography-mass spectrometry. Water Res 36(11):2843–2855. https://doi.org/10.1016/S0043-1354(01)00492-4
19. Lawaetz AJ, Stedmon CA (2009) Fluorescence intensity calibration using the Raman scatter peak of water. Appl Spectrosc 63:936-940. https://doi.org/10.1366/000370209788964548
20. Yu H, Liang H, Qu F, Han ZS, Shao S, Chang H, Li G (2015) Impact of dataset diversity on accuracy and sensitivity of parallel factor analysis model of dissolved organic matter fluorescence excitation-emission matrix. Sci Rep 5:10207. https://doi.org/10.1038/srep10207
21. Wang H-B, Zhang Y-J, Xiao X, Jin D, Zhao N-J, Yin G-F, Guo L-Q, Liu W-Q (2010) Excitation-emission fluorescence characterization study of the three phenolic compounds. Spectrosc Spectral Anal 30(5):1271–1274
22. Geladi P, Isaksson H, Lindqvist L, Wold S, Esbensen K (1989) Principal component analysis of multivariate images. Chemom Intell Lab Syst 5(3):209–220. https://doi.org/10.1016/0169-7439(89)80049-8
23. Pedregosa F, Varoquaux G, Gramfort A, Michel V, Thirion B, Grisel O, Blondel M, Prettenhofer P, Weiss R, Dubourg V (2011) Scikit-learn: Machine learning in Python. J Mach Learn Res 12:2825–2830
24. Osburn CL, Oviedo-Vargas D, Barnett E, Dierick D, Oberbauer SF, Genereux DP (2018) Regional groundwater and storms are hydrologic controls on the quality and export of dissolved organic matter in two tropical rainforest streams, costa rica. J Geophys Res Biogeosci 123(3):850–866. https://doi.org/10.1002/2017jg003960
25. Shutova Y, Baker A, Bridgeman J, Henderson RK (2014) Spectroscopic characterisation of dissolved organic matter changes in drinking water treatment: From PARAFAC analysis to online monitoring wavelengths. Water Res 54:159–169. https://doi.org/10.1016/j.watres.2014.01.053
26. Peleato NM, Legge RL, Andrews RC (2018) Neural networks for dimensionality reduction of fluorescence spectra and prediction of drinking water disinfection by-products. Water Res 136:84–94. https://doi.org/10.1016/j.watres.2018.02.052

Dynamic Multi-year Performance of Bioretention Mesocosms—Patterns of Change

A. Skorobogatov, X. Li, R. Nasrollahpour, J. He, A. Chu, C. Valeo, and B. van Duin

1 Introduction

There has been an increasing demand for sustainable "green" solutions to address the shortcomings of conventional "grey" infrastructure. Low Impact Development (LID) offers an array of such solutions for a more natural approach to managing the urban hydrologic condition, given that urbanization leads to increases in runoff quantity and peak flows, and impairment of water quality [1]. Bioretention systems are among the more popular LID tools offering diverse benefits, such as reduction of peak runoff, attenuation of excess runoff volume, retention of various pollutants, and aesthetic and habitat benefits [2]. The initial focus of many bioretention studies has been on demonstrating how these systems fit into the framework of conventional infrastructure, but the attention has shifted since to characterizing the underlying processes and analyzing the unique benefits. In recent years studies emerged questioning the roles of media, vegetation, biological processes, interactions, and long-term processes in bioretention performance [3].

Very few studies to date had the opportunity to investigate the change in the performance of bioretention systems as they mature and evolve. Many assume that the performance can be predicted based on the initial design parameters, which is potentially limiting as the evolving impacts of the living components would not

A. Skorobogatov (✉) · X. Li · R. Nasrollahpour · J. He · A. Chu
Civil Engineering, Schulich School of Engineering, University of Calgary, 2500 University Drive NW, Calgary, AB T2N 1N4, Canada
e-mail: askorobo@ucalgary.ca

C. Valeo
Mechanical Engineering, University of Victoria, 3800 Finnerty Road, Victoria, BC V8P 5C2, Canada

B. van Duin
Water Resources, City of Calgary, 625-25 Ave S.E., Calgary, AB T2G 4K8, Canada

S. Walbridge et al. (eds.), *Proceedings of the Canadian Society of Civil Engineering Annual Conference 2021*, Lecture Notes in Civil Engineering 249,
https://doi.org/10.1007/978-981-19-1061-6_32

be adequately represented. The temporal evolution of bioretention performance is also one of the key research areas that needs more data to support practical understanding and future decision-making [4]. Moreover, it is notoriously challenging to make inferences about interactions when different factors are studied in isolation. Therefore, this study was set up to offer unique insights on interactions by utilizing a factorial experimental design. The research presented here spans four years of monitoring data with multiple factors acting simultaneously and interacting with one another. This project analyzed the effects of media, vegetation, and IP (Impervious to Pervious) ratio on bioretention performance while also investigating the changes in performance as the bioretention mesocosms matured. The IP ratio represents the hydrologic loading as it reflects the size of contributing catchment to the bioretention bed area [5]. Hydrological performance was assessed as volumetric retention (in %) and infiltration, whereas water quality performance was assessed from the perspective of effluent pollutant concentrations. The pollutants included nutrients (phosphorus and nitrogen species) as well as organics.

2 Materials and Methods

A bioretention research site was constructed for this project in the Town of Okotoks, Alberta, Canada in Fall 2016/Spring 2017 (Fig. 1). The research site consists of 24 fully lined bioretention mesocosms designed to receive no natural runoff and to be drained by pumping. Each cell is 1.8 × 1.8 × 1.2 m (LxWxH) in size. The depths of media (60 cm) and drainage layer (30 cm) are the same in all mesocosms. They were constructed with three different bioretention media. Two of those, referred to as CoC 70 and CoC 40, are based on local LID guidelines [5]. The third one is a mix of clay loam and wood chips (CL for clay loam). The mesocosms were planted with three vegetation types including herbaceous, woody, and turfgrass (as control). In addition, the cells were exposed to two hydrologic loadings, IP of 15 and 30.

Over the study period, each mesocosm was subject to 72 simulated events (3, 25, 24, and 20 in 2017, 2018, 2019, and 2020, respectively). The seasonal hydrologic loading, event magnitude, and inter-event period were taken into consideration in the design of the simulated events, which was determined by analyzing historical

Fig. 1 Okotoks bioretention research site after construction and planting

precipitation for the area. A typical application regime was designed and largely adhered to, but there were some variations due to logistic constraints.

The water used in simulated events was sourced from a local stormwater pond on the day of simulation. Sediments were added to the water to better represent the total suspended solids concentration of typical runoff (400 mg/L). Water was applied into each mesocosm using garden hoses at 2 L/s flow rate. Each cell had a perforated standpipe extending from the liner to above the freeboard elevation. Free drainage was simulated by pumping the effluent into a volumetric tank. Once pumped, the volume of exfiltrate was recorded and a composite sample was taken for water quality analysis.

The dataset in question is rather complex, as it involves factorial setup, true replication, multiple independent and dependent variables, and repeated measurements over time. Within each simulated event, factorial analysis of variance (ANOVA) was used to analyze the effect significance, its size, and pairwise comparisons of the design parameters, i.e. media, vegetation, and IP ratio on hydrological and water quality performance. Comparative summaries of significance of the design parameters and their interactions were created based on within-event analysis. All statistical analyses were performed using IBM SPSS Statistics Version 25 at the significance level of 5%.

3 Results and Discussion

3.1 Hydrological Performance

Volumetric retention varied across the different cell types within each simulated event and across the years. As shown in Table 1, media type had a pronounced impact at the early stages of the study period, but its significance decreased dramatically over the years. The CL media cells retained significantly less volume than the traditional media in the first few seasons, yet the differences lessened with each year of simulation. On the other hand, the impacts of vegetation and IP ratio were consistently significant (Table 1). Control vegetation was the least effective at retention, whereas woody vegetation became progressively more effective. Higher IP ratio resulted in

Table 1 The percentage of individual events within each season where a respective design parameter had a significant effect on volumetric retention based on ANOVA analysis

Parameter	2017	2018 (%)	2019 (%)	2020 (%)
Media	100%	48	21	20
Vegetation	67%	36	67	50
IP	n/a	60	75	50
Interactions	0%	32	29	20

lower retention. For the long-term, it appears that media selection might not be particularly relevant to the systems that are lined or installed in poorly permeable native soils. The reality might be that the natural processes (macropore formation, biofilm accumulation, root growth and decay, etc.) dictated the evolution of available storage and evapotranspiration controlled how much of the storage capacity was replenished, even though media porosity and intrinsic retention capacity were dissimilar at the onset of bioretention lifetime.

Another hydrologic factor that impacts the longevity of bioretention systems and media selection is infiltration. Within individual events, media type significantly affected infiltration across the years. The effect of vegetation was not as pronounced, and appeared to decrease in significance in 2020, complicating the inter-year comparison. The role of IP ratio, which also reflects the sediment loading, appeared to be significant and increasing in significance across the years. The infiltration rates were consistently lower for IP30 cells than they were for IP15, which is consistent with the notion of accelerated clogging under a higher loading.

3.2 Water Quality Performance

The water quality data also showed substantial inter-event variability, and indicated that there were significant impacts of media, vegetation, and IP ratio within the events and across the years. A key finding was that the mesocosms were leaching nutrients rather than providing retention. As such, the data presented here are of effluent concentrations. The parameters that were analyzed are reactive phosphate, total phosphorus, nitrate, total nitrogen, and total organic carbon. The overall leaching patterns were similar for the two phosphorus species, as well as for the two nitrogen species and the organics.

The results highlighted herein are of reactive phosphate, as it is thought to be a leading cause of eutrophication in freshwater aquatic systems. Media and vegetation had a significant and consistent impact on reactive phosphate and total phosphorus effluent concentrations for most events (Table 2). The CL media cells released significantly less phosphorus compared to the other two. However, they also had the highest

Table 2 The percentage of individual events within each season where a respective design parameter had a significant effect on reactive phosphate (in concentration) of effluent based on ANOVA analysis

Parameter	2017	2018 (%)	2019	2020
Media	100%	100	95	100
Vegetation	0%	81	86	100
IP	n/a	38	23	0
Interactions	0%	56	64	85

infiltration rates, which could mean that little interaction between media and percolating runoff took place. The significance of vegetation effects appeared to have increased over the years. As for vegetation type, control cells released the most phosphorus, whereas woody cells released the least, especially at the later stages of the study period. The impact of vegetation on phosphorus release has been debated in the literature, as some studies point to significant impacts of vegetation, whereas other argue lack thereof. This study, however, showcased the vegetation effects and their evolution over time. In addition, IP ratio had little and diminishing effect on the release of phosphorus. After four years of observation, it is still not clear whether there is a decreasing trend in reactive phosphate leaching, but there appears to be one for total phosphorus.

As for the nitrogen species, there was a key difference from that of phosphorus species as the extent of leaching generally decreased over time and decreased dramatically in 2017 and 2018 seasons. Media, vegetation, IP ratio, and their interaction all had a pronounced impact on the release of nitrogen species. The significance of the media impact appeared to have lessened over the years based on the analysis within events. Fairly pronounced decreases over time in the impact of IP and interactions on nitrate release were also observed. Similar patterns were observed for the total organics, with the exception that there was almost no impact of the vegetation type.

4 Conclusions

Overall, media, vegetation, IP ratio, and time had a significant impact on the percentage of runoff retained and the concentration of nutrients released over the years. The traditional bioretention media that were based on the local guidelines produced more nutrient leaching as compared to the CL media. In addition, the effects of media type on hydrological and water quality performance were significant from the very onset of this study, which supports the notion of bioretention media playing a key role in the performance. However, after four seasons of observation, vegetation effects became more apparent. Turfgrass appeared to be the least effective at volumetric and nutrient release, whereas herbaceous and woody vegetation performed in a generally similar manner during early stages, while woody cells performed significantly better in the later stages of the study. As system's performance appeared to change with time, further long-term studies that assess such impacts are recommended to shed further light on this important issue.

Acknowledgements The authors would like to thank the multiple sponsors and partners that contributed to this project—Bow River Basin Council, Alberta Environment and Parks, University of Calgary, City of Calgary Water Resources, Source2Source Inc., Alberta Low Impact Development Partnership, Environment Canada EcoAction, Natural Sciences and Engineering Research Council, MITACS, TD Bank Friends of Environment Foundation, and FortisAlberta.

References

1. LeFevre GH, Paus KH, Natarajan P, Gulliver JS, Novak PJ, Hozalski RM (2015) Review of dissolved pollutants in urban storm water and their removal and fate in bioretention cells. J Environ Eng 141(1)
2. Li H, Davis AP (2009) Water quality improvement through reductions of pollutant loads using bioretention. J Environ Eng 135:567–576
3. Funai JT, Kupec P (2018) Evaluation of three soil blends to improve ornamental plant performance and maintain engineering metrics in bioremediating rain gardens. Water Air Soil Pollut 230:3
4. Ayers MEE, Kangas P (2018) Soil layer development and biota in bioretention. Water (Basel) 10(11):1587
5. Calgary (2016) Low impact development guidelines: module 2—bioretention and bioswales. Final Report

How to Identify Cities on the Path Towards Real Sustainability?

M. Vigier, J. Moore, and C. Ouellet-Plamondon

1 Introduction

Accounting for 80% of global greenhouse gas (GHG) emissions and 75% of the planet's material resources, cities' overconsumption is a crucial issue regarding the environmental crisis [13, 39, 47]. Already home to half of the world's population, this urbanizing trend is projected to increase to 70% by 2050, according to the latest report by the United Nations [48]. Concentrating important monetary, material and energetic flows, cities have a great potential for resource conservation and could be catalysts to a global sustainable transition [17, 32]. As a result, a growing interest has been given to cities regarding urban sustainability in the literature [3, 25, 29, 47]. However, despite this rising awareness concerning climate change, ecological footprint, natural resource consumption and GHG emissions, are all foreseen to increase in the years to come, exceeding our planet's limits [12, 30, 43, 47]. The purpose of this article is to reflect on how to identify cities that have reduced their pressure on the environment and are aiming towards a life within our only planet's means. A first review of the discrepancies in meaning when talking about sustainability is performed and compared to what Earth's carrying capacity (ECC) really entails. ECC compliant sustainability indicators and accounting approaches are described, and the importance of their correspondence with cities' dynamics is put forward. Finally, the common gaps and biases encountered in a search for cities on the path towards real sustainability are listed. Real sustainability is defined as a recognition that human manufactured capital is not substitutable for natural ecological capital, commonly referred to as ecosystem services or biocapacity [37].

M. Vigier (✉) · C. Ouellet-Plamondon
Ecole de Technologie Supérieure, Montreal, Canada
e-mail: marie.vigier.1@ens.etsmtl.ca

J. Moore
British Columbia University of Technologies, Burnaby, Canada

S. Walbridge et al. (eds.), *Proceedings of the Canadian Society of Civil Engineering Annual Conference 2021*, Lecture Notes in Civil Engineering 249,
https://doi.org/10.1007/978-981-19-1061-6_33

2 Various Definitions Around Sustainability

In a world where terms like "sustainability", "green growth", or "green cities" are flourishing, some must wonder how is it that scientists keep talking about global warming. Although the meaning of "sustainable development" was universally agreed upon in the Brundtland report in 1987, the term "sustainability" bears several meanings [11, 18, 32, 41]. As an example, Metro Vancouver is often cited in the literature as a sustainable city, because of its engagement and actions towards environmental challenges [32]. However, when looking at its global impact, it appears like most Canadian cities: rather unsustainable and typical of high-consuming cities [20]. Indeed, when measured with an overarching indicator such as the ecological footprint, the city was found in a clear overshoot, at the point that if everyone on earth were to live alike Metro Vancouver's residents, almost four planets would be needed to supply resources and assimilate the waste and pollution of their lifestyles [32]. This dependency on other regions for food and natural resources, exacerbated by the globalized context of our societies, highlights the pressure cities induce on territory outside their physical boundaries and their "lack of self-sufficiency" [12, 18, 23, 39]. Hence, for accuracy purposes not only shall one refer to these urban regions as "cities on the way to sustainability" rather than "sustainable cities", but also consider a more holistic approach when assessing urban environmental impact, in order to consider cities' widespread impact [3, 12, 23, 32]. This discrepancy between usual terms employed and actual status sheds light on the distortion that can happen regarding the perception people have on the overall environmental situation, and can further hinder decision-makers from acting according to the urgency of the matter [18, 28]. Indeed, "One Planet" is not a mere target for our societies, it is the context within which we evolve and must respect in order for future generations to be able to live and thrive [12]. The Earth's Carrying Capacity (ECC) sets quantitative environmental limits, or planetary thresholds, within which our societies can operate without causing irreversible degradation [44]. These environmental thresholds would be accurate objectives for policy-makers because not only do they give quantitative objectives, but they can also be used for evaluating sustainability indicators of various materiality [17, 24, 46, 47].

3 How to Assess Earth Carrying Capacity at City Scale?

Cities are complex systems for which various challenges need to be considered in order to fully understand their dynamics and correctly assess their impacts compared to ECC [29, 31]. First, their physical urban boundaries and accounting approach need to be coherently set and clearly defined. The indicators used to evaluate the city's environmental impact shall then be comparable with quantitatively characterized planetary boundaries.

3.1 Boundaries and Accounting Approaches

To correctly assess the environmental impact associated to a city, a clear definition of its spatial delineation must be specified. However, there is a lack of consensus regarding what constitutes a 'city', for different definitions represent different perspectives, and choosing the most appropriate one relies on the aims and targets of the environmental assessment [1, 4, 28]. As the focus is placed on identifying active cities leading the way towards ECC, considering their administrative boundaries, the area over which they have jurisdictional power, is a sensible choice. Once the system delineation is defined, another challenge lies in the accounting method used for the assessment. The selected approach determines whether impacts are attributed according to a consumption-based (CB), production-based (PB) or territorial (TE) point of view. Depending on the method chosen, the responsibility is then either placed on the consumer, the producer or merely where the impacts physically occur, as represented in the Fig. 1 [25, 28].

Hence, for a sustainability assessment to adequately represent the pressure that a certain city induces on its ecosystem, it must reflect the city's dynamics [4, 23, 28, 47]. As connectivity of urban regions develops with the rest of the world, it spreads ecological pressure to further territories [24, 28, 39]. As a result, to reflect the city's economic structure, CB inventories should be reported for high-consuming cities (typically based on services) and a PB inventories for low-consuming ones (generally based on manufacturing) [7, 35, 53]. Both CB and PB approaches can be used for cities, regardless of their emission profile, as they bring different insights to their decision-makers, either regarding the emissions linked to the production of goods consumed within their cities' boundaries or in locally generated emissions. The use

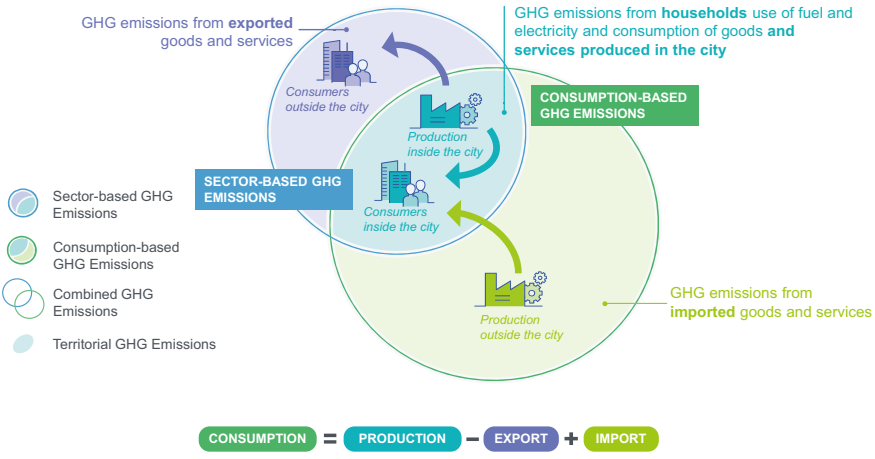

Fig.1 Scheme of different accounting approaches. *Source*: adapted from Cities [7]

of these different approaches also helps preventing any "burden-shifting" from high-consuming cities, whose embodied emissions and impacts are bigger than direct ones, to low consuming ones [4, 13, 35, 39, 53]. Then categorizing urban clusters depending on their typology of emissions (whether consumer cities or producer ones) could help develop more efficient transfer knowledge among cities facing the same issues and limit a "front runner paradox effect" [4, 38, 50]. The latter describes the lack of adequacy that can occur when knowledge transfer is done from a small group of seemingly leading cities to the urban majority where solutions do not resonate with their realities and main issues, making the whole process inefficient [18, 50].

3.2 ECC Compatible Sustainability Indicators

As of today, no single indicator can evaluate environmental urban impacts in their entirety although several proxies can be measured. Among the most used at the city scale are footprints assessments such as material, ecological, carbon or water [6, 29]. They reflect main urban flows and can thus direct policy makers to take action, and develop more sustainable practices regarding several fields, such as for instance monitoring solid waste and wastewater footprints to develop more sustainable municipal waste management [32]. Moreover, these footprints bear the advantage to be ECC compliant for they can be compared to planetary thresholds that have been scientifically evaluated for their corresponding metrics.

3.2.1 Material Footprint

Natural resource consumption is generally evaluated using Domestic Material Consumption (DMC) which accounts for the annual quantity of raw material a territory extracts and uses domestically or physically imports and is expressed in tonnes per capita per annum [47]. A DMC range of 6–8 tonnes has been proposed as an indicative threshold for staying within planetary boundaries, given current population, and associated averaged material standard of living, i.e., a fair material share. This could therefore serve as a target for economic decoupling efforts [47, 49]. However, because it omits the upstream impacts of resource consumption—which represents 80–90% of the material footprint—and the unused extraction, this indicator fails at representing the real impact of a territory's consumption [31]. Hence, another indicator referred to as the Total Material Consumption (TMC) has been proposed, as it encompasses these lacking aspects and allows for a better guidance as it deconstructs material footprint into three different flows [6, 47]. The corresponding thresholds have been set for biotic, abiotic and Raw Material Consumption (RMC) respectively to 2, 6–12 and 3–6 tonnes per person per year [6, 47]. This corridor for sustainability would allow a better use of natural resources and could also serve as a basis for reducing different bundles of environmental pressure induced by our societies [6, 42].

3.2.2 Ecological Footprint

The ecological footprint (EF) accounts for the human pressure a specific population induces on its natural capital and expresses it in terms of global hectares of productive land necessary to produce the resources needed for consumption and assimilates the generated wastes [23, 46]. It either compares it to the biocapacity (BC) of the same supportive ecosystem (the bioproductivity of the land), or to the Fair Earth Share. The latter is a dynamic indicator evaluated by dividing the global biocapacity of the planet by the total number of its inhabitants. Using the data for 2019, the Fair Earth Share was evaluated at 1.6 gha/cap/year, for a world's total biocapacity of 12.2 billion hectares, to be shared by 7.7 billion people [15]. This reflects the fact that environment is a common good, hence everyone shall be legitimate to pretend to an equal share of it [34]. Although, one should bear in mind that as population increases and available biocapacity goes down, due to climate warming's side effects, this Fair Earth Share is likely to shrink over the coming years [30, 48].

3.2.3 Carbon Footprint

The carbon footprint (CF) is a subpart of the ecological footprint and represents the quantity of air pollutants (carbon dioxide and other carbon compounds) emitted directly or indirectly by a particular entity. These emissions are generally expressed using the universally unified metric of tonnes of CO_2e which stands for their global warming potential [25, 54]. An upper global limit of 387 gigatons of CO_2e has been set, referred to as the carbon budget. It represents the cumulative amount of emission that our societies must not exceed in order to respect Paris Agreements and remain within a temperature elevation of 1.5 °C [8]. In a scenario where our societies do not rely on carbon capture technologies, the equivalent per capita target would be of 3.4 tCO_2e in 2030 and gradually decrease to 1 tCO_2e by 2050 [19].

3.2.4 Water Footprint

The water footprint (WF) is the amount of water used by a territory for its activities and considers the indirect flows through either a lens of production or consumption [2]. The WF comprises three main categories of blue, grey and green water according to the source of the flow considered, respectively groundwater and surface water, evapotranspiration from soil or assimilated with waste flows [2, 40]. Analogous to EF, the WF threshold is either expressed in terms of local attributes (here water availability), or in terms of planetary boundaries. The latter corresponds to the global amount of freshwater our societies can use (for their industries, agriculture and domestic consumption), while avoiding excessive perturbation of the natural environmental flows in all river basins. It has been set at 2800 km^3/year, or for a global population of 7.7 billion people, a limit of 363.6 m^3/cap/year [14, 24].

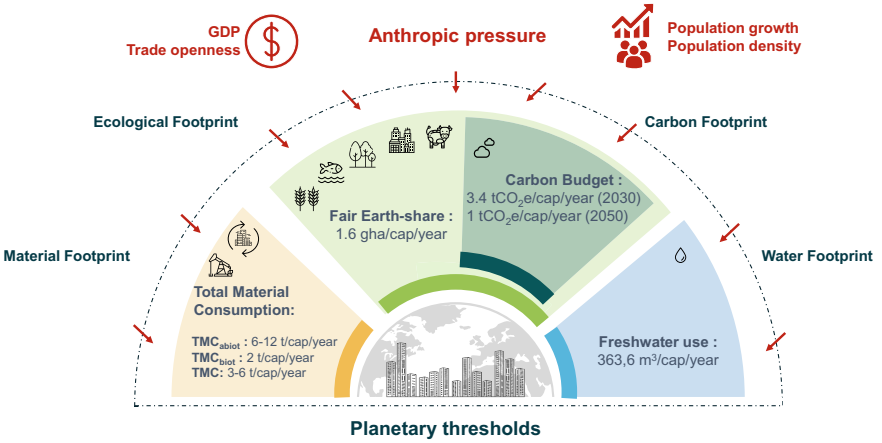

Fig. 2 Scheme of the four planetary threshold identified and their interaction with anthropic pressure

3.2.5 Anthropic Pressure and Mitigation Responsibility

It is worth mentioning that although planetary boundaries have been set for these sustainability indicators, their value is not constant over time and are particularly sensitive to parameters like population, population density or economic globalization and GDP, as represented in Fig. 2 [13, 35, 39].

As a result, the identification of cities on the way towards ECC must be done through absolute reductions of their overall pressure on the ecosystem. Only monitoring reductions based on normalized indicators at the urban scale (i.e., CO_2e per capita) would dismiss the population as a driver for environmental degradation and would fail to reflect a city's situation in its integrality. Another parameter that must be considered relates to attributive approaches [5]. Indeed, all the threshold presented in Fig. 2 are based on equality principles (same share of natural remaining capital among all individuals) rather than on equity one (fair share of natural remaining capital among individuals according to their context). Several attributive methodologies have been investigated, from approaches considering natural capital stokes such as local biocapacity or quantity of natural resources available in a specific area, to effort sharing approaches, based on parameters alike GDP, GDP per capita or cumulative environmental impact. Although local threshold evaluation is a good tool for implementing policies for regional sustainability management, it lacks fairness regarding mitigation responsibility [16, 26]. Indeed, high-consuming societies have much more contributed to global environmental deterioration compared to low-consuming ones, and also have a better capacity, both in economical and technological terms, to mitigate their environmental impact [26, 39].

Having in mind all these aspects prevent misrepresentation and allows to better target active cities on the way towards ECC. However, there are other practical obstacles that stand in the way of identifying these leading urban regions which must also be acknowledged.

4 Obstacles for ECC Assessment at Urban Scale

When trying to pinpoint leading cities transitioning towards a life respecting our only planet's means, several gaps and biases are encountered, that can be separated among four main categories: definitions and materiality, scopes and methodology, urban accounting standards, and data at the urban scale.

4.1 Definitions and Materiality

As described in Sect. 2, there is a significant discrepancy concerning frequently used sustainability terms and actual situations regarding environmental impact assessment. As a result, the misemployed words can distort reality to the point of being in antagonism with it. This ambiguity in definition can make it difficult for urban decision-makers to make the right decision in designing policies that could reduce cities' environmental impact according to the urgency of the matter [18]. This is corroborated by the fact that nowadays, despite the critical situation regarding climate change, only a few cities really monitor their environmental impact against ECC, or in a planetary boundary perspective [12, 33]. Moreover, although carrying capacity assessment promotes a holistic approach to assess the environmental impact, the most used indicator at urban scale remains about GHG emissions quantification despite its narrow focus [21]. Although an important driver of global change, affecting biodiversity, water availability, and some natural resources, particularly those related to food crops, a singular focus on GHG emissions is less comprehensive than other indicators like ecological footprint., It does not account for direct drivers of crucial aspects such as loss of biodiversity, due in large part to land use change, water shortages or depletion of natural resources [21, 29]. This lack of completeness is problematic because in the case where an absolute reduction in GHG emissions is achieved by a trade-off in another kind of ecological capital, a carbon footprint assessment would fail to capture it and only present the situation as an improvement [27, 55]. For example, converting to biofuels as a way to reduce carbon intensity could increase timber harvest from forests with a negative impact on biodiversity. Not only do those parameters make it difficult the identification of leading cities aiming for a life within ECC, but it also unveils a lack of comprehensiveness concerning the scopes and boundaries considered.

4.2 Scopes and Methodology

Selecting cities based on a global and absolute reduction (as suggested in Sect. 3.2.5) implies comparing the same urban system's footprint for various years. However, both these temporal and physical scopes are limited in some ways. Indeed, if we consider urban ecological footprint assessment for instance, most of the evaluation worldwide have been performed for a single year, and do not specify the urban delineation considered, which hinders comparability for evaluation and monitoring of improvements [33]. Hence, although EF is considered an overarching indicator, the lack of urban longitudinal studies prevent its broader use as a selection criteria for identifying cities going toward ECC [12, 33]. Another bias that affects the identification of leading urban regions in terms of impact reduction is the lack of consistency among cities' typologies and the accounting methods used to evaluate their emissions. Indeed, most of the studies performed are on high-consuming cities and yet, there is a clear lack of comprehensive consumption-based assessments [28, 35, 53]. This gap is partly explained by the inconsistency in urban accounting standards [25, 53].

4.3 Urban Accounting Standards

To facilitate interurban comparison on sustainability performance, international accounting standards were designed. However, some inconsistencies have been pointed out for different materiality assessment. For example, standards for ecological footprint or material footprint assessment at urban scales are directly adapted from their national versions, respectively Global Footprint Network or Eurostat, using a top down approach [3, 45, 51]. While it allows for a comparison between different cities, it also hinders the accuracy of their evaluation. For a more precise assessment, a bottom up approach can be used, however, it can hinder comparison, as various approximations and adaptations might be done differently from a study to another [45, 51, 52]. As a result, a choice between accuracy and comparability is to be made. For water and carbon footprints, although international urban standards already exist, shortcomings in their accounting protocols have been expressed [2, 25, 28]. As highlighted in Sect. 4.2, there is a lack of comprehensive consumption-based assessment at the urban scale, despite the fact that most urban clusters have significantly larger consumption embodied emissions, as compared to direct ones [35]. Indeed, for the main international standards concerning carbon footprint, the report of indirect emissions is both incomplete and facultative for cities, which can partly explain inadequacy in assessment [9, 25, 28]. Only considering direct emissions can lead to under-reporting by up to three times a city's real impact, and indirectly promotes burden shifting from high-consuming urban clusters to low consuming ones [28, 39]. Life cycle analysis (LCA) methods, that encompass embodied emissions, are gaining momentum in the urban academic literature and several researchers request that they further complement actual standards to solve this issue of unfairness and

incompleteness [1, 13, 29]. However, LCA methods are data-intensive approaches that can be hard to use in regions where qualitative data are hardly accessible [13].

4.4 Data at Urban Scale

When listing the limitations and gaps of one's research in the domain of urban sustainability, the lack of accessible, comprehensive, and qualitative data is typically mentioned [9, 13, 22]. Either they lack transparency, have a weak precision or are merely unavailable, which directly impacts the identification of cities going towards ECC [33]. International comprehensive urban databases for sustainability assessment are lacking water, material, and ecological footprint, which limits their use in the search for leading cities [33]. For carbon footprint, although the Carbon Disclosure Project (CDP) database helps with gathering information on cities' emissions around the globe, the platform is self-reported by cities and data are not further verified, which brings uncertainty on their quality [36]. Reporting qualitative and comprehensive data for urban sustainability requires dedicated infrastructure, staff and is time-consuming, requiring a subsequent budget. These kinds of constraints are one of the reasons why low-consuming cities are generally poorly represented in existing databases [10, 17]. This regionality in qualitative data accessibility further prevents the unbiased identification of cities going towards ECC and sheds light on the importance of assessing an intentionality parameter.

5 Conclusion

Identifying cities on the way towards real sustainability, that is, pursuing a life respecting our only planet's means, remains a difficult task. Indeed, actual main urban sustainability terms, assessment methods, approaches and standards lack the completeness and accuracy needed for this selection. To remediate these issues, a first step would be to set quantitative objectives according to fair effort-sharing methodologies, that would reflect cities' mitigation responsibility and financial capacity, while ensuring reduction level targets. Hence, international urban standards must be complemented with guidelines for using holistic indicators and coherent attributive methodologies in order to adequately evaluate urban environmental impact in function of cities' typology and dynamics. This fairer attribution and more comprehensive assessment methods would both prevent burden shifting among different cities and trade-off between distinct aspects of environmental degradation. A more inclusive representation of cities must also be reached in databases, for the lack of quantitative information on low-consuming cities hinders their identification as ones aiming at an ECC goal. To conclude, ECC must be put forward as the absolute goal for every city wanting to achieve real sustainability, and be the subject of major knowledge transfer among urban regions. To ensure the efficiency of this interurban capacity

building, further research must be done on developing standards for ECC compliant indicators and on complete and comparable urban assessing methodologies. Finally, an effort-sharing approach, must be universally acknowledged to set realistic targets for cities, allowing to optimize global environmental impact mitigation.

Acknowledgements The authors would like to thank the Canadian agencies of Social Sciences and Humanities Research Council (SSHRC), the Canadian Institutes of Health Research (CIRH) and the Natural Sciences and Engineering Research Council (NSERC) for their grant for research in the theme Living within the Earth's Carrying Capacity.

References

1. Albertí J, Balaguera A, Brodhag C, Fullana-i-Palmer P (2017) Towards life cycle sustainability assessment of cities. a review of background knowledge. Sci Total Environ 609(December):1049–1063. https://doi.org/10.1016/j.scitotenv.2017.07.179
2. Aldaya M (2012) The water footprint assessment manual: setting the global standard, 1st ed. Routledge.https://doi.org/10.4324/9781849775526
3. Baabou W, Grunewald N, Ouellet-Plamondon C, Gressot M, Galli A (2017) The ecological footprint of mediterranean cities: awareness creation and policy implications. Environ Sci Policy 69(March):94–104. https://doi.org/10.1016/j.envsci.2016.12.013
4. Balouktsi M (2020) Carbon metrics for cities: production and consumption implications for policies. Build Cities 1(1):233–259. https://doi.org/10.5334/bc.33
5. Berg Nicole van den J, van Soest HL, Hof AF, den Elzen MGJ, van Vuuren DP, Chen W, Drouet L et al (2020) Implications of various effort-sharing approaches for national carbon budgets and emission pathways. Clim Change 162(4):1805–1822. https://doi.org/10.1007/s10584-019-02368-y
6. Bringezu S (2015) Possible target corridor for sustainable use of global material resources. Resources 4(1):25–54. https://doi.org/10.3390/resources4010025
7. C40 Cities (2017) Consumption based GHG emissions of C40 Cities. https://www.c40.org/researches/consumption-based-emissions
8. C40 Cities, ARUP (2016) Deadline 2020—how cities will get the job done. https://www.c40.org/researches/deadline-2020
9. Chen G, Shan Y, Yuanchao H, Tong K, Wiedmann T, Ramaswami A, Guan D, Shi L, Wang Y (2019) Review on city-level carbon accounting. Environ Sci Technol 53(10):5545–5558. https://doi.org/10.1021/acs.est.8b07071
10. Dietz T (2018) Online representation of sustainable city initiatives in africa: how inclusive? In: International Development Policy | Revue Internationale de Politique de Développement, vol 10 (October). Institut de hautes études internationales et du développement, pp 139–61. doi:https://doi.org/10.4000/poldev.2674
11. Eyong CT, Foy II (2006) Towards alternative strategies for sustainable development in africa. Int J Sustain Dev Plan 1(2):133–156. https://doi.org/10.2495/SDP-V1-N2-133-156
12. Galli A, Iha K, Pires SM, Mancini MS, Alves A, Zokai G, Lin D, Murthy A, Wackernagel M (2020) Assessing the ecological footprint and biocapacity of portuguese cities: critical results for environmental awareness and local management. Cities 96(January):102442. https://doi.org/10.1016/j.cities.2019.102442
13. Ghaemi Z, Smith AD (2020) A review on the quantification of life cycle greenhouse gas emissions at urban scale. J Clean Prod 252(April):119634. https://doi.org/10.1016/j.jclepro.2019.119634

14. Gleeson T, Wang-Erlandsson L, Zipper SC, Porkka M, Jaramillo F, Gerten D, Fetzer I et al (2020) The water planetary boundary: interrogation and revision. One Earth 2(3):223–234. https://doi.org/10.1016/j.oneear.2020.02.009
15. Global Footprint Network (2019) Glossary. https://www.footprintnetwork.org/resources/glossary/
16. Guo J, Yue D, Li K, Hui C (2017) Biocapacity optimization in regional planning. Sci Rep 7(1):41150. https://doi.org/10.1038/srep41150
17. Hachaichi M, Baouni T (2020) Downscaling the planetary boundaries (Pbs) framework to city scale-level: de-risking MENA region's environment future. Environ Sustaina Indic 5(February):100023. https://doi.org/10.1016/j.indic.2020.100023
18. Hassan AM, Lee H (2015) The paradox of the sustainable city: definitions and examples. Environ Dev Sustain 17(6):1267–1285. https://doi.org/10.1007/s10668-014-9604-z
19. IGES (Institute for Global Environment Strategies), Aalto University, and D-mat ltd. (2019) 1.5-Degree lifestyles: targets and options for reducing lifestyle carbon footprints. Technical Report. Institute for Global Environmental Strategies, Hayama, Japan. https://enfuce.com/wp-content/uploads/2020/06/15_degree_lifestyles_mainreport.pdf
20. Isman M, Archambault M, Racette P, Konga CN, Llaque RM, Lin D, Iha K, Ouellet-Plamondon CM (2018) Ecological footprint assessment for targeting climate change mitigation in cities: a case study of 15 canadian cities according to census metropolitan areas. J Clean Prod 174(February):1032–1043. https://doi.org/10.1016/j.jclepro.2017.10.189
21. Kalbar PP, Birkved M, Karmakar S, Nygaard SE, Hauschild M (2017) Can carbon footprint serve as proxy of the environmental burden from urban consumption patterns? Ecol Ind 74(March):109–118. https://doi.org/10.1016/j.ecolind.2016.11.022
22. Khalil HAEE, Al-Ahwal A (2020) Reunderstanding Cairo through urban metabolism: formal versus informal districts resource flow performance in fast urbanizing cities. J Ind Ecol August(jiec):13056. https://doi.org/10.1111/jiec.13056
23. Kissinger M, Rees WE (2010) An interregional ecological approach for modelling sustainability in a globalizing world—reviewing existing approaches and emerging directions. Ecol Model 221(21):2615–2623. https://doi.org/10.1016/j.ecolmodel.2010.07.003
24. Li M, Wiedmann T, Liu J, Wang Y, Yuanchao H, Zhang Z, Hadjikakou M (2020) Exploring consumption-based planetary boundary indicators: an absolute water footprinting assessment of Chinese Provinces and Cities. Water Res 184(October):116163. https://doi.org/10.1016/j.watres.2020.116163
25. Lombardi M, Laiola E, Tricase C, Rana R (2017) Assessing the urban carbon footprint: an overview. Environ Impact Assess Rev 66(September):43–52. https://doi.org/10.1016/j.eiar.2017.06.005
26. Maguire R, Jiang X (2015) Emerging powerful southern voices: role of BASIC nations in shaping climate change mitigation commitments. In: Alam S, Atapattu S, Gonzalez CG, Razzaque J (eds) International environmental law and the global South, pp 214–36. Cambridge University Press, Cambridge. https://doi.org/10.1017/CBO9781107295414.011
27. Merino-Saum A, Halla P, Superti V, Boesch A, Binder C (2020) Indicators for urban sustainability: key lessons from a systematic analysis of 67 measurement initiatives. Ecol Indic 119(September). https://doi.org/10.1016/j.ecolind.2020.106879
28. Mirabella N, Allacker K (2021) Urban GHG accounting: discrepancies, constraints and opportunities. Build Cities 2(1):21–35. https://doi.org/10.5334/bc.50
29. Mirabella N, Allacker K, Sala S (2019) Current trends and limitations of life cycle assessment applied to the urban scale: critical analysis and review of selected literature. Int J Life Cycle Assess 24(7):1174–1193. https://doi.org/10.1007/s11367-018-1467-3
30. Moore D, Cranston G, Reed A, Galli A (2012) Projecting future human demand on the earth's regenerative capacity. Ecol Indic State Art Ecol Footprint: Theo Appl 16(May):3–10. https://doi.org/10.1016/j.ecolind.2011.03.013
31. Moore J (2013) Getting serious about sustainability : exploring the potential for one-planet living in Vancouver. University of British Columbia. https://doi.org/10.14288/1.0074187

32. Moore J, Kissinger M, Rees WE (2013) An urban metabolism and ecological footprint assessment of Metro Vancouver. J Environ Manage 124(July):51–61. https://doi.org/10.1016/j.jenvman.2013.03.009
33. Moore J, Ouellet-Plamondon C, Olsen C, Spiliotopoulou M, Kennedy E, Vigier M, Harte A, Warmbersie L (2021) Forthcoming report : measuring and managing for living within earth's carrying capacity at the city scale. SSHRC—knowledge synthesis grant living within earth's carrying capacity
34. Moore J, Rees W (2013) Getting to one-planet living. In: State of the world report: is sustainability still possible? The Worldwatch Institute, Washington, DC, USA. http://library.uniteddiversity.coop/More_Books_and_Reports/State_of_the_World/State_of_the_World_2013-Is_Sustainability_Still_Possible.pdf
35. Moran D, Kanemoto K, Jiborn M, Wood R, Többen J, Seto KC (2018) Carbon footprints of 13 000 cities. Environ Res Lett 13(6):064041. https://doi.org/10.1088/1748-9326/aac72a
36. Nangini C, Peregon A, Ciais P, Weddige U, Vogel F, Wang J, Bréon F-M et al (2019) A global dataset of CO2 emissions and ancillary data related to emissions for 343 cities. Sci Data 6(1):180280. https://doi.org/10.1038/sdata.2018.280
37. Neumayer E (2003) Weak versus strong sustainability: exploring the limits of two opposing paradigms. Edward Elgar Publishing
38. Noiva K, Fernández JE, Wescoat JL (2016) Cluster analysis of urban water supply and demand: toward large-scale comparative sustainability planning. Sustain Cities Soc 27(November):484–496. https://doi.org/10.1016/j.scs.2016.06.003
39. Ortega-Montoya CY, Johari A (2020) Urban ecological footprints. In: Filho WL, Azul AM, Brandli L, Özuyar PG, Wall T (eds) Sustainable cities and communities. Springer International Publishing, Cham. https://doi.org/10.1007/978-3-319-95717-3_76
40. Paterson W, Rushforth R, Ruddell B, Konar M, Ahams I, Gironás J, Mijic A, Mejia A (2015) Water footprint of cities: a review and suggestions for future research. Sustainability 7(7):8461–8490. https://doi.org/10.3390/su7078461
41. Rees W (1989) Defining sustainable development. CHS Res Bull https://scarp.ubc.ca/sites/scarp.ubc.ca/files/1989%20May_Defining%20Sustainable%20Devt_Rees.pdf
42. Sala S, Crenna E, Secchi M, Sanyé-Mengual E (2020) Environmental sustainability of European production and consumption assessed against planetary boundaries. J Environ Manage 269(September):110686. https://doi.org/10.1016/j.jenvman.2020.110686
43. Spratt D, Dunlop I, Taylor L (2020) Climate reality check 2020. breakthrough—national centre for climate restoration. https://469804a7-ae0f-4ba4-926a-0f4778d88216.filesusr.com/ugd/148cb0_c4cb345518ad4669bafa7c31d205edf4.pdf
44. Steffen W, Richardson K, Rockström J, Cornell SE, Fetzer I, Bennett EM, Biggs R et al (2015) Planetary boundaries: guiding human development on a changing planet. Science 347:6223. https://doi.org/10.1126/science.1259855
45. Świąder M, Lin D, Szewrański S, Kazak JK, Iha K, van Hoof J, Belčáková I, Altiok S (2020) The application of ecological footprint and biocapacity for environmental carrying capacity assessment: a new approach for european cities. Environ Sci Policy 105(March):56–74. https://doi.org/10.1016/j.envsci.2019.12.010
46. Świąder M, Szewrański S, Kazak JK, Van Hoof J, Lin D, Wackernagel M, Alves A (2018) Application of ecological footprint accounting as a part of an integrated assessment of environmental carrying capacity: A case study of the footprint of food of a large city. Resources 7(3):52. https://doi.org/10.3390/resources7030052
47. Swilling M, Hajer M, Baynes T, Bergesen J, Labbé F, Musango JK, Ramaswami A, et al. (2018) The weight of cities: resource requirements of future urbanization. the International Resource Panel. United Nations Environment Programme, Nairobi, Kenya
48. UNDESAPD (United Nations Department of Economic and Social Affairs Population Division) (2019) World urbanization prospects: 2018 : highlights
49. UNEP (2011) Decoupling natural resource use and environmental impacts from economic growth. Kenya, UNEP

50. Van der Heijden J (2018) From leaders to majority: a frontrunner paradox in built-environment climate governance experimentation. J Environ Plan Manage 61(8):1383–1401. https://doi.org/10.1080/09640568.2017.1350147
51. Voskamp IM, Stremke S, Spiller M, Perrotti D, van der Hoek JP, Rijnaarts HHM (2017) Enhanced performance of the eurostat method for comprehensive assessment of urban metabolism: a material flow analysis of Amsterdam. J Ind Ecol 21(4):887–902. https://doi.org/10.1111/jiec.12461
52. Wang X, Li Y, Liu N, Zhang Y (2020) An urban material flow analysis framework and measurement method from the perspective of urban metabolism. J Clean Prod 257(June):120564. https://doi.org/10.1016/j.jclepro.2020.120564
53. Wiedmann T, Chen G, Owen A, Lenzen M, Doust M, Barrett J, Steele K (2020) Three-scope carbon emission inventories of global cities. J Ind Ecol September(jiec):13063. https://doi.org/10.1111/jiec.13063
54. WRI, C40 Cities, and ICLEI (2014) Global protocol for community-scale greenhouse gas emission inventories—an accounting and reporting standard for cities. In: *Global protocol for community-scale greenhouse gas emission inventories—an accounting and reporting standard for cities.* https://ghgprotocol.org/sites/default/files/standards/GHGP_GPC_0.pdf
55. Yu H, Wang Y, Li X, Wang C, Sun M, Anshu D (2019) Measuring ecological capital: state of the art, trends, and challenges. J Clean Prod 219(May):833–845. https://doi.org/10.1016/j.jclepro.2019.02.014

An Emission Model for Regional Biogenic Oxygenated Volatile Organic Compounds from Crops

Mengfan Cai, Chunjiang An, Christophe Guy, Chen Lu, and Qi Feng

1 Introduction

Biogenic oxygenated volatile organic compounds (BOVOCs), such as methanol (CH_3OH), are mainly emitted from living organisms in terrestrial ecosystems (particularly vegetation and soil microbes). Agriculture crops have been found to the important emission source of methanol to the environment [9]. Wheat was selected for this study because it is the principal crop in Canada, and it is a fast-growing crop species that are potentially large methanol emitters [2].

Empirical models have been widely adopted to estimate BVOC emissions based on various factors including vegetation, emission activity, and environments. Biogenic Emissions Inventory System (BEIS) was the earliest emission model of large-scale BVOCs emissions, considering land use areas, leaf biomass, emission activity, and environments, but its scope of application was very limited [12]. Subsequently, the second generation of this model (BEIS2) applied high-resolution land-use data to increase the number of vegetation types to 76 and the time resolution from monthly to hourly [13]. However, BEIS2 lacked reliable leaf energy balance models and canopy models, and the Global Biosphere Emissions and Interactions System (GloBEIS)

M. Cai (✉) · C. An · Q. Feng
Department of Building, Civil and Environmental Engineering, Faculty of Engineering and Computer Science, Concordia University, Montreal, QC 3G 1M8, Canada
e-mail: mengfan.cai@mail.concordia.ca

C. Guy
Department of Chemical and Materials Engineering, Concordia University, Montreal, QC 3G 1M8, Canada

C. Lu
Institute for Energy, Environment and Sustainable Communities, University of Regina, Regina, SK S4S 02, Canada

S. Walbridge et al. (eds.), *Proceedings of the Canadian Society of Civil Engineering Annual Conference 2021*, Lecture Notes in Civil Engineering 249,
https://doi.org/10.1007/978-981-19-1061-6_34

was introduced, which indicated that the BEIS series has evolved from a regional model to a global model [5].

After a further improvement in the emission mechanism and land-use database through a large number of experimental data in several years, the Model of Emissions of Gases and Aerosol from Nature (MEGAN2.0) was proposed [7]. MEGAN2.1 [6] was an update version from MEGAN2.0 focusing on isoprene emissions [7] and MEGAN2.02 modelling monoterpene and sesquiterpene emissions [14], and it has been updated into MEGAN3 [11]. However, there are still few studies on modelling BOVOC emissions from crops.

In this study, a simple emission model for regional BOVOCs will be developed to estimate the net emission of methanol from wheat in Saskatchewan using weather data, such as temperature, solar radiation, etc. This study aims to assess methanol emissions during different developmental stages of wheat. The results can be used to develop an appropriate strategy for regional emission management.

2 Methods

In this study, combined with BEIS and MEGAN, the emission rates of methanol (*ER*, $\mu g \cdot m^{-2} \cdot h^{-1}$) are estimated as follows:

1. $ER = \varepsilon \times B \times \gamma \times \rho$
2. $B = PAR_i \times f_{PAR} \times LUE_{max} \times T_s \times W_s \times CUE/((1 + RSR) \times CR)$
3. $\gamma = \left[(1 - LDF) \cdot \gamma_{T-li} + LDF \cdot \gamma_P \cdot \gamma_{T-ld}\right]$

In these equations, ε is the standard emission factor for methanol from wheat ($\mu g \cdot g^{-1} \cdot h^{-1}$), and the standard condition includes a temperature equal to 303 K and a photosynthetically active radiation (PAR) flux being 1,000 $\mu mol \cdot m^{-2} \cdot s^{-1}$ photons in the range of 400–700 nm. A constant value of 1.0 $\mu g \cdot g^{-1} \cdot h^{-1}$ is used to simulate the methanol emission rates of spring wheat based on the results from Gomez et al. [4].

B is the dry weight of wheat biomass ($g \cdot m^{-2}$) in different months. It can be simulated using the vegetation photosynthesis model (VPM) [15]. According to these studies, f_{PAR} is the fraction of *PAR*, which can be calculated using empirical algorithms from Acevedo et al. [1]. LUE_{max} is the maximum light use efficiency of spring wheat and is set to 2.55 $gC \cdot MJ^{-1}$; CUE is the carbon use efficiency and is set to 0.5; RSR is the belowground to aboveground biomass ratio and is set to 0.2; CR is the carbon content and is set to 0.45.

γ is the environmental correction factor mainly related to light and temperature, which is calculated using empirical algorithms from Stavrakou et al. [16].

ρ is a factor explaining the production and loss of methanol within plant canopies, which is set to be 0.96 [7].

Weather data, such as air temperature and solar radiation, can be found from the Government of Canada. All the statistical analyses and figures were conducted and prepared using Microsoft Excel 2016 and SPSS 16.0.

3 Results and Discussion

Figure 1 showed the methanol emission rates of spring wheat among four regions of Saskatchewan during May–September 2018. The mean methanol emission rates were 52 $\mu g\ m^{-2}\ h^{-1}$. They have significant changes among different months ($F = 48.22$, $p < 0.001$, $n = 20$) but negligible spatial variations ($F = 0.241$, $p = 0.866$, $n = 20$). From the temporal perspective, methanol emission rates changed with leaf development, i.e., increasing from 3 to 112 $\mu g\ m^{-2}\ h^{-1}$ when leaf area expansion and growth during May–August but decreasing to 41 $\mu g\ m^{-2}\ h^{-1}$ when leaf senescence and defoliation in September.

Although mean methanol emission rates varied slightly among four regions, it was observed that methanol emission rates increased from cold north to warm south in August, with values ranging from 116 to 139 $\mu g\ m^{-2}\ h^{-1}$. Spatial and temporal differences in methanol emissions are closely correlated with air temperature, solar radiation, and leaf development.

These results were consistent with some previous studies [3, 10]. These studies proposed that higher biogenic methanol emissions are observed in spring and early summer because leaf methanol is typically produced through pectin biosynthesis during cell wall growth and expansion. More importantly, the temperature is reported to be the primary driver of seasonal changes in methanol emissions [3, 8]. For example, a 10 °C rise in leaf temperature may lead to a 2.4-fold increase in methanol emissions [9].

The findings of this study can provide appropriate strategies for regional cropping management considering the balance of leaf biomass and pollutant emission.

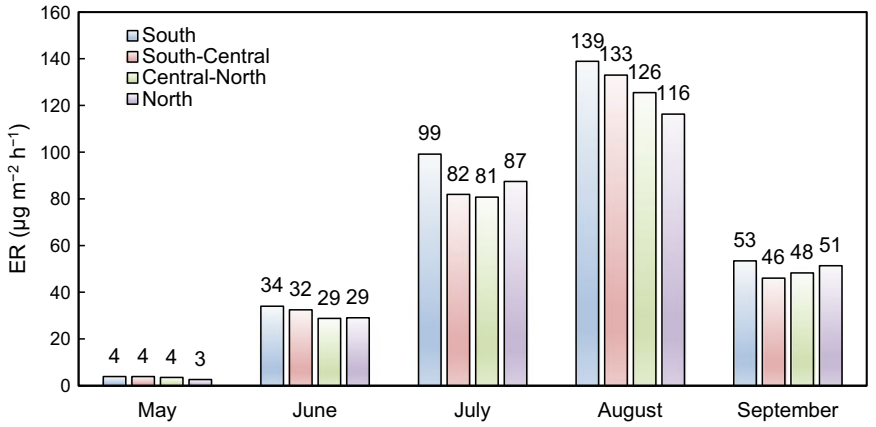

Fig. 1 Methanol emission rates (*ER*, $\mu g\ m^{-2}\ h^{-1}$) among four regions of Saskatchewan during May–September 2018

4 Conclusions

A simple emission model for regional BOVOCs was developed to estimate the net emission of methanol from wheat in Saskatchewan using weather data, such as temperature, solar radiation, etc. Overall, the mean methanol emission rates were 52 $\mu g\ m^{-2}\ h^{-1}$. They have no obvious spatial variations but significantly changed among different months. These spatial and temporal differences are closely correlated with air temperature, solar radiation, and leaf development.

Acknowledgements This research was supported by the Natural Science and Engineering Research Council of Canada.

References

1. Acevedo E, Silva P, Silva H (2006) Growth and wheat physiology, development. In: Laboratory of soil-plant-water relations. faculty of agronomy and forestry sciences, vol 1004. University of Chile, Casilla
2. Custer T, Schade G (2007) Methanol and acetaldehyde fluxes over ryegrass. Tellus Series B-Chem Phys Meteorol 59(4):673–684. https://doi.org/10.1111/j.1600-0889.2007.00294.x
3. Galbally IE, Kirstine W (2002) The production of methanol by flowering plants and the global cycle of methanol. J Atmos Chem 43(3):195–229
4. Gomez LG, Loubet B, Lafouge F, Ciuraru R, Buysse P, Durand B, Gueudet JC, Fanucci O, Fortineau A, Zurfluh O, Decuq C, Kammer J, Duprix P, Bsaibes S, Truong F, Gros V, Boissard C (2019) Comparative study of biogenic volatile organic compounds fluxes by wheat, maize and rapeseed with dynamic chambers over a short period in northern France. Atmos Environ 214:16. https://doi.org/10.1016/j.atmosenv.2019.116855
5. Guenther A, Archer S, Greenberg J, Harley P, Helmig D, Klinger L, Vierling L, Wildermuth M, Zimmerman P, Zitzer S (1999) Biogenic hydrocarbon emissions and landcover/climate change in a subtropical savanna. Phys Chem Earth Part B-Hydrol Oceans Atmos 24(6):659–667. https://doi.org/10.1016/s1464-1909(99)00062-3
6. Guenther AB, Jiang X, Heald CL, Sakulyanontvittaya T, Duhl T, Emmons LK, Wang X (2012) The model of emissions of gases and aerosols from nature version 2.1 (MEGAN2.1): an extended and updated framework for modeling biogenic emissions. Geosci Model Dev 5(6):1471–1492. https://doi.org/10.5194/gmd-5-1471-2012
7. Guenther A, Karl T, Harley P, Wiedinmyer C, Palmer PI, Geron C (2006) Estimates of global terrestrial isoprene emissions using MEGAN (Model of emissions of gases and aerosols from nature). Atmos Chem Phys 6:3181–3210. https://doi.org/10.5194/acp-6-3181-2006
8. Guenther AB, Monson RK, Fall R (1991) Isoprene and monoterpene emission rate variability: observations with eucalyptus and emission rate algorithm development. J Geophys Res: Atmos 96(D6):10799–10808
9. Harley P, Greenberg J, Niinemets Ü, Guenther A (2007) Environmental controls over methanol emission from leaves
10. Hu L, Millet DB, Mohr MJ, Wells KC, Griffis TJ, Helmig D (2011) Sources and seasonality of atmospheric methanol based on tall tower measurements in the US upper midwest. Atmos Chem Phys 11(21):11145–11156. https://doi.org/10.5194/acp-11-11145-2011
11. Jiang X, Guenther A, Potosnak M, Geron C, Seco R, Karl T, Kim S, Gu L, Pallardy S (2018) Isoprene emission response to drought and the impact on global atmospheric chemistry. Atmos Environ 183:69–83

12. Pierce TE, Waldruff PS (1991) PC-BEIS—a personal computer version of the biogenic emissions inventory system. J Air Waste Manag Assoc 41(7):937–941. https://doi.org/10.1080/10473289.1991.10466890
13. Pierce T, Geron C, Bender L, Dennis R, Tonnesen G, Guenther A (1998) Influence of increased isoprene emissions on regional ozone modeling. J Gerontol Ser A Biol Med Sci 103(D19):25611–25629. https://doi.org/10.1029/98jd01804
14. Sakulyanontvittaya T, Duhl T, Wiedinmyer C, Helmig D, Matsunaga S, Potosnak M, Milford J, Guenther A (2008) Monoterpene and sesquiterpene emission estimates for the United States. Environ Sci Technol 42(5):1623–1629. https://doi.org/10.1021/es702274e
15. Sánchez ML, Pardo N, Pérez IA, García MA (2015) GPP and maximum light use efficiency estimates using different approaches over a rotating biodiesel crop. Agric For Meteorol 214:444–455
16. Stavrakou T, Guenther A, Razavi A, Clarisse L, Clerbaux C, Coheur PF, Hurtmans D, Karagulian F, De Maziere M, Vigouroux C, Amelynck C, Schoon N, Laffineur Q, Heinesch B, Aubinet M, Rinsland C, Muller JF (2011) First space-based derivation of the global atmospheric methanol emission fluxes. Atmos Chem Phys 11(10):4873–4898. https://doi.org/10.5194/acp-11-4873-2011

Porous Media Classification Using Multivariate Statistical Methods

M. Elmorsy, W. El-Dakhakhni, and B. Zhao

1 Introduction

Subsurface porous media characterization is important in many natural and industrial processes such as groundwater movement, oil extraction, and geologic CO_2 sequestration. Classifying the type of porous media (e.g., sandstone, carbonate) is often the first step in the characterization process, and it provides critical information regarding the physical properties of the porous media. Conventionally, trained experts classify subsurface porous media samples via laboratory analyses [22]. More recently, advances in remote sensing technologies such as laser-induced breakdown spectroscopy (LIBS) have made in-situ characterization of porous media possible, whereas computed micro-tomography (μCT) technologies have made characterization of porous media samples much more efficient [4, 14]. For example, modern desktop X-ray μCT machines are capable of scanning a rock sample in as little as a few minutes. As a result, we now have unprecedented access to three-dimensional (3D) visualizations of various subsurface materials, which are readily available in online repositories [15].

Digital classification of porous media samples is now possible via the combination of imaging, chemical analysis and multivariate statistical methods. Multivariate statistical methods analyze the common behaviour of multiple independent variables, and they include principal component analysis (PCA), soft independent modeling of class analogy (SIMCA), and partial least squares discriminant analysis (PLS-DA). They have been utilized to analyze and classify porous media samples based on their chemical composition, textural features, pore characteristics, and physical properties.

M. Elmorsy (✉) · W. El-Dakhakhni · B. Zhao
Department of Civil Engineering, McMaster University, Hamilton, ON L8S 4L7, Canada
e-mail: elmorsym@mcmaster.ca

S. Walbridge et al. (eds.), *Proceedings of the Canadian Society of Civil Engineering Annual Conference 2021*, Lecture Notes in Civil Engineering 249,
https://doi.org/10.1007/978-981-19-1061-6_35

Multivariate statistical method based classification make in-situ classification of porous media possible, in situations where sample collection and retrieval is exorbitantly expensive or infeasible. For example, Sirven et al. [17] studied the feasibility of remotely identifying rocks on the Martian surface, using LIBS spectra data and multivariate methods including PCA, SIMCA, and PLS-DA. Their results show that SIMCA outperforms PLS-DA in discriminating materials that share similar features, however, combination of both models achieves the highest classification rate (97%). Kim et al. [9] used PCA and PLS-DA methods to classify three types of soil samples based on LIBS spectral data. Guang et al. [6] classified different rocks and soils using PLS-DA and support vector machine (SVM) algorithms based on LIBS spectra. Similarly, Xie et al. [22] used PLS-DA for soil type identification using near-infrared (NIR) spectra. Lepistö et al. [11], and Kachanubal and Udomhunsakul [8] utilized neural networks to categorize rocks into homogeneous and non-homogenous groups based on their color and textural features using RGB images. Valentín et al. [19] used Naïve Bayes classifier to classify rock textures based on 31 different combinations of 520 textural and spectral features. In order to reduce the computational cost of the classification process, they used PCA to reduce the problem dimensionality followed by a genetic algorithm to define the most statistically significant input configuration.

While LIBS spectra-based analysis has shown success in classifying rocks and soils based on their chemical composition [6], LIBS cannot provide precise information about the inner domain structure. μCT scans capture 3D information of porous media's inner structure with micron-scale precision, enabling precise characterization at the pore-scale. Adhikari et al. [1] studied the variability of CT-measured pore characteristics and physical properties of three soil samples obtained from different locations. The CT-measured pore characteristics are macroporosity, mesoporosity, number of pores, circularity and fractal dimension, while the soil physical properties are bulk density, hydraulic conductivity, sand, silt and clay content. They employed PCA to perform a redundancy analysis that reduced pore features, and soil physical properties into three principal components. Their analysis shows that the soil porosity and the sample number of pores are the most governing characteristics in constructing the principle components.

Here, we present a fast and robust data-driven model for rock classification using 3D μCT images. We find OPLS is the most efficient at extracting latent variables of domain features (e.g., porosity, convexity, etc.) from μCT images compared to other commonly used methods such as PCA, SIMCA, and PLS. In addition, our work provides quantitative insights into the homogeneity of the rock sample, and uncovers the relative influence between different domain features in rock classification, which improves our understanding of rock formation and evolution.

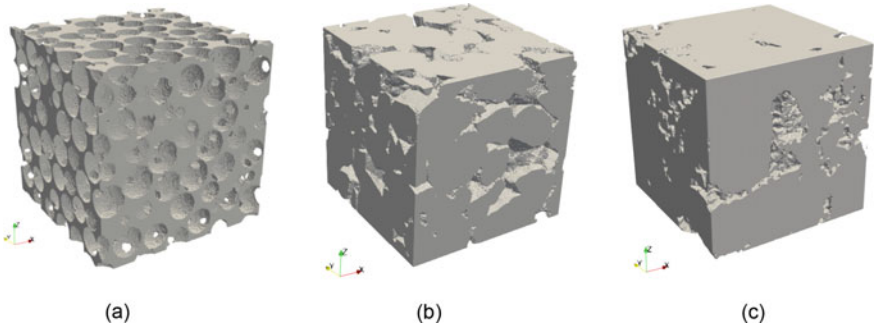

Fig. 1 3D visualization of μCT scans of **a** synthetic rock, **b** sandstone, and **c** limestone

2 Data

2.1 Description

The μCT imaging dataset used in our analysis is obtained from Muljadi et al. [13] and it is accessible via the digital rock portal [15]. Specifically, the dataset contains a 1500^3 μm^3 sandstone sample (3 μm/pixel), a 1655^3 μm^3 limestone sample (3.31 μm/pixel), and a 1000^3 μm^3 synthetic rock sample (2 μm/pixel) (Fig. 1). The synthetic rock was stochastically generated such that the pore bodies are spherical. The synthetic rock sample has homogeneous pore sizes in all spatial directions, while the sandstone and limestone samples have spatially heterogeneous pore sizes and irregular pore shapes.

2.2 Pre-processing and Feature Visualization

We perform pre-processing of the data by slicing the segmented 3D μCT scans and obtaining 500 sequential, equally-spaced 2D binary images for each sample dataset (Fig. 2). We then transform the 2D binary images of the porous media to extract the contours of the void space. The contours are used to calculate different geometric features including perimeter, area, porosity, convexity, moments, etc. (Fig. 3). Convexity is the ratio between the contour area and its convex hull area, where a convex hull of a contour is the minimum perimeter that contains the contour (e.g. a convex contour will have a convexity ratio = 1, while a concave contour will have convexity ratio <1). Convex hull descriptor is an important geometrical feature to detect shapes' similarities and it has been used for a variety of computer vision applications [7]. Similarly, moments and functions of moments are common contour-based shape features used in object recognition [12]. We calculated three groups of moments, (i) spatial moments: m01, m02, m03, m10, m11, m12, m20,

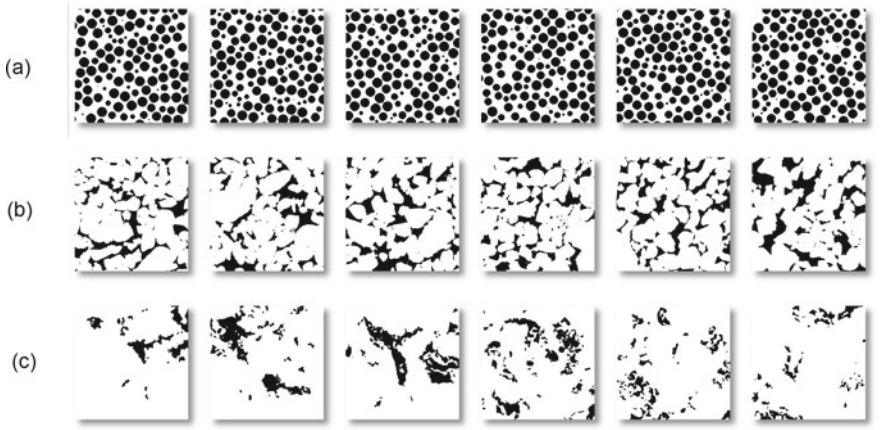

Fig. 2 Sequential 2D slices of 3D μCT scans of **a** synthetic rock, **b** sandstone, and **c** limestone. The void fractions of the porous media are shown in black, while the solid fractions are shown in white

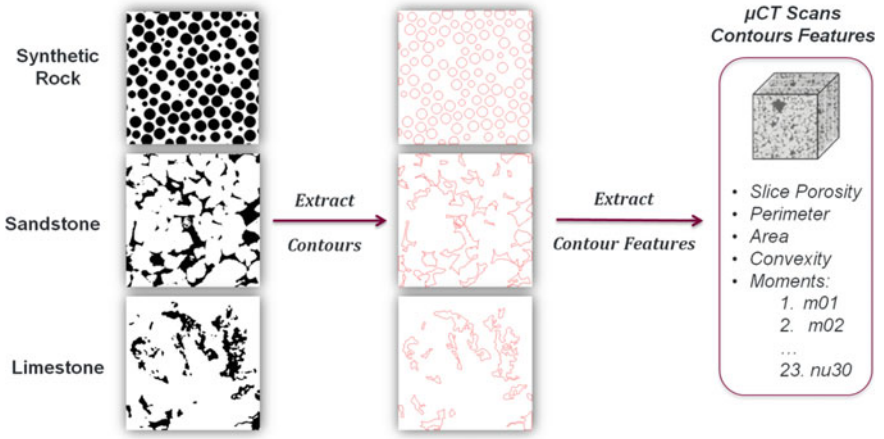

Fig. 3 We transform the 2D binary images of the porous media to extract the contours of the void space. We extract different geometric features of the contours including perimeter, area, porosity, convexity, moments, etc. using the OpenCV library in Python [3]

m21, m30, (Eq. 1), (ii) central moments: mu02, mu03, mu11, mu12, m20, mu21, mu30, (Eq. 2) and (iii) normalized central moments: nu02, nu03, nu11, nu12, nu20, nu21 and nu30 (Eq. 3). Their mathematical derivations are defined by,

Spatial moments (m_{ji}):

$$m_{ji} = \sum_{x} \sum_{y} x^j y^i I(x, y) \tag{1}$$

where I(x, y) = contour pixel intensity.

Central moments $\left(\mathrm{mu_{ji}}\right)$:

$$mu_{ji} = \sum_{x} \sum_{y} (x - \overline{x})^{j} (x - \overline{y})^{i} I(x, y) \tag{2}$$

where $\overline{x}$, $\overline{y}$ are the contour centroid: $\overline{x} = \frac{\mathrm{m_{10}}}{\mathrm{m_{00}}}$, $\overline{y} = \frac{\mathrm{m_{01}}}{\mathrm{m_{00}}}$.

Normalized central moments $\left(\mathrm{nu_{ji}}\right)$:

$$nu_{ji} = \frac{mu_{ji}}{m_{00}^{(i+j)/2+1}} \tag{3}$$

Then, the slice porosity for each contour was calculated, and the contour perimeter to area ratio (P/A). The final multivariate dataset consists of 3000 contours (i.e., 1000 contours for each porous media) and the extracted features. We divide this dataset into a training set and a testing set, whose sizes have a ratio of 4:1.

We develop a correlation heat map to visualize the correlation matrix between all rock features and the rock types (Fig. 4). Correlation matrix is a useful tool for exploratory data analysis, it inform us the degree and direction of correlation between data variables and their corresponding target. Correlation heat maps transform the correlation matrix information and present them in a visually appealing format. The developed correlation heat map shows that porosity and convexity are the most strongly correlated to the rock type, while area and moments (m01-3, m10-12, m20-21, m30, mu30, nu02 and nu11) exhibits intermediate correlation to the rock type. The remaining features (P/A ratio, mu03, mu12, mu20-21, mu30, nu30, nu12 and nu20-21) have weak correlation to the rock type. This illustrates that not all pore features have a statistically significant correlation to the rock type.

3 Methodology

We test three multivariate statistical methods—principal component analysis, partial least squares, and orthogonal partial least squares—to classify porous media samples using the geometric features extracted from pre-processing of the 3D μCT scans. We briefly describe each of the methods below.

Principal component analysis (PCA) is a mathematical procedure that reduces the dimensionality of large datasets by finding linear combinations of large number of correlated variables to create a smaller number of uncorrelated variables (orthogonal to each other), known as principal components, while preserving as much variability as possible [20]. PCA is commonly used as a pre-processing step to reduce dimensionality of multivariate data prior to using machine learning classification algorithms [16]. In addition to the PCA popularity as a dimensionality reduction technique, it is also a useful technique for data visualization and feature discovery [10]. Based

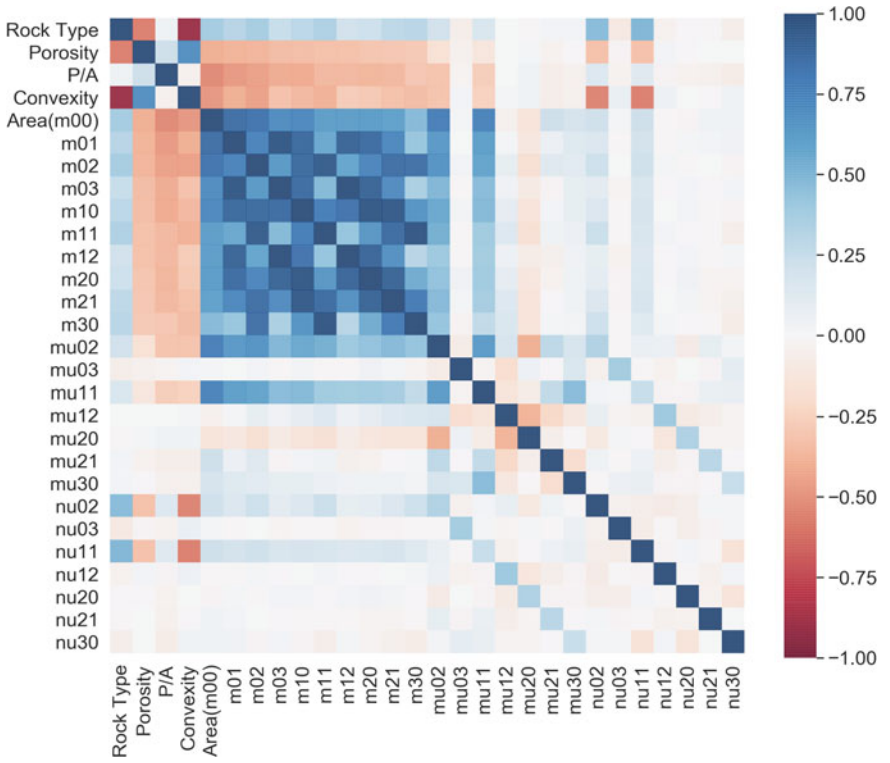

Fig. 4 Correlation heat map of the correlation matrix between the extracted rock features and rock types. The color bar displays the correlation coefficient. Dark blue indicates strong positive correlation, dark red indicates strong negative correlation and white indicates no correlation exists

on the PCA technique, the soft independent modeling of class analogy (SIMCA) method is used for complex classification tasks where a single PCA model does not encompass all of the dataset's variability. SIMCA is collection of PCA models, in which each class in the dataset has its own PCA model [21]. Here, we first develop a PCA model for each rock type, by fitting and calculating the scores and loadings of the model components. Then, we use the developed models to classify porous media samples in a supervised manner by projecting them onto each PCA model and calculating the corresponding residual. The porous media sample is classified as the rock type that yields the lowest residual and that is within its statistical limit. Partial least squares (PLS) is a mathematical method that finds latent variables of dataset variables and sequentially extracts each component. PLS differs from PCA in that it uses two blocks of data, X (variables) and Y (target), where X is used to predict Y, and Y can have multiple variables. PLS maximizes the relationship between X and Y while explaining the best variability in both X and Y, where scores and loadings are calculated for both blocks simultaneously [2]. PLS can handle multi-class

datasets using one model and it use cross-validation to check the number of components. We assign the dummy variable Y to each porous media sample (synthetic rock = 0, sandstone = 1, limestone = 2) in the training process. Orthogonal PLS (OPLS) method divides variability in the X block into systematic variability and residual variability. OPLS further splits systematic variability into two parts—one part is correlated to the Y block (predictive), while the other part is uncorrelated to Y (orthogonal). By evaluating the variation explained in each PLS component, OPLS can filter the systematic variability extracted from the input block but not related to the Y block. Therefore, an effective model with reduced complexity is obtained while maintaining the predictability of the model [18]. As a result, usually, one or two components are enough to represent variation when using the OPLS technique. By the end, rock features components generated by PLS and OPLS models were used in conjunction with discriminant analysis. The multivariate data analyses were carried out using SIMCA® software (Version 16.0, Umetrics).

4 Results

4.1 PCA Analysis

PCA model was developed and R^2 and Q^2 for each component of the X matrix in the training set were calculated. R^2 is the percentage of the variance explained by the model. It indicates how well the model fits the data. Q^2 is the percentage of the variance of the training set predicted by the model according to cross validation. By increasing the number of components, the value of R^2 increases for incorporating more variability, however, the value of Q^2 has decreased after the second component. In fact, Q^2 is calculated the same way as R^2, but it is applied on validation set which is not used in fitting the model. Therefore, by increasing more components and including more variability representing more variables from the data, this leads to over-fitting due to noise. This shows that weakly correlated moment variables discussed in the data visualization section contribute negatively to Q^2 of the model. So by adding more components to explain more variability of the X matrix this weakness the model's predictive capability since it incorporate more noise. The highest Q^2 was recorded at the first component and equals to 0.31 with R^2 equals to 0.344. Then, the t_1-t_2 scores plot was developed and it shows good separation between the synthetic rock, and the two natural rocks, sandstone and limestone; however the natural rocks scores are totally overlapped (Fig. 5).

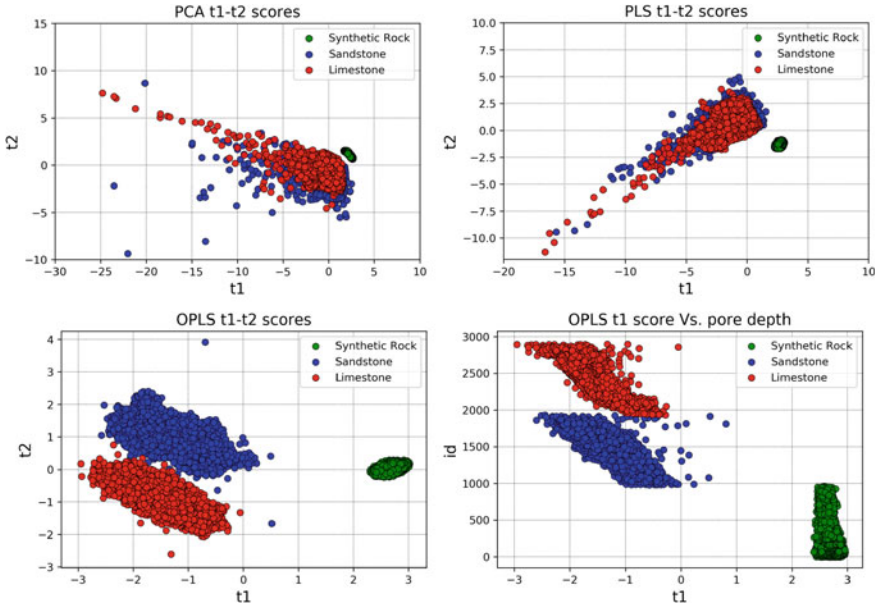

Fig. 5 Scores plot for PCA, PLS and OPLS models. The t_1-t_2 PCA scores were the most scattered and have a near complete overlap of the sandstone and limestone scores, making the separation task between these two rocks difficult; however, it is easier to separate the synthetic rock samples. Similarly, the PLS t_1-t_2 scores show similar distribution with narrower ranges and less outliers. On the other hand, the OPLS t_1-t_2 scores have a neat separation in the t_2 scores dimension, with few outliers. Finally, the OPLS t_1-id plot illustrates two information regarding the homogeneity of rocks, (i) the synthetic rock has a narrow t1 range for a given rock slice indicating close pore features values; on the other hand, real rocks t_1 scores have a wider range indicating wider pore features values range on the slice level. (ii) the synthetic rock t_1 scores almost stabilize when the pore depth increases in the X direction; unlike, real rocks t_1 scores that shift to the left (negative direction), indicating change in the features values. This concludes that, the synthetic rock has a homogeneous pore structure, whilst, real rocks are heterogeneous

4.2 SIMCA Classification Model

We perform supervised classification of porous media samples using an SIMCA model. SIMCA is collection of PCA models, each fitted for a specific rock type. In the classification process, we calculate the average orthogonal distance of the test sample to each model. The orthogonal distance is the Euclidian distance of the test sample to the PCA model of a given class. If the orthogonal distance of a new sample was found to be within the class model border (or below its statistical limit) then the sample belongs to that class, and vice versa. Similarly, to the PCA model, by increasing the number of components for each class model, we obtain a higher R^2 value, however Q^2 value decreases. The best fit models were used to classify rock samples by using two components for sandstone, limestone and synthetic rock models. The SIMCA classification recorded accuracy of 96.63% for training set and

Table 1 SIMCA model classification results on the testing set using two components

Rock type	Pores	Synthetic rock	Sandstone	Limestone	No class	Classification rate
Synthetic rock	200	189	11	0	0	0.945
Sandstone	200	0	197	1	2	0.985
Limestone	200	0	17	182	1	0.91
Total	600	189	225	183	3	0.9467

94.67% for testing set. When the incorporated PCA components were increased to three for the three models, the training and testing accuracies decreased to 96.17 and 92.83% respectively (Table 1).

4.3 PLS-DA Classification Model

PLS-DA model was developed and it was found that by increasing the incorporated components, the R^2 and Q^2 values increases. It was also noted that using two components was not enough to have a robust model since the cumulative R^2, Q^2 values for the second component were below 0.5, however, by adding the third component, the cumulative R^2 and Q^2 values has increased significantly reaching nearly 0.7 for both of them. Also, the scores of the first and second PLS components recorded overlap for the sandstone and limestone samples, as displayed Fig. 5. This emphasized that using only the first two PLS components was not enough for efficient classification. The classification results also matched that observation, since with using only the first two PLS components, total training and testing accuracies recorded 68.63 and 70.5%, respectively, with significant low limestone classification accuracies equals to 29.25 and 34% for the training and testing samples respectively. To further increase the classification accuracies, seven PLS components had to be used to achieve a strong classification, recording training and testing accuracies equals to 98.17 and 98% respectively (Tables 2 and 3).

Table 2 PLS-DA model classification results on the testing set using the first two components

Rock type	Pores	Synthetic rock	Sandstone	Limestone	No class	Classification rate
Synthetic rock	200	200	0	0	0	1
Sandstone	200	1	155	44	0	0.775
Limestone	200	2	130	68	0	0.34
Total	600	203	285	112	0	0.705

Table 3 PLS-DA model classification results on the testing set using the first seven components

Rock type	Pores	Synthetic rock	Sandstone	Limestone	No class	Classification rate
Synthetic rock	200	200	0	0	0	1
Sandstone	200	1	197	2	0	0.985
Limestone	200	0	9	191	0	0.955
Total	600	201	206	193	0	0.98

4.4 OPLS-DA Classification Model

Finally, we developed an OPLS-DA model that achieved cumulative R^2 and Q^2 equal to 0.846 and 0.839 respectively, by using only two components. In addition, the first two components had a cumulative $R^2_{(X)}$ equal to only 0.163, however their contribution to $R^2_{(Y)}$ (Predictive—Y) is equal to 1. This means that only 16.3% of variance in X matrix (rock features) was enough to predict 100% of Y (rock types), and the remaining variance was orthogonal to Y. The first component contributed to 100% of the synthetic rock samples' variance, and below 50% for the sandstone and limestone variance. However, the second component contributed only to explain the most variability in the sandstone and limestone samples. The scores of the first and second components are plotted in Fig. 5, and they showed strong separating capability. The first component could strongly separate between the synthetic rock, and the other two real rock samples, while the second component could separate between the sandstone and limestone samples. The discriminant analysis classification results recorded accuracies of 97.96% and 97.17% on the training and testing sets respectively, outperforming SIMCA and PLS-DA models when using only two principal components. In order to study the homogeneity of the samples, the t_1 scores that represent the highest X variance (pore features) that is predictive to Y (rock types) were plotted versus the contours id, where they are indexed according to their depth order in the X direction in each rock sample. It was noted that synthetic rock pores have smaller variation range of t_1 scores, and they do not change significantly with changing the pore location. This means all the synthetic rock pores have similar characteristics and hence it is a homogenous sample. On the contrary, the sandstone and the limestone had a wider variation range of t_1 scores and display a shift in t_1 scores as the contours depth increases. This means that the characteristics of the sandstone and limestone samples pores change in the three spatial directions, and thus they are heterogeneous. Similar patterns were also found in the t_2 scores values. These findings agree with our observations from visualizing the samples' slices in Fig. 2, but using t1 and t2 scores enables analyzing rock homogeneity in a quantitative way (Table 4).

Finally, we investigated the variables influence in predicting the rock types by utilizing the variable influence in projection (VIP) method. VIP method evaluate the influence of each variable in the projection used in the model by calculating VIP scores that is often used for variable selection in multivariate analysis for big

Table 4 OPLS-DA model classification results on the testing set using the first two components

Rock type	Pores	Synthetic rock	Sandstone	Limestone	No class	Classification rate
Synthetic rock	200	200	0	0	0	1
Sandstone	200	1	195	4	0	0.975
Limestone	200	0	12	188	0	0.94
Total	600	201	207	192	0	0.9717

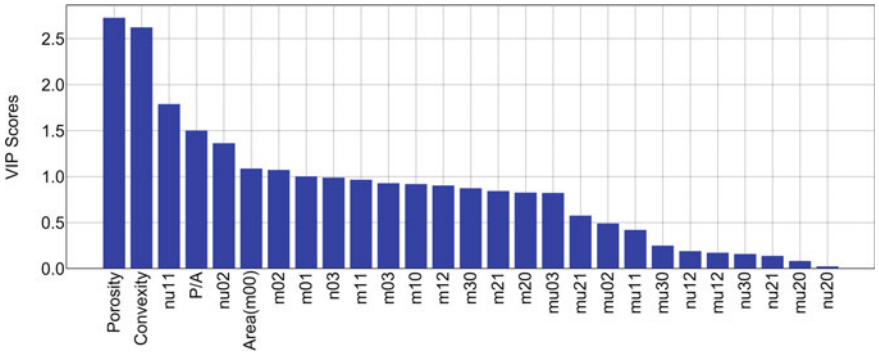

Fig. 6 Variable influence in projection (VIP)

data. Variables with higher VIP scores indicate higher influence in the projection in the model and consequently higher influence in predicting the class of a new data. Specifically, a variable with a VIP Score close to or greater than one ($> = 1$) can be considered influential in a given model, on the contrary, variables with VIP scores substantially less than one (<1) are less influential and might be discarded from the model. For more details about the VIP theory, the reader can refer to [5]. Here we developed the rocks variables VIP scores for the predictive components in the OPLS model, and we illustrate them in Fig. 6. It is illustrated that porosity and convexity have the highest influence on the model with VIP scores greater than 2.5 (>2.5), relatively, less influential variables are nu11 moment and P/A ratio with VIP scores greater than 1.5 (>1.5), and nu02 moment, area and mu02 moment with scores greater than one (>1). The remaining variables are found to be insignificant to the model projection by having VIP scores less than one (<1).

5 Conclusions

In this paper, we carried out a classification analysis over digital rocks dataset, including a synthetic rock and two natural rocks, sandstone and limestone. The digital rocks volumes were sliced in the X direction, and their pore structure contours were

extracted, followed by calculating handcrafted features out of them. We employed four data reduction methods to perform multivariate statistical analysis, namely PCA, SIMCA, PLS-DA and OPLS-DA. The PCA model showed a poor capability to explain the whole dataset in one single model. On the other hand, the SIMCA model demonstrated higher prediction capability by building a single PCA model for each rock type. We found the PLS model to be more capable of dealing with the analyzed dataset because of its ability to deal with noise and uncorrelated variables to the sample class. However, its t1-t2 plot showed that the first 2 PLS components were not enough to separate rock samples effectively. On the other hand, the OPLS method effectively filtered the variables that did not correlate to the sample class. It resulted in only two components that predicted 100% of the Y matrix (rock type) while explaining only 16.3% of the X matrix (rock features) variance. The t1-t2 scores plot of the OPLS model showed a near clear separation between all rock types with few outliers. That emphasized the OPLS capability in filtering the uncorrelated variables to the classified classes, and consequently, it uses less information with higher prediction ability. Therefore, the OPLS-DA model achieved the highest classification rate equals to 0.9717 when using only 2 components. Finally, we utilized the VIP method to uncover the most influential rock features in classifying rock types. Variables such as porosity, convexity, P/A ratio, nu02 and nu11 moments were revealed to be the key features to distinguish rock types.

References

1. Adhikari P, Anderson SH, Udawatta RP, Kumar S (2016) Analysis of CT-measured pore characteristics of porous media relative to physical properties. Procedia Comput Sci 95:442–449
2. Barker M, Rayens W (2003) Partial least squares for discrimination. J Chemom 17(3):166–173
3. Bradski G (2000) The OpenCV library. Dr. Dobb's J Softw Tools 120:122–125
4. Díaz Pace DM, Gabriele NA, Garcimuño M, D'Angelo CA, Bertuccelli G, Bertuccelli D (2011) Analysis of minerals and rocks by laser-induced breakdown spectroscopy. Spectrosc Lett 44:399–411
5. Galindo-Prieto B, Eriksson L, Trygg J (2014) Variable influence on projection (VIP) for orthogonal projections to latent structures (OPLS). J Chemom 28:623–632
6. Guang Y, Shujun Q, Pengfei C, Yu D, Di T (2015) Rock and soil classification using PLS-DA and SVM combined with a laser-induced breakdown spectroscopy library. Plasma Sci Technol 17(8):656–663
7. Jayaram M, Fleyeh H (2016) Convex hulls in image processing: a scoping review. Am J Intell Syst 6(2):48–58
8. Kachanubal T, Udomhunsakul S (2008) Rock textures classification based on textural and spectral features. Int J Geotech Geol Eng 2(3):658–664
9. Kim G, Kwak J, Kim K-R, Lee H, Kim K-W, Yang H, Park K (2013) Rapid detection of soils contaminated with heavy metals and oils by laser induced breakdown spectroscopy (LIBS). J Hazard Mater 263:754–760
10. Landgraf AJ, Lee Y (2020) Dimensionality reduction for binary data through the projection of natural parameters. J Multivar Anal 180:104668
11. Lepistö L, Kunttu I, Autio J, Visa A (2003) Rock image classification using non-homogenous textures and spectral imaging. In: Skala V (ed) WSCG 2003, the 11th international conference in central Europe on computer graphics, visualization and computer vision 2003, short papers, 3–7 February 2003. Czech Republic, Iniversity of West Bohemia, Plzen, pp 82–86

12. Mercimek M, Gulez K, Mumcu TV (2005) Real object recognition using moment invariants. Sādhanā 30(6):765–775
13. Muljadi BP, Blunt MJ, Raeini AQ, Bijeljic B (2016) The impact of porous media heterogeneity on non-Darcy flow behaviour from pore-scale simulation. Adv Water Resour 95:329–340
14. Pak T, Archilha NL, Mantovani IF, Moreira AC, Butler IB (2019) An X-ray computed micro-tomography dataset for oil removal from carbonate porous media. Sci Data 6:190004
15. Prodanovic M, Esteva M, Hanlon M, Nanda G, Agarwal P (2015) Digital rocks portal: a sustainable platform for imaged dataset sharing, translation and automated analysis.
16. Reddy GT, Reddy MPK, Lakshmanna K, Kaluri R, Rajput DS, Srivastava G, Baker T (2020) Analysis of dimensionality reduction techniques on big data. IEEE Access 8:54776–54788
17. Sirven J-B, Sallé B, Mauchien P, Lacour J-L, Maurice S, Manhès G (2007) Feasibility study of rock identification at the surface of Mars by remote laser-induced breakdown spectroscopy and three chemometric methods. J Anal At Spectrom 22(12):1471–1568
18. Trygg J, Wold S (2002) Orthogonal projections to latent structures (O-PLS). J Chemometr J Chemometr Soc 16(3):119–128
19. Valentín M, Bom C, Albuquerque M, Albuquerque M, Faria E, Correia M, Surmas R (2017) On a method for rock classification using textural features and genetic optimization. Notas Técnicas 7(1):18–30
20. Wold S, Esbensen K, Geladi P (1987) Principal component analysis. Chemom Intell Lab Syst 2(1–3):37–52
21. Wold S, Sjöström M (1977) SIMCA: a method for analyzing chemical data in terms of similarity and analogy. Chemometr: Theor Appl 52(12):243–282
22. Xie H, Zhao J, Wang Q, Sui Y, Wang J, Yang X, Zhang X, Liang C (2015) Soil type recognition as improved by genetic algorithm-based variable selection using near infrared spectroscopy and partial least squares discriminant analysis. Sci Rep 5(1):10930

Prediction of Waste Disposal During Covid-19 Using System Dynamics Modeling

Sanaalsadat Eslami, Kelvin Tsun Wai Ng, and Golam Kabir

1 Introduction

Due to rapid development of economy and increase in the population during the last few decades across the globe, sustainable solid waste management has become an important issue. Waste management organizations and researchers have realized the importance of proper solid waste management, and published studies to better control and manage solid waste [5, 23, 25]. For example, some studies proposed various novel performance indicators to assess the efficiency and effectiveness of waste management systems [2, 16]. Some studies focused on specific aspects of sustainable solid waste management systems, including waste generation characteristics [3, 27], waste collection efficiency [26], waste diversion models [6, 20, 21], and the use of landfill technology [4, 13–15].

The amount of waste generation is generally affected by various socio-economical factors such as population, GDP, and family income [3, 20]. Unexpected phenomena such as the COVID-19 pandemic can significantly impact waste management operations and system performance [1, 22]. During the pandemic and the subsequent lockdown, the pattern and quantity of the waste generation changed dramatically [1, 22, 28]. Proper waste management is important to the health and safety of the residents, and should be taken more seriously to protect the surrounding environment, especially during the COVID-19 period. Various waste management researchers have reported waste management issues during COVID-19 [22, 23, 28].

Numerous personal protective equipment and disposal health care products such as masks, gloves, and disinfection wipes have been used to prevent spread of COVID-19. Van Fan et al. [25] reported that the recent pandemic could affect different types of waste differently, meaning that it could cause increase in some waste streams and

S. Eslami (✉) · K. T. W. Ng · G. Kabir
University of Regina, Regina, Canada
e-mail: SEP403@uregina.ca

S. Walbridge et al. (eds.), *Proceedings of the Canadian Society of Civil Engineering Annual Conference 2021*, Lecture Notes in Civil Engineering 249,
https://doi.org/10.1007/978-981-19-1061-6_36

decrease in other streams. For example, the consumption of plastics has increased considerably because of online orders for food and other products [25]. Richter et al. [22] examined the variability of waste disposal data in Regina, the capital city of Saskatchewan, and found similar results. To effectively operate a waste management system during and after the pandemic, information regarding the amount and type of waste generated is needed. The amount and type of waste generation can be used in predictive models to identify trends and obtain useful insights regarding waste generation characteristics and recycling behaviors during and after the COVID-19 pandemic. System dynamics is known as an effective tool to complex model and non-linear problems such as waste management. In this study, a system dynamic model is proposed to model the amount of municipal solid waste (MSW) in the city of Regina, and to forecast the amount of various waste streams during and after the COVID-19 pandemic. Specifically, we develop a system dynamics (SD) model to analyse and investigate the possible factors on MSW disposal in Regina during and after pandemic. This model can be used for the other cities in Canada to investigate the waste disposal behaviors during pandemic. The results will help decision makers to evaluate waste management system efficiency and develop new regulations and by-laws regarding waste management during emergencies.

1.1 Research Area and Data Source

City of Regina, with population of 258,960, is the capital and the second-largest city in Saskatchewan [17]. Regina, with an area of 118.4 square kilometers, is located centrally of a Prairie province, with Alberta to the west and Manitoba to the east [19]. Due to population and economic growth, Regina continues to advance several Official Community Plan (OCP) of environmental policies to reduce emissions, energy consumption, and organizations environmental impact [18]. The GDP and population have strong influences on waste generation, as suggested by Aldaco et al. [1]. The population of the city depends strongly on the birth, death, and immigrant rates [11]. The estimated GDP growth rate in the city is 0.8435 from 2013 to 2020.

This city has a detailed plan for waste management and resourcing conservation goals. The bi-weekly curb-side residential waste collection program includes the provision of different size of carts to households, and the establishment of a comprehensive recycling program. Educating of the residents on residential waste management is another important component of the city's waste minimization goal. For example, the city developed waste reduction plan to inform residents regarding the importance of component separation of the recyclables. The waste plan has provided sufficient information to residents regarding different ways that they can help the city to achieve its established sustainability goals. For instance, simple actions such as using reusable bags for grocery shopping, purchasing products with less packaging, or leaving grass trimmings on the lawn have been recommended [11].

Due to the blooming economy, city of Regina is attracting more immigrants nationally and internationally. Regina is an immigrant city with a considerable population

growth in recent years, with a recent immigrant rate of 2.4%. As a result, the city has witnessed a population growth with about 1.38% per year from 2011 to 2016 [10]. Based on the Conference Board of Canada Forecast for Regina in April 2020, despite of Regina's weaker economy over the prior couple of years, net migration remained positive. Based on this information, it is estimated that Regina's net population would rise roughly 1.7% each year between 2019 and 2023 [7].

1.2 Related Works

In recent years, the rapid increase in the waste generation has caused serious impact to the environment. Xiao et al. [28] developed a system dynamic model to investigate the effects of waste policies on MSW management in Shanghai, China. In Xiao et al. [28], system dynamic model was used to model overall waste generation. However, this model was not used for a particular type of waste. According to Xiao et al. [28], GDP growth rate and MSW generation rate per capita are significant factors. Higher GDP growth rate generally results in higher MSW generation per capita and therefore the total amount of MSW generation. Although strict demographic policy increased MSW generation per capita, it did not considerably affect total amount of MSW generation [28].

To simulate and study the positive influence of waste minimization in construction sector on the environment, Ding et al. [8] developed a system dynamic approach to analyse the amount of construction and demolition (C&D) waste and examine the relationship between source deduction and C&D generation rate. Ding et al. [8] showed that by reducing sources of could reduce the total waste generation by 27.05%. According to Ding et al. [8], waste sorting can improve the ratio of reused to generated waste by 15.49%. They concluded that paying more attention to source reduction by using modern equipment and tools could help to minimize environmental impacts.

Zulkipli et al. [29] proposed a system dynamic model for waste management in Malaysia and used stock flow diagram to investigate the amount of waste generation. The model was developed based on three variables, population, recycling rate, and total waste generation. Their results suggested increasing recycling rate and reducing waste generation rate in Malaysia. Recently, Sharma et al. [24] conducted a numerical study on waste management during COVID-19 pandemic using multiple waste streams and reported promising results.

Literature review suggested that SD modeling approach is versatile and applicable for many nonlinear and complex problems. SD seeks to understand the dynamic behaviours in a system, and SD model explicitly presents the relationships among the components [12]. SD analysis can be presented by multiple loop structures [5]. SD uses what-if scheme simulation, indicating the relations between comportments in a system. This model is suitable for different variables, which is the key to the protect public health and minimize risk.

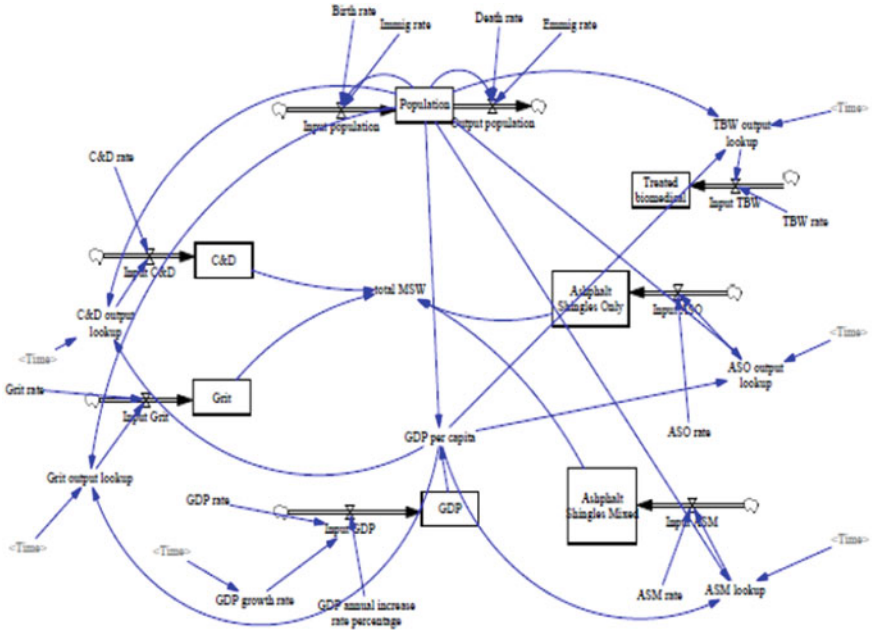

Fig. 1 Proposed system dynamics model

2 Methodology

In this study, a SD model is designed to investigate the city of Regina waste disposal behaviors during the COVID-19 pandemic. The model is built using waste disposal data at the Regina landfill from 2013 to 2020. Unlike other models, different waste fractions we separately modeled. Figure 1 illustrate the SD model with five main stock-flow processes for (i) Construction and Demolition (C&D), (ii) Grit, (iii) Treated Biomedical Waste (TBW), (iv) Asphalt Shingles Only, and (v) Asphalt Shingles Mixed to predict the waste disposal rate at the landfill. The temporal changes of the five waste streams are separately examined with respect with time. Rate associated with each waste streams is defined to describe the waste disposal trend during the period. Finally, the total MSW is also considered in this study to present an overview of Regina waste disposal behaviors.

3 Results and Discussion

The average annual GDP rate in Regina was 2.7%, so there will be an increase of per capita GDP from $16,194 to $20,172 at the end of the simulation period in 2025. In

addition, population is expected to increase from 210,000 to 224,895 at the end of the 5-year period.

Figures 2 and 3 present the various waste generation during 2019 and 2025 which is indicated an increase in the prediction of waste generation. It is believed the increase in waste generation rate is mainly due to the changes in population and per capita GDP.

C&D waste, with an average 15,000 tonnes per year, represents the largest share of the total waste stream in Regina. Figure 2 shows and estimates on C&D waste generation with respect to time. A sharp increase is observed between 2019 and 2020. The slope of the C&D generation curve however appear less steep between 2020 and 2021. A slower C&D generation rate may be due to the newly imposed COVID-19 physical distancing at the city, as well as a quieter construction season during the

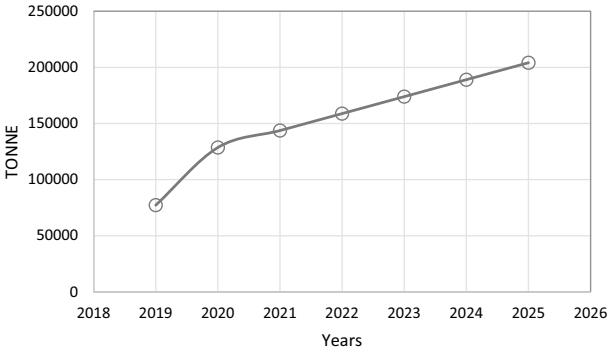

Fig. 2 Estimates of C&D waste in Regina

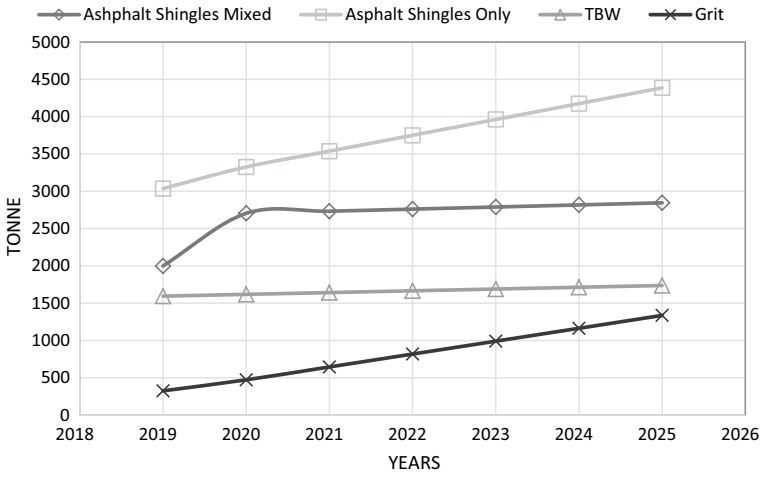

Fig. 3 Estimates of other waste streams in Regina

second wave of COVID-19. Most major construction projects were put on hold in 2020. However, it appears there was a slightly increase in smaller renovation projects carried by the homeowners in 2020. This was probably due to government's work from home recommendation. These smaller scale individual renovation projects, nonetheless, produced much less C&D waste than full scale infrastructure and civil engineering projects. A relatively linear trend is observed from 2021 to 2025.

Figure 3 shows, different trends that are observed for different waste streams in Regina. There is a linear increasing trend of the grit generation. Grit generation in Regina is mainly derived from road maintenance projects and street sweepings. Regina has long, harsh winters, and the city crew uses large quantity of sand and salt to maintain roads and create safe driving condition. Asphalt Shingles Only has similar slope with the Grit. Both Grit and Asphalt shingles only increased linearly with time. It appears the pandemic has little impact on the generation of Grit and Asphalt Shingles Only.

TBW are collected from hospitals and clinics in Regina. Surprisingly, the generation of TBW is relatively constant during the study period. It may be because residents avoid visiting hospitals and clinics and cancelling non-essential medical appointment to lower the possible exposure of the virus. However, more research is needed before a definite conclusion can be made.

Asphalt Singles Mixed has generation trend similar to C&D (Fig. 2), probably due to the similarity between the materials. A change of slope is observed between 2019 and 2020. As discussed before, Asphalt Singles Mixed may be related to the slowdown of larger scale infrastructure projects in the city.

4 Conclusion

In this paper, we investigated the impact of COVID-19 on the amount of MSW in Regina, and modeled the waste generation rates from 2021 to 2025 using a SD model. Five waste streams were considered. C&D, grit, Asphalt Shingles Only, Asphalt Shingles Mixed, and TBW were separately considered to forecast the amount of MSW during and after the pandemic. SD model was developed by the historical waste disposal data at Regina landfill. The preliminary results showed that the pandemic has impacts on waste generation characteristics and recycling behaviors in the city, particularly the generation of C&D and Asphalt Shingles Mixed.

An abrupt change of C&D generation is observed between 2019 and 2020. A slower C&D generation rate may be due to the physical distancing regulation at the city, as well as a quieter construction season during the second wave of COVID-19. Major construction projects were put on hold in 2020. However, it appears there was a slightly increase in smaller renovation projects carried by the homeowners in 2020.

Both Grit and Asphalt Shingles Only increased linearly with time. It appears the pandemic has little impact on these waste streams. TBW generation is surprisingly constant during the study period. Asphalt Singles Mixed has generation trend similar to C&D, and is affected by the pandemic.

Preliminary results suggested that SD model is effective for predicting MSW generation rates in Regina. The project is on-going, and more variables and regulations will be included to study the factors affecting MSW generation in Regina.

Acknowledgements The research reported in this paper was supported by a grant from the Natural Sciences and Engineering Research Council of Canada (ALLRP 551383-20) to the second and third authors. We would also like to thank City of Regina Environmental Services branch for supporting this project. The authors are grateful for their support. The views expressed herein are those of the writers and not necessarily those of our research and funding partners.

References

1. Aldaco R, Hoehn D, Laso J, Margallo M, Ruiz-Salmón J, Cristobal J, Kahhat R, Villanueva-Rey P, Bala A, Batlle-Bayer L, Fullana-I-Palmer P (2020) Food waste management during the COVID-19 outbreak: a holistic climate, economic and nutritional approach. Sci Total Environ 742:140524
2. Bolingbroke D, Ng KTW, Vu HL, Richter A (2021) Quantification of solid waste management system efficiency using input-output indices. J Mater Cycles Waste Manag. https://doi.org/10.1007/s10163-021-01187-7
3. Bruce N, Asha A, Ng KTW (2016) Analysis of solid waste management systems in Alberta and British Columbia using provincial comparison. Can J Civ Eng 43(4):351–360. https://doi.org/10.1139/cjce-2015-0414
4. Bruce N, Ng KTW, Vu HL (2018) Use of seasonal parameters and their effects on FOD landfill gas modeling. Environ Monit Assess 190:291. https://doi.org/10.1007/s10661-018-6663-x
5. Chaerul M, Tanaka M, Shekdar AV (2008) A system dynamics approach for hospital waste management. Waste Manage 28(2):442–449
6. Chowdhury A, Vu HL, Ng KTW, Richter A, Bruce N (2017) An investigation on Ontario's non-hazardous municipal solid waste diversion using trend analysis. Can J Civ Eng 44(11):861–870. https://doi.org/10.1139/cjce-2017-0168
7. Community Data (2020) Economic indicator. Retrieved 02 November 2020, from https://economicdevelopmentregina.com/economic-data
8. Ding Z, Yi G, Tam VW, Huang T (2016) A system dynamics-based environmental performance simulation of construction waste reduction management in China. Waste Manage 51:130–141
9. Duan H, Huang Q, Wang Q, Zhou B, Li J (2008) Hazardous waste generation and management in China: a review. J Hazard Mater 158(2–3):221–227
10. Economic Development Regina (2021) Retrieved 05 January 2021, from https://townfolio.co/sk/regina
11. Education & Resources (2020) Retrieved 21 November 2020, from https://www.regina.ca/home-property/recycling-garbage/education-resources
12. Forrester JW (1994) System dynamics, systems thinking, and soft OR. Syst Dyn Rev 10(2–3):245–256
13. Karimi N, Richter A, Ng KTW (2020) Siting and ranking municipal landfill sites in regional scale using nighttime satellite imagery. J Environ Manage 256(109942):1–9. https://doi.org/10.1016/j.jenvman.2019.109942
14. Ng KTW, Lo IMC (2010) Effects of design mix and porosity of waste-derived paste as landfill daily covers on lead retardation. ASCE J Hazard Toxic Radioactive Waste Manage 14(3):195–204. https://doi.org/10.1061/(ASCE)HZ.1944-8376.0000033
15. Ng KTW, Lo IMC (2010) Fines migration from soil daily covers in Hong Kong landfills. Waste Manage 30(11):2047–2057. https://doi.org/10.1016/j.wasman.2010.03.005

16. Pan C, Bolingbroke D, Ng KTW, Richter A, Vu HL (2019) The use of waste diversion indices on the analysis of canadian waste management models. J Mater Cycles Waste Manage 21(3):478–487. https://doi.org/10.1007/s10163-018-0809-3
17. Regina Population (2021) Retrieved 16 January 2021, from https://www.canadapopulation.net/regina-population
18. Renewable Regina (2020) Retrieved 15 November 2020, from https://www.regina.ca/about-regina/renewable-regina/
19. Regina History & Facts (2021) Retrieved 18 January 2021, from https://www.regina.ca/about-regina/regina-history-facts/
20. Richter A, Bruce N, Ng KTW, Chowdhury A, Vu HL (2017) Comparison between Canadian and nova scotian waste management and diversion models—a Canadian case study. Sustain Cities Soc 30:139–149. https://doi.org/10.1016/j.scs.2017.01.013
21. Richter A, Ng KTW, Pan C (2018) Effects of percent operating expenditure on canadian non-hazardous waste diversion. Sustain Cities Soc 38:420–428. https://doi.org/10.1016/j.scs.2018.01.026
22. Richter A, Ng KTW, Vu HL, Kabir G (2021) Waste disposal characteristics and data variability in a mid-sized Canadian city during COVID-19. Waste Manage 122:49–54. https://doi.org/10.1016/j.wasman.2021.01.004
23. Sarkodie SA, Owusu PA (2020) Impact of COVID-19 pandemic on waste management. Environ Dev Sustain 1–10
24. Sharma HB, Vanapalli KR, Cheela VS, Ranjan VP, Jaglan AK, Dubey B, Goel S, Bhattacharya J (2020) Challenges, opportunities, and innovations for effective solid waste management during and post COVID-19 pandemic. Res Conserv Recycl 162:105052
25. Van Fan Y, Jiang P, Hemzal M, Klemeš JJ (2021) An update of COVID-19 influence on waste management. Sci Total Environ 754:142014
26. Vu HL, Ng KTW, Bolingbroke D (2018) Parameter interrelationships in a dual phase GIS-based municipal solid waste collection model. Waste Manage 78:258–270. https://doi.org/10.1016/j.wasman.2018.05.050
27. Wang Y, Ng KTW, Asha A (2016) Non-hazardous waste generation characteristics and recycling practices in Saskatchewan and Manitoba, Canada. J Mater Cycles Waste Manage 18(4):715–724. https://doi.org/10.1007/s10163-015-0373-z
28. Xiao S, Dong H, Geng Y, Tian X, Liu C, Li H (2020) Policy impacts on Municipal Solid Waste management in Shanghai: A system dynamics model analysis. J Clean Prod 262:121366
29. Zulkipli F, Nopiah ZM, Basri NEA, Kie CJ (2016) Stock flow diagram analysis on solid waste management in Malaysia. In AIP Conf Proc 1782(1):040023

Hydrogen Production in Incubated Anaerobic Mesophilic Mixed Culture by Oleic Acid (OA) for Different Periods

Rajan Ray, Laura Cordova-Villegas, Mamata Sharma, and Nihar Biswas

1 Introduction

The propelling factors for the growth of renewable energy resources are increasing global greenhouse gas levels and depleting fossil energy sources. Hydrogen is an important and promising alternative energy carrier to existing fossil carbon containing energy sources from the viewpoint of carbon dioxide emissions mitigation, and production possibilities. Since the 1970s, the idea of a hydrogen economy has made great progress [3].

Biological production of hydrogen is possible through photosynthesis and fermentation [2, 22, 29]. These processes are either light-dependent (photosynthesis) or light-independent (dark fermentation) [11, 13, 24]. The latter is beneficial for the production of hydrogen because it does not rely on light intensity and the dark fermentation reactions are faster and have greater conversion efficiencies compared to photo-fermentation [10, 13, 30]. Mixed microbial cultures degrade complex organic substrates into hydrogen, organic acids and alcohols in the dark fermentation route.

One of the main disadvantages of hydrogen production utilising mixed microbial species is the coexistence of hydrogen-consuming microorganisms. Hydrogen is used as an electron donor by hydrogen eating microorganisms such as hydrogenotrophic methanogens, homoacetogens and bacteria reducing sulphate. Therefore, in these types of systems, extracting hydrogen involves minimising the amount of hydrogen consumed and, consequently, increasing yields. Studies conducted on inhibiting the growth and activity of hydrogenotrophic methanogens using pH has shown compelling evidence of methanogenic growth control on a short-term basis. However, over the long term, after the stress is relieved, microbial growth can resume as the conditions become favourable [9, 10, 23, 26].

R. Ray (✉) · L. Cordova-Villegas · M. Sharma · N. Biswas
University of Windsor, Windsor, Canada
e-mail: rayr@uwindsor.ca

S. Walbridge et al. (eds.), *Proceedings of the Canadian Society of Civil Engineering Annual Conference 2021*, Lecture Notes in Civil Engineering 249,
https://doi.org/10.1007/978-981-19-1061-6_37

In this analysis, OA was added to inhibit hydrogenotrophic methanogens under reduced pH conditions. LCFAs have been reported to inhibit hydrogenotrophic and aceticlastic methanogens at threshold concentrations [19, 20]. LCFAs were derived from lipids and fats by the hydrolytic microorganisms in mixed microbial communities. Fats and lipids are derived from edible oil refineries, slaughterhouses and dairy industries [14, 15, 25]. LCFAs are degraded to shorter chain fatty acids, acetate and hydrogen by acetogen-producing hydrogen using β-oxidation [27]. Repeated β-oxidation steps convert short chain fatty acids to acetate and hydrogen.

This research work exploits the combined favorable hydrogen production conditions as result of methanogenic inhibition due to OA and low pH conditions. Very few studies have been published on hydrogen production using OA incubated cultures for various periods of time. Hence, the main objective of this work was to access hydrogen production from glucose fermentation using OA incubated cultures for varying periods at 37 °C and pH 5.0.

2 Materials and Methods

Inoculum cultures were collected from the Little River Wastewater Treatment Facility in Windsor, Ontario, as well as from the ethanol processing facility in Chatham, Ontario. All microbial experiments to determine the consumption and production of hydrogen have been performed with cultures derived from the ethanol production facility (Designated as mother reactor A). In reactor A, increments of 5000 mg/L glucose and 100 mg/L sulfate were added on a weekly basis to enrich the methanogenic and SRB populations. Eventually, glucose and sulfate concentrations were fixed at 2000 and 1500 mg/L, respectively. Reactor A (8 L semi-continuous) containing 30,000 mg/LVSS was maintained at 37 ± 2 °C. Inoculum from Reactor A was diluted with basal media into a 4 L semi-continuous reactor (Reactor A1) to obtain 5,000 mg/LVSS. The performance of the culture in both reactors (A and A1) was assessed by monitoring the VFA levels, gas production, alkalinity (as $CaCO_3$ mg/L) and VSS/TSS ratio [1]. The reactor temperatures (37 ± 2 °C) were maintained using a thermal tape wrapped around the reactors wall and a variable transformer was used for temperature control.

After glucose was fed (on a weekly basis), the quantity of gas produced was measured over 7 days. Inocula characterization studies have also been conducted to track selected microbial activities. In the characterization experiments, glucose degradation and removal are studied, resulting in methane or methane plus sulphide (in the presence of sulphate). Acidogenesis was defined on the basis of glucose degradation profiles; acetogenesis was monitored by the pattern of formation and removal of VFAs; methanogenesis was monitored by methane levels in cultures; and sulfidogenesis was monitored by the study of sulphate degradation patterns. The characterization experiments were performed in batch reactors comprising 2000 mg/LVSS at 37 °C. All the characterization batch reactors have been prepared in triplicates.

The experiments were designed to investigate the impact of LCFA (OA) on the flow of electron fluxes in an anaerobic mixed culture in the absence of an inorganic electron receptor. The experimental design consisted of the following conditions: (1) Control incubation experiments with LCFA (OA) over a period of 32 days and (2) Incubation experiments with LCFA (OA) and glucose over a period of 32 days. The novelty of this work was to explore hydrogen production using varying incubation periods and to assess the effect of degradation of the parent LCFA on hydrogen production. LCFAs are degraded and removed from the anaerobic cultures within 20–25 days and hence, maximum incubation duration of 25 days was selected to determine the minimum dosage (quantity of LCFAs) that should be added to the cultures for maintaining the high hydrogen yields and also to determine the effect of LCFAs β-oxidation by-products. A pH of 5.0 was maintained using ethanosulfonic acid monohydrate (MES) ($C_6H_{13}NO_4S$, 0.07 M). Control experiments with LCFA (OA) were performed over a span of 32 days. In incubation experiments with LCFA (OA) plus glucose, six triplicate sets (6 incubation periods ranging from 0 to 25 days with an increase of 5 days) of reactors were prepared and injected with LCFA (2000 mg/LOA) (TCI, USA) on day 0. Glucose (5000 mg l-1) (ACP Chemicals, Montreal, Quebec) was injected on the 0th, 5th, 10th, 15th, 20th, and 25th days, respectively, in set 1, 2, 3, 4, 5 and 6 and analyzed for headspace gases, glucose, VFAs and LCFAs for 7 days following each glucose injection.

The objective of the control experiments with LCFAs (OA) was to access the extent of the degradation of LCFAs and to determine whether the accumulation of hydrogen was due to the degradation of LCFAs. Recall the objectives for carrying out these experiments with LCFA plus glucose were to analyse the effect of LCFAs (OA) on the production of hydrogen; to evaluate the effect of different LCFA (OA) incubation periods; to assess the effect of the degradation by-products of OA on the diversion of electron equivalents away from MPB; and to decide whether hydrogen accumulation is feasible amid degradation of the parent LCFAs into LCFA by-products. In addition to the LCFA (OA) controls, three sets (0–10, 10–20, and 20–30 days) of glucose regulation were prepared and analysed for glucose degradation and by-product formation over the entire experimental period.

Analytical parameters consisted of solutes (VFAs, sulfate, glucose, and LCFAs) and headspace gases (H_2, CH_4 and CO_2). Liquid samples were purified before they could be analyzed. The processing procedure adopted for VFAs, sulfate and glucose were the same in all the experiments. A liquid extraction method was adopted for LCFA recovery using MTBE: Hexane (1:1) [18].

A common procedure was adopted for the sampling and processing of samples for VFAs, sulfate and glucose. At selected time intervals, samples were withdrawn using a 2.5 ml syringe, 0.5 ml samples were transferred into 7.5 ml culture tubes containing 4.5 ml of grade water. The 10 times diluted samples were centrifuged at 1750 g for 5 min to remove biological and inorganic solids. The centrate was filtered using 2 filters connected in series. The first filter consisted of a 25 mm diameter syringe filter holder fitted with a 25 mm diameter 0.45 μm polypropylene membrane and the second filter was a 1 ml polypropylene cartridge tube with a 20 μm polyethylene frit and filled with 100 to 200 mesh, sodium resin. The filtrate was transferred to a 5.0 ml

polypropylene vial and stored at 4 °C prior to analysis. Initial glucose degradation rates were calculated using Graphpad Prism software using a non-linear regression by a one-phase exponential decay model.

3 Results

Hydrogen production from glucose was assessed using 6 sets of triplicate cultures incubated to 2000 mg/LOA for varying periods (Fig. 1). The incubation times varied from 0 to 25 days in 5 days consecutive increments. Significantly high levels of

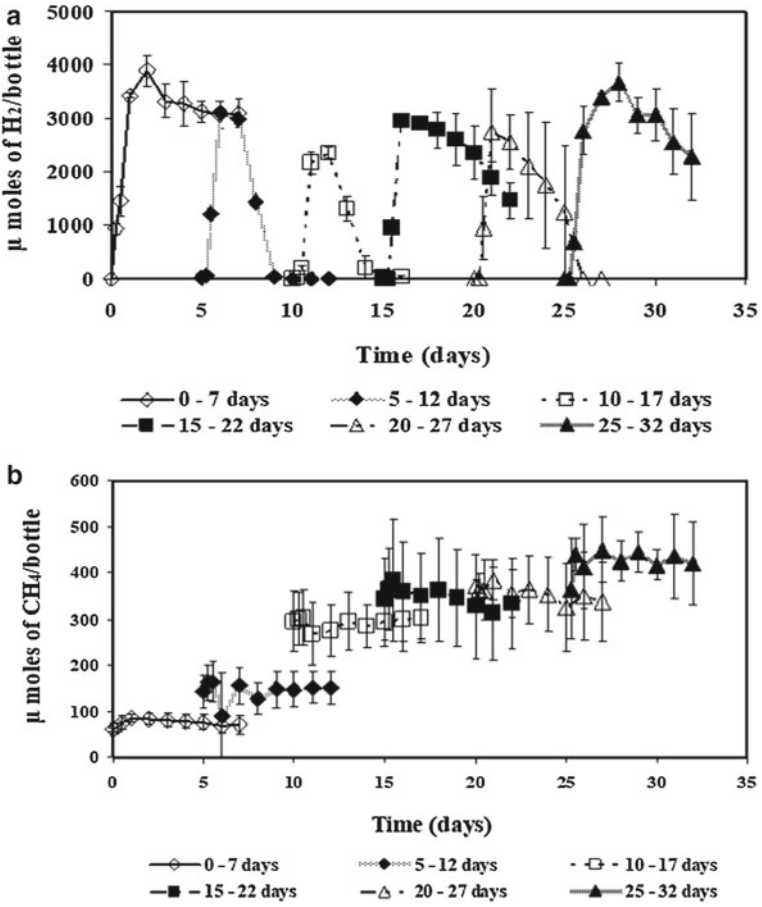

Fig. 1 Hydrogen and methane production in cultures receiving 2000 mg/LOA plus 5000 mg/L glucose. (A = Hydrogen; B = Methane. Values shown are mean and standard deviation for triplicate samples)

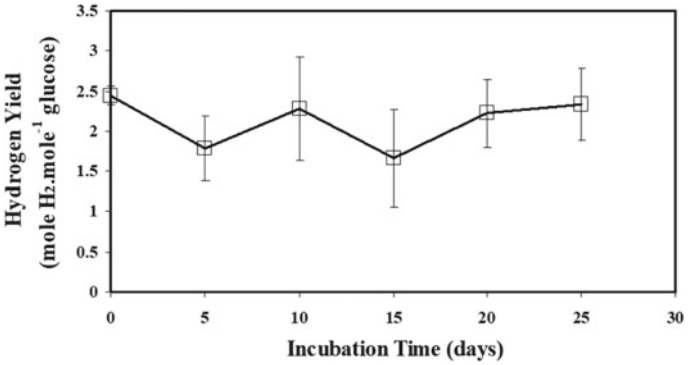

Fig. 2 Effect of varying OA incubation time on hydrogen yield for cultures receiving 2000 mg/LOA plus 5000 mg/L glucose. (Values shown are mean and standard deviation for triplicate samples)

hydrogen were detected in all the cultures receiving OA plus glucose for all the conditions examined (Fig. 1a). Hydrogen levels peaked on day 1 in all the OA incubated cultures receiving glucose. The maximum hydrogen yield (2.44 ± 0.12 mol H_2 mole^{-1} glucose) was observed in cultures incubated with OA for 0 days and those incubated with for 25 days (2.34 ± 0.45 mol H2 mole^{-1} glucose). Tukey's paired comparison test procedure at 95% confidence level was used to compare the hydrogen yield means [4]. Statistically similar yield values were observed in all the OA incubated cultures. In addition, the trend in hydrogen yields with increasing OA incubation time is shown in Fig. 2. No particular trend was observed in hydrogen yield with increase in incubation time. For all the conditions examined, the average hydrogen yield was 2.12 ± 0.44 H2 mole^{-1} glucose.

Controls containing OA were analyzed to confirm that there was no contribution to the hydrogen yield from hydrogen resulting from OA degradation. A negligible quantity (<1% of the cultures receiving glucose plus OA) of hydrogen was detected in the controls receiving only OA (Fig. 4a) between day 1 and day 4 and after day 4, the levels were undetectable. Control cultures were prepared with glucose to ensure methanogenesis was not inhibited over the duration of the study. Large quantities of methane reaching up to approximately 1268 μmoles were produced while no hydrogen was detected in cultures receiving only glucose (Fig. 3). In the controls receiving OA only, no significant methane (<72% of glucose controls) production was detected when compared to the glucose controls (Fig. 4b). After peak hydrogen levels in the OA incubated cultures for 5, 10 and 20 days were attained, the levels decreased and reached undetectable levels after day 6. The quantity of hydrogen detected on day 7 in the OA incubated cultures for 0 day was 66% of the maximum quantity. In comparison, the residual quantity was 30% of the maximum hydrogen production in the OA incubated cultures for 15 and 25 days.

Methane production profiles in OA incubated cultures receiving glucose are shown in Fig. 3b. The methane levels increased with increasing incubation times in the OA incubated cultures receiving glucose; however, the quantity of methane produced

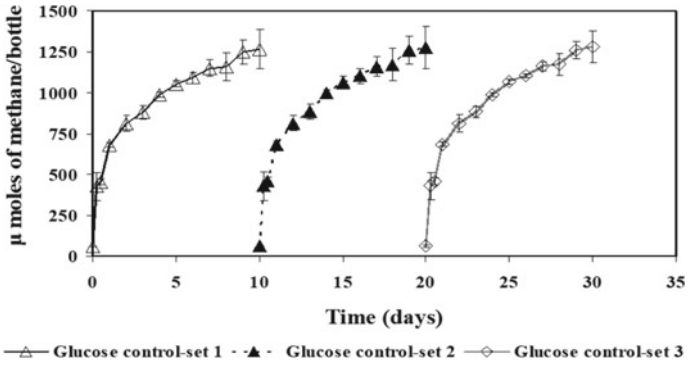

Fig. 3 Concentration profiles for methane control cultures receiving 5000 mg/L glucose. (Values shown are mean and standard deviation for triplicate samples)

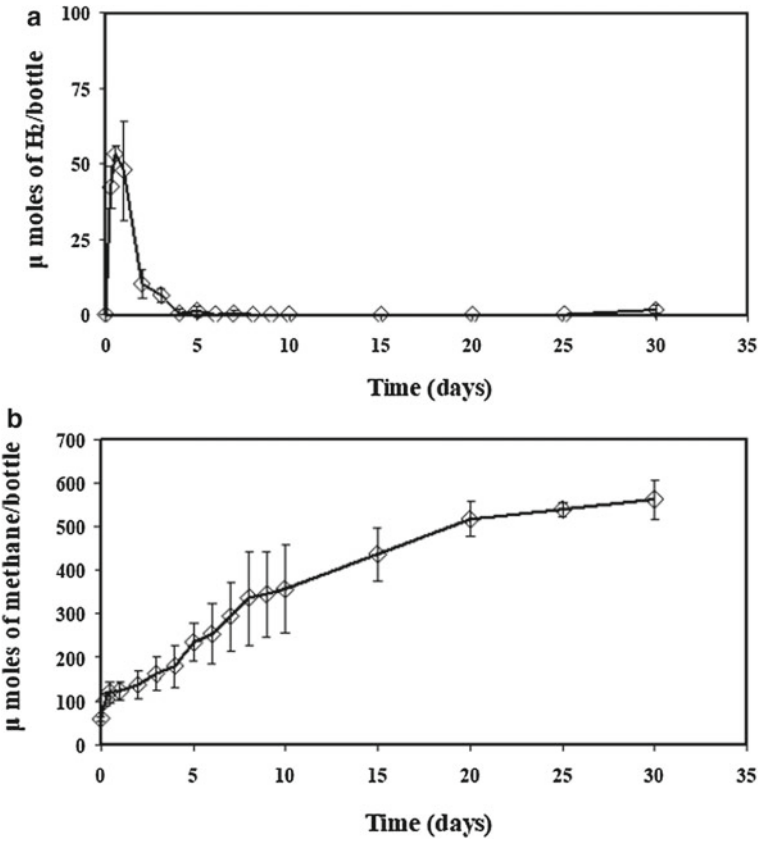

Fig. 4 Concentration profiles for control cultures receiving 2000 mg/L OA. (A = Hydrogen; B = Methane; Values shown are mean and standard deviation for triplicate samples)

was significantly less compared to the methane levels in the cultures receiving only glucose. The maximum quantity of methane was observed in the OA incubated cultures for 25 days, which was less than approximately 70% of the glucose controls. No increase in methane production was observed in any of the OA incubated cultures after glucose injection, while hydrogen was produced. In addition, an increase in methane content was not accompanied with a decrease in hydrogen production.

OA degraded via β-oxidation mechanism to saturated LCFAs bearing carbon atoms ranging from 16 to 12, acetate and hydrogen. The appearance of palmitic, myristic and lauric acid were reported in previous studies on OA degradation [18, 28]. Plamitic acid was the most abundant by-product from OA β-oxidation. OA β-oxidation by-products also inhibited methanogenic organisms when OA was completely degraded and removed from the cultures. Oleic acid exerts a greater inhibitory effect on methanogens than myristic [5, 7, 8] and palmitic acids. Of the β-oxidation by-products detected, lauric acid exerted highest inhibition, which was evident from the hydrogen yields (2.34 ± 0.45 mol H_2 mole^{-1} glucose) in the cultures where lauric acid was predominant (Fig. 5). The hydrogen yields were only 4% less in the cultures where hydrogen was produced under elevated levels of lauric acid compared to cultures where OA was predominant. In granulated methanogenic microbial communities fed with acetate, lauric acid and OA exerts a greater degree of inhibition when compared to myristic acid [17]. In this study, methanogenic inhibition was due to the combined effect of OA or LCFA degradation by-products in the respective incubation studies. However, no SA was detected in any of the cultures, which could be due to two main reasons, either saturation of OA was not required before β-oxidation [5, 8] or the saturation took place inside the cells.

Varying hydrogen yields ranging between 1.66 ± 0.59 to 2.44 ± 0.12 mol H_2 mole^{-1} glucose observed in the OA incubated cultures with incubation periods from 0 to 25 days were likely due to the effect of different OA degradation by-products

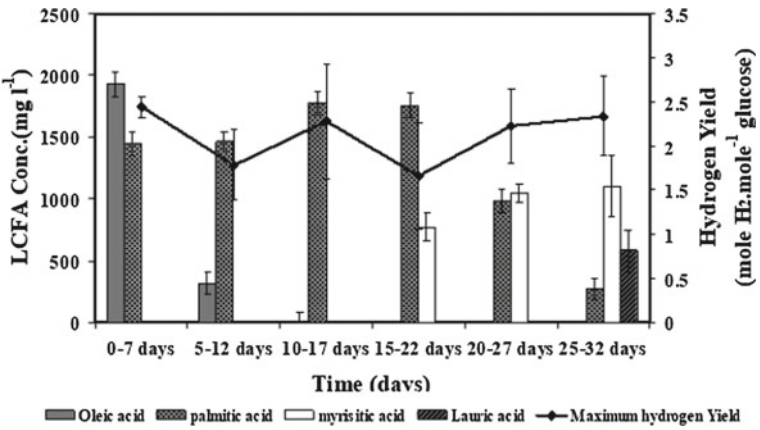

Fig. 5 Hydrogen yields as a function of OA β-oxidation by-products in the OA incubated cultures. (Values shown are mean and standard deviation for triplicate samples)

present in the respective cultures. OA likely exerted a higher degree of inhibition on the methanogenic population compared to its degradation by-products. The latter was clear considering the peak hydrogen yields in the presence of OA (in 0 days OA incubated cultures before injecting glucose) (Fig. 5) and slow hydrogen removal after peak quantities were detected. Examining the effect of longer incubation durations was important to assess the effect of OA degradation and β-oxidation by-products on hydrogen yields. Gurukar [12] and Chowdhury [6] reported lower hydrogen yields than the maximum yields achieved in this work with OA unincubated cultures (0-day incubations). In their work, the effect of longer OA incubation on hydrogen production was not assessed. In this work, the average hydrogen yield in the OA incubated cultures (0–25 days incubations) was 2.12 ± 0.44 mol H_2 mole^{-1} glucose, hence, hydrogen yields were not affected by the increasing incubations.

The maximum hydrogen yields produced in this work (2.44 ± 0.12 mol H_2 mole^{-1} glucose) was greater than the yields reported in studies on hydrogen production at low pH by Mariakakis et al. [21], Fang and Liu [10], Fang et al. [11] and Khanal et al. [16]. At pH 5.5, 2.1 mol H_2 mole^{-1} glucose was reported [10, 11]]. Khanal et al. [16] reported a maximum yield of 1.7 mol H_2 mole^{-1} glucose in a pH range of 4.5 to 6.5.

4 Conclusions

Hydrogen production from glucose fermentation was examined using mixed anaerobic cultures incubated to 2000 mg/L OA for varying periods (0 to 25 days in 5 days consecutive increments) at 37 °C under low pH conditions (pH 5). The conclusions from this work are as follows.

1. Hydrogen was produced and accumulated in all cultures incubated with OA.
2. Based on the hydrogen yields, OA and lauric acid inhibited methanogenic activity to the same extent. However, the inhibitory effect due to myristic and plamitic acids was less.
3. A maximum yield of 2.44 ± 0.12 mol H_2 mole^{-1} glucose was observed in cultures where OA was predominant. During the experiment, lauric acid emerged as a potent methanogenic inhibitor with a yield of 2.34 ± 0.45 mol H_2 mole^{-1} glucose. The average hydrogen yield detected over the duration of the study was 2.12 ± 0.44 mol H_2 mole^{-1} glucose.
4. The combined effect of OA and OA β-oxidation by-products, low pH and high hydrogen partial pressures inhibited the removal of the glucose degradation by-products.

Acknowledgements This research was funded by NSERC Canada.

References

1. APHA, AWWA, WEF (1998). Standard methods for the examination of water and wastewater. 20th ed. Washington, DC, USA
2. Benemann J (1996) Hydrogen biotechnology: progress and prospects. Nat Bitechnol 14:1101–1103
3. Bockris J (2013) The hydrogen economy: its history. Int J Hydrogen Energy 38:2579–2588
4. Box GEP, Hunter WG, Hunter JS (1978) Statistics for experimenters: an introduction to design, data analysis and model building. John Wiley and Sons Inc., Toronto
5. Canovas-Diaz M, Sanchez-Roig MJ, Iborra JL (1991) Myristic and oleic acid degradation by an acclimated anaerobic consortium: synergistic behavior. In: Grassi G, Collina A, Zibetta H (eds) Biomass for energy, industry and environment. 6th E.C. conference. Elsevier Applied Science, London, U.K. pp 580–581
6. Chowdhury N (2005) Microbial production of hydrogen under mesophilic conditions. Master's thesis, University of Windsor, ON., Canada
7. Dasa KT, Westman SY, Millati R, Cahyanto MN, Taherzadeh MJ, Niklasson C (2016) Inhibitory effect of long-chain fatty acids on biogas production and the protective effect of membrane bioreactor. Biomed Res Int 2016:7263974
8. Duarte S, Silva S, Salvador A, Cavaleiro A, Stams A, Alves M, Pereira M (2018) Insight into the role of facultative bacteria stimulated by microaeration in continuous bioreactors converting LCFA to methane. Environ Sci Technol 52
9. Enzmann F, Mayer F, Rother M, Holtmann D (2018) Methanogens: biochemical background and biotechnological applications. AMB Express 8(1):1
10. Fang HHP, Liu H (2002) Effect of pH on hydrogen production from glucose by a mixed culture. Bioresource Technol 82:87–93
11. Fang HHP, Liu H, Zhang T (2004) Biohydrogen production from wastewater. Water Sci Technol 4:77–86
12. Gurukar PS (2005) Hydrogen production from glucose by inhibiting hydrogenotrophic methanogens using C18 long chain fatty acids. Master's thesis, University of Windsor, ON, Canada
13. Hallenbeck PC, Benemann JR (2002) Biological hydrogen production; fundamentals and limiting processes. Int J Hydrogen Energy 27:1185–1193
14. Hanaki K, Matsuo T, Nagase M (1981) Mechanism of inhibition caused by long-chain fatty acids in anaerobic digestion process. Biotechnol Bioeng 23:1591–1610
15. Hwu C, Tseng SK, Yuan CY, Kulik Z, Lettinga G (1998) Biosorption of long-chain fatty acids in UASB treatment process. Water Res 32:1571–1579
16. Khanal SK, Chen W, Li L, Sung S (2004) Biological hydrogen production: effects of pH and intermediate products. Int J Hydrogen Energy 29:1123–1131
17. Koster IW, Cramer A (1987) Inhibition of methanogenesis from acetate in granular sludge by long-chain fatty acids. Appl Environ Microbiol 53:403–409
18. Lalman JA, Bagley DM (2001) Anaerobic degradation and methanogenic inhibitory effects of oleic and stearic acids. Water Res 35:2975–2983
19. Lalman JA, Bagley DM (2002) Effects of C18 long chain fatty acids on glucose, butyrate and hydrogen degradation. Water Res 36:3307–3313
20. Ma J, Zhao QB, Laurens LL, Jarvis EE, Nagle NJ, Chen S, Frear CS (2015) Mechanism, kinetics and microbiology of inhibition caused by long-chain fatty acids in anaerobic digestion of algal biomass. Biotechnol Biofuels 8:141
21. Mariakakis I, Krampe J, Steinmetz H (2012) Effect of pH control strategies and substrate concentration on the hydrogen yield from fermentative hydrogen production in large laboratory-scale. Water Sci Technol 65(2):262–269
22. Nandi R, Sengupta S (1998) Microbial production of hydrogen: an overview. Crit Rev Microbiol 24:61–84
23. Oh S-E, Ginkel SV, Logan BE (2003) The relative effectiveness of pH control and heat treatment for enhancing biohydrogen gas production. Environ Sci Technol 37:5186–5190

24. Petrova EV, Kukarskikh GP, Krendeleva TE et al (2020) The mechanisms and role of photosynthetic hydrogen production by green microalgae. Microbiology 89:251–265
25. Silva SA, Salvador AF, Cavaleiro AJ, Pereira MA, Stams AJ, Alves MM, Sousa DZ (2016) Toxicity of long chain fatty acids towards acetate conversion by Methanosaeta concilii and Methanosarcina mazei. Microb Biotechnol 9(4):514–518
26. Sung S, Raskin L, Duangmanee T, Padmasiri S, Simmons JJ (2002) Hydrogen production by anaerobic microbial communities exposed to repeated heat treatments. In: Proceedings of the U.S. DOE hydrogen program review, pp 1–17
27. Weng CN, Jeris JS (1976) Biochemical mechanisms in the methane fermentation of glutamic and oleic acids. Water Res 10:9–11
28. Wu L-J, Kobayashi T, Li Y-Y, Xu K-Q, Lv Y (2017) Determination and abatement of methanogenic inhibition from oleic and palmitic acids. Int Biodeterior Biodegradation 123:10–16
29. Xia A, Zhu X, Liao Q (2019) Hydrogen production from biological sources. In: Lipman T, Weber A (eds) Fuel cells and hydrogen production. Encyclopedia of sustainability science and technology series. Springer, New York, NY
30. Zhang Q, Zhang Z (2018) Biological hydrogen production from renewable resources by photofermentation. Adv Bioenergy 137–160

Data Analytics Applications for City Resilience Under Climate-Induced Hazards

M. Haggag, A. Siam, W. El-Dakhakhni, and L. Hassini

1 Introduction

Climate amplifies both the frequency and severity of various natural disasters that include floods, droughts, wildfires, ice storms, cyclonic storms, tornados and hurricanes [3, 10, 11]. In addition, Since 1960s, the number of climate-induced hazards worldwide has tripled [12]. The annual liabilities of the Disaster Financial Assistance Arrangement program in Canada have increased from *"$10 million in 1970–1995 to $110 million in 1996–2010 to $360 million in 2011–2016"* [8]. Subsequently, Canadian cities are experiencing, more than ever before, rapid physical transformations which disturb their basic functions. To maintain these functions, Canadian cities have to maximize the resilience of their comprising critical infrastructure systems in the face of these disasters. In that context, resilience can be defined as the ability of a system to bounce back to an original or more desirable state following any disturbance (60). Unfortunately, reaching system resilience under CID is considered a very farfetched goal that could only be realized if throughout disaster planning is conducted.

In that context, the influence of climate change uncertainties on long-lived infrastructure systems was explored in [5]. More specifically, infrastructure planning processes were reviewed to ensure that these systems can be more adaptable to

M. Haggag (✉) · A. Siam · W. El-Dakhakhni · L. Hassini
McMaster University, 1280 Main Street West, Hamilton, ON L8S 4L7, Canada
e-mail: haggagm@mcmaster.ca

A. Siam
e-mail: siamas@mcmaster.ca

W. El-Dakhakhni
e-mail: eldak@mcmaster.ca

L. Hassini
e-mail: hassini@mcmaster.ca

S. Walbridge et al. (eds.), *Proceedings of the Canadian Society of Civil Engineering Annual Conference 2021*, Lecture Notes in Civil Engineering 249,
https://doi.org/10.1007/978-981-19-1061-6_38

climate change uncertainties. The proposed generic climate resilient planning process includes first, acknowledging climate change as a process; second, gathering more information and facts about climate change; and third, planning for flexibility of infrastructures when faced with climatological hazards. Furthermore, components of vulnerability and resilience assessments were selected in [4] with a focus of analyzing exposure to floods, and subsequently five steps of analysis were demonstrated using a geographic information system. Additionally, an online algorithm for incoming alarm flood early prediction was proposed [6]. Moreover, reviews on what was learnt in the last few decades with respect to the predictability of climate and weather extremes were presented in [7]. According to these reviews, improved forecasts and monitoring of extreme weather and climate are necessary if CIDs' impacts are to be alleviated.

Consequently, a pressing need to assess disasters both on the temporal and spatial levels strongly exists. Thus, this work aims to investigate historical CIDs in an attempt to derive meaningful information and assess disaster probability on the spatial level to achieve the ultimate goal of facilitating critical infrastructure systems resilience in Ontario. The current analysis will focus on Ontario's power infrastructure as one of the utmost critical infrastructure systems that all other systems (i.e., water, transportation, telecommunications, etc.) depend on for their operations. The work will be divided into three folds, the first fold involves employing descriptive analytics to derive meaningful information from a CID dataset, while in the second fold unsupervised machine learning will be employed to formulate different disaster probability zones across Ontario. In the last fold, the resilience of hydroelectric power generators across Ontario will be deliberated based on the disaster probability zones evaluated previously. The goal of this work is to identify vulnerable power infrastructure components in Ontario, and subsequently assess their resilience in the face of CID in an attempt to bridge the gap towards achieving city resilience.

2 Data Description

The Canadian Disaster Database used in this paper was created by Public Safety Canada [9]. It tracks about 1000 significant disaster events (i.e., natural and technological events). For each of these events, the database specifies event type, place, start date, and end date, incurred cost, injured and evacuated people and number of fatalities. As this paper focuses only on CID in Ontario, the database was filtered to include only Ontario's records which are in total 137 events. In the second fold, among different CID types only flood, storm, tornado and hurricane disasters were considered, thus, the database was further filtered to include only 95 records. Finally, in the third fold of this paper the locations of 24 hydroelectric power generators which are specified by Ontario Power Generation were used to assess the resilience of Ontario's power infrastructure.

3 Methodology

The purpose of the descriptive analysis herein is to answer key questions related to CID, among these are: Which provinces are more at risk and from which type of disaster?; Which disasters are considered more frequent than others?; What are the average durations of these disasters and does the duration depend on the disaster type?; What is the yearly trend of these disasters and if they increase, is that increase linear or exponential?; Does the season or month influence the disaster type?; Which disasters cause more fatalities and which ones cause more injuries or evacuations?; Are there specific disasters that contribute to rehabilitation cost more than others? The second fold in this work involves disaster spatial analysis using an unsupervised learning technique (i.e., clustering). The analysis aims to spatially assess CID in Ontario. The clustering model divides Ontario into different disaster probability zones and subsequently, the probability of CID occurrence given a specific zone can be evaluated. The methodology for the clustering model is given in Fig. 1. The first step in developing the clustering model involved determining the latitude and longitude of the disasters' locations. As some disasters were spread across more than one location in Ontario, the number of data points considered in the model jumped to 199 instead of 95 data points. Clustering was performed using K-Means and Model-Based Clustering. For K-Means, the number of cluster (i.e., k) was changed from 1 to 10 and within cluster sum of squares was calculated to evaluate model performance and consequently, pick the model with the best number of clusters to represent the data. As for model-based clustering, Bayesian Information Criterion (BIC) was used to assess the model with the best number of clusters. After selecting the model, the probability of disaster occurrence in each cluster was calculated using the number of occurrences recorded within each zone's coordinate limits. Finally, the probability of occurrence of each disaster (i.e., floods, winter storms, thunderstorms, hurricanes and tornados) per zone was evaluated. Finally, the last fold of this work involves laying 24 hydroelectric power generators that are spread across Ontario on the previously determined CID probability zones in an attempt to assess their vulnerability and maximize their resilience accordingly.

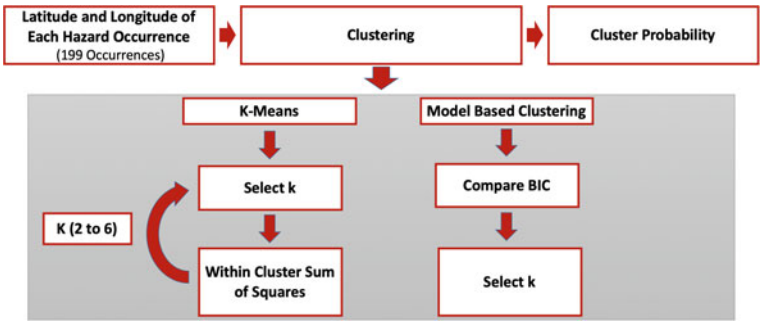

Fig. 1 Clustering model methodology

4 Results and Discussions

Figure 2 shows CID distribution by both province and type. Ontario was the province with the most occurrences recorded, followed by British Columbia, Quebec and Alberta. The significantly higher number of CID in Ontario compared to all other provinces can be attributed to the fact that Ontario is the most populated province with a population of 14.7 million in [2], which is almost double the population in Quebec, the second highest populated province in Canada [2]. Within most provinces, floods accounted for the most frequent CID. Furthermore, Ontario proved to be the province with the most tornado, thunderstorm and winter storm occurrences. Being the province with the overall most frequent CIDs, Ontario was chosen to be the focus of the current work.

Floods are the most frequent type of CID and it accounts for almost 50% of disasters recorded. Wildfires come second, and tornados winter storms, thunderstorms come third, fourth and fifth, respectively. Figure 3 shows hazard distribution by duration and type. Almost 70% of recorded disasters lasted for just a day or less. Moreover, about 25% of the recorded disasters lasted from 2 to 3 days, these disasters were mostly floods, winter storms, thunderstorms and wildfires. Moreover, almost 80% of the CID that lasted from 3 to 8 days were floods.

As per Fig. 4, most of CID occurred in May followed by April and January. Floods were more frequent in April, May and March and tornados were most frequent in August while wildfires were most frequent in May and thunderstorms were more frequent in both July and August, while winter storms were more frequent in January and December. Figure 5 shows CID distribution by year and type. The total number of disasters is increasing rapidly on a yearly basis with 2008 being the year with the highest number of records. Finally, floods, wildfires, winter storms and thunderstorms have increased in frequency since the 2000s.

In fold two, K-Means algorithm was used to cluster the records. The total within cluster sum of squares was calculated for different number of clusters and it was found that the model with four clusters is the best model to represent the data because any

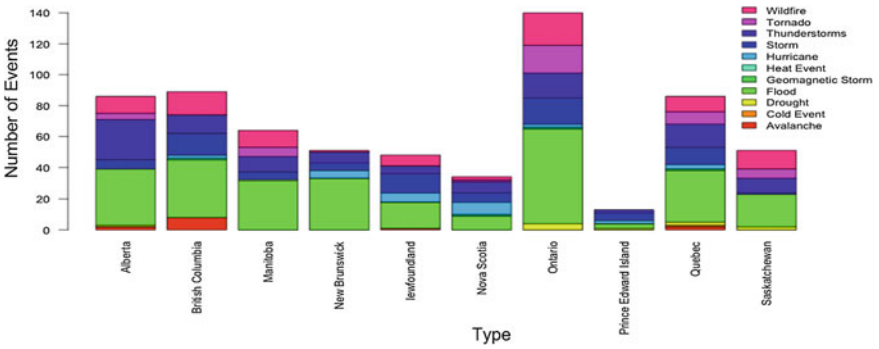

Fig. 2 CID distribution by province and type

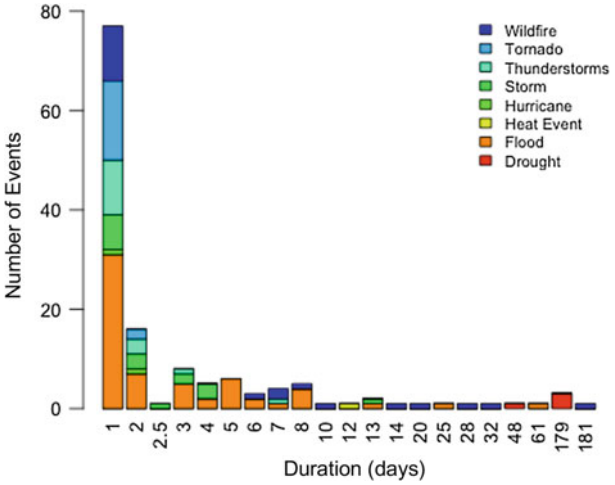

Fig. 3 CID distribution by duration and type

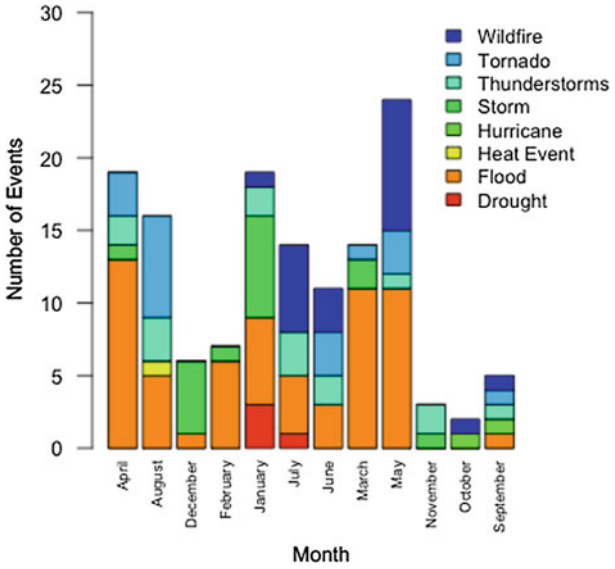

Fig. 4 CID distribution by month and type

further clustering will result in a very small decrease in the total within cluster sum of squares. Subsequently, the cluster plot for the model with 4 clusters is shown in Fig. 6, Cluster 1 (i.e., the green cluster), 2 (i.e., the red cluster), 3 (i.e., the pink cluster) and 4 (i.e., the blue cluster) have 28.6%, 48.7%, 12% and 10.6% CID probability, respectively.

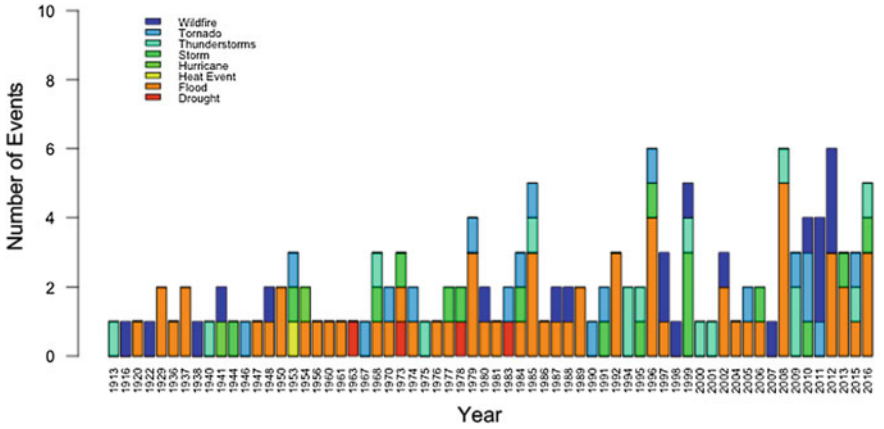

Fig. 5 CID distribution by year and type

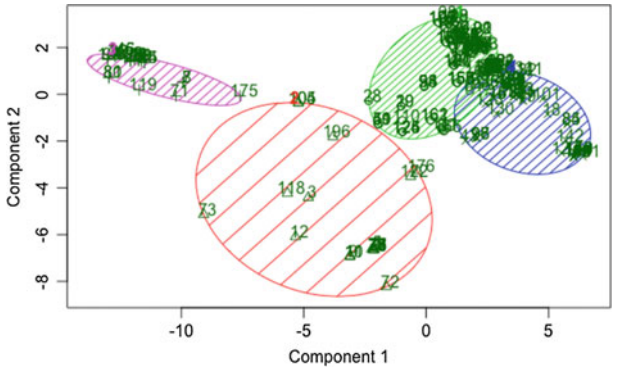

Fig. 6 The four clusters cluster plot

After employing K-Means algorithm, Model Based Clustering was also employed, the BIC showed that the recommended model fitted to the data was VEV (ellipsoidal, equal shape) model with 9 components. Comparing the 9 clusters defined by model-based clustering with the four clusters defined by k-means algorithm, for the region of 42° to 46° latitude and −85° to −75° longitude, the former algorithm fitted 5 clusters while the later one fitted only 2 clusters for the same area. This shows that the model-based clustering algorithm is not the best technique to represent the data herein as it resulted in over clustering. Consequently, the four clusters proposed by the k-means model are mapped as four zones on Ontario in Fig. 7 where Zone 2 (red zone) represents the highest CID probability zone in Ontario. This zone (Zone 2) includes the entire Greater Toronto Area and Niagara Falls. Zone 1 (orange zone), on the other hand, is ranked as second with respect to CID occurrence and includes

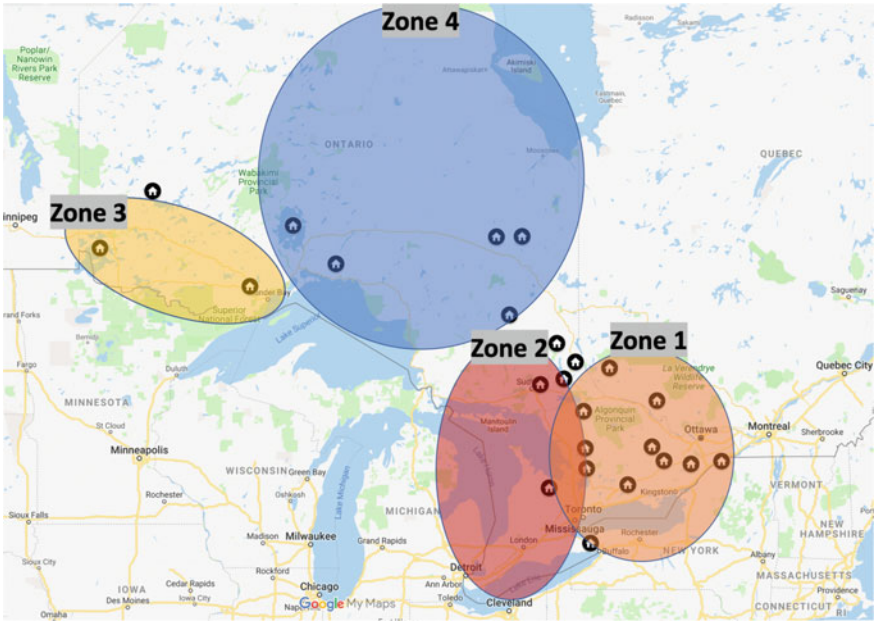

Fig. 7 The four zones mapped on Ontario

Ottawa and Kingston regions. Furthermore, Zone 3 (blue zone) 3 and Zone 4 (yellow zone) have the least probability of CID which is almost quarter that of Zone 2.

Table 1 shows the probability of each CID type in each of the predefined zones. Floods are more likely to occur in zone 2 followed by zones 1, 4 and 3 respectively, while winter storms are more likely to happen in zone 2 followed by zones 3, 1 and 4 respectively. On the other hand, zone 1 has the highest probability of thunderstorms followed by zones 2 and 4, respectively, while zone 3 proved to be thunderstorm free for the examined period. As for tornados, zone 2 is more likely to be hit by tornados compared to zone 1, while zones 3 and 4 experienced no tornados in the examined period and finally, hurricanes have the same likelihood to occur in both zones 1 and 2, while both zones 3 and 4 proved to be hurricane free.

Table 1 Probability of CID in each zone

	Zone 1	Zone 2	Zone 3	Zone 4
Flood	0.21	0.5	0.12	0.16
Winter Storm	0.28	0.38	0.31	0.03
Thunderstorm	0.76	0.19	0	0.05
Hurricane	0.5	0.5	0	0
Tornado	0.22	0.78	0	0

The 24 hydroelectric power generators are shown in Fig. 6 as black home icons. Among the 24 generators, 8 generators (33.33%) fall in Zone 3 and Zone 4. Among these 8 generators, the 3 generators that fall in Zone 3 have 31% probability of winter storm occurrence which indicates their vulnerability as power infrastructure is extremely vulnerable to both winter/snowstorms and thunderstorms. The reason is that these storms can cause the failure of more than two system components at once, which is more than the capacity the system is designed to handle (i.e., > n−2). On the other hand, about 8 generators fall in Zone 2 which is the highest CID probability zone, this indicates the extensive vulnerability of these generators given the fact that Zone 2 has winter storm and thunderstorm probabilities of 38% and 19%, respectively. The 50% flood probability of Zone 2 doesn't affect much the vulnerability of generators, but the very high (i.e., 78%) probability of tornados adds to the high vulnerability of these components. The last 8 generators which are in Zone 1 are most vulnerable to thunderstorms which have a 76% probability of occurrence I. that zone. Thus, the most vulnerable generators are the ones located in Zone 1 and Zone 2 as the highest probabilities of thunderstorms and winter storms are found in these zones, respectively. This indicates the need for resilience assessment and throughout planning to make sure these generators won't lose their functionality under CID. Two notions have to be planned for to be able to consider these generators as resilient components of the power infrastructure, which are: redundancy and resourcefulness [1]. Redundancy ensures the availability of replacement components within the generator that would allow it to perform smoothly in time of disasters, while resourcefulness ensures the availability of resources that can help in timely detection of disasters before they occur, and throughout diagnosis of damage if any. Figure 8 shows the change in system performance when the notions of redundancy and resourcefulness are adopted for the most vulnerable system components. The non-resilient system lost 70% of its functionality and took more time to be restored (i.e., $t_{nr}-t_d$), whereas the resilient system lost only 30% of its functionality and was restored in much less time compared to the non-resilient system (i.e., t_r-t_d). Subsequently, after maximizing the redundancy and resourcefulness of the system, the area under the functionality curve decreased dramatically. The shrinkage in the area under the system functionality curve can be attributed to an increase in the ability

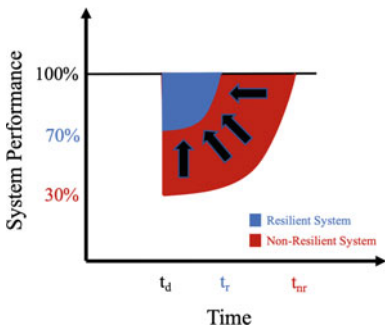

Fig. 8 System performance (resilient versus non-resilient)

of the system to stay functional under a disaster (i.e., robustness), and a decrease in the time it takes the system to get back to its initial operations after an extreme event (i.e., rapidity).

5 Conclusions

In this work, descriptive analytics was employed to answer several significant questions related to CID in Ontario, while unsupervised machinic learning was employed to evaluate the probability of CID (i.e., floods, storms, tornados and hurricanes) and thus, assess power infrastructure components resilience in Ontario. Based on the descriptive analytics results, Ontario was the province with the most occurrences recorded. The analysis also showed that the total number of CID is increasing rapidly on a yearly basis with 2008 being the year with the highest number of disasters. Clustering was used to divide Ontario into different CID probability zones; thus, four different probability zones were uncovered with the highest probability zone being the one encompassing the Greater Toronto Area and Niagara Falls, and the second highest zone included both Ottawa and Kingston regions. The 24 hydroelectric power generators in Ontario were laid on the clustered zone and the most vulnerable generators were specified. Subsequently, two notions were proposed to decrease component vulnerability, and thus increase system resilience, being redundancy and resourcefulness. This paper is considered as a step in CID prediction, based on historical hazard data, global climate models, and climate change measures, in an attempt to maximize critical infrastructure systems resilience and mitigate CID risks on cities.

Acknowledgements The authors are grateful to the financial support of the Ontario Trillium Scholarship Program and the Natural Sciences and Engineering Research Council (NSERC) of Canada. The authors would also like to acknowledge the fruitful discussions with the research teams of the NSERC-CaNRisk-CREATE program and the INViSiONLab.

References

1. Bruneau M, Chang S, Eguchi R, Lee G, O'Rourke T, Reinhorn A, Von Winterfeldt D (2003) A framework to quantitatively assess and enhance the seismic resilience of communities. Earthq Spectra 19(4):733–752
2. Canada—Population Projection by Province 2020–2043 | Statista (2020)
3. Climate Change | EU Science Hub (2018). https://ec.europa.eu/jrc/en/research-topic/climate-change
4. Fekete A, Tzavella K, Baumhauer R (2017) Spatial exposure aspects contributing to vulnerability and resilience assessments of urban critical infrastructure in a flood and blackout context. Nat Hazards 86(1):151–176. https://doi.org/10.1007/s11069-016-2720-3
5. Giordano T (2012) Adaptive planning for climate resilient long-lived infrastructures. Utilities Policy 23:80–89. https://doi.org/10.1016/j.jup.2012.07.001

6. Lai S, Yang F, Chen T (2017) Online pattern matching and prediction of incoming alarm floods. J Process Control 56:69–78. https://doi.org/10.1016/j.jprocont.2017.01.003
7. Nicholls N (2001) Atmospheric and climatic hazards: improved monitoring and prediction for disaster mitigation 137–155
8. Public Safety Canada (2017) 2016–2017 evaluation of the disaster financial assistance arrangements. https://www.publicsafety.gc.ca/cnt/rsrcs/pblctns/vltn-dsstr-fnncl-ssstnc-2016-17/vltn-dsstr-fnncl-ssstnc-2016-17-en.pdf
9. Public Safety Canada (2019) The Canadian disaster database (2019). https://www.publicsafety.gc.ca/cnt/rsrcs/cndn-dsstr-dtbs/index-en.aspx
10. Shaftel H (2018a) Causes | facts—climate change: vital signs of the planet. NASA's Jet Lab Propulsion Laboratory California Institute of Technology. https://climate.nasa.gov/causes/
11. Shaftel H (2018b) Evidence | facts—climate change: vital signs of the planet. NASA's Jet Lab Propulsion Laboratory California Institute of Technology. https://climate.nasa.gov/evidence/
12. World Health Organization (2018) Climate change and health. https://www.who.int/news-room/fact-sheets/detail/climate-change-and-health

The PIEVC Protocol for Assessing Public Infrastructure Vulnerability to Climate Change Impacts: National and International Application

D. Sandink and D. Lapp

1 Introduction

The rate of climate warming in Canada is twice that of the global average, with faster rates of warming in Canada's arctic regions [4]. Climate change impacts, including changing temperature and precipitation regimes and increasing frequency of extreme events, present a significant risk to the built environment across the country [4, 11]. Already climate-related hazards and disaster events represent a significant disruption to critical services provided by buildings and infrastructure in Canada. For example, disaster events driven by a combination of flood, hail, high wind, and wildland-urban interface fire resulted in ~$11 billion in insured losses in Canada from 2015 to 2019 [7]. These damages were largely attributed to impacts on residential and commercial property. Significant uninsured losses attributed to the above hazards include most coastal and river flood damage, interruptions in critical services, societal impacts caused by displacement during and after disaster events, and a multitude of additional social, environmental and cultural effects of disasters are not represented in disaster loss figures (see for example [19]).

Responding to historical climate events and potential future impacts of climate change, infrastructure and asset owners have increasingly worked to develop and apply formalized processes to account for the potential impacts of climate change on built, natural, and human systems [5, 8, 14, 17, 18]. Further, given the role of the engineering community in designing, managing and operating infrastructure, the engineering community can make critical contributions with respect to understanding and managing these risks, and ultimately offering evidence-based risk management

D. Sandink (✉) · D. Lapp
Institute for Catastrophic Loss Reduction, Toronto, Canada
e-mail: dsandink@iclr.org

D. Lapp
e-mail: dlapp@iclr.org

S. Walbridge et al. (eds.), *Proceedings of the Canadian Society of Civil Engineering Annual Conference 2021*, Lecture Notes in Civil Engineering 249,
https://doi.org/10.1007/978-981-19-1061-6_39

policy recommendations under changing climate conditions [9]. The PIEVC Protocol was developed by Engineers Canada with the support of NRCan as a tool to identify inherent risks of failure or damage to infrastructure systems associated with climate change and climate-related hazards. It was developed to meet the needs and professional obligations of engineers to identify and address climate impacts through climate consideration in professional practice [15].

The PIEVC process assesses the negative impacts of extreme weather and changing climate to physical infrastructure and its operation, and assists infrastructure decision makers in managing uncertainty associated with future climate change impacts. The scope of assessments includes the impact of the loss or damage that infrastructure would have on societal and worker health and safety, and economic, social and environmental factors of concern to the public served by the infrastructures. The Protocol was designed to assess all types and scales of civil infrastructures including buildings.

The Protocol uses the best information available for "project assessments" including design parameters, operational and maintenance data that include performance records from past severe climate events. It requires climate data and future projections of climate parameters provided by climate scientists/specialists and often delivered through nationally or regionally based climate services. It includes the engagement of infrastructure operators and maintenance staff who have intimate knowledge of the infrastructure and memories of impacts and corrective actions undertaken at the time to minimize the impacts of a climate event. This human element and engagement is critical to a credible and defensible assessment.

A multi-disciplinary, multi-stakeholder team is needed to assure a fulsome assessment. The team can be customized to focus on the priorities of the owner, but would normally include engineers (of one or more disciplines depending on the type of infrastructure), climate scientists, representatives of the infrastructure owner (such as risk manager, operator(s)) and other stakeholders (e.g. planners, managers, emergency response, decision and policy makers, natural scientists) as required. It is a highly collaborative and iterative process that depends on the collective expertise, experience and perspective of these experts and stakeholders.

Further to the above, the Protocol supports "mixed methods" with respect to climate vulnerability assessment for infrastructure and buildings [5]. Vulnerability assessments conducted using the PIEVC Protocol typically rely on both quantitative and qualitative data and the process can be adjusted to reflect data and expertise available for any given assessment. Further, the processes may applied as either a "top-down," screening or narrow-scope assessment driven and completed by a small team of experts, or as a "bottom-up" approach, relying on insights and consensus drawn from a range of experts through facilitated workshops.

The Protocol's ability to facilitate top-down assessments is exemplified by its wide use to support "climate lens" and screening assessments (see for example [25]). Conversely, "bottom-up" assessments include those that rely on input gained from multiple stakeholder engagement workshops. Workshops may include systematic collection of input from a wide variety of infrastructure stakeholders, from political decision makers to operations staff with an equal say in workshop decision

processes (see for example [21], where building operators to medical practitioners were engaged in assessment workshops of a hospital building). Further, the Protocol may be applied for specific, highly localised infrastructures (see for example [20]—an airport assessment), as well as assessment for a variety of infrastructure types for extremely large geographic areas (see for example [26]—an assessment of multiple infrastructure types across the whole of the Northwest Territories).

2 The PIEVC Protocol

Engineers Canada began development of the PIEVC Protocol in 2005 in partnership with, and co-funding from NRCan. It involved the formation of technical and strategic guidance committees, comprised of a cross section of infrastructure and climate experts, federal, provincial, municipal government representatives, local utilities, various infrastructure owners, academics, standards organizations, and several non-government organizations involved in climate change adaptation. The development included an extended period of validation and refinement through the execution of case studies and a "learn by doing" approach across a wide variety of infrastructure types and types of owners—from large cities to small communities. The development was completed in 2012 with publication of Version 9 and the end of co-funding support from NRCan. The PIEVC Protocol was incorporated into an ongoing program (the "PIEVC Program") operated by Engineers Canada until 2020 when it was divested to a partnership including the Institute for Catastrophic Loss Reduction (ICLR), the Climate Risk Institute (CRI) and Deutsche Gesellschaft für Internationale Zusammenarbeit (GIZ) GmbH (the PIEVC Program Partnership).

The Protocol is a qualitative risk identification and assessment process that defines climate risks and vulnerabilities at a screening level. It is adopted from CAN/CSA Standard Q850-97 (R2009) Risk Management: Guideline for Decision-Makers [6]. Unlike quantitative risk tools, it does not require comprehensive nor complete data to undertake an assessment. The trade-off is that it does not provide quantitative estimates of risk, but rather "risk scores" that can be ranked into levels of risk, qualitatively described (and defined) with terms such as high, medium and low risk. It provides a high level understanding of climate risks that is often sufficient to support adaptation and resilience decision-making, especially for smaller infrastructures and for small communities. It can also inform more detailed quantitative risk assessments and help focus these types of studies on the key issues that may need deeper, more quantitative analysis before decisions can be made on action and budget allocation.

Through the PIEVC Protocol process, "infrastructure" is defined as a series of structural and non-structural components. Structural components are normally the physical sub-systems that are assembled to enable the infrastructure to operate—for example foundation, building envelop, roof, electrical and mechanical systems for buildings. Non-structural components include items such as the personnel that operate and maintain the infrastructure, policies and procedures as well as codes and standards, and local regulation. An additional layer of component definition

concerns the users of the infrastructure and/or the external suppliers of services to the infrastructure (e.g., utilities).

Each of these components interacts with, or is affected by, climate in varying ways and to varying degrees. Some components will only be affected or interact with certain climate elements. Understanding infrastructure component/climate interactions is a key element of the analysis. A further key element of the Protocol process is identifying the appropriate level of component definition. The more components that are defined, the larger the scope of effort to identify the climate-component interactions followed by the analysis of risk for each one. Normally components are defined at a system or sub-system level since further granularity does not provide additional insight for the level of effort required.

The scoping of the risk and vulnerability assessment is scalable in that the breadth and depth of the component definition can be limited. Scaling will affect what information is required and who should be involved. Ideally the stakeholders that should be at the table would represent or support all of the structural and non-structural elements of the infrastructure. However, in normal practice this is not always possible nor practical and it may not serve the interests of the infrastructure owner. It is important however to record components or stakeholders which were not considered, or who did not participate, and to include these limitations in the final assessment report.

2.1 The PIEVC Protocol Steps Explained

Figure 1 and Table 1 summarize the basic tasks within each step in the process. Preparation is key to a successful assessment with useable outcomes. Preparation includes understanding the type and location of infrastructure that is to be assessed. Step 1 requires the project parameters to be refined and adjusted to meet constraints such as budget, time and the detail needed from the assessment. The more components that are identified for assessment, the greater the depth and breadth of data compilation and analysis, with additional time and budget likely required. With respect to stakeholder engagement, many PIEVC assessments have organized a workshop of key stakeholders to achieve consensus on project definition while others have used interviews. The aim is gain a shared understanding and agreement of the scope to manage expectations and execution.

Step 2 requires working with the infrastructure owner/management as well as operations and maintenance personnel to secure items such as drawings, operational records, local codes, standards, jurisdictional constraints and so forth. The availability of local historical climate data and climate projections is another significant task that requires a climate specialist. Interviews with management and operational personnel are sometimes used in data and information collection. Understanding the condition of and where an infrastructure is in its life cycle is fundamental to the process.

In every assessment there are data gaps or missing information that must be supplemented by local knowledge and consultations with operations and maintenance personnel. Data gaps, either climate or infrastructure, can be augmented by

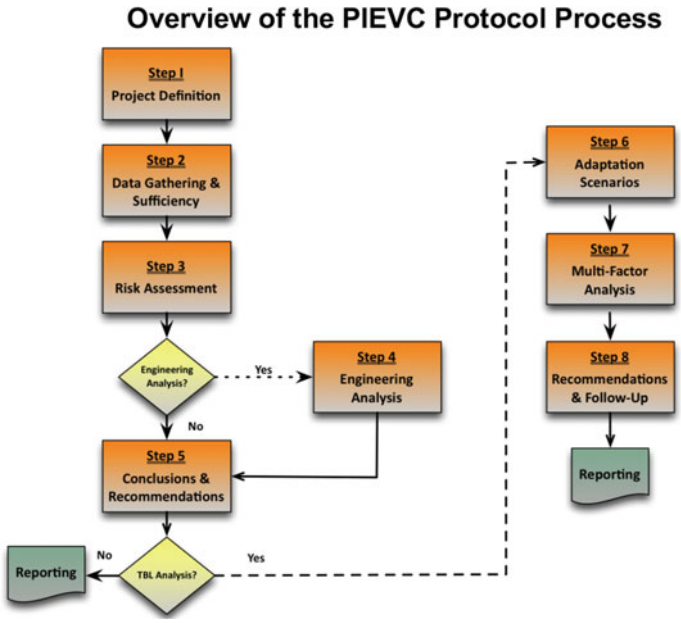

Fig. 1 Overview of the PIEVC protocol process

the experience and professional judgment of the assessment team members working with the infrastructure owner and their operations/maintenance personnel. Ideally these consultations and judgments are combined with, and informed by, a site visit.

Step 3 is normally carried out through one or more workshops where the stakeholders are brought together to define and score the consequences of exceeded climate thresholds. The climate specialist should have determined the likelihood score in advance so the focus of workshops is on consequences. Consequence scores are determined by consensus or voting procedures. The consequence scores are multiplied by the climate likelihood score to produce a climate risk score. The results are normally tabulated in a risk matrix—one for current climate and one for the future climate as a means to document results. The difference in the current and future climate score is the increase or decrease in risk attributed to climate change. Of greatest concern are increases in risk scores from current to future climate especially where the risk level is shifted into the range that is considered high. High risk interactions require earlier and possibly immediate adaptation action.

Step 4—Engineering Analysis is an optional step in the process. The analysis is complex and requires more engineering data on capacity and loading that may be limited or not available in some cases, and is limited to a few cases where the infrastructure component is critical to the integrity or operation of the infrastructure.

Once the risk is identified, adaptation solutions are normally developed to address the high and medium level risks. These can be structural actions that involve "grey" solutions, nature-based solutions, or a combination of both. "Non-structural" actions

Table 1 PIEVC steps and main tasks

Step	Description	Main tasks
–	Preparation	• Identify infrastructure for assessment (existing or new)
		• Determine scope of assessment, including budget, timeline, and participants
		• Assemble project assessment team (owner and consultant, if applicable)
1	Project definition	• Define structural and non-structural infrastructure components
		• Define climate parameters of interest/concern
		• Define future climate period(s) of interest—tie to infrastructure life cycle
		• Define geographic location and boundaries
		• Determine risk levels and scoring (e.g., three, five or seven levels—defined by owner and consultant
		• Determine high, medium and low risk scores
2	Data collection, compilation and analysis	• Define climate parameter thresholds that would include component failure
		• Compilation and analysis of historical climate data to determine probability of threshold exceedance and conversion to a likelihood score
		• Utilize climate projection models to determine probability of exceedance in future climate period of interest
		• Assemble infrastructure component information (design drawings, age, condition assessments, operational records (if available))
3	Risk assessment	• Conduct a yes/no analysis—is there an interaction with/between the component and climate parameter (?)
		• Determine probability/likelihood score for exceedance of climate thresholds, for current and future climate
		• Determine the consequence score for a component climate parameter interaction, given that there is an interaction and that the climate threshold has been exceeded
		• Calculate the risk score for all climate/component interactions

(continued)

Table 1 (continued)

Step	Description	Main tasks
		• Classify risk scores into risk levels to develop a current and future climate risk profile
4	Engineering analysis (optional)	• Analysis of climate loads and component capacity on selected structure components to determine vulnerability
5	Conclusions and recommendations	• Describe risk profile (climate parameter/component interactions classified into risk levels—e.g., high, medium, low)
		• Identify high risk interactions for early action, medium for future action, low for monitoring
		• Develop recommended adaptation actions to reduce risk levels
–	Reporting	• Complete project assessment report
		• Document all executed steps, include risk matrix or risk profile for current and future climate
		• Disclose limitations, gaps, unknowns

are part of the suite of adaptation solutions and may include changes to policies or procedures. The actions may include timelines and estimated costs.

It should be noted that within an assessment all system elements including physical built systems, interconnected systems (e.g., power supply to water distribution), management, personnel, operational and maintenance procedures can be included or not included. Thus, the PIEVC Protocol is a scalable process.

2.2 The PIEVC High Level Screening Guide

Long term use of the PIEVC Protocol has demonstrated that full applications of the Protocol generally require considerable resourcing and time to complete. Further, in specific cases, more streamlined approaches would provide a level of information more suitable to the particular phase of an infrastructure's life cycle, prove more cost and time efficient, and still be highly technically defensible.

The Protocol was originally developed for comprehensive screening-level assessments of existing assets. Though the Protocol has since been used on various occasions to assess projects still in their planning or design phases, it was not originally established with this particular use in mind. Considerably more attention is now placed on screening-level assessments of the climate vulnerability and related risks of *projects in their pre-planning (project identification) and planning phases.* From

a Canadian perspective, the Federal Climate Lens has been an especially important driver of this type of assessment.

To better support practitioners conducting the resiliency portion of Climate Lens assessments, other such assessments focused on the project identification or planning phases of a new asset, as well as rapid assessments of one or more (e.g. a portfolio) of existing assets, the PIEVC Protocol needs to be modified. Numerous stakeholders have called for the development of a new, supplemental version of the PIEVC Protocol, better aligned with screening-level climate vulnerability and risk assessments conducted during the planning phase of proposed infrastructure projects. This new version has been referred to as "PIEVC High Level Screening Guide." This new version of the PIEVC Protocol is currently in development and will be available in the latter half of 2021.

3 PIEVC Protocol Applications

3.1 Application in Canada

Table 2 provides a summary of completed and in progress assessments by infrastructure category. The Protocol has been applied to several types of linear infrastructures e.g. roads and highways, as well as for infrastructures at a specific location. Most

Table 2 Canadian PIEVC assessments by category of infrastructure

Infrastructure category	Number of completed assessments[a]	Number of assessments in progress[a]
Buildings (all types)	23	2
Water supply and treatment	4	2
Storm water and wastewater collection, treatment and conveyance	18	4
Roads, highways, bridges and associated structures	12	1
Urban transit systems	1	1
Coastal infrastructures and ports	13	4
Airports	7	2
Utilities (e.g., power distribution)	5	1
Indigenous/first nations	8	4
Other, including screening of assets across a large geographic region	1	1

[a] These figures do not include all uses of the PIEVC protocol for infrastructure Canada's climate lens requirement

of the reports from these assessments are publicly available at the website www.pievc.ca, operated and maintained by ICLR as part of the PIEVC Program. Some reports are not included for reasons of confidentiality on the request of the infrastructure owner. This collection of assessment reports provides valuable references to inform the planning and execution of future assessments as well as for research purposes. For example, the reports could be used to determine the need and provide evidence for adjustments to infrastructure codes, standards and related instruments.

Owners of these infrastructures are from all three levels of government in Canada and, at the municipal level, from small communities with populations in the thousands to Canada's largest cities. A majority of the completed assessments are for existing infrastructures. The recommendations from these assessments center primarily on adjustments to operations and maintenance procedures and policies including worker health and safety in times of extended high heat or more intense storms. An example of recommendations related to operations is seen in the assessment of the G. Ross Lord and Claireville water retention dams operated by the Toronto and Region Conservation Authority [3].

A an additional example of an operational adjustment resulting from a PIEVC assessment includes a change in the frequency and nature of inspection of more than 300 large culverts in the City of Toronto following an assessment of the climate risks and vulnerabilities to three representative culvert types installed by the city. The impetus for the assessment was the failure of a culvert crossing Finch Avenue from an intense localized rainfall in August 2005. The PIEVC assessment provided the evidence to justify the changes in procedure, and to improve the climate resiliency of Toronto culverts to extreme rainfall events in the future [12].

The Municipality of the District of Shelburne, Nova Scotia sought to upgrade and expand their existing sewage treatment plant. The municipality included a climate risk and vulnerability assessment task as part of the design contract. The assessment influenced the location of the expansion relative to the coast to accommodate future as well as the selection of treatment technologies [1].

The Protocol was used to evaluate the climate risks and vulnerabilities for a conceptual design of an extension to an engineering building at the University of Saskatchewan. The results of the assessment triggered adjustments to the design to accommodate future climate risks from higher temperatures as well as increased frequency and intensity of storm water events [2].

These are a few examples of the application of the PIEVC Protocol and how the results influenced or triggered adaptation actions to improve climate resilience.

In 2016, Engineers Canada was approached by the Ontario First Nations Technical Services Corporation (OFNTSC) to explore the application of the PIEVC Protocol to First Nations (FN) infrastructure in Ontario. The PIEVC Protocol was used to assess the potable water supply system for the Akwesasne First Nation located near Cornwall Ontario [22]. The pilot study was intended to demonstrate the utility of the Protocol for FN infrastructure systems. The Protocol was subsequently applied in two other case studies—Moose Factory (example of a remote northern community) and Oneida First Nation (example of a southern community) [23, 24].

The success of these projects led to the development of a variant to the PIEVC Protocol that was referred to as the PIEVC FN Protocol. Further development by OFNTSC with financial support from the federal government enabled the development of an Asset Management module that is integrated with the PIEVC FN Protocol to create the FN (PIEVC) Asset Management Toolkit. Since this development the OFNTSC has conducted an extensive training program among almost all FN communities in Ontario. Efforts are underway to offer the Toolkit to other FN communities outside of Ontario and two further PIEVC assessment one in Saskatchewan and the other in Quebec are nearing completion at the time of writing.

3.2 International Applications

Through its participation in the World Federation of Engineering Organizations (WFEO), and encouragement and funding support from NRCan and Environment Canada (now Environment and Climate Change Canada), Engineers Canada was able to engage with national engineering organizations in Costa Rica and Honduras to conduct PIEVC assessments for infrastructures located in these countries. Following these first two projects, Engineers Canada continued its international promotion of the PIEVC Protocol, organizing workshops and side events at UNFCCC COP and intersessional meetings. It was at these meetings that an interest was sparked with GIZ which eventually led to collaboration on the GIZ "Climate Services for Infrastructure Investment" (CSI) project. A component of the project was the application of the Protocol in three countries and the Nile Basin for projects listed in Table 3.

Table 3 International PIEVC assessments by country

Project location	Year	Type of infrastructure assessed
City of Limon, Costa Rica Road Bridges, Honduras	2010–2011 2013–2014	Storm water and wastewater four road bridges
Guanacaste Province, Costa Rica	2017 to present	Regional water supply
Mekong Delta, Vietnam	2018–2019	Sluice gates
Mekong Delta, Vietnam	2020–2021	Update and further assessment of multiple small scale sluice gates
Itaaji Port, Brazil Electrosul Hydro Authority, Brazil	2018–2020 2018–2020	Port facilities Transmission lines
Nile Basin	2018–2020	Hydro-electric and water control dams

4 The PIEVC Partnership and the PIEVC Program

In 2019–2020, Engineers Canada conducted a divestment process for the PIEVC Protocol and associated PIEVC Program elements. The process involved inviting a small group of non-profit associations to submit proposals to assume the full PIEVC Program. A total of seven organizations were invited to submit bids. A partnership involving ICLR, CRI and GIZ submitted a bid and were awarded the program and assumed ownership in March 2020.

The objective of the "PIEVC Program Partnership" is to maintain and expand the PIEVC Program, while maintaining its primary tenants of free Protocol access for public infrastructure applications in Canada and ensuring that, to the extent possible, PIEVC Protocol assessment reports remain publicly accessible via the www.pievc.ca website. ICLR and CRI will provide administrative and technical support for the PIEVC Program in Canada, while GIZ will focus on continued international implementation of the PIEVC Protocol.

Under the partnership, the guiding principles and objectives of the PIEVC Program include:

- Providing freely accessible, open, credible resources to support improved understanding of the impacts of climate change on Canada's infrastructure and buildings.
- Providing a Community of Practice to engage and work directly with infrastructure policy and decision-makers from the public and private sectors.
- Improving the understanding, capacity and expertise of policy makers, decision makers, infrastructure professionals and practitioners to adapt infrastructure based on current and future climate risks and vulnerabilities.
- Providing ongoing advice to, and engagement with, governments, and other regulatory authorities on reviews and adjustments to infrastructure codes standards and related instruments to account for and mitigate climate risks and vulnerabilities.

Training for PIEVC Protocol practitioners is available as part of a parallel program to the PIEVC Program—the Infrastructure Resilience Professional (IRP) program. This program includes a series of courses that lead to an "IRP" credential, and includes a course focussed on the PIEVC Protocol.

Publication of PIEVC Protocol assessment reports is considered the primary "public good" of the program, and is intended to facilitate increased application of infrastructure climate change vulnerability assessment methods nationally and internationally, as well as facilitate academic research, policy discussions and strategic climate change adaptation initiatives at all levels of government and in private industry, both in Canada and internationally. Each user of the PIEVC Protocol is requested to complete a licence agreement, which includes a condition that a final assessment report is submitted to the PIEVC Program Partnership. Reports are placed on the www.pievc.ca website for public access. Publication exceptions have been made in several instances where assessment reports contain confidential information.

5 Conclusion

The PIEVC Protocol is a nationally recognized tool for the assessment of climate risks and vulnerabilities for public infrastructure in Canada. It has been applied to a wide variety of infrastructures and a community of practice is developing among practitioners as well as owners. It is a "Made in Canada" tool for the highly specialized and focused task of infrastructure climate risk and vulnerability assessment to inform climate adaptation decision-making and the subsequent actions to reduce risks and improve the climate resilience of the infrastructure.

The development and application of the PIEVC Protocol by engineers working with other practitioners and stakeholders has provided a practical means to assess risk and determine structural and non-structural adaptation actions to improve climate resilience. The fact that the Protocol has been applied to a wide variety and scale of infrastructures, through both top-down and bottom-up applications, demonstrates its versatility, flexibility and practicality. The process fosters collaboration among a wide cross-section of professional and scientific disciplines working with the managers, operators and maintainers of the infrastructure, which is one of its greatest strengths.

Acknowledgements The authors wish to acknowledge ICLR, CRI and GIZ for their support of the PIEVC Program. We would also acknowledge the leadership of Engineers Canada who initiated, and contributed extensive resources during the development and operating stages of the Program. We further acknowledge NRCan for their partnership and encouragement during the development years and their many years of ongoing support.

References

1. ABL Environmental Consultants Ltd. (2011) Vulnerability of Sandy point STP upgrade to climate change. Prepared for the Municipality of the District of Shelburne. Available via www.pievc.ca.
2. Associated Engineering (Sask.) Ltd. (2012) University of Saskatchewan assessment of the engineering building's vulnerability to climate change. Available via www.pievc.ca.
3. Bourgeois G, Dickson S, Ness R, Lapp D (2010) Is your dam vulnerable to climate change? Using the PIEVC engineering protocol. In: Proceedings of the Canadian dam association conference 2010: partnering for a safer future. Canadian Dam Association, Canada, p 175
4. Bush E, Lemmen DS (eds) (2019) Canada's changing climate report. Government of Canada, Ottawa
5. Canadian Council of Ministers of the Environment (2021) Guidance on good practices in climate change risk assessment. Canadian Council of Ministers of the Environment
6. Canadian Standards Association (2009) Risk management: guideline for decision-makers CAN/CSA Q850-97 (R2009). https://www.scc.ca/en/standardsdb/standards/6777
7. CatIQ. 2021. Disaster Bulletins. Toronto: CatIQ. Accessed May 2021 from catiq.com.
8. Debortoli NS, Sayles JS, Clark DG, Ford JD (2018) A systems network approach for climate change vulnerability assessment. Environ Res Lett 13(10):104019
9. Dixon M (2009) Climate change, politics and the civil engineering profession. Proc Inst Civ Eng Municipal Eng 162(4):207–210
10. Engineers Canada (2008) Adapting to climate change: Canada's first national engineering assessment report see: http://www.pievc.ca/e/doc_list.cfm?dsid=4

11. ECCC (2016) The public infrastructure engineering vulnerability committee protocol, version 10. PIEVC Program Partnership, Toronto/Ottawa
12. Genivar Inc. (2011) Climate change vulnerability assessment for culverts. Prepared for the City of Toronto. Available via www.pievc.ca.
13. Government of Canada (2016) Pan canadian framework on clean growth and climate change: Canada's plan to address climate change and grow the economy. Environment and Climate Change Canada, Ottawa
14. Infrastructure Canada (2019) Climate lens—general guidance. Infrastructure Canada, Ottawa. Accessed May 2021 from https://www.infrastructure.gc.ca/pub/other-autre/cl-occ-eng.html
15. Lapp D (2005) What engineers should know about climate change. PEO Eng Dimensions 51–53
16. McConnach JS, Zobaa AF, Lapp D (2011) Impacts of climate change on the power industry and how it is adapting. In: Mcconnach J, Zobaa A (eds) Climate change—research and technology for adaptation and mitigation
17. Naylor A, Ford J, Pearce T, Van Alstine J (2020) Conceptualizing climate vulnerability in complex adaptive systems. One Earth 2(5):444–454
18. Ordóñez C, Duinker PN (2015) Climate change vulnerability assessment of the urban forest in three Canadian cities. Clim Change 131(4):531–543
19. Porter KA, Scawthorn CR, Sandink D (2021) An impact analysis for the national guide for Wildland-Urban interface fires. Prepared for the National Research Council of Canada. Institute for Catastrophic Loss Reduction, Toronto, ON, p 136
20. Prism Engineering (2020) Penticton airport climate change risk assessment report. Prism Engineering. Prepared for Transport Canada & Public Service and Procurement Canada (PSPC), Burnaby. Available via pievc.ca.
21. RDH Building Science (2018) Nanaimo regional general hospital vulnerability assessment report. RDH Building Science. Available via pievc.ca.
22. Stantec/OFNTSC 2017 Climate change impacts on water and wastewater infrastructure at Akwesasne. Ontario First Nations Technical Services Corporation. Available via pievc.ca.
23. Stantec/OFNTSC (2018a) Climate change impacts on the housing infrastructure at Oneida Nation of the Thames. Ontario First Nations Technical Services Corporation. Available via pievc.ca.
24. Stantec/OFNTSC (2018b) Climate change impacts on water and wastewater infrastructure at moose factory. Ontario First Nations Technical Services Corporation. Available via pievc.ca.
25. Wood (2021) Climate lens assessment: G.H. daw community centre enhancements. Prepared for the City of Red Deer. Available via pievc.ca.
26. WSP (2021) Government of northwest territories assessment of climate change impacts on infrastructure in all NWT communities. Prepared for Government of Northwest Territories. WSP Canada Inc., Montreal. Available via pievc.ca.

Prediction of C&D, Grit, Asphalt and Treated Biomedical Wastes During COVID-19 Using Grey Model

Sanaalsadat Eslami, Golam Kabir, and Kelvin Tsun Wai Ng

1 Introduction

According to the increasing trend of waste generation around the world, proper waste management is going to be a critical research subject for the protection of our environment. The rapid growth of population, urbanization, and industrial activities have all impacted waste generation characteristics and recycling behaviors. This is especially important in Canada, as Canadians heavily rely on landfill disposal as the primary solid waste treatment technology. Compared to other industrialized nations, we have a higher per capita waste generation rate and a lower diversion rate [1, 4, 11].

The COVID-19 pandemic has brought many changes to our societies and surrounding environment. Waste generation is one of the important issues that was affected by the pandemic [18]. Different generation trends of municipal solid waste (MSW) for different waste streams are observed during the pandemic in cities. For example, there is a study that shows the total MSW has decreased during the pandemic, however some waste streams have increased [21]. Distinct waste generation characteristics are also reported by Richter et al. [18] during COVID-19 in a Canadian city. To better manage the spread of the virus, countries are paying more attention to allocate appropriate resources [21]. Although the threat of the virus is the same everywhere the policies should be location-specific [21]. Much personal protective equipment such as disposal face masks and gloves have been generated during the pandemic [20]. And due to the lockdown situation in most of the countries, restaurants, and stores have been closed, therefore the online ordering of products and foods increased which led to an increase in packaging wastes. Recycling activities are also reduced, and it is challenging to control the volume of plastics waste [20].

S. Eslami (✉) · G. Kabir · K. T. W. Ng
University of Regina, Regina, Canada
e-mail: SEP403@uregina.ca

S. Walbridge et al. (eds.), *Proceedings of the Canadian Society of Civil Engineering Annual Conference 2021*, Lecture Notes in Civil Engineering 249,
https://doi.org/10.1007/978-981-19-1061-6_40

1.1 Study Area and Data Source

The city of Regina with the population of 258,955 by end of 2021 is the capital and second-largest city in Saskatchewan [15]. Regina with 118.4 km^2 area is located in the middle of the Prairie Province with Alberta to the west and Manitoba to the east (Regina History & Facts 2021). It is expected to witness growth equal to 1.8% in Regina's GDP in 2021. Over the previous two years, Regina city has witnessed a positive immigration rate which can be considered as positive sign for the city. It is predicted to have 3300 new arrivals each year in Regina, until 2023. Therefore, one can expect that the growth in the population of the city by a ratio equal to 1.7% each year, from 2019 to 2023 [5]. In this study, seven years of municipal solid waste disposal data (2013–2020) at Regina city landfill was used to investigate the amount of MSW generation during and after the pandemic.

City of Regina landfill, located at the North-East corner of the city, is the only municipal landfill in the surrounding area. New landfill sites near urban centers are increasingly difficult to locate, and the Regina landfill was extended in 2010. Recently, there is a trend in using remote sensing and satellite imagery in quantifying the impacts of landfills [7] and the planning waste management system [19].

Landfill design standards and guidelines vary across Canadian provinces [17], and the northern part of the Regina landfill was built in 1960 without an engineered liner. Landfill gas and leachate are generated during the anaerobic decomposition of buried organic wastes. Minimizing rainwater infiltration rates may reduce the generation rates of landfill gas and leachate. Alternative daily covers may be used to encourage surface runoff [9, 10] and reduce these harmful landfill by-products. Studies on landfill gas generation [2, 3] and leachate leakage [12, 13] at the Regina landfill have been reported previously.

Prediction of the amount of MSW during the pandemic can be beneficial to control and manage waste generation. In this study, Grey model GM (1,1) and TBGM (1,1) are used to predict the quantities of different waste streams, including the amount of construction and demolition (C&D), Grit, Asphalt Shingles Only, Asphalt Shingles Mixed and Treated Biomedical waste (TBW).

1.2 Related Works

There is research that used TBGM (1,1) and traditional GM (1,1) to predict the energy usage of Shanghai city [8]. In Li et al. [8], the authors implemented the improved GM (1,1) to compare which model generate the best result. According to Li et al. [8], the results achieved by TBGM (1,1) are very promising and comparable to results achieved by present GM (1,1). In order to have appropriate energy policies, we need to have an accurate predictions for the energy consumption of that region Li et al. [8]. In Rahman et al. [16] authors forecast the key performance indicators (KPI) of healthcare with secondary data by GM (1,1). The secondary data has uncertainty and

lack information, therefore the grey model is suitable for this situation. The errors are calculated to show the accuracy of prediction KPIs. The results indicate that two KPIs, bed turnover rate and bed occupancy rate declined process in the time but the other KPIs such as average length of stay increased by the time [16]. This type of research can conduct to predict the KPIs during the COVID-19 pandemic. Thus, the grey model is a useful model to research and investigate the KPIs.

2 Methodology

Deng presented Grey System theory in 1982 Julong [6]. Grey model GM (1,1) is the first structure of the Grey models family which is working by one variable and its appropriate for issues with lack and weak information. GM (1,1) is using and excavating the available data to implement and improve the unknown information in a system. GM (1,1) can be applied to non-linear and time series analysis data. Due to the uncertainty in data in problems, GM (1,1) was considered by many researchers that working with shortage information Julong [6]. Because of the obscure and lack information system has an uncertainty. The GM (1,1) steps are presented below:

Step1: First assumption there is a non-negative data sequence $x^{(0)} = (x^{(0)}(1), x^{(0)}(2), \ldots., x^{(0)}(n))$.

Step2: Make an accumulated generating operator (AGO) of $x^{(0)}$, $x^{(1)} = (x^{(1)}(1), x^{(1)}(2), \ldots., x^{(1)}(n))$ and $x^{(1)}$ is increasing linearly to smoothen the noises of the data which is $\sum_{i=1}^{k} x^{(0)}(i)$, k = 1, 2, 3,..., n.

Step3: Present grey developed coefficient (a) and the grey controlled variable (b) and developed the first order grey differential equation of GM (1,1).

$$\frac{dx^{(1)}(t)}{dt} + ax^{(1)}(t) = b, \tag{1}$$

The Eq. (2) is grey difference,

$$x^{(0)}(k) + aZ^{(1)}(k) = b \tag{2}$$

If $\hat{u} = [a, b]^T$, the least square method by a and b can be developed as:

$$\hat{u} = [a, b]^T = \left[B^T B\right]^{-1} B^T Y, \tag{3}$$

where $Y = \left[x^{(0)}(2), x^{(0)}(3), \ldots, x^{(0)}(n)\right]^T$ and the matrix $\mathrm{B} = \begin{vmatrix} -Z^{(1)}(2)1 \\ -Z^{(1)}(3)1 \\ .. \\ .. \\ .. \\ -Z^{(1)}(n)1 \end{vmatrix}$

The mean value sequence of $x^{(1)}$ is $Z^{(1)} = \left(Z^{(1)}(2)..., Z^{(1)}(n)\right)$, and the GM (1,1) background value is modeled as

$$Z^{(1)}(k+1) = \frac{1}{2}\left[x^{(1)}(k+1) + x^{(1)}(k)\right], \quad k = 1, 2, 3, \ldots, n-1 \tag{4}$$

Step 4: The solution of GM (1,1) can be estimated as:

$$\hat{x}^1(k+1) = \left(x^{(0)}(1) - \frac{b}{a}\right)e^{-ak} + \frac{b}{a} \tag{5}$$

The prediction data at time k presented as:

$$\hat{x}^{(k+1)} = \left(1 - e^a\right)\left(x^{(0)}(1) - \frac{b}{a}\right)e^{-ak} \quad k = 1, 2, 3, \ldots, n \tag{6}$$

TBGM is an developed model of GM (1,1), which is presented by transformation the original data sequence. The steps are using algorithm to add a constant c in data sequence in the front of $x_1^{(0)}$

$$x_2^{(0)} = \left\{c, x_1^{(0)}(1), x_1^{(0)}(2)..., x_1^{(0)}(n)\right\}, \quad c \geq 0 \tag{7}$$

Finally take exponentials for the prediction which is estimated as:

$$\hat{x}_3^{(0)}(k) = \exp\left(\hat{x}^{(0)}(k)\right) \tag{8}$$

For the optimization of background value using the bellow equation:

$$Z^{(1)}(k+1) = \frac{x^{(1)}(k+1) - x^{(1)}(k)}{\ln[x^1(k+1) - x^{(1)}] - \ln x^{(1)}(k)} - \frac{x^{(1)}(1) \cdot x^{(1)}(k)}{x^{(0)}(k+1) - x^{(0)}(1)} \tag{9}$$

3 Results and Discussion

The predictions amount of MSW for waste generation of Regina are shown in Figs. 1, 2, 3, 4 and 5. GM (1,1) and TBGM (1,1) are proposed to predict the amount of MSW

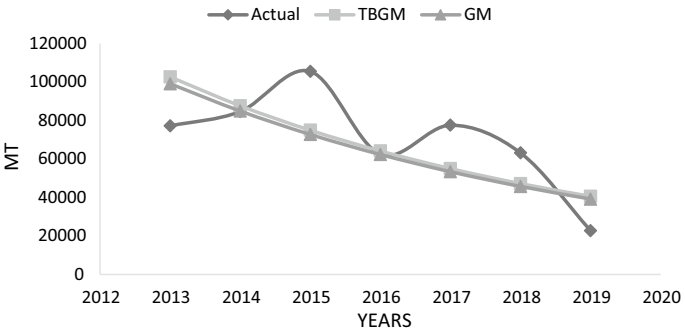

Fig. 1 C&D actual value and prediction value by TBGM (1,1) and GM (1,1)

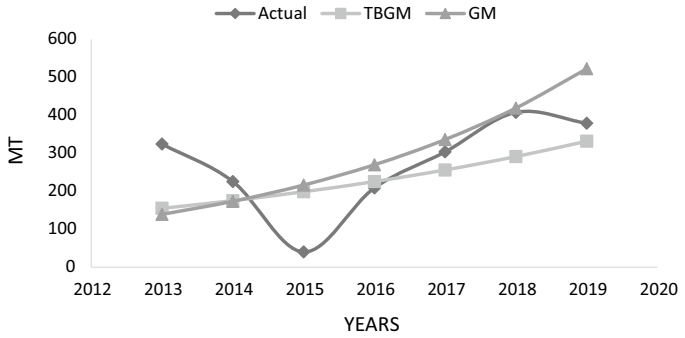

Fig. 2 Grit actual and prediction value by TBGM (1,1) and GM (1,1)

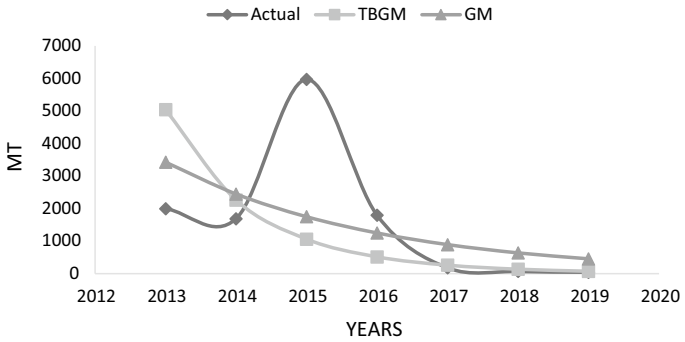

Fig. 3 Asphalt shingles mixed actual and prediction amount by TBGM (1,1) and GM (1,1)

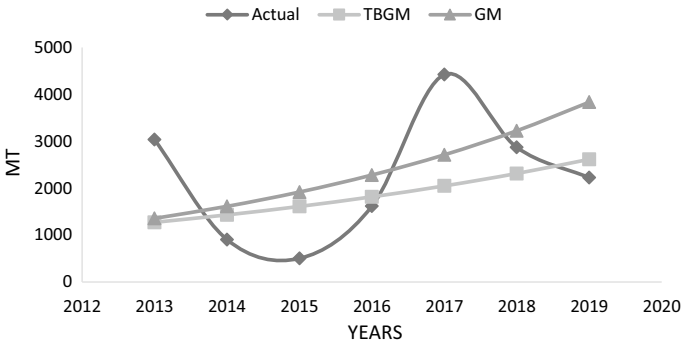

Fig. 4 Asphalt shingles only actual and prediction value by TBGM (1,1) and GM (1,1)

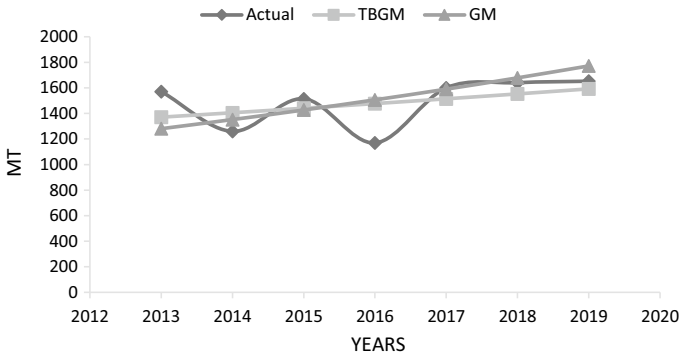

Fig. 5 Treated biomedical waste actual and prediction value by TBGM (1,1) and GM (1,1)

and the MAPE and RMSE are calculated to show which model indicates better prediction. The actual and predicted values for two models during 2013 and 2019 in Figs. 1, 2, 3, 4 and 5 presents the closest value for the TBGM system. It can be deduced from the predictions that more waste generation is predicted in GM (1,1).

The results of TBGM (1,1) indicate that most of the wastes increase during the seven years prediction. C&D and asphalt shingles mixed in Figs. 1 and 3 have predicted to decrease in seven years which is indicates that projects have been put on hold for a while. We can see that the C&D generation forecasts are close to each other in models. The prediction amount of C&D waste generation have been measured 100,000 million tonnes to reach 40,000 million tonnes from 2013 to 2019. Due to the some policies of permission to construct there are two picks in C&D actual value waste generation line in 2015 and 2018, which can be deduced that construction has flourished in some points [14].

Grit generation in Fig. 2 and asphalts shingles only waste in Fig. 4 grow during the time, therefore it can be seen the projects related to roads have not been stopped. The highest amount of Grit generation is predicted in the last few years which is

in the COVID-19 period (near 300 and 500 tonnes by TBGM (1,1) and GM (1,1) respectively). The grit generation amount indicates due to the icy road condition we cannot see the significant impact of the pandemic on grit generation. The largest amount of grit has been generated (around 500 million tonnes) during the pandemic, since due to the lockdown people have been forced to stay at their homes, and therefore the crews could work without interruption.

Asphalt Shingles Mixed values are the same as C&D with an 80% decrease in the amount of asphalt shingles mixed generation during the seven years. From the asphalt shingles mixed actual value during 2014 and 2015, we can see there is an increase in asphalt shingles mixed generation, which may be due to the Residential Road Renewal Program (RRRP). RRRP was issued in 2014 to improve the quality of roads. Figure 3 indicates fewer projects have been done during the pandemic. Moreover, there is a slight increase in asphalt shingles only value. There can be seen no significant changes during the pandemic years which can illustrates the stopping on some projects. There are up and down trends in the actual value of asphalt shingles only but the changes value during this six years was from 3000 million tonnes to reach around 2000 million tonnes between 2013 and 2019.

In Fig. 5 TBGM (1,1) and GM (1,1) prediction value for TBW increase slightly so we can speculate that due to the fear of COVID-19, people didn't refer to hospitals for any issues. Although in the first three years the prediction of GM (1,1) is smaller than TBGM (1,1), but in the following years, the GM (1,1) prediction process grow to reach 1600 tonnes generation in 2019. Although these predictions values are vary in the biomedical waste generation from the middle of the period, the TBGM (1,1) creates closer values to the actual values.

The accuracy of two model can be indicated by MAPE and RMSE. The equations of the errors are as follow:

$$\text{MAPE} = \frac{1}{n}\sum_{i=1}^{n}\left|\frac{\hat{x}^{(0)}(i) - x^{(0)}(i)}{x^{(0)}(i)}\right| \tag{10}$$

$$\text{RMSE} = \sqrt{\frac{1}{n}\sum_{i=1}^{n}\left(\hat{x}^{(0)}(i) - x^{(0)}(i)\right)^2} \tag{11}$$

Figure 6 is presented the amount of MAPE for TBGM (1,1) and GM (1,1) for C&D, Grit, Asphalt Shingles Only, Asphalt Shingles Mixed, and TBW. From Fig. 6 we can see that the errors associated with TBGM (1,1) in most of the waste types are less than GM (1,1). However, GM (1,1) performs better in predicting values for C&D with around 1.5% less MAPE error than TBGM (1,1). According to the Fig. 3, the asphalt shingles mixed decrease in actual value, there is a big difference in asphalt shingles mixed MAPE error (163.995%) for the models, which is shown TBGM (1,1) can better predict this reduction trend.

Figure 7 and 8 indicates RMSE value for different wastes prediction for TBGM (1,1) and GM (1,1). From Fig. 7 we can see that TBGM (1,1) model has better performance than GM in terms of the RMSE error on waste prediction. Asphalt

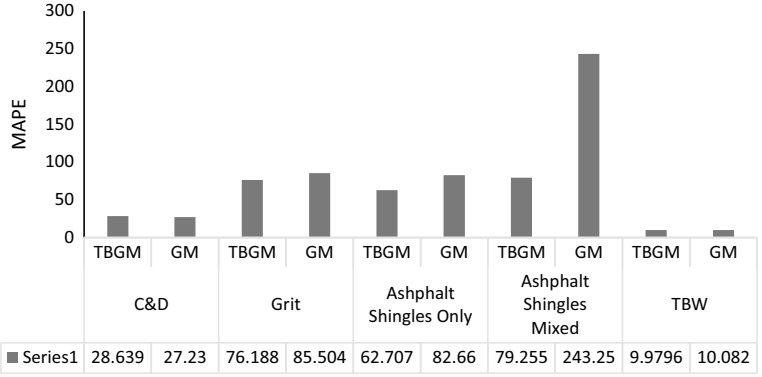

Fig. 6 MAPE value for TBGM (1,1) and GM (1,1)

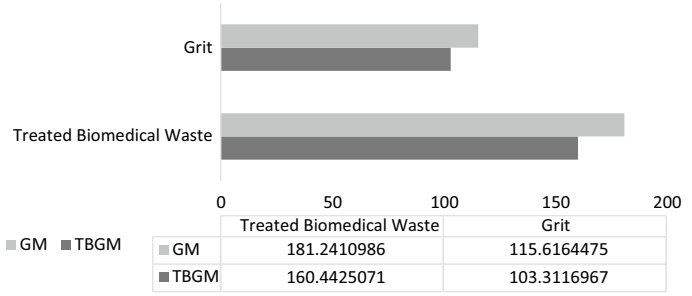

Fig. 7 RMSE value for C&D, asphalt shingles mixed and asphalt shingles only for TBGM (1,1) and GM (1,1)

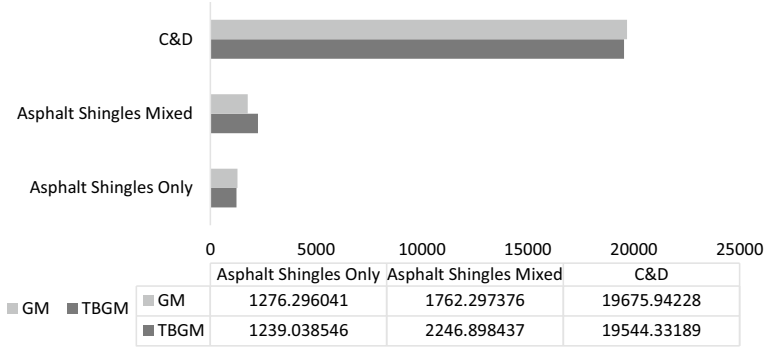

Fig. 8 RMSE value for grit and treated biomedical wastes for TBGM (1,1) and GM (1,1)

shingles Mixed was the only waste that presents the higher RMSE error for TBGM (1,1) than GM (1,1), and it caused by the sudden increase in 2015 of asphalt shingles mixed actual value.

4 Conclusion

In this paper, we predicted the amount of C&D, Grit, Asphalt Shingles Only, Asphalt Shingles Mixed, and TBW based on the data that was provided by the City of Regina. Models namely, GM (1,1) and TBGM (1,1) were used to make a prediction on the amount of the different wastes. We used MAPE and RMSE errors as accuracy metrics to validate and compare the performance of the models. The results showed that TBGM (1,1) generated better predictions for waste generation. Also, the results of the TBGM (1,1) can provide better insights into waste generation during the COVID-19 period. Although, in some type of wastes the RMSE and MAPE of the GM (1,1) were smaller, in general TBGM (1,1) provide the more accurate prediction. Therefore, we can conclude that the TBGM (1,1) model which is the advanced version of GM (1,1), performs better in prediction, overall.

Acknowledgements The research reported in this paper was supported by a grant from the Natural Sciences and Engineering Research Council of Canada (ALLRP 551383-20) to the second and third authors. We would also like to thank City of Regina Environmental Services branch for supporting this project. The authors are grateful for their support. The views expressed herein are those of the writers and not necessarily those of our research and funding partners.

References

1. Bolingbroke D, Ng KTW, Vu HL, Richter A (2021) Quantification of solid waste management system efficiency using input-output indices. J Mater Cycles Waste Manage 1–11. https://doi.org/10.1007/s10163-021-01187-7
2. Bruce N, Ng KTW, Richter A (2017) Alternative carbon dioxide modeling approaches accounting for high residual gases in landGEM. Environ Sci Pollut Res 24(16):14322–14336. https://doi.org/10.1007/s11356-017-8990-9
3. Bruce N, Ng KTW, Vu HL (2018) Use of seasonal parameters and their effects on FOD landfill gas modeling. Environ Monit Assess 190:291. https://doi.org/10.1007/s10661-018-6663-x
4. Chowdhury A, Vu HL, Ng KTW, Richter A, Bruce N (2017) An investigation on Ontario's non-hazardous municipal solid waste diversion using trend analysis. Can J Civ Eng 44(11):861–870. https://doi.org/10.1139/cjce-2017-0168
5. Economic Indicators (2021). Retrieved 05 January 2021, from https://economicdevelopmentregina.com/economic-data/economic-indicators
6. Julong D (1989) Introduction to grey system theory. J Grey Syst 1(1):1–24
7. Karimi N, Ng KTW, Richter A, Williams J, Ibrahim H (2021) Thermal heterogeneity in the proximity of municipal solid waste landfills on forest and agricultural lands. J Environ Manage 287(112320):1–10. https://doi.org/10.1016/j.jenvman.2021.112320

8. Li K, Zhang T (2019) A novel grey forecasting model and its application in forecasting the energy consumption in Shanghai. Energy Syst 1–16. https://doi.org/10.1007/s12667-019-00344-0
9. Ng KTW, Lo IMC (2007) Mechanical behaviors of a synthetic paste of tire chips and paper sludge in MSW landfill daily cover applications. Can Geotech J 44:928–941. https://doi.org/10.1139/T07-041
10. Ng KTW, Lo IMC (2010) Effects of design mix and porosity of waste-derived paste as landfill daily covers on lead retardation. ASCE J Hazard Toxic Radioactive Waste Manage 14(3):195–204. https://doi.org/10.1061/(ASCE)HZ.1944-8376.0000033
11. Pan C, Bolingbroke D, Ng KTW, Richter A, Vu HL (2019) The use of waste diversion indices on the analysis of Canadian waste management models. J Mater Cycles Waste Manage 21(3):478–487. https://doi.org/10.1007/s10163-018-0809-3
12. Pan C, Ng KTW, Fallah B, Richter A (2019) Evaluation of the bias and precision of regression techniques and machine learning approaches in total dissolved solids modeling of an urban aquifer. Environ Sci Pollut Res 26(2):1821–1833. https://doi.org/10.1007/s11356-018-3751-y
13. Pan C, Ng KTW, Richter A (2019) An integrated multivariate statistical approach for the evaluation of spatial variations in groundwater quality near an unlined landfill. Environ Sci Pollut Res 26(6):5724–5737. https://doi.org/10.1007/s11356-018-3967-x
14. Regina residential construction (2017). Retrieved 16 January 2021, from https://leaderpost.com/news/local-news/regina-residential-building-permits-surpass-300-million-in-2016
15. Regina Population (2021). Retrieved 16 January 2021, from https://www.canadapopulation.net/regina-population
16. Rahman MH, Tumpa TJ, Ali SM, Paul SK (2019) A grey approach to predicting healthcare performance. Measurement 134:307–325
17. Richter A, Ng KTW, Fallah B (2019) Bibliometric and text mining approaches to evaluate landfill design standards. Scientometrics 118(3):1027–1049. https://doi.org/10.1007/s11192-019-03011-4
18. Richter A, Ng KTW, Karimi N (2021) The role of compactness distribution on the development of regionalized waste management systems. J Clean Prod 296(126594):1–12. https://doi.org/10.1016/j.jclepro.2021.126594
19. Richter A, Ng KTW, Vu HL, Kabir G (2021) Waste disposal characteristics and data variability in a mid-sized Canadian city during COVID-19. Waste Manage 122:49–54. https://doi.org/10.1016/j.wasman.2021.01.004
20. Sharma HB, Vanapalli KR, Cheela VS, Ranjan VP, Jaglan AK, Dubey B, Goel S, Bhattacharya J (2020) Challenges, opportunities, and innovations for effective solid waste management during and post COVID-19 pandemic. Resour Conserv Recycl 162:105052
21. Van Fan Y, Jiang P, Hemzal M, Klemeš JJ (2021) An update of COVID-19 influence on waste management. Sci Total Environ 754:142014

Characteristics of Excavated Waste from a 14-Year-Old Landfill Bioreactor: Calgary Biocell Case Study

H. Jalilzadeh, J. P. A. Hettiaratchi, P. A. Jayasinghe, T. Abedi Yarandy, and Z. Tan

1 Introduction

Waste disposal practices have evolved over the years from open dumping to the current conventional practice of sanitary landfilling using the dry-tomb landfill approach [3]. However, in recent years, the practices have further advanced with the introduction of the landfill bioreactor concept [1]. In a landfill bioreactor, waste degradation occurs relatively quickly; therefore, granting the option to mine the waste cell to recover degraded waste residue and the landfill space [10]. The excavated waste residue may contain material of value, including recyclables, refuse derived fuel and others, depending on the characteristics of the excavated waste [2, 8].

Hettiaratchi [3] proposed a novel approach for landfill waste disposal known as "sustainable landfill BioCell concept" or the BioCell. The BioCell is a variation of the landfill bioreactor approach and involves the operation of a landfill cell under sequential anaerobic—aerobic conditions with leachate recirculation to take advantage of both forms of biodegradation [5]. The BioCell operation consists of three stages. In the first stage, the BioCell performs the function of an anaerobic bioreactor and enhances methane (CH_4) production. In the second stage, the BioCell is converted to an aerobic bioreactor. Aerobic biodegradation is carried out up to the point where all the waste is decomposed. The third stage is cell mining to recover resource and space thus making the landfill operation sustainable [3].

The Calgary BioCell construction started in 2006 at the Shepard landfill in Calgary, Alberta, Canada owned by the City of Calgary. BioCell covers an area of 100 m ×

H. Jalilzadeh · J. P. A. Hettiaratchi (✉) · P. A. Jayasinghe · T. Abedi Yarandy
Department of Civil Engineering, University of Calgary, Calgary, Alberta, Canada
e-mail: jhettiar@ucalgary.ca

Z. Tan
Department of Mechanical and Mechatronics Engineering, University of Waterloo, Waterloo, Ontario, Canada

S. Walbridge et al. (eds.), *Proceedings of the Canadian Society of Civil Engineering Annual Conference 2021*, Lecture Notes in Civil Engineering 249,
https://doi.org/10.1007/978-981-19-1061-6_41

100 m with a waste footprint of 85 m × 85 m and was designed for a maximum height of 15 m. With a base of 50 m × 50 m, the shape of the BioCell is similar to a pyramidal square frustum increasing sectional area with side slope of 3H: 1 V up to ground level. The cell was designed to accept residential solid waste with feedstock placed in three lifts of 5 m each. Once the shell of the waste cell was constructed, a total of 15,500 tonnes of waste were placed in the first lift. The first intermediate cover of 0.5 m thickness of material compatible with residential waste was then placed over the waste with embedded leachate recirculation and gas extraction pipes and sensors. A total of 17,052 tonnes of waste and 13,312 tonnes of waste were placed respectively in the second and third lifts, bringing the total mass of waste in the cell to 45,860 tonnes [6]. The BioCell produced about 150 m^3/h of landfill gas in early stages. Given that currently minimal gas is being produced, the waste is assumed to be fully stabilized and ready for mining.

2 Methodology

Efforts were made to take a representative sample from the BioCell by developing an appropriate sampling plan. Waste samples were collected from three boreholes aerially, every 1.5 m deep, up to 10 m depth. Initial drilling for pilot holes was carried out with a LS 250 Minisonic Rig (R-45) at three locations with the highest, lowest, and average settlements shown in Table 1. Waste was excavated at every 1.5 increments from each location. Every increment was then visually inspected and logged. The first 0.6 m of each location was observed to be topsoil. Visual inspection showed mostly plastics as the main component in samples. Lack of a strong smell indicated that there are not many biodegradable organics left as they are mostly decomposed. Sampling was carried out with a large drilling hole rig (DR-24) casing up to 0.6 m in diameter. Waste was excavated at every 1.5 m increments from each location providing a total of 18 sample buckets. Waste composition for each sample point was carried out via hand separation method and then compared to the initial composition. The Moisture contents (MC) of waste samples were determined by drying 10 g of waste sample in an oven (model 1510 E, Sheldon Manufacturing Inc.) at 105 °C for 24 h until a constant weight was obtained. Drilling rigs and the excavated material are shown in Fig. 1.

Table 1 Sampling points locations and elevations

Point No.	Northing	Easting	2020 Elevation (m)	2006 Elevation (m)	El. difference (m)
(01)	5,644,676	4005	1031.397	1035.57	−4.173
(02)	5,644,669	4031	1032.407	1035.40	−2.993
(03)	5,644,644	4007	1031.400	1034.90	−3.500

Fig. 1 Drilling rigs and excavated material

3 Results and Discussion

The moisture content is an important factor affecting the rate of waste degradation. The moisture content of the collected samples was measured, and results are shown in Fig. 2.

The MC of the samples varied significantly in the vertical direction along the depth of the landfill cell. The aerial variation (in a horizontal direction) of the moisture content was less significant compared to the vertical variation, as expected. Moisture content, ranging from 40 to 68%, was observed to be increasing with depth of the waste cell highlighting the effectiveness of leachate recirculation system and confirming that intermediate cover layers are letting the moisture through as they were designed to. Comparing the range of MC with other landfill mining case studies around the world shows that BioCell waste is carrying more moisture (10 to 20% more

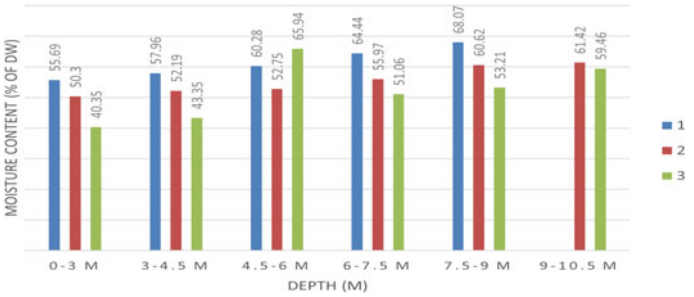

Fig. 2 Moisture content (%) for waste samples collected at different depths and locations

Table 2 Excavated waste composition at different depths compared to the initial composition

Category	Initial composition (weight %)	Composition after 14 years (weight %)	Breakdown of composition per depth interval (m) after 14 years (weight %)				
			0–3	3–4.5	4.5–6	6–7.5	7.5–9
Food waste	14.00	–	–	–	–	–	–
Garden waste	19.00	–	–	–	–	–	–
Paper/cardboard	24.00	15.91	28.81	20.94	14.43	12.08	8.65
Wood	2.00	0.47	1.50	0.13	0.66	0.26	0.00
Glass	1.00	–	–	–	–	–	–
Metal	9.00	4.55	4.24	5.41	4.13	3.95	5.29
Plastic	13.00	10.92	12.99	12.55	9.69	11.02	10.14
Other	18.00	7.64	11.40	10.72	8.46	6.49	3.93
Unidentifiable	–	60.51	41.07	50.25	62.63	66.20	72.00

compared to the average MC reported in literature), highlighting the effectiveness of leachate recirculation [4, 7, 11].

Waste composition of the collected samples at various depths and their comparison to the initial waste are shown in Table 2.

As shown in Table 2, the level of degradation increases with the depth of the landfill. Food and garden waste are degraded to a level that are not identifiable anymore showing the effectiveness of BioCell in degrading organics at a much faster rate compared to conventional landfills.

4 Conclusion

The preliminary results show that the Calgary BioCell operating as a bioreactor landfill with leachate recirculation system in place degraded the waste at a much faster pace compared to conventional landfills and the excavated materials exhibit properties compatible with fully degraded waste that could be used in a productive manner. Going forward, to maximize the energy production from the excavated waste, several thermal methods are being investigated. Among various thermal conversion methods, high-temperature gasification processes (e.g. slagging gasification) are considered as viable options for combined energy and material valorizations in the form of syngas and ash residue [12]. Gasification is also preferred as it can provide a hydrogen rich syngas when steam is used as the gasifying agent [13]. The use of steam as a gasifying agent also results in products with minimal environmental impacts, preventing the formation of NO_x and producing low CO_2 emissions in the gasifier and downstream processes [9].

References

1. Benson CH, Barlaz MA, Lane DT, Rawe JM (2007) Practice review of five bioreactor/recirculation landfills. Waste Manage 27(1):13–29. https://doi.org/10.1016/j.wasman.2006.04.005
2. Chiemchaisri C, Charnnok B, Visvanathan C (2010) Recovery of plastic wastes from dumpsite as refuse-derived fuel and its utilization in small gasification system. Biores Technol 101(5):1522–1527. https://doi.org/10.1016/j.biortech.2009.08.061
3. Hettiaratchi JPA (2007) New trends in waste management: north American perspective. In: International conference on sustainable solid waste management, pp 9–14
4. Hull RM, Krogmann U, Strom PF n.d. Composition and characteristics of excavated materials from a new Jersey landfill. https://doi.org/10.1061/ASCE0733-93722005131:3478
5. Hunte CA, Hettiarachchi CH, Meegoda JN, Hettiaratchi JPA (2012) The city of calgary biocell landfill: data collection and settlement predictions using a multiphase model. In, 4202–11. American Society of Civil Engineers (ASCE). https://doi.org/10.1061/9780784412121.432
6. Hunte CA, Hunte C (2010) Performance of a full-scale bioreactor landfill submitted to the faculty of graduate studies in partial fulfilment of the requirements for the degree of doctor of philosophy department of civil engineering Calgary, Alberta
7. Pecorini I, Iannelli R (2020) Characterization of excavatedwaste of dierent ages in view of multiple resource recovery in landfill mining. Sustainability (Switzerland) 12(5). https://doi.org/10.3390/su12051780
8. Rotheut M, Quicker P (2017) Energetic utilisation of refuse derived fuels from landfill mining. Waste Manage 62:101–117. https://doi.org/10.1016/j.wasman.2017.02.002
9. Shayan E, Zare V, Mirzaee I (2018) Hydrogen production from biomass gasification; a theoretical comparison of using different gasification agents. Energy Convers Manage 159(March):30–41. https://doi.org/10.1016/j.enconman.2017.12.096
10. Slezak R, Krzystek L, Ledakowicz S (2015) Degradation of municipal solid waste in simulated landfill bioreactors under aerobic conditions. Waste Manage 43:293–299. https://doi.org/10.1016/j.wasman.2015.06.017
11. Ximenes FA, Cowie AL, Barlaz MA (2018) The decay of engineered wood products and paper excavated from landfills in Australia. Waste Manage 74:312–322. https://doi.org/10.1016/j.wasman.2017.11.035
12. Zaini IN, Gomez-Rueda Y, López CG, Ratnasari DK, Helsen L, Pretz T, Jönsson PG, Yang W (2020) Production of H2-rich syngas from excavated landfill waste through steam co-gasification with biochar. Energy. https://doi.org/10.1016/j.energy.2020.118208
13. Zaini IN, Nurdiawati A, Aziz M (2017) Cogeneration of power and H2 by steam gasification and syngas chemical looping of macroalgae. Appl Energy 207:134–145. https://doi.org/10.1016/j.apenergy.2017.06.071

Identification and Mitigation of By-Products Formed During an Advance Oxidation of Emerging Contaminants: Example of Pharmaceutical Sulfamethoxazole

S. Fazeli and M. Elektorowicz

1 Introduction

The widespread detection of emerging contaminants (ECs) in wastewater effluents, rivers and even in drinking water in the range from μg/L to ng/L have been reported in many studies [6, 10, 24, 25, 36]. The traces of ECs in drinking water [11, 22, 23, 26, 34] and water resources have been proven even at ng/l concentrations [1, 18, 19, 29, 35]. Emerging contaminants are a wide range of synthetic chemicals in global use that have recently been monitored due to advancement in toxicological knowledge, analytical instruments, and risk assessments [9, 38]. A wide range of ECs include hormones, pharmaceuticals and personal care products (PPCPs), endocrine disrupting chemicals (EDCs), detergents, flame-retardants, pharmaceutical active compounds (PhACs, and textile chemicals [11]. Sulfamethoxazole (SMX) is amongst ECs that its traces (in ppb to ppt) have been found in surface water [4, 8, [12, 32, 40]. This pollutant persists in the environment due to insufficient removal at the wastewater treatment plants (WWTPs) [3, 13]. Many reports on advanced oxidation processes (AOPs) address degradation and removal of micropollutants with a relatively high efficiency. Thus, AOPs might be recognized as promising water treatment systems [17, 25, 28]. However, these reports have never investigated a possible formation of by-products during the advanced oxidation process. Nevertheless, other works emphasized an imminent possibility of by-products' formation while oxidizing micropollutants [39, 37, 15]. In fact, the by-products' formation using AOP, such as UV/H_2O_2 for emerging micropollutants treatment, is very likely [16]. More than 600 disinfection by-products (DBPs) have been identified in the literature, but only

S. Fazeli (✉) · M. Elektorowicz
Concordia University, Montréal, Canada
e-mail: s_fazel@encs.concordia.ca

M. Elektorowicz
e-mail: mariae@encs.concordia.ca

S. Walbridge et al. (eds.), *Proceedings of the Canadian Society of Civil Engineering Annual Conference 2021*, Lecture Notes in Civil Engineering 249,
https://doi.org/10.1007/978-981-19-1061-6_42

a limited number was investigated with respect to their impact on health and environment [20, 27, 31, 33]. The content of DBPs varies between μg/L and ng/L; while more than 50% of DBPs, formed by ozonation and chlorination, have been considered as non-classified and non-identified DBPs [5, 14, 20]. Insufficient data, inaccurate experimental conditions and analytical methods as well as a variation in water quality make characterization of BPs difficult in most cases. Nevertheless, an investigation through evolution of an EC, such as SMX, during AOP treatment of water, would define the risk associated with by-products. The objective of this study is to identify SMX by-products generated during AOP oxidation in water matrix. Furthermore, impact of operational conditions, including oxidant dose, pH and aeration on parent ion and on its BPs' evolution were defined.

2 Materials and Method

2.1 Materials

AOPs experiments were conducted using DI water matrix which was spiked with sulfamethoxazole (SMX) as target EC. The target EC pollutant, SMX, (CAT-No. S7507) was purchased from Sigma Aldrich. Known amounts of target pollutant, SMX, were spiked to the DI water matrix for treatment by AOP. Analytical grade chemicals (acetonitrile, methanol, acetic acid, methylene chloride, ammonium acetate, formic acid) and hydrogen peroxide (H_2O_2) solution (35% w/w) were provided by Fisher Scientific. For measuring chemical oxygen demand (COD) and total organic carbon (TOC), the ultra-low COD (TNT 820, part number 2415815, method 8000) and TOC (part number 2760345, method 10,129) kits from HACH were used.

2.2 Experimental Method, UV/H_2O_2 AOP Setup

The experimental setup was made of a stainless steel (316 L) tubular reactor (10 cm diameter, 45 cm length) equipped with a LP-UVC 40-W lamp (Trojan Company validated UV Lamp, 40 cm length, 2.8 cm sleeve OD, ON, Canada) located on the center of the reactor. The UV intensity was recorded in mJ/cm^2. To deliver the water samples to the reactor at adequate rate, a peristaltic pump with a Tygon ELFL tubing was installed into the system. The water samples placed in a 4-L Erlenmeyer flask, then, it was recycled through a closed loop: passed to the reactor and then came back to the flask. This method allowed the SMX spiked water samples to receive H_2O_2 dose, desired aeration, as well as an adequate nitrogen and oxygen flows and mixing the solution.

2.3 Analytical Methods for Identification of SMX By-Products

Treated water samples' analyses were carried out with UV-Spectrophotometer, HPLC, LC-MS-MS and using COD and TOC Hack kits. For preliminary qualification tests of transformation by-products, LC–MS 6210 QTOF was applied. Ionization sources were ESI+, ESI−. The mass analyzer was Time of Flight MS-2 with mass range: 40–4000 m/z and a resolution of 10,000 FWHM (full width at half maximum). The FWHM was used to define resolution. For quantification analysis at ppb levels the Micromass Quattro LC Waters (triple quadrupole) was applied. Its ionization sources were ESI+, ESI− and mass analyzer was Tandem Quadrupole MS with mass Range: 20–4000 m/z and resolution of 1000 FWHM. Sample introduction was to the HPLC (Agilent HP 1200) where applied column was C18 reversed- phase, X-Select HSS T3 XP column purchased from the Waters with 100 Å, 2.5 μm packing size and 3 mm × 50 mm dimensions and 2–8 pH range. Protocols for analytical experiments such as US-EPA method 1694 (2007) and standard method 6810 (2013), were developed based on the compound nature and instrument conditions. For measuring anions and cations (as SMX mineralization end-products), Metrohm Ion Chromatography (IC) machine (model 530 Compact IC Flex, OpenLab CDS software) was applied with two sensitive columns.

3 Results and Discussion

3.1 Identification of SMX By-Products

This study permitted to found several by-products (BPs) during conducting UV/H_2O_2 advance oxidation of water polluted with SMX. Some of these BPs had much abundance and more persistence in the water samples, others had higher molecular weight in comparison to low molecular weight transformation compounds. The intermediate products with lower molecular weight, such as oxalic acid and formic acid were not persistent in the solution, while for the other by-products with higher molecular weight, such as BP-270 (m/z = 270) and BP-288 (m/z = 288), degradation and removal were difficult. Based on information obtained from LC-MS QTOF and LC-MS-MS analyses, several SMX transformation products were identified. However, the intensity of peaks for some by-products was not high enough and/or their lifetime was short; then, four major degradation products of SMX were selected due to their higher stability in medium and much higher abundances. The structure of four major by-products (BP-99, BP-270, BP-288, BP-172) were assigned based on their accurate mass to charge ratio and information regarding the SMX structure and possible forms of new transformation products. Figure 1 depicts degradation of SMX by UV/H_2O_2 AOP and the evolution of SMX four major BPs. All BPs formed from the

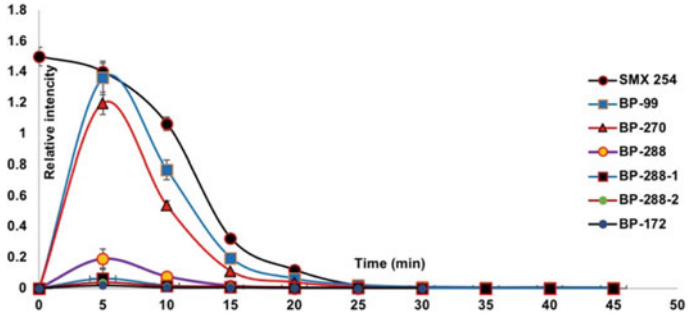

Fig. 1 Evolution of SMX and its four major by-products during the time. Experimental conditions: reaction time = 60 min, air flow rate = 1.5 L/min, H_2O_2 dose = 6 mM, pH = 5.5

beginning of SMX oxidation. The concentration of BPs increased along with degradation of SMX and reached the maximum at initial time of reaction. At maximum SMX removal conditions, the abundance of BPs reduced after 10 min of reaction. However, as long as SMX existed in the medium, the BPs were present even after the complete removal of SMX. Two major BPs, namely BP-99 and BP-270, having higher concentration and longer life time, were selected for further investigations.

3.2 Effect of Technological Parameters on BPs Evolution

The effect of technological parameters (pH, aeration rate and H_2O_2 dose) on BPs evolution, was investigated. The study was conducted in DI water samples. Mineralization with respect to end-products (mineral ions produced from SMX degradation) evolution were considered.

3.2.1 Effect of Aeration on BPs Evolution

The air flow can provide oxygen as an electron receiver for subsequent AOP reactions and produce superoxide radicals ($O_2^{\bullet -}$). Superoxide radicals are highly reactive and can decompose organic pollutant structure and eliminate it from water samples (Eq. 1). During advanced oxidation of target compounds, SMX by-products were affected by aeration of water samples. The by-products behaved similarly to the pattern of SMX parent ions. Figure 2 depicts the evolution of BP-99 and BP-270 by-products. Both BPs had the minimum abundance when the rate of aeration was between 0.5 and 1.5 L/m showing contribution of superoxides to the by-product's removal. However, by increasing the air flow rate from 1.5 to 4 L/m, the aeration had lower effect or even adverse effect on treatment. These conditions contributed to scattering the UV light by air bubbles in addition to the bubbles' behaviour as UV light barriers. Therefore, by decreasing the UV light, the OH radical's concentration

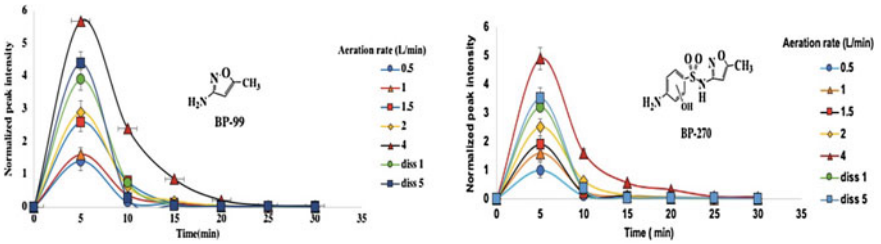

Fig. 2 The effect of aeration rate (L/min) on BP-99 (left) and BP-270 (right) evolution; peak areas were normalized; treatment conditions: reaction time = 30 min, airflow rate = 0.5–4 L/min, H_2O_2 dose = 6 mM, pH = 5.5

decreased and BPs revealed a lower destruction rate.

$$O_2 + e^- \rightarrow O_2^{\bullet -} \qquad (k = 2.0 \times 10^{10}\ M^{-1}s^{-1}) \tag{1}$$

The study showed a difference between behavior of BP-99 and BP-270 with respect to the water aeration rate. At a rate between 0.5 and 1.5 L/m, the abundance of BP- 99 was by about 10% higher in comparison to BP-270. This can be attributed to the contribution of superoxides to cleavage of S–N bound of SMX. At the aeration of the sample over 2 L/m, the concentration of OH radical decreased in the medium while superoxide might increase. Therefore, hydroxylation of the aromatic ring of SMX for production of BP-270 decreased that led to 20% lower abundance of BP-270 in comparison to BP-99.

3.2.2 Effect of pH on BPs Evolution

The pH change has a significant effect on SMX degradation and removal rate. In acidic condition, i.e. from 3 to 5, there is more degradation and a slight increase of degradation from 3 to 5. However, under basic conditions (pH = 7.5–10), the degradation rate has been highly decreased. These findings are compatible with previous studies on SMX degradation [2, 19, 21]. The phenomena could be elucidated by hydroperoxyl radical generation (Eqs. 2 and 3):

$$HO_2^- + OH^{\cdot} \rightarrow HO_2^{\cdot} + OH^- \tag{2}$$

$$H_2O_2 + HO_2^- \rightarrow H_2O + O_2 + OH^- \tag{3}$$

Hydroperoxyl is a strong OH radical scavenger and can lead to lower SMX degradation rate. The more alkaline the condition, the more hydroperoxyl radical generated resulting in lower degradation.

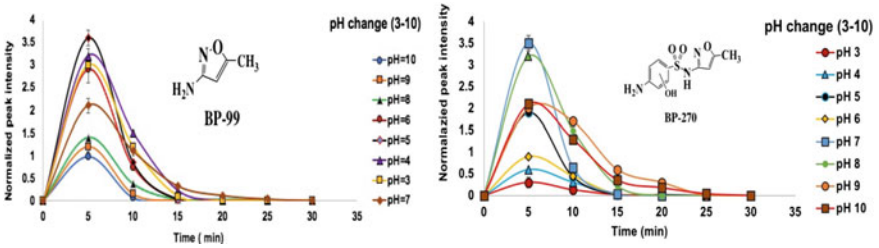

Fig. 3 The effect of pH changes on BP-99 (left) and BP-270 (right). Peak areas were normalized; treatment conditions: reaction time = 30 min, airflow rate = 0.5 L/min, H_2O_2 dose = 6 mM, pH = 3–10

BP-99 Evolution with a pH Change

The evolution of BP-99 during oxidation of SMX was investigated with respect to pH change (Fig. 3). It was found that in acidic conditions more by-products were formed; however, when pH shifted from 3 to higher basic condition, the abundance of BP- 99 slightly decreased. The evolution of BP-99 with respect to pH change can be described by the SMX degradation process. It has been suggested that formation of BP-99 is the effect of the cleavage of sulfonamide (S–N) bound in SMX molecules, which has the highest abundance during oxidation reaction of SMX. In acidic conditions, the OH radical's concentration is not favorable. Moreover, cleavage of S–N bound is more likely at higher pH values. Therefore, by shifting toward alkaline condition (from pH = 3 to 5), there was an increase of the OH radical's concentration, which led to an increasing the rate of BP-99 formation, and simultaneously, degradation of the parent SMX compound. Therefore, in more acidic condition (pH 3–4) there was less BP-99 because of a lower number of OH radicals than at pH 5 (Fig. 3).

The most probably at pH = 5, there was a balance between OH radicals' formation and its abatement at acidic conditions. So, the highest concentration of BP-99 was observed at pH = 5. From pH 5 to 10, the concentration of OH radicals increased; however, the conditions were not favorable for the SMX degradation. Therefore, a reduction of BP-99 from pH 5 to 10 was seen. At pH = 5, higher rate of reduction was observed between 5 to 15 min of treatment period. At other pH values, slower reduction rate of the BP-99 was observed. An abundance trend of the BP- 99 with respect to pH has been found as follows:

$$\text{BP - 99 abundance} : pH5 < pH4 < pH3 < pH6 < pH8 > pH7 > pH9 > pH10$$

It can be concluded that in neutral waters (pH = 6–7) a moderate formation of BP-99 can be observed.

BP-270 Evolution with a pH Change

Formation of BP-270 is probably the effect of attacking the aromatic benzene ring by OH radical. In alkaline condition, the abundance of OH radicals are higher than at acidic pH values. Therefore, from pH 3 to 5, there is an increase of the BP-270 concentration (Fig. 3). At pH from 5 to 6, there is a substantial increase of the BP-270 concentration due to higher dose of OH radicals. In basic conditions (from 7 to 10), there is a reverse behavior of BP-270 in terms of its abundance. At pH = 8, BP-270 had the highest concentration. However, from pH 8 to 10, there is a reverse behavior in which the by-product abundance decreases as pH increases because of the scavenging effect of higher dose of OH radicals. The following abundance trend of BP-270 formation in function of pH was observed:

$$\begin{aligned} &\mathrm{BP}-270\,\text{abundance}: pH3 < pH4 < pH5 < pH6 \\ &< pH8 > pH7 > pH9 > pH10 \end{aligned}$$

Moreover, at the pH value around 5, there was much less BP-270 formation compared to higher pH values. Simultaneously at this pH, the maximum amount of another BP (BP-99) was formed, but a faster removal rate in comparison to other pH values was observed. It was concluded that at the pH = 5for SMX removal, much less by-product 270 was formed and a high-rate removal of BP-99 was observed.

3.2.3 Effect of H_2O_2 Dose on BPs Evolution

One of the most important parameters which affect BPs formation and destruction during AOPs is the oxidant dose. As the H_2O_2 (oxidant) dose was increased from 0.5 to 12 mM, the rate of the SMX degradation was increased but to a limited value of 12 mM. After 12 mM, the excess H_2O_2 behaves as scavenger leading to a decrease in the SMX degradation rate.

BP-99 Evolution with H_2O_2 Dose

The water treatment showed that BP-99 formation rate is faster than its degradation rate. In fact, in SMX molecule, (S–N) bond cleavage needs 300 kJ/mole to form BP-99; however, benzene ring dissociation energy, for the BP-99 degradation, requires around 3200 kJ/mole energy. At low H_2O_2 dose (between 0.5 and 1.5 mM), more BP 99 in comparison to higher doses has been observed (Fig. 4). Nevertheless, at 1.5 mM dose, the highest BP value was recorded because its formation rate was faster than its degradation rate. Between 3 and 6 mM H_2O_2 dose, the lowest concentration of BP-99 was observed. This finding may be attributed to a balance between formation and destruction rate of BP-99. At this oxidant dose, there is much higher concentration of OH radicals for degradation of BP-99. Between 12 and 24 $_{\mathrm{mM}}$, the H_2O_2 behaves

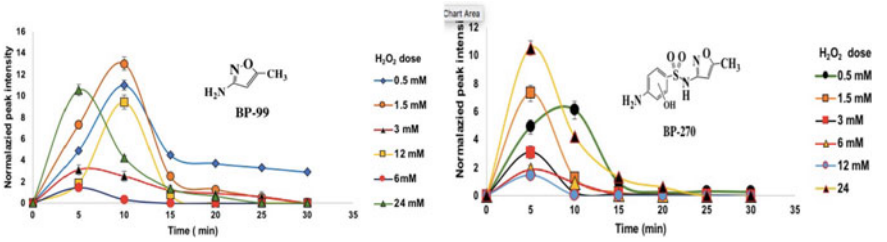

Fig. 4 The effect of H_2O_2 dose change on BP-99 (left) and BP-270 (right); Peak areas were normalized; treatment conditions: reaction time = 30 min, airflow rate = 0.5 L/min, water pH = 5.5, H_2O_2 dose = 0.5–24 mM

as OH radical's scavenger; therefore, there are not enough OH radicals to destroy the BP-99 aromatic ring (Fig. 4).

The study showed that the H_2O_2 dose range between 3 and 6 $_{mM}$ was the optimum value for mitigation of BP-99 abundance. Furthermore, H_2O_2 dose = 6 mM, was the best one for the parent SMX removal.

BP-270 Evolution with H_2O_2 Dose

The evolution pattern of BP-270 is much different than those of BP-99. Based on data depicted in Fig. 4 (right), the lowest BP-270 abundance was reported for 6–12 mM dosage and the highest for 24 mM. At an oxidant dosage around 12 mM, the formation of BP-270 was maximal while the destruction rate was recorded at a maximum level either. Therefore, the minimum concentration of BP-270 was observed around 12 mM H_2O_2 dosage. On the other hand, at 24 mM, the scavenging effect was the highest. Therefore, BP-270 molecules have much higher possibility for formation at initial time of reaction. For lower H_2O_2 doses (between 0.5 and 1.5 mM), a similar evolution pattern was observed for both BP-270 and BP-99. Relatively, the abundance of BP-270 between 0.5 and 1.5 mM was much higher than H_2O_2 doses between 3 and 12 mM. This behavior may be attributed to the faster formation of BP-270 than its degradation rate. At the dose ranges between 6 and 12 mM, BP-270 showed the minimum abundance; while H_2O_2 dose of 6 mM create the best conditions for the maximum SMX removal.

3.3 SMX Mineralization; End-Products Evolution

Results showed an accumulation of SMX's BPs in the first 60 min of reaction (Fig. 5 left). At longer reaction time, the COD concentration, which is an indicator of BPs accumulation, was reduced. The flattering rate of the COD and TOC curves

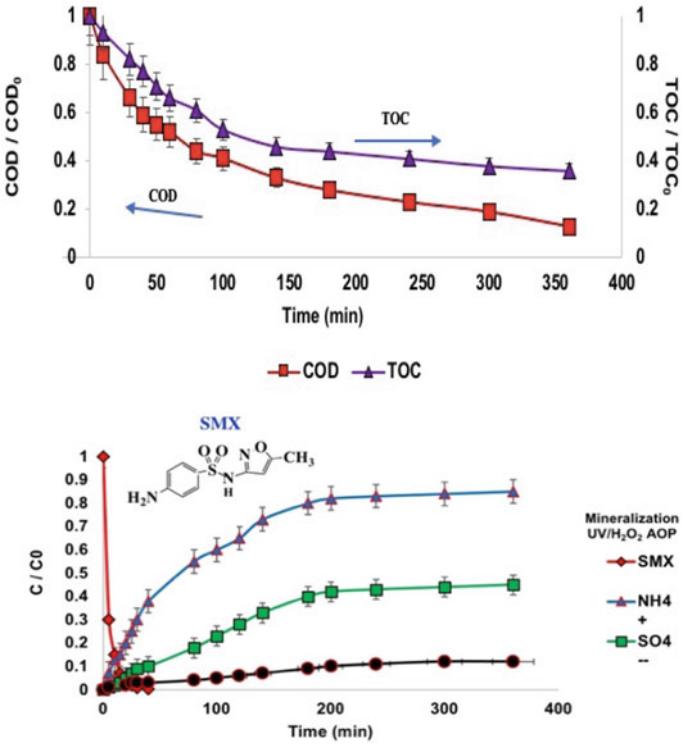

Fig. 5 Degradation of SMX: chemical oxygen demand (COD) rate as degree of mineralization (left). Oxidation of SMX and formation of end-products' ions as mineralization indicators (right). Experimental conditions, reaction time = 360 min

increased after the 120 min reaction time—an evidence of the presence of identified and unidentified BPs during this period.

During 360 min of reaction, COD curve descended and its concentration decreased by 87% (Fig. 5, left); However, the concentration of the ions in the water sample increased (Fig. 5, right). Mineralization of the SMX molecule was carried out by continuing the oxidation over longer period, i.e. more than two hours. Formation of ammonia, nitrate and sulfate as oxidation end-products was a strong indicator of the mineralization reaction. The DOC removal and formation of ammonia (NH_4^+), nitrate (NO_3^-) and sulfate (SO_4^{-2}) ions are shown in Fig. 5 (right). Evaluation of mineralization process was performed on account of reaction end-products. It was found out that the final products contained: $CO_2 + H_2O + SO4^{-2} + NO_3^- + NH4^+$. Based on the abundance of by-products and their lifetime, the major pathway for SMX degradation in this study may be proposed by hydroxylation of molecule aromatic ring, S–N bound cleavage and subsequent sulfone moiety abstraction.

4 Conclusion

Advanced oxidation of sulfamethoxazole (SMX), as one of the important pharmaceutical emerging contaminants, was comprehensively analyzed and monitored in DI water matrix. Accurate mass of SMX ion and its four major by-products including BP-99, BP-270, BP-288, BP-172, identified and quantified by an LC-Q-TOF and LC-MS-MS spectrometry respectively. The results of the total organic carbon analysis confirmed partial mineralization of target pollutants. A high abundance of degradation products might bring a potential hazard to the water resources. However, optimal operational conditions can lead to minimization of the by-products' formation. At pH = 5 for SMX parent ion removal, much less by-product 270 was generated, in addition to the higher removal rate of BP-99, which was the most persistent by-product. Moreover, a moderate abundance for both BPs was recorded at pH = 6. This study showed a significant influence of pH on water treatment by using UV/H_2O_2 advanced oxidation systems. Results showed the high concentration of degradation by-products during the UV/H_2O_2 oxidation of the parent compound. The high concentrations of BP-270 and BP-99 were present even after an entire removal of SMX. Overall at pH = 5, lower concentration of BP-270 and faster degradation of BP-99 was observed. However, at pH = 6, a moderate abundance of both BPs was recorded. At aeration between 0.5 and 1.5 mM, the minimum concentrations of BPs were obtained. At the H_2O_2 dose of 6 $_{mM}$, both BPs were controlled and minimized. Therefore, the best parameters for controlling and minimizing the BPs were obtained at: H_2O_2 dose = 6 mM, aeration = 0.5 to 1.5 L/min, and pH = 6. By continuing the treatment time, SMX by-products disappeared in the medium. However, TOC and COD remained in the medium until the certain time. Formation of ammonia (NH_4^+), nitrate (NO_3^-) and sulfate (SO_4^{-2}) as SMX end-products were strong indicators of mineralization process.

References

1. Alder AC, Schaffner C, Majewsky M, Klasmeier J, Fenner K (2010) Fate of β-blocker human pharmaceuticals in surface water: comparison of measured and simulated concentrations in the Glatt Valley Watershed, Switzerland. Water Res 44(3):936–948
2. Alharbi SK, Price WE (2017) Degradation and fate of pharmaceutically active contaminants by advanced oxidation processes. Curr Pollut Rep. https://doi.org/10.1007/s40726-017-0072-6
3. Almuktar SAAAN, Abed SN, Scholz M (2018) Wetlands for wastewater treatment and subsequent recycling of treated effluent: a review. Environ Sci Pollut Res. https://doi.org/10.1007/s11356-018-2629-3
4. Behera SK, Kim HW, Oh JE, Park HS (2011) Occurrence and removal of antibiotics, hormones and several other pharmaceuticals in wastewater treatment plants of the largest industrial City of Korea. Sci Total Environ. https://doi.org/10.1016/j.scitotenv.2011.07.015
5. Bond T, Huang J, Templeton MR, Graham N (2011) Occurrence and control of nitrogenous disinfection by-products in drinking water—a review. Water Res. https://doi.org/10.1016/j.watres.2011.05.034

6. Brion F, Tyler CR, Xavier Palazzi B, Laillet J-M, Garric J, Flammarion P (2004) Impacts of 17β-estradiol, including environmentally relevant concentrations, on reproduction after exposure during embryo-larval-, juvenile-and adult-life stages in zebrafish (Danio Rerio). Aquat Toxicol 68(3):193–217
7. Cabrera-Rodríguez R, Luzardo OP, González-Antuña A, Boada LD, Almeida-González M, Camacho M, Zumbado M, Acosta-Dacal AC, Rial-Berriel C, Henríquez-Hernández LA (2018) Occurrence of 44 elements in human cord blood and their association with growth indicators in newborns. Environ Int. https://doi.org/10.1016/j.envint.2018.03.048
8. Drillia P, Dokianakis SN, Fountoulakis MS, Kornaros M, Stamatelatou K, Lyberatos G (2005) On the occasional biodegradation of pharmaceuticals in the activated sludge process: the example of the antibiotic sulfamethoxazole. J Hazard Mater. https://doi.org/10.1016/j.jhazmat.2005.03.009
9. Eriksson U, Haglund P, Kärrman A (2017) Contribution of precursor compounds to the release of per- and polyfluoroalkyl substances (PFASs) from waste water treatment plants (WWTPs). J Environ Sci. https://doi.org/10.1016/j.jes.2017.05.004
10. Fazeli S, Elektorowicz M, Ibeid S (2019) CSCE annual conference. In: 17th international environmental conference. Laval (Greater Montreal). June 12–15. Cnadian socoety of civil engineering
11. Furlong ET, Batt AL, Glassmeyer ST, Noriega MC, Kolpin DW, Mash H, Schenck KM (2017) Nationwide reconnaissance of contaminants of emerging concern in source and treated drinking waters of the United States: pharmaceuticals. Sci Total Environ. https://doi.org/10.1016/j.scitotenv.2016.03.128
12. Göbel A, Thomsen A, McArdell CS, Joss A, Giger W (2005) Occurrence and sorption behavior of sulfonamides, macrolides, and trimethoprim in activated sludge treatment. Environ Sci Technol. https://doi.org/10.1021/es048550a
13. Haiba E, Nei L, Ivask M, Peda J, Järvis J, Lillenberg M, Kipper K, Herodes K (2016) Sewage sludge composting and fate of pharmaceutical residues—recent studies in Estonia. Agron Res
14. Hammes F, Salhi E, Köster O, Kaiser H-P, Egli T, Von Gunten U (2006) Mechanistic and kinetic evaluation of organic disinfection by-product and assimilable organic carbon (AOC) formation during the ozonation of drinking water. Water Res 40(12):2275–2286
15. Huang W-J, Fang G-C, Wang C-C (2005) The determination and fate of disinfection by-products from ozonation of polluted raw water. Sci Total Environ 345(1):261–272
16. IJpelaar, Guus F, Danny J H Harmsen, Minne Heringa, and W R Kiwa. (2007) UV disinfection and UV/H2O2 oxidation: by-product. Environ Eng Sci 4:S51-56
17. Jiménez S, Micó MM, Arnaldos M, Medina F, Contreras S (2018) State of the art of produced water treatment. Chemosphere. https://doi.org/10.1016/j.chemosphere.2017.10.139
18. Kasprzyk-Hordern B, Dinsdale RM, Guwy AJ (2009) The removal of pharmaceuticals, personal care products, endocrine disruptors and illicit drugs during wastewater treatment and its impact on the quality of receiving waters. Water Res. https://doi.org/10.1016/j.watres.2008.10.047
19. Kim TH, Kim SD, Kim HY, Lim SJ, Lee M, Yu S (2012) Degradation and toxicity assessment of sulfamethoxazole and chlortetracycline using electron beam, Ozone and UV. J Hazar Mat. https://doi.org/10.1016/j.jhazmat.2012.05.038
20. Krasner SW (2009) The formation and control of emerging disinfection by-products of health concern. Philos Trans Royal Soc London A Math Phys Eng Sci 367(1904):4077–4095
21. Lee SH, Kim KH, Lee M, Lee BD (2019) Detection status and removal characteristics of pharmaceuticals in wastewater treatment effluent. J Water Proc Eng. https://doi.org/10.1016/j.jwpe.2019.100828
22. Leung HW, Jin L, Wei S, Po Tsui MM, Zhou B, Jiao L, Cheung PC, Chun YK, Murphy MB, Lam PKS (2013a) Pharmaceuticals in tap water: human health risk assessment and proposed monitoring framework in China. Environ Heal Perspec 121(7):839
23. Leung HW, Jin L, Wei S, Po Tsui MM, Zhou B, Jiao L, Cheung PC, Chun YK, Murphy MB, PK Sing Lam (2013b) Pharmaceuticals in tap water: human health risk assessment and proposed monitoring framework in China. Environ Heal Perspec. https://doi.org/10.1289/ehp.1206244

24. Luis, SV, Jover E (2014) 14th EuCheMS international conference on chemistry and the environment ICCE 2013: IEC-WTC, Barcelona, Spain, 25–28 June 2013. Environ Sci Poll Res https://doi.org/10.1007/s11356-014-2756-4.
25. Luo Y, Guo W, Ngo HH, Nghiem LD, Hai FI, Zhang J, Liang S, Wang XC (2014) A review on the occurrence of micropollutants in the aquatic environment and their fate and removal during wastewater treatment. Sci Total Environ. https://doi.org/10.1016/j.scitotenv.2013.12.065
26. Machado KC, Grassi MT, Vidal C, Pescara IC, Jardim WF, Fernandes AN, Sodré FF et al (2016) A preliminary nationwide survey of the presence of emerging contaminants in drinking and source waters in Brazil. Sci Total Environ. https://doi.org/10.1016/j.scitotenv.2016.07.210
27. Miklos DB, Remy C, Jekel M, Linden KG, Drewes JE, Hübner U (2018) Evaluation of advanced oxidation processes for water and wastewater treatment—a critical review. Water Res. https://doi.org/10.1016/j.watres.2018.03.042
28. Munter R (2001) Advanced oxidation processes-current status and prospects. Proc Estonian Acad Sci Chem 50(2):59–80
29. Peña-Guzmán C, Ulloa-Sánchez S, Mora K, Helena-Bustos R, Lopez-Barrera E, Alvarez J, Rodriguez-Pinzón M (2019) Emerging pollutants in the Urban water cycle in Latin America: a review of the current literature. J Environ Manage. https://doi.org/10.1016/j.jenvman.2019.02.100
30. Richardson SD (2003) Disinfection by-products and other emerging contaminants in drinking water. TrAC—Trends Anal Chem. https://doi.org/10.1016/S0165-9936(03)01003-3
31. Richardson SD, Postigo C (2011) Drinking water disinfection by-products. In: Emerging organic contaminants and human health, pp 93–137. Springer
32. Roberts PH, Thomas KV (2006) The occurrence of selected pharmaceuticals in wastewater effluent and surface waters of the lower tyne catchment. Sci Total Environ. https://doi.org/10.1016/j.scitotenv.2005.04.031
33. Sillanpää M, Ncibi MC, Matilainen A (2018) Advanced oxidation processes for the removal of natural organic matter from drinking water sources: a comprehensive review. J Environ Manage. https://doi.org/10.1016/j.jenvman.2017.12.009
34. Snyder SA, Wert EC, Lei HD, Westerhoff P, Yoon Y (2007) Removal of EDCs and pharmaceuticals in drinking and reuse treatment processes (91188). Denver, CO, USA: American Water Works Association Research Foundation (AWWARF).
35. Teodosiu C, Gilca AF, Barjoveanu G, Fiore S (2018) Emerging pollutants removal through advanced drinking water treatment: a review on processes and environmental performances assessment. J Clean Prod. https://doi.org/10.1016/j.jclepro.2018.06.247
36. Terzić S, Senta I, Ahel M, Gros M, Petrović M, Barcelo D, Müller J et al (2008) Occurrence and fate of emerging wastewater contaminants in Western Balkan Region. Sci Total Environ. https://doi.org/10.1016/j.scitotenv.2008.03.003
37. Weinberg HS, Krasner SW, Richardson SD, Thruston AD Jr (2002) The occurrence of disinfection by-products (DBPs) of health concern in drinking water: results of a nationwide DBP occurrence study. National Exposure Research Laboratory, Athens, Ga
38. Zhang R, Wang X, Zhou L, Liu Z, Crump D (2018) The impact of dissolved oxygen on sulfate radical-induced oxidation of organic micro-pollutants: a theoretical study. Water Res. https://doi.org/10.1016/j.watres.2018.02.028
39. Zimmermann SG (2011) Enhanced wastewater treatment by Ozone and Ferrate: kinetics, transformation products and full-scale ozonation. Dissertation ETH Zurich. https://doi.org/10.3929/ethz-a-006657068
40. Zojaji et al (2019) Occurrence of ibuprofen and 2-hydroxy ibuprofen in saint Laurent river. CSCE Annual Conference. In: 17th international environmental conference. Laval (Greater Montreal). June 12–15. Canadian society of civil engineering

Development of Microfluidic Photocatalytic Oxidation System for Drinking Water Treatment

B. Liu, B. Chen, G. H. Dong, F. Wu, and B. Y. Zhang

1 Introduction

Drinking water safety in small communities in rural Newfoundland and Labrador (NL) has risen in concern for many years [6, 9]. Though most communities have high drinking water quality, others could face lack of potable water. According to the Department of Environment and Conservation's annual report, 213 boil water advisories, the preventative measure for protecting public health from waterborne disease, were in effect (this includes long-term boil water advisories), affecting 156 communities in the province with an impacted population of 45,124 [2]. These communities generally use surface pond water or well water as their drinking water source and chlorination to disinfect drinking water, in which over 67% use sodium hypochlorite and 31% use gas chlorination. Therefore, the disinfection by-products (DBPs) generated from chlorination are a big concern in these communities [2]. Typical DBPs, include trihalomethanes (THMs), haloacetic acids (HAAs) and other iodinated and fluoride by-products, are commonly detected after the chlorination of natural organic matter (NOM) in source water. Regarding health risks, there has been links found between long-term exposure to DBPs and certain cancers, particularly cancer of the liver, kidneys, bladder, and colon, as well as other health impacts [8, 12]. Therefore, removal of NOM in source water is a key to decreasing the level of DBPs.

Photocatalysis has been studied on the inactivation of pathogenic bacteria and the oxidation of NOM in drinking water for decades [1]. It generates reactive oxidation species such as hydroxyl radicals that can non-selectively oxidize the organic compounds into carbon dioxide and water [4]. The previous studies have showed

B. Liu · B. Chen (✉) · G. H. Dong · F. Wu · B. Y. Zhang
Northern Region Persistent Organic Pollution Control (NRPOP) Laboratory, Memorial University of Newfoundland, St. John's, NL A1B 3X5, Canada
e-mail: bchen@mun.ca

S. Walbridge et al. (eds.), *Proceedings of the Canadian Society of Civil Engineering Annual Conference 2021*, Lecture Notes in Civil Engineering 249,
https://doi.org/10.1007/978-981-19-1061-6_43

promising results in mineralizing different organics with various types of nanocatalysts [5, 7]. However, the mineralization takes much longer time than the degradation of the parent compounds. The intermediates may have a high DBP formation potential (DBPfp) which was not favorite to the DBP control during the treatment [3]. By comparing with conventional photocatalytic oxidation processes, the microfluidic photocatalysis in small reaction channels have advances in enhancing the interfacial reactions (e.g., catalytic generation of reactive oxidative species), and utility rate of reactive oxidative species [11]. These advantages would help enhance the removal of NOMs and diminish intermediate production.

Therefore, this research aimed at developing a novel green technology based on microfluidic photocatalytic oxidation to effectively reduce NOM and DBPfp in treated drinking water. A novel microfluidic reactor coupling with UV-A LED light and TiO_2 nanoparticles were fabricated to degrade humic acids (HA), widely recognized as a typical representative of NOM. Microfluidic photocatalytic oxidation of HA in ultrapure water was tested in various pH values and flow rates.

2 Methodology

2.1 Reagents and Standards

Aeroxide® P25 TiO_2 nanoparticle (anatase: rutile is 9:1, average particle size is around 21 nm) was purchased from Fisher Scientific (Canada). Humic acids, THMs and HAAs reference standards were purchased from Sigma-Aldrich (Canada). Methyl tert-butyl ether (MTBE, HPLC grade) was used for preparing stock solutions and aqueous sample extraction. The commercial products were used as received without any further purification. Ultrapure water was produced on-site from a double fused-silica distillation unit followed by a Barnstead™ Nanopure™ water purification system.

2.2 Microfluidic Photocatalytic Degradation of HA

The microreactor for photocatalytic degradation consists of syringe pump, LTF-V chip reactor and UV-LED light with a 35 V DC power supply (365 nm, 3.98 mw/cm^2) (Fig. 1). LTF-V chip reactor with a 1 mm width channels with a total volume of 1.7 mL. Ten mg/L HA solution was first adjusted pH to 5, 7, and 9. P25 was then added to the system at a ratio of 0.1 g/L. The mixture was vigorously stirred for 20 min and then syringed in a microreactor at a certain flow rate (0.5, 0.75, and 1 mL/min). The irradiation time for HA water sample at the flow rates of 0.5, 0.75, 1 mL/min was 3.4, 2.3, 1.7 min, respectively. Around 50 mL of water samples from outlet of chip reactor in each run was collected and filtered by a 0.45 μm membrane for

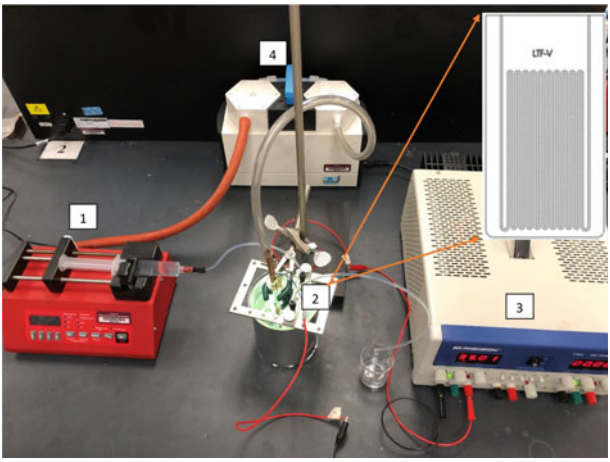

Fig. 1 Microfluidic photocatalysis system: **1** syringe pump, **2** microfluidic photocatalytic reactors, **3** DC power supply, and **4** light cooling system

further analysis. In comparison, a conventional photocatalytic degradation test was performed in a 250 ml bottle. Ten mg/L HA was mixed with 0.1 g/L P25 nanoparticle and irradiated under the LED UV lamp at 35 V DC (365 nm, 7.88 mw/cm^2) for 1 h.

2.3 Characterization of Water Samples

HA concentration in water samples was determined by Thermo Scientific™ Genesys™ 10S UV–Vis spectrophotometer, and total organic compounds (TOC) were examined by SHIMADZU TOC-L analyzer with ASI-L autosampler. The DBPfp were quantified by the following method. The water samples were mixed with chlorine solution and stored at room temperature in darkness for 24 h. After 24 h, THMs and HAAs in water samples were extracted following the EPA methods 551.1 and 552.3 and analyzed by an Agilent 7890A/5975C gas chromatograph – mass spectrometer (GC–MS).

3 Results and Discussion

Microfluidic photocatalytic oxidation system showed an enhanced degradation rate of HA. For example, the degradation rate of HA at 0.75 ml/min and pH of 9 was 44.6%, which was much higher than that of 7.6% in the bottle test under the same irradiation time (2.3 min). However, it was observed that HA degradation was the least at the slowest flow rate but the longest exposure time. Slow flow rate may

lead to the precipitation of catalyst on the surface of microchannels, blocking the permeability of light. The degradation of HA was then inhibited. This phenomenon was also found at other pHs (Fig. 2). As the increase of flow rate, the degradation rate was first increased to a peak at 0.75 mL/min, then decreased due to a shorter retention time.

Further, at pH of 9, the TOC in water samples showed a removal rate of 31% by the microfluidic photocatalytic oxidation system. In comparison, 80% of HA in the bottle test was removed in one hour, while the TOC removal was 40%. The result showed a significantly enhancement of mineralization by the microfluidic system.

Incomplete mineralization of HA can result in the formation of small but more reactive intermediates thus increase THMs and HAAs formation [3, 10]. Photocatalysis can well control the formation of THMs, as the reduction of THMfp in the microfluidic system and the bottle system was 63.6% and 48.7%, respectively. However, it was observed in the bottle test that a higher value of HAAfp in the treated

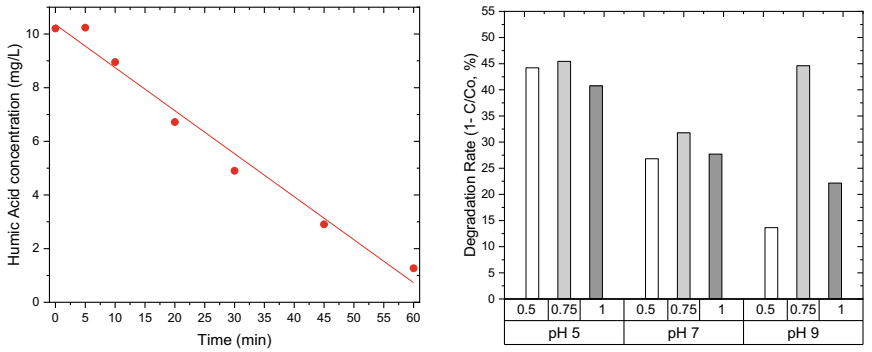

Fig. 2 Photocatalytic degradation of HA in the bottle test (left) and in the microfluidic reactor at different pHs and flow rates (mL/min) (right)

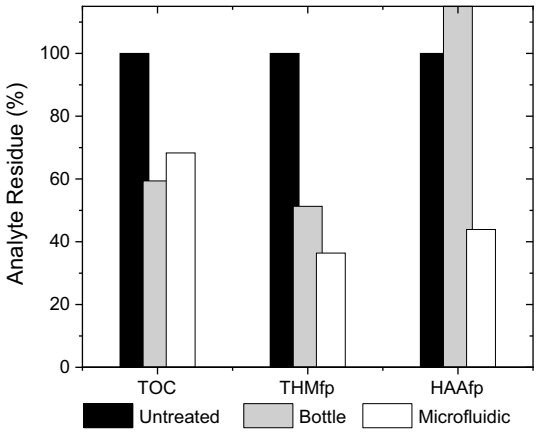

Fig. 3 Changes of TOC, THMfp and HAAfp after the photocatalytic oxidation at 0.75 ml/min and pH 9

sample than in the untreated sample. It is implicated that the photocatalytic oxidation intermediates of HA in the bottle test were favorite to HAA formation. Meanwhile, the removal rate of HAAfp was 56.1% in the microfluidic system, showing better mineralization of the activate intermediates. The microfluidic photocatalytic oxidation can efficiently and constantly inhibit the generation of DBPs, indicating high potential in the field application.

4 Conclusion

A microfluidic photocatalytic oxidation system was developed to remove NOM and control DBPs in drinking water after chlorination. The results showed that the system could efficiently remove HA within minutes, and the best performance was observed to be 45% at pH of 5 in 2.3 min. At pH of 9, the reduction rates of THMfp and HAAfp were 63.6% and 56.1%, respectively. Comparing with conventional system, the microfluidic system had a higher efficiency in HA removal and better performance in mineralization and the control of DBPs production. These results demonstrated that the system can quickly and effectively control DBP levels in drinking water disinfection.

Acknowledgements This research was supported by the Harris Centre-RBC Water Research and Outreach Fund and Memorial University.

References

1. Bekbolet M (2020) An overview of photocatalytic drinking water treatment. Front Water Energ Nexus Nat Bas Sol Adv Technol Best Pract Environ Sustain 247–248
2. ENVC (2016) Drinking water safety in Newfoundland and labrador annual Report 2015. Retrieved from: https://www.gov.nl.ca/eccm/files/waterres-reports-drinking-water-annual-report-2015.pdf
3. Gora S, Sokolowski A, Hatat-Fraile M, Liang R, Zhou YN, Andrews S (2018) Solar photocatalysis with modified TiO_2 photocatalysts: effects on NOM and disinfection byproduct formation potential. Environ Sci Water Res Technol 4(9):1361
4. Hoffmann MR, Martin ST, Choi W, Bahnemann DW (1995) Environmental applications of semiconductor photocatalysis. Chem Rev 95(1):69–96
5. Jing L, Chen B, Zhang BY, Li P (2015) Process simulation and dynamic control for marine oily wastewater treatment using UV irradiation. Water Res 81:101–112
6. Ling J, Husain T (2014) Technologies to remove DBPs in drinking water in Newfoundland and labrador—a review. In: Exploring solutions for sustainable rural drinking water systems, Memorial University of Newfoundland, St. John's, Canada
7. Liu B, Chen B, Zhang B, Song X, Zeng G, Lee K (2020) Photocatalytic ozonation of offshore produced water by TiO_2 nanotube arrays coupled with UV-LED irradiation. J Hazard Mater 402:123456
8. Lyon BA, Milsk RY, Deangelo AB, Simmons JE, Moyer MP, Weinberg HS (2014) Integrated chemical and toxicological investigation of UV-chlorine/ chloramine drinking water treatment. Environ Sci Technol 48(12):6743. https://doi.org/10.1021/es501412n

9. Minnes S, Vodden K (2014) Exploring solutions for sustainable rural drinking water systems: a study of rural Newfoundland and Labrador drinking water systems. The Harris Centre, St.John's, Canada
10. Uyguner-Demirel CS, Birben NC, Bekbolet M (2017) Elucidation of background organic matter matrix effect on photocatalytic treatment of contaminants using TiO_2: a review. Catal Today 284:202–214
11. Wang N, Zhang X, Wang Y, Yu W, Chan HLW (2014) Microfluidic reactors for photocatalytic water purification. Lab Chip 14(6):1074
12. Wang H, Zhu Y, Hu C, Hu X (2015) Treatment of NOM fractions of reservoir sediments: effect of UV and chlorination on formation of DBPs. Sep Purif Technol 154:228

Parameter Analysis in Simulating Transport of Metformin in a Sandy Medium

Q. Kang, A. Datta, and B. Chen

1 Introduction

Metformin is a prescription drug for type 2 diabetes treatment and one of the most prescribed medicines globally [1]. Since metformin cannot be metabolized by the human body, 70% of its intake is excreted and eventually reaches the environment. Although metformin in the environment has not been shown to affect human health, it can affect vegetables and animals. It was demonstrated that 6–10 mg/kg metformin in soils could inhibit the growth of carrots [4]. Besides, metformin has been considered to be a potential endocrine disruptor. When *Pimephales promelas* (a freshwater fish) was exposed to metformin solutions, the gene expression related to endocrine was changed, and they showed amphoteric traits. Metformin can also influence the metabolism and development of *Rana striata tadpole*. It is expectable that metformin's future consumption rate is unlikely to decrease, considering the recent reports on its anti-cancer effectiveness and the increasing rate of type-2 diabetes. Therefore, the environmental fate of metformin deserves attention.

Metformin is mainly discharged into the environment through effluents from municipal wastewater treatment plants (WWTPs), hospitals and industries. It was reported that the mean concentrations of metformin in influents of WWTPs were highest in Germany, followed by Canada, Netherland and the US, where there are more diagnosed cases of diabetes. In 2018, it was reported that the concentrations of metformin in influents of WWTPs in Germany were 14–95 μg/L. The latest

Q. Kang · B. Chen (✉)
The Northern Region Persistent Organic Pollution Control (NRPOP) Laboratory, Faculty of Engineering and Applied Science, Memorial University of Newfoundland, St. John's, NL, Canada
e-mail: bchen@mun.ca

A. Datta
Faculty of Engineering and Applied Science, Memorial University of Newfoundland, St. John's, NL, Canada

S. Walbridge et al. (eds.), *Proceedings of the Canadian Society of Civil Engineering Annual Conference 2021*, Lecture Notes in Civil Engineering 249,
https://doi.org/10.1007/978-981-19-1061-6_44

investigation in 2019 indicated that mean concentrations of metformin were 2.42–53.6 μg/L in 21 WWTPs in the Northeast of China [2]. In WWTPs, the traditional treatment technology, such as flocculation and active carbon filtration, cannot remove metformin effectively. Therefore, large amounts of metformin residues remained in the effluents of WWTPs and finally enter the surface water, which makes metformin one of the most abundant drugs in surface water. Metformin is widely occurred in drinking water and sea water worldwide, and the concentrations of metformin in surface waters were at the range of ng/L–μg/L. In China, the detection frequency of metformin in 217 surface water samples was 99%. The concentrations were at μg/L level; the median concentration was approximately one to two orders magnitude higher than most other pharmaceuticals and personal care products. Metformin can adhere to the activated sludge, in which the concentration of metformin was detected up to 2.96 mg/kg. By soil remediation with activated sludges, metformin can permeate into soils. Irrigation is also an important way for metformin entering soils because metformin widely occurs in wastewater and surface water. Although metformin can adsorb onto soils, the adsorption affinity is weak for its high solubility and low Kow and low vapour pressure. Moreover, metformin's adsorption mechanism includes electrostatic attraction, which is weak and results in high desorption from soils. Thus, once metformin enters soils, it will transport downward and leach into the groundwater, especially during rainstorms. Now, the occurrence of metformin has been determined in groundwater. In Mexico, high metformin concentrations were determined in all canals in a sewage irrigation district, and metformin was also detected in two wells with concentrations smaller than 30 ng/L [6].

Though the presence of metformin has been more frequently reported, studies on its fate and transport processes in the environment are few. Apart from the adsorption, the dynamic migration of metformin in soils was investigated, which showed that metformin's mobility in agriculture soils remediated by biosolids was increased. However, metformin's transport behaviour, especially in groundwater compartments, has not been thoroughly studied. As a link between surface water and groundwater, the vadose zone plays a vital role in the migration of pollutants. Hence, this paper aims to investigate metformin's transport behaviour in groundwater, especially in the sandy vadose zone. A comprehensive experimental approach, including static batch tests and column experiments, was applied. Three types of sand with different grain size distributions were investigated in the experiment to explore metformin's adsorption behaviour in other porous mediums. Hydrus 1-D model was used to simulate the breakthrough curves. The simulation focused on identify essential transport parameters of metformin while supporting future environmental management practice [3, 7].

2 Method

Metformin hydrochloride (98%, manufactured by MP Biomedicals™) and Sodium Azide Crystalline (NaN_3) were purchased. All chemicals were used without further

treatment. Metformin solutions in multiple concentrations were prepared by diluting the stock solution with de-ionized water (>18.2 MΩ.cm). Commercial quartz sand (>98%) was purchased and screened by #40 (0.425 mm) coupled with #80 (0.180 mm) mesh, #80 coupled with #120 (0.125 mm) mesh, and 2 mm mesh, to represent medium, fine and natural mixed sand, respectively. All the sands were gone through acid (HCl) and alkaline (NaOH) wash and then rinsed with distilled water multiple times to ensure the removal of all impurities. An acrylic soil column with a 5-cm inner diameter and a 40 cm height was used.

High-performance liquid chromatography with an ultraviolet detector (HPLC-UV, Agilent Technologies) was used to determine concentrations of metformin in the collected samples. A Shimadzu HILIC column (250 mm * 4.6 mm, 5 μm) was used with a mobile phase of acetonitrile and 10 mM ammonium acetate (pH adjusted to 3 by acetic acid). The volume ratio of acetonitrile to ammonium acetate is 20/80. The mobile phase's flow rate was 1.2 mL/min, and the injected sample volume was 20 μL; the UV detection wavelength was 233 nm. The retention time of metformin was 4.9 min. A particle size analyzer (Mastersizer 2000) is used to examine the grain size distribution of different sandy mediums. The concentrations of Cl^- in the breakthrough experiment were determined by an electrical conductivity meter (Thermo Fisher).

A computer program Rosetta was used for estimating porous medium hydraulic parameters. The tool implemented five hierarchical pedotransfer functions and has been proved effective by many researchers [5, 8]. Given the bulk density of the sand column, two parameters *a* and *n* in the corresponding soil water retention function can be estimated by the tool. Meanwhile, an inverse method for model parameterization embedded in the HYDRUS-1D software package is used in the study to determine unknown parameters in both medium and solute. In the inverse method implemented in the HYDRUS-1D software package, the governing flow and solute transport equations will be solved using a Galerkin-type linear finite element method coupled with a Crank–Nicholson time weighting scheme. By inputting the observed NaCl breakthrough curves into HYDRUS-1D, some soil hydraulic parameters can be determined by the inverse method module embedded in the software. The method is used to determine the soil hydraulic conductivity K_s, which will be further utilized in metformin breakthrough curve simulations. By using the same inverse method in metformin breakthrough curve simulation, fraction f of adsorption sites classified as type-1 in the mobile zone can be determined, as well as the first-order rate coefficient *a* for nonequilibrium adsorption [8]

3 Results and Discussions

Breakthrough curves of metformin were displayed in Fig. 1. From Fig. 1, it can be seen that after a relatively drastic rise of metformin breakthrough concentration, the breakthrough curves exhibited sharp leading and long trailing edges, which indicate time-dependent type-2 sites adsorption limited transport, which tailed the transport

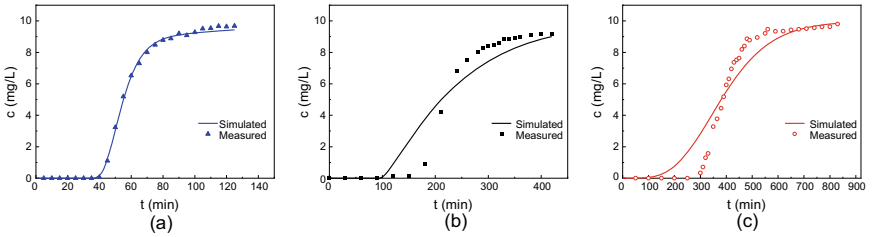

Fig. 1 Breakthrough curves of metformin in different sand columns **a** medium sand column; **b** fine sand column; **c** mixed sand column

process. The breakthrough time of metformin in the three columns was as follows: Mixed > Fine > Medium. Compared with the breakthrough curves of NaCl, such sequence is not quite following the patterns in Fig. 1.

The fit between the measured values and the simulated ones are good in general, with R^2 ranged between 0.9352 and 0.9987. In this case, using the two-site nonequilibrium model to describe the transport and sorption processes of metformin in sandy columns is appropriate. It can be found that the fraction of type-1 site sorption in the fine sandy column is the largest among the three, yet only reached 0.505. f values in medium and mixed sandy columns are only 0.355 and 0.236, respectively. It indicates that type-1 adsorption is not the main contributing factor of the system's total metformin adsorption. The first order adsorption rate coefficients α for type-2 nonequilibrium adsorption were from 0.08 to 0.6.

By using the same inverse method in metformin breakthrough curve simulation, fraction f of adsorption sites classified as type-1 in the mobile zone can be determined and the first-order rate coefficient a for nonequilibrium adsorption. By using the same inverse method in metformin breakthrough curve simulation, fraction f of adsorption sites classified as type-1 in the mobile zone can be determined and the first-order rate coefficient a for nonequilibrium adsorption.

4 Conclusion

The transport velocity of metformin in the sandy vadose zone is approximate 1/5 to 1/3 of the water's velocity, which is generally slow. According to the static experiment, Freundlich and Langmuir isotherm equations can describe metformin's adsorption in the corresponding medium. A two-site nonequilibrium model is suitable to describe the adsorption of metformin in the investigated sandy columns. According to low fractions of type-1 site sorption f values in all three sandy columns, type-1 instantaneous adsorption is not a significant contributor to the total adsorption, which implies that type-2 nonequilibrium adsorption is the primary metformin adsorption process in all three of the sandy columns.

Acknowledgements Special thanks for the supports from the Natural Sciences and Engineering Research Council of Canada (NSERC) and the Canada Foundation for Innovation (CFI).

References

1. Briones RM, Sarmah AK, Padhye LP (2016) A global perspective on the use, occurrence, fate and effects of anti-diabetic drug metformin in natural and engineered ecosystems. Environ Poll 219:1007–20. 10/f9hbqz
2. Bu Q, Wang B, Huang J, Deng S, Yu G (2013) Pharmaceuticals and personal care products in the aquatic environment in China: a review. J Hazard Mater 262:189–211. 10/gfkr8j
3. Datta AR, Kang Q, Chen B, Ye X (2018) Fate and transport modelling of emerging pollutants from watersheds to oceans: a review. In: Advances in marine biology, Vol 81, pp 97–128. Elsevier. https://doi.org/10.1016/bs.amb.2018.09.002
4. Eggen T, Lillo C (2012) Antidiabetic II drug metformin in plants: uptake and translocation to edible parts of cereals, oily seeds, beans, tomato, squash, carrots, and potatoes. J Agric Food Chem 60(28):6929–6935. https://doi.org/10.1021/jf301267c
5. Fernández-Gálvez J, Simmonds LP (2006) Monitoring and modelling the three-dimensional flow of water under drip irrigation. Agric Water Manage 83(3):197–208. 10/d6wchx
6. Kong L, Kadokami K, Wang S, Duong HT, Cam Chau HT (2015) Monitoring of 1300 organic micro-pollutants in surface waters from Tianjin, North China. Chemosphere 122:125–30. 10/f6zdxw
7. Xie WP, Yang JS, Yao RJ, Wang XP (2020) Impact study of impoundment of the three gorges reservoir on salt-water dynamics and soil salinity in the Yangtze River Estuary. J Environ Inf. https://doi.org/10.3808/jei.202000432
8. Zhou Q, Kang S, Zhang L, Li F (2007) Comparison of APRI and hydrus-2D models to simulate soil water dynamics in a vineyard under alternate partial root zone drip irrigation. Plant Soil 291(1–2):211–23. 10/chtdwc

Biomethane Recovery from Brewer's Yeast Using Two-Stage Anaerobic Digestion

A. Jariwala, A. ElGhanam, S. Singh, D. Lee, H. Yeo, R. Seth, H. Hafez, and N. Biswas

1 Introduction

At present in the global market, the brewing industry is a major contributor to the economy. Average beer consumption is estimated at around 23 L per capita, making it the fifth-highest consumed drink [3]. From the brewery industry, Apart from wastewater, Beer Spent Grain (BSG) and Residual Beer Yeast (RBY) are two major by-products produced at the end of the beer production process. The production of RBY is about 1.5–3% of the total volume of beer produced. Only a small fraction (4–6%) of RBY is reused for frementation, while the remainder (94–96%) is either post-treated and pasteurized to sell as livestock food, or ends up in landfills [3]. RBY is rich in organic content [6]. Ifutilized to generate bioenergy, RBY could be an asset in reducing the dependency on fossil fuel. However, the economics of biomethane recovery as biomethane is not always favorable. Pretreatment is often used to help increase biomethane generation from organic wastes. Many pre-treatment processes are available, Greenfield Global's High-Rate Hydrolysis/Acidification (HRHA) process is one of them and has been shown to be quite effective in previous studies. HRHA process works on the principle of decoupling Solids Retention Time (SRT) and Hydraulic Retention Time (HRT) [5]. It consists of a Biohydrogen Reactor (BHR), operated at an HRT of about 12 h, and an SRT of about 2.5 days. followed by a Solids Storage Tank (SST) where the solids are concentrated in combination with a membrane. After membrane treatment, solids are recycled back to SST for further decomposition, and permeate are discharged in permeate tank. After the system is stabilized, The HRT for the HRHA process was

A. Jariwala · A. ElGhanam · S. Singh · R. Seth (✉) · N. Biswas
University of Windsor, Windsor, Canada
e-mail: rseth@uwindsor.ca

D. Lee · H. Yeo · H. Hafez
Greenfield Global Inc., Toronto, Canada

S. Walbridge et al. (eds.), *Proceedings of the Canadian Society of Civil Engineering Annual Conference 2021*, Lecture Notes in Civil Engineering 249,
https://doi.org/10.1007/978-981-19-1061-6_45

achieved about 12 h whereas SRT was near about 2.5 days. The treated effluent was collected from the BHR unit after the treatment process. The scope of this project was to investigate the biomethane potential of untreated RBY and compare it with that of RBY after treatment using HRHA process.

2 Materials and Methods

2.1 Substrate and Pre-Treatment

Residual Brewer's Yeast (RBY) from a brewery in Quebec, Canada was used as the substrate in the current study. A pilot-scale set-up for the HRHA process at the Environmental Engineering Laboratories, University of Windsor was used for the pre-treatment of RBY. The set-up includes a Biohydrogen Reactor (BHR), operated at an HRT of about 12 h. BHR is followed by a Solids Storage Tank (SST), where the solids are concentrated in combination with a membrane unit and recycled back to the BHR to help maintain an SRT of about 2.5 days. The treated RBY is the effluent from the HRHA process and consists of the permeate from the membrane unit and the excess solids from the SST. The pilot system was operated 30 days to help achieve stable operation. Three samples each of the untreated RBY and treated RBY were collected during the last week of operation for biomethane potential (BMP) testing.

2.2 Biomethane Potential Testing

BMP testing was conducted using a batch Automated Methane Potential Test System (AMPTS) [2]. Three samples each of the untreated RBY and RBY treated using the HRHA process were tested. Characteristics of the untreated RBY samples in presented in Table 1 and those for the treated RBY are presented in Table 2.

Batch testing was conducted in bottles with a working volume of 200 mL. The Food to micro-organism (F/M) ratio was set at 1. Anaerobically Digested Sludge

Table 1 Characteristics of untreated RBY samples

Parameter	Units	Untreated (1)		Untreated (2)		Untreated (3)	
		Average	STD	Average	STD	Average	STD
TCOD	g/l	252	18.2	260	21	254	20.6
SCOD	g/l	178	8.2	192	9.1	188	10.4
VFA	g/l	11	0.6	11.4	1.1	11.7	0.9
TSS	g/l	73	6.9	87	6.1	90	6.4
VSS	g/l	65	5.4	76	5.9	85	7.1

Table 2 Characteristics of treated RBY samples

Parameter	Units	Treated (1)		Treated (2)		Treated (3)	
		Average	STD	Average	STD	Average	STD
TCOD	g/l	238	18.9	252	18.2	244	20.1
SCOD	g/l	157	8.5	184	7.5	187	6.8
VFA	g/l	17.7	1.6	19.2	1.3	20.1	1.5
TSS	g/l	78	7	73	5	73	6
VSS	g/l	55	4	63	5	67	5

(ADS) from the Stratford Wastewater Treatment Plant, Stratford, Canada was used as the inoculum and the same ADS volume was used in each bottle. Substrate volume needed to maintain the F/M ratio was then calculated using Eq. (1).

$$\text{F/M} = \frac{\text{TCOD of Substrate} * \text{Volume of Substrate}}{\text{VSS of ADS} * \text{Volume of ADS}} \quad (1)$$

The operational temperature for the process was in the mesophilic range (37–38 °C). To create an anaerobic condition in each bottle, Nitrogen (99.999%, PraxAir, ON, Canada) purging at 10 psi pressure was applied for one minute. Characterization of untreated samples and treated samples are shown in Tables 1 and 2.

2.3 Analytical Techniques

Ammonia Nitrogen, Chemical Oxygen Demand, Sulfate, Total Alkalinity, Total Phosphorous, Volatile Fatty Acids were measured using Hach Standard kits [4]. Total Solids and Volatile Solids were measured using the Standard Methods [1].

3 Results and Discussion

The cumulative biomethane production during BMP testing over 44 days for all samples in presented in Fig. 1. The total cumulative methane produced from treated RBY is observed to be 24 ± 2% higher than from untreated RBY samples. On the basis of volume of substrate added, average methane yield from the untreated RBY was 72 ± 7 L CH_4/L substrate added compared to 83 ± 7 L CH_4/L substrate added from treated RBY, respectively. On the basis of TCOD added, the average methane yield was 273 ± 15 mL CH_4/g TCOD for untreated RBY and 338 ± 20 mL CH_4/g TCOD for the treated RBY samples.

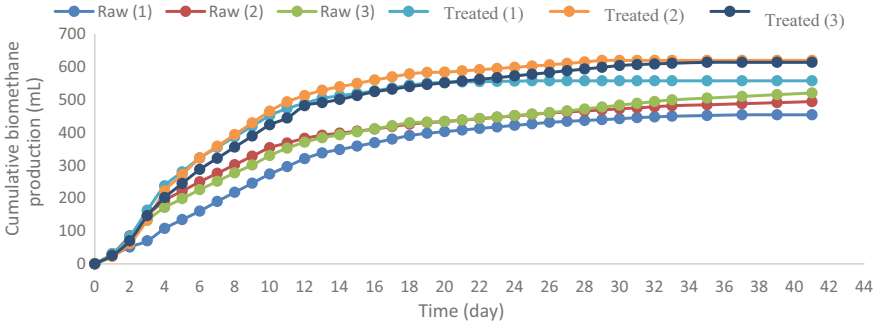

Fig. 1 Cumulative methane production for untreated (raw) RBY and treated RBY samples

4 Conclusions

The current study shows that Residual Brewer's Yeast (RBY) on its own can be a good substrate for bioenergy recovery as biomethane. Pre-treatment of RBY using HRHA process resulted in about 24% increase in biomethane recovery.

Acknowledgements The authors would like to thank Greenfield Global Inc. for partnering and sponsoring the project. We also acknowledge the support received from the University of Windsor.

References

1. APHA, AWWA and WEF (2005) Standard methods for examination of water and wastewater, 21st edn. DC, USA, Washington
2. Badshah M, Lam DM, Liu J, Mattiasson B (2012) Use of an automatic methane potential test system for evaluating the biomethane potential of sugarcane bagasse after different treatments. Biores Technol 114:262–269
3. Fillaudeau L, Blanpain-Avet P, Daufin G (2006) Water, wastewater and waste management in brewing industries. J Clean Prod 14(5):463–471
4. Hach C (2002) Water analysis handbook. Loveland, Colorado, USA, pp 61–62
5. Hafez H, Baghchehsaraee B, Nakhla G, Karamanev D, Margaritis A, El Naggar H (2009) Comparative assessment of decoupling of biomass and hydraulic retention times in hydrogen production bioreactors. Int J Hydrogen Energy 34(18):7603–7611
6. Sosa-Hernández O, Parameswaran P, Alemán-Nava GS, Torres CI, Parra-Saldívar R (2016) Evaluating biochemical methane production from brewer's spent yeast. J Ind Microbiol Biotechnol 43(9):1195–1204

A Study on the Control of Indoor Temperature in Typical Canadian Homes

E. Shen, C. Liao, and D. Yang

Nomenclature

$T(i, t)$	Temperature value recorded by the instrument/set by the model in room i at a time t. Note $T(0, t)$ defines the temperature at the thermostat at a time.
$S_{i,x}$	Set of instances in which the deviation between the temperature/set by the model in room i/recorded by instrument i and the instrument at the thermostat was at most x degrees.
s_i	Total instances in which weather station i recorded/model at room i set temperature.
$R(I, x, y)$	Relative frequency of the temperature of room i being within the interval $(x, y]$.

1 Introduction

In Canada, most existing residential houses are conditioned by a HVAC system known as a forced-air central heating system (Natural Resources Canada's Office of Energy Efficiency 2016), in which the conditioned air is distributed to individual rooms through an air-duct system. Contrary to what the name suggests, it can be operated in both heating and cooling mode. The central equipment, or the furnace in the heating mode and the split-type air-conditioning unit in the cooling mode, is controlled by a room thermostat which measures the air temperature and relative humidity at only one point within the house. In such a system, the indoor thermal environment of

E. Shen · C. Liao · D. Yang (✉)
University of Toronto Schools, Toronto M6J 1M5, Canada
e-mail: yanda@utschools.ca

S. Walbridge et al. (eds.), *Proceedings of the Canadian Society of Civil Engineering Annual Conference 2021*, Lecture Notes in Civil Engineering 249,
https://doi.org/10.1007/978-981-19-1061-6_46

each room cannot be regulated according to its unique occupancy schedule due to the lack of ability to control the heating/cooling capacity delivered into the room. Consequently, the desired thermal environment cannot be maintained in many rooms during a large amount of time whilst energy is wasted for over-conditioning some rooms.

This research is aimed to investigate how serious this problem is within typical Canadian homes and to identify the potential and method to improve the situation by proposing strategies to maximize the thermal comfort of the indoor environment. This goal is to be achieved through a combination of an experimental and a simulation study. This paper first addresses and summarizes existing literature and research done on thermal comfort. The following section describes the methodology for temperature data collection in a Canadian home and the structure of the model used for simulating different cases. The next section presents an analysis of the temperature recorded in a Canadian home using instruments placed in rooms and locations throughout the building. To illustrate various solutions to this thermal comfort problem, Building Energy Simulation (BES) models are employed to test different scenarios. The model used in this study is based on the first principle of thermodynamics and is implemented in Simulink. This model represents a single-family residential building, similar to the case study observed. Three different HVAC zoning models are implemented—the current convention of a single zone thermostat, a dual zone thermostat (floor-level zoning), and an idealized HVAC system with room-level zoning through the control of each individual air register. An analysis of each systems' results is presented, comparing their temperature distributions with their respective scheduled temperatures. The conclusion of this work expands on these findings, proposing the best solution to implement in new construction based on experimental results and analysis in order to optimize thermal comfort.

2 Literature Review

People spend more than 80% of their time indoors [6]. As a result, it is imperative to consider the effects of thermal comfort on occupants.

Studies have shown that within various forms of Canadian housing, significant issues regarding the level of thermal comfort arise during the winter. Bennet and O'Brien [3] surveyed 20 condominium units in Ottawa of varying window sizes and HVAC systems, and found that less than half of the occupants of the units reported comfortable conditions during the winter. Rassam [10] more specifically reported that indoor temperatures in Canada feel "too warm during winter", due to how the temperatures are often "set at specific temperatures" and not accommodating of each occupant's needs.

This latter point may be attributed to the prevalence of single-zone HVAC systems, which according to [4] have been installed in most residential buildings. They also note that single-zone HVAC systems inefficiently distribute air across the building, and do not maintain thermal comfort across all rooms in accordance with occupant

scheduling. This viewpoint is shared by multiple articles—for example, [7] states that fewer zones within an HVAC system leads to significant reductions in "temperature control performance". Sookoor et al. [12] also specifically notes that single-zone HVAC systems will inevitably result in warmer top floors and/or colder bottom floors. Thus, given the various drawbacks of the single-zone HVAC system, along with its widespread use within residence buildings, it is imperative to investigate possible alternatives to the single-zone HVAC system, along with the measured benefits of these alternatives.

A proposed improvement to the single-zone HVAC systems typically implemented in Canadian homes is through a process called HVAC/thermal zoning. For a typical home, it is natural to consider two possible zoning divisions: floor-level zoning and room-level zoning. A study by [12] investigated room-level zoning in a practical setting and found significant (20.5%) energy savings over the existing single-zoned thermostat system. Floor-level zoning systems have also resulted in similar energy savings [12]. In this paper, we investigate the impacts of floor-level zoning and room-level zoning on the maintenance of thermal comfort within a house.

Within relevant literature, thermal comfort is most often measured in experimental studies through questionnaires [3], with these questionnaires often being based on the ASHRAE thermal sensation scale [11]. When objective measurements are taken to determine thermal comfort, they are also often based on what is considered acceptable according to the guidelines provided in the ASHRAE Standard 55 [1], in particular the temperature variation recommendations [14]. Since in a simulation study questionnaires cannot be used to evaluate thermal comfort, such references to official guidelines must be used instead as a benchmark.

The topic of this paper is unique as little research has been done regarding the impact of such HVAC system modifications in Ontario (or Canada in general), or more specifically in the warm-summer humid continental climate zone where this case study was conducted.

3 Methodology

3.1 Overview

The following section outlines the procedure followed to conduct the study and analysis presented in this paper. The first part details how data was collected and analyzed to provide context and experimental data to determine the performance of the current building conventions (single point thermostat) in a real-world setting. The second part of this section pertains to how the modeling used for Building Energy Simulation (BES) was built and how it will be used to simulate the building performance under different scenarios.

The performance of three models with different HVAC systems are compared. These models will be referred to as the Type 1, Type 2, and Type 3 Models, where:

- The Type 1 Model is the reference model. It represents the current convention of a single-zoned HVAC system controlled by a single point thermostat.
- The Type 2 Model represents the use of two smaller HVAC systems, each separately controlled by single point thermostats and each supplying heating/cooling for half of the home. This is an example of floor-level zoning, as each thermostat controls one floor of the house.
- The Type 3 Model represents the use of a terminally controlled system with automated air registers that will close, thence preventing warm airflow into the room, when the desired temperature is achieved. This is an example of room-level zoning, as the temperature of each room is controlled by the air registers.

Note that this study only investigates the heating system of the house.

3.2 Data Collection

A typical Canadian house in Markham, Ontario was chosen as the subject for the investigation of current issues regarding temperature control (the evenness of the distribution of heat from the HVAC systems) in Canadian housing. This two-storey detached house is a light wood-framed structure with a 2×6 stud wall built in compliance with [9]. The floor area is roughly 3000 square feet.

The temperature and relative humidity of each room were measured from January 4, 2020 to January 26, 2020. The outdoor condition was monitored using a weather station located in the backyard of the house.

Relative frequencies of the deviations in temperature recorded by various instruments within the house are calculated to determine the magnitude of the current issue. The set of instances $S_{i,x}$ in which the deviation in temperature recorded by instrument i and the instrument located at the thermostat (hereafter referred to as the "thermostat temperature") was at most x °C, is calculated as follows using Eq. 1:

$$S_{i,x} = \{t | T(i,t) - T(0,t) \leq x\} \tag{1}$$

The relative frequency $R(i, x, y)$ of the deviation in temperature recorded by instrument i and the instrument located at the thermostat being within the interval $(x, y]$ °C is calculated as follows using Eq. 2:

$$R(i, x, y) = \frac{|S_{i,y}| - |S_{i,x}|}{s_i} \tag{2}$$

3.3 Simulation Studies

Three models were developed and implemented in Simulink for the simulation studies. These models take Canadian climatic weather data as an input parameter and simulate the transfer of heat and airflow in a house. The Type 1 Model was created as a reference model to simulate the results of an HVAC system controlled by a single set-point thermostat, which is the current norm for typical Canadian houses. The systems of the Type 2 Model and Type 3 Model were proposed to mitigate the shortcomings of the reference model observed in the experimental case study. The Type 2 Model uses two smaller furnaces to heat half of the house each, enabling a more precise control of the temperature in the house in theory. The Type 3 Model uses a terminal control system, which further improves the precision of the HVAC system's heat transfer. The structure of the models will be discussed further in depth in Sect. 5.

The Simulink model is used to determine how to mitigate significant deviations in thermal comfort across rooms. Two objectives are to be completed in this investigation:

1. Objective 1 is to investigate the performance of the Type 1 model and to identify significant issues regarding heat distribution within the household. The thermostat for the Type 1 Model is located in room 1, and the performance of the model is evaluated across two schedules
2. Objective 2 is to investigate the performance of Type 2 and Type 3 models and to compare their thermal comfort efficacy with the results of Objective 1. The thermostats for the Type 2 Model are located in rooms 1 and 4 (one on each floor), and the performance of the model is evaluated across two schedules.

Table 1 presents the two winter operation schedules. The temperature setpoints are 16 °C during setback and 21 °C during occupancy. Schedule 1 consists of a constant temperature setpoint at 21 °C to test the capabilities of the Type 1 model in maintaining small temperature deviations, while Schedule 2 is designed to reflect real-life scenarios more accurately, by modelling the typical workday of an adult. The scheduled temperature changes to the temperature shown within the table in accordance with the corresponding time (which denotes when the temperature changes are first implemented). F1 and F2 denote floor 1 and floor 2 of the house, respectively.

Table 1 Four winter operation schedules

Time	0:00	6:00	7:00	17:00	22:00
Schedule 1	All 21 °C F1, F2				
Schedule 2	16 °C F1, 21 °C F2	21 °C F1, F2	16 °C F1, F2	21 °C F1, F2	16 °C F1, 21 °C F2

3.3.1 Objective 1

While Sect. 4 investigates the empirical reasons to the significant deviations in temperature, another theoretical investigation must be done to confirm that it is the HVAC system and not any external factor (i.e. a faulty HVAC system, exceptional geography of the house) that is causing this issue. In addition, to confirm that this is a regular issue, this investigation must examine all reasonable scenarios under which the HVAC system operates.

To conduct this experiment, the temperatures of all six rooms are recorded over a period of 151 days from November to March, in 2 distinct simulations. As only climate data from winter (November to March) is used, the climate data used in the simulation accurately reflects temperatures in which only the heating system would be active.

To analyze the data collected in Objective 1, similar methods to the procedure described in Sect. 3.2 are used. The model provides the deviation $T(i, t)$ between the temperature of room i and its scheduled temperature at any time t. The set of instances in time $S_{i,x}$ of the deviation in the temperature of room i and its scheduled temperature being at most x is determined as follows using Eq. 3:

$$S_{i,x} = \{t | T(i, t) \leq x\} \tag{3}$$

Finally, the relative frequency $R(i, x, y)$ of the temperature of room i being within the range $(x, y]$ can be calculated by applying Eq. 2.

3.3.2 Objective 2

In order to propose an effective solution to this problem, we must verify that the proposed modifications to the HVAC model work theoretically. To do this, the Type 2 and Type 3 Models were used to simulate different scenarios.

The data is collected in a similar manner to the methods described for Objective 1. For both model types, the temperatures of all six rooms are recorded over a simulation period of 151 days, from November 1 to March 31.

4 Experimental Study of a Canadian House

This experimental study is aimed to understand the extent of the issue regarding uneven distribution of heat by the HVAC system within typical Canadian houses. The temperature and relative humidity are measured in 12 rooms of a typical Canadian home using battery driven instruments, in addition to a weather station that measures the outdoor weather at the backyard of the house. The data collected is analyzed to highlight the existence of significant temperature deviations between rooms in typical Canadian housing.

Throughout this section, temperature deviations are considered significant if they are greater than 1 °C in magnitude. This is based off of ASHRAE Standard 55 [1], which allows a "Cyclic Operative Temperature Variation" of at most 1.1 °C. With this definition, 5 instruments in the house (numbered 1–5) frequently experience significant temperature deviations. Instruments 1 and 5 are located in distinct bedrooms within the house, instrument 2 is located in the kitchen-family room, instrument 3 is located by the master bedroom window, and instrument 4 is located in the basement.

Figure 1 displays the relative frequencies of the deviations in the temperature recorded by select instruments, and the instrument located at the thermostat. The shaded region in Fig. 1 indicates deviations up to ±1 °C compared with the thermostat temperature. Figure 1 plots the values of $R(i, x - 0.5, x)$ against x, where x is an integer multiple of 0.5 ranging from −9 to 9.

Figure 1 depicts the deviations between the temperatures recorded in rooms 1, 2, 3, 4, 5, and the thermostat temperature. Of these 5 rooms, the temperatures of rooms 2, 3, and 4 are most frequently below the thermostat temperature, while the temperatures of rooms 1 and 5 are most frequently above the thermostat temperature. The temperatures of rooms 2 and 4 are most often 2.5–3.0 °C lower than the thermostat temperature, while Room 5 is even colder, experiencing temperatures often 4–4.5 °C lower than that of the thermostat temperature. In contrast, the temperatures of rooms 1 and 5 are most often 0.5–1 °C higher than the temperature recorded at the thermostat. All 5 rooms experience a temperature deviation less than 1 °C in magnitude (illustrated by the shaded region) at a relative frequency of less than 38%, and rooms 2, 3, and 4 experience a temperature deviation of less than 1 °C at a frequency of less than 2%. All rooms experience a temperature deviation greater than 2 °C at a frequency of at least 25%.

These observations demonstrate that multiple rooms within this typical Canadian house experience frequent (>50%) temperature deviations of at least 1 °C in magnitude from the thermostat temperature. In addition, all rooms occasionally (>20%) experience temperature deviations greater than 2 °C. Finally, one room is extremely

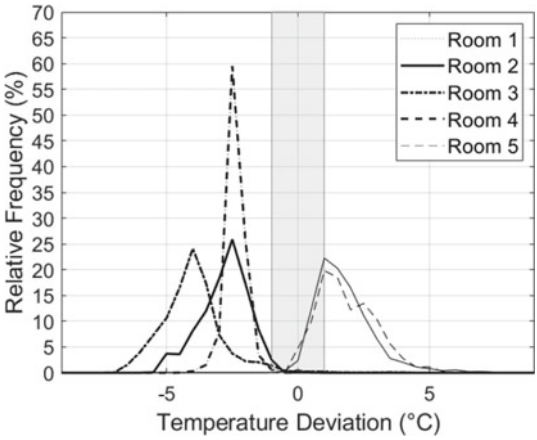

Fig. 1 Relative frequencies of the deviations in temperature recorded between selected instruments within the house and the instrument located at the thermostat

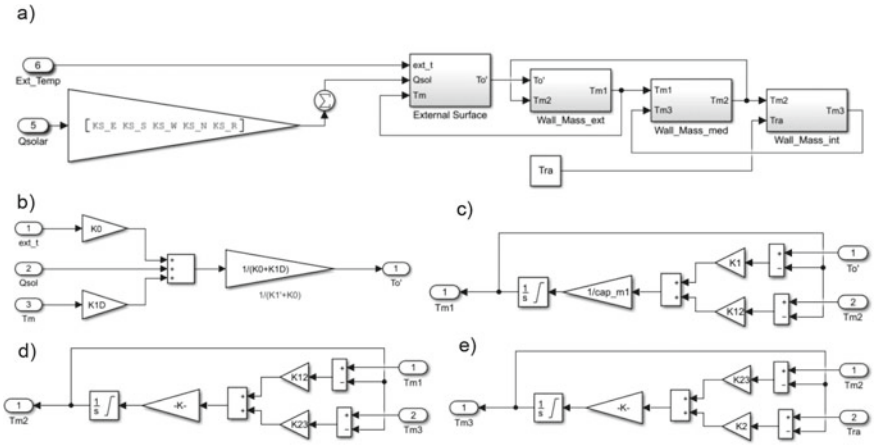

Fig. 2 **a** Three-layer external wall model. **b** External surface subsystem. **c** Outer wall subsystem. **d** Middle wall subsystem. **e** Inner wall subsystem

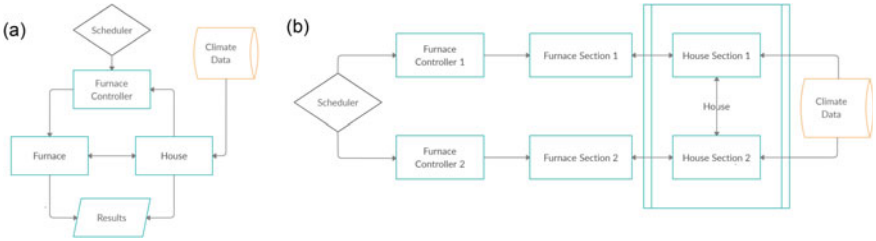

Fig. 3 **a** Subsystems for type 1 model. **b** Subsystems for type 2 model

cold and experiences frequent temperature deviations greater than 4 °C from the thermostat temperature.

These results thus confirm the existence of significant temperature deviations within typical Canadian housing. As described in Sect. 1, these large temperature deviations within residential housing may be explained because the HVAC system cannot individually regulate the distribution of conditioned air to each room in order to accommodate for unique occupancy schedules. Thus, we conduct a simulation study to confirm whether the demonstrated issue regarding temperature deviations is influenced by the aforementioned inadequacies of the Single-Zone HVAC system.

5 Model Development

The house model is based on the first principle of thermodynamics. A 3TC model is used to represent the thermodynamics of building envelope and zone model [5,

13]. All the models presented have been implemented in Simulink (MATLAB). As an example, Fig. 2 shows the implementation of a three-layer external wall model in Simulink (Tra represents the mean radiant temperature of the room).

The model is configured into three models, each with a different HVAC system.

5.1 Type 1 Model

The Type 1 Model is the reference model and it represents the most common HVAC heating system currently implemented in typical Canadian homes. The Type 2 and Type 3 Models are based on the Type 1 Model. Figure 3a depicts the structure of the model and how each component contributes to the final output.

5.2 Type 2 Model

The Type 2 Model represents a control system with two set-points. This model consists of two smaller furnaces, each individually controlling the temperatures for one floor of the house. The other sections of the model are identical to those described in the Type 1 Model. Figure 3b depicts the structure of the model and how each component contributes to the final output.

5.3 Type 3 Model

In the Type 3 Model, each air register is controlled individually according to the difference between the air temperature and the setpoint in the room. This controls the airflow from the furnace into each of the rooms and allows for highly regulated temperatures within each of the rooms. Additionally, in such a system, each room may have a unique temperature setpoint schedule. As shown in Fig. 4, the air registers are controlled using an anti-windup PID controller, which prevents integration windup

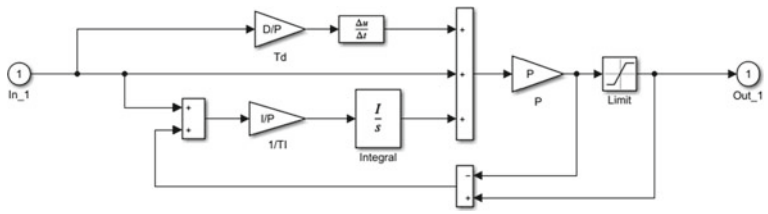

Fig. 4 Anti-windup PID controller implementation

in the PID controllers when the damper values are saturated. The PID controllers are manually tuned using the Ziegler-Nichols method with minimal overshoot.

All other control aspects, including the furnace and scheduler, are implemented identically to the design outlined in the Type 1 Model.

6 Simulation Results

6.1 Objective 1

2 simulation scenarios regarding the setup of the Type 1 Model are investigated in the first objective of the simulation study. Note that as with Sect. 4, in this section temperature deviations are considered significant if they are greater than 1 °C in magnitude. Also note that in the following analysis, "Scenario 1" will be used as a shorthand for the simulation where the Type 1 Model is used with Schedule 1, and "Scenario 2" will be used as a shorthand for the simulation where the Type 1 Model is used with Schedule 2.

As with Fig. 1, the shaded region in Fig. 5 indicates a deviation of up to 1 °C from the setpoint temperature in either direction.

Figure 5 shows that Room 6 in the Type 1 Model under both scenarios experiences frequent (>50%) temperature deviations of at least 1 °C compared to the scheduled temperatures. In scenario 1, the range of this distribution is at least 6 °C: the distribution reaches as low as −4 °C, and as high as 2 °C. In scenario 2, rooms 3–5 also experience frequent temperature deviations of at least 1 °C in magnitude, with the distribution of each said deviation having a large spread and reaching as low as −7 °C. In fact, only 43.2% of the temperatures for scenario 2 fall within ±1 °C of the scheduled temperature.

In conjunction with the conclusions drawn in Sect. 4, this indicates that there are significant issues regarding the forced-air central heating system model that result in

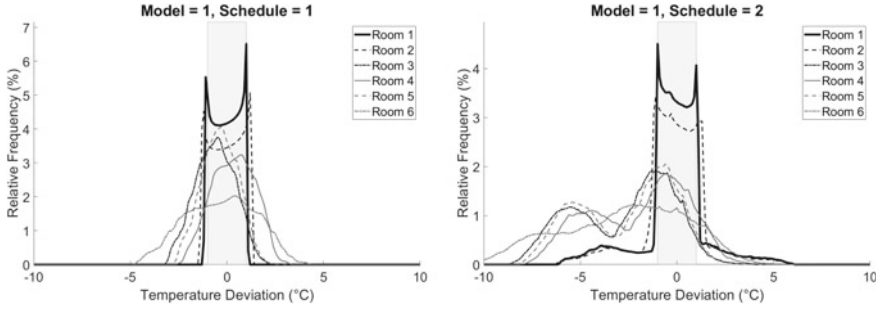

Fig. 5 Relative frequencies of temperature deviations of each room from the scheduled temperature, for scenarios 1, 2

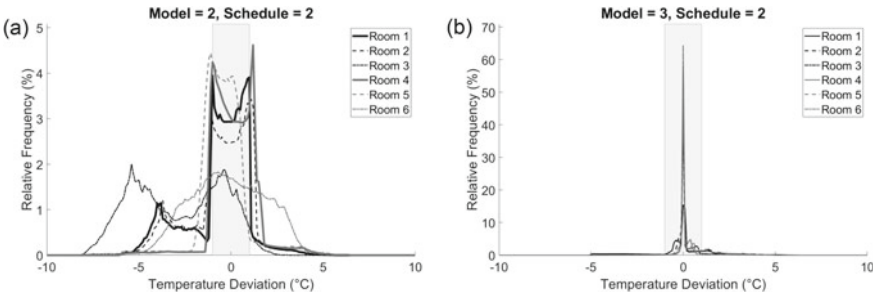

Fig. 6 Histogram plots of temperature deviations from scheduled temperatures

large temperature deviations. Thus, it is necessary to investigate alternative models for the heating component of the HVAC system in order to mitigate the current issues surrounding the uneven distribution of heat in typical Canadian housing.

6.2 Objective 2

In Fig. 6, the central shaded band represents a maximal temperature deviation of ±1 °C from the scheduled temperature, which is also the hysteresis range of the simulated thermostat in the Type 1 and 2 models. Additionally, the bolded lines in the graphs for the Type 2 Model represent rooms 1 and 4, the two setpoint rooms.

Figure 6a depicts the histograms of the temperature deviations in the Type 2 Model for Schedule 2, while Fig. 6b depicts the histogram plots for the temperature deviations in the Type 3 Model for Schedule 2. The impact of using two setpoints can be clearly observed from plot (a), in which 70.7% of the total temperatures in the two setpoint rooms fall within the desired range of ±1 °C of the scheduled temperature. However, the remaining rooms do not perform as well, as only 55.8% of temperatures across all rooms fall within the desired range.

These deviations are completely mitigated in the Type 3 model, which manages to consistently keep the temperatures within the acceptable ±1 °C limits. In plot (b), 81.3% of the temperatures fall within the desired range, which is a significant improvement over the other two models. Note that much of this deviation from the desired temperature range arises as a result of the sudden change of the setpoint temperature at the specified times.

7 Conclusion

Based on the results presented above, we can conclude that the practice of using HVAC systems controlled by a single setpoint thermostat in typical Canadian homes

is very ineffective in managing the thermal comfort of the internal environment, and it is not possible for such a single setpoint thermostat HVAC system, like the Type 1 Model, to maintain the desired temperatures of each individual room. Using the Type 1 Model with Schedule 2, only 43.2% of the temperatures fall within ±1 °C of the scheduled temperature. In addition, an HVAC system comprised of two smaller furnaces and controlled by two setpoints, such as the Type 2 Model, still often experiences temperature deviations from the scheduled setpoints. With Schedule 2, the total temperatures in the two setpoint rooms while controlled by the Type 2 Model fell within ±1 °C of the scheduled temperature 70.7% of the time, while the other rooms experienced temperatures within said desired range only 55.8% of the time. An HVAC system with automatically controlled air registers, such as the Type 3 Model, consistently maintains temperature in an acceptable range from the scheduled setpoints. With Schedule 2, the Type 3 model was able to maintain temperatures within the desired range 81.3% of the time.

While the Type 2 model did not perform perfectly, our findings indicated that either proposed HVAC system would perform better than the current system used in typical Canadian homes. Further experimental research will need to be done in order to validate these conclusions in a real-life setting.

Conflicts of Interest The authors declare no conflict of interest.

Funding This research received no external funding.

References

1. ASHRAE (2010) ANSI/ASHRAE/IES 55-2010 thermal environmental conditions for human occupancy, American Society of Heating. Refrigerating and Air-Conditioning Engineers, Atlanta, GA
2. ASHRAE (2016) ANSI/ASHRAE/IES 90.1-2016 energy standard for buildings except low-rise residential buildings, American Society of Heating. Refrigerating and Air-Conditioning Engineers, Atlanta, GA.
3. Bennet IE, O'Brien W (2016) Field study of thermal comfort and occupant satisfaction in Canadian condominiums. Archit Sci Rev 60(1):27–39. doi:https://doi.org/10.1080/00038628.2016.1205179
4. Jornet-Monteverde JA, Galiana-Merino JJ (2020) Low-cost conversion of single-zone HVAC systems to multi-zone control systems using low-power wireless sensor networks. Sensors 20(13):3611
5. Liao Z, Dexter AL (2004) A simplified physical model for estimating the average air temperature in multi-zone heating systems. Build Environ 39(9):1013–1022. https://doi.org/10.1016/j.buildenv.2004.01.034
6. Liu Z, Ma S, Cao G, Meng C, He B-J (2018) Distribution characteristics, growth, reproduction and transmission modes and control strategies for microbial contamination in HVAC systems: a literature review. Energ Build 177:77–95. https://doi.org/10.1016/j.enbuild.2018.07.050
7. Mcdowall R (2007) Fundamentals of HVAC systems, SI. American Society of Heating, Refrigerating and Air-Conditioning Engineers eLearning, Atlanta, Ga
8. Natural Resources Canada's Office of Energy Efficiency (2016) Energy efficiency trends in Canada 1990 to 2013. Crown copyright, Ottawa

9. Ontario Building Code 1983. Reg.583/83, Ministry of Municipal Affairs and Housing, Housing Development and Buildings Branch, 1983. Accessed 1 Aug 2020
10. Rassam S (2004) Climate, energy, and sustainable design in Southern Ontario. Dalhousie University, PhD Diss
11. Schiavon S, Yoni Donner BY, Chang VWC, Nazaroff WW (2017) Thermal comfort, perceived air quality, and cognitive performance when personally controlled air movement is used by tropically acclimatized persons. Indoor Air 27(2):690–702. doi:https://doi.org/10.1111/ina.12352
12. Sookoor T, Holben B, Whitehouse K (2013) Feasibility of retrofitting centralized HVAC systems for room-level zoning. Sustain Comp Inform Syst 3(3):161–171. https://doi.org/10.1016/j.suscom.2013.01.006
13. Tindale A (1993) Third-order lumped-parameter simulation method. Build Serv Eng Res Technol 14(3):87–97. https://doi.org/10.1177/014362449301400302
14. Wang Y, Kuckelkorn J, Zhao F-Y, Liu D, Kirschbaum A, Zhang J-L (2015) Evaluation on classroom thermal comfort and energy performance of passive school building by optimizing HVAC control systems. Build Environ 89:86–106. https://doi.org/10.1016/j.buildenv.2015.02.023

Covid-19 Monitoring Using Wastewater-Based Epidemiology: The Promise and Peril of Seeking Useable Data in a Pandemic

J. Hollman, N. Acosta, M. Bautista, J. McCalder, L. Man, A. Buchner Beaudet, B. Waddell, J. Chen, D. Kuzma, R. G. Clark, N. Ruecker, K. Frankowski, C. Hubert, M. Parkins, M. C. Ryan, and G. Achari

1 Background

The COVID-19 pandemic has had profound impacts, with government health agencies around the world rushing to collect adequate and timely data to inform decision making. Wastewater-based epidemiology (WBE) presents a unique opportunity as a novel data source in pandemic management. Infected individuals excrete billions of copies of SARS-CoV-2 RNA in their stool daily, creating great opportunity for large-scale data collection of municipal wastewaters to monitor the spread of infections.

Considerable research has taken place globally to rapidly advance WBE, with research primarily focused on detection and quantification of SARS-CoV-2 RNA at wastewater treatment plants (WWTPs) [2, 6, 7]. Conventional epidemiological data obtained through clinical testing and hospitalizations are lagging indicators, given that clinical testing typically occurs a few days after symptom onset, with hospitalization on average 7 days after symptom onset [3]. As COVID-19 infected individuals typically begin shedding SARS-CoV-2 in stool shortly after becoming infected, WBE has the potential to serve as an early warning system as infections increase, with available current examples demonstrating 2–4 days of advanced warning [5]. Conventional testing also underestimates disease burden, as asymptomatic and pauci-symptomatic individuals are not accounted for, which represent 40–50% of infections.

J. Hollman (✉) · N. Acosta · M. Bautista · J. McCalder · L. Man · A. B. Beaudet · B. Waddell · J. Chen · D. Kuzma · R. G. Clark · N. Ruecker · K. Frankowski · C. Hubert · M. Parkins · M. C. Ryan · G. Achari
University of Calgary, Calgary, Canada
e-mail: jordan.hollman@ucalgary.ca

S. Walbridge et al. (eds.), *Proceedings of the Canadian Society of Civil Engineering Annual Conference 2021*, Lecture Notes in Civil Engineering 249,
https://doi.org/10.1007/978-981-19-1061-6_47

A notable challenge in the evolving field of WBE is the need for effective sampling strategies, the informed selection of sampling sites, and proper utilization of collected data [4, 9]. The case study presented here examines multiple sampling strategies undertaken to monitor SARS-CoV-2 in municipal wastewater. Major challenges with each approach are discussed and use of results from each sampling approach is demonstrated.

2 Methods

SARS-CoV-2 RNA was monitored from three diverse locations representing a continuum of wastewater samples: at a WWTP, at a location in a sewer network that is fed by high-case communities, and outside a non-residential building. Samples were collected using ISCO GLS or ISCO 6712 composite samplers programmed to achieve time-weighted sampling over 24 h collecting 100 mL of wastewater every 15 min, for a total composite sample of 10 L. Approximate wastewater flowrates at locations sampled were 350,000 m^3/d for the WWTP and 25 m^3/d for the community sewer network sample (flow rates at the individual buildings were not determined due to sporadic low-flow conditions). Samples were collected from Nov 10, 2020 for three WWTPs in the City of Calgary and from Dec 1, 2020 from sewer networks. Samples from a workplace were collected from Nov 14, 2020. All samples were collected until Feb 10, 2021.

Subsamples (40 mL) from each composite were spiked with a positive internal control - Bovine coronavirus, cleaned and concentrated using a 4S-silica column method [8]. A blank control was used with each sample batch to verify an absence of contamination during processing. Quantification of SARS-CoV-2 RNA in the samples used a TaqMan-based RT-qPCR assay, with the N1 primers and probe used to amplify a region of the nucleocapsid gene (N), as described elsewhere ([1], under review).

3 Results and Discussion

3.1 Findings

Results from the three sampling locations are shown as genome copies of SARS-CoV-2 per mL, providing an indication of the population that is shedding SARS-CoV-2 in stool. Results are shown in Fig. 1.

The most integrated results available were from WWTP influents serving a large municipal population. Results showed an upward trend as the second wave of COVID-19 began in the Fall of 2020, with a few data points showing substantial sudden spikes. When comparing WWTP data to neighbourhood-level sampling

from the sewer collection network, neighbourhood samples also broadly followed population trends, but also demonstrated significantly larger spikes in SARS-CoV-2 as overall cases in the municipality increased and then decreased. As these samples were taken in a location considered to be a "COVID-19 hotspot" as determined through contract tracing, the increased SARS-CoV-2 signal demonstrates that cases in this region are considerably higher than the municipal average, with sharper spikes and dips than WWTP data. Results from the individual building that experienced an outbreak during the time of testing showed a substantial spike in SARS-CoV-2 signal, corresponding to the high proportion of active cases in the building, as compared to the municipal average. As the outbreak was managed, a sudden and drastic decrease in SARS-CoV-2 RNA signal was observed.

Comparing the results demonstrates two major findings: (1) WWTP data provides population level trends, but masks local outbreaks. (2) Increasingly granular data results in a significantly resolved SARS-CoV-2 RNA signal as well as showing greater spikes and fluctuation.

3.2 Use Case and Major Considerations

The significant difference in signal strength and the ability to accurately monitor trends demonstrates that consideration of sampling locations directly influences how results can be interpreted and utilized. Practical considerations must also be accounted for when planning a WBE monitoring program. A summary of potential use cases and major considerations is shown in Fig. 2.

Given the need for sampling devices in a building for granular results, residential testing may be strategic for high-risk locations (e.g., nursing homes, hospitals, meat processing plants) where regional authorities have resources to clinically test all occupants when a positive wastewater result is returned. Highly granular results may also find use in workplaces where employers can quickly respond by instituting

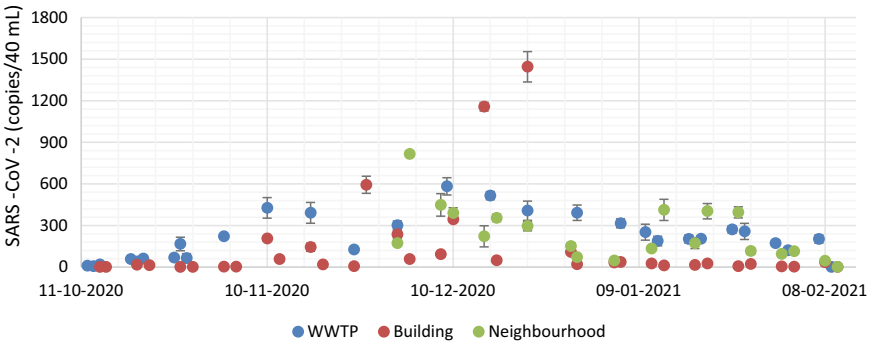

Fig. 1 SARS-CoV-2 copies/mL in wastewater at different sampling locations semi-weekly from November 2020 to February 2021

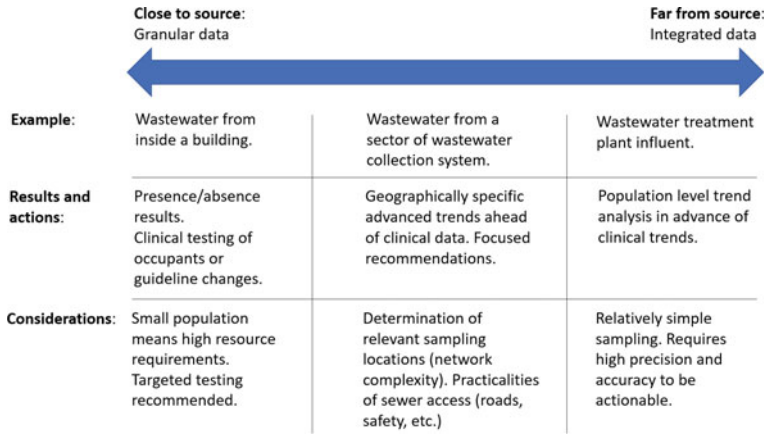

Fig. 2 Sampling location considerations

extra/increased measures that will reduce spread of the virus such as at warehouses, or other cases where people otherwise work in close proximity, and work at camps.

The application of WBE using WWTP influent is currently the most common WBE approach, in part due to the relative ease in obtaining samples by taking advantage of WWTP infrastructure. The primary use of integrated data from WWTPs is to monitor population level trends, with an anticipation that WBE data will precede clinical testing by as much as by one week. Additional research is required to properly interpret data and ensure testing reliability.

Data collected from within the sewershed presents an underutilized opportunity, as regional outbreaks result in significantly higher signal strength than what is seen in WWTP influents. Such spikes present an entirely new data source to regional health authorities. However, mechanisms of responding to early warning of localized outbreaks are only now being explored. Despite the promise of this sampling approach, significant considerations must be managed, such as identifying ideal sampling locations within complex sewer networks and the practicality and safety of installing samplers. Such considerations include determining sample locations that collect water from designated communities that are primarily residential, while minimizing road closures, and collecting adequate metadata to aid in interpreting results. Resolving these issues requires significant buy-in from the local municipality.

The presented case study shows how the design of sample planning in WBE can inform the use of results. With adequate support from authorities, appropriate sampling programs can be established to provide an additional data source to decision makers and support pandemic response.

Acknowledgements The authors acknowledge support from of the City of Calgary, particularly the Industrial Monitoring Group for their contributions of planning and sample collection in the sewershed. The work was supported by grants from the Canadian Institute of Health Research

(Parkins: 448242) and the Canada Foundation for Innovation (Hubert: 41054) as well as discretionary funding from the Cumming School of Medicine (Parkins) and the Campus Alberta Innovates Program (Hubert).

References

1. Acosta N, Bautista M, Hollman J, McCalder J, Buchner Beaudet A, Man L, Waddell B, Chen J, Li C, Kuzma D, Shatnagar S, Leal J, Meddings J, Hu J, Cabaj J, Ruecker N, Naugler C, Pillai D, Achari G, Ryan MC, Conly JM (2021) Wastewater monitoring of SARS-CoV-2 from acute care hospitals identifies nosocomial transmission and outbreaks. Prepint available at https://www.medrxiv.org/content/https://doi.org/10.1101/2021.02.20.21251520v1
2. Ahmed W, Angel NA, Edson J, Bibby K, Bivins A, O'Brien JW, Choi PM, Kitajima M, Simpson SL, Li J, Tischarke B (2020) First confirmed detection of SARS-CoV-2 in untreated wastewater in Australia: a proof of concept for the wastewater surveillance of COVID-19 in the community. Sci Total Environ 728:138764
3. Garg S, Kim L, Whitaker M, O'Halloran A, Cumming C, Holstein R, Prill M, Chai SJ, Kirley PD, Alden NB, Kawasaki B (2020) Hospitalization rates and characteristics of patients hospitalized with laboratory-confirmed coronavirus disease 2019—COVID-NET. Morb Mortal Week Rep US Dep Heal Hum Serv Centers Dis Control Prev 69(15):458–64
4. Medema G, Been F, Heijnen L, Petterson S (2020) Implementation of environmental surveillance for SARS-CoV-2 virus to support public health decisions: opportunities and challenges. Curr Opin Environ Sci Heal
5. Nemudryi A, Nemudraia A, Wiegand T, Surya K, Buyukyoruk M, Cicha C, Vanderwood KK, Wilkinson R, Wiedenheft B (2020) Temporal detection and phylogenetic assessment of SARS-CoV-2 in municipal wastewater. Cell Rep Med 1(6):100098
6. Randazzo W, Truchado P, Cuevas-Ferrando E, Truchado P, Simón AA, Sánchez G (2020) SARS-CoV-2 RNA in wastewater anticipated COVID-19 occurrence in a low prevalence area. Water Research 181
7. Rosa G, Iaconelli M, Mancini P, Ferraro GB, Veneri C, Bonadonna L, Lucentini L, Suffredini E (2020) First detection of SARS-CoV-2 in untreated wastewaters in Italy. Sci Total Environ 736:139652
8. Whitney O (2020) Sewage, salt, silica and SARS-CoV-2 (4S): an economical kit-free method for direct capture of SARS-CoV-2 RNA from wastewater, pp 1–24
9. Zhu Y, Oishi W, Maruo C, Saito M, Chem R, Kitajima M, Sano D (2021) Early warning of COVID-19 via wastewater-based epidemiology: potential and bottlenecks. Sci Total Environ 767:145124

Utilization of Recycled Plastic in the Construction Industry

Sakr Nancy and Abouzeid Mohamed

1 Introduction

The world is facing a challenge of managing the amount of generated MSW. According to Chinese Roots Global Impact, "Despite plastics being the source of energy, replacing the non-renewable resources and diminishing carbon foot print, only 9% of the plastic wastes have been recycled, 12% incinerated and 79% still in the landfills as of 2015" [1].

Based on previous researches, tests and statistics are seeking plastic utilization and recycling in many countries. These researches can be used, as a strong base for finding solutions for this current situation in 2020.The main reasons of focusing on plastic waste is the high population rates, which have caused high pollution rates, especially in the Mediterranean area, as a result. In addition, the high rates of carbon foot print, which the world is looking for new alternatives for energy sources" [1].

2 Problem Statement

The construction industry is one of the most energy consuming industries. This is because the construction process is passing through many stages that are consuming different types of energy sources. Wide platform of sustainable implementation processes is being carried out in the construction industry, which can open the doors for using/testing different types of energy alternatives. Based on research,

S. Nancy (✉) · A. Mohamed
The American University in Cairo, Cairo, Egypt
e-mail: noor@aucegypt.edu

A. Mohamed
e-mail: mnagiba@aucegypt.edu

S. Walbridge et al. (eds.), *Proceedings of the Canadian Society of Civil Engineering Annual Conference 2021*, Lecture Notes in Civil Engineering 249,
https://doi.org/10.1007/978-981-19-1061-6_48

some countries are trying to use some types of recycled plastic in the construction building materials. This is measured as one of the promising approaches that are going in the three-dimensional sustainable development pillars of economic, social and environmental.

Furthermore, based on research, field experts and interviews with key persons in the construction field in the Middle East, there are big developing countries, such as Egypt, did not experiment applications using recycled plastic in the building materials in the construction industry. Plastic wastes are either transferred to landfills or being exported to other countries for recycling, such as India and Japan. This can be a promising start for assessing the implementation process, especially in developing countries, where wide platform of plastic wastes exist, including the different types used in road construction. This also will initiate unseen sustainable approaches in the construction industry.

3 Objectives

As Introducing recycled plastics in the construction industry is an implemented approach in international countries, yet there are no promising initiatives to use this technology in some countries. For example, although Egypt has high percentage of plastic wastes, as illustrated earlier in the research. The main reason behind exporting plastic wastes is that there is no high demand to the commodity of recycled plastics from owners or entities in different industries. While it is a treasure that should be taken into consideration on the sustainable development factors. In order to achieve success in assessing recycled plastics, all of the environmental, social and economic levels should be well evaluated. The environmental approach is tackling the material assessment and how it will be evaluated in relation with sustainability and green materials. Introducing this environmental analysis to the community and the industry is the social aspect in this equation.

The key objective of this research is serving the proficiency of bringing this approach to developing countries, such as Egypt, as it has the promising qualifications to start assessing recycled plastic in the concrete mix design for road pavers.

Environmental Objectives.

- Reduction of total plastic waste versus disposed quantities in landfills
- Introducing a sustainable source of energy in building materials
- Green Construction
- Minimizing the use of non-renewable energy

Social and Economic objectives.

- Introducing a new technique in the construction industry, rather than the traditional approach that could lead to introducing a policy for encouraging people using recycled materials in the construction industry.

- The technology is not expensive. PET plastic, such as plastic bottles are inexpensive

4 Literature Review

The combination between recycled plastic and concrete mix is implemented in developing and developed countries, which make it feasible to build on these approaches and implementations. Starting with the analysis of plastic waste and the recycled plastics, there are various types of recycled plastic types. Each type has its own specifications and method of implementation. The following table illustrates the different types of plastic, which the recycling method differs upon the functionality of the recycle plastic. In addition, the recycling approach differs from country to another based on the availability of plastic types. For example, developing countries have large amounts of PET plastics, yet PP are not widely recycled. Based on the existence of the plastic material types and the utilization category for plastic operation. Based on the global plastic waste disposal in 2015 [2]:

- The recycled plastic: 19.5%
- The incinerated plastic: 25.5%
- The discarded plastic: 55%

Polyethylene Terephthalate (PET) is the focus of this research to be used in road construction building materials. The following pie chart reflects the types of plastics produced worldwide parallel with the recycled percentage from each type. PET produced by 20.7%, while recycled by 8%. Although PET is the focus of this research, there are various types of plastic applied in recycling approaches; each type has its unique properties, strengths, limitations and applications. Plastic types, as follow [3]:

Types of Plastic Waste [3]:

- Poly Vinyl Chloride (PVC).
- Low-density poly Ethylene (LDPE).
- Poly Propylene (PP).
- High Density Poly Ethylene (HDPE).
- Polystyrene (PS)
- Poly Ethylene Terephthalate (PET)

Plastic types are categorised under two main plastic sources [3]

- Pre-use plastic source
- Post-use plastic
  - Plastic Bottles
  - Rigid Plastics
  - Plastic Film
  - Plastic Forms.

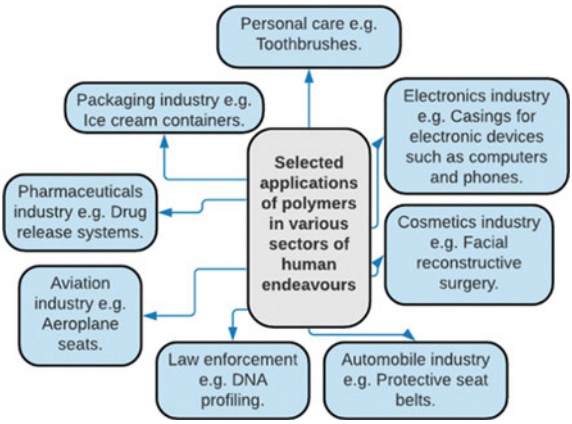

Fig. 1 Applications of plastic polymers [4]

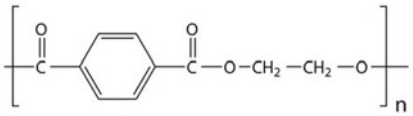

Fig. 2 Molecular structure of PET [5]

As it is shown in Fig. 1, the multiple applications of polymers in various industries.

As shown in the following chart, Polyethylene Terephthalate (PET) is a generated material from family of polymers. Polymers consist of thermosets and thermoplastics, which thermoplastic is the polymer type that can be melted and recycled. As it is formed in two types after melting, which are semi crystalline and amorphous. PET is a semi crystalline thermoplastic polymer, which is known by its durability, chemical, thermal and mechanical resistance with its dimensional stability, as well. (Families of Plastic Polymers (Understanding Plastic and Polymers, Dynisco 2019) (Fig. 2).

In order to make the recycled plastic a ready to be in the concrete mix design, it has to pass through recycling operations, such as sorting, shredding, water treatment after washing and the utilized plastic production to be reading for the concrete mix. There are various types of getting the plastic ready, such as shredding or agglomerating. The operational techniques vary, based on the functionality of this recycled plastic and the operational costs, as well (Understanding Plastic and Polymers, Dynisco 2019).

Chemical properties [5]:

- Excellent resistance to alcohols, aliphatic hydrocarbons, oils, greases and diluted acids
- Moderate resistance to weak alkalis, aromatic and halogenated hydrocarbons.

Advantages [5]:

- High strength and stiffness more than PBT
- Transportation efficiency, as it is lightweight and strong

- It is known for its good gas (oxygen, carbon dioxide) and moisture barrier properties
- Efficient properties while using ass electrical insulating
- Temperature ranges from −60 to 130 °C
- Having low gas permeability (with carbon dioxide)
- Efficient in transparent applications, when stimulating during processing
- Unbreakable; it does not fracture.

Limitations [5]:

Lesser control strength than PBT
Lesser mold capacity than PBT
Can be affected by boiling water
Can be attacked by alkalis; weak burning behavior
Attacked at high temperatures (>60 °C) by ketones, aromatic and chlorinated hydrocarbons and diluted acids and bases

Plastic Contribution in a Sustainable Construction Industry-Paver Blocks

The utilization of recycled plastic in the concrete mix design for paver blocks is an international approach in various countries, such as Mexico, India and countries in South Africa. The use of recycled plastic, mainly PET, in concrete mix design differs according to the replacement material. This means recycled plastic can work as a binder, coarse aggregates substance (by percentage) and fine aggregates, as well. In addition, this is based on the function of the concrete mix made for, whether for reinforcement, lightweight concrete or pavement construction. In this research, the focus on paver blocks, which recycled plastic, will substitute a percentage of coarse aggregates [2].

The effect of using recycled plastic on the environment is important to the sustainability of the environment and the construction industry. This is because the use of recycle plastic reduces the use of fossil fuel (non-renewable energy), reduces the use of aggregates and other resources and reduce the need for landfills to get rid of these plastic wastes; as a result, this reduces of the need for incineration, which has a dangerous effect on the environment and carbon foot print, as well [2].

Furthermore, the chemical and mechanical properties for using this recycled plastic (PET, plastic bottles) in paver, blocks have a high potential of durability. As stated, "The European Union (EU) takes measures to increase plastic recycling, introducing higher targets for recycling in its revised waste legislation. Sweden follows suit, prioritizing actions for improving the management of plastic waste." (European Commission, European Strategy for Plastics 2021). Not only Sweden, but also developing countries, such as India has initial approaches of implementing paver tiles made by recycled plastic [6].

There are various developing and developed countries which have implemented this approach, such as India, Mexico and China. "Across the EU, more than half of

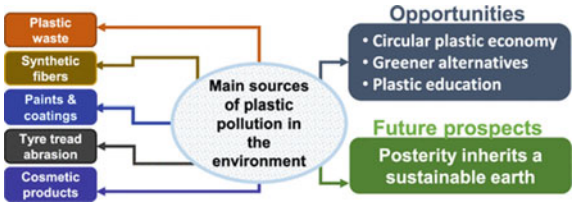

Fig. 3 Sources of plastic and sustainability [4]

the waste from plastics in construction are diverted from landfills, either by recycling them or use in waste-to-energy plants. The energy saved across the lifetime of plastics used in construction outweighs the energy used in their manufacturing" [2].

Since some countries have started engaging recycled plastic in their construction industries, an analysis for the plastic waste is being generated in a model, which calculates the impacts of environmental and socio economic pillars for sustainable environment. Waste management model indicators that is being used in the model reflects the effect of the following factors on the environment [2]:

- GHG emissions
- Economic costs and benefits
- Job Opportunities.

As illustrated from Fig. 3, In order to reach to the approach of sustainability, opportunities/pillars of sustainability should be fulfilled in the criteria of sustainability. GHC emissions, economic costs and job opportunities are covering sustainability and Resource efficiency, as well. According to EU, some environmental policies are being approached for materials, in order to reduce consumption. This is will be through recycling them. The EU approach is also tackling the circular economy, which is to keep products in use, reuse and recycle (the frequent use of waste). "A Plastic industry is making significant input to the economic development and expansion of various key sectors in the country such as: Automotive, Construction" [3].

5 Conclusion

The utilization of recycled plastic in the construction industry is a promising approach on all levels of sustainability, which some countries started to tackle. Recycled plastic is a resource efficient recycled material; wide platforms are collaborated through recycled plastic in the construction industry. The sustainable chain and the circular economy are playing an important rule in the reproduction of this plastic wastes and minimizing the consumed energy in the construction industry. Paver blocks production is a promising and a cheap technology since the used plastic type in constructing paver tiles is PET (plastic bottles), which will replace a measured percentage of coarse aggregates. This will raise the re-use of PET and reduce dumping these massive

amounts of plastic waste in landfills. This approach implemented in developing and developed countries, which reflects the cost affordability on the sustainable economic level, as well. As stated in one of the credible technical report, "Manufacturing a hydraulic concrete paver has a cost that ranges between 358 and 450 Colombian pesos, while manufacturing a paver with recycled plastic and sand costs 479 and 500 Colombian pesos" [7].

It also has public health, social and environmental impacts. This technology will generate a new construction material in the industry market, while reducing the amount of plastic wastes and energy consumed in the conventional concrete mix design process. Furthermore, this utilization of plastic wastes will transform the material from a pollutant factor to an efficient alternative to consumed energy sources.

5.1 Key Conclusions from the Study

- Collaboration between the construction industry and packaging industry should be achieved
- Achieving the integration between the recycled plastic wastes and the concrete mix design for paver blocks is part of waste management systems seeking circular economy
- Circular economy is one of the important approaches towards sustainability and energy conservation
- The re-utilization of recycled wastes in the production line will save energy and costs
- Having various precedents from other developing and developed countries, such as India, Mexico and China is a promising step towards implementing such a sustainable approach in Egypt.

References

1. Devasahayam S, Raju GB, Hussain CM (2019) Utilization and recycling of end of life plastics for sustainable and clean industrial processes including the iron and steel industry. Mater Sci Energy Technol 2(3):634–646
2. Lenkiewicz Z (2019) Innovation in plastic recycling. WasteAid
3. Das S, Das B (2017) Waste plastic green construction. Euro J Biomed Pharma Sci 4(12):307–319
4. Iroegbu AOC, Ray SS, Mbarane V, Bordado JC, Sardinha JP (2021) Plastic pollution: a perspective on matters arising: challenges and opportunities. ACS Omega 6(30):19343–19355
5. AZoM (2018) Polyethylene terephthalate polyester (PET, PETP)—properties and applications—supplier data by good fellow. AZoM.com
6. Environmental Sustainability of Plastics in Construction (2021) Modern building alliance. Accessed 21 Feb 2021
7. Saieth B, Ernesto, Carlos W, Miguel A, Jaime O (2020) Technical and economic comparison between recycled plastic and hydraulic concrete pavers